ORDERED MIXING OF DRUGS WITH PARTICULATE EXCIPIENTS

by

John Nicholas Staniforth

A thesis submitted for the degree of

DOCTOR OF PHILOSOPHY

in the

Department of Pharmacy

of the

University of Aston in Birmingham

August 1980

Ordered Mixing of Drugs with Particulate Excipients

by John Nicholas Staniforth

submitted for the degree of Doctor of Philosophy, 1980

A novel direct compression tableting excipient has been made by recrystallisation of lactose. The particles produced had high porosity, high specific surface area and high surface roughness.

The resistance to segregation of ordered mixes formed between a model drug; potassium chloride and the excipients recrystallised lactose, spray crystallised maltose-dextrose (Emdex) and a direct compacting sugar (Dipac) was studied using a vibrational segregation model. The highly porous excipients, Emdex and recrystallised lactose formed ordered mixes which did not segregate even at high accelerations and low frequencies whereas the relatively smooth excipient, Dipac, displayed marked segregation in most vibration conditions. The vibrations were related to practical conditions measured in pharmaceutical process machinery. The time required to form an ordered mix was inversely related to the stability of the mix when subjected to vibration.

An ultracentrifuge technique was developed to determine the interparticle adhesion forces holding drug and excipient particles together as ordered units. Excipient powders such as Emdex and recrystallised lactose, which formed non-segregating ordered mixes, had high interparticle adhesion forces. Other ordered mixes that segregated when subjected to different vibration conditions were found to have large quantities of weakly-bound drug particles; such mixes included those with Dipac as the carrier excipient as well as those containing a high concentration of drug.

The electrostatic properties of different drug and excipient powders were studied using a Faraday well and an electrometer. Excipient powders such as Emdex and recrystallised lactose which formed stable ordered mixes also had a widely different surface charge in comparison with drug particles, whereas Dipac had a similar surface charge to the drug particles and formed unstable ordered mixes.

A specially constructed triboelectric charging apparatus based on an air cyclone was developed to increase the affinity of drug particles for different excipient particles. Using tribo-electrification to increase the interparticle adhesion forces, the segregation tendencies of unstable ordered mixes were greatly reduced.

The stability of ordered mixes is shown to be related to both the surface physical characteristics and the surface electrical properties of the constituent carrier (excipient) particles.

Keywords

Ordered Mixing, Vibrational Segregation,

Interparticle Adhesion Forces, Triboelectric charging

Acknowledgements

It is my great pleasure to thank Dr. John Rees for supervising this work and for his help, guidance, useful criticism and constant encouragement. I also wish to thank Dr. John Kayes who became my academic supervisor in 1978.

My thanks are due to Profs. M. R. W. Brown, D. G. Wibberley and C. B. Ferry for providing laboratory facilities and to the Science Research Council for the award of a Research Studentship.

I should like to express my grateful thanks to the Winston Churchill Memorial Trust for awarding a Travelling Fellowship which enabled me to carry out research at the Victorian College of Pharmacy in Melbourne, Australia. I am indebted to Prof. John Hersey for help and guidance in the work on adhesion forces in ordered mixes. This work was carried out at V.C.P. with Felix Lai to whom I am grateful for technical assistance and useful discussions.

In addition I should like to thank all those who provided research facilities and help in any way: Dr. John Fell of Manchester University for use of the Ströhlein Areameter; Mr. Alan Faley of the Railway Technical Centre, Derby for use of Quantimet 720; Dr. John Stevens of Boots Ltd., Nottingham for use of Quantasorb surface area equipment; The Dept. of Mechanical Engineering for the equipment used in the vibration study; The Dept. of Construction Engineering for use of the mercury porosimeter; Dept. of Chemical Engineering for use of apparatus to prepare the large batch of lactose crystals. I also wish to express my thanks to Mr. Peter Dixon of Aston Technical Services Ltd., for constructing the ultracentrifuge rotor tube insert, Faraday Well and the charging cyclone apparatus.

I should also like to thank the National Research Development Corporation for their interest in this research and for patenting the recrystallised lactose excipients.

My thanks to Lynda Page for typing this thesis.

To My Parents

And

To My Wife,

Andrea.

List of Contents

List of Figures

List of Tables

List of Symbols

A	Area under sample curve (Quantasorb)
A_{cal}	Area under calibration curve (Quantasorb)
A_{cs}	Adsorbate cross-sectional area (Quantasorb)
a	Constant radius of small particle
a_m	mth order Fourier coefficient
a_o	Fourier coefficient
a_q	Particle radius of maximum charge, q
a_r	Adherent particle radius
b	Acceleration due to vibration
C	Distance between particle centres ($C = R_1 + R_2 + d_R$)
C_c	Condenser capacity of a charged particle
C_p	Corrected counter reading (mercury porosimetry)
C_t	Initial counter reading (mercury porosimetry)
C_v	Coefficient of variation of a binary mix
c	Rate constant of mixing
D	Carrier particle diameter
D'	Particle diameter
D''	Diameter of large sphere
D'_o	Diameter of a smooth sphere
D^o	Diameter of large particles
D_o	Poured or fluff density
D_c	Clump shape coefficient (Danckwerts)
D_e	Equilibrium bulk density
D_p	Diameter of sphere with same volume as particle
D'_s	Segregation coefficient
d	Adherent particle diameter
d'	Diameter of small particle
d^o	Equivalent spherical diameter of drug particles
d_R	Surface separation distance
E	Error variance
E'	Energy of interaction
E_m	Electrostatic field, mono-ionised component

E_y	Young's modulus
E_Y	Composite Young's Modulus of Plate and Particle
e	Exponential
e_c	End count (Quantimet)
$F_{adhesion}$	Force of adhesion obtained experimentally
$F_{applied}$	Applied separation force
F_D	Electrostatic adhesive force (Donald's model)
F_o	Sum of all adhesive forces outside contact area
F^p	Adhesive force
F_X	Charge force
F_x	Fraction of x adhering to carrier y
F_y	Fraction of y adhering to carrier x
F^o_{el}	Electrostatic adhesive forces
F^o_{vdw}	Van der Waals adhesive forces
F_1	Adhesion forces of particles trapped in a pore
F_2	Adhesion forces of particles trapped in a pore
F_g	Maximum field gradient
F_{MAX}	Maximum Coulomb force
f	Weight fraction of a sample within a class interval
f_m	Cell factor (mercury intrusion porosimetry)
f'	Fraction of fines adhering to carrier as a monolayer
G	Percentage by weight of one component of a mix
G^w_o	Weight of drug per sample (g)
H	Hamaker constant
H_i	Busliks universal homogeneity index
H_i^*	Difference between H_i during mixing and H_i required by pharmaceutical specification
H(t)	Hardness of carrier particles
h	Height of flattened portion of 2 spheres in contact
h_p	Distance from particle centre to substrate
I	Danckwerts mixing index
I_c	Current generated
j	Constant of shear mixing

K_o	Vibrational inertia
k	Dielectric constant of charged particle
L	Layer depth of material in a vibrator
L'	Bed length in a non-random mix
L_V	Variable length of small dendrite tip
L_{VIB}	Length of vibration
M	Mass of sample
M_a	Molecular weight of adsorbate (Quantasorb)
M_o	Ordered unit mass
M_{ad}	Mass of adherent particles
m	Integer in fourier series
N	Number of samples taken
n	Number of particles in sample
n'	Number of particles in class interval
n_e	Effective particle numbers in a non-random mix sample
n_o	Number of binding sites
P	Sum of all adhesive forces inside contact area
P_e	Peclet number
P_R	Precision of ultracentrifuge-determined adhesion forces
P_T	Vibrational force of inertia
P_x	Probability of x in a non-random mix
P'	External pressure
$\bar{p}$	Mean proportion of x in a non-random mix
P_d	Constant related to dielectric constant
P_L	Cyclic air pressure at vibrator base
P_o	Atmospheric pressure
$p/_{ps}$	Partial pressure
Q	Effective particle charge contributing to adhesion
Q_o	Point charge on a particle
Q_T	Total particle charge
q	Charge on particle q
q'	Image charge on particle q
q_a	Number of atoms per centimetre

R	Leakage resistance of a charged particle
R'	Particle radius
R_1, R_2	Sphere radii
R_d	Radial dispersion coefficient
$R(r)$	Scale of segregation correlogram axis (Danckwerts)
R.C.F.	Relative centrifugal force (Ultracentrifuge)
r	Distance between different sampling points (Danckwerts)
r'	Distance from axis of rotation
r_1	Unit vector along r
r_c	Radius of contact area
r_q	Vector from q to q'
r_s	Rugosity, or surface roughness
r_v	Variable radius of large dendrite (Dendritic Coarsening)
S	Spot sample standard deviation of random mix
S'	Separation surface
S''	Height of powder throw during vibration
S^2	Spot sample variance of random mix
S_a	Surface area determined by mercury porosimetry
S_d	Equivalent spherical diameter
S'_p	Maximum theoretical separation surface
S_s	Surface area determined by nitrogen adsorption
S_{seg}	Scale of segregation
S_t	Total surface area (Quantasorb)
t	Mixing time
t'	Vibration time
t_c	Residual electrostatic charge half-period
t^k	Rate constant of diffusional segregation
$t_o^{(-)}$	Time at which flight begins (Vibration model)
$t_o^{(+)}$	Time 2 at which flight begins (Vibration model)
u	Mean vertical velocity
u'	Superficial air velocity in vibrator

V	Total volume
V^*	Velocity modifying term
V_c	Contact potential difference
V_{clump}	Volume of drug particle clumps or aggregates (Danckwerts)
V_e	Equilibrium bulk volume
V_m	Mercury volume (mercury porosimetry)
V_n	Bulk volume after n taps (Jolting Volumeter)
V_o	Particle velocity
V_o'	Poured or fluff volume
V_p	Residual potential or charge on powder particles
V_{po}	Original potential or charge on powder particles
V_s	Volume of sample cell (mercury porosimetry)
v	Sample volume
W	Mean weight of particles in a non-random mix
W_c	Weight of empty sample cell (mercury porosimetry)
W_c'	Weight of single carrier particle
W_d	Dose weight
W_o	Sample weight required to produce a standard deviation of 1%
W_p	Mass flow rate of powder
W_Q	Sample weight for Quantasorb area determinations
W_s	Sample weight before mercury penetration
W_t	Weight of cell, sample & mercury following penetration
w	Individual particle weight
$\bar{w}$	Mean particle weight of ingredients
W_e	Effective particle weight
$\bar{w}_g$	Average weight, per piece, of size being investigated
X	Gas weight
X_{cal}	Calibration gas weight
x	Proportion of ingredient x
$\bar{x}$	Mean proportion of component x
x_1, x_2 etc.	Concentration of component x in units 1, 2, etc.
x_j	Proportion of ingredient x in jth sample
y	Proportion of ingredient y
$\bar{y}$	Mean proportion of component y
y_d	Yield pressure

z	Distance above base
z'	Distance of particle from substrate
z_o	Distance of maximum force of adhesion

Greek Type

α	Dimensionless charge parameter ($\alpha = R/3d_R^{0.7}$)
α'	Shock forces in handling
β	Cycle fraction of bed flight
β_r	Roundness of particle ($\beta_r = 2R_1/D_p$)
Δ_t	Effective duration of contact
δ	Wedge angle
δ^o	Penetration depth of surface charge
$\delta_{cs}(r,t)/\delta_r$	Boundary condition of diffusional segregation
δ_m/δ_t	Unit mass flow of drug particles
ε	Bed voidage in vibrated bed
ε_c	Capacitivity constant for medium
ε_d	Dielectric constant of air
ε_o	Influence constant ($\varepsilon_o = 8.86 \times 10^{-4}$ Asec/V_{cm})
ε_o'	Dielectric constants
ε_p	Powder porosity
η	Fluid viscosity
γ	Eulers constant (0.5772)
θ	Angle of inclination of target plane
θ'	Mercury contact angle
θ''	Phase angle of vibration
κ	Permeability constant of vibrating bed
Λ	Constant length of large dendrite
λ	London-van der Waals constant (Hamaker)
μ	Mass median diameter before friabilation
μ_f	Mass median diameter after friabilation

v_o	Horizontal velocity
v^p	Poisson ratio
$2\pi\hbar$	Planck's constant
Ψ_o	Vibration coefficient 2
$\Psi_{(+)}$	Vibration coefficient 1
Φ	Friability index
ρ	Mean particle density
ρ_β	Bulk density
ρ'	Air density
ρ^o	Drug density ($g.cm^{-2}$)
ρ_m	Density of mercury
ρ_o	Density at atmospheric pressure in vibrating bed
ρ'_o	Circular contact area
ρ_r	Dielectric resistivity of a particle (e.s.u.)
ρ'_r	Dielectric resistivity of a particle (ohm. cm^{-1})
ρ_s	Sample true density
ρ_x	Density of x
ρ_y	Density of y
Σ	Summation
σ_A	Specification standard deviation of a pharmaceutical mix
$\sigma_{(lr)}$	Long range segregation in non-random mix
σ_n	Inter-sample standard deviation of non-random mix
$\sigma_{(n)}$	Any randomness contributing to std. deviation of non-random mix
σ_{NR}	Theoretical standard deviation of non-random mix
σ_o	Standard deviation of totally unmixed system
σ_{POR}	Standard deviation of partially ordered random mix
σ_R	Theoretical standard deviation of random mix
$\sigma_{(sr)}$	Short-range dilution of aggregates in non-random mix
σ_{TOTAL}	Standard deviation of Total Mix
σ_∞	Standard deviation of theoretical random mix after infinite mixing

ζ	Point at which R(r) cuts r axis
ζ'	Zenith angle
τ	Time constant of model condenser produced by two particles
ξ_1	mth order phase lag
ξ_z	Surface tension of mercury
ω	Angular velocity
ω'	Angular vibration frequency
$\bar{\omega}$	Angular frequency
$\hbar\omega$	Lifshitz - van der Waals constant

Russian Type

Ш	Re-entrant shape factor
$Ш_m$	Mean re-entrant shape factor

Chapter One

1. Introduction and Theory

1.1 Pharmaceutical Powder Technology

In the preparation of tablets, capsules and other pharmaceutical dosage forms, particulate solids must normally be mixed and processed to ensure homogeneity of drug content and uniform distribution of excipients. A generally accepted definition of an excipient, as quoted by Cooper (1), is: "any component other than the claimed therapeutic ingredient or ingredients".

Pharmaceutical powder technology involves the characterisation and processing of drug and excipient powders both at the formulation stage and during normal manufacture of the dosage form (2). In pharmaceutical research and development, evaluation of individual particle properties and bulk material characteristics is often necessary. This involves an investigation of the chemical and physical performance of the drug itself and in the formulated dosage form, as well as studies of the processing behaviour of the powder mix. At the pharmaceutical production stage, powder technology is used in quality control for characterisation of the raw materials, including drug and excipient powders. In-process control measurements are made on the powders and granules and final quality control checks are carried out on the finished products.

Despite the problems associated with bioavailability and homogeneity when formulating drugs into solid oral dosage forms, delivery systems such as tablets and capsules offer many advantages. The main reason for compacting pharmaceutical powders is to

produce an easily administrable dosage form by reducing the bulk volume of the formulation and providing a precisely metered dose of drug. The solid dose is a single unit which, especially when packed individually, offers improved stability, child safety and reduced microbial contamination (3). The compressed tablet is the most widely used of the different solid oral dosage forms.

There are several different ways of preparing a tablet from its constituent drug and excipient powders (4). One technique which is becoming increasingly popular is the method known as direct compression.

1.1.1 Direct Compression

The process of direct compression is the simplest method of preparing a tablet from a mixture of drug and excipient powders. The simplicity of the process leads to improved reliability with a reduction in the complexity of tablet formulation (5). The process has many advantages over other methods of tablet production, both economic and technical (6). Most direct compression excipients are still derived from natural products of either animal, e.g. lactose, or plant origin, e.g. celluloses (7). Shangraw (8), lists some of the commercially available direct compression excipients.

The direct compression excipient should possess certain specific properties in addition to those of any other type of excipient. As well as being completely compatible with the drug, the direct compression excipient must also produce a tablet of the required physical, mechanical and biopharmaceutical properties. The properties of an ideal direct compression excipient have been listed by Kanig (9):

1. The material should have a high fluidity or flowability.
2. The material should have high "compressibility".
3. Direct compression excipients should be physiologically inert.
4. Excipients should not show any physical or chemical changes on ageing and should be stable to heat, moisture and air.
5. Excipients should have a high "capacity", which is defined as the amount of active ingredient which the diluents can carry without adversely affecting the direct compression of tablets.
6. Excipients should be colourless and tasteless.
7. Excipients should be relatively inexpensive.
8. Excipients should not interfere with the bioavailability of active ingredients.
9. Excipients should be compatible with all types of active ingredients.
10. Excipients should be able to be re-worked without loss of flow or compressibility.
11. Excipients should have a good strength profile.

In addition to these criteria, Mendell (10) lists hygroscopicity as an undesirable characteristic and "acceptability" as an excipient requirement. "Acceptability" of an excipient is its ability to comply with pharmacopoeial requirements relating to purity, inertness and compatibility. Most excipients are unable to satisfy at least one of these criteria. Spray-dried lactose, for example, has a tendency to discolour particularly in the presence of amines (11). Microcrystalline cellulose has very poor flow properties (12). Although individual excipients may have a weakness in one particular area, direct compression excipients as a whole have two major

disadvantages. The first is that unless the drug itself is easily compressible, the amount of drug which may be added to the excipient is restricted to about 30% of the compression weight (4). For this reason, the direct compression process is often confined to tableting low-dose, high potency drugs. This compounds the second disadvantage, namely the tendency for excipient powders to segregate from the drug powder in a free flowing direct compression mix.

Although segregation of drugs from excipients can also occur with wet granulations (13, 14), the completely free movement of particles in a direct compression random mix means that any segregation tendency during processing will almost inevitably produce dosage variations.

In setting standards for tablets, the British Pharmacopoeia (15) uses the test of uniformity of weight as a control of content uniformity. This same criterion is employed by other national and trans-national pharmacopoeias. However, Train (16) used a statistical approach to show that in formulations where the drug constitutes less than half the gross compression weight, the tablets could comply with the pharmacopoeial standards despite many individual tablets being outside the specified dose range. The variation could be as high as four times the official assay limits in most cases and eight times or more with one or two formulations. Analysing practical systems, Moskalyk et al. (17) found excessive dosage variation in individual tablets from batches which had passed the official tests for content uniformity.

It is possible that some of these dose uniformity problems in the case of direct compression systems may be overcome by careful design of a new direct compression excipient. One of the

hypotheses which form the basis of this thesis is that control of the crystallisation process can produce crystalline powders with optimal physical properties for mixing and direct compression.

1.2 Crystallisation of direct compression excipients

1.2.1 Crystal growth

Crystal growth occurs by a three-stage mechanism (18):

1. Diffusion of solute molecules from the bulk of the solution (mother liquor) to the crystal-solution interface.
2. A subsequent surface reaction as the solute molecules arrange themselves into the crystal lattice.
3. Diffusion of heat of crystallisation from crystal solution interface back into the mother liquor.

Crystal growth rates in systems where growth conditions are identical and crystal shape factors remain constant are governed by the McCabe - ΔL Law. Under these conditions growth rate is independent of crystal size (19). Abegg *et al.* (20) developed a model to account for size dependent crystal growth not governed by the McCabe - ΔL Law. This model has been further modified by Nyvlt (21) to allow for the crystal residence time in the crystalliser.

The physical properties of a crystalline powder are largely governed by the crystal growth conditions. The crystal size distributions are influenced by the nucleation rate, growth rate and hydrodynamic behaviour of the suspension in the crystalliser (22).

1.2.2 Alteration of crystalline habit

The external shape of a crystal is determined by the relative development of the various crystallographic faces governed by their growth kinetics. The slowest growing faces have the greatest

influence on the final habit (23). In general, the rate of cooling, degree of supersaturation, mother liquor impurities and the nature of the crystallising solvent all affect the crystal habit (24). Torgeson and Strassburger (25) described the growth of oxalic acid crystals from different aqueous concentrations of acetone. The crystal habit of the oxalic acid changed from pinacoid to prismatic with increasing acetone concentration. Davey et al. (26) have shown the dependence of crystal growth rates linked to the strength of habit modifying dislocation groups, on supersaturation. Solvents such as acetone may be used to increase supersaturation by decreasing solubility. This leads to high crystallisation pressures and can produce altered physical properties by agglomeration of rapidly growing crystallites. In multiparticulate systems particle-particle collisions frequently occur, leading to secondary nucleation. These collisions can also produce crystal agglomeration (27). The rate of agglomeration is greatest when the crystallisation rate is high, and when the diameter of the particles is small.

The effect of the crystallisation conditions on the habit of α-lactose monohydrate has been studied by Herrington (28, 29), (Figure 1). The crystal habit changes from the prismatic dendrites formed when growth velocity is high (A), through the intermediate pyramids (D) and "tomahawks" (E, F) to the fully-developed crystal exhibiting 13 faces (G, H). In cases where lactose is crystallised from an organic solvent solution, the fully-developed crystal will rarely form due to the high crystallisation pressure. The effect of the crystallising solvent on the habit of the lactose powder has been studied by Majd and Nickerson (30). They found that at high concentrations of ethanol (90%), dendritic crystals of the

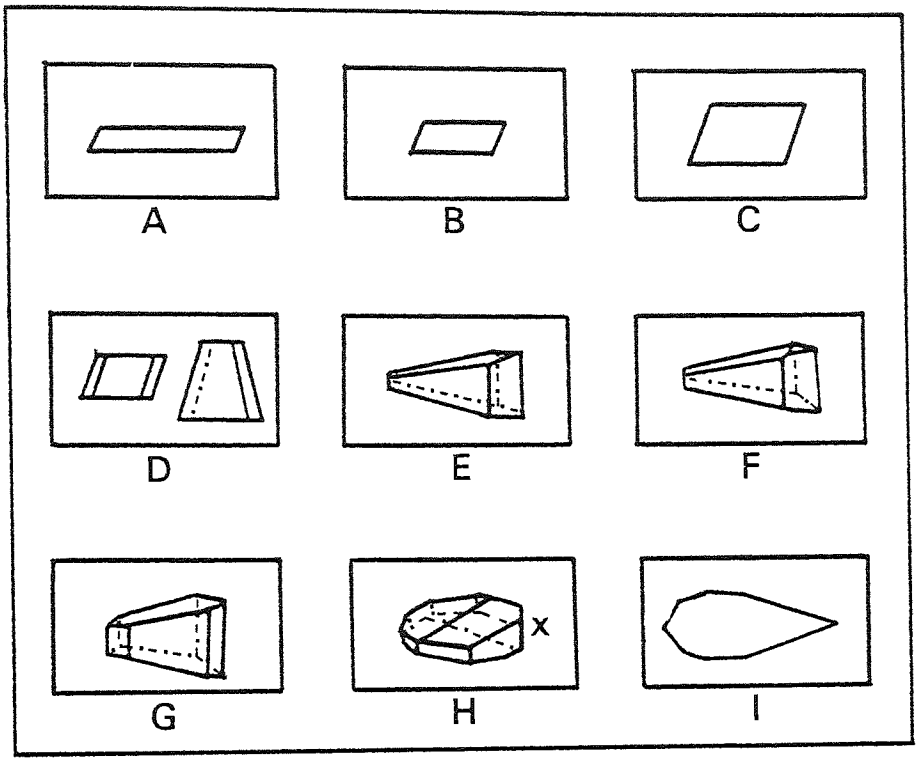

Figure 1. The crystalline habit of α-lactose monohydrate (after Herrington, 28, 29)

A. Prism, formed when growth velocity is high.

B. Prism, formed more slowly.

C. Transition diamond, between prism and pyramid.

D. Pyramids produced by diamond thickening.

E. Tall pyramid or tomahawk.

F. Tomahawk with an additional face to E.

G. Lactose "fully-developed" crystal.

H. Lactose crystal with 13 faces.

I. Profile of H with tomahawk blade pointed.

X. For explanation see text.

polymorphs, anhydrous α- and β-lactose were formed (type A, Fig. 1). At lower concentrations of ethanol (60%), most crystals were partially or fully developed tomahawks of α-hydrated lactose (E, F Fig 1). The polymorph, α-(stable) anhydrous lactose crystals were formed by mixing with pure methanol to remove the water of crystallisation (31). The effect of additives, including alcohols, on the growth rates of the individual crystal face of lactose has been studied by Michaels and van Kreveld (32). They discovered that ethanol and methanol had similar effects: in 1% solution they accelerated growth of the (010) face (end face X, crystal I, Fig. 1) by a factor of 1.6 and by 1.3 for the other faces. Although all the alcohols depressed lactose solubility it was considered that change in growth rates were caused by alcohol adsorption onto crystal faces producing step generation. Crystallisation of lactose from alcohol can produce dendrites which become agglomerated by multiple twinning. The crystallite complex formed is known as a spherulite and consists of dendrites radiating from a central nucleus. By appropriate selection of crystallisation techniques it might therefore be possible to produce crystalline powders in a suitable form for use as non-segregating, free-flowing direct compression tableting excipients.

1.3 The Process of Powder Mixing

Although unsatisfactory content uniformity of tablets may result from the segregation of powder mixes during processing it may be attributable to incomplete mixing of the drug and excipient during initial processing prior to tableting. To minimise the probability of a batch of tablets or capsules failing a content

uniformity test it is necessary to understand the intermediate processes taking place between the initial preparation of the powders and the final compression or encapsulation (33). One of the major intermediate operations is the process of powder mixing.

The problems associated with producing a consistently homogeneous mix are linked to the constituent particles molecular properties. Unlike a Newtonian fluid, solid particles have no intrinsic mobility; they are constrained to remain in their relative positions by interparticulate forces and the force of gravity. In the case of two fluids the intrinsic mobility of the fluids combines with the law of increasing universal entropy to produce homogeneous fluid mixtures, without any external applied force. However, to produce a solid-solid mix, work must be done to overcome the influence of gravity on the particles. The mechanisms which govern this operation and the different methods involved are all part of the process of powder mixing.

A recent literature survey was carried out on various aspects of powder mixing (34). The survey lists 650 references classified into 17 separate categories relating to powder mixing processes.

In a review of powder mixing theory, Hersey (35) considers the influences of various powder properties on the ultimate homogeneity of a mix, and the mechanisms which affect the final degree of mixedness. The review also investigates the relative importance of randomisation, ordering and non-random mixing in producing a powder mix. Rees (36) reviewed the process of powder mixing, with special attention to the requirements of the pharmaceutical industry.

The different types of powder mixes may be divided into two main groups: those formed by randomisation and those formed by mechanisms other than randomisation. The second group can be sub-divided into those formed by ordering and by other non-random mixing mechanisms. Linking the two main divisions there exist mixes which owe their homogeneity to a combination of randomisation and processes other than random mixing. These systems include partial ordered random mixes and total mixes.

The theory of random mixing was the first attempt to scientifically evaluate the formation of powder mixes.

1.3.1 Random mixing theory

Random mixing is a statistical process in which the bed of particles is repeatedly split and recombined until there is an equal chance of any individual particle being at any given point in the mix at any one time (37). Weidenbaum and Bonilla (38) used the concept of a change in relative frequency of spot sample compositions in various composition ranges to illustrate the process of random mixing. According to their scheme, random mixing occurs when motion is imparted to two sets of particles, x and y, causing them to rearrange producing a continuous narrowing of the frequency distribution of sample composition. This approaches the binomial distribution at equilibrium. Since, as random mixing proceeds, the probability of locating a given particle at any point is described by a binomial curve it is possible to determine statistically the quality of a mix according to its variance or standard deviation. Lacey's treatment (39) of such a binary powder mix is based on equidimensional particles, indistinguishable from one another except by properties not affecting their mechanical

behaviour. These particles proceed towards an ideal mix via randomisation (Figure 2). Lacey defined this transition mathematically:

$$\sigma_o = x \cdot y \qquad (1)$$

$$\sigma_R = \frac{x \cdot y}{n} \qquad (2)$$

where σ_o represents the standard deviation of the totally unmixed state and σ_R, that of the completely randomised (ideal) mix; x and y are the proportions of the ingredients (black and white particles in Figure 2) and n is the number of particles in the sample. From Figure 2 it can be seen that in this theoretical treatment, mixing proceeds from a highly ordered un-mixed state, through a disordered random state to a highly ordered ideal state.

Stange (40) derived an alternative relation to calculate σ_R for practical mix components having a range of physical properties such as size, shape and density:

$$\sigma_R^2 = x.y \Big/ \left(\frac{M}{\left[y\{\bar{w}(1 + \bar{s}^2/\bar{w}^2)\}_x + x\{\bar{w}(1 + \bar{s}^2/\bar{w}^2)\}_y \right]} \right) \qquad (3)$$

where M is the mass of sample removed, $\bar{w}$ ($\bar{w}_x$ & $\bar{w}_y$) is the mean particle weight of the ingredient and $\bar{s}$ ($\bar{s}_x$ & $\bar{s}_y$) is the standard deviation of particle weight for the respective mix components. To solve this equation for σ_R it is necessary to know the mean and standard deviation of particle frequencies for each component. Poole, Taylor and Wall (41) simplified this formula for calculation purposes using the relationship

$$fM = n'w \qquad (4)$$

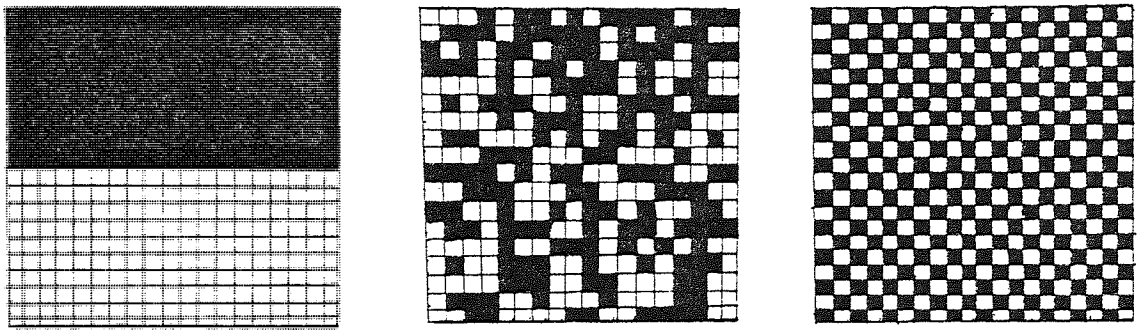

(a) (b) (c)

Figure 2. Theoretical treatment of mixing process a) unmixed state b) randomised state c) ideal state

(where f is the weight fraction in each class; w, the individual particle weight and n', the number of particles in the class interval) $\bar{w}$ and $\bar{s}$ in equation (3) may be replaced by a single term (Σfw):

$$\sigma_R^2 = x.y \Big/ \left(\frac{M}{y(\Sigma fw)_x + x(\Sigma fw)_y} \right) \qquad (5)$$

Johnson (42) further simplified this equation for mixes containing less than 1% of one ingredient. In this situation the value of y will approach unity and: $x(\Sigma fw)y << y(\Sigma fw)x$ thus equation (5) will simplify to:

$$\sigma_R^2 = {}^{x}/_{M}\left[(\Sigma fw)_x\right] \qquad (6)$$

In a mix where the proportions of one excipient are between 0.01 and 0.1, an approximation based on $y \geq 90\% = 0.9$ and $x \leq 10\% = 0.1$ produces:

$$\sigma_R^2 = \frac{x.y^2}{M} \cdot (\Sigma fw)_x \qquad (7)$$

Kristensen (43) developed a relationship to describe the theoretical variance of a two-component mix. The equations are based on samples of constant volume, to mirror the situation when solid dosage forms are prepared. Unfortunately, under these conditions, changes in particle properties would lead to a change in compression volume to maintain constant compression weight rather than the reverse. The expressions do not account for interparticle porosity in assessing sample volumes. In its full form the relationship for the variance of a binary mix based on particle volume is given by:

$$\sigma_R^2 = \frac{1}{N} \sum_{i=1}^{N} \cdot \sum_{j=1}^{n'} \frac{1}{n'_2} \left(x_{j,i} - \frac{x\rho}{\rho_x}\right)^2$$

$$+ \frac{1}{N} \sum_{i=1}^{N} \cdot \sum_{j \neq k}^{\frac{1}{2}n'(n'-1)} \frac{2}{n'^2} \cdot \left(x_{j,i} - \frac{x\rho}{\rho_x}\right)\left(x_{k,i} - \frac{x\rho}{\rho_x}\right) \qquad (8)$$

where ρ & ρ_x are the mean particle densities and the density of component particle x respectively. Equation (8) can be subdivided into three component variances each of which can be developed separately. In the random state these components may be brought together and reduced to give:

$$\sigma_R^2 = \frac{x.y}{M} \cdot \frac{\rho^4}{\rho_x^2 \cdot \rho_y^2} \cdot \left[x.\bar{w}_y \cdot y.\bar{w}_x \right] \qquad (9)$$

This becomes the same as the relationship of Poole, Taylor and Wall if the particle densities are the same. This equation however has been derived without any assumptions regarding particle size distribution.

If the components consist of the same particle weight, w, equation (9) can be further reduced to re-generate Lacey's relationship (2) in the form:

$$\sigma_R^2 = x \cdot y \cdot \left\{\frac{w}{M}\right\} \qquad (10)$$

Manning (44) modified Lacey's equation (2) by replacing the proportional relationship of x & y by a percentage term:

$$\sigma_R^2 = \frac{G(100 - G)_w}{M} \qquad (11)$$

where G is the percentage of one component of the powder mix.

Buslik developed equation (11) to measure the variance σ_g^2 of the percentage of any particle size W_g in random samples of constant weight M from any given size distribution (45):

$$\sigma_g^2 = G.\ (100 - G)\ \bar{w}_g + G^2(\bar{w} - \bar{w}_g) \ /\ M \qquad (12)$$

This equation only holds true whilst all particles are of the same density. The inter-relationship of the equations of Buslik, Stange, Poole et al. and Lacey has been described by Harnby (46).

Another way of mathematically describing a random mix is given in equation (13). Beaudry (47) developed a relationship to compare blender efficiencies according to their ability to reduce inter-batch variance. Part of this expression can be arranged to give:

$$\sigma_R^2 = \frac{\Sigma x_j^2 - \bar{x}^2}{N} \qquad (13)$$

where x_j is the proportion of ingredient x in the j^{th} sample; $\bar{x}$ is the mean proportion of x in the mix and N is the number of samples removed. It can be seen that as the mix approaches the ideal state, σ_R^2 becomes zero. This form of σ_R^2 can be used to calculate intersample variance which has some practical significance (48).

Under certain circumstances, most of the foregoing expressions reflect the theoretical variance of the ingrediert distribution in a random mix. The final distribution of particles in a random mix is produced by several different mechanisms.

1.3.1.1 Mechanisms of random mixing

Mixing of bulk solids begins from a static powder bed in which all the particles are in spatial equilibrium, under the force

of gravity. The first step in any mixing process is a dilation of the powder bed (49). The importance of the principle of dilatancy of a powder bed was first described by Jenkin (50). Dilatancy is a fundamental property of a granular material on which its behaviour and the forces it exerts ultimately depend. The function of dilatancy in random mixing is to allow relative particle motion. Mixing then proceeds according to either a single mechanism or a combination of mechanisms. The interrelationship of different mixing mechanisms has been described in a review by Bridgwater (51). The most widely accepted mechanisms of mixing are those outlined by Lacey (52). They include shear, diffusion and convection as the basis of particle mixing.

1.3.1.1.1 Shear Mixing

This mechanism of mixing occurs when slip planes are formed in a powder bed causing bulk rearrangement of different sections within the mass. This same mechanism was described by Brothman et al. (53) as "three dimensional shuffling" in which mixing took place across planes of separation. They used the magnitude of these separation surfaces, S', and the time of mixing, t to produce a kinetic expression based on the law of mass action:

$$S' = S'_p (1 - e^{-tc}) \qquad (14)$$

where S'_p is the maximum theoretical separation surface and c is a rate constant for the mixing process. Lacey (52) extended this expression by using the fraction R of a mix component in a sample of the separation surface (interface) as a measure of S' the instantaneous surface of equation (14). To allow for the fact

that R will intersect more than one separation surface as mixing proceeds, thereby reducing the number of mixed samples in relation to the actual number of surfaces he introduced the exponential term:

$$R = 1 - e^{-j.S'.v / V} \qquad (15)$$

Equation (14) then rearranges to give:

$$R = 1 - \exp\left\{-jS'm\,(1 - e^{-ct})\,{}^{v}/_{V}\right\} \qquad (16)$$

By assessing R at different mixing times, S_m' and C can be determined separately. Lacey was able to show (52) that S_m' increases with decreasing particle size. Weydanz (54) considered a similar mechanism according to the system variance rather than the expansion of interfaces:

$$\sigma = \left\{e^{-2ct} + \sigma_\infty^2\,(1 - e^{-2ct})^2\right\}^{\frac{1}{2}} \qquad (17)$$

where σ_∞ is the variance of the system after infinite mixing time.

1.3.1.1.2 Diffusive mixing

This mechanism is described as the distribution of particles over a freshly developed surface (52). This involves the transfer of individual particles across boundaries linking adjacent zones of different materials. These zones occur along shear planes and in the tumbling regions of the powder (55). Diffusive mixing also occurs by the percolation of fines through the interparticle voids under the influence of gravity. The analogy between particle diffusion and gaseous diffusion is possible because of the behaviour of moving material. As each particle rolls down a slope

it has an equal chance of deflecting to either side of another particle at each collision. The particle has a component of random motion during flight following collision which allows the application of the classical diffusion theory. From theoretical considerations of Fick's second law of diffusion, Lacey (52) produced a relationship for diffusive mixing based on the distribution variance:

$$s^2 = \frac{2}{\pi^2} \cdot e^{-2\pi^2 c} \cdot \sin^2 \cdot x\pi \qquad (18)$$

c is a rate constant linking the diffusion coefficient and mixing time as a function of the length of the mixer.

Percolation rates of fine particles through a powder bed have been modeled (56) using a diffusion coefficient for the bulk powder based on Einstein's diffusion coefficient. This system is also dependant on the strains in the bed, such as those which exist in failure zones. Scott and Bridgwater (56) treat percolation as a separate fundamental mixing mechanism. Simulation of diffusional mixing based on a random walk process has been carried out by Cahn and Fuerstenau (57) with good correlation between diffusion coefficients obtained in theory and practice. Strek et al. (58) have developed a mathematical model based on the mechanism of diffusive mixing.

1.3.1.1.3 Convective mixing

This mechanism is described by Lacey (52) as the transfer of groups of adjacent particles from one location to another. The process by which this is achieved is not described, and it is completely omitted from a description of mixing mechanisms by Valentin (59). Williams (60) considers that convective mixing cannot occur without the formation of some slip planes, and in this

way it is related to shear mixing. Under certain conditions convective mixing is analogous to diffusive mixing (51) and longitudinal diffusion of individual particles is produced as if pure diffusion is occurring. Hogg et al. (61) consider that convective and shear mixing are merely a combination of effects which involve diffusion and the breaking up of agglomerates. Convective mixing, if it could be induced as the sole mixing mechanism, could be a useful tool to promote good mixing whilst minimising segregation (60), since it may be the only mechanism unaffected by particle size and density effects.

Although the different mechanisms of mixing have been considered separately, it is probable that whilst one form may predominate, no one mechanism will be responsible for the formation of a random mix (60).

1.3.2 Non-Random Mixing Theory

In the theory of random mixing (Section 1.3.1) it was assumed that the component particles proceeded from complete separation to complete integration so that the probability of finding a particle of either system was equal. A practical powder mix will rarely, if ever, be truly random. Williams (62) called this process of incomplete mixing, non-random. The theory of non-random mixing accepts that the probability of finding any constituent particle in a mix is not equal. The probability, Px, of finding a given component, x, is a function of the sampling pattern. The variance σ^2_{NR} of samples from a non-random mix containing n particles at a distance X from a reference plane is given by:

$$\sigma^2_{NR} = \int_0^1 \left[(\bar{P} - P_x)^2 + P_{x/n} (1 - P_x) \right] . dX \qquad (19)$$

where $\bar{P}$ is the mean proportion of the x component in the whole mix. The variance can also be calculated from a knowledge of the bed length, L' which is a constant for any mix:

$$\sigma^2_{NR} = L' + \frac{\sigma_o^2 + L}{n} \qquad (20)$$

These equations derived by Williams (62) are continuous with random mixing theory, since when randomisation is complete $P_x = \bar{P}$ and equation (19) reduces to:

$$\sigma^2_{NR} = \frac{\bar{P}(1 - \bar{P})}{n} \qquad (21)$$

which is the expression of Lacey (equation 2). Kristensen (43) used the correlation coefficient r to follow the non-random mixing process, where r diminishes from unity to zero as mixing proceeds. He derived the following expression for a theoretical non-random mix:

$$\sigma^2_{NR} = r.\sigma_o^2 + \frac{\sigma_o^2 + r\sigma_o^2}{n_e} \qquad (22)$$

where n_e is the effective particle number in a sample of mean weight, W and effective particle weight, w_e, given by:

$$n_e = W/w_e \qquad (23)$$

This treatment of the particle number count in a sample is based on densities and can thus be used to derive equation (20) without assumption of uniform particle size. By substituting $L' = r\sigma_o^2$ in equation (22), equation (20) can be regenerated in the form:

$$\sigma^2_{NR} = L' + \frac{\sigma_o^2 + L'}{n_e} \qquad (24)$$

Kristensen introduced the concept of mixture correlograms to account for long-range and short-range segregation effects

preventing complete mixing in non-random systems (63). An aggregate or cluster of particles, size r(k) composed of the correlation coefficient r and a lag coefficient k to account for the sampling range measured relative to the unit size produces an omni-directional correlogram (64):

$$r(k) = \begin{cases} 1 - \alpha k & k \leq {}^{1}/_{\alpha} \\ 0 & k < {}^{1}/_{\alpha} \end{cases} \qquad (25)$$

where α is a constant and ${}^{1}/_{\alpha}$ is a measure of mean cluster size. For the completely unmixed system where, $\alpha = 0$, a correlogram is produced in which the number of lags, k varies from 0 to the dimensions of the whole system. This gives a cluster size of +1. As mixing proceeds, r (k) decreases although the clusters are still assumed randomly distributed. Decreasing r (k) increases α to its limit at unity when the cluster size is equal to the unit size. If α increases above 1 then each unit must contain several clusters.

The use of the mixture correlogram in assessing real systems is impractical because it requires that the composition of the clusters at any position are known (65). Since the minimum number of meaningful lags is 20 this corresponds to a minimum sample size of about 10^4 units.

Random mixes and non-random mixes such as those described above are formed between two or more sets of particles which do not interact physically except under the force of gravity. Under some circumstances particles of one powder component may form a physical link with particles of another component. This effect can cause ordering in a system of particles.

1.3.3 Ordered Mixing Theory

The phenomenon of ordered mixing was first delineated by Hersey (66), and was used to explain the mixing of cohesive or interacting fine particles. Cohesive particles which do not mix randomly adhere to other, usually coarser particles (67). Cohesion between individual particles in a powder mix was recognised previously (68) and has been reported to affect powder flow (69) and the efficiency of mixers (50). Travers and White (70) were the first to note that adsorption of fine particles onto "host" crystals prevented the segregation normally associated with differences in particle size predicted by the theory of random mixing.

In ordered powder mixes a system of fine particles adheres to a system of coarser carrier particles. In the random mix (Figure 3b) any group of discrete particles may be composed of all component x (drug) or all component y (excipient) or different combinations of both components. Viewed as a whole the non-ideal mix produced by randomisation is unsymmetrical (Figure 3b). A perfect ordered mix (Figure 4a) consists of groups of discrete units each one of which must be composed of a combination of drug and excipient; the units cannot be composed of only one component. An excipient unit always lies adjacent to another excipient unit and each unit carries the same number of drug particles; this gives the mix total symmetry.

However, if each excipient unit carries different numbers of drug particles as shown in Figure 4(b), this partially destroys the symmetry. Under these conditions an ordered mix displays broken symmetry. The broken symmetry displayed by the model of a

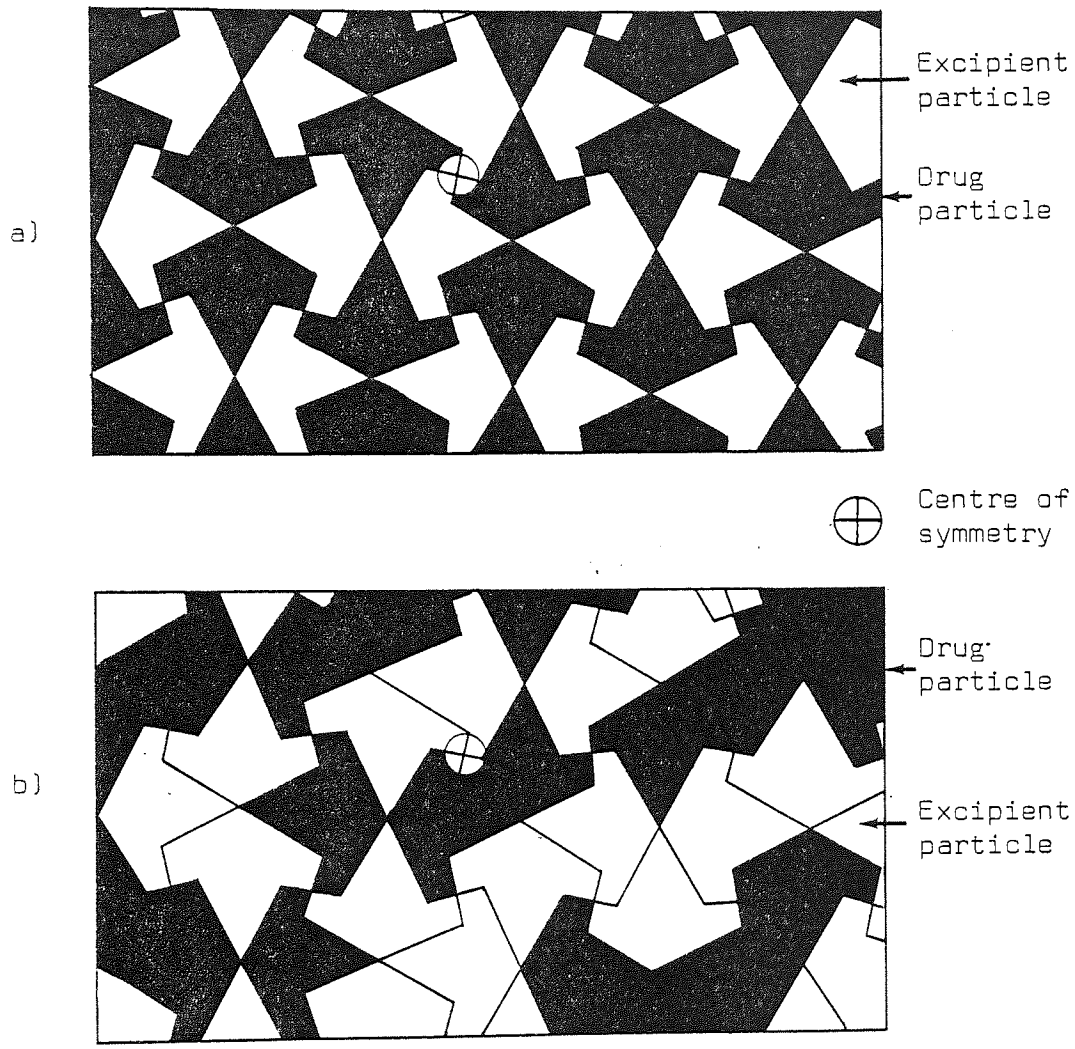

Figure 3. The formation of random mixes a) ideal mix produced by ideal randomisation b) random mix

practical ordered mix (Figure 4b) compared with the model of a random mix (Figure 3b) which is unsymmetrical, reflects the increased homogeneity of the ordered mix.

Unlike the process of random mixing, ordered mixing does not progress to an ideal state by a method analogous to statistical randomisation. When ordered mixing is carried to completion an even coating of particles from the fine system adheres to particles of the coarse system. In such an ordered mix which approaches a perfect state, the standard deviation of the distribution of the fine system will be zero, provided the sample size is greater than a single ordered unit (71). In practice, results obtained for a real ordered mix will have a finite variance due to errors associated with the sampling and analytical procedures. These errors may be listed in the form of a summation term related to the measured error variance obtained for an ordered mix, σ^2_{OM} (72):

$$\sigma^2_{OM} = \sigma^2_{MIX} + \sigma^2_{ANAL.} + \sigma^2_{SAMPLING} + \sigma^2_{PURITY} + \ldots \quad (27)$$

σ^2_{MIX} is the variance introduced by processes which separate ordered units into drug rich or drug poor areas, for example by carrier particle size differences (73). A similar variance may occur where ordered units carry significantly different quantities of fine particles. For the case of a near-perfect ordered mix in which carrier particles are monosized and have the same number of adherent particles, equation (27) reduces to:

$$\sigma^2_{OM} = \sigma^2_{ANAL.} + \sigma^2_{SAMPLING} + \sigma^2_{PURITY} + \ldots \quad (28)$$

Assuming that the problems associated with formation of a perfect ordered mix can be overcome, then the measured small

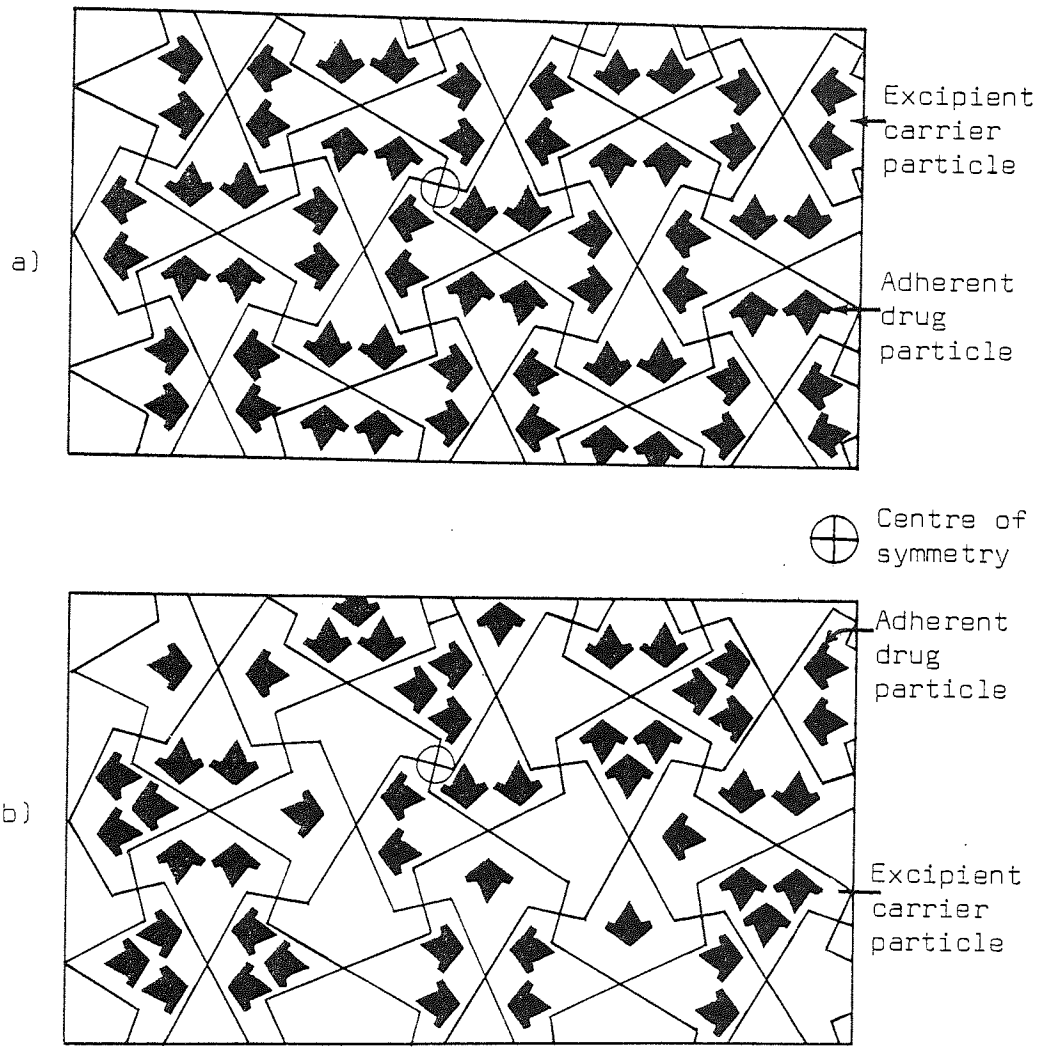

Figure 4. The formation of ordered mixes a) perfect ordered mix b) ordered mix

variance will be unaffected by a sample size exceeding one carrier particle diameter. In a random mix the variance falls as the sample size increases (41) (Figure 5).

Yeung and Hersey (74) used the characteristic plateau variance as a criterion for the formation of an ordered mix. They used different sample sizes to analyse the variances of powder mixes and found that those of ordered mixes were unaffected by sample size. However, the standard deviations were so low, 1.7×10^{-5} to 2.7×10^{-6}, that they were of a similar order to those introduced by error standard deviations: 1×10^{-5} to 3×10^{-5}, (75). It is therefore necessary to use additional methods for assessing the formation of an ordered mix (76).

Yip and Hersey (71) used Buslik's concept of a universal homogeneity index (77) to calculate the effect of increasing carrier particle size on the homogeneity of an ordered mix. The homogeneity index, H_i, expresses the various degrees of homogeneity according to the negative log of the sample weight, W_o, required to obtain a standard deviation of 1%:

$$H_i = -\log W_o \qquad (29)$$

In an ordered system, W_o becomes the weight of a single carrier particle. An increase in carrier particle size from 300 to 655 µm, decreases the theoretical absolute homogeneity, H_i, from 4.65 to 3.63 (72).

The areas on coarse particles which act as adherence sites for fine particles are called binding sites. An increase in carrier particle size increases the theoretical number of binding sites calculated from equation 30 (66).

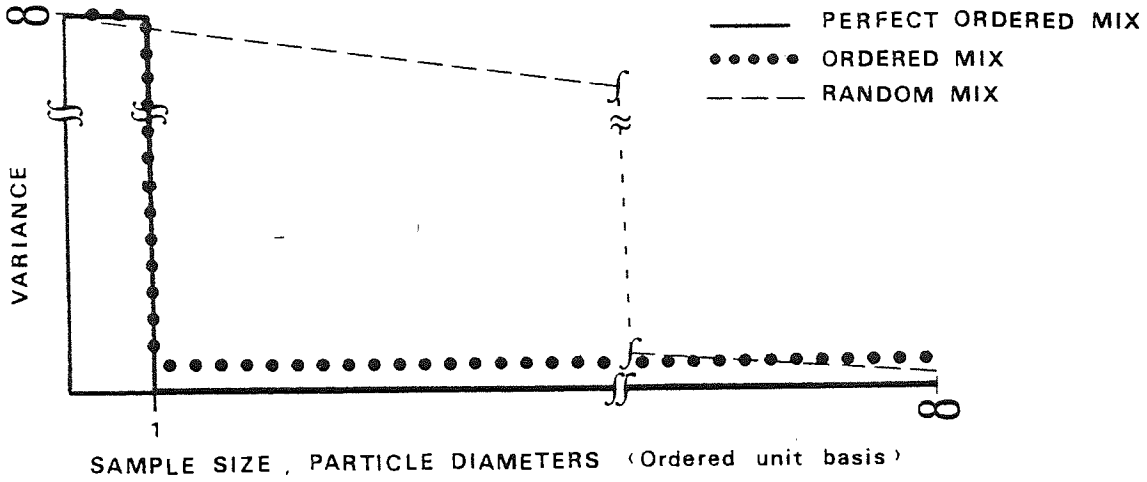

Figure 5. The relationship between increasing sample size and the variance of three types of powder mix.

$$n^{o} = \frac{2\pi(D + d)^2 . f'}{3.d^2} \qquad (30)$$

where n^{o} is the number of binding sites; D, the coarse particle diameter; d, the fine particle diameter and f', the fraction of fine particles not adhered to the carrier particles because of a shortage of binding sites.

Since an increase in the number of binding sites on a carrier particle should decrease the fraction of unadhered particles and increase the amount of ordered mixing in the system, the homogeneity should rise with increasing carrier particle size. However, the absolute homogeneity, H_i, will be largely unaffected by other particle properties, whereas the value of n_o in equation (30) is based only on the stereometry of the particle systems and will be modified by particle interactions.

The processes involved when an ordered mix is formed have recently been reviewed (78, 79). Ordered mixes have been demonstrated in practical systems, particularly in the pharmaceutical field. Ampolsuk et al. (80) described the use of a "frictional force" to increase the rate and reproducibility of dissolution of digoxin and hydrocortisone by forming ordered mixes in which the drug was dispersed as fine particles on the surface of coarser lactose carrier particles. The process of ordered mixing has also been described in the manufacture of microdose drug delivery systems (a mix containing less than 1% w/w drug) (81). Ordered mixes of 2% sulphaphenazole with the direct compression excipients Dipac and Emdex (Celutab) have been studied (82) and their mixing properties attributed to differences in surface irregularities of the carrier particles. Adhesion of fine material to irregularly

shaped coarse material was also noted by Jones (83). Travers (84) found that some sites of adherence in an ordered mix were "stronger" than others. The ability of these strong sites to hold on to fine adherent particles was associated with plateaux on the coarse crystal particles where point charges accumulate. Lattice defects such as these may act in the same way as low humidity by increasing the homogeneity of an ordered mix through an increase in the interparticle adhesion forces (85, 86). The process of drying as a method of deliberately producing crystal defects to facilitate ordering has been described (87).

Although ordered mixing has mainly been considered as a mechanism operating between coarse carrier particles and fine particles less than 100 μm diameter (88), it has also been used to describe mixing where both constituents are fine powders (89). Orr and Shotton (90) found that where two sets of fine powders were mixed, large inhomogeneities were produced. The time required for complete mixing was also prolonged under some circumstances.

When an ordered mix is formed, whether the constituent particles are coarse-fine or fine-fine, one set adheres to the other set. In a random mix there can be no particle interactions. The formation of an ordered or a random mix cannot be chosen by selecting a particular mixing apparatus; the over-riding criterion which determines whether an ordered or a random mix will be formed is the diameter of the powder particles. If both powders have particles well above 100 μm diameter it is likely that they will mix randomly. But if one or both of the powders are well below 100 μm then ordering will occur. In a grey area on either side of the arbitrary 100 μm diameter the processes of ordering and

randomisation will occur together. The likelihood that both mechanisms occur together in any practical mix is increased because most powders have wide particle size distributions. I have described this process of simultaneous ordered, random and non-random mixing as total mixing.

1.3.4 Total Mixing Theory

The major forces which stabilise powder mixes are gravitational and surface forces. Both of these types of forces are present in ordered and random mixes. In the ordered mix, the gravitational force is less predominant than the surface force; in the random mix the reverse is true. This situation arises merely as a consequence of the particle size distribution of the two types of mix. The larger the particles of the mix become, the greater will be the influence of the gravitational force. As the particles become smaller, the increasing dominance of the surface force will swamp the gravitational force acting on these fine particles. It would therefore appear that the forces which stabilise mixes by randomisation and ordering are two facets of a total mix. In most practical mixes of powders with wide size distributions the only requirement is a homogeneous final mix (91). Under these circumstances it is acceptable from a practical standpoint that both ordering and randomisation are produced in a dynamic equilibrium (92).

Johnson (93, 94) realised that a real system owed its final mixedness to a combination of ordered and random mixing. This is the total mix shown in Figure 6.

To assess the theoretical variance of a total mix the variance of its two facets - the random system and the ordered system - must be considered. Lacey (39) described the theoretical variance of a

Figure 6. The formation of total mixes a) stoichiometric total mix b) real total mix

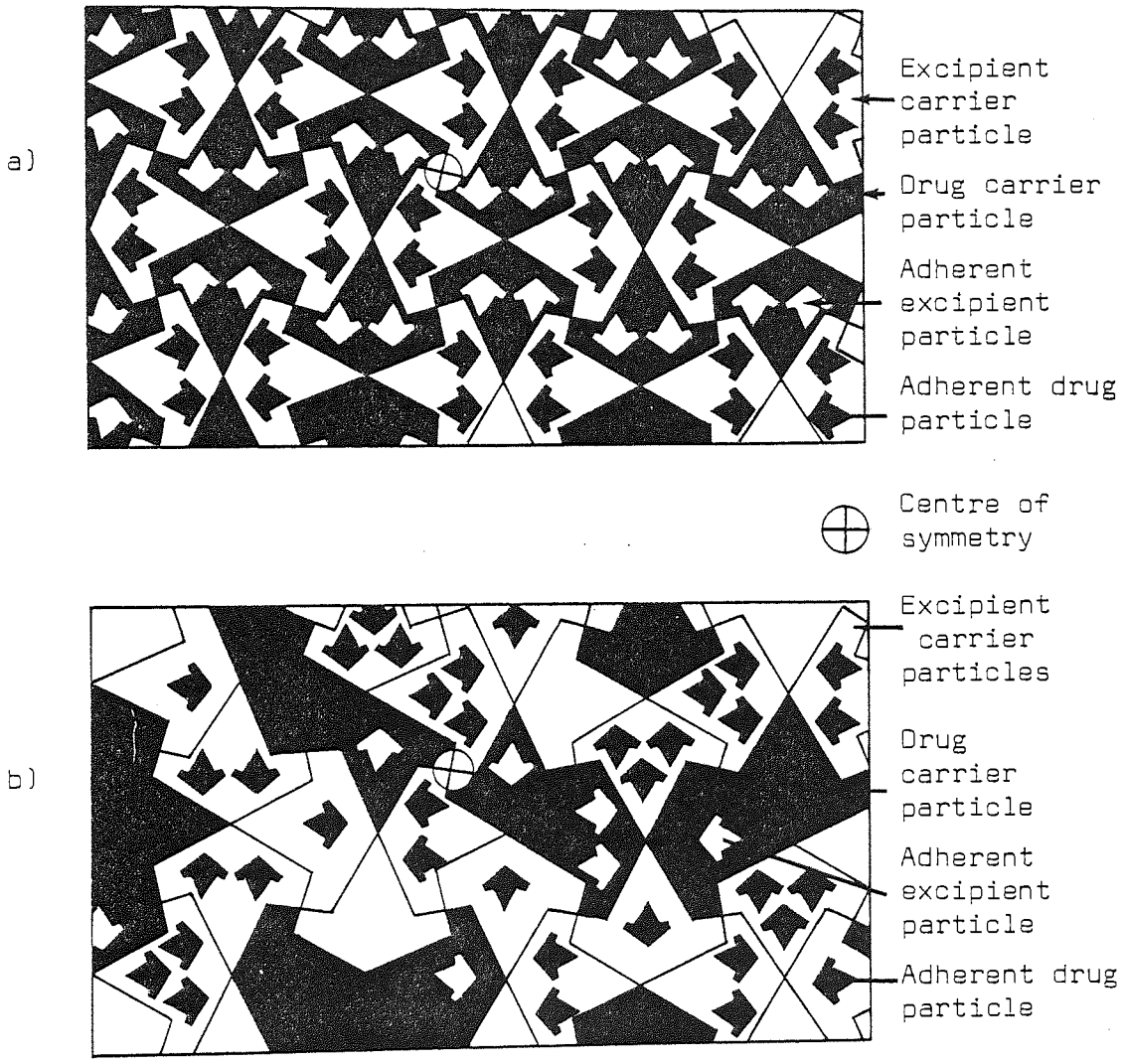

two-component mono-sized powder by the relationship in equation (2), shown schematically in Figure 7. This equation only applies to

Figure 7. Representative constituent particles of a random mix

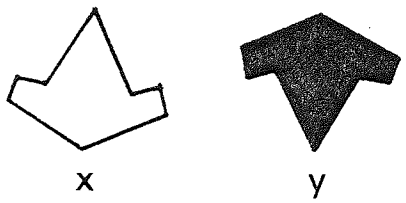

binary powder mixes where randomisation is the only mixing process. In mixes produced solely by ordering, the theoretical variance of the two components should be zero. However, in a random mix where some particles from one component powder adhere to particles of the other component powder, without altering the overall particle size, so that Lacey's assumptions are still valid, the theoretical variance will be altered. Hersey, Thiel and Yeung (95), called this type of mix "partially ordered random" (POR). The theoretical variance of a POR mix is given by:

$$\sigma^2_{POR} = \frac{(x + Fy)(y - Fy)}{n} \qquad (31)$$

where Fy is the fraction of component y which adheres to component x (Figure 8). The theoretical variance of a total mix depends not only on the amount of component y adhering to component x, but also the fraction of component x adhering to component y without altering

Figure 8. Representative constituent particles of a partially ordered mix

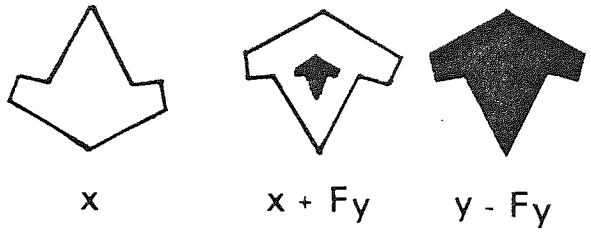

the physical properties of the final powder mix:

$$\sigma^2_{TOTAL} = \frac{(x + Fy - Fx)(y - Fy + Fx)}{n} \qquad (32)$$

The different fractional quantities of constituent particles adhering to particles of the other component powder, affect the overall variance of the total mix. Figure 9 shows different combinations of the same number of two sets of constituent particles which are identical in every respect except colour (the particles designated, x, are represented by white circles and those of y are represented by black circles in Figure 9). The theoretical variance of each total mix is also shown. When total mixes contain constituent particles which do not adhere to each other (Figure 9a) the values of Fx and Fy in equation (32) fall to zero and the theoretical variance is the same as that usually described as a random mix. An increase in interparticle adhesion causes some particles of both systems to bind to one another, but also leaves some particles as single units (Figure 9b). The variance of this type of total mix can be larger than that of a random mix, although the particular combination shown in Figure 9(b) has a lower variance. If only one set of particles has an affinity for the other set of

Figure 9. Five different types of total mixes, three of which are special cases and are described by random, partially ordered random and ordered mixes. The theoretical variances of each mix are calculated according to the relative proportions of components.

○ — x particles ● — y particles

	APPEARANCE	DESCRIPTION	THEORETICAL VARIANCE
a	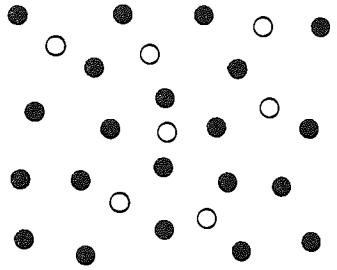	RANDOM	x=0·25 y=0·75 Fx=0 Fy=0 n=28 $\sigma^2_{TOTAL} = 6{\cdot}7 \times 10^{-3}$
b	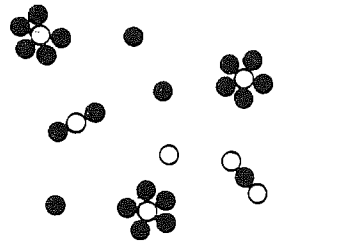	TOTAL	x=0·25 y=0·75 Fx=0·07 Fy 0·61 n=28 $\sigma^2_{TOTAL} = 5{\cdot}9 \times 10^{-3}$
c	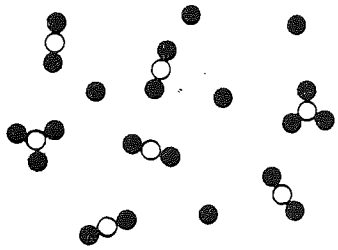	P.O.R.	x=0·25 y=0·75 Fx=0 Fy=0·57 n=28 $\sigma^2_{TOTAL} = 5{\cdot}3 \times 10^{-3}$
d	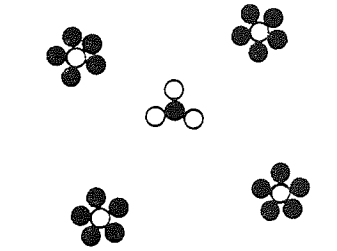	TOTAL	x=0·25 y=0·75 Fx=0·11 Fy=0·71 n=28 $\sigma^2_{TOTAL} = 3{\cdot}2 \times 10^{-3}$
e	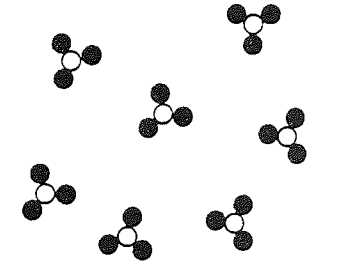	ORDERED	x=0·25 y=0·75 Fx=0 Fy=0·75 n=28 $\sigma^2_{TOTAL} = 0$

particles, a special type of total mix, called a partially-ordered random mix, is formed (Figure 9c). An increase in the interparticle adhesion force of both powders causes each particle in the component powders to be associated with at least one particle of the other constituent system (Figure 9d). The variance of this type of total mix is much lower than that of a total mix where no interparticle adhesive forces are present (e.g. random mixes). The type of total mix with the lowest variance is produced when all the component particles of one powder system are adhered to particles from the other system (ordered mix, Figure 9e) and in this special type of total mix with $F_x = 0$ & $F_y = y$, the theoretical variance is zero.

Equation (5), proposed by Poole, Taylor and Wall (25) can be used to explain differences in particle characteristics, such as size distributions and densities when determining the variance of a random mix, not accounted for in the relationship of Lacey which was developed in equations (31) and (32); figure 10 is a diagrammatic representation of such a system:

$$\sigma_R^2 = \frac{x.y}{M} . \; x(\Sigma fw)_y + y(\Sigma fw)_x \qquad (5)$$

Figure 10. Representative constituent particles of a random mix.

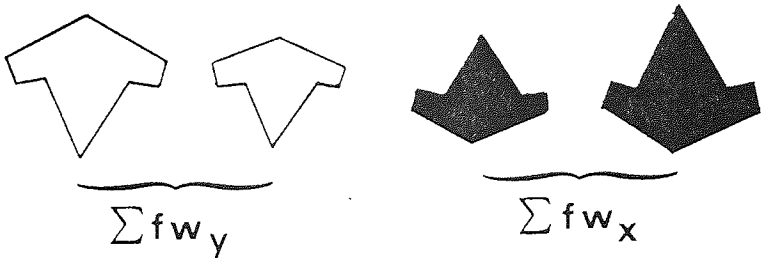

In the partial ordered random system shown diagramatically in Figure 11, where a proportion of the fine component y adheres to the coarse component x, equation 5 can be modified to the one developed by Hersey et al. (95):

$$\sigma^2_{POR} = \frac{(x + Fy)(y - Fy)}{M} \cdot \left\{ x + Fy(\Sigma f(1 - Fy/x)w)_y + y - Fy(\Sigma f(1 + Fy/x)w)_x \right\} \quad (33)$$

where M is the sample weight. Small particles of component y are randomly mixed with coarser particles of component x and adherent particles of y. A constant weight fraction, F of y particles in each size range adheres to the surface of the x particles which thus gain in weight by a similar constant fraction. The fractional weight, fw, of the x particle fraction is assumed to gain in weight by a constant amount, represented by Fy/x.

Figure 11. Representative constituent particles of a partially ordered random mix.

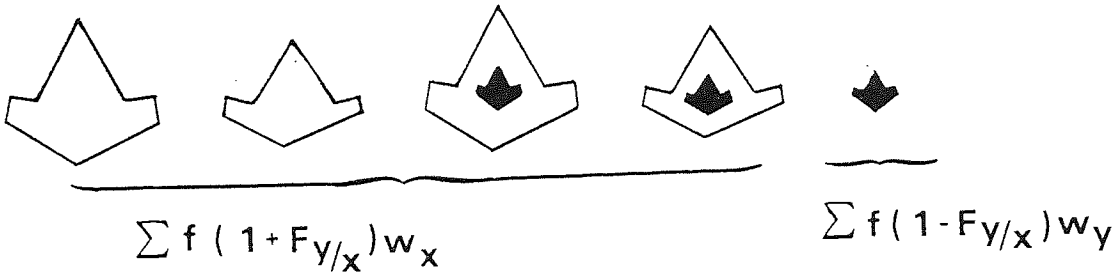

For a total mix, equation (33) can be further modified to account for the alterations caused by some fine particles of each component leaving the random system by adhering to coarse particles of both systems (Figure 12). In the relationship developed here, the proportions of x and y are further altered to account for the adherent fraction of x particles, Fx, as well as the adherent

Figure 12. Constituent particles of a total mix.

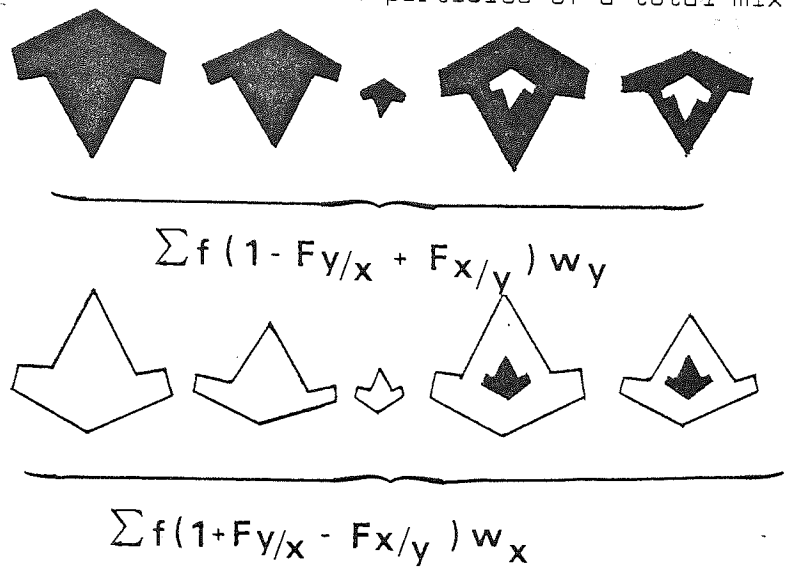

fraction of y, Fy. Similarly coarse y particles gain in weight by a constant amount in each size fraction, represented by Fx/y:

$$\sigma^2_{TOTAL} = \frac{(x + Fy - Fx).(y - Fy + Fx)}{M}\left[\left\{x + Fy - Fx\right\}(\Sigma f(1 - Fy/x + Fx/y)_w)_y + \left\{y + Fx - Fy\right\}(\Sigma f(1 + Fy/x - Fx/y)_w)_x\right] \quad (34)$$

The same estimated values for fractional powder weights, size distributions and powder densities, were used to recalculate the variances of different total mixes shown in Figure 9 according to equation (34). Powders mixed randomly without any adhesion forces (Figure 9a) had an estimated variance of 4.10×10^{-3} and this decreased to 3.63×10^{-3} in total mixes with a small inter-particle adhesion influence similar to the monosize particle distribution shown in Figure 9b. The estimated variance decreased further to 2.79×10^{-3} in total mixes with more extensive inter-particle adhesion (Figure 9d). In total mixes described as partially ordered random (Figure 9c), the variance was 3.78×10^{-3}, but in total mixes which were completely ordered (Figure 9e) the estimated variance calculated from equation 34 was zero.

Kristensen (64) attempted a complete description of a powder mix in an extension of several previous models. He considered that the variance of samples taken from a non-random mix is affected by several different component variances:

$$\sigma_n^2 = \sigma_n^2(lr) + \sigma_n^2(sr) + \sigma_n^2(e) \qquad (26)$$

where σ_n^2 is the variance between n samples; $\sigma_n^2(lr)$ the degree of segregation (long-range); $\sigma_n^2(sr)$, is the variance due to short-range segregation effects causing incomplete mixing of particle clusters, and $\sigma_n^2(e)$, any randomness in the system.

A theoretical model is developed here which incorporates variances in a total mix produced by randomisation, ordering and non-randomisation processes. The model is based on the equation which Williams (10) used to describe a non-random mix:

$$\sigma_{NR}^2 = \int_0^1 \left[(\bar{P} - P_X)^2 + \frac{P_X (1 - P_X)}{n} \right] . dX \qquad (19)$$

Substituting $(P(x)_X + P(y/x)_X)$, the probability of finding a sample containing discrete particles of $x(P(x)_X)$ or a sample containing particles of x with adherent y particles $(P(y/x)_X)$, for P_X, the probability of finding a sample containing discrete particles of x at a distance X from a reference plane gives:

$$\sigma_{TOTAL}^2 = \int_0^1 \left[(\bar{P} - \{P(x)_X + P(y/x)_X\})^2 + (P(x)_X + P(y/x)_X).[1 - P(x)_X + P(y/x)_X] \right] . dX \qquad (35)$$

In a total mix there is also a probability that some particles of x will be adhered to particles of y. This means that there is a probability that some of this adherent x fraction will be located in some samples and is represented by $P_{(x/y)X}$:

$$\sigma^2_{TOTAL} = \int_0^1 \left[\bar{P} - \{ P(x)_X + P(y/x)_X - P(x/y)_X \} \right)^2 + \frac{(P(x)_X + P(y/x)_X - P(x/y)_X).(1 - P(x)_X + P(y/x)_X - P(x/y)_X)}{n} \right] .dX$$

(36)

There are several special cases of total mixes where equation (36) can be modified. In total mixes that are non-cohesive and mixing is completely random (shown schematically in Figure 9a) $P(x)_X = \bar{P}$ and $P(y/x)_X$ and $P(x/y)_X = 0$, equation (36) reduces to that of Lacey (2) written in the form:

$$\sigma^2_{TOTAL} = \frac{P(x)_X \,.\, 1 - P(x)_X}{n} = \frac{(\bar{P})(1 - \bar{P})}{n}$$

In total mixes that are completely ordered (Figure 9e) $P(y/x)_X = \bar{P}$, and $P(x/y)_X = 0$ and $P(x)_X = 0$ and the variance of the mix becomes zero, the theoretical variance of an ordered mix. When partially ordered random mixing is the only mechanism by which powders are blended (Figure 9c) $P(x/y)_X$ becomes zero and equation (36) for a total mix reduces to equation (35). If non-randomisation is the sole mixing mechanism, $P(y/x)_X$ and $P(x/y)_X$ become zero and the variance of the total mix reverts to that described by equation (26) of Williams.

Using equation (34) or (36), the theoretical variances of all possible combinations of component particles in a total mix can be calculated. Equation (34), based on the relationship of Poole, Taylor and Wall (25) is probably the easier of the two equations to apply to experimental situations, because although it does not account for non-random mixing it expresses a variance of samples from total mixes based on constituent particles with different physical properties.

The theoretical variance of a powder mix can be significantly altered by different contributions of random, non-random and ordered mixing to the final homogeneity of the powders. The

theoretical variance of total mixes calculated using equation (34) or (36) takes account of the different random, non-random and ordered mixing processes and describes all combinations of particles in a binary powder mix.

1.3.5 Mixing Equipment

To achieve any type of powder mixing, the location of individual particles must be changed. The mechanisms which produce powder movement have been divided into two broad categories by Bates (96): a) powder movement in relation to machine walls, beds, blades and other boundary layers which may be either static or sliding, b) the internal particle structure within the powder bed may be virtually rigid (static) or moving. The powder bed may possess narrow failure planes where one section is moving relative to another or be in bulk shear (general rearrangement).

A brief review of the different types of mixing equipment and their uses has been made by Griffin (97). Some new mixing techniques have also been described (98).

Powder mixers can be divided according to their use into those for either continuous or batch processing. Williams and Rahman (99) and Williams (100) have reviewed some of the literature relating to continuous mixing. Williams and Rahman (99) achieved near perfect mixing for non-segregating particles at optimum rotation speeds of a continuous drum blender and they considered that in powders prone to segregation, continuous mixing had some advantages over batch processing.

Batch mixers have normally been used by the pharmaceutical industry in powder processing operations. Screw and paddle mixers are popular for both dry powder blending and in wet massing. The Nauta mixer is an example of a screw mixer, which has been evaluated by Cook and Hersey using mixes of starch, sucrose, lactose with an

active ingredient, fenfluramine hydrochloride (101). They found that dry pre-blending was sufficient to satisfy pharmacopoeial requirements, but continuation of blending after 10 minutes produced partial segregation of the components. A similar effect was noted after 8 minutes mixing of phenobarbitone, butobarbitone, quinalbarbitone and lactose (102). The results suggest the necessity for manufacturing limits such as mixing time specifications on batch mixers of this type. The behaviour of paddle blades in mixing granular material has been studied theoretically by Bridgwater et al. (103) who used tracer particles to study the importance of height, immersion and velocity of a mixing blade. Novosad used a kinematic analysis of moving blades to examine slip lines under different conditions (104).

Tumbling mixers are of various geometries including double cone, cube, y-cone and v-cone. Whatever their shape the tumbling mixers operate by lifting the powder bed on the rising side of the container until it exceeds its normal angle of repose. The powder particles then fall down in a riffling motion, or are thrown clear of the turning face; as they reach the base they may be recombined as occurs in cone and cube blenders or they may be successively split and recombined as with the v-cone and y-cone mixers. Carley-Macaulay and Donald (105) studied tumbling blenders of various geometries using granular materials differing only in colour. They found that the system variance decreased with time in an exponential manner although the slope of the variance-time curve altered with the type of mixer. Kaufman (106), used a double-cone and twin-shell blender to evaluate mixing of penicillin G and dihydrostreptomycin powders. The progress of mixing was found to be rapid and low variances were produced after 10 to 100 revolutions. After this period the variance did not decrease but varied

erratically in a manner similar to that described by Cook and Hersey (101). Yip and Hersey (107) described the use of a tumbling blender, the Revolvocube, for producing ordered as well as random powder mixes. They found that ordered mixing occurred during tumbling when particles were free to slide over one another facilitating cohesion (108). Tumbling mixers are recommended for producing ordered mixes with one coarse particle component, provided that dead spots in the mix can be avoided (109).

Where an ordered mix of two fine powders is required, a mixer producing higher shear is desirable. For such conditions and for all random mixes, Yip and Hersey have recommended internally agitated, stationary mixers (105), such as the cascade mixer.

Williams has suggested a classification of powder mixers based on their ability to produce a segregating or a non-segregating mix (60). This suggestion may need to be modified to include the type of mix being processed, viz randomised/non-randomised or ordered. Yip and Hersey (107, 108) have shown that a tumbling blender normally considered as a segregating mixer can produce homogeneous non-segregating ordered mixes. Nevertheless, it can be useful to classify the mixer according to its ability to produce or prevent segregation. Harnby (110) used a mix of millet and salt with wide, non-overlapping particle size distributions as a searching test of different mixing equipment. He found that the Nauta mixer and Ribbon blender produced better quality mixes more efficiently than the tumbler mixers. Harnby's systems probably mixed by randomisation. Rogers and Clements (111) studied the segregation of granular material in a tumbling mixer and found that mixes were formed non-randomly. Segregation of material with dissimilar physical properties produced a sucrose-rich central

core in a mix containing citric acid. Williams and Khan (112) also used segregation data to select powder mixers.

Although several types of mixing equipment may cause segregation of powders, the intensity and type of segregation can also vary from different mixes produced by the same equipment. Any differences in powder properties can facilitate segregation of two or more components; this effect may be enhanced by the mode of mixing.

1.4 The Process of Powder Segregation

The processes of mixing and segregation occur simultaneously, they are two extremes of one phenomenon. Forces and properties which increase mixing can also decrease or increase segregation. A random mix is also randomly segregated and a totally unmixed system is perfectly segregated. The two conditions exist in dynamic equilibrium (113). The effect of powder segregation begins well above the molecular level, when particles reach a size beyond which Brownian motion cannot occur. As in powder mixing, the first step in any segregation process is dilation of the powder bed (50). Dilation can be produced in several different ways which lead to different segregating mechanisms. Williams has described the causes and mechanisms of particulate segregation in a recent review (114).

1.4.1 Causes of Powder Segregation

Segregation of a powder is caused by differences in the physical and mechanical properties of the constituent particles. Williams (60) defined segregation as "the preference of particles, possessing a similar property, for being at some part of the system". This is the antithesis of the definition of a random mix where

particles possessing similar properties have an equal probability of being located anywhere in the system. The properties of powders which are known to cause segregation include relative density, shape or roughness, resilience and relative size of the particles. Of all the causes of segregation, particle size is considered to be the most important (115).

1.4.1.1 Relative Particle Size Differences

The influence of relative particle sizes and size distributions on the segregation of powders has long been recognised in powder flow (116, 115) and other processing conditions (117, 118). Williams and Khan (119) found that the diameter ratio and the mean component diameter were the most critical variables influencing segregation of sand and fertiliser granules. With a constant diameter ratio they found that the intensity of segregation fell if the mean component diameter was less than 500 μm. Lawrence and Beddow (120) found that radial segregation during filling of lead powder mixes into dies reached a maximum when the relative size difference (R.S.D.) was in the range 0.58 to 0.8

$$R.S.D. = (D^{o} - d) / D^{o} \qquad (37)$$

where D^{o} is the large component diameter and d the fine component diameter.

In a powder bed subjected to strain it has been shown (121) that large particles tend to move towards the centre of the failure zone, away from the fine particles. The difference in mobility of the two sets of particles and thus their segregation depends on the strain rate being constant throughout the powder bed. Ripple et al. (122) have demonstrated the ability of different particle size soils to undergo radial segregation. The process of radial

segregation appears to occur in response to disturbance in a limited depth "active" layer less than 15 cm from the soil surface, where the different particle sizes are separated by jostling.

1.4.1.2 Relative Density Differences

Ripple et al. (123) studied the interactions of particle size and density relationships. They found that density differences alone had a negligible effect on segregation, but when combined with particle size differences a marked non-linear increase in segregation tendency occurred.

Syskov and Lyon (124) studied a mix of an ore of density 4.00 to 4.25 with coal of density, 1.29. They found that the denser ore was concentrated at the centre of a poured cone. However, they used a wide size distribution (2 - 3 mm) and the coal at the cone periphery was of larger particle size as well as lower density than the ore. Their conclusion that the density differences were mainly responsible for segregation therefore appear to require further investigation. Tanaka (125) produced a model for density segregation based on the possible combinations of heavy and light particles of similar diameters. The "pushaway" action in relation to friction and other factors of each packing combination was calculated. Using this model, Tanaka was able to identify three different powder zones: the segregation zone where the pushaway process occurs and two outer heaping zones. In one heaping zone, light and heavy spheres co-existed, having been pushed away from the segregation zone. Light particles alone are distributed as far as the second heaping zone by the pushaway process. The model was also verified experimentally for binary mixes.

1.4.1.3 Particle Shape

Particle shape has had little experimental attention although it has been listed as a potential cause of powder segregation (114, 115, 121). Campbell and Bauer (126) found that a mix of acicular soda ash particles and angular sand was best able to resist segregation when the component particles had the same equivalent diameters, although this was not synonymous with equal particle size.

Rippie et al. (127) found that by pairing spheres of the fine component the segregation intensity of a mix could be decreased. They explained this effect of a change in particle shape in terms of competition for void spaces. They also found that highly angular particles such as crushed quartz, required less energy input to produce segregation than did spherical particles.

A number of other factors including surface friction can influence powder segregation (128). Surface effects will be particularly important in determining the stability of ordered mixes (37).

Particles possessing similar or disimilar physical properties can be segregated from other particles by a number of different mechanisms.

1.4.2 Mechanisms of Segregation

Segregation mechanisms can be considered according to the processes producing segregation (60, 115, 125) or by the forces acting on the particles (114). The second approach is analogous to Lacey's classification of the mechanisms of mixing (52) and is used here:

1.4.2.1 Trajectory Segregation

Trajectory segregation occurs when particles with different properties are set in horizontal motion. Each set of similar particles has a different stopping distance. According to Williams (114) a particle of diameter D and density ρ, which is projected horizontally with velocity, V_o, into a fluid of viscosity, η, will travel, after infinite time, a distance given by:

$$\text{Stopping distance} = V_o.\rho.(D)^2/18\eta \qquad (38)$$

The difference in stopping distances and hence the particle segregation increases in a geometric progression according to the square of particle diameter. This mechanism is analogous to Lacey's convective mixing in which particles are spread horizontally. Particles in flight will travel different distances according to their relative sizes though the predicted distances from equation (38) can be modified by fine particles interacting in a cloud (114). The actual stopping distances for particles in the centre of a stream in flight could also be increased. The particles at the stream centre could be projected up to 18 times further than particles near the edge; because air drag on particles in the centre of a stream is minimised. As well as affecting stopping distances this phenomenon can also alter the geometry of particle trajectories (128).

1.4.2.2 Percolation Segregation

Particle percolation has been identified in both mixing and segregation and the mechanism in each case may be related (129). Spontaneous inter-particle percolation of fines occurs through voids in the powder bed. This motion is produced by the action of

gravity and is affected by a number of powder properties already described (Section 1.4.1). The velocity of spontaneous percolation is influenced by the packing diameter ratio of fine and coarse particles. The coefficient of restitution is also important, the more elastic the collisions, the lower the resulting velocity of the particles (130). Percolation segregation can also occur in powders where the void diameters are smaller than the fine particle diameters when the powder is at rest (114). Under conditions when slip planes are formed in a powder bed, particle motion up to ten particle diameters in width can occur. Within this failure zone deformation of the mix allows percolation of fines around coarse particles. Radial percolation or dispersion has been observed and can be characterised by a radial Peclet number P_e, which is related to the Reynolds number and Prandtl number:

$$P_e = \frac{u.D''}{R_d} \qquad (39)$$

where u is the mean vertical velocity of a small sphere; D", the large sphere diameter and R_d, the radial dispersion coefficient (130).

In general, percolation of fines occurs vertically producing a concentration of smaller particles towards the base of a powder bed.

1.4.2.3 Densification Segregation

This mechanism occurs when powders of very dissimilar size distribution are vibrated. It has been demonstrated by covering a single large particle with finer powder (115). During vibration the coarse particle rises to the surface. This mechanism occurs with large particles regardless of their density, although density can affect the rate of segregation. The effect may be caused by

the large particle producing an increased pressure on the region below it. This compacts the material preventing the particle moving downwards, so that when upward movement occurs, fine particles flow under the large particle and the process is repeated. In some respects this mechanism is similar to that demonstrated by the pushaway theory of density segregation described earlier (125).

1.4.3 Segregation of Ordered Mixes

Yip and Hersey (131) have defined two distinct types of segregation occurring in ordered mixes, "ordered-unit segregation" and "constituent segregation".

1.4.3.1 Ordered Unit Segregation

Ordered unit segregation occurs in mixes containing multi-sized carrier particles (82). The mechanisms by which ordered unit segregation occurs are analogous to those described in Sections 1.4.1 and 1.4.2, for random mixes. When ordered unit segregation occurs, carrier particles of different sizes, with different numbers of adherent particles, move to a specific area of the powder bed. In pharmaceutical mixes this can lead to drug-rich and drug-lean areas of powder even though no change has occurred in the distribution of adherent particles on individual carrier particles.

1.4.3.2 Constituent Segregation

This type of segregation occurs when the fine particles are dissociated from the coarse particles. This can happen in two ways. The fine particles may become dislodged from the coarse carrier particles as a result of weak interparticle forces. A second method of segregation is produced when a true ordered mix

is not formed. Such a situation arises when there are more fine particles in a mix than the coarse particles can carry, either as a monolayer or a multilayer (132). What is more, fine particles which are free to move within a mix have been shown to produce aggregates which exacerbate any segregation tendency (131). Since, in such cases, an ordered mix has not been formed, initially, this type of effect is probably better described as segregation in a total mix (Section 1.3.4). Constituent segregation probably occurs by percolation, although this may be modified by the ability of some fine particles to become re-ordered as they fall down the powder bed.

Segregation of ordered mixes can be minimised by using monosized carrier particles (133). Bryan et al. (132) found no segregating tendency in an ordered mix of fine salicylic acid particles with a starch/lactose granulatum, whereas in a random mix of coarse salicylic acid powder with the same granulation under the same conditions considerable segregation was found.

Another possible segregating mechanism in ordered mixes has been reported by Lai and Hersey (134). They found that magnesium stearate particles added to a binary ordered mix of a and b caused "stripping" of the adherent b particles from the coarse a particles. The mechanism may be one of competition for active sites, where magnesium stearate is preferentially adsorbed on to the carrier particles, leaving no sites for other fine particles. The mechanism may also be linked with the charge dispersing ability of magnesium stearate, which will be discussed later in Chapter 5.

1.4.4 Conditions Facilitating Segregation of Powder Mixes

1.4.4.1 Pouring in a Heap

One of the first methods which was used to demonstrate powder

segregation, flow into a heap, is also an important practical condition (116). When powders are poured into a heap, larger non-cohesive particles roll down the sloping surface of the heap leaving a central cone rich in cohesive fines (115). In addition, the high velocity gradient in the particle bed at the cone apex produces the conditions under which percolation segregation can occur. Another reason for segregation in a heap is described by Johanson (128). Particles with different angles of repose segregate to different areas of the cone. The cohesive material having the steeper angle of repose concentrates in the core, whereas the less-cohesive powder with the flatter angle of repose concentrates on the outside. This is undoubtedly a result of the different coefficients of friction for the two materials. Friction can also modify the cone segregation formed when powder is poured from a chute (128). Particles with high frictional coefficients have longer residence times on the chute and reduced free-fall velocity. These particles congregate on the chute side of the powder cone, whereas other particles fall away from the chute.

Flow in bins and hoppers is a special case of heap formation which is of practical importance. The amount of segregation produced in discharging a bin has been described by Matthée (135). He related segregation to bin diameter, charge height and orifice diameter. Segregation is probably a greater problem when pouring into a bin than when flow occurs from the bin or hopper. Schofield (136) has described a number of hopper designs which can remix a segregated powder during discharge.

1.4.4.2 Fluidisation

The process of fluidisation can be used to mix dry powders, but as in other mixing operations, differences in particle properties

combined with adverse operating conditions can produce segregation. Rowe and Nienow (137) have recently reviewed the processes involved in powder mixing and segregation during fluidisation. Nienow et al. (138) found that mechanisms of powder segregation in a fluidised bed were more dependent on density differences than on particle size differences. This contrasts with the situation affecting most conventional mixers (139), possibly because of the different segregation mechanisms which influence fluidisation mixing (140). Fan and Chang (141) developed a stationary random-walk model to describe axial or radial segregation of large particles in fluidised bed mixers. This may be analogous to diffusive percolation in conventional mixing, where a random-walk approach can also be adopted. Thiel (142) found that fluidisation of an ordered mix containing microfine salicylic acid and coarse sucrose or Emdex carrier particles caused no significant constituent segregation. This should enable ordered mixes to be produced by fluidisation without any segregation problems.

1.4.5 Vibrational Segregation

Vibration is a major cause of segregation during processing of powders ranging from coal to pharmaceuticals. The Pharmaceutical Codex (143) recognises that "there is a possibility of segregation of the constituents if powders for mixtures are stored for long periods or subjected to mechanical vibration".

1.4.5.1 Vertical Sine Wave Vibration

Coarse particle constituents of a vibrating powder move up or down the bed according to the packing arrangement of the particles (116). In a moving bed, Hirst (144) showed that elimination of interparticle contact forces allowed large particles to sink. However,

Williams found that under most conditions, particles much larger than the rest of the powder rose to the surface (115). This phenomenon was further studied by Khan and Smalley (145). They found that reducing vibration frequency at any acceleration reduced the time taken for a large sphere to rise to the surface of a packed bed of sand. Similarly, the segregation time could be reduced by increasing the acceleration at any vibration frequency. The size of the large particles also affected the rise time. The higher the ratio of large particle diameter to particle size of sand the greater the segregating effect.

In powders containing smaller particles and where particle size distributions are narrower, different behaviour occurs. Lawrence and Beddow (146) showed that vertical vibration of lead mixtures in a die produced downward movement of fines. This probably occurs by the mechanism of percolation and is affected by the stability of the powder bed. At low amplitudes and frequency, Lawrence and Beddow found that dilation of the powder is minimal and segregation does not occur. At high frequency and high amplitude the powder bed moves out of phase with the vibrating die and causes bouncing. Bouncing produces little vertical segregation. At intermediate frequency and amplitude the powder bed begins churning and it was under these conditions that segregation increased.

Harwood (147) studied the effect of vertical vibration on free-flowing and cohesive powders. He found that whilst segregation could be readily produced in free-flowing systems, truly cohesive powders exhibited very little tendency to segregate. Upward movement of fine iridium-192-labelled sand was produced in a vibrated powder bed of flint particles. Harwood explained this

action in terms of vibratory mixing. Use of banding sand with a particle size distribution closer to that of the tracer sand caused segregation in both directions although upward movement was more marked; the time required for segregation was also somewhat increased. Further studies were carried out using cohesive lactose powder. Segregation was very low at low frequency and acceleration, probably because cohesion prevented free powder movement. When vibration conditions were adjusted to minimise interparticle friction, some segregation by upward movement of the coarse sand was noticed. Harwood's explanation for this was that the semi-fluidisation produced large voids through which the large particles moved by their greater upward momentum. The concept of segregation during vibrofluidisation was further described in the segregation of cohesive milled zircon, although aggregation of fines such as those produced in milling (148) does not appear to have been considered. Harwood's model inevitably emphasises the wall effects of vibration segregation because of the radio-tracer sampling technique. Particles at the wall nearest the counter-probe will contribute more to the sample count than particles deeper in the bed.

1.4.5.2 Percolation Segregation in Vibration

Percolation segregation of different sized particles is actively encouraged in vibratory sieving. Williams and Shields (149) investigated the sieving conditions which produced optimum powder segregation on a vibrated screen. Segregation was most marked when the direction of vibration was 30^{o} to the horizontal. Maximum segregation under these conditions was produced by an acceleration of 6.6 G with a vertical component of 4.5 G. Percolation is the main mechanism by which segregation is produced

during vibratory sieving; this may occur through interparticle void spaces in the bed or by the production of failure zones. Hudson et al. (150) studied the behaviour of different particle sizes of glass Ballotini spheres during sieving. They measured the time for 60% of the fines to be sieved out and found that increasing bed depths prolonged sieving times in two different mixes. To explain these results they proposed that the effective rate of flow of fine grains through the powder bed was proportional to the concentration gradient of fine particles. This assumption is analogous to the diffusion mechanism of mixing. Shinohara and Tanaka (151) proposed a model of sieving based on tapping in which the stratification process (layered packing) of larger particles above the screen controls the flow rate. According to this theory, flow is rate-limited by the layer with the smallest void spaces and the effective minimum void space decreases with an increasing number of complete layers (bed depth). This model obviously breaks down in conditions of bulk shear.

1.4.5.3 Vibrational Segregation in Simulated Transportation

Movement of fines to the base of containers often occurs as a result of vibrations produced in transportation and handling of powders. Parsons (152) studied the segregation of fine powders, such as cathode ray tube phosphors, in a tapped drum. He found that tapping generally produced increased fines at the base of the container, with a concurrent rise in coarse particles and agglomerates to the top. Turczyn (153) discussed the implications of different types of vibration profiles on the contents of containers during transportation. The effect of shock waves on the packing of granular materials has been studied by Nunziato and

Walsh (154). They showed that the way in which different materials respond to shock depends on the initial porosity of the solid; this alters the wave behaviour as it passes through the granules and thus affects the stress on the material.

1.4.5.4 Equations of Vibration-Induced Particle Motion

Kroll (155), in proposing a model for the motion of material in a vibrated bed, assumed an absolutely rigid porous medium not touching the container walls. Others have shown experimentally that this model is only accurate if the bed depth in the vibrated vessel is small and Ryzhkov and Baskakov (156) used a membrane strain gauge embedded in the container walls to show that the powder exerts a pressure on the wall throughout vibration. Based on this work Ryzhkov and Baskakov derived equations of motion for material in the vibration vessel. At certain vibration displacements corresponding to a vibration coefficient $\psi(+)$, which is related to acceleration and the frictional force, and low inertial vibration forces, K_o, material is thrown off the container base. The flight stage begins at time, $t_o^{(+)}$ when the stress at the lower boundary of the layer decreases to zero according to:

$$\sin \omega . t_o^{(+)} = \frac{\psi(+)}{K_o} \qquad (40)$$

where ω is the angular frequency ($2\pi f$). However, if $\psi(+) < \Psi_o$, particle flight begins earlier at a time $t_o^{(-)}$ given by:

$$\sin \omega . t_o^{(-)} = \frac{\Psi_o}{K_o} \qquad (41)$$

where Ψ_o is another vibration coefficient related to the vessel diameter and the damping factor. Over the time $t_o^{(+)}$ to $t_o^{(-)}$ the powder moves over the vessel wall exerting no pressure on the base. The phase angle θ" at which the direction of particle velocity changes can be found from the expressions:

$$\frac{d\bar{s}_1}{d\theta} \cdot (\theta'') = 0 \; ; \; \frac{d^2.\bar{s}_1}{d\theta^2} (\theta'') = 0 \qquad (42)$$

where $\bar{s}_1$ is the mean height to which the powder is thrown above the base; θ is given by $\theta = wt$. These equations were checked experimentally using a layer of graphite powder inserted into a bed of sand, subjected to vibration conditions of 10 - 30 Hz frequency and 2.73 mm amplitude.

Gutman (157) has also modified the Kroll model of particle movement during vibration after studying the propagation of a pulsating air pressure through a fixed bed of 250 - 300 μm diameter sand during vibration. He found that up to 100 Hz vibration frequency Darcy's law, which predicts a linear dependence of pressure drop on fluid (air) velocity held true. In addition, he discovered that the compression and expansion of air in the porous layer of powder occurred isothermally.

Gutman (158) has extended the Kroll model, based on the isothermal compression of air in the vibrating cylinder. The pressure at the base of the cylinder was found to change in a cyclic manner which Gutman expressed mathematically as a Fourier series. Considering the height to which the bed is thrown, S", with respect to this cyclic pressure change P_L, the equation of motion of the vibrated bed is given by:

$$d(\rho's'')/dt' = \rho_o'u' = -\rho_o'(\kappa\varepsilon/P_o)(\delta P/\delta z)_L \qquad (43)$$

where ρ' is the air density; ρ_o', the density at atmospheric pressure; κ, is a permeability constant related to the air velocity in a section of powder; ε, the bed voidage; u, the superficial air velocity; t, the vibration time; z, the distance of particle flight

above the bed base; L, the layer depth of material; P_o, the atmospheric pressure, related to P_L by the fourier series:

$$P_L = P_o + a_o + \sum_{m=1}^{m=\infty} a_m \sin(m.\omega t + \xi_m) \qquad (44)$$

where, a_o is a fourier coefficient; a_m, an mth order fourier coefficient and ξ_m the mth order phase lag. When the density changes are small it was assumed that $\rho' \approx \rho'_o$ and $s''d\rho'/dt' << \rho'_o\, ds''/dt'$ so that equation (43) becomes:

$$ds''/dt' = -(\kappa\varepsilon/\rho_o)(\delta\rho'/\delta z)_L \qquad (45)$$

This equation was used as a basis for deriving four simultaneous equations which by limited continual iteration can be used to yield the coefficients along with other unknown values, such as β, the fraction of a cycle when the bed is in flight. The predictions of vibrated particle motion produced by this model are shown in Figure 13 compared with the Kroll model under the same conditions. Both models predict that the bed lifts off the vessel base on the upstroke of vibration. The Kroll model (Figure 13(b)) predicts that when the bed collides with the vessel base at the start of the next upstroke (Figure 13(b)), the pressure will return to zero instantaneously (Figure 13(c)). However, the compressible gas model assumes that the air pressure following collision decays in a finite time so that the bed base is above atmospheric pressure at the start of the next cycle (Figure 13(c)). As a consequence of these influences, the Gutman compressible gas model (Figure 13(c)) predicts a much higher bed throw than the Kroll model, for which the particles are in flight longer but the trajectory is shallower. When tested experimentally

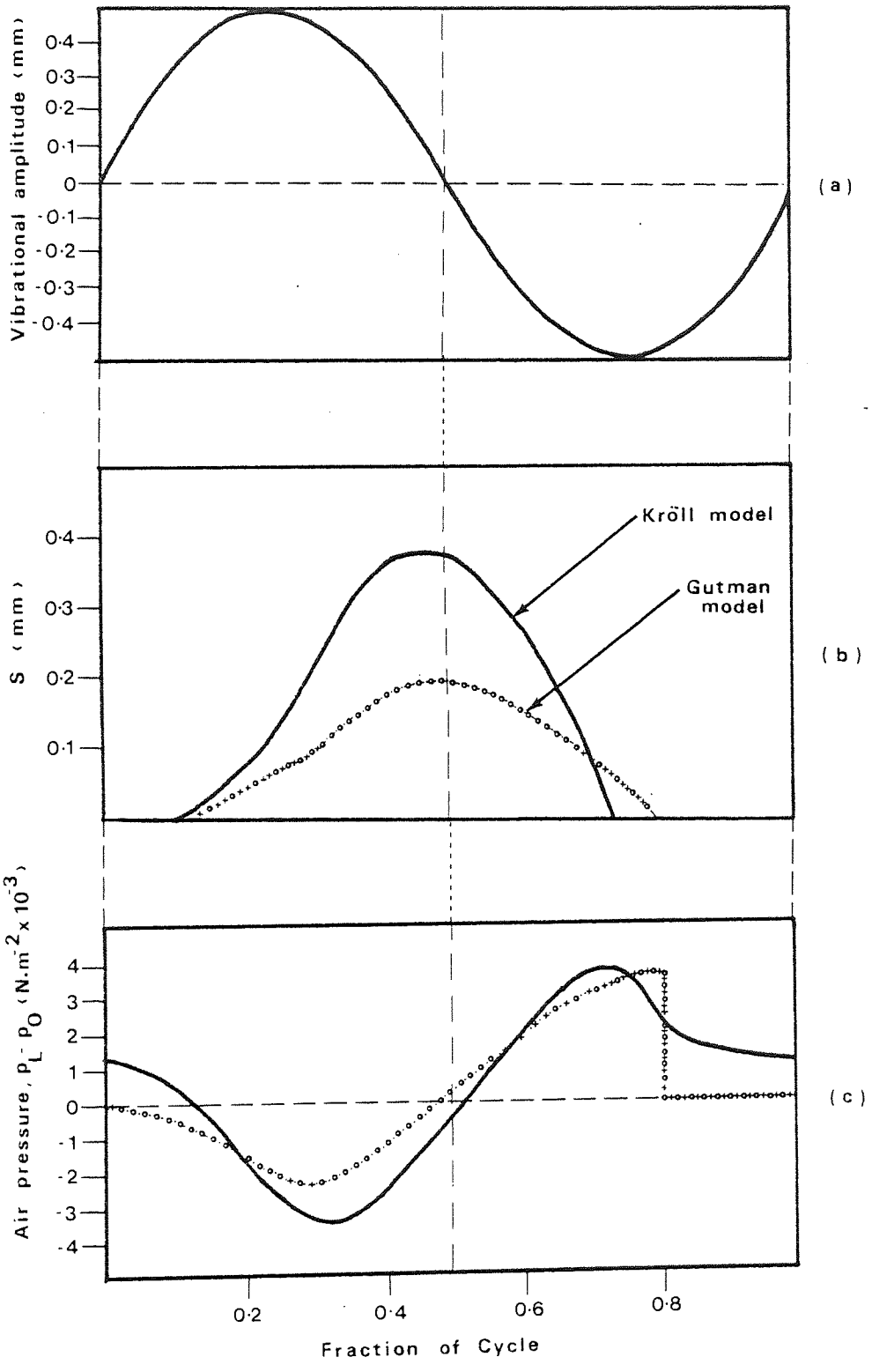

Figure 13. (a) The cyclic vibrational amplitude, (b) the displacement height of a vibrated powder bed, (c) the air pressure at the powder base. The different measurements are all related to the fraction of the cycle during which events occur. Figs. (b) and (c) show predictions based on the Kroll model and the Gutman model of powder vibration.

the Gutman model broke down in deep beds. It has the same limitations as the Kroll model, being based on the assumption of zero wall friction, and therefore requires modification according to the equations of Ryzhkov and Baskakov (156).

1.4.6 Reduction of Segregation

During the preceding sections it has been shown that systems which contain particles with similar properties are less likely to segregate. Successful attempts to reduce segregation are normally based on this principle; for example, Harris and Hildon (159) have used narrow size-range powders to reduce segregation of non-cohesive powders. Ordered mixes are a notable exception to this general rule, since they can provide homogeneous, non-segregating ordered systems of two or more components with widely divergent properties.

It is desirable to obtain information about the homogeneity of a powder mix at each stage during its processing. Many methods of assessing the quality of a powder mix have been developed, some based on heterogeneity, others on homogeneity.

1.4.7 Quality of a Mix

When defining the quality of a powder mix the requirements depend on the final use of the mix, but in all cases quality is best expressed quantitatively. An assessment of a powder mix is generally achieved by studying a limited number of spot samples, since only in exceptional circumstances will it be feasible to analyse the entire mix. These spot samples are then compared statistically to generate a single figure which best describes the state of mixing in that group of samples at that instant. Weidenbaum (160) illustrated the use of different statistical

techniques in quantifying mixing processes and also reviewed the early work on quantification of the degree of mixing. The review by Schofield (161) includes more recent work in the quality assessment of solid mixes.

1.4.7.1 Statistical Analysis of Powder Mixes

The application of various statistical analyses to powder mixing has been described by Harnby (162). In general, the sample data to be analysed are assumed to follow a normal distribution, although the central limit theorem has also been used in known non-normal distributions (163). Most segregating mixes and also non-segregating systems at the start of mixing have non-random distributions. However, Schofield and Valentin (164) have shown that errors introduced by using measures based on the standard deviation of a normal population do not exceed the uncertainty limits for most practical mixing situations. They conclude that no serious errors result from assuming a normal distribution.

The quality of a powder mix is frequently measured by calculating the standard deviation of representative spot samples. The standard deviation s, of a random mix will lie between the limits σ_R for a completely randomised system and σ_o, for a totally unmixed system:

$$\sigma_o \leqslant s \leqslant \sigma_R \qquad (46)$$

Equation (46) forms the basis of most mixing indices which assess the homogeneity of a system by comparing the standard deviation or variance of spot samples taken in the totally mixed and unmixed states.

1.4.7.2 Mixing Indices

Most mixing indices are based on statistical analysis although some use direct measures based on photometry (160) and kinetic approaches (53). A mixing index is usually a single real number lying somewhere between zero and one, which expresses the state of mixedness from a number of spot samples. Fan et al. (165) presented a summary of 35 different mixing indices. Later, Fan and Wang (166) produced a table matrix relating each of nine frequently used mixing indices to one another. Some of these indices, as reported by Schofield (161), are listed in Table 1. Each of these mixing indices becomes a more accurate description of the system homogeneity as the number of spot samples used to calculate the standard deviation increases. The theoretical standard deviation of samples taken from random mix varies inversely with sample size. The observed standard deviation of the various mixing indices will also be affected by sample size, according to the scale of scrutiny (170). Harvey (171) has claimed to develop independently of other workers, a theory of ideal mixing based on the concept of "sufficiently small volumes" which is the scale of scrutiny term used by others. Marc de Chazal and Hung (172) found that indices of mixing are dependent on both the shape and size of the samples removed. Kristensen (173), developed a relationship between variance and sample size for non-random mixtures based on correlation coefficients. The observed total variance of a random or non-random mix of particles will be composed of elements which include long range and short range segregation effects as well as systematic errors such as those produced by sampling (Section 1.3.3). A mixing index determined from an observed inter-sample variance will therefore include both

Table 1. Relationships between different mixing indices, M, and their numerical values as mix quality improves. C^*, C_r are coefficients of variation of practical and random mixes respectively, χ_o^2 is the practical chi-squared value for a mix and χ_R^2 and χ_S^2 are expected chi-squared values for the random and unmixed state respectively.

Author	Reference	Mixing index	Equation no.	Range of index and change (→) as mixing improves
Lacey	(39)	$M = \frac{\sigma^R}{S}$	(47)	$<1 \rightarrow 1$
Weidenbaum & Bonilla	(38)			
Kramer	in (52)	$M = \frac{\sigma_o - S}{\sigma_o - \sigma_R}$	(48)	$0 \rightarrow 1$
Lacey	(52)	$M = \frac{\sigma_o^2 - S}{\sigma_o^2 - \sigma_R^2}$	(49)	$0 \rightarrow 1$
Ashton & Valentin	(167)	$M^2 = \frac{\log \sigma_o^2 - \log S^2}{\log \sigma_o^2 - \log \sigma_R^2}$	(50)	$0 \rightarrow 1$
Poole, Taylor & Wall	(41)	$M = \frac{C^*}{C_R}$ or $\frac{S}{\sigma_R}$	(51)	$>>1 \rightarrow 1$
Carley-Macaulay & Donald	(105)	$M^2 = \frac{S^2 - \sigma_R^2}{(1 - 1/n)}$	(52)	$>>0 \rightarrow 0$
Rumpf & Sommer	(168)			
Gayle, Lacey and Gary	(169)	$M = \frac{\chi_o^2 - \chi_R^2}{\chi_S^2 - \chi_R^2}$	(53)	$1 \rightarrow 0$

long and short range segregation effects and will be unable to locate different units of scrutiny within a mix. Danckwerts (174) developed two separate indices to account for long and short range segregation of particles. The intensity of segregation, I (equation 54) is related to the mixing indices in Table 1:

$$I = \frac{s^2}{\bar{x}.\bar{y}} \qquad \frac{s^2}{\bar{x}(1-\bar{x})} \tag{54}$$

I, has a value of one when segregation is complete (i.e. when the concentration of x or y at every sampling point is either 1 or 0) and 0 when the content is uniform. Danckwerts second parameter, the scale of segregation, is based on the correlation coefficient R(r) between pairs of sample scrutiny units a distance r apart. The relationship is given by:

$$R(r) = \frac{\overline{(x_1 - \bar{x})\,(x_2 - \bar{x})}}{\overline{(x - \bar{x})^2}} \tag{55}$$

where x_1 and x_2 are the concentrations of x (or y) in any pair of scrutiny units; $\bar{x}$ is the mean of the individual sample concentrations, x. R(r) should be averaged over all possible pairs of scrutiny units. Danckwerts plotted a correlogram of R(r) against r. The area under the curve was used as a measure of clump (aggregate) size. The curve can also be used to identify long-range segregation, demonstrated by a negative value of R(r). In systems not displaying long range segregation R(r) has a value between zero and unity. When r = 0, x_1 and x_2 are identical. Lacey and Mirza (175, 176) used the Danckwerts coefficients to describe the structure of a practical (imperfect) mix of particles. Chou *et al*. (177) took a different approach to the use of scalar mixing indices described previously. They used the stochastic (randomisation) theory of mixing applied

to a Markov chain with stationary or non-stationary transition matrices between the arrays. This method is applicable to binary or multicomponent mixes and can be used to simultaneously study particle distributions and particle mobilities.

1.4.8 Quality of Pharmaceutical Mixes

The scale of scrutiny of a pharmaceutical powder mix is defined by the volume or weight of the finished dosage form. The objective in all pharmaceutical powder mixing operations is to obtain and subsequently maintain an adequate degree of drug content uniformity. This is recognised by most pharmacopoeias in their standards for weight uniformity of tablets (15). However, as Train (16) observed, this method is unreliable, particularly with microdose drug systems. The British Pharmacopoeia 1973 (and subsequent addenda) (15) requires that for certain microdose preparations, individual assays must be carried out on a specified number of unit doses. The required content uniformity for these tablets is listed in Table 2.

DRUG	TABLET STRENGTH (mg)	VARIATION ABOUT MEAN %	LIMIT FOR 9 OUT OF 10 TABLETS %	LIMIT FOR ALL TABLETS %
Dexamethasone —	0·05	±10	±10	±20
Digoxin — — — —	0·125	±10	±20	±25
Ergotamine — —	1	±10	±15	±20
Glibenclamide —	5	±10	±10	±15
Methysergide —	1	±10	±15	±20
Nicoumalone —	1	±10	±15	±20

Table 2. Content uniformity for microdose preparations (B.P. 1973 and subsequent addenda)

The United States Pharmacopoeia (178) requires that all tablets containing less than 50 mg of drug should be assayed individually, although the U.S.P. requirements for content uniformity are based on a 'range' about the mean of ± 15%.

The implications of these standards and other indices of mixing in relation to pharmaceutical operations have been described by Hersey (179).

1.4.8.1 Specification Indices

Mixing indices (such as those in Table 1) which describe the quality of a mix can be misleading in pharmaceutical systems (180). Hersey (181), has suggested a specification index, σ_A, based on the variance required by a pharmacopoeial standard or by a pharmaceutical company. The variance may be chosen as a percentage about the mean, and the 3σ level proposed by Train (16) has been widely used. In these circumstances, tablets which must contain ± 15% of the mean drug content in a 1% active formulation, the 3σ level is given by:

$$3\sigma = 0.15 \times 0.01 \qquad (56)$$

and the corresponding σ_A value will be 0.0005. The specification index, S/σ_A has been shown to produce a more realistic representation of the quality of a pharmaceutical powder mix than the index S/σ_R (171).

Hersey and Cook (182) applied the universal homogeneity index of Buslik (equation 29) to pharmaceutical systems. The relationship between σ_A, the desired content uniformity and H_i the homogeneity index is given by the following relationships:

$$\sigma_A = \left\{ G(100 - G)\ W/Wd \right\}^{\frac{1}{2}} \qquad (57)$$

where W_d is the dose size and G, the proportion of component weight, w. By substituting equation (57) in equation (29):

$$H_i = -\log W_1 = -\log \sigma_A^2 W_d \qquad (58)$$

Hersey (183) suggested the use of $H_i^* - H_i$ as a pharmaceutical mixing index. H_i^* is the difference between the homogeneity at any instant during mixing and the specification homogeneity calculated from equation 58. $H_i^* - H_i$ approaches zero as mixing progresses and can be further related to the specification index, S/σ_A, according to the relationship (163):

$$H_i^* - H_i = -\log \sigma_A^2 W + \log S^2 W$$

$$= \log S^2 w/\sigma_A^2 W \qquad (59)$$

or

$$H_i^* - H_i = 2 \log (S/\sigma_A) \qquad (60)$$

Hersey et al. (184) used these principles to determine the limiting particle size requirements for a three-component pharmaceutical system which would allow the required homogeneity to be achieved. Johnson (185) used the same approach to calculate the required particle size distributions which he considered to be of more practical significance than particle size alone. Johnson used the coefficient of variation, C_v, of a theoretical random mix in place of standard deviations:

$$C_v = \frac{100(\pi \rho^o)^{\frac{1}{2}} (\Sigma f d^{o3})^{\frac{1}{2}}}{6G^w} \qquad (61)$$

where ρ^o is the drug density; G^w, the weight of drug in a sample and d^o is the equivalent spherical diameter of the drug particles in a given size range. The coefficient of variation was derived

from equation 3 (42). The dose variation limits in USP XIX (178) of ± 15% correspond to a C_v of 5% at the 99.7% (3σ) probability level. To allow for practical limitations due to differences in particle properties and deviations from the normal distribution in microdose systems, Johnson (42) recommends a coefficient of variation of 1% as the limit for an ideal mix.

The use of different quantitative analyses in pharmaceutical micro-dose systems has been reviewed by Crooks (81).

The problem of dose variation encountered in free flowing direct compression microdose systems can be overcome by forming stable ordered mixes (82). The surface forces stabilising an ordered mix and the fine components of a total mix produce powder particle adhesion.

1.5 Powder Particle Adhesion

The forces acting at particle interfaces include:

(a) The Colour Force (chromodynamic interaction). Binds quarks in protons, extremely strong, short in range (10^{-13} cm) carried by gluons.

(b) The Strong Force (nuclear interaction). Binds atomic nuclei, acts on quarks, strong, short in range (10^{-13} cm) carried by mesons.

(c) The Weak Forces (weak interactions via neutral or charged current). Acts on quarks and electrons. 10^{-11} strength of the Electric Force, very short in range (10^{-15} cm) carried by W^o, W^- and W^+ particles.

(d) The Electric Force (electromagnetic interaction). Binds atoms, acts on all charged particles, infinite in range, carried by photons.

(e) The Gravitational Force (gravity interaction). Binds matter, extremely weak in atoms, infinite in range, acts on matter and energy, carried by gravitons.

For particles less than 60 μm diameter, the gravitational force is swamped by the electric adhesive forces (186). The distances between particles are so great in relative terms that the colour force and the strong and weak nuclear forces play no part in stabilising powder mixes; they do not even influence the adhesive bonds in ordered or total mixes. Thus the only interactions which remain of interest are those with electrical origin which can be divided into two main types:

1. Short-range forces: These arise when molecules come close enough for their electron probability-distribution clouds to overlap. They have been called chemical bonds.

2. Long-range forces: Other bonds produced when electron clouds do not overlap, often called physical forces.

1.5.1 Particle Adhesion Theory

The influence of physical forces in adhesion has been studied by Krupp (187). The electric potentials arising from long-range forces vary as the inverse power of intermolecular separation, and can be classified according to their electrostatic and dispersion contributions.

1.5.1.1 Electrostatic Forces

The electrostatic contribution produces potential energy from interactions between multipoles. These multipole moments can be charges (monopoles), dipole moments, quadrupole moments etc. Application of Coulomb's law of electrostatic attraction yields the potential functions for various types of charge

distribution interactions in multipoles (188):

$$F_x = \frac{q.q'}{4\pi\varepsilon r^2} \cdot r_1 \qquad (62)$$

where F_x is the force on the image charge of q'coulombs due to the applied charge, q; r , the vector from $q'$to q ; r_1, a unit vector along r and ε , the capacitivity constant for the medium (ε_{vacuum} = 8.85×10^{-12} $F.m^{-1}$). Coulombs law applies only to charged bodies whose dimensions are small in comparison with the distances between them, and may only be of interest at molecular level. Donald (189) distinguishes between electrostatic multipole interaction at molecular distances and the integration of those forces leading to macroscopic charge effects. By consideration of space-charge depths at particle interfaces Krupp (172) derived an expression for the electrostatic attractive force between two macroscopic particles, F^o_{el}:

$$F^o_{el} = Q^2/16\pi\varepsilon_o R'\delta_o \cdot \frac{Ln(1 + \delta_o/Z)}{\left\{\gamma + \frac{1}{2}Ln(2R'/Z')\right\}\left\{\gamma + \frac{1}{2}Ln\left[2R'/(Z + \delta_o)\right]\right\}} \qquad (63)$$

where Q is the effective particle charge contribution to the adhesive force; ε_o, the influence constant; δ_o, the penetration depth of surface charge; Z, the distance of the particle from the other particle or substrate; γ, Eulers constant (0.5772) and R', the particle radius.

1.5.1.2 Van der Waals Forces

Van der Waals forces are produced by interactions of multipoles induced within neighbouring charge distributions. These forces also include London's forces and are known collectively as the

dispersion effect. For spherical molecules, the dispersion potential function for an induced dipole-induced dipole varies as the inverse sixth power of separation distance. Over distances greater than 10^{-8} m this relation must be modified to account for electromagnetic retardation so that the energy now varies as the inverse 7th power of distance. This increases to the 8th power for induced dipole-induced quadrupole and the 10th power for induced quadrupole-induced quadrupole interactions (186). The overall effect of these interactions on macroscopic particles can be seen by integrating over all multipole pairs of atoms or molecules in a powder to produce an energy of interaction, E' (190):

$$E' = \frac{-\pi^2 q_a^2 \lambda}{C} \int_{C-R_2}^{C+R_2} \left\{ R_2^2 - (C - R)^2 \right\} . dR \times$$

$$1/12 \left\{ \frac{2R_1}{(R + R_1)^3} + \frac{2R_1}{(R - R_1)^3} + \frac{1}{(R + R_1)^2} - \frac{1}{(R - R_1)^2} \right\} \qquad (64)$$

where C is the distance between particle centres; R_1 and R_2 are the two particle diameters; q_a, the number of atoms per cm and λ is the London - van der Waals constant. Equation (63) can be expressed as a force by differentiation with respect to d_R, the surface separation distance.

The integration method of calculating van der Waals forces in macroscopic bodies will only be valid in rarefied systems, such as gases where interactions are simplified, although Kiefer and Parsegian (191) have modified some of the assumptions of the integration method. Lifshitz (192) developed a relationship for

van der Waals adhesion, F^{o}_{vdw}, based on macroscopic interaction of two particles in a fluctuating electromagnetic field:

$$F^{o}_{vdw} = \hbar / 2\pi^{2}C^{3} \qquad (65)$$

where $2\pi\hbar$ is Planck's constant. Krupp (187) modified equation (65) to account for gap C becoming filled with a dielectric:

$$F^{o}_{vdw} = \frac{\hbar\bar{\omega}}{8\pi C^{2}} \cdot R' \qquad (66)$$

where $\bar{\omega}$ is the angular frequency in $\hbar\bar{\omega}$, the Lifshitz - van der Waals constant.

1.5.1.3 Unified Adhesion Theory

Krupp (187) derived a relationship for the adhesive force F^{P}, between a plane solid and a spherical solid particle:

$$F^{P} = F^{o}(1 + P/H\{t\}) \qquad (67)$$

where F^{o} is the sum of all attractive forces acting outside the contact area and producing deformation; P, the sum of all the attractive forces acting within the contact area; H(t) is related to the deformation resistance of the softer material given by a property such as Brinell hardness (Figure 14).

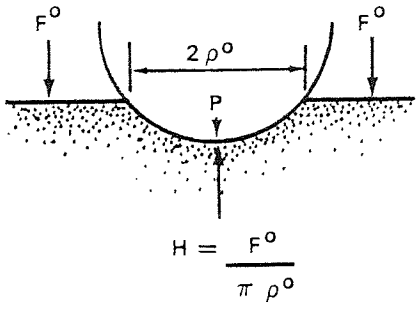

Figure 14 Diagramatic representation of adhesion forces between a small and large sphere or plate. For definition of symbols see text.

Usually the electrostatic component, P_{el} of P is small compared with the van der Waals component P_{vdw}:

$$P \approx P_{vdw} \qquad (68)$$

F^o is composed of the short range forces F^o_{vdw} acting only around the contact area, plus F^o_{el}:

$$F^o = F^o_{el} + F^o_{vdw} \qquad (69)$$

Kottler et al. (193) produced a relationship for the theoretical force of adhesion between particles based on equation (66), (67) and (68):

$$F^o = (F^o_{el} + F^o_{vdw}) \left\{ 1 + P_{vdw}/H_{(t)} \right\} \qquad (70)$$

They compared the theoretical behaviour of fine particle adhesion in particle multilayers with results obtained experimentally.

Donald and Watson (194), found that in a system of fine powder adhering to coarse beads, the electrostatic contribution to adhesion was larger than the short range van der Waals contribution. Bozorg and Klinzing (195) noticed a similar effect in a system of aluminium powder. Donald developed a model to account for loosely bound as well as tightly bound particles (196). The model calculates the force of electrostatic adhesion, F_D, in relation to the point charge Q_o or total charge Q_T of a spherical particle radius R , whose centre is a distance h^P from the substrate according to equation (71):

$$F_D = (Q_o^2 / 4h^{P2})\,\alpha \qquad (71a)$$

$$= (Q_T^2 / 4R'^2)\,\alpha \qquad (71b)$$

where α is a dimensionless parameter given by:

$$\alpha = (R'/3d_R)^{0.7} \qquad (72)$$

The difference between the two solutions for F_D (equations (71a) and (71b)) is the number of triboelectric contacts the adherent particle has made.

1.5.2 Triboelectric Charging

A general description of the processes and applications of electrostatic charging has been given by Moore (197). There are many different methods of producing an electrostatic charge on a material, but the one which has been known for a considerable time is that produced by friction. It is generally supposed (188, 197) that Thales of Miletus in 600 B.C. first observed the effect which is now called triboelectric charging (from tribos, to rub), by rubbing amber. Rudge (198), found that an electrostatic charge could be produced by blowing powder off a surface. He showed that, in general, metallic powders charged negatively as did strongly basic materials, whereas non-metallic and strongly acidic powders charged positively. The experiments were repeated and Rudge (199) further discovered that unweighable quantities of powder produced measurable charges. The sign of these charges was the same no matter what surface the powder was blown from. Masuda and Iinoya (200) used the opposite approach, by blowing powders on to a surface to produce a triboelectric charge. They found that impact electrification occurs through deformation as well as friction. This is analogous to the prediction of Krupp (Figure 14) (187). Masuda and Iinoya (200) derived an equation relating the current generated, I, to the contact transition region of the plastic-elastic collision for impact velocities at the elastic limit and assuming the conservation of electric charge:

$$I = \frac{-2.45.\varepsilon_o.V_c.\Delta t.W_p}{d_R.\tau.D_p}\sqrt{\beta/\rho.y_d}.\ (\nu_o.\cos\theta - \nu^*) \qquad (73)$$

where ε_o is the dielectric constant of air; V_c, the contact potential difference; Δt, the effective duration of contact; W_p, mass flow rate of powder; τ, time constant of model condenser produced by interparticle gap; D_p, the diameter of a sphere with the same volume as the particle; β, roundness of the particle ($\beta = 2R_1/D_p$); Y_d, yield pressure; ν_o, particle velocity; θ, angle of inclination of the target plate and ν^*, the velocity modifying term given by:

$$\nu^* = 0.04\quad Y^5.\beta^3/Ey^4.\rho \qquad (74)$$

where E_y is the composite Young's modulus of the particle, E_y and plate, Ey_2 ($Ey = \frac{Ey1 \times Ey2}{Ey1 + Ey2}$). They found that the current produced varied inversely with particle diameter and directly with powder flow rate, W_p when Wp was small. Pope et al. (201) had previously demonstrated the same effects in triboelectrically charged alkaline earths using perspex and brass cyclones. They also showed that particle charge was proportional to surface area and that re-cycling the charged material increased powder particle charge up to a limiting value. Pearse and Reid, also using a charging cyclone, produced a triboelectric series for several alkaline earths (202). The highest negatively-charged powder was biotite and the highest positively charged powder was dolomite. These two powders retained their positions in the series when triboelectrically charged on different surfaces. However, some of the intermediate members of the series changed rank order. Pearse and Pope (203) successfully reversed the triboelectric charge of calcite and apatite powders

by surface treatment with oleate ions prior to charging. The ions apparently adsorbed on to the powder surface and changed a weak negative charge into a strong positive charge. In powders normally having like triboelectric charges, this effect could be used to increase particle collection, as discussed in the following section.

1.5.2.1 Triboelectric Particle Collection

Triboelectrically charged filters have been used to remove minute particles from air streams with a very high efficiency (204). Walton (205) described the collecting action of charged resin particles in a filter. He found that the radius over which the charge was effective extended about 3 μm from the resin-carrying fibre boundary. Nielsen and Hill (206) calculated particle trajectories and target efficiencies for the collection of inertialess particles on spherical collectors in a gaseous flow field. They found (207) that the electrostatic forces significantly enhanced particle collection in comparison with that produced by inertial impact alone. Particle collection on filters can be considered analogous to the objectives in achieving an ordered powder mix.

1.6 Aims of the Present Study

The aims of the present study are to utilise the principles of crystallisation outlined in Section 1.2 to produce a habit-modified, free-flowing, microdose direct-compression excipient (Section 1.1.1). This excipient should ideally be capable of forming stable mixes (Section 1.3) which do not segregate during processing (Section 1.4) with a model drug.

The phenomenon of triboelectric charging (Section 1.5.2) will also be studied as a method of controlling and modifying the surface

electrical forces (Section 1.5.1) which influence the mixing of fine particles.

The ultimate aim of the study reported here is to establish a basis for eventual development of a special blending process by which a variety of active ingredients can be mixed with standard excipients to produce non-segregating homogeneous systems (208).

Chapter Two

2. Preparation and Characterisation of a Novel Direct Compression Excipient

Modifications of the crystal growth patterns of lactose were attempted in order to produce crystals with various external habits, including increased surface irregularities which might be capable of entrapping fine particles.

2.1 Crystallisation of lactose

As an initial feasibility study, systems were studied in which lactose powder of European Pharmacopoeia standard (209) (British Drug Houses Ltd., Poole, U.K. Batch No. 1184680) was dissolved in a binary solvent system.

Method (i). In the first method one solvent was water and the second solvent (co-solvent) was miscible with water but reduced the overall solubility of the lactose. Crystals were recovered using a vacuum filtration apparatus consisting of a Buchner flask and filter funnel. Following drying the crystals were examined under a low-power light stereomicroscope (Zeiss, Jena, W. Germany).

Method (ii). The second method used was similar to that of Majd and Nickerson (30) adapted to take account of the super-solubility profile of lactose given by Jelen and Coulter (210). The lactose powder was dissolved in water at 70^{o}C to produce a supersaturated mother liquor. This was allowed to equilibrate for ten minutes to remove any crystal ghosts (18). Aliquots of lactose mother liquor were added to solutions of co-solvents (see later for details of different solvents) which produced

final solvent concentrations of 40%, 50% and 60% in aqueous lactose solution. The crystals were examined microscopically after growth times of 15 and 30 minutes.

Method (iii). The third method was essentially similar to the previous one except that the co-solvent was added to the mother liquor. Several different concentrations of co-solvents in the mother liquor were employed to examine the effect of increased proportions of solvent on crystallisation; solutions containing 70, 80 and 90% co-solvent were prepared and the recovered crystals were examined microscopically. The effect of mechanical stirring and ultrasonic vibration on the size of crystal agglomerates produced was also studied.

Following each crystallisation method dry sieving was used as a final process to control agglomerate size, and the crystals produced were examined using a stereo optical microscope. Several co-solvents were evaluated using each of these three methods, propan-2-ol (isopropanol) acetone (of analytical grade) and ethanol (as industrial methylated spirits), all obtained from Fisons Scientific Apparatus, Loughborough, U.K. Crystals were recovered on filter paper (Whatman Number 1, Whatman Ltd., London, U.K.). Secondary growth, which occurs from the residual mother liquor surrounding the filtered crystals (211), and causes caking during drying, was avoided by washing with pure acetone immediately after filtration. Drying was carried out in a vacuum oven (Edwards High Vacuum, London, U.K.) at 70^{o}C and a pressure of 250 mm of mercury.

All the methods used in these initial experiments produced lactose spherulites of various particle sizes. Method (iii), in which co-solvent was added to the mother liquor, produced lactose crystallites with more dendrites than the other methods.

The various co-solvents produced similar results in each of the methods. Ethanol in the form of industrial methylated spirits was chosen as the co-solvent for further study in preparing small-scale lots of lactose spherulites, primarily because it is pharmaceutically most acceptable as a processing solvent. Both mechanical agitation and ultrasonic vibration caused agglomerate breakdown and produced small single dendritic crystals in a manner similar to that described by Mullin and Ang (212). Dry screening was chosen as the most convenient method of controlling agglomerate size in the small-scale experiments.

2.1.1 Small-scale crystallisation of lactose spherulites

Several batches of crystal agglomerates were produced using method (iii) in the initial crystallisation experiments. The crystals were grown in 250 ml conical flasks surrounded by a constant temperature water bath at 25°C. In lots A and B, ethanol concentrations of 40, 50, 60, 70, 80 and 90% $^{w}/_{w}$ in mother liquor were used to prepare crystals which were recovered after growth times of 5, 15, 30, 60 and 90 minutes. A third set of crystals, lot C, was prepared; here, the mother liquor was seeded with 0.5% $^{w}/_{w}$ lactose crystals, less than 60 µm diameter, and crystals were recovered after 90 minutes. Filtration of the mother liquor was carried out in two stages: (i) a 53 µm test sieve (Endecotts Ltd., London, U.K.) was used to collect the larger agglomerates which otherwise blocked the fibre back-up filter, (ii) the smaller crystals were recovered in a Buchner filter funnel. Following drying, the crystal agglomerates were screened on an 850 µm test sieve. Any agglomerates still retained after ten minutes shaking (Endecotts sieve shaker, Endecotts Ltd., London) were transferred

to a wire mesh processing sieve and gently brushed through. Using a sieve shaker (Endecotts Ltd., London, U.K.) operated for twenty minutes, each batch in lot C was separated into six size fractions ranging from 1000 μm to below 45 μm diameter.

The yields of crystals in all size fractions were calculated as a percentage of the quantity of lactose powder used as the starting material. All the crystalline raw material dissolved was assumed to be recoverable and no allowance was made for transference losses. It was found that the values for percent yield were related in rank order to the concentrations of ethanol used to recrystallise the lactose and varied with the crystallisation time (Figure 15). Particles recrystallised from a 90% solution of ethanol in water were recovered as 94% of the starting material. However, only 40% of the original lactose powder was recovered in 90 minutes from the solution containing 40% ethanol. The high concentrations of ethanol produced the fastest recovery of crystals, growth being virtually complete after 30 minutes. The low concentration solutions (60% ethanol and below) crystals were still growing steadily even after 90 minutes.

2.2 Characterisation Methods for Lactose Crystals

2.2.1 X-ray Powder Diffraction

Mutarotation of lactose in solution can lead to preferential crystallisation of either the α- or β- forms. The ratio of the two polymorphs alters according to the crystallising conditions (213). Although the crystal habit of the original lactose can be changed by recrystallisation, the crystal lattice packing and hence the crystal type may remain the same. Differences in the

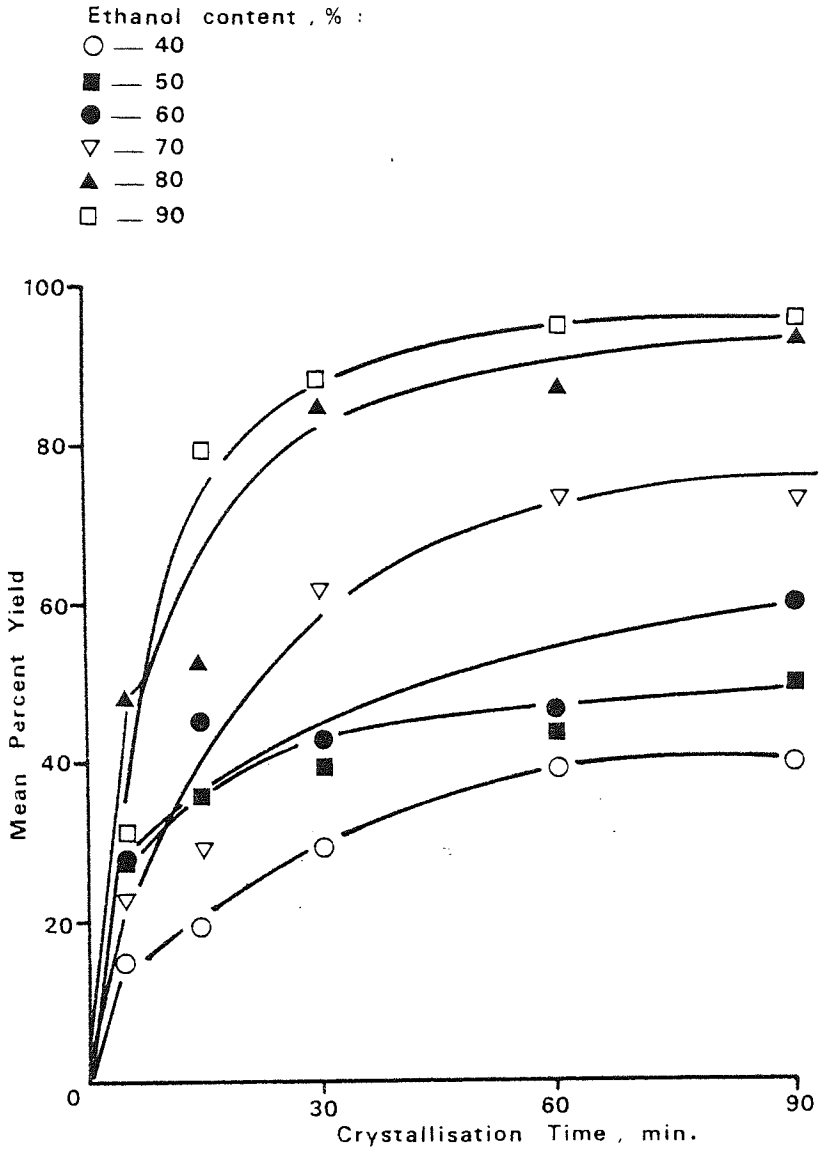

Figure 15 Mean percent yield of lactose spherulites after different growth times in solutions of different ethanol content.

internal crystal lattice can be detected by x-ray powder diffraction

The samples were assumed to consist of very large numbers of minute crystal fragments in a completely random orientation. This assumption meant that every possible lattice plane was present in every possible orientation with respect to the incident electron beam. The Bragg equation: $\lambda_B = 2.d_B.\sin\theta_B$, will thus be satisfied for all three crystal planes, h, k and l, where λ_B is the wavelength; d_B, the crystal lattice spacing and θ_B, the incident angle of the impinging x-rays. Each of the three crystal planes gives rise to a cone of diffracted beams corresponding to a solution of the Bragg equation. The diffraction pattern was scanned by a counting device which plotted counter output against Bragg angle. The random orientation of crystallites produced by sample preparation was enhanced by slow rotation of the sample normal to the x-ray beam. The line of focus of the x-ray tube and the entrance slit of the counter were always equidistant from the sample on a focussing circle. During scanning, the counter was rotated about the centre of the specimen whilst remaining on the focussing circle.

2.2.2 Flow and Packing Properties

2.2.2.1 Flow Rate Measurements

The flow rate of the different particle size fractions of lactose spherulites were measured. The powders were measured in flow from a hopper removed from a tableting machine (Type STD1, Wilkinson Ltd., Loughborough, U.K.). The hopper (Figure 16) was mounted vertically using a laboratory stand and was filled to a

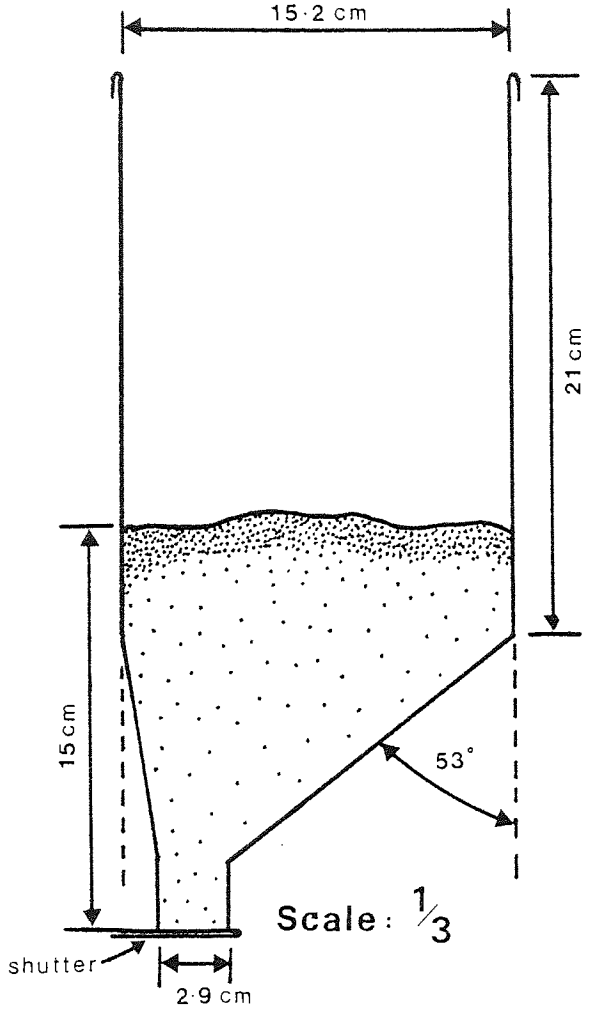

Figure 16 Dimensions of tableting machine hopper used to determine powder flow rates

constant depth of 15 cm with powder stored under ambient conditons. A broad-bladed metal spatula was used as a simple shutter to cover the hopper exit. Measurements were made by removing the shutter and recording the time taken for all the powder to leave the hopper (Figure 16).

2.2.2.2 Bulk Density Measurements

Bulk density measurements were made on all the batches of crystal agglomerates in lots A and B. Bulk density is a function of the packing behaviour of powder particles. For any type of packing, failure of the powder bed, for example during flow or mixing, is determined by interparticle friction and alters according to particle size, shape and the material composition.

A weight of 10 g of lactose spherulites was filled into a 50 ml measuring cylinder using a smooth-walled glass funnel. The 50 ml cylinder was used because of the small quantities of powder available in each batch of crystals; it is recognised that the small cylinder size may lead to an increase in wall effects which could modify the packing geometry and decrease the recorded bulk density. The initial volume, V_o, was recorded and the cylinder was placed on a jolting volumeter (J. Engelsmann A-G, Ludwigshafen am Rhine, W. Germany), which operated at approximately 4 Hz. Subsequent volumes, V_n, were recorded after the cylinder had been tapped 50, 100, 200, 500, 1000, 2000 and 3000 times. Under the experimental conditions, all the powder samples had reached equilibrium volume, V_e, after 3000 taps. The consolidated bulk density at equilibrium (D_e) and the poured or fluff density, D_o, were used to calculate what Carr termed the "percentage compressibility" of the lactose spherulites, according to the equation proposed by

Carr (214):

$$(D_e - D_o) / D_e \cdot 100 = \% \text{ Compressibility} \qquad (75)$$

The Hausner ratio was also calculated from the ratio: D_e/D_o (215).

2.2.3 Particle Size Analysis

2.2.3.1 Sieve Analysis

Test sieves were used which complied with B.S. 410 (1962) (Endecotts Ltd., London, U.K.). A nest of six sieves was used with 1000 µm, 710 µm, 500 µm, 250 µm, 90 µm and 45 µm mesh sizes. The sieves were shaken for twenty minutes on a sieve shaker (Endecotts Ltd., London, U.K.). Each size fraction in Lot C was tested individually.

2.2.3.2 Quantitative Image Analysis

An image analysing computer, the Quantimet 720 (Imanco, Metals Research Ltd., Cambridge, U.K.) was used to determine the projected particle diameters of lactose spherulites in Lots A and B. Sample specimens were prepared on slides similar to those used in light microscopy. The sample was mixed prior to sampling by rotating the container for one minute. A sample was removed with a spatula and dispersed on the slide using propan-2-ol. The slides were dried at room temperature for five minutes before analysis. The particle counting mode known as the "full-feature count" was used. The full-feature count always registers a count of one for each particle (or feature) irrespective of its shape. Particle counts were carried out at six pre-set size levels: 1 µm, 50 µm, 100 µm, 200 µm, 350 µm and 500 µm. For each count only particles with maximum projected chords greater than or equal to the selected

size level were counted. Each size-count was the average of 50 fields and each field count was the mean of 16 separate counts. The counting program was set to submit fields containing particles with diameters greater than 500 μm.

2.2.4 Surface Area Measurements by Nitrogen Adsorption

The Ströhlein Areameter (Ströhlein, W. Germany) was used to produce a single-point surface area determination by nitrogen adsorption. The Ströhlein Areameter operates by a simplification of the method developed by Brunauer, Emmett and Teller (B.E.T.). The sample vessel was connected with a blank vessel across a manometer (Figure 17).

Figure 17 The Ströhlein Areameter nitrogen adsorption apparatus used to determine the specific surface area of lactose powders.

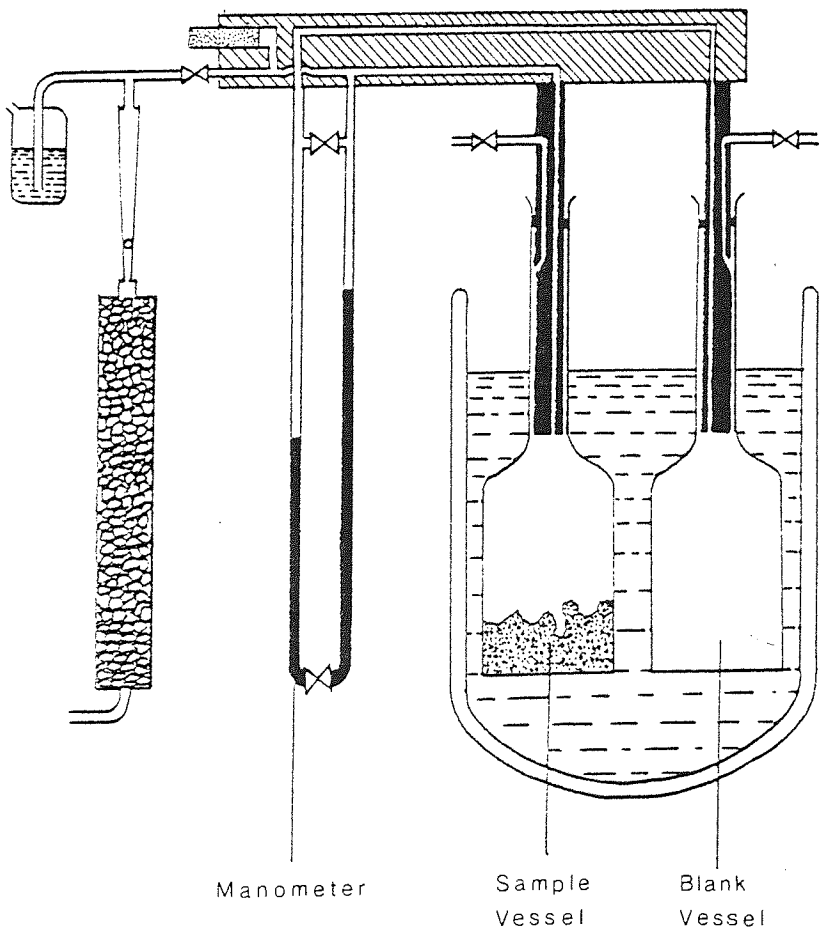

Adsorption of nitrogen caused an imbalance in the pressure of the system which produced a change in the manometer fluid level. This differential measuring system makes it unnecessary to correct for dead volume - a procedure which is carried out in the B.E.T. method by using a non-adsorbing gas such as Helium and the equilibrium pressure is not determined separately but at the same time as the pressure difference. The single point determination method assumes a nearly linear B.E.T. plot passing close to the origin which, according to the manufacturer's claim, introduces an error of only 10% to the specific surface area determinations.

Samples of lactose spherulites were prepared by drying for 16 hours at 70^{o}C under a vacuum of 735 mm Hg to remove any adsorbed water on the crystal surfaces. Sample weights between 4 and 5 g produced pressure differences in the range recommended for the apparatus. The accurately weighed samples were introduced into the measuring vessel which was then connected to the gas lines for de-gassing (Figure 18). De-gassing (or outgassing) is the removal of a physically adsorbed surface film of impurities.

De-gassing was achieved by flushing the samples for 3 hours at 50^{o}C with nitrogen gas. The nitrogen flow rate to all 8 adsorption vessels was 45 litres per hour. Following de-gassing the sample vessels were transferred to the measuring apparatus (Figure 19). The valves were operated sequentially as described in the operating manual and the sample vessels were cooled under fresh liquid nitrogen for 15 minutes. The surface areas were calculated from the differences in the manometer levels using the Strönlein nomogram.

Figure 18 Heating block and nitrogen gas lines for degassing powder samples

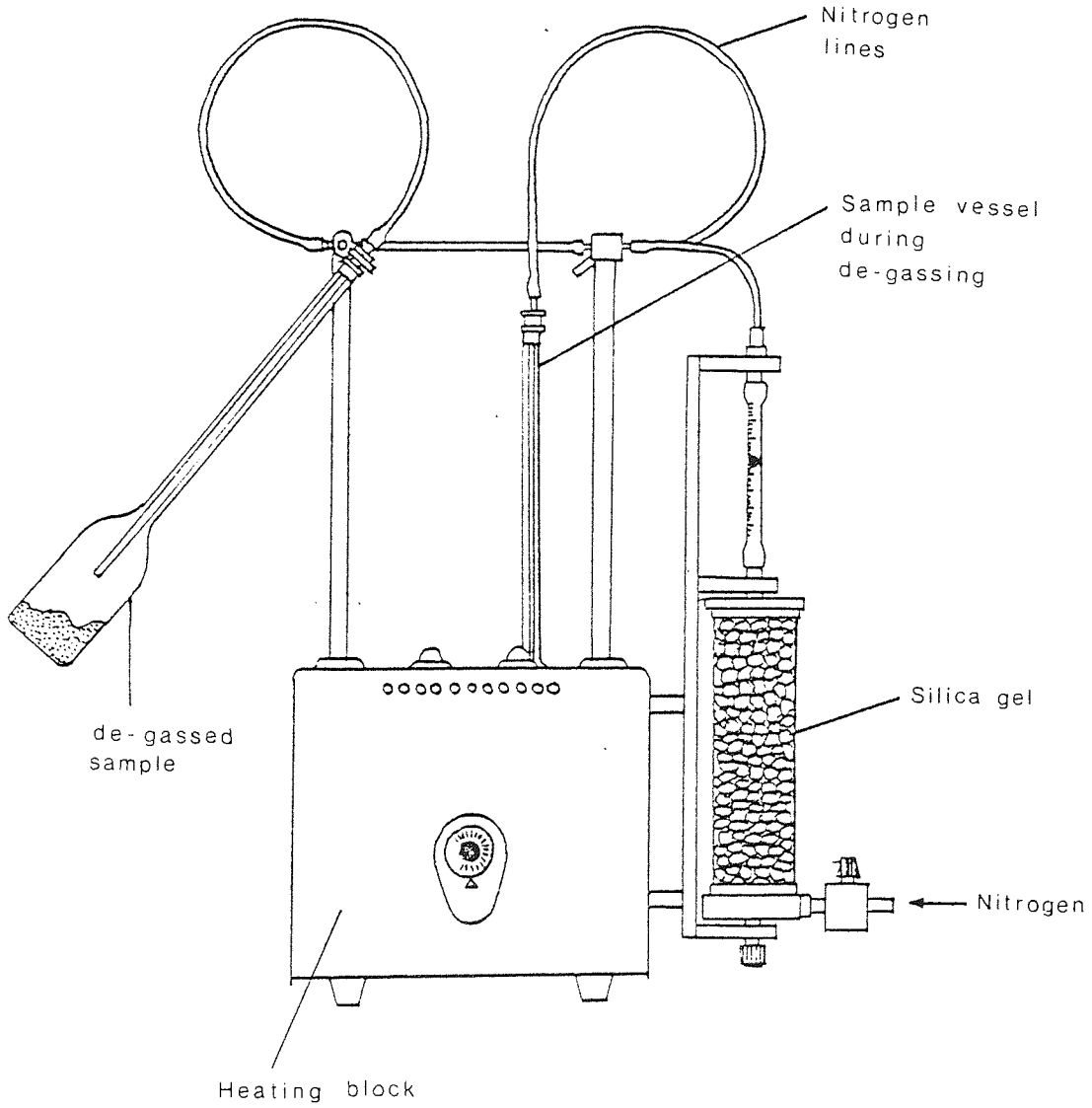

2.2.5 Mercury Intrusion Porosimetry

Mercury intrusion porosimetry was used to determine the pore volume distributions, interparticle porosities, pore size distributions, pore shapes, and accessible surface areas (defined later) of the lactose spherulites.

In mercury porosimetry, intruding fluid enters all open pores in a sample up to a limiting diameter governed by the size of the

Figure 19 Schematic representation of Strohlein Areameter measuring apparatus.

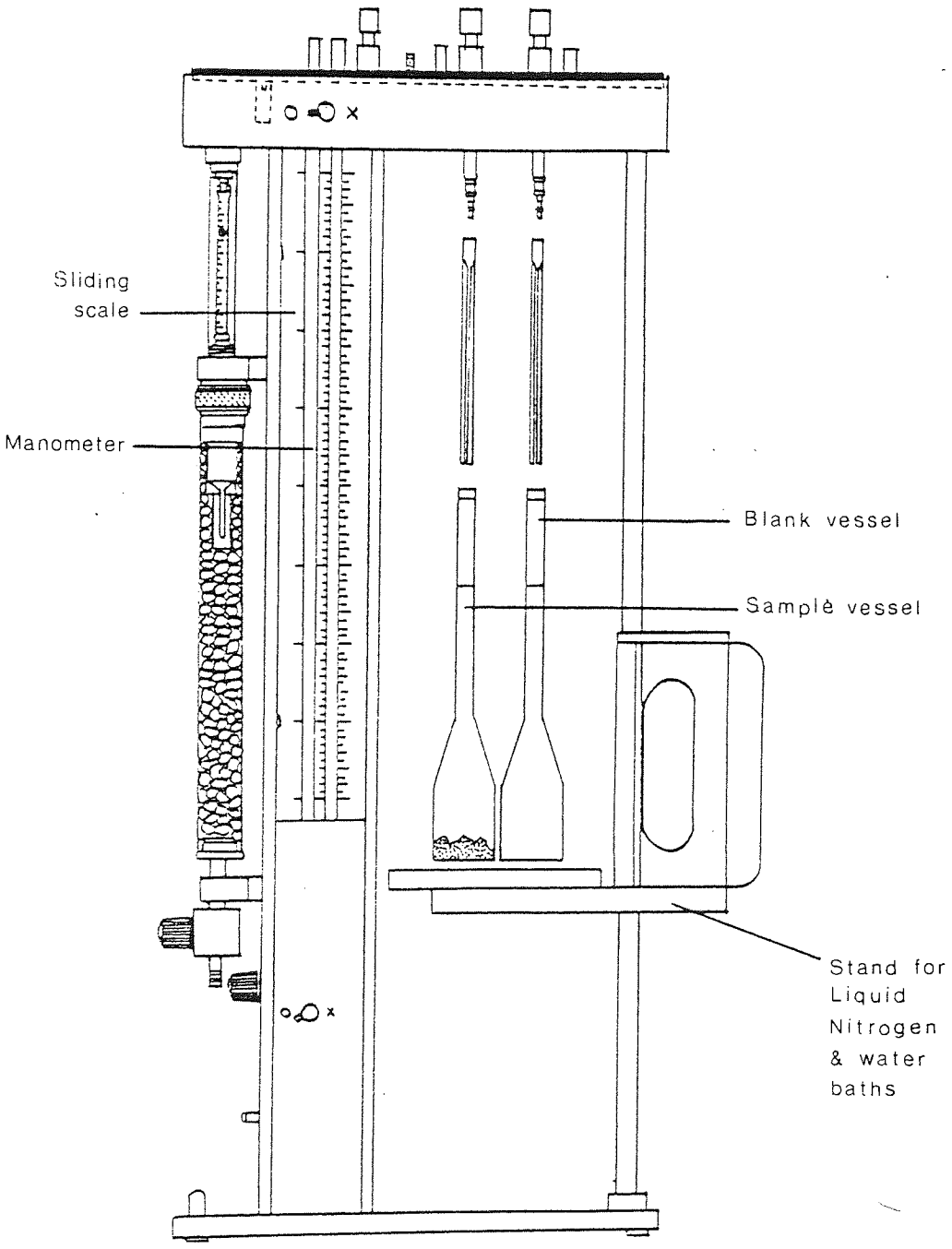

mercury molecule, the surface tension of mercury and the applied pressure. Mercury enters a pore when the applied pressure is large enough to overcome the surface tension (474 dyne.cm^{-1} at 25^{o}C).

Above zero pressure (absolute vacuum) pores are filled sequentially up to the maximum applied pressure. In the Coulter Model 910 series mercury penetration porosimeter (Micromeritics Instrument Corp., Norcross, U.S.A.), applied pressures could be varied between 1 and 50,000 psia (6895 N.m^{-2} to 3.4 x 10^{8} N.m^{-2}). This pressure range was capable of filling voids and pores with radii between 1.76 nm and 88.6 µm. Approximately 2 g of dry sample was accurately weighed and introduced around the gallery of the sample cell (Figure 20) which was then sealed and clipped to the head unit of the measuring apparatus (Figure 21). The head unit carried a fixed electrical contact which dipped into the cup on the top of the sample cell (Figure 20). It also carried a moveable contact (probe) that followed the mercury meniscus down the constant bore tube as pressure forced mercury into the sample voids and pores. The extent of this movement was monitored electrically and displayed as a digital readout related to the penetration volume of mercury.

At each chosen pressure the digital readout was noted and the pressure further increased until no more pores were filled. In the samples of lactose analysed, the maximum applied pressures were between 16,000 and 30,000 psia (1.1 x 10^{8} N.m^{-2} to 2.1 x 10^{8} N.m^{-2}) depending on the sample. Hysteresis analysis was carried out to examine the shape of the pores; when the maximum pressure was reached, the digital readout was set to zero and as pressure was released from around the sample, the probe followed the rising mercury level as fluid flowed from the pores and voids back into

Figure 20 Base Unit (a) and top unit (b) for holding powder samples during mercury intrusion porosimetry determinations.

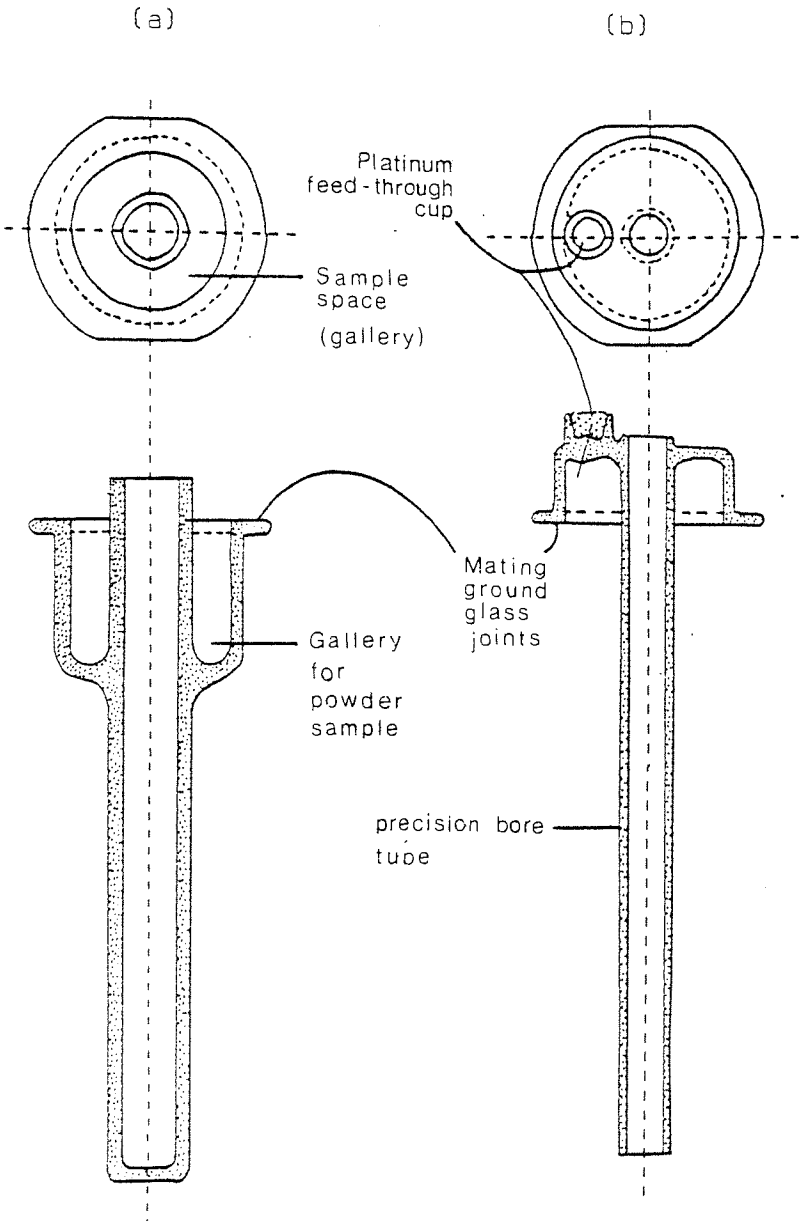

the tube. Discrepancies between the values for the pore volumes at set pressures when applied pressure was increasing compared with the corresponding values determined when pressure was decreasing were used to give approximate pore shapes in the lactose spherulites.

Figure 21 Schematic representation of mercury intrusion porosimeter.

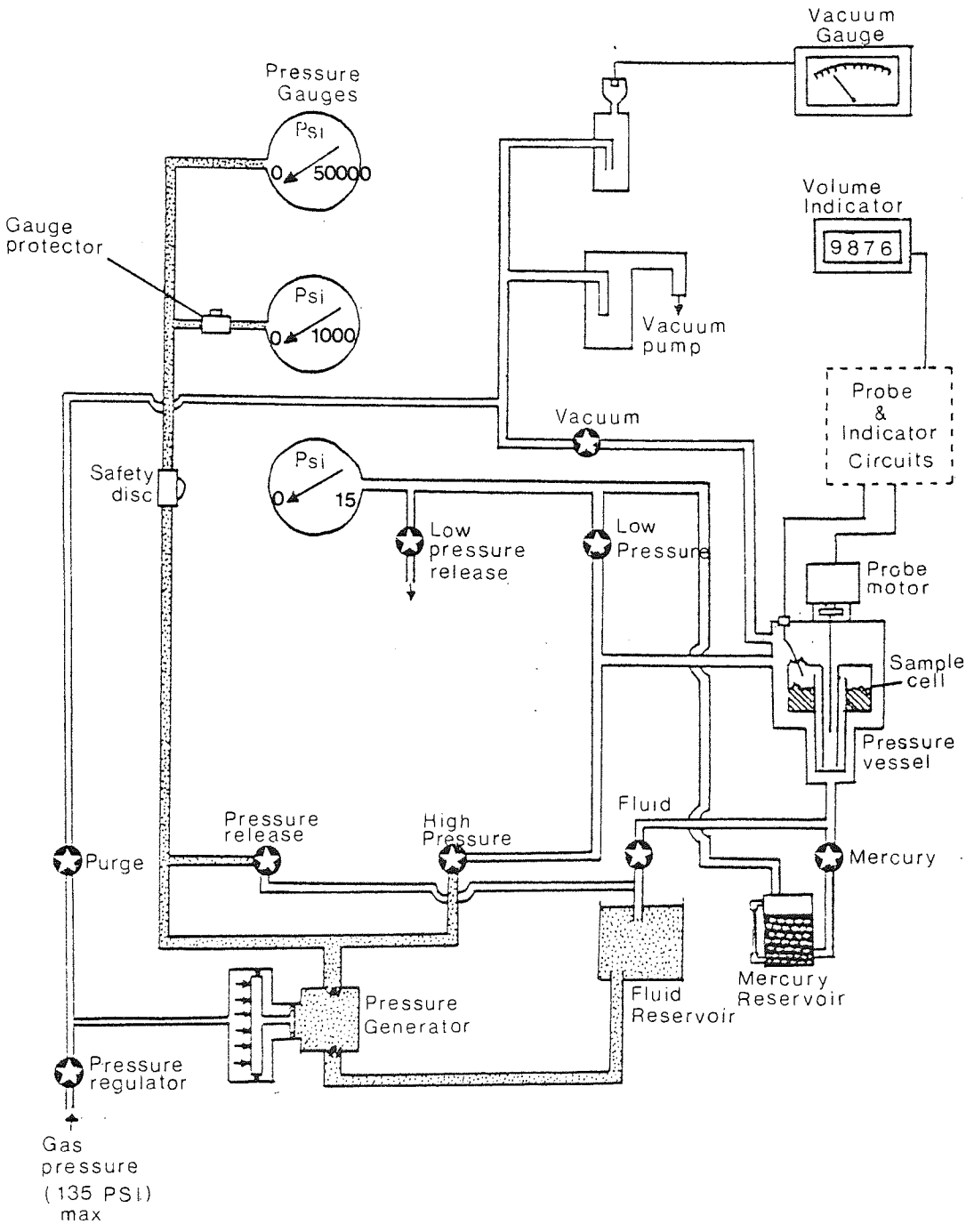

2.2.6 Scanning Electron Microscopy

Specimens were prepared for examination by scattering representative particles of lactose samples on to adhesive-covered aluminium stubs. The stubs were dried and coated with an electrically conducting material. The only coating found suitable to prevent sample charging under the electron beam was gold applied by the following sputter coating technique. The sample stub was placed under a gold plate electrode at a distance of about 5 cm. The area was evacuated and argon gas was introduced around the sample to act as an ion carrier. Ionisation of the gold was produced by applying a high voltage across the gold plate and the sample stub, causing gold ions to be deposited over the lactose surface. The prepared specimens were examined in a scanning electron microscope (Pye Stereoscan, Pye Unicam, Cambridge, U.K.). The incident electron beam produced back-scattered electrons and characteristic x-rays. Both of these beams could be collected and displayed on a video screen. The back-scattered electrons produced the usual electron photomicrographs. The scanning electron microscope was especially suitable for examination of the lactose spherulites because of the depth of focus achieved which was 300 times that of the light microscope. This allowed the whole particle to be in focus simultaneously.

2.3 Results for Characterisation of Lactose Crystals

The general appearance of the lactose crystals prepared by different methods was similar - each set of crystals had a wide particle size range and the individual particles were agglomerates of several crystallites. The crystallites, usually dendritic crystals, radiated from the centre of each particle and the

agglomerate thus formed was described as a spherulite. Spherulites recovered from different crystallisation solutions were composed of crystallites with different dimensions arranged in different patterns. The constitution of spherulites recovered from different crystallisation solutions governed many of the physical properties of the lactose powders.

2.3.1 X-ray Powder Diffraction

X-ray powder diffraction plots were produced for samples of the lactose spherulites. The output varied between samples at different Bragg angles (θ_B). This was probably caused by unequal quantities of crystallites in the sample spherulites. All the samples, including the original material, had similar d_B spacings at different Bragg angles, from which it was concluded that although the external habit of the spherulites and crystals changed on recrystallisation, the internal arrangement of the crystal lattice remained the same . All the recrystallised lactose powders prepared by different methods and the original lactose powder used as the starting material, were all composed of particles of stable α-lactose monohydrate.

2.3.2 Particle Size Analysis

The particle size distributions of the spherulites recrystallised as Lots A and B were found to be similar irrespective of crystallisation conditions. This was largely due to the final agglomerate breakdown process using a 1000 μm wire-mesh sieve, which gave all of the lactose powders a similar size distribution. However, the high concentrations of IMS in the mother liquor, above 60% $^{w}/_{w}$, were found to produce an increased quantity of fine particles. Lot C was separated into different particle size ranges before further characterisation.

2.3.3 Flow and Packing Properties

2.3.3.1 Flow Rate

The flow rates of different particle size fractions of lactose spherulites from Lot C are given in Table 3. At particle sizes

Table 3. Flow rates of different particle size fractions of lactose spherulites in lot C from a tableting hopper.

Particle size distribution, μm	Flow rate, $g.s^{-1}$
< 45	N/A
45 - 90	N/A
90 - 250	N/A
250 - 500	36·67
500 - 710	52·44
710 - 1000	83·05

below 250 μm powder flowed when the shutter was removed but stopped almost immediately. The initial flow was probably caused by particles falling from a failure zone beneath a powder arch formed over the hopper exit. A cohesive powder arch prevented further powder flow in these fine powder fractions. At particle sizes above 250 μm, powder flowed uniformly from the hopper. Powder flow rate increased with increasing particle size.

2.3.3.2 Bulk Density

The poured densities of the recrystallised lactose fractions from Lot C were in the range 0.18 to 0.50 g ml^{-1} compared with a poured bulk density of 0.62 g ml^{-1} for the original lactose powder.

The consolidated bulk densities of the lactose spherulites were in the range 0.28 to 0.64 g ml^{-1}, whereas the original lactose powder had a consolidated density of 0.96 g ml^{-1} (Table 4). The poured and consolidated bulk densities of the recrystallised lactose powders were smaller than the original lactose powder and this reduction was probably caused by differences in particle shape and size. The larger dendritic recrystallised lactose spherulites were unable to pack as closely as the finer original lactose powder. Both the poured and consolidated densities showed a tendency to increase with increasing crystal growth time. An increased consolidated bulk density would be advantageous in tableting operations because the volume of die-fill would be correspondingly reduced; an improved flow rate could well combine with this effect to maintain good weight uniformity and content uniformity of the compressed tablets. The lighter powders of low bulk densities had a lower consolidating strength in hoppers and were less likely to form strong powder arches or bridges, nevertheless they may have a high inertia at rest which can produce flooding from a hopper. The heavier lactose powders of higher bulk densities, such as those produced after 60 minutes crystallisation time from 40% to 70% IMS solution and 90 minutes from 50, 60, 80 and 90% IMS solutions, are likely to be more easily consolidated and possess better flow properties. The marked differences in bulk densities (both poured and consolidated) which were seen between powders recovered after short crystallisation times and those grown for longer periods indicated alterations in packing geometries attributable to particle shape differences. This will be discussed in more detail in section 2.3.6.

Table 4

Poured and consolidated bulk densities of lactose spherulites crystallised under different conditions (Lots A and B)

Lactose sample (percent IMS in mother liquor and crystallisation time)	Poured (fluff) bulk density (D_o) g ml^{-1}	Consolidated (Equilibrium) bulk density (D_e) g ml^{-1}
40% IMS 5 mins	0.26	0.37
40% IMS 15 mins	0.24	0.37
40% IMS 30 mins	0.39	0.50
40% IMS 60 mins	0.50	0.64
40% IMS 90 mins	0.38	0.51
50% IMS 5 mins	0.32	0.46
50% IMS 15 mins	0.30	0.42
50% IMS 30 mins	0.30	0.45
50% IMS 60 mins	0.41	0.53
50% IMS 90 mins	0.42	0.53
60% IMS 5 mins	0.27	0.37
60% IMS 15 mins	0.30	0.40
60% IMS 30 mins	0.30	0.42
60% IMS 60 mins	0.37	0.50
60% IMS 90 mins	0.40	0.53
70% IMS 5 mins	0.18	0.28
70% IMS 15 mins	0.21	0.28
70% IMS 30 mins	0.20	0.33
70% IMS 60 mins	0.27	0.41
70% IMS 90 mins	0.25	0.38
80% IMS 5 mins	0.31	0.44
80% IMS 15 mins	0.29	0.44
80% IMS 30 mins	0.25	0.40
80% IMS 60 mins	0.30	0.47
80% IMS 90 mins	0.31	0.51
90% IMS 5 mins	0.28	0.43
90% IMS 15 mins	0.33	0.52
90% IMS 30 mins	0.37	0.61
90% IMS 60 mins	0.35	0.56
90% IMS 90 mins	0.38	0.58
BDH Lactose Original Material	0.62	0.96

2.3.3.3 The Hausner Ratio

Hausner found that the ratio D_e/D_o was a measure of interparticle friction and as such could be used to predict powder flow properties (215). Hausner showed that powders with low interparticle friction, such as spheres, had ratios of approximately 1.2. The high Hausner ratio of the original lactose powder (Fig. 22) was probably due to the high interparticle cohesion

Figure 22 Relationship between the Hausner ratio and the IMS concentration of the solution from which the lactose spherulites in lots A and B were recovered.

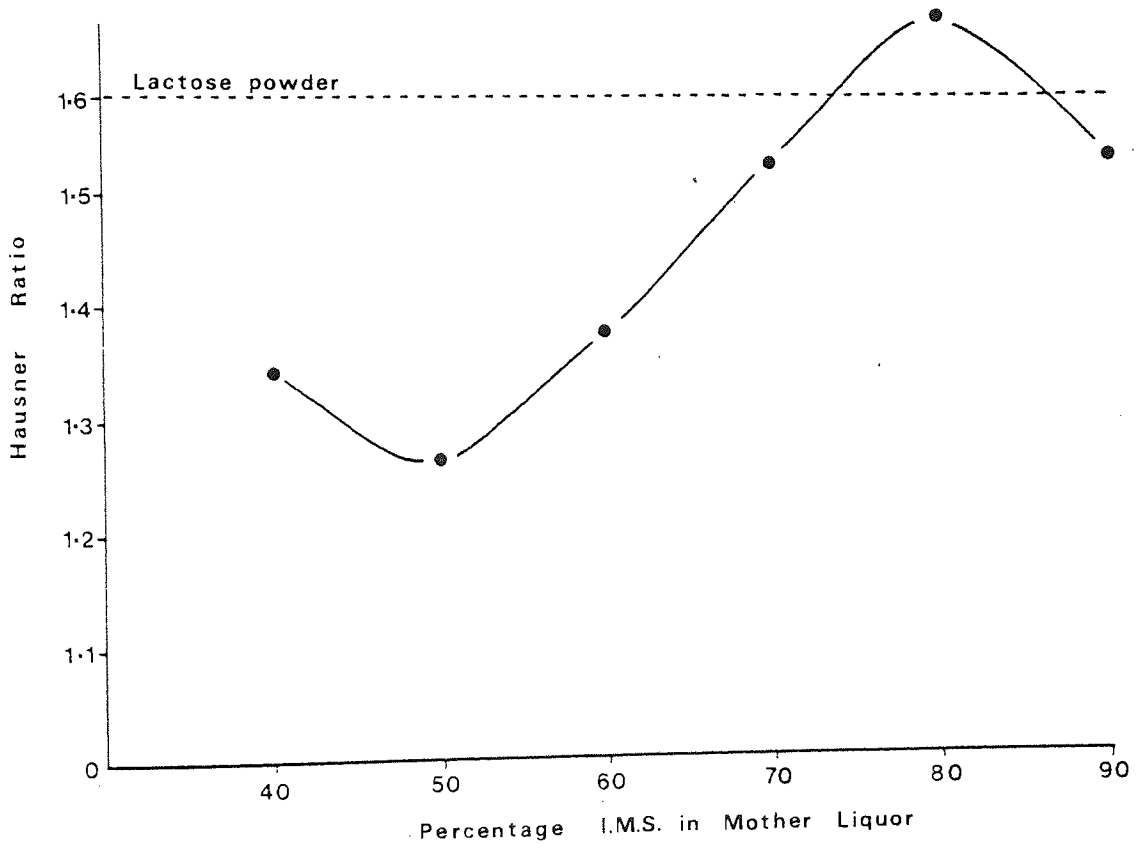

associated with low particle size; in contrast the differences in ratios of lactose spherulites recovered from different crystallising solutions was caused by other surface properties such as shape

and roughness. The Hausner ratios increased with increasing IMS concentration in the lactose mother liquor, to a maximum of 1.7 in spherulites recrystallised from 80% IMS solution. High ratios of this order were associated with high interparticle friction such as that produced between thin powder flakes (215).

2.3.3.4 Percentage Compressibility

The percentage compressibility of a powder is a useful indirect method of measuring powder flow. It is a direct measure of the potential powder arch or bridge strength and stability. Table 5 shows the generalised relationship between descriptions of powder flow and Carr's compressibility values:

Table 5

Relationship between powder flow and percentage compressibility, according to Carr (214)

Percent Compressibility Range	Description of probable flow conditions
5 - 15	Excellent (free-flowing granules)
12 - 16	Good (free-flowing powdered granules)
18 - 21	Fair (powdered granules)
23 - 28	Poor (very fluid powders)
28 - 35	Poor (fluid cohesive powders)
33 - 38	Very poor (fluid cohesive powders)
>40	Extremely poor (cohesive powders)

A comparison of the values in Table 5 with the results in Fig. 23 for lactose spherulites from Lot C show that the fine original lactose powder had very poor flow properties. The recrystallised lactose powders also had poor flow properties, the

Figure 23 Relationship between the Percent Compressibility and the IMS concentration of the solution from which the lactose spherulites in lots A and B were recovered.

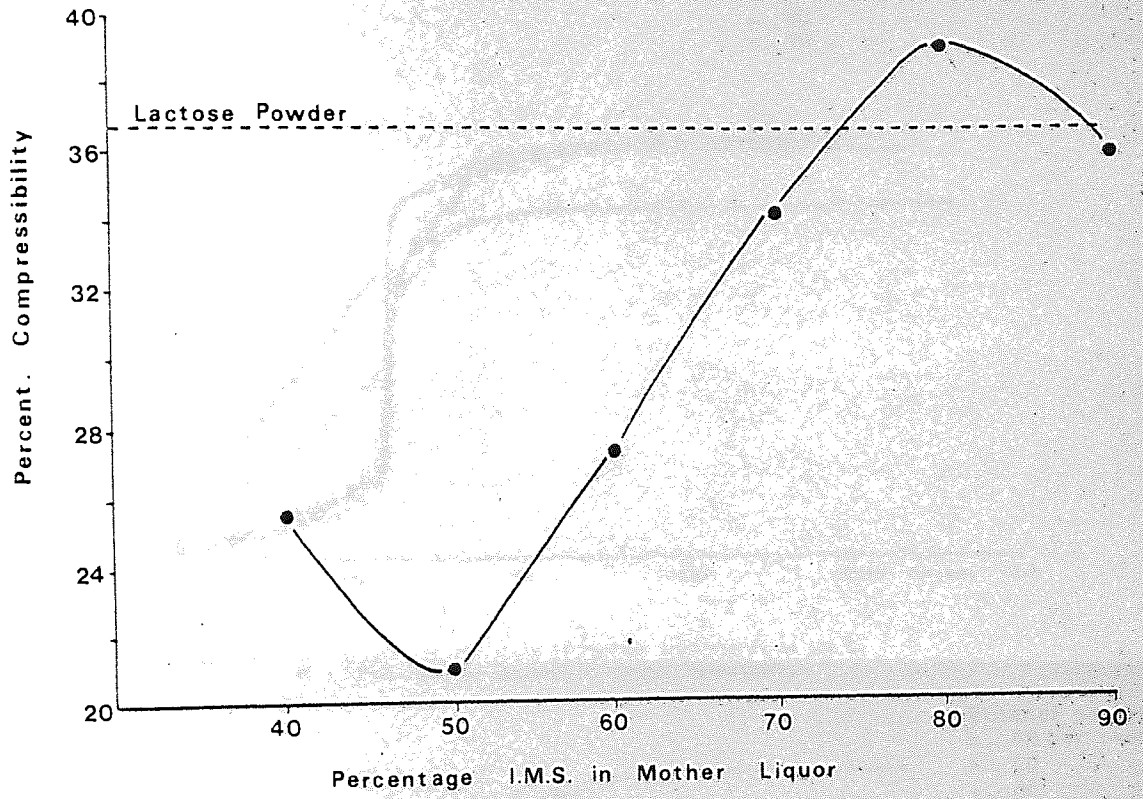

percent compressibility reached a maximum in spherulites recrystallised from 80% IMS. The general curve followed that of the Hausner ratio, as would be expected.

2.3.4 Powder Porosity

2.3.4.1 Total Porosity (Penetration Volume)

Unless the powders measured are extremely porous, the measured powder porosity is, in effect, the volume of voids (interparticle pores) in a powder bed and is representative of its packing geometry.

Pore volumes of spherulites collected after 90 minutes from solutions containing different ethanol concentrations (Lot C) were compared in the same particle size range (Figures 24 to 29). In

Figure 24 Pore volume distributions of lactose spherulites in lot C, < 45 µm diameter obtained by mercury porosimetry.

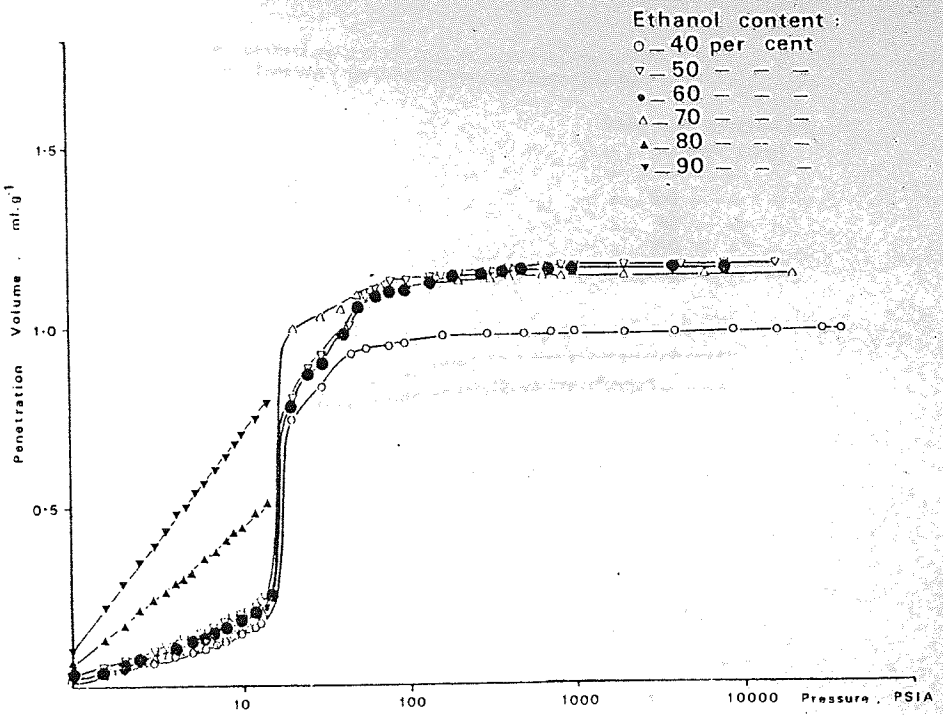

Figure 25 Pore volume distributions of lactose spherulites in lot C, 45 - 90 µm diameter obtained by mercury porosimetry.

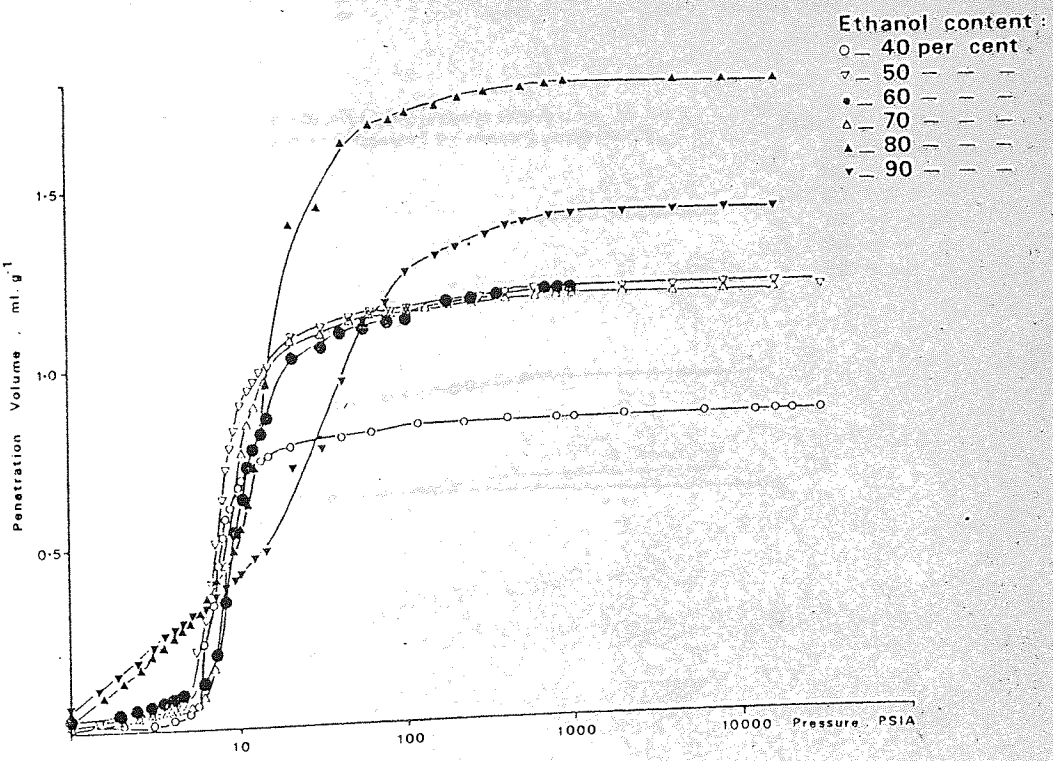

Figure 26 Pore volume distributions of lactose spherulites in lot C, 90 - 250 μm diameter obtained by mercury porosimetry.

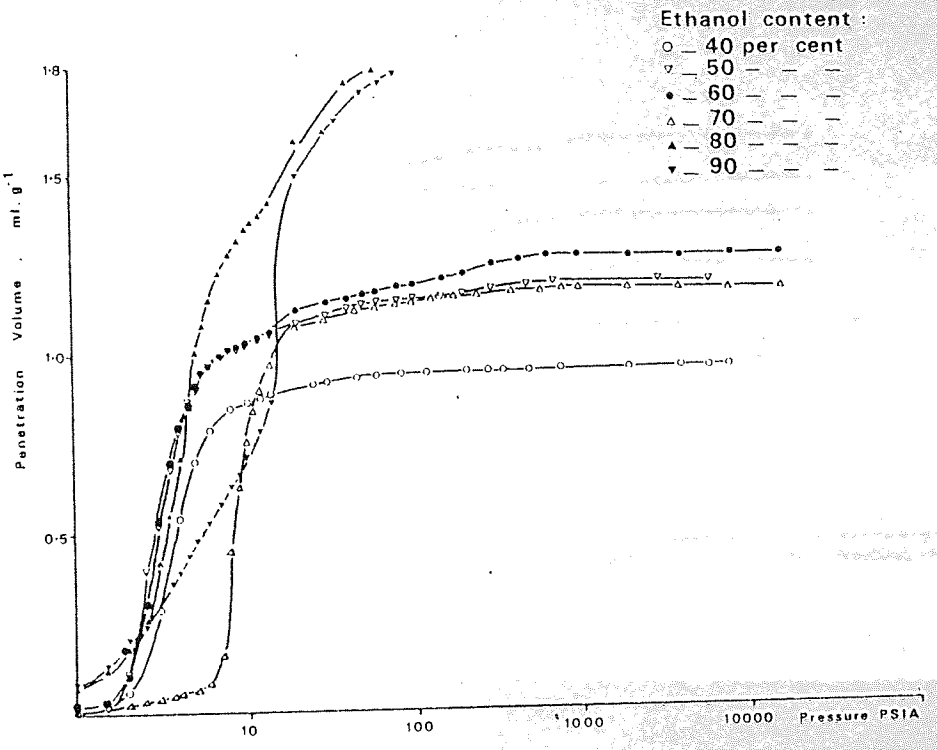

Figure 27. Pore volume distributions of lactose spherulites in lot C, 250 - 500 μm diameter obtained by mercury porosimetry.

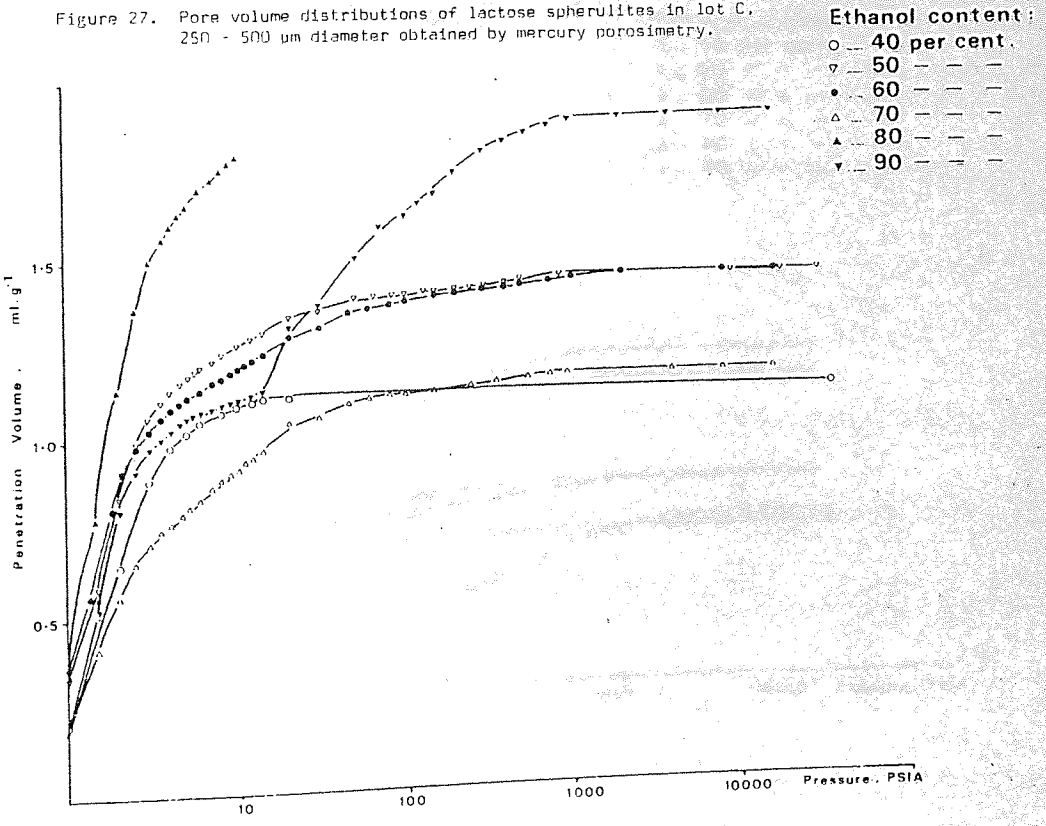

Figure 28 Pore volume distributions of lactose spherulites in lot C 500 - 710 µm diameter obtained by mercury porosimetry.

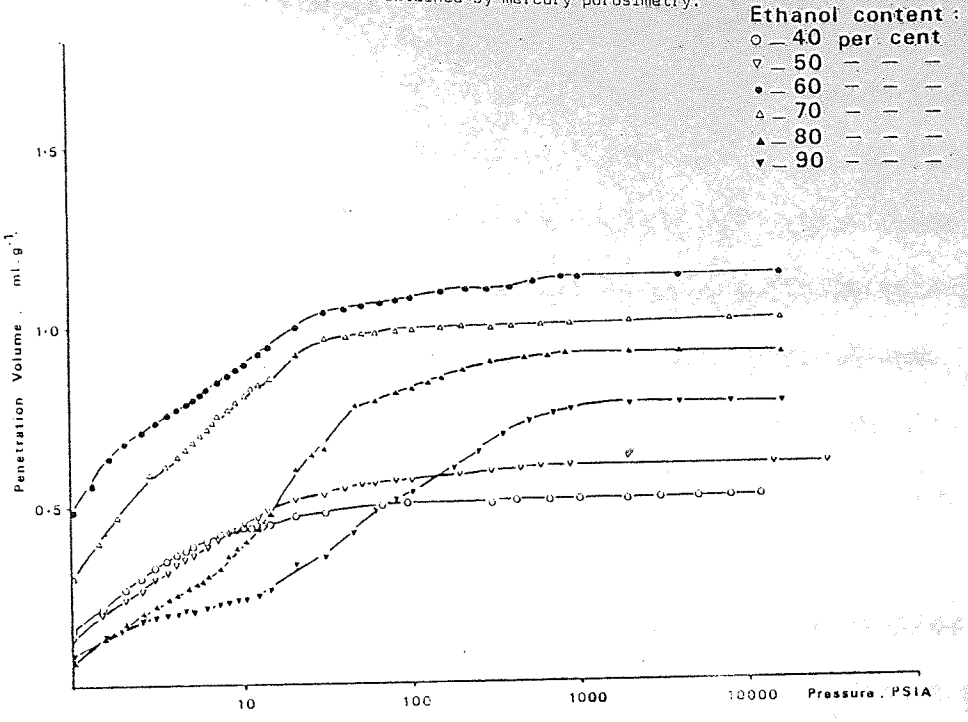

Figure 29 Pore volume distributions of lactose spherulites in lot C, 710 - 1000 µm diameter obtained by mercury porosimetry.

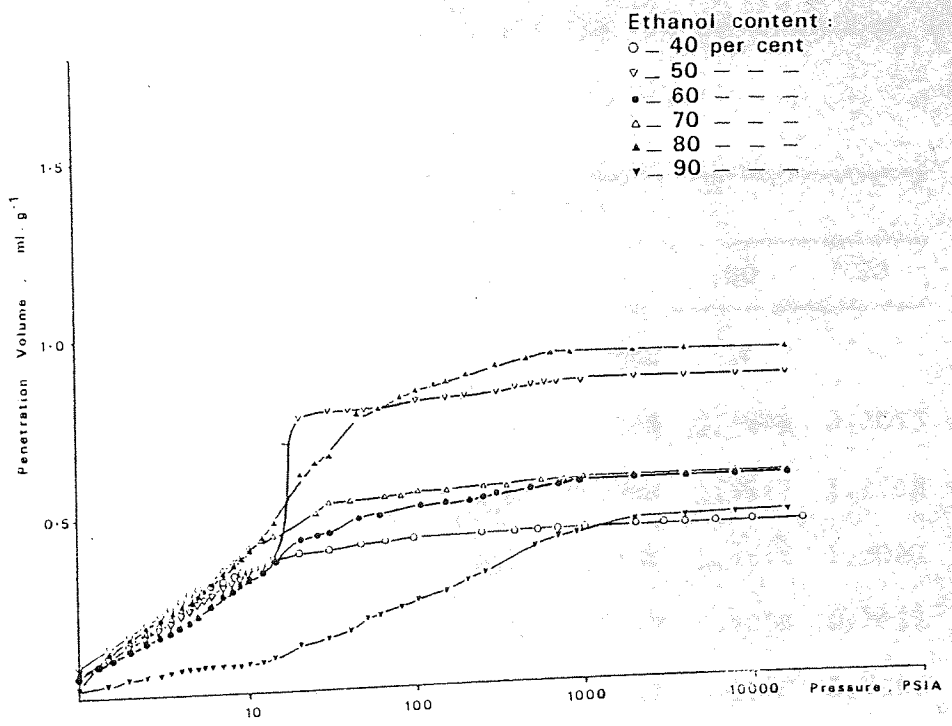

each particle size range, the spherulites containing pores of the largest volume were those recrystallised from 80% ethanol solution, an exception being the 500 - 710 µm particle size fraction (Figure 28). The spherulites with the lowest pore volumes were those recrystallised from 40% ethanol solutions (except in Figure 29). The spherulites from the 50, 60, 70 and 90% ethanol solutions lay within these two extremes. The increase in pore volumes up to a particle size of 250 and 500 µm was due to a rising interparticle void volume. Above this particle size range, the void volume became too large to be measured by porosimetry and the penetration volume was mainly due to intraparticle pores.

In order to calculate the total intraparticle porosities of the spherulites in each size fraction (Table 6), a correction was applied to remove the void contribution to pore volume.

Table 6

Relationship between total intraparticle specific pore volume (ml/g) of spherulites in various particle size fractions and the IMS concentration in the mother liquor

Particle Size Distribution	IMS Concentration (%)					
	40	50	60	70	80	90
<45 µm	0.0673	0.1043	0.1358	0.1054	-	-
45 - 90 µm	0.0593	0.1213	0.1882	0.1078	0.2848	0.7053
90 - 250 µm	0.4290	0.4986	0.5020	0.7934	1.3872	1.8588
250 - 500 µm	0.4807	0.9341	0.8967	0.7836	1.4518	1.3080
500 - 710 µm	0.5257	0.6227	1.1582	1.0279	0.9314	0.7952
710 - 1000 µm	0.4391	0.8583	0.5729	0.5746	0.8292	0.4651

The intraparticle porosity was calculated as the volume of pores (ml) per gram of powder using mercury porosimetry penetration volumes. The maximum intraparticle porosities were reached in the high particle size ranges recrystallised from solutions with IMS concentrations less than 80%. The maximum porosities for particles recovered from 80 and 90% IMS were found in the lower particle size ranges of 90 - 500 µm, possibly because particle growth occurred more quickly than dendrite coarsening in the faster-growing small crystals (Section 2.2.2.5.1). The maximum porosities in spherulites recovered from different lactose solutions tended to increase with increasing IMS concentration.

2.3.4.2 Pore Size Distributions

Corrected intraparticle pore size distributions were calculated by plotting the small increase in pore volume (dP_V) as a percentage of the total pore volume against the corresponding pore size. This allowed determination of the maximum pore diameters and identification of the samples with the largest pore volume at a specific pore diameter. These values varied with the particle size distributions as well as the IMS concentration in the solution from which the lactose spherulites were recrystallised (Figures 30 to 35).

The maximum pore diameters of particles less than 45 µm diameter (Fig. 30 a, b) occurred between 1 and 2 µm. The pore size with the greatest pore volume varied from about 2 µm for spherulites recrystallised from 50 and 70% ethanol solutions, to 1 µm for those recovered from 40 and 60% solutions. The maximum pore diameters increased with increasing particle size. The percentage volume contribution of pores with different diameters to the total pore volume decreased with decreasing pore diameter. In particles with

Figure 30(a) Pore size distributions of lactose spherulites < 45 μm diameter obtained by mercury porosimetry.

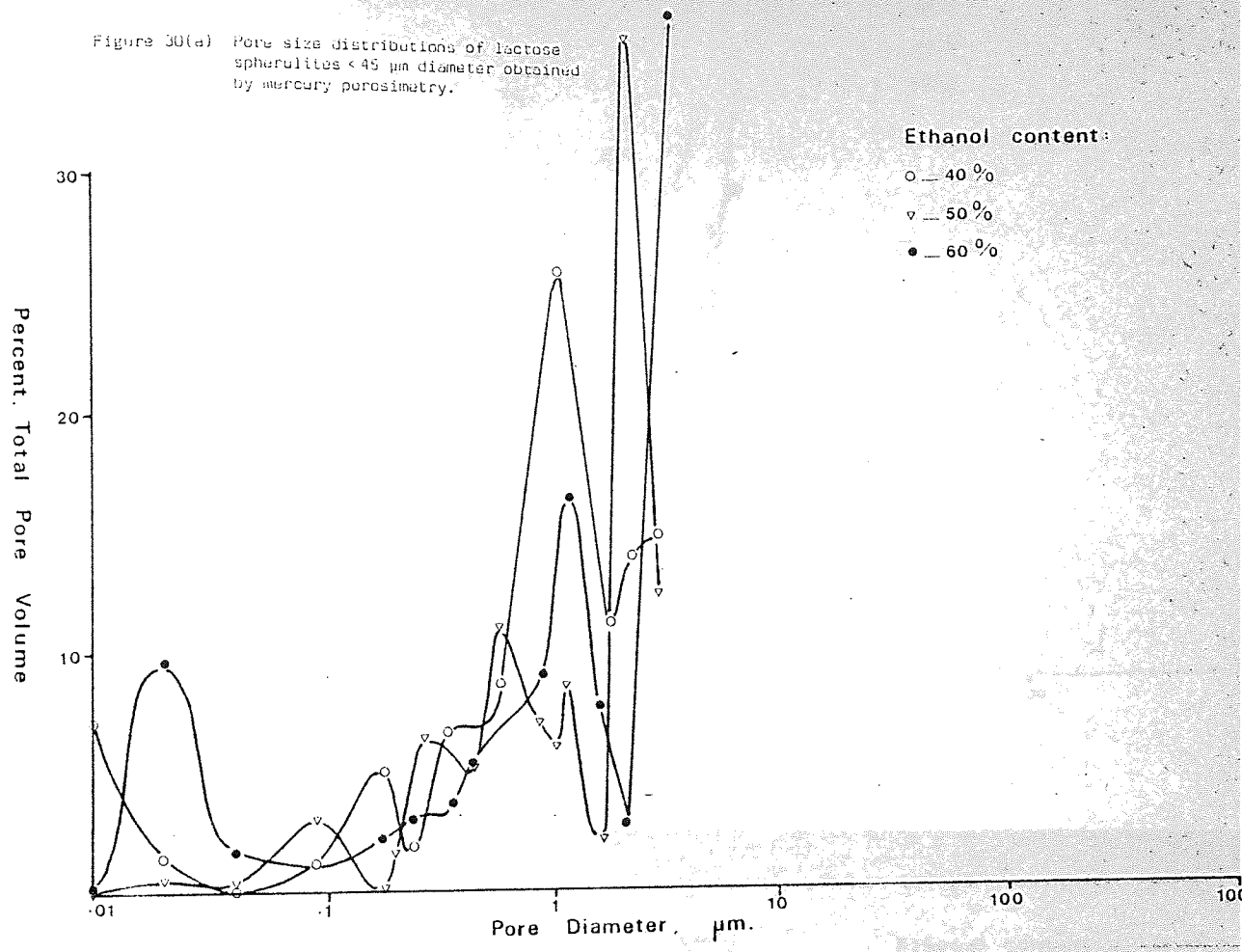

Figure 30(b) Pore size distributions of lactose spherulites < [illegible] μm obtained by mercury porosimetry.

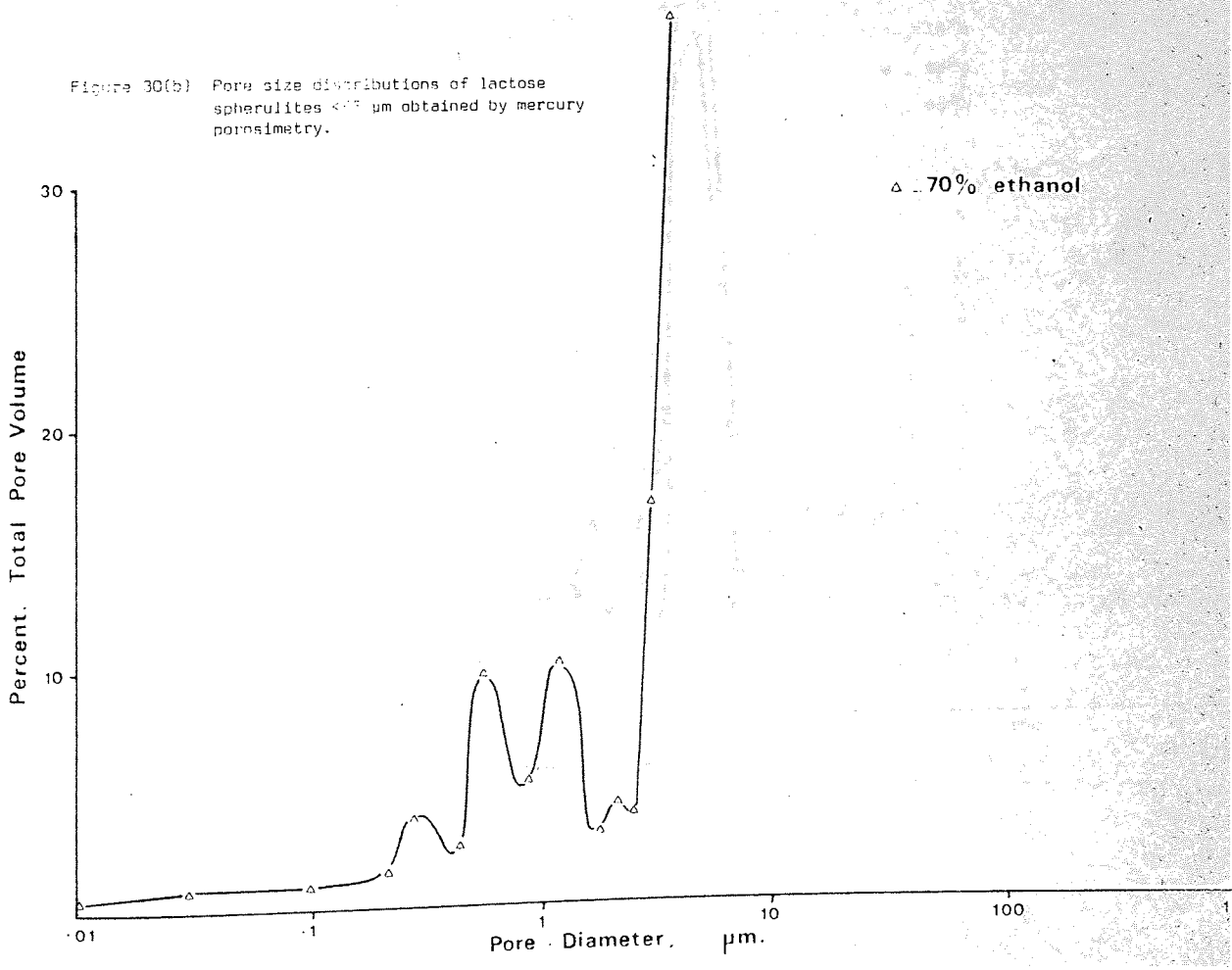

Figure 31(a) Pore size distributions of lactose spherulites 45 - 90 µm diameter obtained by mercury porosimetry

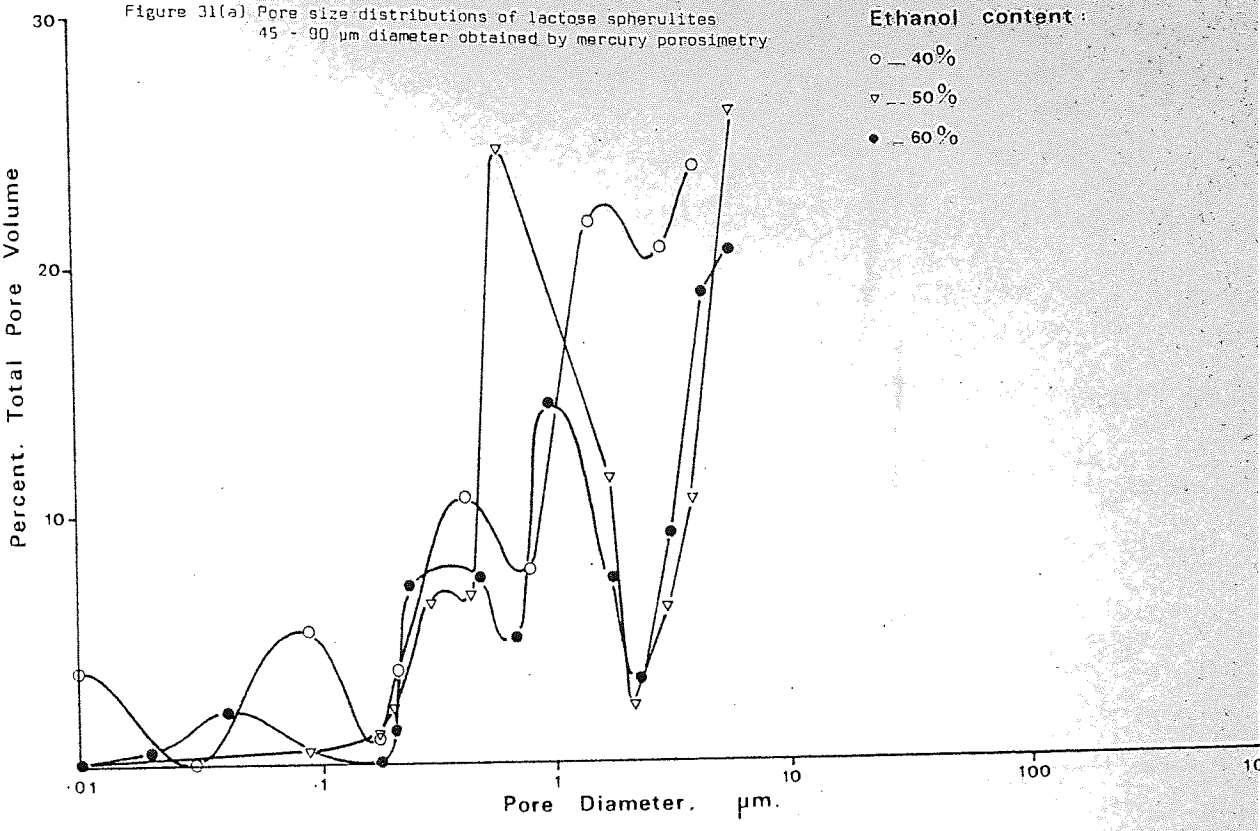

Figure 31(b) Pore size distributions of lactose spherulites 45 - 90 µm diameter obtained by mercury porosimetry

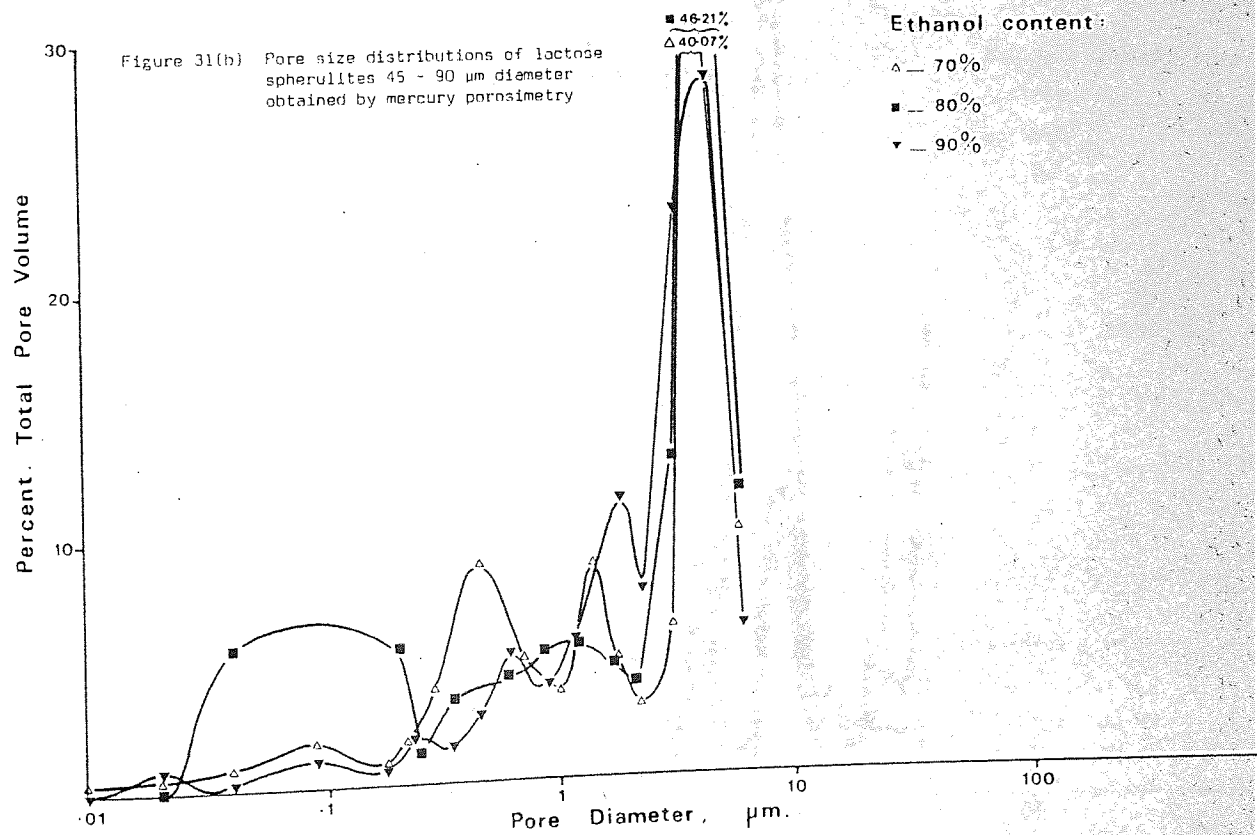

Figure 32(a) Pore size distributions of lactose spherulites 90 - 250 um diameter obtained by mercury porosimetry.

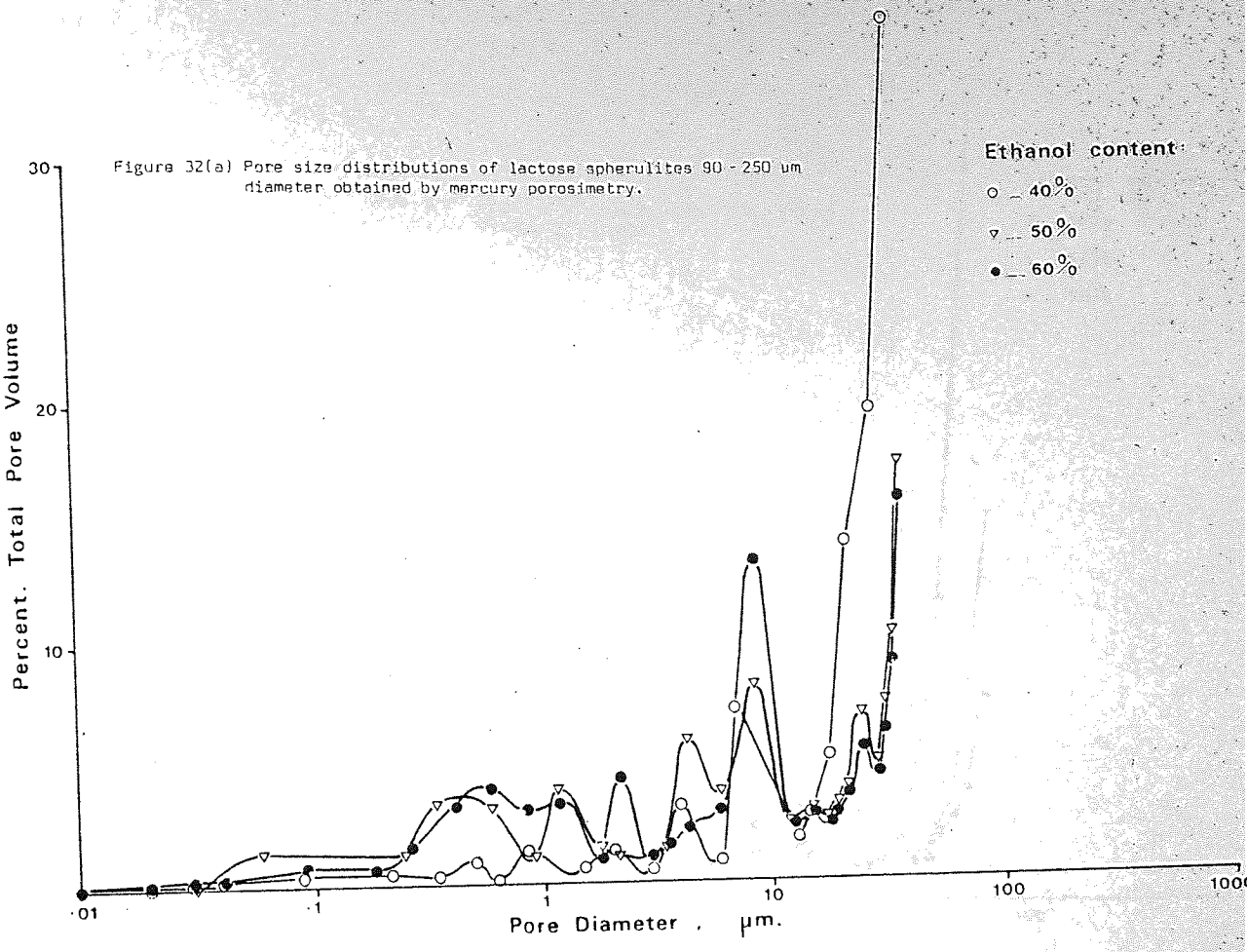

Figure 32(b) Pore size distributions of lactose spherulites 90 - 250 um diameter obtained by mercury porosimetry

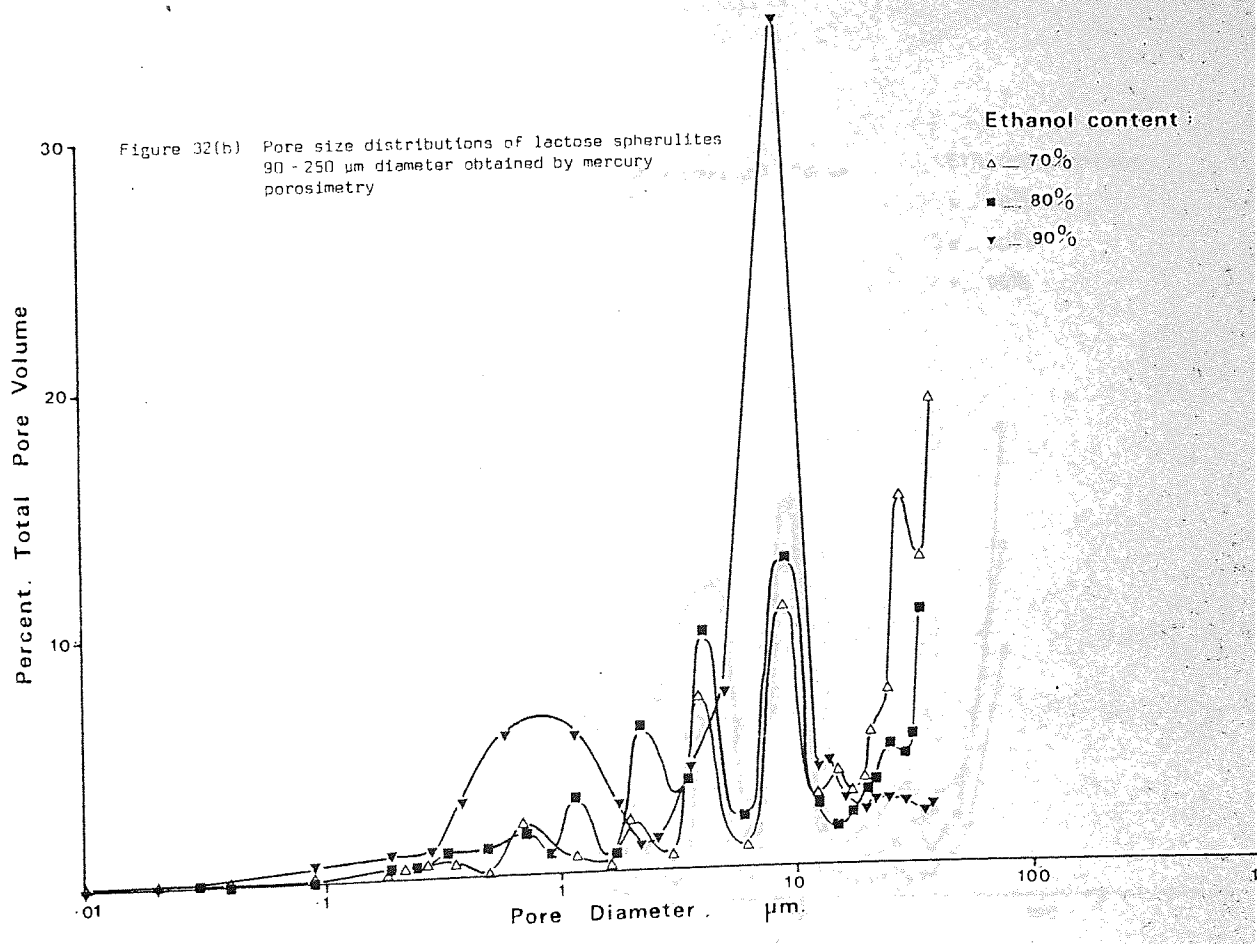

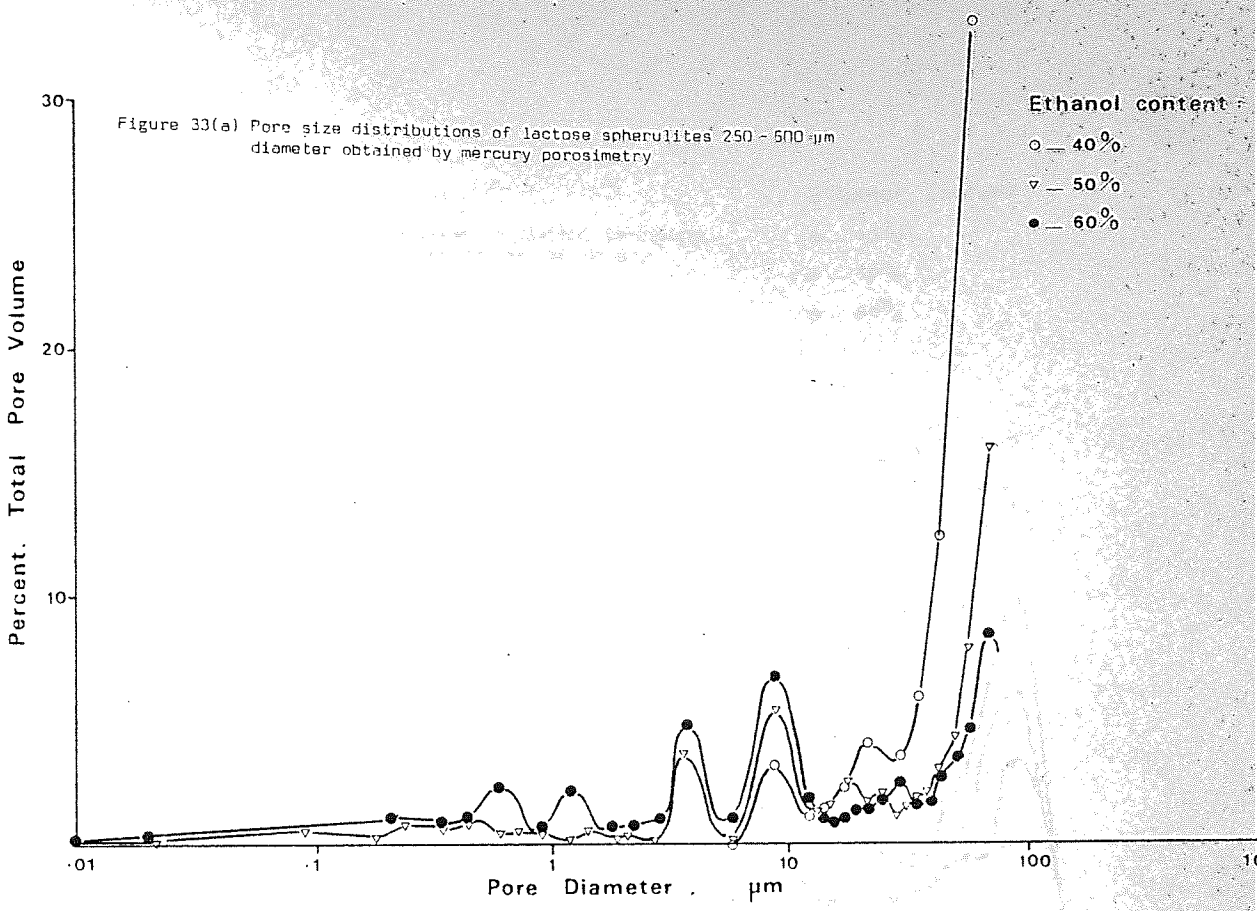

Figure 33(a) Pore size distributions of lactose spherulites 250 - 500 µm diameter obtained by mercury porosimetry

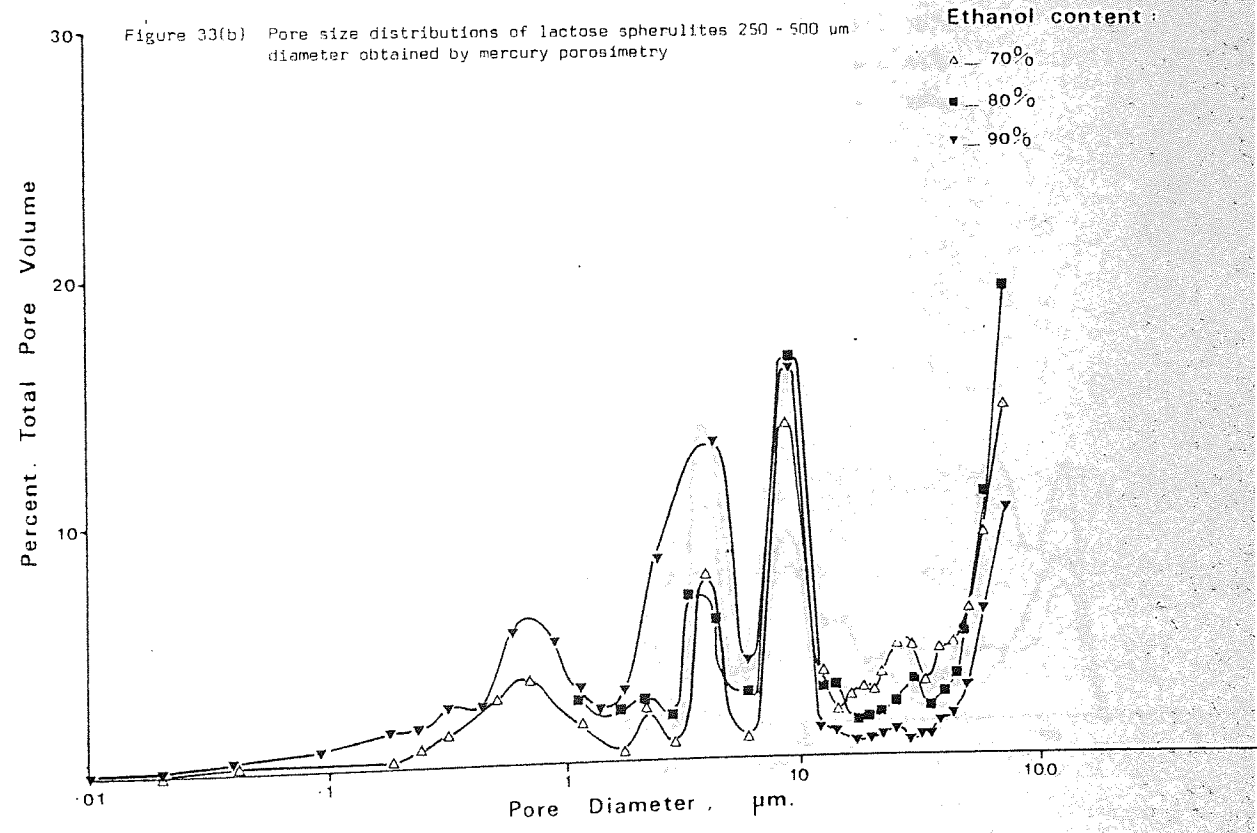

Figure 33(b) Pore size distributions of lactose spherulites 250 - 500 µm diameter obtained by mercury porosimetry

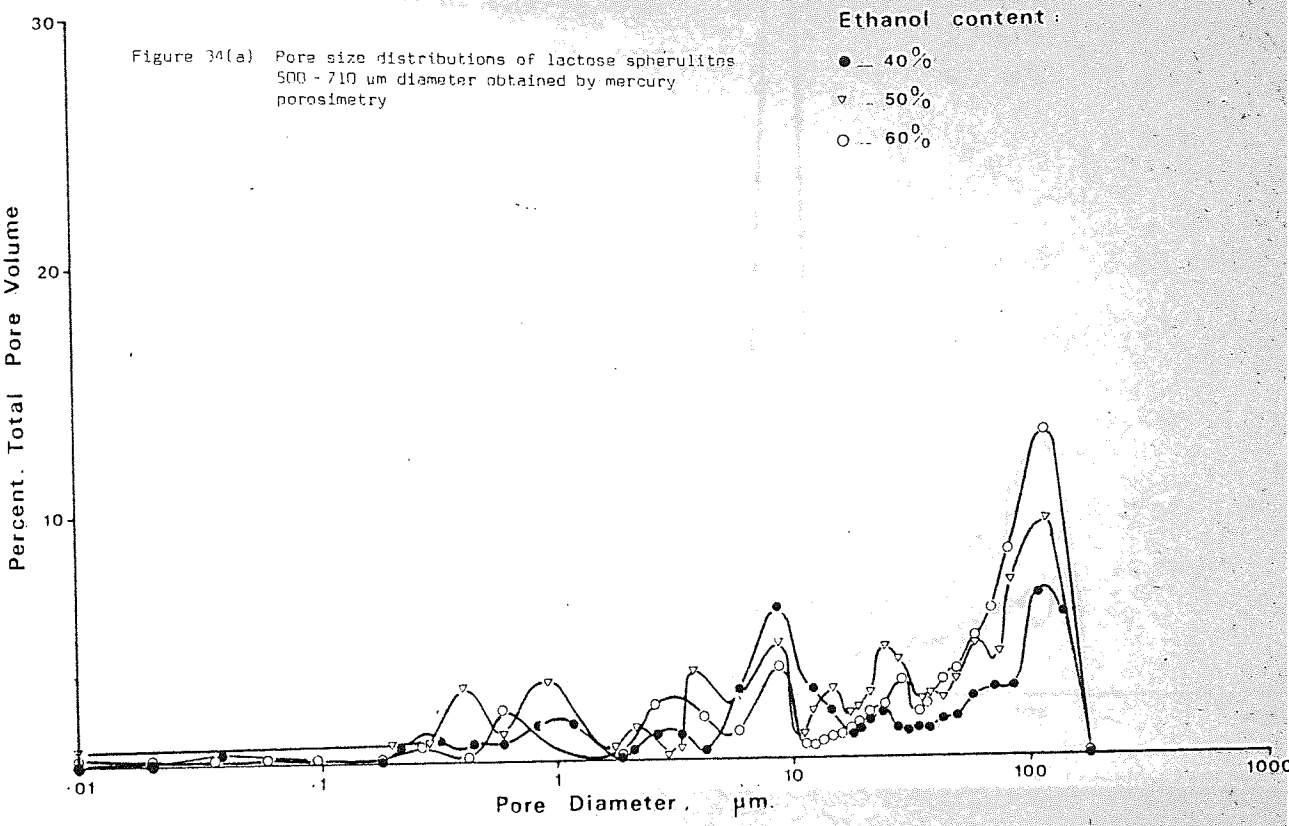

Figure 34(a) Pore size distributions of lactose spherulites 500 - 710 µm diameter obtained by mercury porosimetry

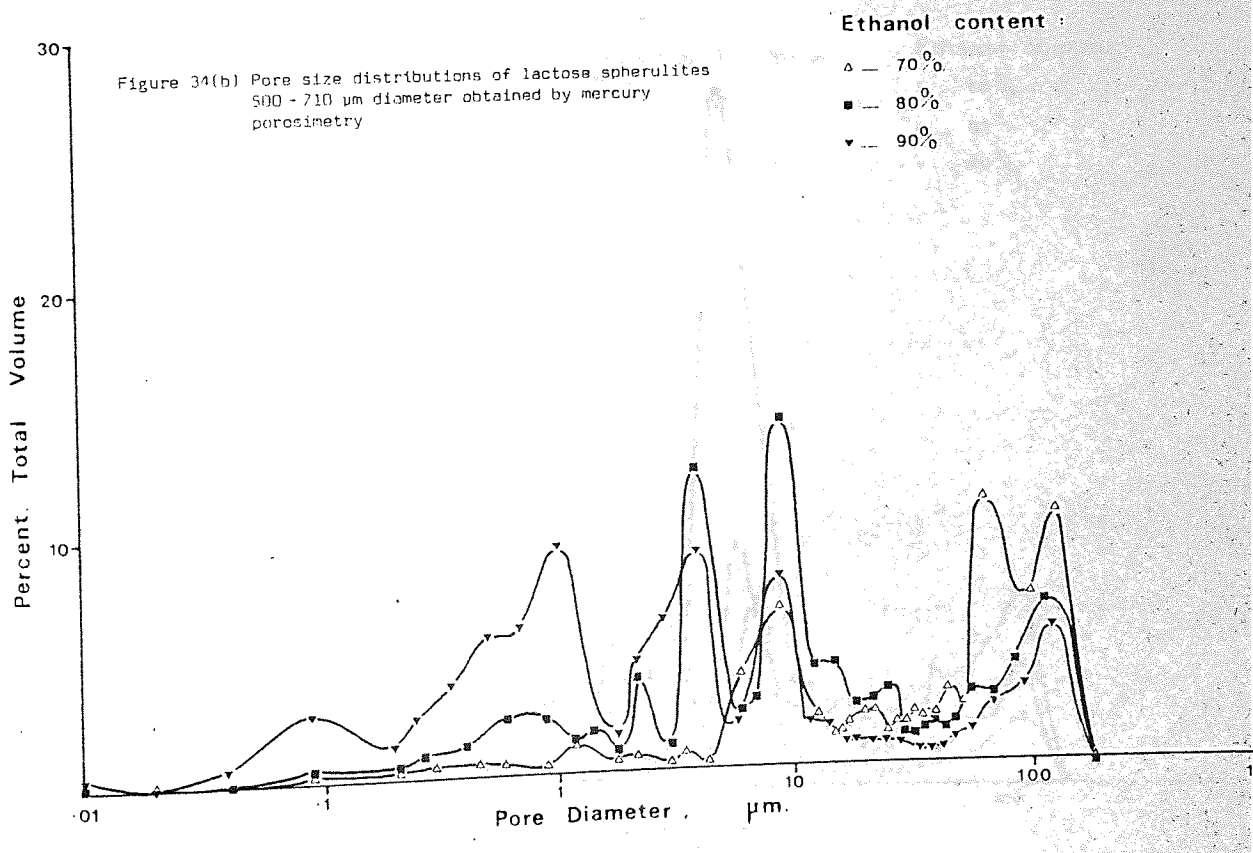

Figure 34(b) Pore size distributions of lactose spherulites 500 - 710 µm diameter obtained by mercury porosimetry

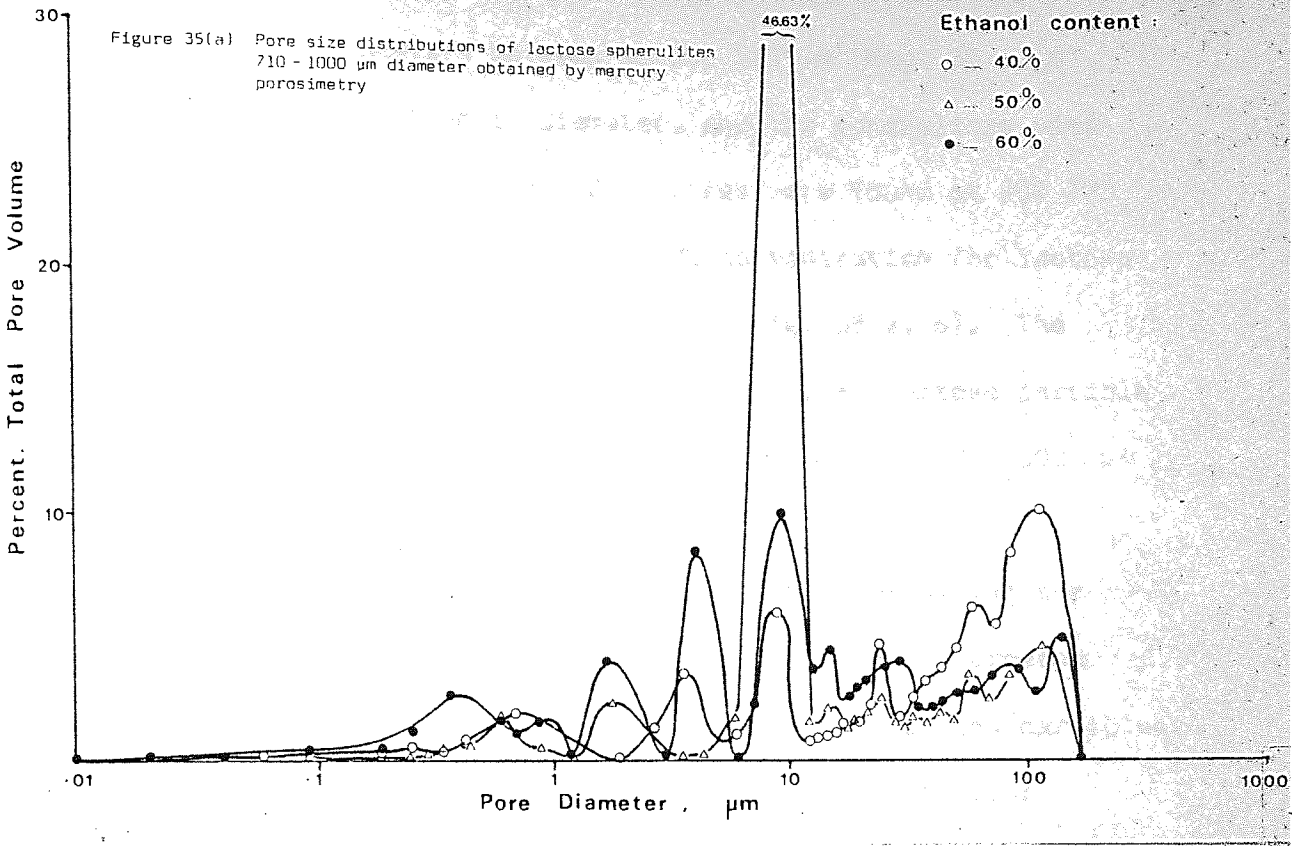
Figure 35(a) Pore size distributions of lactose spherulites 710 - 1000 µm diameter obtained by mercury porosimetry
46.63%
Ethanol content :
○ — 40%
△ — 50%
● — 60%
Percent. Total Pore Volume
30
20
10
·01
·1
1
10
100
1000
Pore Diameter , µm

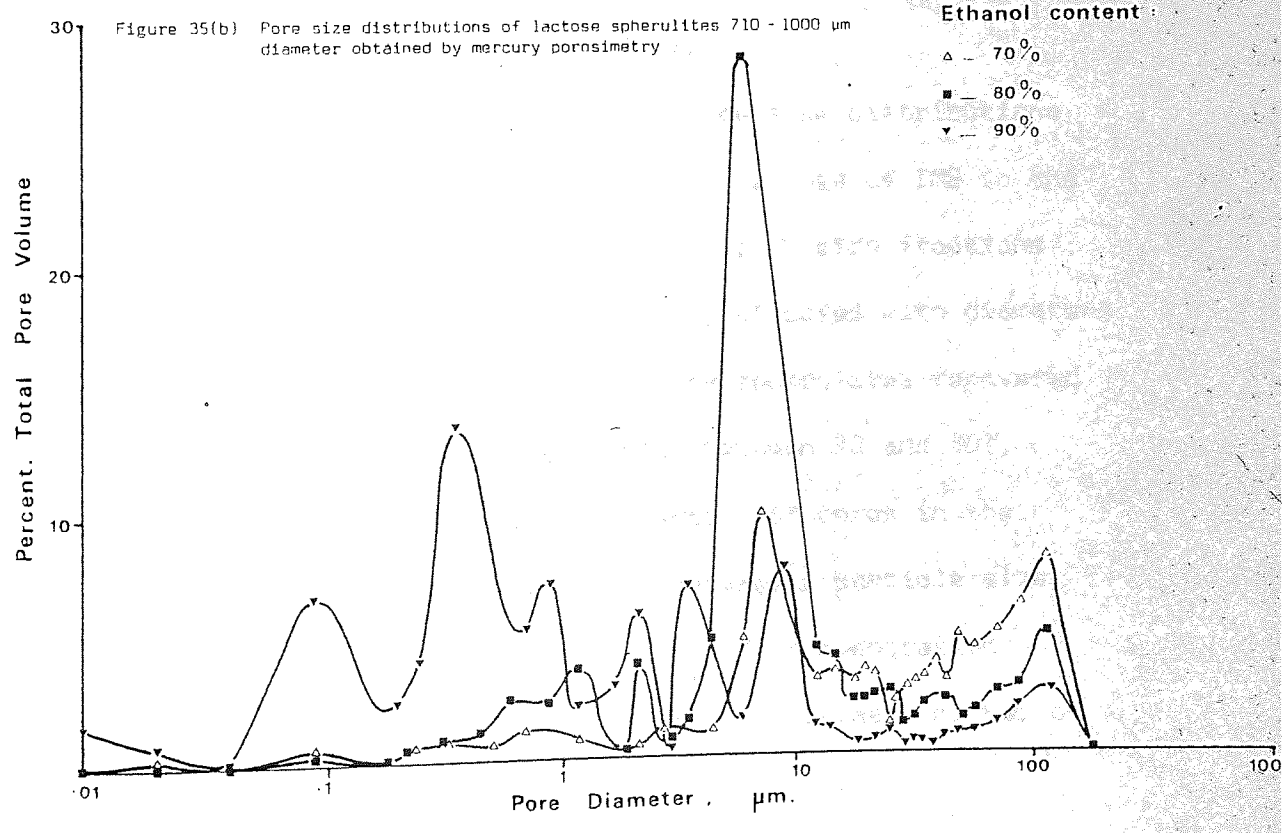
Figure 35(b) Pore size distributions of lactose spherulites 710 - 1000 µm diameter obtained by mercury porosimetry
Ethanol content :
△ — 70%
■ — 80%
▼ — 90%
Percent. Total Pore Volume
30
20
10
·01
·1
1
10
100
Pore Diameter , µm.

diameters between 45 and 90 µm (Fig. 31 a, b) the highest pore volume at any pore size occurred at pore diameters around 5 µm. In particles with diameters between 90 and 250 µm (Fig. 32 a, b), most pores were about 10 µm in diameter, and the spherulites with the largest percentage volume of 10 µm pores were found at 90% IMS concentration. This decreased to 80% IMS concentration for lactose spherulites of particle sizes 250 - 500 µm (Fig. 33 a, b). The maximum percentage pore volume decreased further at lactose particle size distributions of 500 - 710 µm (Fig. 34 a, b) and 710 - 1000 µm (Fig. 35 a, b).

The pores which would be of most interest in assessing the ability of a powder to provide active adherence sites in ordered mixes are those with dimensions large enough to entrap fine particles. Pore diameters in the range 10 - 100 µm will be of particular interest. A composite analysis of the effect of ethanol concentration in the solutions from which the lactose spherulites were recovered, was produced by measuring the area under the curves in Figures 30 to 35 in the pore size range 10 - 100 µm.

The areas under the curves of the pore size distributions were calculated and plotted against the percentage of IMS in the recrystallisation liquor for different particle size fractions (Figures 36 and 37). The largest quantity of pores with diameters between 10 and 100 µm was found in lactose spherulites recovered from solutions with an IMS concentration between 70 and 80%, irrespective of particle size. The quantity of pores in the desired diameter range increased with increasing particle size and the area distribution with respect to IMS concentration broadened at higher particle sizes due to an increased number of pores over the whole range of 10 to 100 µm.

Figure 36 The relationship between the concentration of IMS and the total volume of large pores 10 - 100 µm diameter in lactose spherulites of different particle size

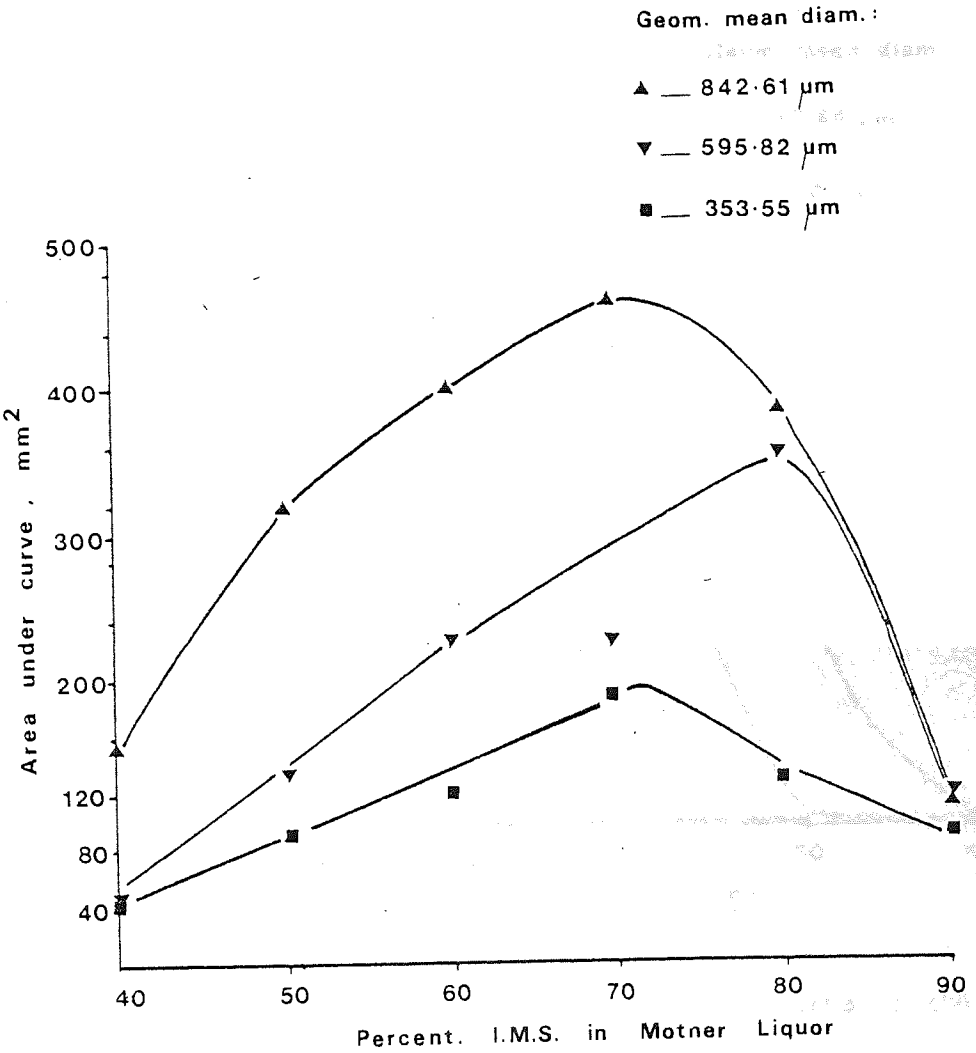

2.3.4.3 Pore Shape

The shape of pores can be determined from a hysteresis analysis of the mercury penetration data (Figure 38). If the mercury leaves the pores along the same pressure line as the penetration curve, the pores present no resistance to the mercury as it flows out of the pores. Pores which produce this type of hysteresis curve are probably wide-necked and V-shaped. The more

Figure 37 The relationship between the concentration of IMS and the total volume of large pores 10 - 100 µm diameter in lactose spherulites of different particle size

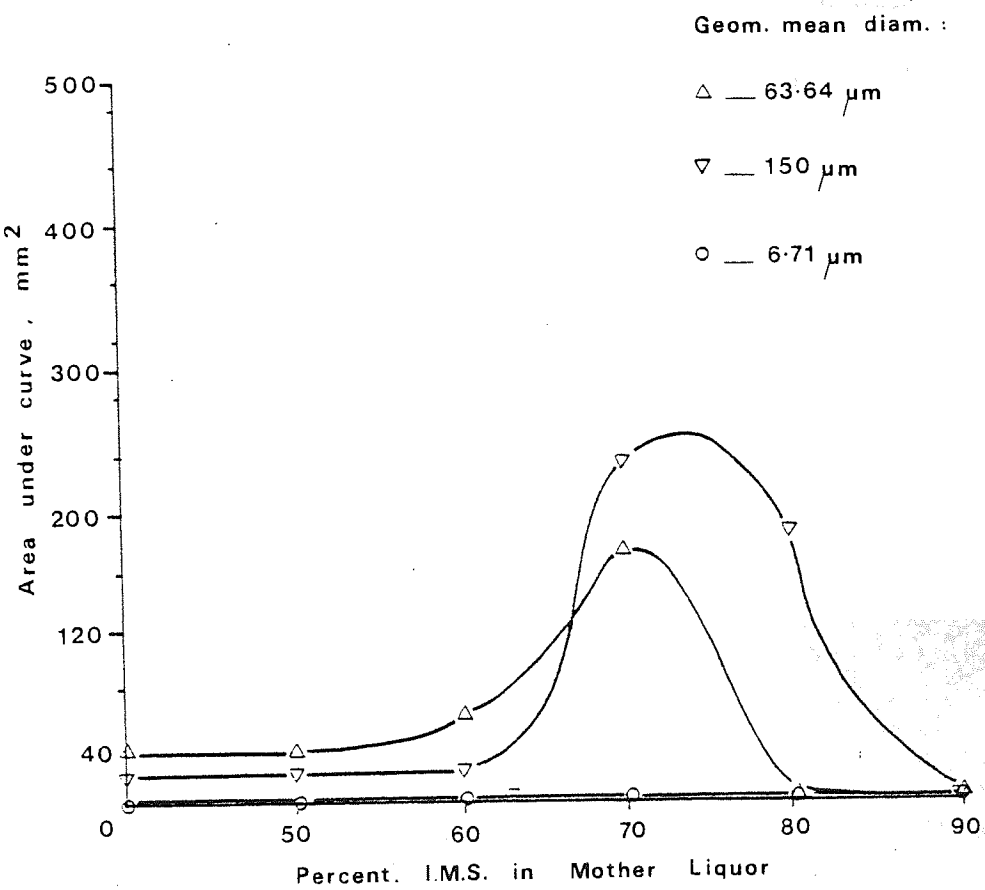

resistance the mercury encounters as it leaves pores as the pressure decreases, the wider the hysteresis curve becomes. A widely separated hysteresis curve indicates the presence of pores which are narrower at their entrance than at their base; these are described as "ink-bottle" shaped.

The lactose spherulites had pores with different shapes depending on the crystallisation conditions. Spherulites recrystallised from solutions of different ethanol concentration had pores with different shapes, but within a particle size range

Figure 38 Assessment of pore shape based on the area between the hysteresis curves of increasing and decreasing applied pressures in mercury intrusion porosimetry

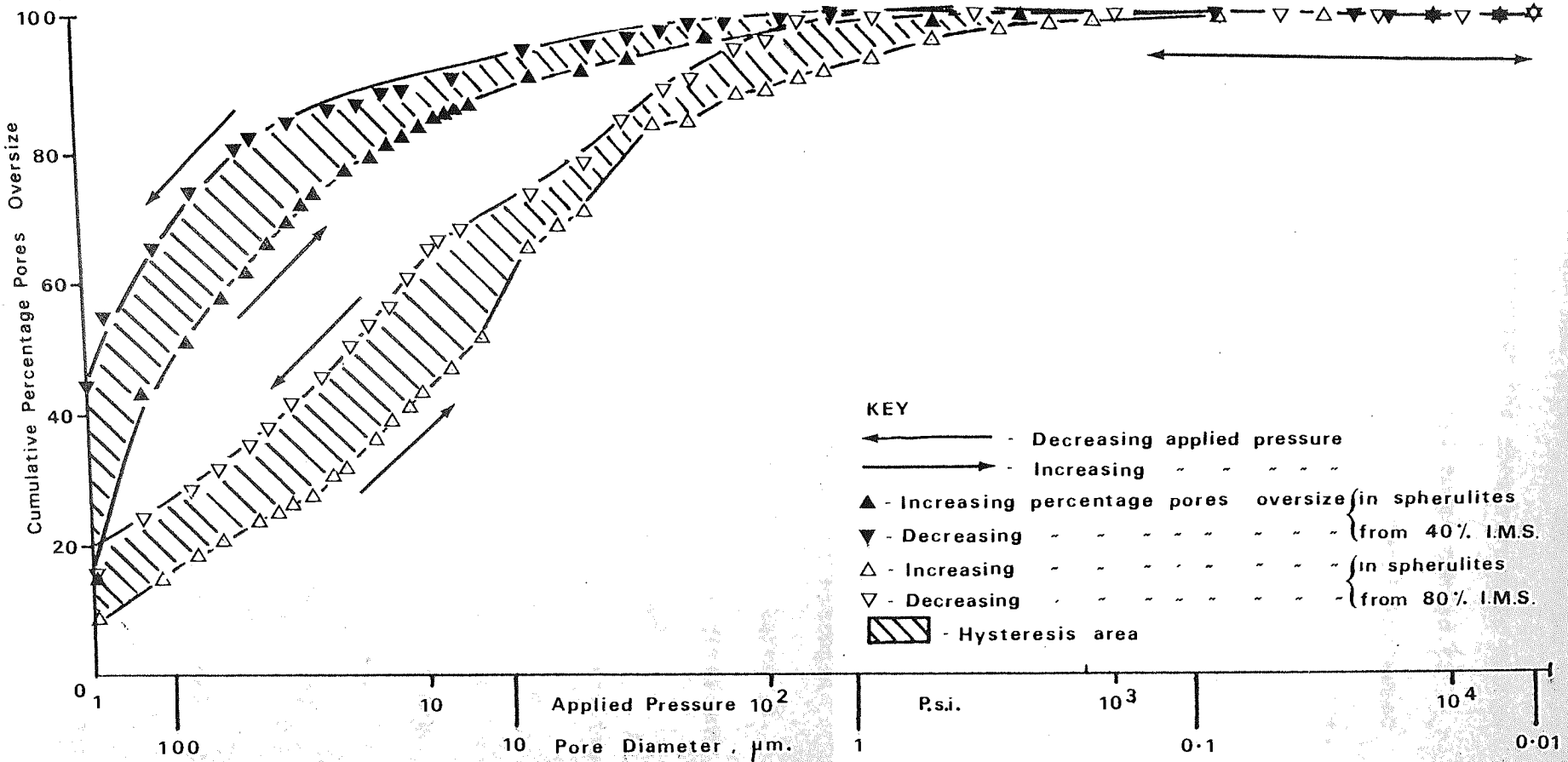

the pore shapes were similar. Lactose solutions containing 40% ethanol produced spherulites which had virtually open-ended capillary-shaped pores. At 50% IMS concentration the pore structure changed to open-ended wedge shapes. The wedge-shaped pores tended to become more wide-necked as the concentration of ethanol increased up to 80%. At 90% ethanol concentration the spherulites had pores which had bottle-necked entrances (ink-bottle pores).

The shapes of pores may be important in the formation of active adherence sites for an ordered mix. Wide necked, open-ended pores will be more likely to capture fine particles in a powder mix, than pores with narrower necks.

2.3.5 Surface area measurements

2.3.5.1 Nitrogen adsorption determinations

Surface area determinations were carried out by nitrogen adsorption using the Ströhlein Areameter (Ströhlein, W. Germany). The specific surface areas of spherulites recovered from different concentrations of ethanol in the lactose mother liquor were measured (Figure 39). The specific surface areas of the spherulites increased to a maximum at an ethanol concentration of 80%. The concentration of IMS in the lactose mother liquor affected the dimensions of their constituent dendrites. Spherulites which are composed of thin dendritic crystals will have a higher surface area than spherulites with large quantities of coarse dendrites.

Kahlweit (216) studied the ageing of dendritic crystals during the precipitation of ionic solutions. He found that the dendrite arms dissolved from their tips towards their roots. During this process, the dendrite radii remained virtually unaffected.

Figure 39. The relationship between specific surface area and ethanol content of the mother liquor from which the lactose crystals were recovered after 90 minutes crystallisation time. Ranges bounded by dotted lines represent 95% confidence limits.

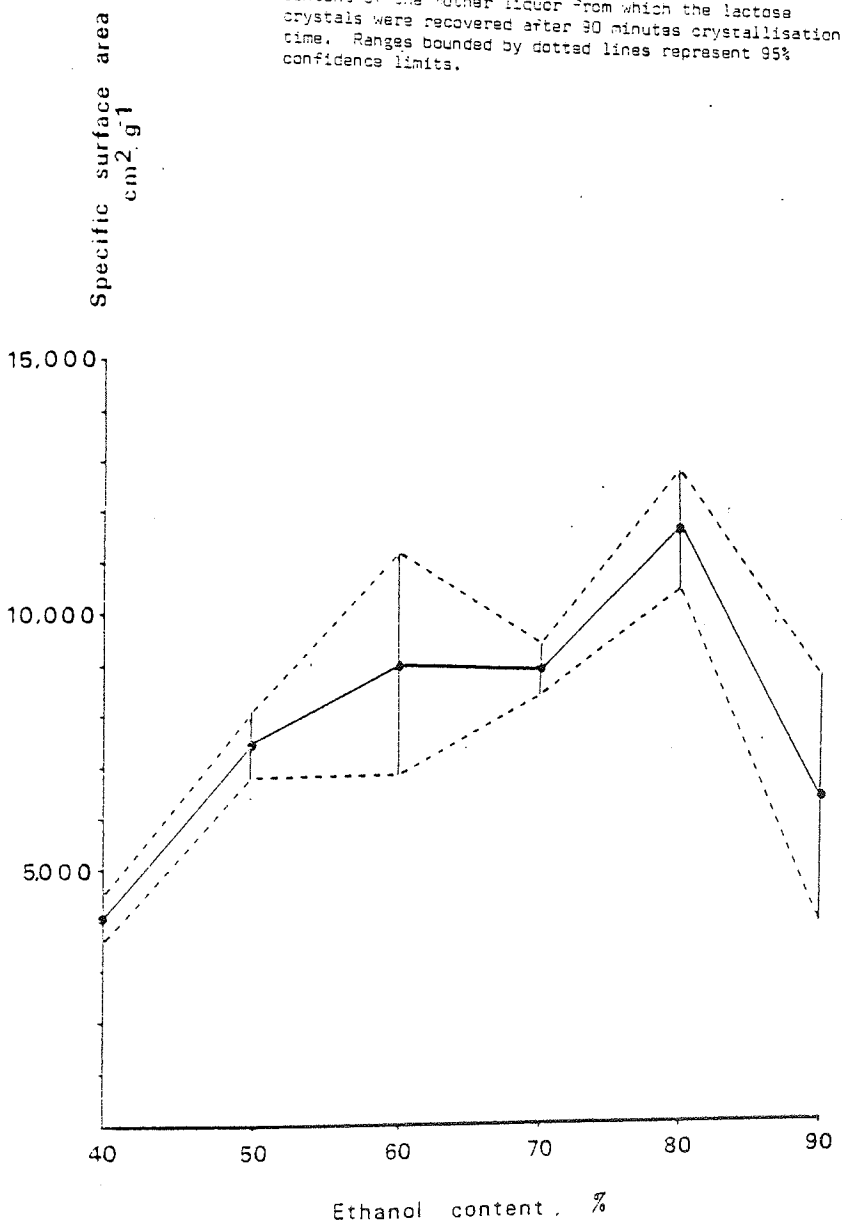

The solubility was twice as high at the tip as at the dendrite root wall; however, since the mean solute concentration in the mother liquor is determined by the mean radius of all curved interfaces in the system, the arms with the smallest radii dissolve first (217). A theoretical model of dendritic coarsening was developed by Reeves and Kattamis (217), (Figure 40). The model

Figure 40. Model of dendritic coarsening developed by Reeves and Kattamis.

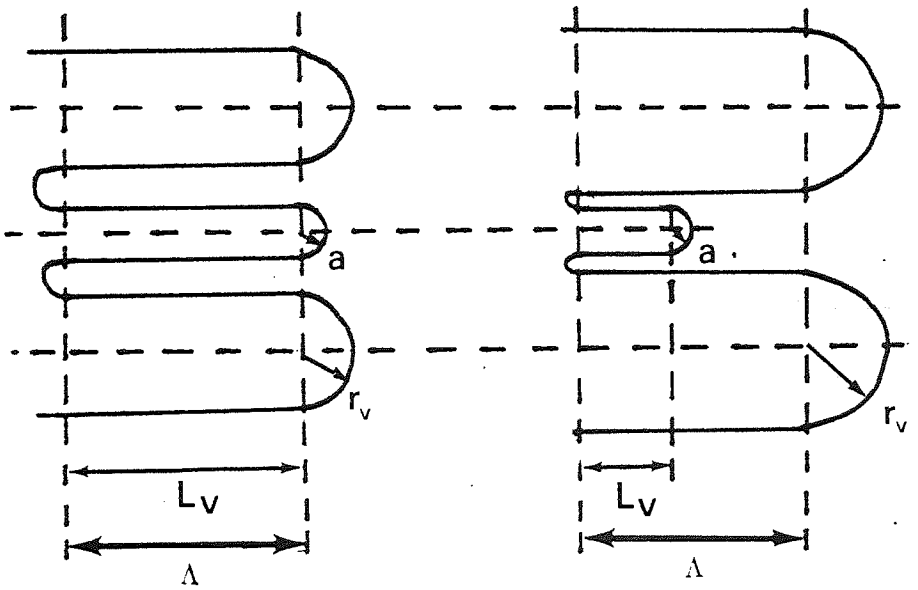

assumes that coarsening occurs by three mechanisms:

1. Dissolution at the small dendrite tip, of constant radius, a, and variable length, L_v.

2. Diffusion of material to the larger dendrites adjacent to it, of variable radius, r_v and constant length, Λ.

3. Deposition along the surface of the arms of the larger dendrites, Λ.

The small dendrites shrink back and finally disappear. Dendritic coarsening occurs by the removal of small dendrites and

the deposition of new material on progressively fewer arms.

This model can be used to explain the trends in Figure 39. Up to 80% IMS concentration the rate of production of new crystallites by secondary nucleation exceeded the reduction of surfaces by dendritic coarsening, and the measured surface area consequently increased. However, in the 90% IMS solution such a high proportion of crystals were removed from solution at the point of crashing that crystal growth was virtually complete after 30 minutes. During the last 60 minutes of crystal residence time in the 90% IMS solution, the dynamic equilibrium between dendritic coarsening and new crystallite formation was shifted and was probably dominated by the processes of dendritic coarsening which produced a corresponding reduction of spherulite surface area.

2.3.5.1.1 Surface Roughness

The determined surface areas, S_s, of the spherulites were compared with their theoretical areas when considered as spheres, S_d (measured from projected particle diameters) to determine the surface roughness or rugosity, r_s, of the particles:

$$r_s = S_s/S_d \qquad (78)$$

Figure 41 shows the relationship between the concentration of IMS in the solution from which the spherulites were recrystallised and the particle rugosity. The rugosity reached a maximum at an IMS concentration of 80%. Assuming that these spherulites did not deviate markedly from an overall spherical shape, they had a high individual roughness produced by surface asperities.

2.3.5.2 Mercury Penetration Porosimetry Determinations

Surface areas can be calculated from pressure penetration-

Figure 41 Relationship between increasing IMS concentration and surface rugosity of lactose spherulites.

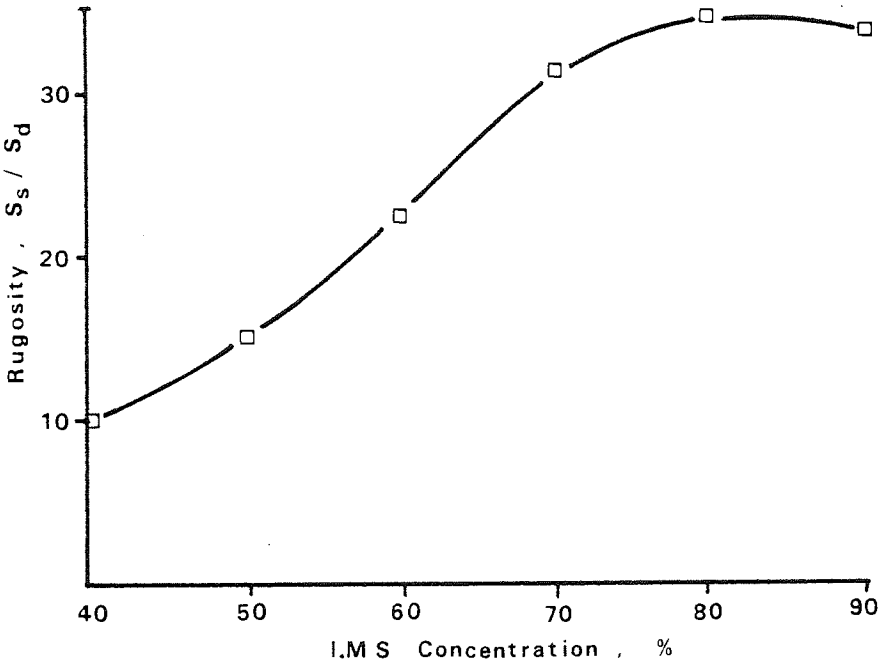

volume curves of a powder (218), according to the equation

$$S_a = -\int P'. \, dV_m / \xi'. \cos\theta \qquad (79)$$

where P' is the external (applied) pressure; dV_m, the small change in mercury volume; ξ', the surface tension; θ , the contact angle and S_a, the surface area of the powder sample. The equation assumes that the pores at any measured pressure have entrances larger than internal dimensions, and that at the highest pressure mercury is forced into the smallest pores. This last assumption may not be valid in the very narrowest pores, approaching molecular dimensions, but in the pore size range of interest here the assumptions are probably valid. The smallest pore diameter used to calculate

the "accessible surface areas" of lactose spherulites was 2 µm. The term "accessible surface area" was used to describe the surface area of porous spherulites for all pores with dimensions greater than a specific limiting diameter. As with the pore size distributions (Figures 36 and 37), the limiting diameters were chosen to include only those surfaces which would be relevant to the formation of active adherence sites in an ordered mix. For this reason limiting diameters were selected to calculate surface area contributions from only those surfaces accessible to small powder particles, such as those in the fine component of an ordered mix. In the calculations of accessible surface areas it was assumed that pores with a diameter greater than say, $d_{lim.}$, would be accessible to all particles whose largest dimension was smaller than this value, $d_{lim.}$. For the spherulites studied, the accessible surface areas decreased as the limiting diameter increased. Figure 42 a, b shows the surface areas of pores accessible to particles having diameters greater than 2 µm, for lactose spherulites in different size fractions. For the larger particle size fractions (Figure 42b), all the curves showed a maximum accessible surface area for particles recrystallised from 80% ethanol solution. Spherulites with a geometric mean diameter of 64 µm had the highest surface area of pores with diameters greater than 2 µm.

The accessible surface areas of pores with diameters greater than 10 µm (Figure 43 a, b) also reached a maximum with spherulites recrystallised from 80% IMS solution, although at higher particle sizes the difference between accessible surface area in spherulites recovered from solutions containing 60 to 80% IMS was less marked. For a limiting diameter of 10 µm the particle size fraction with

Figure 42(a) The relationship between surface areas of pores accessible to particles greater than 2 μm and the IMS concentration from which the lactose spherulites were grown. The three curves present data for different particle size distributions of spherulites.

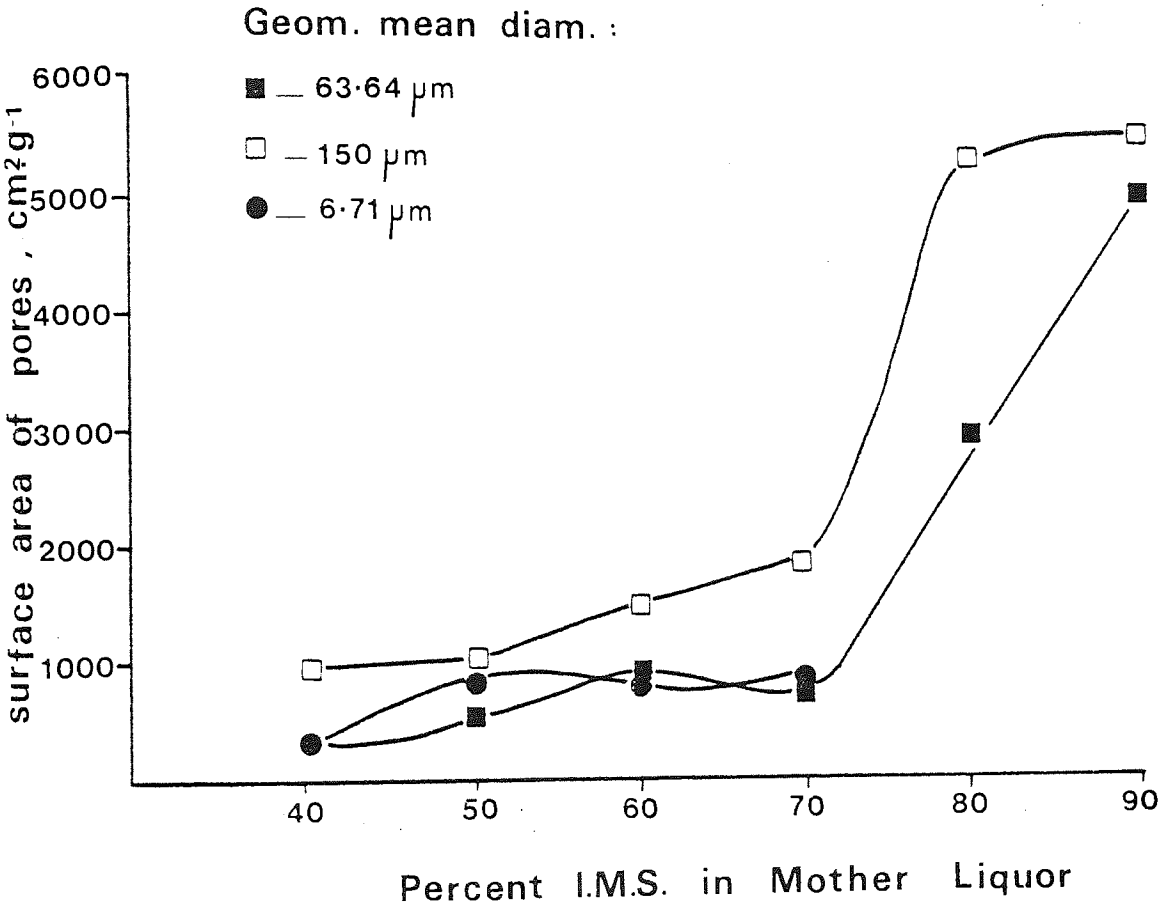

the largest accessible surface area had a geometric mean diameter of 354 μm.

2.3.6 Particle Shape Analysis

2.3.6.1 The Shape Factor, Ш

To determine the potential usefulness of different spherulites in an ordered mixing process, the irregularity of the particle surface needs to be known. A shape factor is required which is capable of distinguishing quantitatively between re-entrant and

Figure 42(b) The relationship between surface areas of pores accessible to particles greater than 2 μm and the IMS concentration from which the lactose spherulites were grown. The three curves present data for different particle size distributions of spherulites.

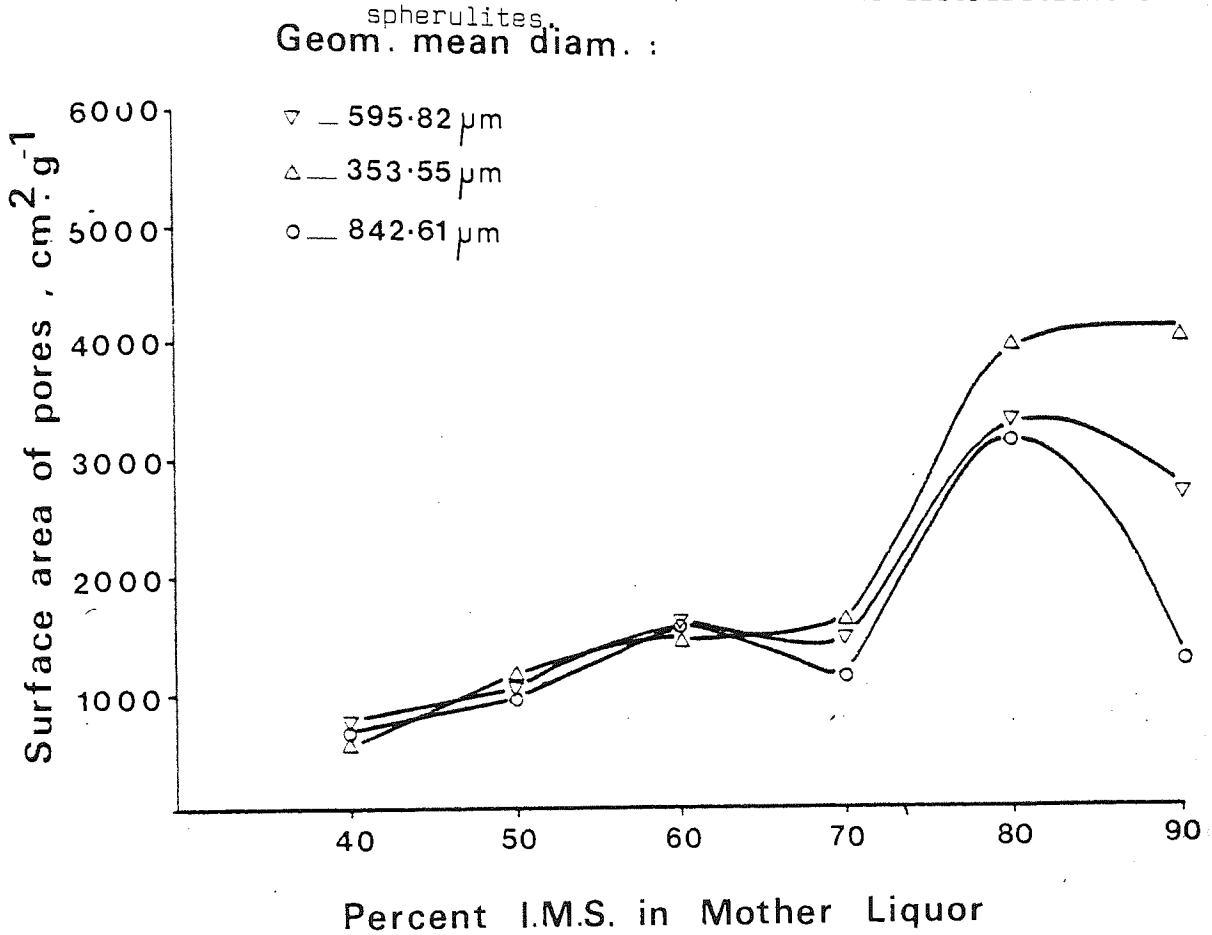

non-re-entrant particle shapes from a bulk powder sample. An empirical shape factor was developed for this purpose being machine-generated and capable of quantifying particle irregularities, such as re-entrant surface morphology. The surface asperities on coarse particles have been implicated in the production of active adherence sites in ordered mixes (84). Surface asperities are associated with re-entrant particle shapes; the more re-entrant the particles the larger and more numerous the asperities, and consequently the greater the number of possible adherence sites. The Quantimet 720 image analysing computer was used to generate a

Figure 43 The relationship between surface areas of pores accessible to particles greater than 10 μm and the IMS concentration from which the lactose spherulites were grown. The four curves present data for different particle size distributions of spherulites.

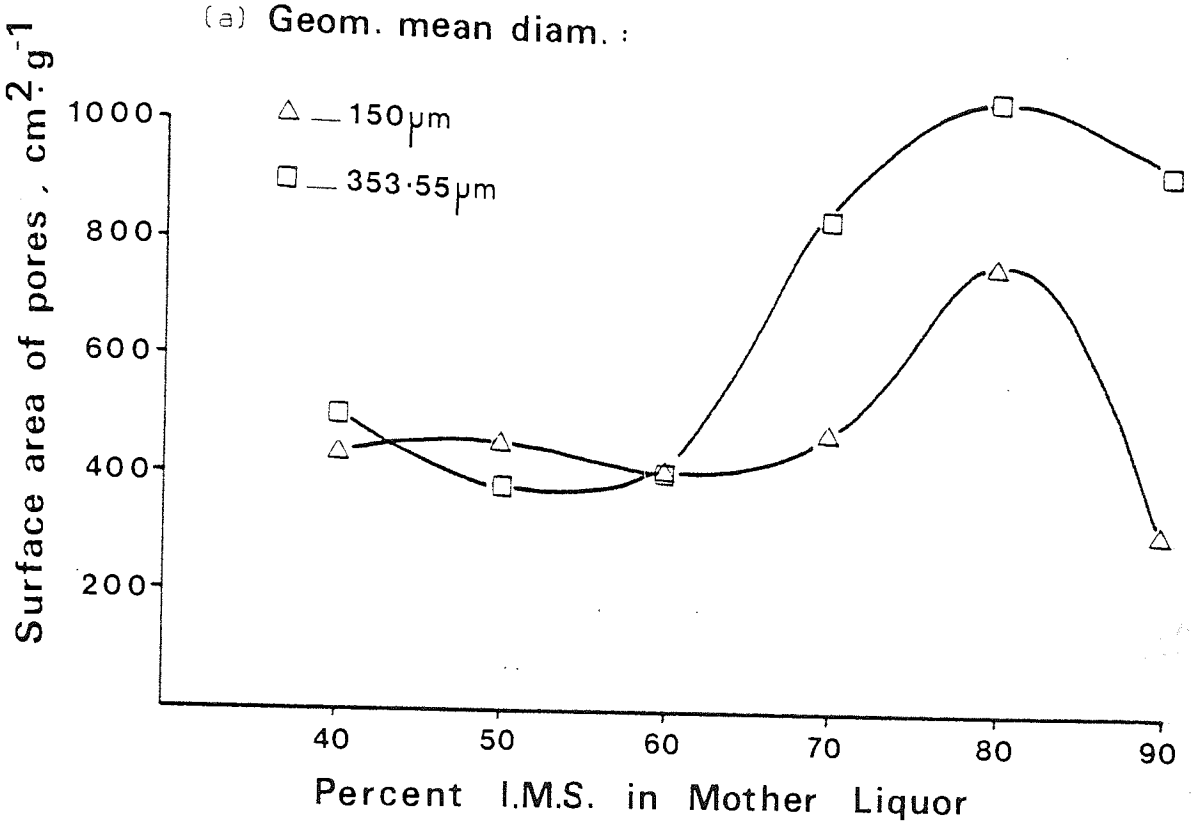

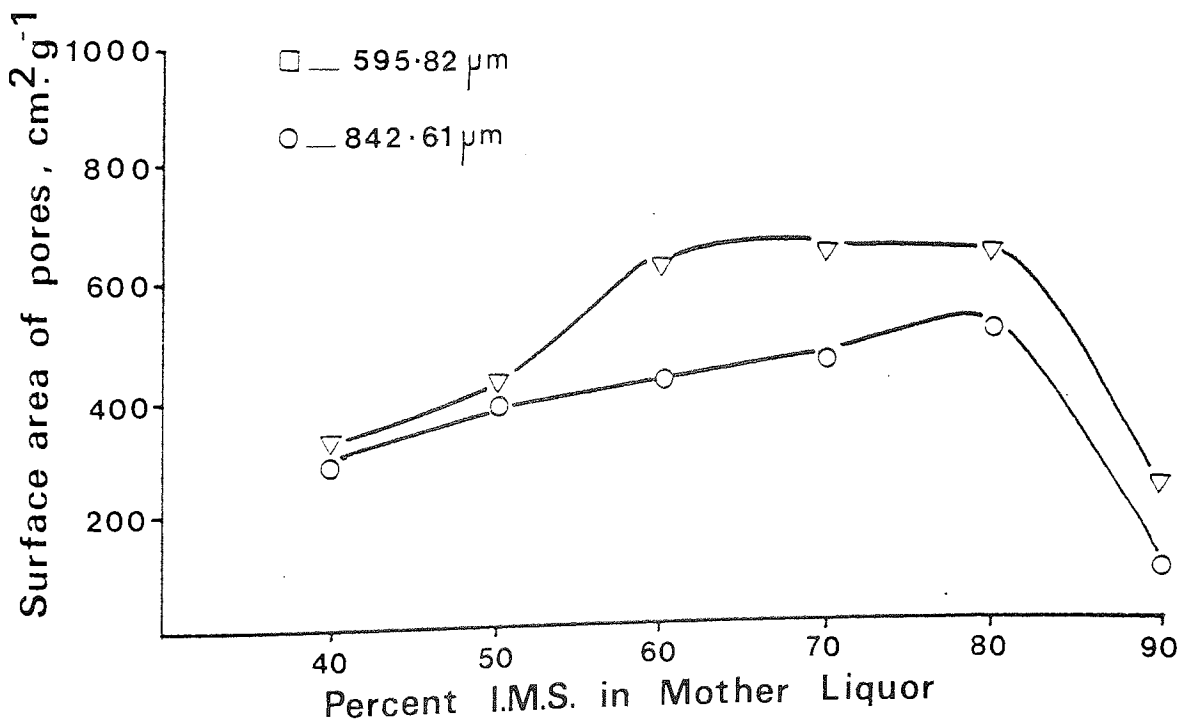

shape factor specifically designed to quantify re-entrant particles. The image analysing computer is capable of analysing large numbers of particles and it can produce mean shape factors, for example, of particles in selected size ranges. As well as the full-feature count, described earlier (Section 2.2.3.2), the Quantimet is capable of detecting particles by another method, called the "end count". Whereas the full-feature count recognises detected particles (features) only once at a fixed position, the end count recognises all downward pointing projections within the detected region of the live frame (Figure 44 a, b). Using the end-count, a re-entrant particle is counted more than once. The number of counts per particle is a function of its re-entrancy. The shape factor, $\underline{\underline{\mathrm{III}}}$ (shar) of a re-entrant particle was based on the number of downward pointing projections in a powder sample, related to the total number of particles, n, calculated from the full-feature count. Expressed in terms of end counts, e_c, the shape factor, $\underline{\underline{\mathrm{III}}}$, is therefore given by:

$$\underline{\underline{\mathrm{III}}} = e_c/n \qquad (80)$$

For completely non-re-entrant particles such as spheres or cubes, $\underline{\underline{\mathrm{III}}}$ has a value of unity. The value of $\underline{\underline{\mathrm{III}}}$ for re-entrant particles increases to a maximum which is governed by the resolution at each magnification.

The particle shape factor, $\underline{\underline{\mathrm{III}}}$, was calculated for each of the particle size fractions of the different lactose powders. For each sample analysed, $\underline{\underline{\mathrm{III}}}$ was calculated as the mean of approximately 6,000 different particles. Tables 7 to 11 show the effect of different particle sizes, and the concentration of IMS in the lactose mother liquor, as well as the effect of crystallisation

Figure 44(a)

Diagram of particle (feature) recognition of the Quantimet 720. Only part (b) of the total chord (a) lies within the live frame and is detected. Part (c) lies outside the live frame and is undetected. Only particles falling wholly in the live frame are counted.

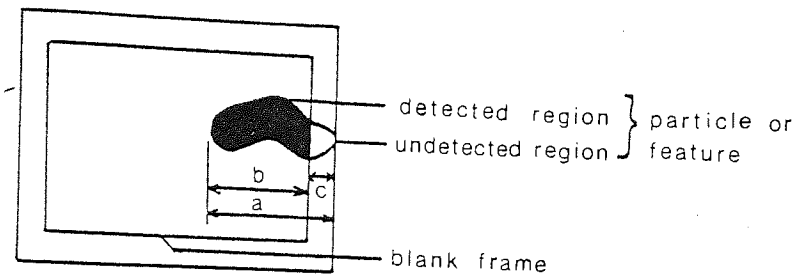

Figure 44(b) Difference between end and full-feature counts on the same particle in the Quantimet 720.

Re-entrant particle or agglomerate

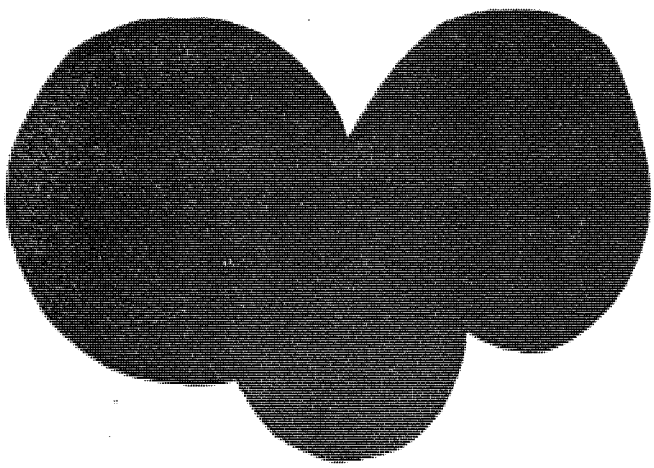

End count = 3

Full feature count = 1

Tables 7 to 11

Shape factors ($\frac{11}{}$) for lactose spherulites of different particle sizes recovered from different concentrations of ethanol solutions after different crystallisation times.

Table 7 Crystallisation time : 5 minutes

	Projected Particle Diameter (µm)					
%IMS	1	50	100	200	350	500
40	2.5	4.2	4.1	4.1	4.6	6.2
50	3.3	3.0	3.2	3.4	3.6	2.3
60	4.4	4.3	3.6	5.0	5.0	5.5
70	3.2	3.2	2.4	2.4	3.7	3.1
80	3.7	4.6	5.3	5.1	8.5	10.4
90	3.5	2.7	2.2	2.5	2.5	2.9

Table 8 Crystallisation time : 15 minutes

%IMS	1 µm	50	100	200	350	500 µm
40	4.2	3.9	3.7	3.5	3.4	2.8
50	2.9	2.7	3.8	5.8	9.3	12.9
60	5.6	3.1	2.8	3.3	4.4	12.5
70	2.8	2.5	2.4	2.3	2.7	3.6
80	3.1	2.4	2.5	3.4	4.0	4.0
90	2.4	2.1	2.1	2.7	3.5	N/A

Table 9 Crystallisation time : 30 minutes

%IMS	1 µm	50	100	200	350	500 µm
40	2.9	3.2	3.7	4.7	5.0	11.3
50	2.7	3.1	3.6	3.7	3.9	4.8
60	2.5	2.7	2.8	3.6	2.2	5.3
70	3.5	3.0	3.0	3.3	2.6	4.7
80	3.6	3.1	3.1	3.7	4.7	7.7
90	2.8	2.8	2.8	3.0	2.8	6.4

Table 10 Crystallisation time : 60 minutes

%IMS	1 µm	50	100	200	350	500 µm
40	3.3	2.7	2.3	2.8	2.3	4.0
50	3.8	3.3	3.6	3.4	4.8	8.1
60	3.0	3.2	3.1	3.4	4.2	3.7
70	2.5	3.0	2.7	3.1	4.0	6.8
80	3.0	2.8	2.8	2.4	N/A	N/A
90	3.1	2.7	3.4	3.3	2.1	2.0

Table 11 Crystallisation time : 90 minutes

	Projected Particle diameter					
%IMS	1	50	100	200	350	500
40	3.9	2.6	3.1	2.9	3.0	3.3
50	2.3	3.5	4.0	3.7	4.8	2.5
60	3.6	3.3	3.4	3.3	4.1	8.1
70	3.2	3.5	4.7	3.8	5.5	9.0
80	3.1	2.8	2.8	2.5	N/A	N/A
90	3.0	3.2	2.8	2.2	2.5	4.2

Table 12 Mean shape factor ($\amalg_M$) of lactose spherulites recovered from different IMS concentrations after different crystallisation times

%IMS	5	15	30	60	90
40	2.5	4.1	3.0	3.2	3.7
50	3.3	3.0	2.8	3.7	2.4
60	4.4	5.0	2.5	3.0	3.4
70	3.2	2.8	3.4	2.5	3.2
80	3.8	2.6	3.7	3.0	3.1
90	3.4	2.4	2.8	3.1	3.0

time on the re-entrant particle shape of lactose spherulites. The tables show a general increase in re-entrant particle shape with increasing particle size. The effect of IMS concentration on particle shape within a spherulite size range was shown by plotting the shape factor $\underline{III}$ against IMS concentration (Figure 45).

Figure 45 The relationship between the concentration of IMS and the re-entrant shape factor $\underline{III}$ for two different particle sizes.

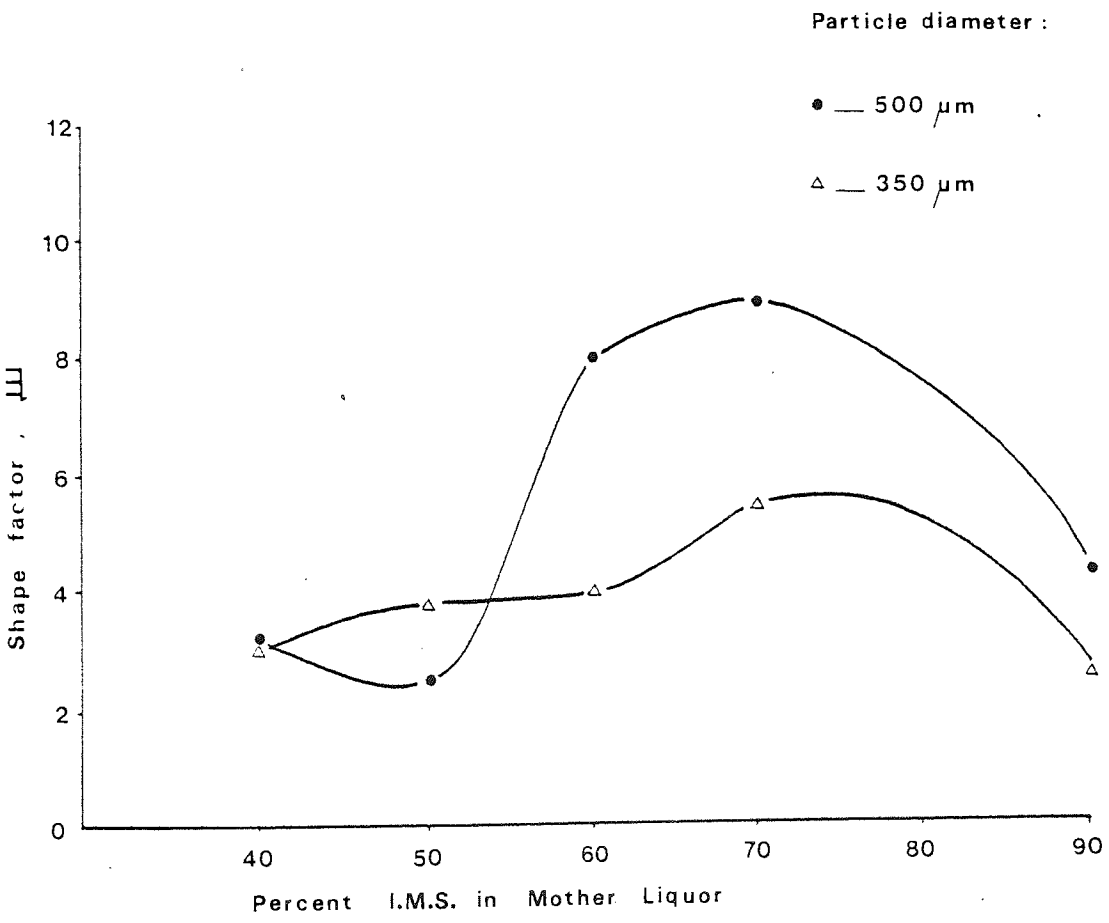

In spherulites recovered after 90 minutes crystallisation time, the shape factor $\underline{III}$ reached a maximum between 70 and 80% ethanol concentrations. When each bulk sample of crystals was considered as a whole, using the mean shape factor, $\underline{III}_M$ (Table 12), for the total size range, the effect of ethanol concentrations on re-entrant

particle shape appeared to be negligible. This can be explained by the massive contribution to the mean shape factor of the fine particles in comparison with the smaller number of the generally more re-entrant coarse particles (Tables 7 to 11).

2.3.6.2 The Heywood Shape Factor

A different shape factor was developed by Heywood to classify irregularly-shaped particles (219). In Heywood's system each particle is allocated into a different shape group depending on which one of four geometric forms best describes the particle: angular tetrahedral; angular prismoidal; sub-angular; rounded. The allocation of particles into a shape group is done either by measurement or by estimation of the volume coefficient, f, and its relationship with the surface coefficient, k or k_e. The ratio f/k can vary from unity to infinity, but in practice a particle with a minimum f/k value of 3 or 4 would be represented by a flattened sphere or disc, whilst a sphere has a value of 6. A cube has $f/k = 6.8$ and if split into 100 equally thin plates, the f/k value would rise to 228. In general, the higher the ratio of surface area to volume, the greater the f/k value.

The Heywood shape coefficients were calculated for the lactose spherulites recrystallised from different concentrations of ethanol (Figure 46). As the ethanol concentration increased the value of f/k increased from 6 to a maximum 42 at an ethanol content of 80%. Over this f/k range, the particle shape description changed from near spherical for spherulites recrystallised from 40% ethanol, to flaky or dendritic particles with an f/k value of about 40 at 80%. This increasing f/k value indicated an increasing surface to volume ratio, probably caused by increasing dendrite

Figure 48 Relationship between the Heywood shape coefficient and the concentration of ethanol from which the lactose spherulites were recovered after 30 minutes crystallisation time. The ranges bounded by dotted lines represent 95% confidence limits.

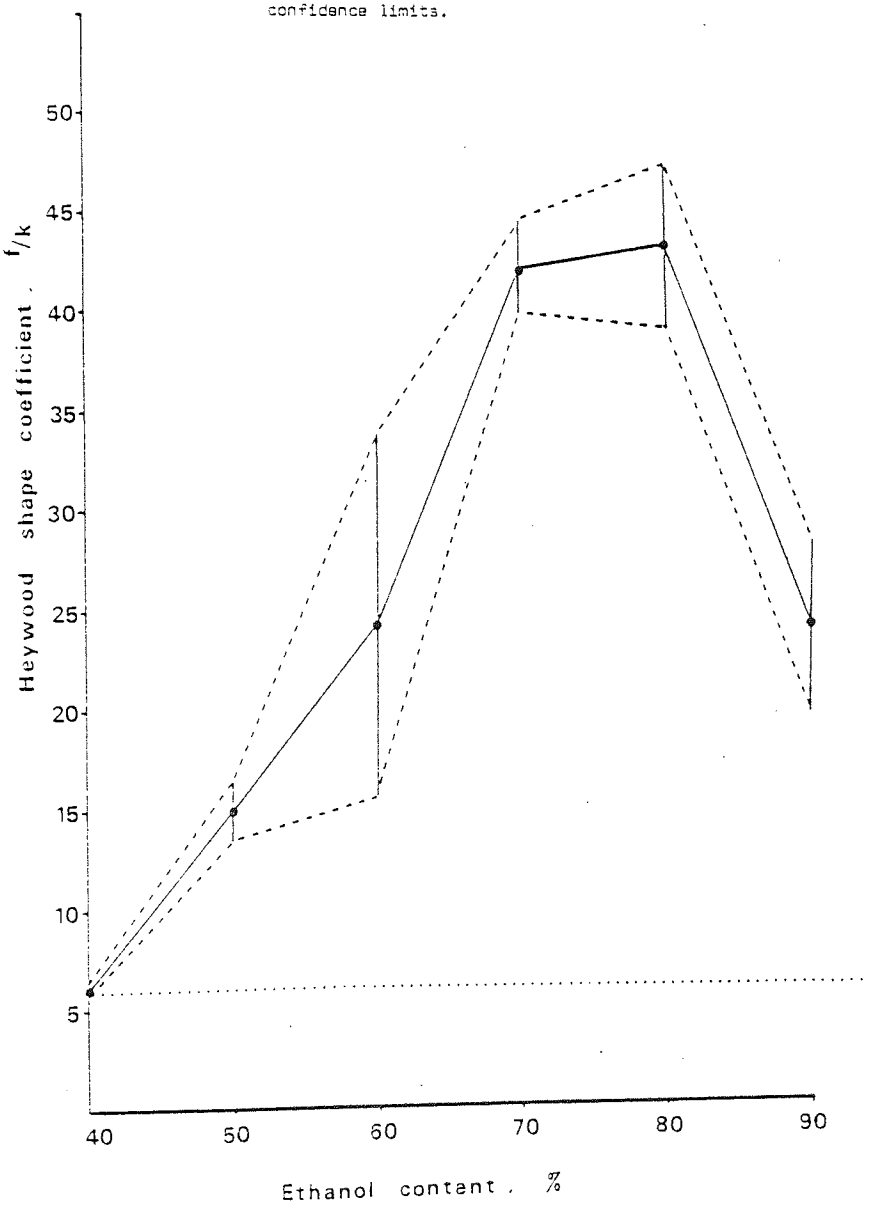

formation. When the component dendrites coarsen the $^{f}/_{K}$ value should fall. This occurred above 80% ethanol concentrations.

The shape coefficient, $^{f}/_{K}$ is based on calculation of the specific surface area of a powder. A powder which has a high surface area is likely to be assigned a biased $^{f}/_{K}$ value because of the calculation method. In particular, a highly re-entrant particle which has a high specific surface area due to large numbers of small pores or increased surface roughness (rugosity), will have a disproportionately high $^{f}/_{K}$ value. In these cases assumptions regarding particle shape will therefore be inaccurate. This occurs because the small pores and fine asperities produce powder surfaces which do not contribute to the overall particle shape, but which nevertheless contribute a high proportion to the measured surface area. This bias is unimportant in plane or re-entrant particles that are relatively smooth and non-porous, but for powder particles that are porous or have a high rugosity, a correction should be made.

To ensure that the measured $^{f}/_{K}$ value was an accurate representation of particle shape, a technique was developed to filter out that proportion of the surface area which did not contribute to the overall particle shape. The specific surface area is accurately measured by nitrogen adsorption, but this method is based on quantifying the number or volume of nitrogen molecules which are adsorbed onto a powder surface. The nitrogen molecule is capable of penetrating virtually all open-ended pores and irregularities in a powder particle in the range of 0.004 μm diameter at a pressure of 50,000 psia to 177 μm pore diameter at 1 psia. Nitrogen adsorption measures the total surface area of a powder. By using mercury porosimetry to calculate the accessible

surface area of a powder, (Section 2.3.5.2) only those surfaces are measured which contribute to the level of particle shape of interest, such as irregularities producing large cavities capable of trapping drug particles, or affecting the formation of active sites in ordered mixes.

The accessible surface areas (S_a) were used to calculate the adjusted Heywood shape coefficient, $(f/k)^*$. Table 13 shows the differences in predicted shape for lactose spherulites recrystallised from different concentrations of IMS, compared with the Heywood Shape Coefficient (f/k) for the same groups of particles shown schematically in Figure 47.

Table 13 Heywood shape coefficients for lactose spherulites derived from 2 alternative values for surface area

%IMS	$(f/k)^*$ calculated from S_a	(f/k) calculated from nitrogen adsorption surface areas
40	1.7	6.1
50	1.1	18.1
60	3.4	24.0
70	3.5	40
80	10.4	42
90	11.4	23

The values of the shape coefficients calculated from S_a were consistently lower than the (f/k) values calculated from surface areas determined by nitrogen adsorption (S_s). The ratios between $(f/k)^*$ and (f/k) for the same IMS concentration ranged from about 3 for 40% IMS to about 18 at 50% concentration. Table 14 presents a descriptive interpretation of the Heywood shape coefficient listed in Table 13.

Figure 47. Relationship between the modified Heywood shape coefficient $(f/k)^*$ and the re-entrant shape factor,

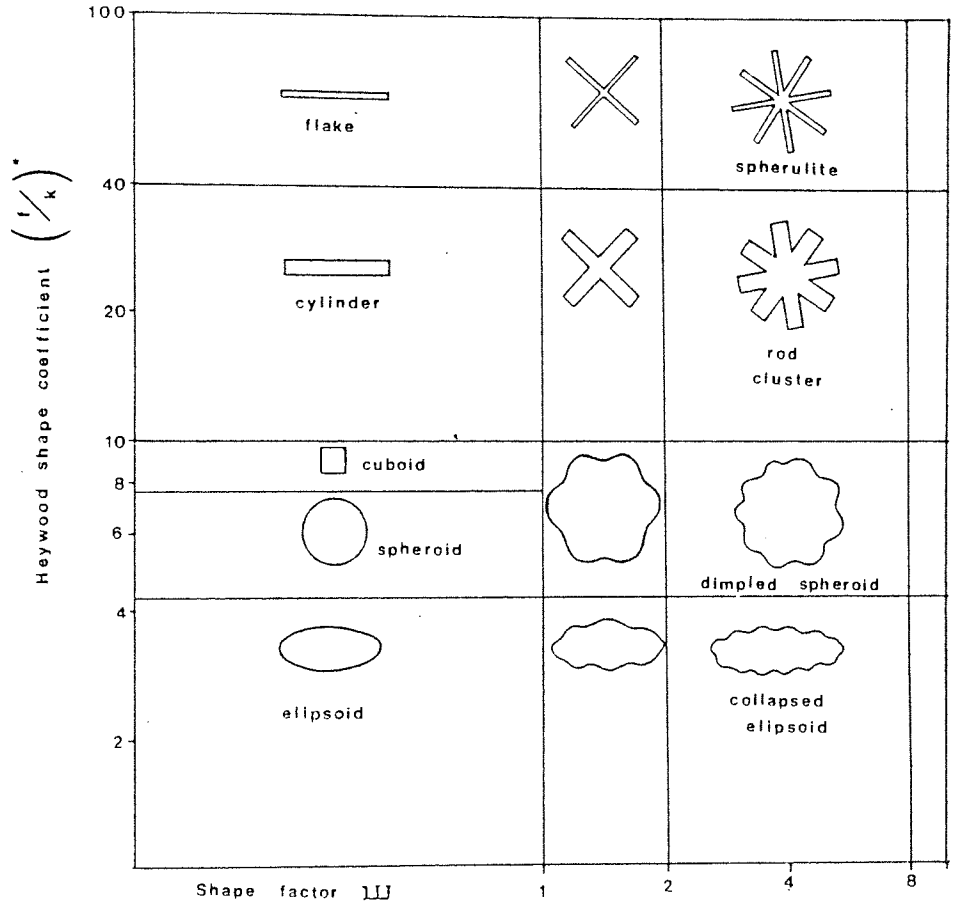

Table 14 Literal interpretation of the Heywood shape coefficients calculated from the two different surface area measurements (see Table 13)

%IMS	Shape description based on: $(f/k)^*$	(f/k)
40	Flattened sphere	Sphere
50	Flattened sphere	Flat Plate
60	Flattened sphere	Flat Plate
70	Flattened sphere	Thin plate
80	Cuboid, rectangular prism	Thin plate
90	Cuboid, rectangular prism	Flat plate

Although all the particles described in Table 14 were re-entrant, the interpretation of the modified Heywood Shape Coefficients $(f/k)^*$ gave a more accurate description of the overall particle shape than those obtained using conventional surface area values to calculate (f/k).

By combining the modified Heywood shape coefficients $(f/k)^*$ and the shape factor, III , a table matrix was constructed capable of describing both the geometric form of a particle and the degree of re-entrancy (Figure 47). Using this matrix most of the spherulites prepared in the crystallisation studies were found to have similar overall particle shapes which were best described by the term "collapsed ellipsoid".

2.3.6.3 Scanning Electron Microscopy

The scanning electron microscope was used to produce photomicrographs of the lactose spherulites recrystallised from different ethanol concentrations. Particles crystallised from

ethanol solutions of 80 and 90% concentration (Figures 48 e & f) showed a marked difference in surface morphology from the other samples (Figures 48 a, b, c, d). At 80% the particles still showed some fairly large surface cavities, although these appear to be much shallower than those in particles recrystallised from lower ethanol concentrations and none of the cavities appeared to have mouths wider than 60 - 80 µm diameter. Individual dendrites were not discernible and the surface was generally covered with many small crystallites less than 10 µm long. The particles recrystallised from 90% ethanol solutions had no large surface cavities although the particle surface was totally covered with many small crystallites. The size of these crystallites was approximately 20 µm in the longest dimension. The lactose starting material, from which all the spherulites were recrystallised appeared to be microscopically relatively smooth and non-re-entrant (Figure 49). Most of the spherulites shown in Figure 48 were those described as "dimpled discs" according to the matrix system.

2.4 Discussion

The various qualitative and quantitative examinations of the lactose spherulites revealed differences in their surface properties depending on their particle size and the content of IMS in the crystallising solution. In many of the measurements carried out on the lactose spherulites optimum values were obtained for particles recrystallised from solutions containing a concentration of 80% IMS.

The flow rate measurements revealed that increasing particle size of spherulites graded into different size ranges improved flow, but bulk density measurements showed that the ungraded spherulites had similar poor flow properties, probably as a result of increased fine interparticle contact causing high friction.

Figure 48. Surface morphology of lactose spherulites recrystallised from different I.M.S. concentrations.

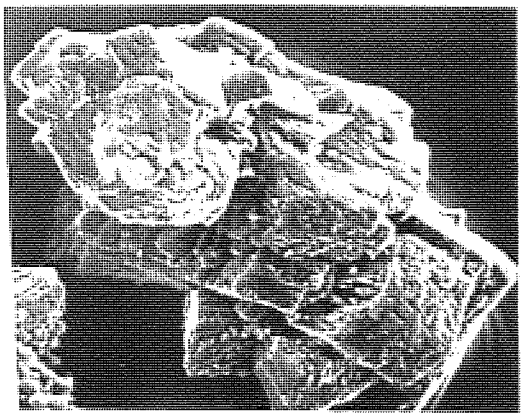

Whole particle

120 μm

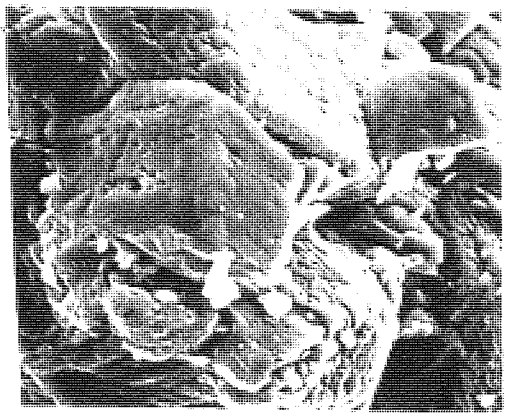

Surface detail

40 μm

A. 40% I.M.S.

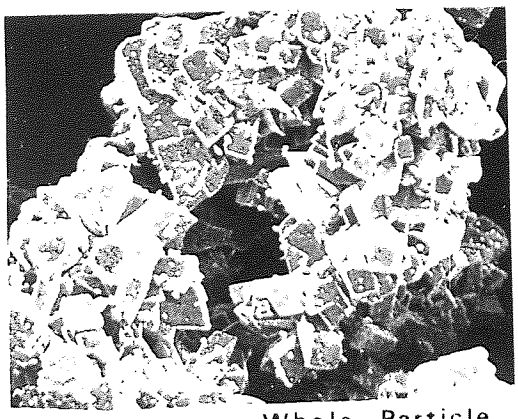

Whole Particle

120 μm

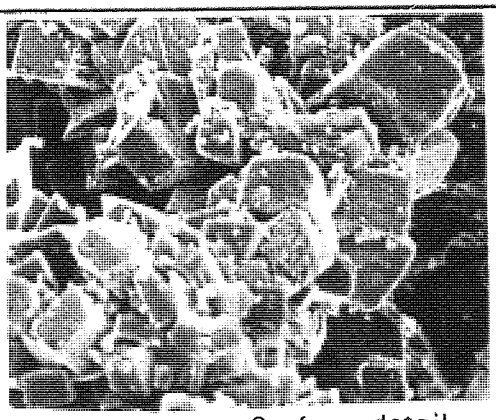

Surface detail

80 μm

B. 50% I.M.S.

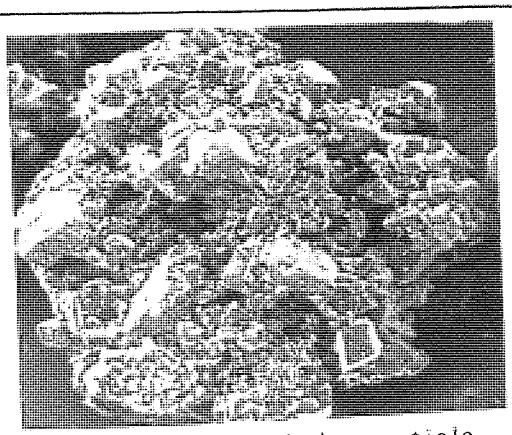

Whole particle

120 μm

Surface detail

40 μm

C. 60% I.M.S.

Figure 48 continued.

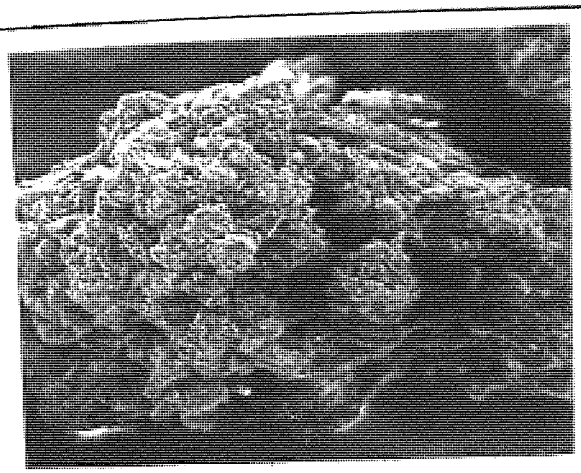

120 µm

Whole particle

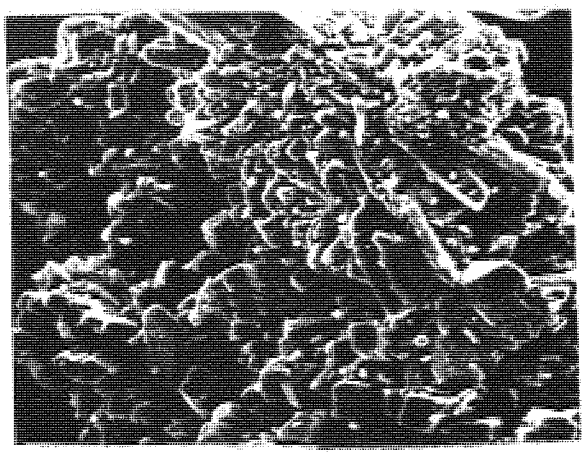

40 µm

Surface detail

D. 70% I.M.S.

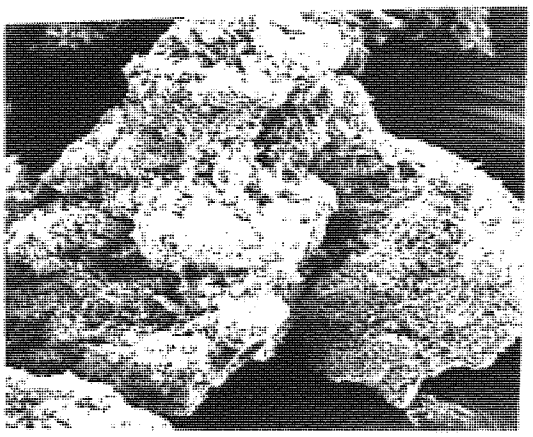

120µm

Whole particle

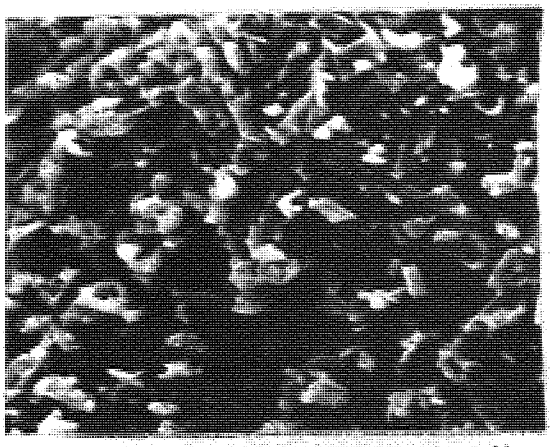

30 µm

Surface detail

E. 80% I.M.S.

120 µm

Whole particle

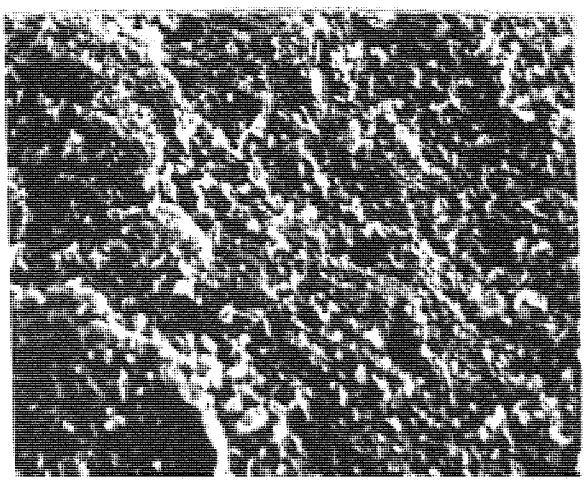

40 µm

Surface detail

F. 90 % I.M.S.

Figure 49. Surface morphology of original lactose material.

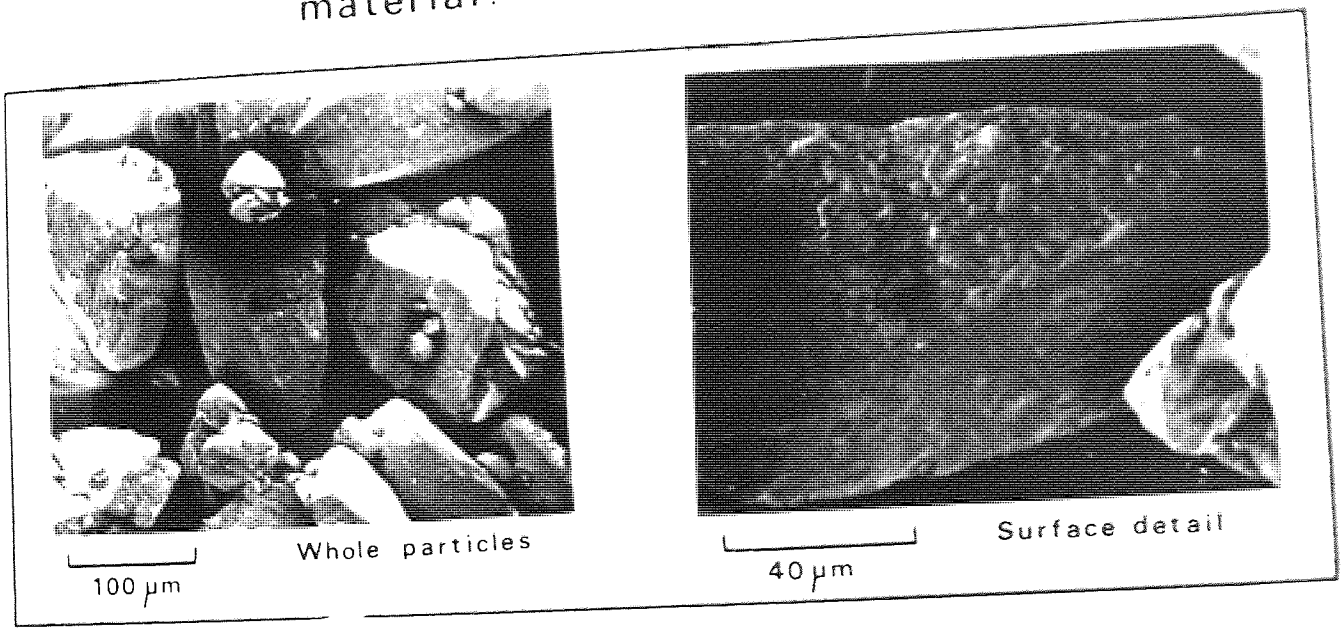

The measurements of surface properties of lactose spherulites, showed that the particles were made much more re-entrant by the re-crystallisation process. The most re-entrant lactose spherulites were those with a particle size of 500 μm, recrystallised from different concentrations of IMS. The effect of the concentration of IMS on particle shape was shown by the Heywood shape coefficient, $(^{f}/_{k})$ which reached a maximum value of 42 in lactose spherulites recrystallised from 80% IMS. The modified Heywood shape coefficient $(^{f}/_{k})^{*}$ increased from 1.7 for particles recrystallised from 40% IMS to 11.4 for spherulites recovered from 90% IMS. The modified Heywood shape coefficient and the shape factor, $\underline{III}$, together showed that the most re-entrant collapsed ellipsoids were spherulites with a diameter of 500 μm recrystallised from 70 or 80% IMS after 90 minutes crystallisation time.

The influence of IMS concentration on the particle surface properties was demonstrated by measurements of several other parameters.

The maximum spherulite surface area determined by nitrogen adsorption was achieved by crystallisation of particles from 80% IMS. Similarly these crystallisation conditions produced the maximum accessible surface areas of lactose spherulites. In bulk density determinations, both the Hausner ratio and the curves for percent compressibility reached a maximum at 80% IMS.

The high values for surface area and interparticle contact, inferred from bulk density studies, in spherulites recrystallised from 80% IMS probably result from the peak values of surface rugosity and porosity shown at this concentration. The pore size determinations showed that the most porous spherulites were those

recrystallised from an 80% IMS solution. This was also the concentration of IMS which produced crystals with the highest percentage of large pores greater than 10 μm in diameter. At particle sizes of 350 μm and 500 μm, spherulites with the most re-entrant surfaces were those recrystallised from 80% IMS. Stereoelectronphotomicrographs also demonstrated the noticeable change in surface morphology between those lactose spherulites recrystallised from ethanol concentrations at or below 70% and those at or above 80%. The ultrastructure of the particle surface showed a change from coarse dendrites to a finer total covering of small crystallites; this gave the particles recrystallised from 80% IMS their increased surface rugosity and high porosity.

Consideration of the factors influencing the formation of ordered mixes indicates that carrier particles with surface asperities and high porosities are more able to form adherence sites for small particles and produce non-segregating mixes, than smoother, non-porous carrier particles. The results obtained in the previously described experiments on the surface properties of lactose particles suggested that spherulites recrystallised from 80% IMS solution should be capable of trapping the highest quantity of fine drug particles and should therefore form more stable ordered mixes.

For this reason a larger, pilot-scale batch of spherulites was recrystallised from a solution containing 80% IMS in the lactose mother liquor.

2.5 Preparation of pilot-scale batch of lactose excipient

A supersaturated solution of lactose was made in a tank with a volume of approximately 50 litres, continuously stirred using

an electrically-operated single marine paddle (L. A. Mitchell Ltd., Manchester, U.K.). The solution was heated from below by an electric mantle (type 52TY, Heatrae Ltd., Norwich, U.K.) to a constant temperature of 70°C. The large mass of supersaturated lactose solution (20 kg) was allowed to cool overnight. At a temperature of 25°C, IMS was added to produce a final mother liquor concentration of 80%. Lactose crystals were grown for 90 minutes, during which time the tank was continuously stirred by one deep marine paddle (L. A. Mitchell) to prevent caking at the base of the crystalliser and two slowly rotating shallow paddle stirrers (Type KQTS 9, Citenco Ltd., Boreham Wood, U.K.). The crystals were discharged from the crystalliser through an exit valve at the base of the tank and filtered through a vacuum filtration apparatus consisting of a large Buchner flask and funnel. The lactose was immediately washed by pouring acetone over the crystals and allowing the vacuum to draw the acetone through the filtered bed of crystals and thus remove any remaining mother liquor. The washed crystals were dried in a fan-assisted tray-drier (Weyco Ltd., Loughborough, U.K.) at 60°C for ten hours. The agglomerates of dried crystals were initially broken up by sieving through a 2 mm aperture wire mesh sieve. The smaller spherulites were than removed from any remaining agglomerates by shaking the powder for twenty minutes on a 1 mm test sieve (Endecotts Ltd., London) using a mechanical sieve shaker (Endecotts Ltd., London).

The properties of the crystals derived from this procedure are described in Chapter 3 and the trials carried out with this bulk material are described in Chapters 4, 5 and 6.

Chapter 3

3. Characterisation of excipients for mixing and segregation

3.1 Materials

Three free-flowing commercial direct-compression tableting excipients were studied in addition to various size fractions of a batch of lactose spherulites recrystallised according to the method described in Section 2.3 of Chapter 2.

The three commercial excipients tested were:

1. Dipac : a direct compacting 'sugar' (Amstar Corporation, New York, U.S.A., supplied by Wilfrid Smith Fine Chemicals Ltd., Edgware, U.K.).
2. Elcema G250 : a granular form of microfine cellulose (Degussa, Frankfurt, W. Germany)
3. Emdex : a spray crystallised, porous, maltose-dextrose direct tableting excipient (Edward Mendell Inc., New York, U.S.A., supplied by K & K-Greeff Fine Chemicals Ltd., Croydon, U.K.).

All excipients were tested as received and particular attention was given to assessment of the surface characteristics of the excipient powders.

3.2 Methods

Some of the methods used to characterise excipients for mixing and segregation studies were the same as those described in Section 2.2.1 for the characterisation of lactose crystals.

3.2.1 Particle Densities

3.2.1.1 Bulk Density Measurements

The apparatus and methods used to determine the bulk densities of the different excipient powders were the same as those described

in Section 2.2.2.2 for recrystallised lactose. However, in these experiments a 250 ml measuring cylinder was used to hold the powder during tapping in the jolting volumeter. The larger volume of the 250 ml cylinder reduced the wall effects which can affect consolidated bulk densities of powders in small cylinders such as those of 50 ml volume.

3.2.1.2 True Density Measurements

The true density of a powder is the density of individual particles without any contributions from void spaces in the powder bed. The method for calculating true particle densities was based on measurements obtained by mercury penetration porosimetry. The particle densities were determined from the volumes of mercury forced into the powder sample. High applied pressures were used to ensure that the smallest pores were filled with mercury. The following equation was used to calculate powder density ρ_s:

$$\rho_s = W_s / \left(V_s - \left\{ (W_t - W_s - W_c) / \rho_M + (C_p + C_t) + f_M \right\}\right) \quad (81)$$

where, W_s is the sample weight; V_s, the volume of the sample cell; W_t, the weight of the sample cell and mercury following mercury penetration; W_c, the weight of the empty sample cell; ρ_M, the density of mercury; C_p, the corrected mercury penetration counter reading; C_t, initial counter reading (C_p & C_t are used to calculate the volume of mercury penetrating pores at each applied pressure) and f_M, the cell factor (a constant for each cell).

The mercury porosimetry method of determining the densities of porous powders has advantages over the use of conventional liquid pycnometry because of the extremely efficient degassing procedure

which removes all the entrapped air and due to the high applied pressures which ensures that all the open-ended pores are penetrated by mercury.

3.2.2 Particle Size Analysis

Each of the four excipients had a relatively coarse particle content and were analysed by sieving. A 100 g sample of excipient powder was obtained using a chute sample divider - Endecotts (Test Sieves) Ltd., London. The sample was placed on the top screen of a nest of eight wire mesh test sieves assembled on a mechanical sieve shaker (Endecotts (Test Sieves) Ltd., London). Sieving was carried out according to the method described in B.S. 1796; 1952. The amount of material retained on each screen after sieving was weighed, and the cumulative percentage oversize was calculated.

3.2.3 Pore Size Determinations

The same methods and apparatus were used to characterise the various excipient powders as those described in Section 2.2.5 for the pore size determinations of recrystallised lactose.

3.2.4 Powder Surface Area Determinations

A multi-point determination of the surface areas of the excipient powders was carried out using a Quantasorb surface area analyser (Quantachrome Corp., Greenvale, U.S.A.).

The principle of operation is based on a modification of gas-adsorption chromatography, where the column packing is the actual powder sample and the mobile gas phase is a mixture of nitrogen as adsorbate gas, and an inert gas, helium. A known mixture of helium and nitrogen gas was passed through the small U-shaped cell containing the powder sample. After a suitable degassing period (16 hours)

the U-cell was immersed in liquid nitrogen. At this temperature, helium is not adsorbed on any surface, while the nitrogen gas is. When the liquid nitrogen bath was removed a corresponding desorption occurred. Changes in the helium to nitrogen ratio in the out-flowing gas stream were sensed by a thermal conductivity detector, and plotted as a near-normal distribution curve. The instantaneous signal height of this normal curve was proportional to the adsorption rate and the total area under the curve was proportional to the quantity of gas adsorbed on the powder sample. This value was automatically digitally integrated by the Quantasorb.

Measurements were made at different partial pressures (10, 20 and 30% nitrogen in helium), following desorption calibration with known adsorbate gas volumes. A "small-piece" sample cell was used and all samples were de-gassed without heat. The surface areas were calculated from adsorption isotherms of the partial pressures P/P_s plotted against the volume, $1/X \left\{(P_s/p) - 1)\right\}$. In this volume term, X is the weight of adsorbing gas, given by:

$$X = (A/A_{cal.}) \cdot X_{cal} \tag{82}$$

where A is the area under the sample desorption volume curve; A_{cal}, the area under the volume calibration curve and X_{cal} is the calibration gas weight.

The total surface area, S_t, of the sample powder was then calculated from the following expression:

$$S_t = \left\{X_M \cdot (6.02 \times 10^{23}) A_{cs}\right\}/M_a \tag{83}$$

where A_{cs} is the adsorbate gas cross-sectional area; M_a, the molecular weight of the adsorbate gas and X_M is given by the reciprocal of

the sum of slope and intercept of the partial pressure curve. Where nitrogen is the adsorbate gas, equation 83 can be reduced by combining the Avogadro Number, the cross-sectional molecular area and the molecular weight of nitrogen into a single constant;

$$S_t = X_M(3.483 \times 10^3) \quad (84)$$

The specific surface area, S_s, was determined from the total surface area S_t using the known sample weight, W_Q:

$$S_s = S_t/W_Q \quad (85)$$

3.2.5 Powder Flow Determinations

The flow rates of different excipient powders were measured using a tableting machine hopper as described in Section 2.2.2.1. The flow rates were calculated as the mean of four separate determinations.

3.2.6 Particle Friability Measurements

The friability of granular materials is a measure of abrasion resistance and powder strength. High particle friability can result in a powder developing poor flow properties, poor tablet weight uniformity and unsatisfactory compression properties. The "universal" friability test for tablet granules described by Rubenstein and Musikabhumna (220), was modified for measurements on Dipac, Emdex and lactose spherulites. A 10 g sample of powder was placed on a nest of eight test sieves which was vibrated on a mechanical sieve shaker for 5 minutes. The fraction retained on each sieve was weighed and a graph of cumulative percentage oversize material was plotted against sieve diameter. The mass median diameter of the powders was then determined. The procedure was repeated three

times on replicate samples and the mean mass median diameter was calculated. A fresh 10 g sample of powder was introduced into a Roche Friabulator (J. A. Engelsmann, Ludwigshafen, W. Germany) together with five polyethylene balls of 19 mm diameter, and the apparatus was rotated at constant speed for 10 minutes. A sieve analysis of the friabilated powder was carried out and the mean mass median diameter was again calculated. The friabilation procedure was then repeated on a new sample using ten polyethylene balls.

The friability index, Φ, was determined from the ratio of mean mass median diameters of the particle size distributions before friabilation, μ, and after friabilation, μ_f.

$$\Phi = \mu_f/\mu \cdot 100\% \qquad (86)$$

The less friable, or harder, the powder analysed, the higher the friability index.

3.2.7 Moisture Content Determinations

The moisture content of powders can affect their compressibility, flow characteristics and may also influence the formation of ordered mixes.

The moisture content of the excipient powders was determined using an infra-red moisture balance (Sauter Inframatic, Ebingen, W. Germany). The powders were dried to constant weight and the corresponding percentage moisture content was read directly from the balance.

3.2.8 Scanning Electron Microscopy

The methods used for specimen preparation were the same as those described in Section 2.2.6. The specimens were examined using a Pye Model 150 a stereoelectronmicroscope (Pye Ltd., Cambridge U.K.) with zoom lens control.

3.3 Results and Discussion

3.3.1 Particle Density and Bulk Density

The poured and consolidated bulk densities and the equivalent Hausner ratios and percent compressibilities are shown in Table 15, along with the corresponding true densities of the different excipient powders.

Table 15

True and bulk densities of different direct compression tableting excipients

Sample	Bulk density determinations				True density ($g.ml^{-1}$)
	Poured density ($g.ml^{-1}$)	Consolidated density ($g.ml^{-1}$)	Hausner Ratio	Percent Compress-ibility	
Dipac	0.69	0.75	1.09	8.00	1.24
Elcema G250	0.34	0.43	1.26	20.93	1.04
Emdex	0.68	0.72	1.06	5.56	1.24
Lactose 710 - 1000 µm	0.44	0.49	1.11	10.20	0.63
500 - 710 µm	0.33	0.38	1.15	13.16	N/A
250 - 500 µm	0.39	0.48	1.23	18.75	0.46
180 - 250 µm	0.27	0.40	1.48	32.50	0.26
90 - 180 µm	0.25	0.40	1.60	37.50	0.48
<90 µm	0.23	0.39	1.70	41.03	0.26

The Emdex and Dipac excipient powders had higher bulk and true densities than the lactose excipient samples, whereas the Elcema G250 had comparable bulk densities with the 250 - 500 µm particle size lactose powder. The Hausner ratio and percent compressibility of Dipac and Emdex were comparable with those of the larger particle sizes of

lactose excipient, but the percent compressibility of Elcema G250 was high and comparable with "mid-particle-size" ranges of lactose. The bulk densities and true densities of lactose excipient powders decreased with decreasing particle size and the Hausner ratios and percent compressibilities showed a corresponding increase as a result of increasing interparticle cohesion in the finer powders. The fall in bulk densities resulted from altered packing properties whereas the fall in true densities was probably caused by large quantities of blind pores but may be due to the presence of extremely narrow pores with entrances too small to be penetrated by mercury even at high applied pressures.

The values for the different bulk density determinations showed that the recrystallised lactose particles had packing properties comparable with those of the commercial excipients tested, down to a particle size of 250 µm. Below this diameter, the lactose powders had an increased interparticle cohesion which would prevent uniform flow and impede die filling during tableting. The larger particle sizes of lactose with diameters above 250 µm had improved packing properties which would make them suitable for processing as free-flowing direct compression excipients.

3.3.2 Particle Size Distributions

The particle size distributions of the four excipients were determined. Table 16 shows the cumulative percentage oversize material at each sieve diameter. Emdex and Dipac had particle size distributions in which nearly 50% of the particles by weight had diameters between 250 µm and 500 µm. The lactose spherulites had a bimodal size distribution, caused by size reduction of crystal agglomerates larger than 1000 µm diameter.

Table 16

Particle size distributions of excipient powders by sieve analysis

Sieve Diam. (μm)	Cumulative percentage oversize by weight			
	Elcema G250	Emdex	Dipac	Lactose spherulites
710		0.46	0	16.04
500	0	8.06	0.03	23.71
355		25.56		28.34
250	26.734	54.51	46.96	29.22
180	91.174	78.04	74.29	34.24
125	99.244		95.52	
90	99.270	97.23	99.43	55.65
63	99.289	99.16	99.72	73.11
45	99.306		99.81	
0	0	100	100	100

Lactose contained the largest proportion of particles in the range 355 - 710 μm.

3.3.3 Pore Size Distributions

The pore size distributions of Emdex, Elcema G250 and Dipac along with three particle size ranges of lactose spherulites were determined as described in Section 2.3.4.2 (Figure 50). The pore size distributions of all the powders included both interparticle voids and intraparticle pores. The excipient powder with the highest total bed porosity was Elcema G250, followed by the 250 - 500 μm particle size fraction of lactose and then Emdex. The powders with the lowest total porosities included the 500 - 710 μm particle size fraction of lactose, Dipac and the lactose

Figure 50. Pore size distributions of various direct compression tableting excipients.

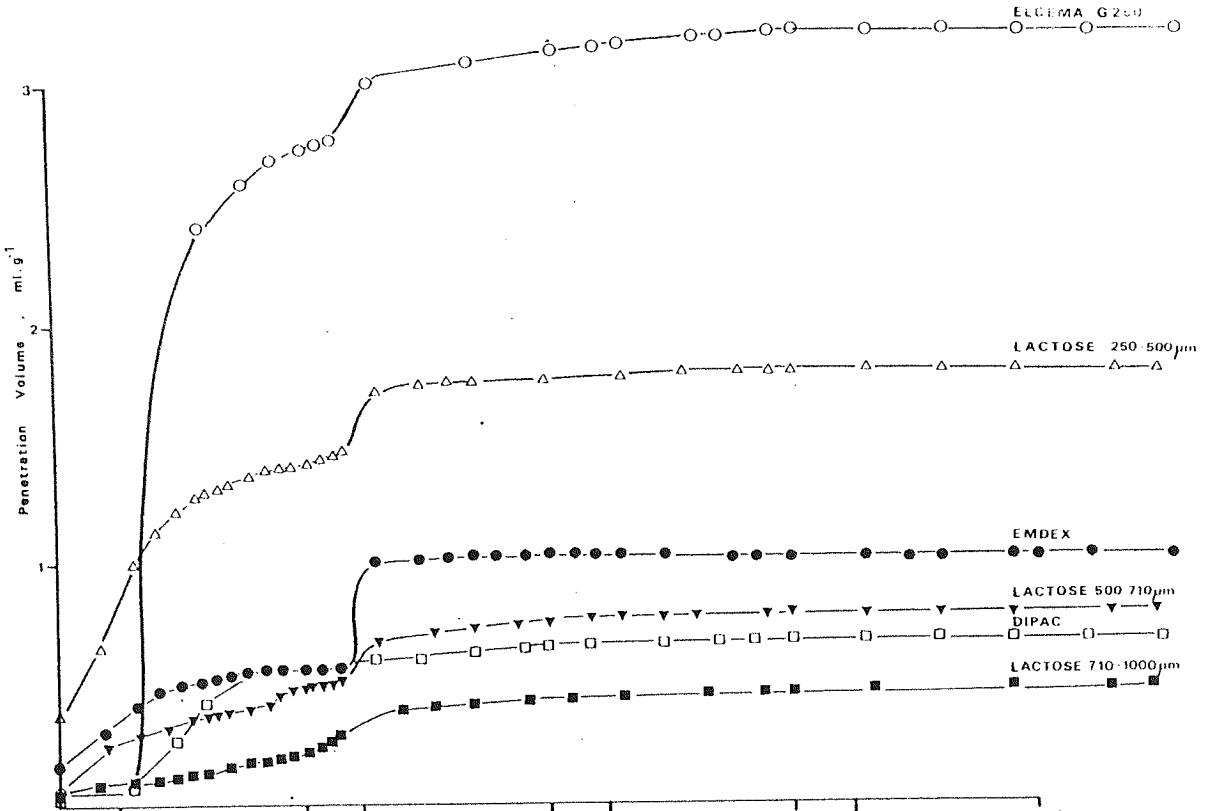

powder of highest particle size (710 - 1000 μm). However, the porosities of the two lactose powders with large particle sizes were essentially measures of interparticle pores alone, since both these size ranges contained voids too large to be determined by mercury porosimetry since the pore size distribution contained no large vertical rise. The Emdex, Elcema G250 and Dipac powders had minimum interparticle void diameters of about 13 - 14 μm. Above this diameter, the mercury only penetrated interparticle void spaces, whereas below this size the intraparticle pores were filled. The 250 - 500 μm lactose fraction had a minimum interparticle void diameter comparable with those of the three commercial excipients.

Although Elcema G250 had the highest total bed porosity, it had a lower proportion of intraparticle pores. Table 17 shows the intraparticle pore volumes of the three commercial excipients and of the different particle size fractions of lactose spherulites.

Figure 51 a, b, shows the distribution of the intraparticle pore volumes listed in Table 17, at different applied pressures. The fairly porous excipients, Emdex and Elcema G250 were found to

Table 17

Intraparticle pore volumes of tableting excipient powders

Excipient	Pore Volume ($ml.g^{-1}$)
Dipac	0.1012
Elcema G250	0.5204
Emdex	0.6401
Lactose 710 - 1000 μm	0.4785
500 - 710 μm	0.7990
250 - 500 μm	1.2473

Figure 51a. Pore volume distributions of three commercial excipients

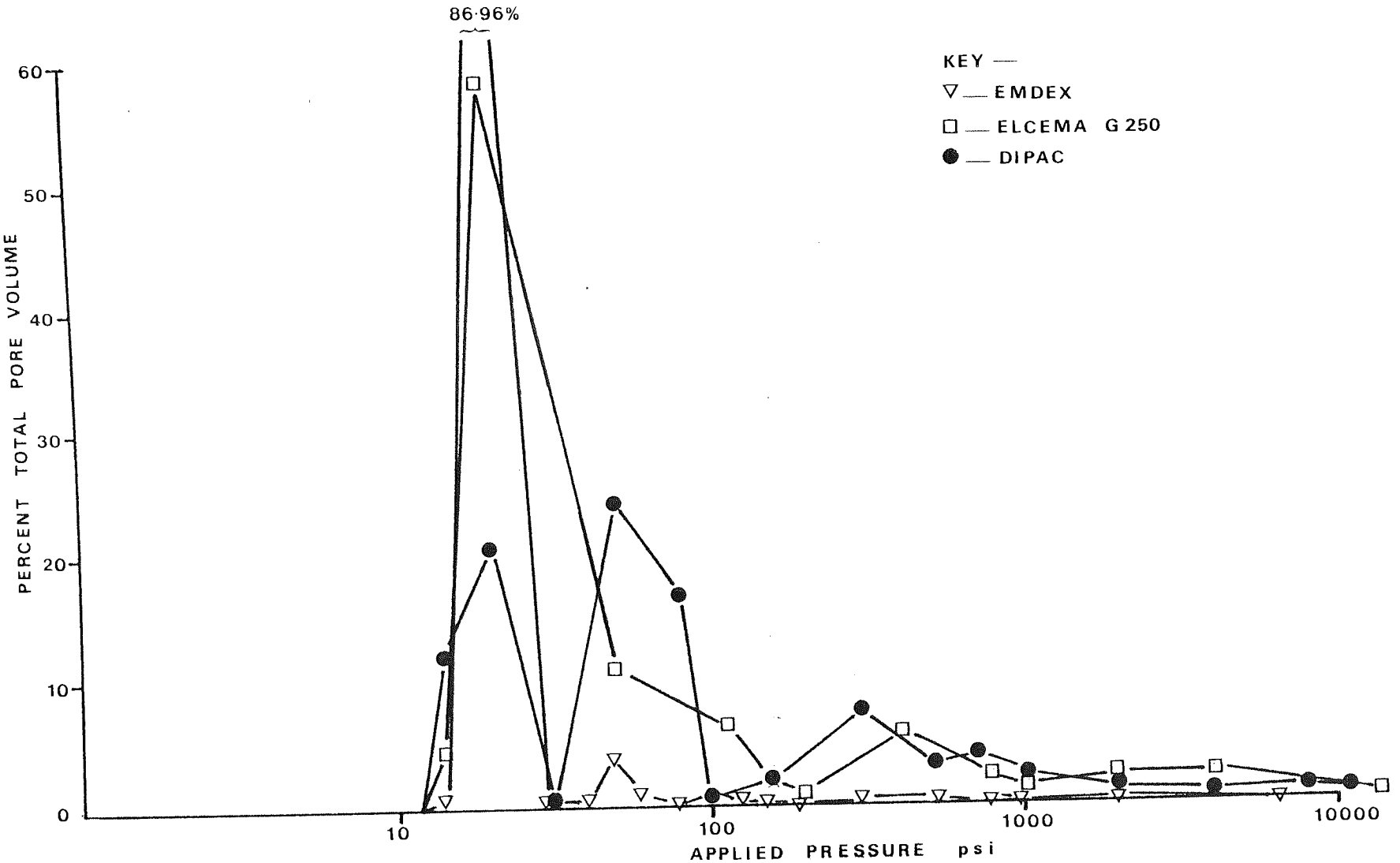

Figure 51b. Pore volume distributions of three different particle-size ranges of lactose excipients

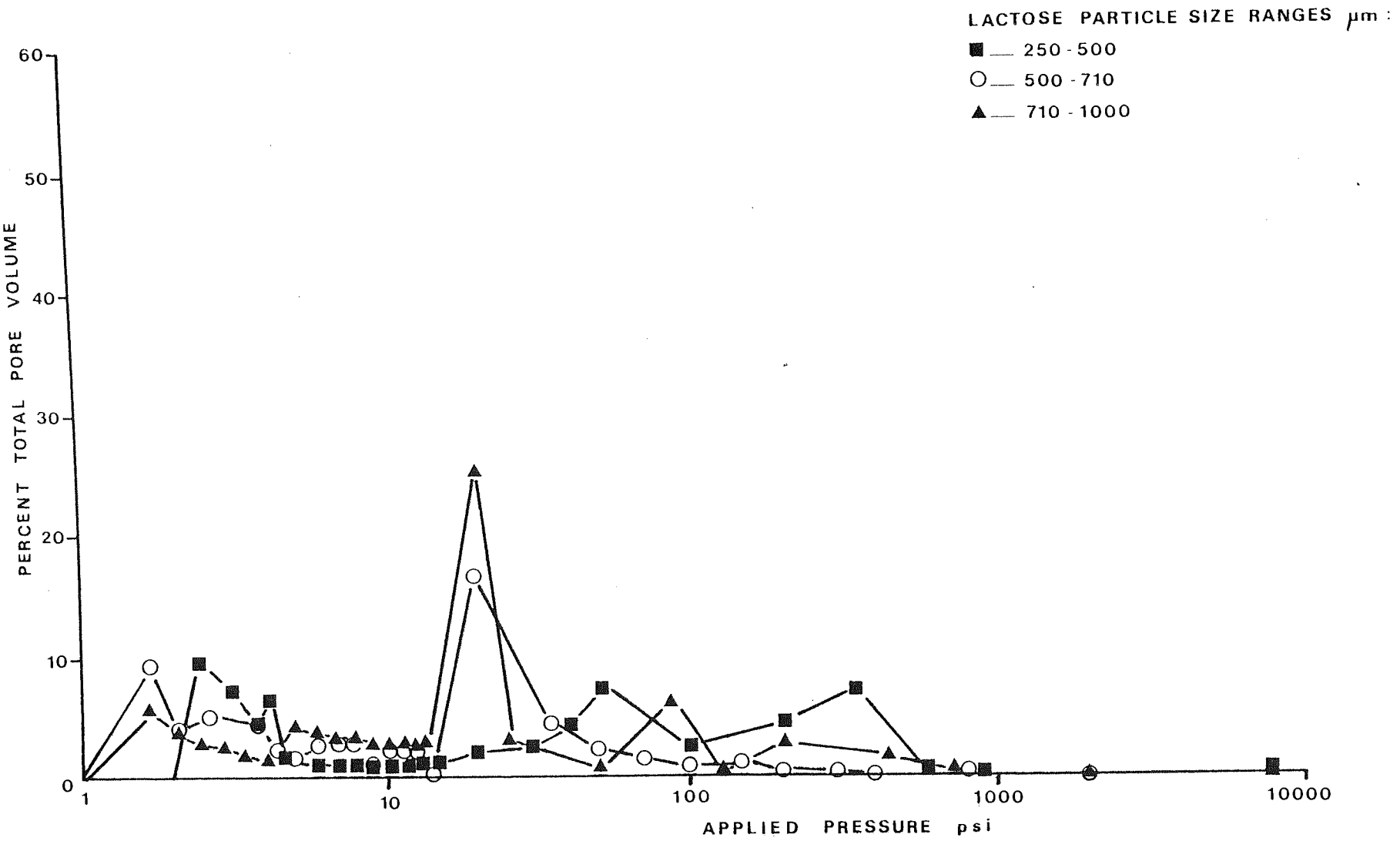

have narrow pore volume distributions. Although the 250 - 500 μm particle size lactose excipient had a very high pore volume (Figure 51 b), this was distributed over a wide pore size range. The Dipac excipient powder had a very low porosity (both void and intraparticle pore volumes) with a virtually bimodal distribution.

The interparticle voids represent the gaps between particles in a powder bed and the void dimensions depend upon the geometry of particle packing. Intraparticle pores are the spaces lying within the projected outline of the particle. The intraparticle pore sizes of an excipient particle may be important in the formation of adherence sites for fine particles in an ordered powder mix. The interparticle voids can also influence the stability of an ordered mix; a powder bed with large voids may be more susceptible to downward movement of dislodged fine particles by spontaneous percolation between the void spaces separating particles. A desirable combination for an ordered mix excipient is high intraparticle porosity and low interparticle void volume. The various particle sizes of lactose spherulites and the Emdex excipient exhibit the property of maximum intraparticle porosity combined with minimum interparticle void volume. The Dipac excipient has a low void volume but it also has a low pore volume and the Elcema G250 excipient powder has a large pore volume but this is combined with a very high interparticle void volume.

3.3.4 Powder Surface Area

3.3.4.1 Nitrogen Adsorption Determinations

The surface areas of Dipac and Emdex were compared with those of the different size ranges of recrystallised lactose excipient using the multipoint B.E.T. method. The specific

surface areas of the different excipient powders are shown in Table 19.

Table 19

The surface areas of different excipient powders determined using the Quantasorb analyser

Excipient	Surface Area $cm^2.g^{-1}$
Dipac	1,780
Emdex	1,170
Lactose 710 - 1000 µm	8,300
500 - 710 µm	5,200
250 - 500 µm	5,600
180 - 250 µm	5,400
90 - 180 µm	4,000
<90 µm	3,600

All of the lactose powder fractions had a much higher specific surface area than either of the two commercial excipients. This is almost certainly explained by the increased porosity and surface rugosity of the lactose excipients.

3.3.4.1.1 Powder Rugosity

The surface roughness or rugosity of the different excipient powders was calculated from the surface area determinations described in Section 3.3.4.1 using the method previously set out in Section 2.3.5.1.1. The different powder rugosities are shown in Table 20. The two commercial excipients had smooth surfaces compared with the larger particle size ranges of recrystallised lactose excipient.

Table 20

Rugosities of Dipac, Emdex and six different particle size ranges of lactose excipient

Excipient	Rugosity
Dipac	5.56
Emdex	3.35
Lactose 710 - 1000 µm	31.94
500 - 710 µm	24.83
250 - 500 µm	14.61
180 - 250 µm	5.20
90 - 180 µm	5.30
<90 µm	1.34

3.3.4.2 Mercury porosimetry determinations

The "accessible surface areas" of the different excipients were calculated on the basis of mercury porosimetry data as described in Section 2.3.5.2. The surface areas accessible to particles above 2 µm diameter and to those above 10 µm diameter are shown in Table 21. These data indicate that the lactose spherulites, particularly those particles in the range 180 - 500 µm have a much larger pore surface area accessible to fine particles with diameters above 2 µm than the commercial excipients; Dipac, Elcema and Emdex. All the lactose spherulites in the size range 90 - 1000 µm had surface areas accessible to fine particles with diameters larger than 10 µm, whereas the three commercial excipients had no pore surface area in this range. The increased accessible surface areas of the lactose spherulites indicate that these carrier particles could form more active adherence sites for fine particles in ordered mixes than Emdex, Dipac or Elcema G250 particles.

Table 21

Accessible surface areas of three commercial direct compression tableting excipients and six different particle size ranges of lactose spherulites

Excipient	Surface areas accessible to adhering particles with diameters: >2 μm($cm^2.g^{-1}$)	>10 μm($cm^2.g^{-1}$)
Dipac	817	No pores in this range
Elcema G250	2,241	"
Emdex	1,985	"
Lactose 710 - 1000 μm	1,795	399
500 - 710 μm	1,829	1,083
250 - 500 μm	4,848	583
180 - 250 μm	6,649	1,226
90 - 180 μm	3,203	424
0 - 90 μm	2,198	No pores in this range

3.3.5 Powder Flow

The flow rates of different excipient powders were measured using a tableting machine hopper. The flow rates were calculated as the mean of four separate determinations (Table 22).

Dipac and Emdex powders had the fastest flow rates but even Elcema G250 powder and lactose spherulites in the size fraction 250 - 500 μm where the rate was slower, the powder exhibited uniform flow. In lactose size fractions below 250 μm, there was no flow. These results indicated that lactose spherulites with diameters larger than 250 μm had flow properties which were comparable with those of the three free-flowing commercial direct compression excipients.

Table 22

The flow rates of different excipient powders

Excipient	Flow Rate ($g.s^{-1}$)
Dipac	164.8
Elcema G250	29.5
Emdex	164.0
Lactose bulk	15.3
Lactose 710 - 1000 µm	96.4
500 - 710 µm	72.6
250 - 500 µm	32
180 - 250 µm	No flow
90 - 180 µm	No flow
<90 µm	No flow

3.3.6 Particle Friability

The friabilities of the different excipients were determined and the friability indices are shown in Table 23. The higher the index, Φ, the lower the amount of particle attrition. The two lactose powders tested both had lower friability indices than either of the two commercial excipients. Emdex showed no measurable attrition at the mass median diameter, and therefore had a friability index, $\Phi = 100$.

Figure 52 a, b, c, d shows the particle size distributions before and after friabilation for different excipient powders. The only powder which was not abraded by the friabilation process using either 5 or 10 balls was Emdex. The two size fractions of lactose spherulites tested were more friable than either Emdex or Dipac and this is probably due to the large numbers of fine

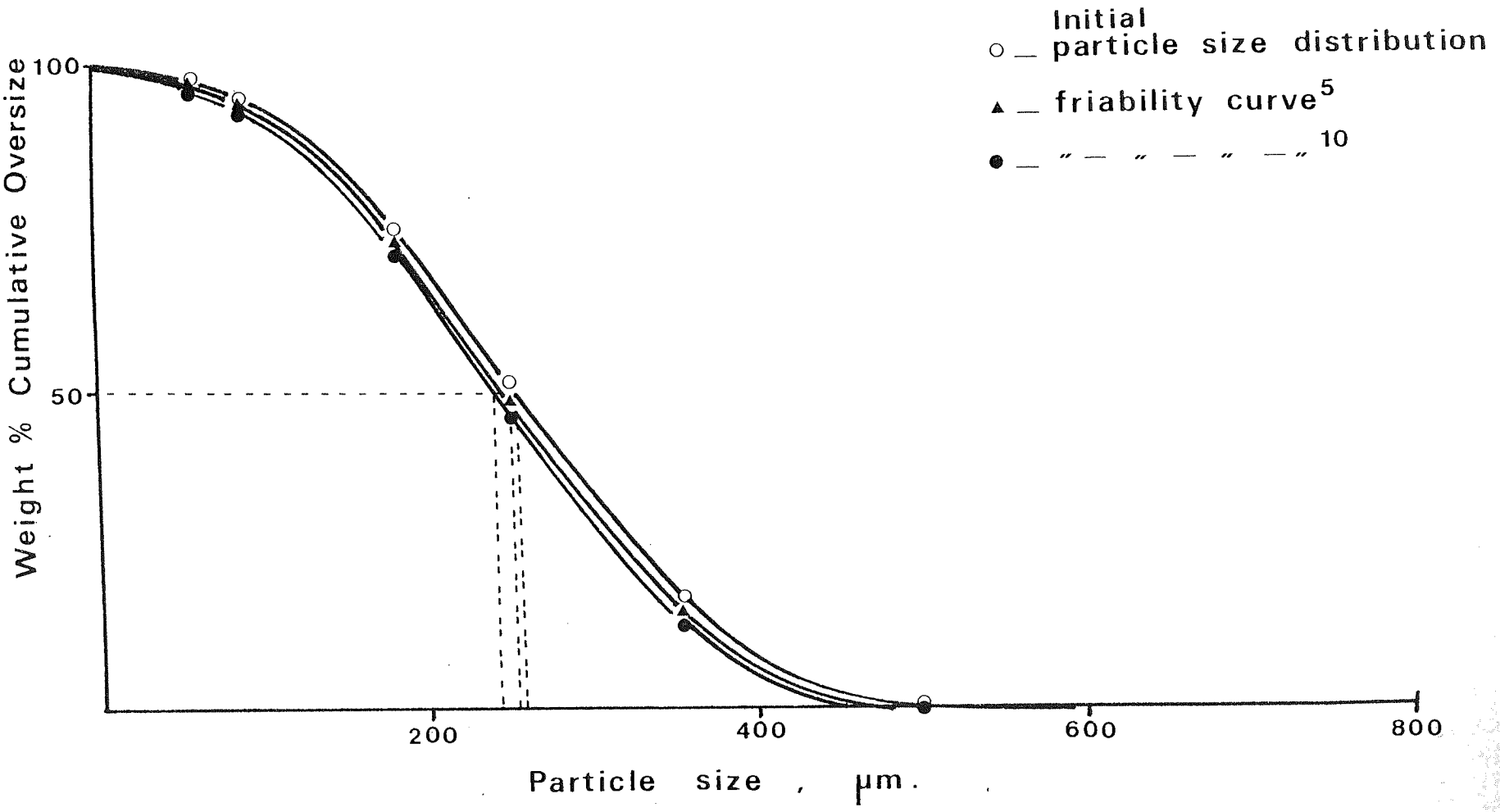

Figure 52a. Relationship between particle size distributions of Dipac powder before and after friabilation with 5 and 10 balls

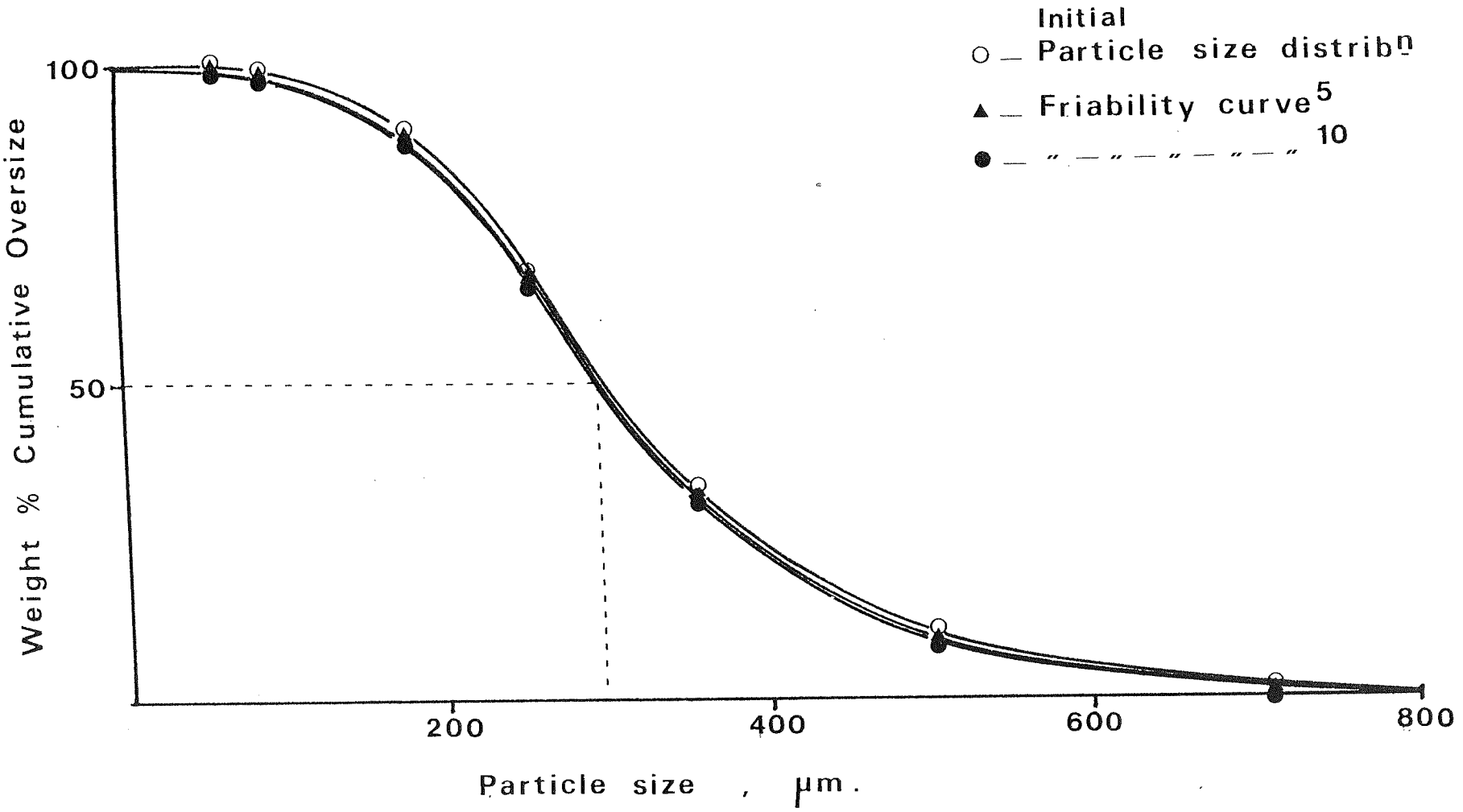

Figure 52b. Relationship between particle size distributions of Emdex powder before and after friabilation with 5 and 10 balls

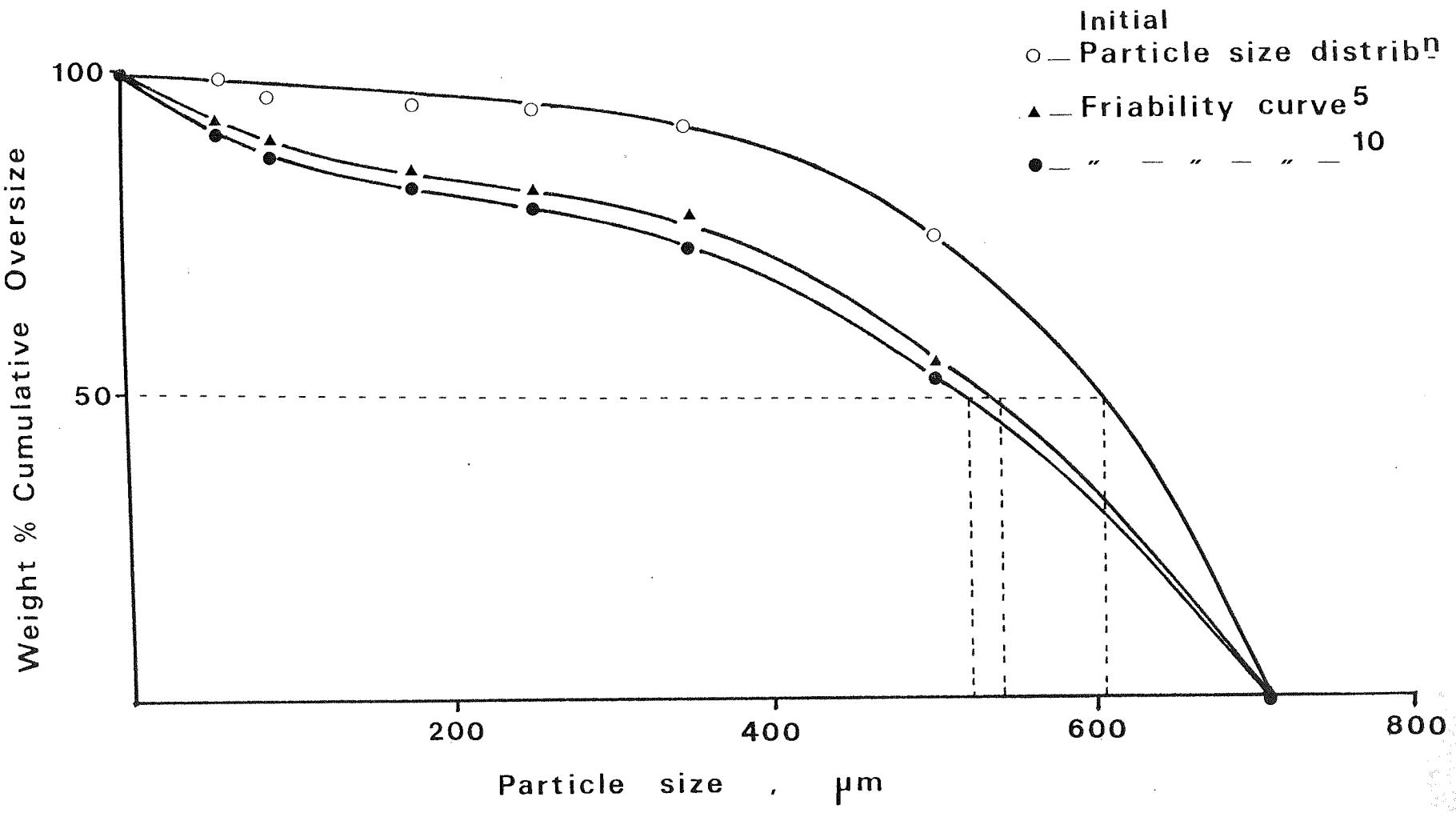

Figure 52c. Relationship between particle size distributions of lactose spherulites (500 - 710 µm) before and after friabilation with 5 and 10 balls

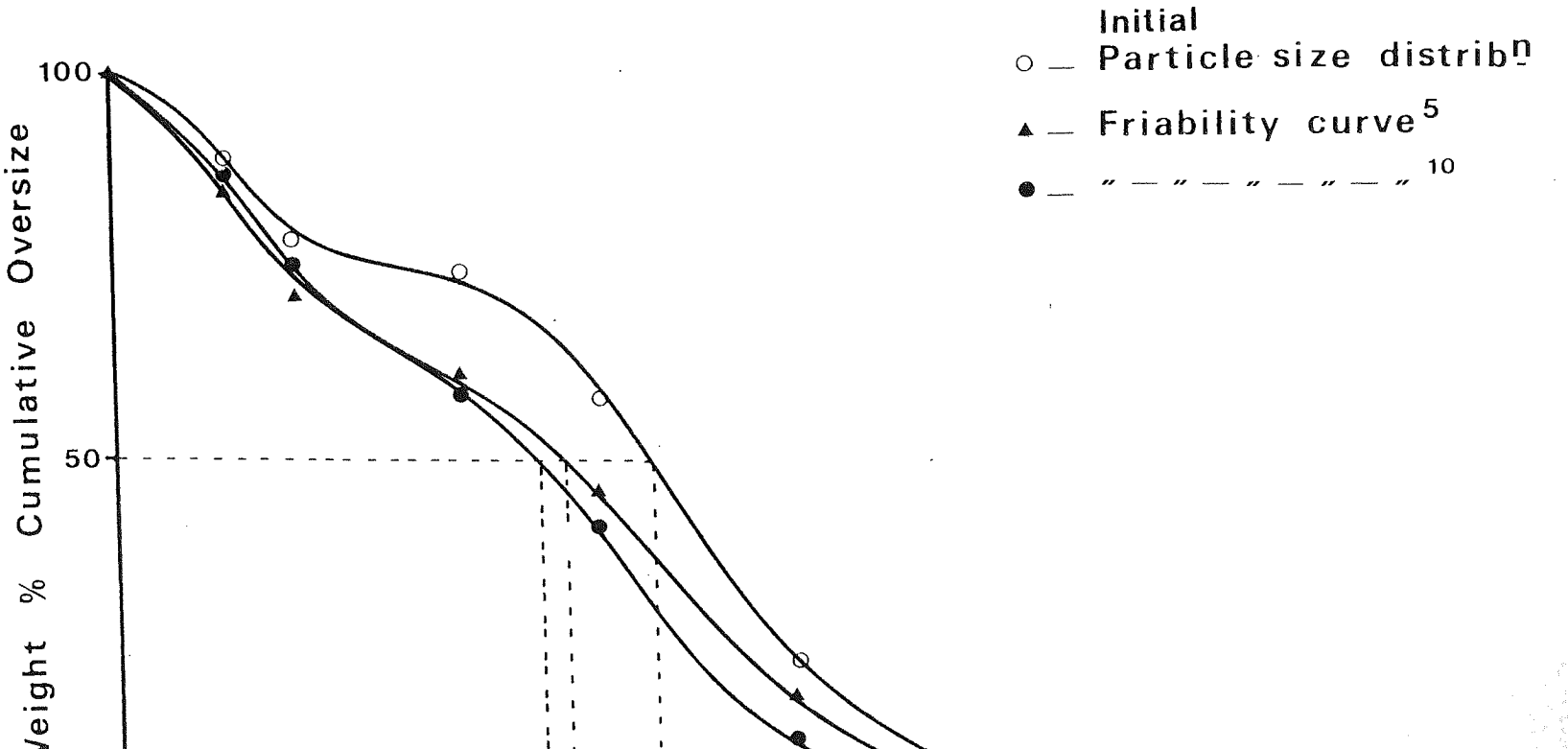

Figure 52d. Relationship between particle size distributions of lactose spherulites (250 - 500 µm) before and after friabilation with 5 and 10 balls

Table 23

Friability indices (Φ) of different excipient powders friabilated with different numbers of balls (5 and 10)

Excipient	$\Phi_{5\ BALLS}$	$\Phi_{10\ BALLS}$
Dipac	96.92	91.73
Emdex	100	100
Lactose 500 - 710 µm	90.91	88.81
250 - 500 µm	84.06	79.71

dendrites on the lactose surface which were abraded by the friabilation process. With the exception of Emdex the powders were abraded more by friabilation with 10 balls than with 5 balls.

3.3.7 Moisture Content

The moisture content of the different powders was calculated as the loss in weight on drying expressed as a percentage of the initial sample weight. Table 24 shows the different moisture contents of the various excipient powders tested.

Table 24

Moisture content of different excipient powders

Excipient	Loss on drying (%)
Dipac	0.1
Elcema G250	3.5
Emdex	6.1
Lactose spherulites (ungraded)	0.1
Lactose 250 - 500 µm	0.1

3.3.8 Scanning Electron Microscopy

Scanning electron photomicrographs were taken of specimens from each of the excipient powders. Figure 53 shows the differences in shape and surface of the various excipients.

The lactose spherulite appears to have the roughest surface of the four excipient powders. The particle of Emdex is virtually spherical but the surface is very porous. Dipac appears to have the smoothest and least porous surface.

Figure 53. Scanning electron photomicrographs of four different excipient powder particles.

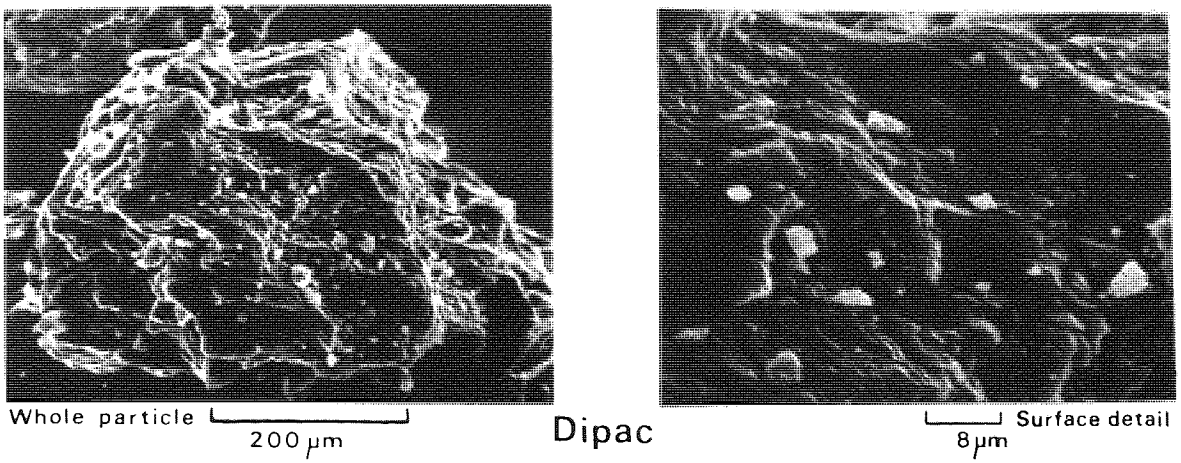

Dipac

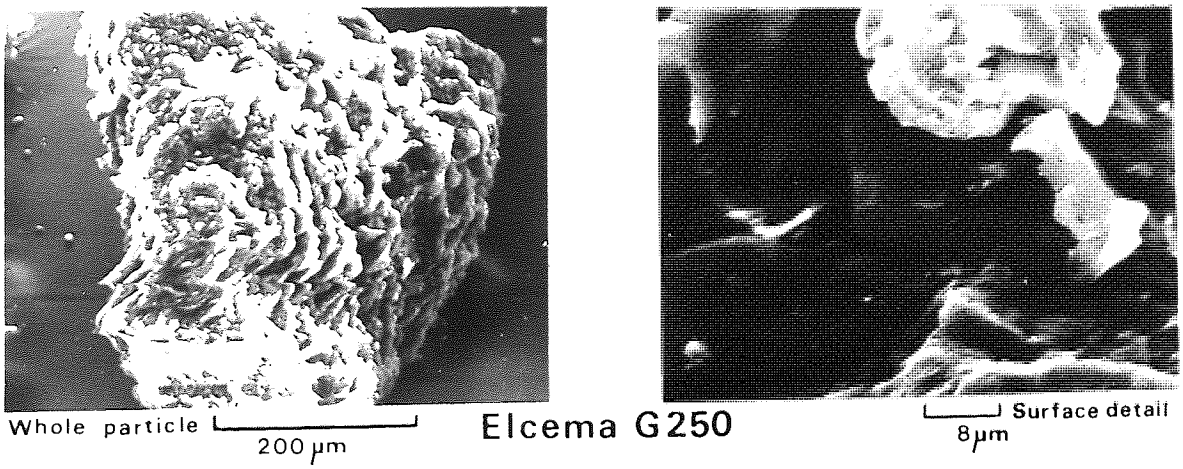

Elcema G250

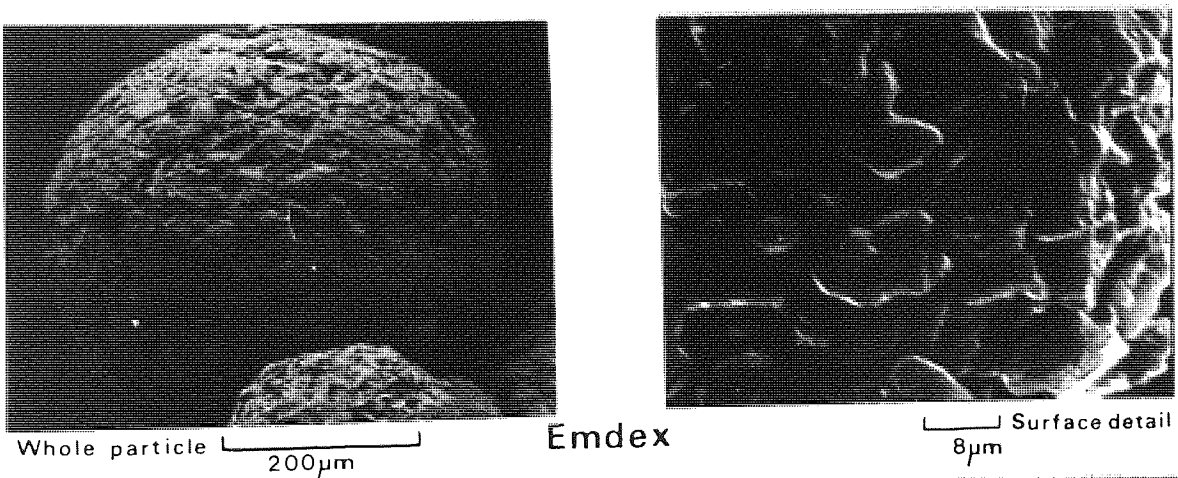

Emdex

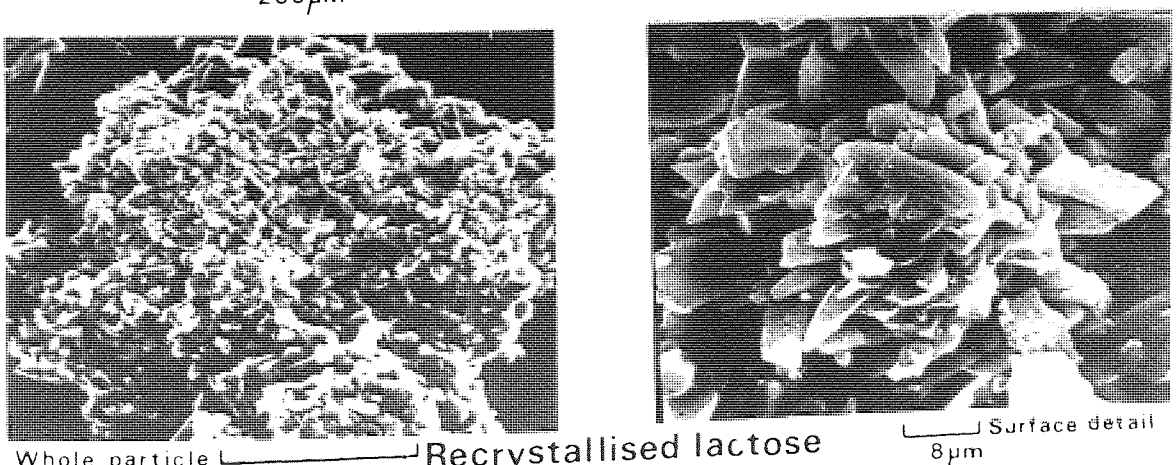

Recrystallised lactose

Chapter 4

Vibrational Segregation of Ordered Powder Mixes

4.1 Preparation of Perfect Ordered Mixes

Ordered mixes of different free-flowing direct compression excipients were made with either fine-particle potassium sorbate or fine-particle potassium chloride used as model drugs. Each excipient was pre-blended with 0.5% fine particle drug, less than 45 μm diameter, by serial dilution to break down any drug agglomerates and to disperse the drug particles throughout the excipient system. The pre-blend of 0.5% w/w drug and excipient powder was then mixed with the remainder of the powders in a Y-cone blender (Erweka A.G., Frankfurt, W. Germany). The mixed powders were filled into a sampling cylinder described in detail later and twenty samples with scales of scrutiny ranging from 200 mg to 1000 mg were analysed. Powder mixes containing the model drug potassium sorbate were analysed by ultraviolet spectrophotometry (Pye Unicam, SP500, Cambridge, U.K.) at the wavelength of maximum U.V. absorbance, 264 nm. Over the potassium sorbate concentration range analysed the U.V. absorbance was directly proportional to potassium sorbate concentration showing recti-linear compliance with the Beer-Lambert relationship. The powder mixes containing excipient and drug particles were dissolved in 0.01 molar hydrochloric acid (Concentrated Volumetric Solutions, BDH Ltd., Poole, U.K.) and diluted to produce an absorbance between zero and one. Powder mixes containing the excipient Elcema G250 were dispersed in 0.01 molar hydrochloric acid and the insoluble Elcema particles were removed by filtration using a microfilter (Millipore, N.Y., U.S.A.) attached to a syringe.

Powder mixes containing the model drug potassium chloride were analysed using conductivity measurements with an autobalance universal bridge (Model B642, Wayne Kerr Ltd., New Malden, U.K.). A calibration curve prepared over a wide range of known potassium chloride concentrations showed a linear relationship between solution conductance and drug concentration in the required range. Samples of drug and excipient were removed from the mixes and dissolved in de-ionised water. The containers were placed in a constant temperature water bath and a conductance cell consisting of two platinum electrodes separated by a constant distance was immersed in the solution. The electrical conductance (reciprocal resistance) between the electrodes, which is influenced by the concentration of potassium chloride electrolyte, was measured using the universal conductance bridge. The use of a conductance bridge to measure concentrations of ionic drug solutions had the advantage that dilution of solutions was unnecessary because of the instruments extremely wide measuring range. Any errors introduced by multiple dilutions were therefore removed using this method. The drug concentrations of twenty samples were used to calculate the coefficient of variation as an assessment of the statistical variance of the mix.

4.1.1 Theoretical Variance of Powder Mixes

Johnson (42, 91, 93, 94) and others (41, 92, 106, 133) have used the coefficient of variation of samples removed from a powder mix to assess the homogeneity. The coefficient of variation is calculated from measurements of the standard deviation of several samples and the sample mean. The use of the mean as a denominator has a standardising effect for comparison of powders with different

theoretical mean drug concentrations. Johnson developed a relationship for calculating the theoretical coefficient of variation of samples containing less than 1% drug (42):

$$C_V = 100 \left(\frac{\pi.\rho}{6.6}\right)^{\frac{1}{2}}.(\Sigma f d^3)^{\frac{1}{2}} \qquad (61)$$

Applying this formula to the mixes used in this study containing potassium sorbate the powders would have a theoretical homogeneity described by a coefficient of variation of 0.11%. Ideally mixed powders containing potassium chloride would have a theoretical coefficient of variation of 0.35%.

Using the specification index, σ_A, described by Hersey (181) it was possible to calculate the mixture homogeneity required to produce mixes within pharmacopoeial standards. The minimum coefficient of variation for an acceptable powder mix was calculated for each drug according to a dose variation of $\pm$10% such as that required by the B.P. for several microdose drugs (Table 2). The specification coefficient of variation of the powder mixes containing potassium sorbate is therefore required to be less than 2.22% in order for the mix to comply with the pharmacopoeial standards. The pharmacopoeial specification for mixes containing potassium chloride required a coefficient of variation less than 2.78%.

Hersey (180) used the difference between the specification variance of a mix and the theoretical variance of a perfect mix to assess the ease of mixing, which he called the mixing margin. A wide difference between the two variances indicated that the mixing operation would produce a homogeneous system with maximum efficiency, whereas identical theoretical and specification variances indicated a potentially difficult mixing process. In systems where the specification index was less than the theoretical

variance, mixing could in theory never produce powders with the required pharmacopoeial homogeneity. In this investigation, for powder mixes containing the model drugs potassium sorbate and potassium chloride, the specification coefficients of variation were considerably larger than the theoretical coefficients of variation. All the powders were mixed so that they had coefficients of variation less than 2%, and could therefore be considered to have reached an acceptably high degree of homogeneity in terms of pharmacopoeial requirements.

4.1.2 Formation of Ordered Mixes

In addition to producing mixes with the required homogeneity it was also considered desirable to form ordered mixes of the drug and excipient powders so that the stability of such systems could be assessed. Yip and Hersey (72) took samples of different sizes to demonstrate the formation of ordered mixes. In theory, an ordered mix should have a constant, very low, standard deviation regardless of sample size, whereas powder mixes produced by randomisation show a reduction in standard deviation with increasing sample size. Different sample sizes ranging from 200 mg to more than 1 g were removed from mixes containing potassium sorbate and the various excipient powders. The sample standard deviation was in all cases found to be very low and did not change with an alteration in sample size. According to the model of Yip and Hersey an ordered mix had been formed between the two sets of constituent particles. However, as Orr (75) demonstrated, the variances of ordered powder mixes can be of the same magnitude as the error variances and therefore should not be used alone to confirm the formation of an ordered mix.

In addition to measuring the variance of drug concentration in different sample sizes, for systems used in this study, the location of drug particles in a mix was assessed directly using the technique of x-ray microanalysis (221, 222). X-ray microanalysis utilises the characteristic x-rays which are emitted by a specimen when irradiated with a finely focused electron beam in a scanning electron microscope. By comparing the normal electron photomicrograph with an x-ray image of the sample shown as a series of dots, it is possible to locate a specific element or compound in the specimen. Samples of the mixes of potassium sorbate and potassium chloride with excipient were analysed for the characteristic x-rays released from potassium ions.

The dot micrograph in Figure 54(b) shows the areas of the specimen surface which contain potassium ions. By comparing this distribution with the photomicrograph of the same part of the specimen produced by back-scattered electrons (Figure 54(a)), the areas of high potassium concentration can be located. The schematic diagram of the specimen (Figure 54(c)) is an interpretation of the two photomicrographs to distinguish those particles adhering to the surface of the carrier excipient which are in fact potassium sorbate from those which are adhering fine particles of excipient. X-ray microanalysis can also locate particles of drug not adhering to carrier particles. By careful examination of a representative powder specimen using x-ray microanalysis in the scanning electron microscope it was therefore possible to demonstrate the formation of ordered units of drug and excipient particles and also to show qualitatively the degree of ordering in a powder mix. Figure 55 shows the locations of fine potassium sorbate particles in mixes

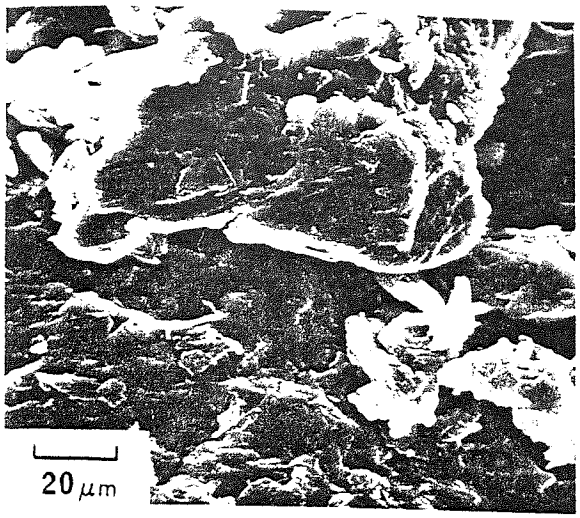

(a)

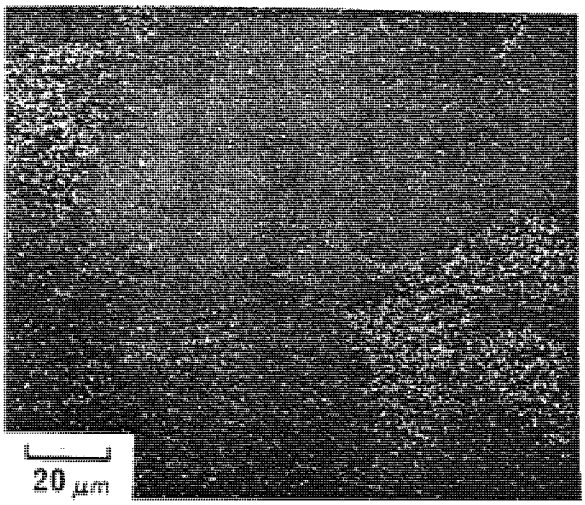

(b)

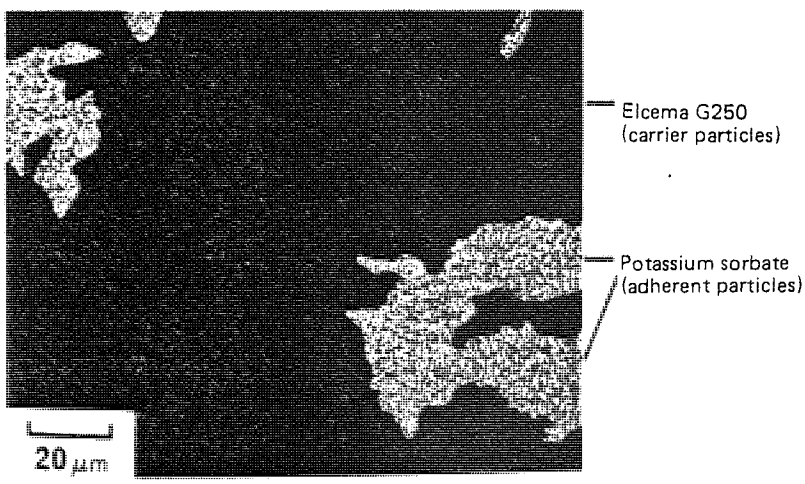

(c)

Fig.54 (a) Photomicrograph produced by backscattered electrons (magnification × 1K.) showing a sample of Elcema G250 with adherent particles. (b) Photomicrograph of the identical field of view of Elcema G250 produced by characteristic X-rays. The white dots correspond to areas of potassium sorbate. (c) Schematic interpretation of Fig.54(b), to differentiate between potassium sorbate particles and those of Elcema G250.

containing different excipient particles. The porous Elcema G250 acts as a carrier for several relatively large particles of potassium sorbate, shown as high dot concentrations of potassium in the x-ray micrograph of Figure 55(a). In contrast, the smoother Dipac particles carry only very fine particles of drug on their surface (Figure 55(b)). The particles of potassium sorbate adhering to the surface of Elcema G250 appear to be mainly located in pores or surface irregularities (Figures 54 and 55(a)). In the case of Dipac (Figure 55(b)) many of the adhering particles are apparently not potassium sorbate; some of these fine particles are small fragments of the carrier material. This confirms that in the absence of the corresponding x-ray micrograph, visual inspection of the photomicrograph produced by back-scattered electrons could lead to false conclusions regarding the detailed structure of an ordered mix. It was concluded that x-ray microanalysis could be used to determine the structure of a powder mix and in particular to demonstrate the formation of an ordered mix.

4.2 Powder Segregation in a Modified Jolting Volumeter

4.2.1 Method

A modified jolting volumeter was used as a vibrational segregation model. Elcema G250 and Dipac, two direct compression excipients which may produce segregation in powder mixes because of their large particle size and good flow properties, were mixed separately with 0.5% potassium sorbate particles of less than 45 μm diameter. Mixes with coefficents of variation less than 2% were filled into an open-ended brass cylinder (Figure 56) and the homogeneity was again measured. A P.T.F.E. plug was fitted at one end of the cylinder to provide a base for the powder bed. The

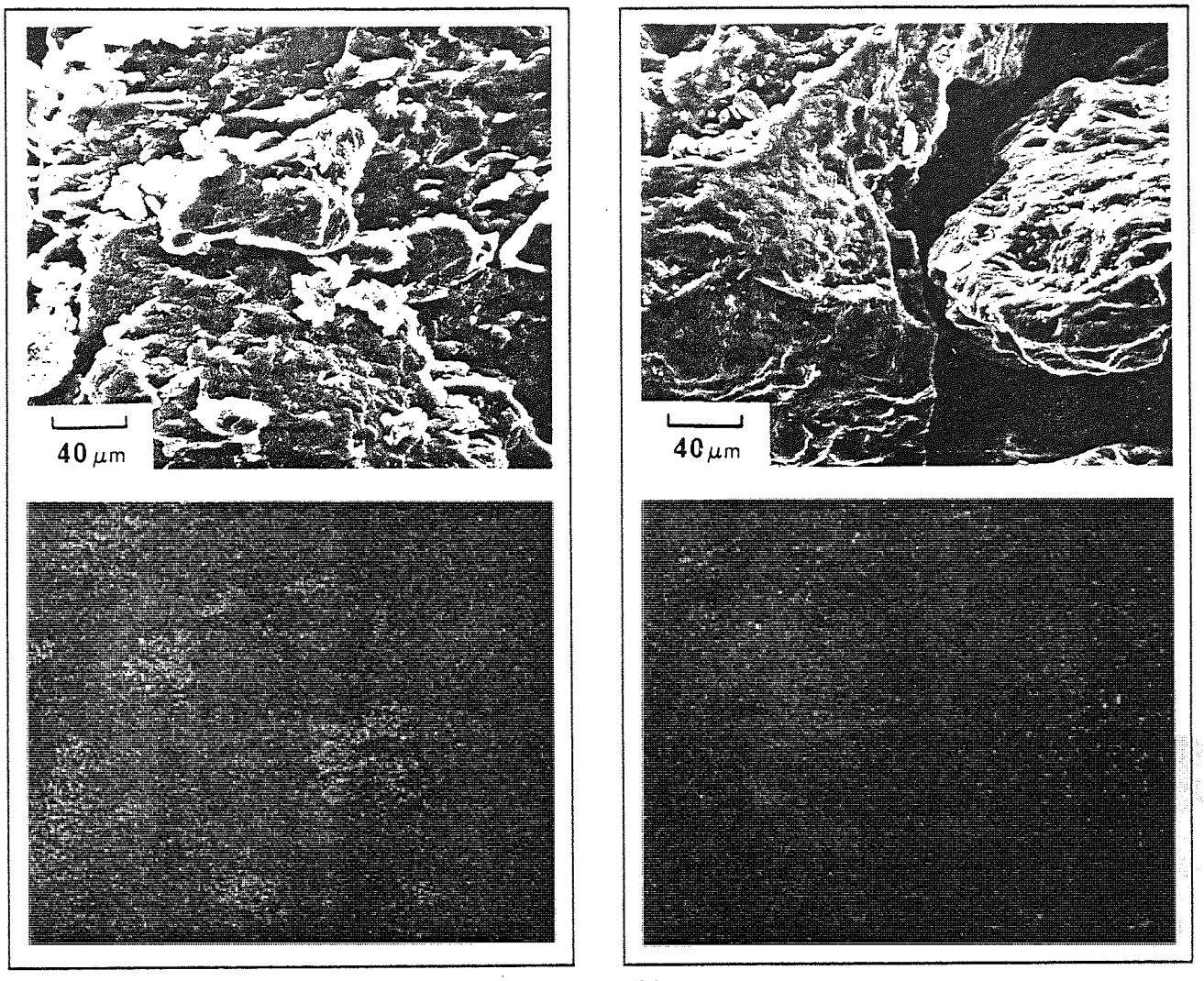

(a) (b)

Fig.55 Electron photomicrographs of (a) Elcema G250 and (b) Dipac with the corresponding photomicrographs produced by characteristic X-rays of potassium.

Figure 56.

Arrangement for securing the sample cylinder in the jolting volumeter.

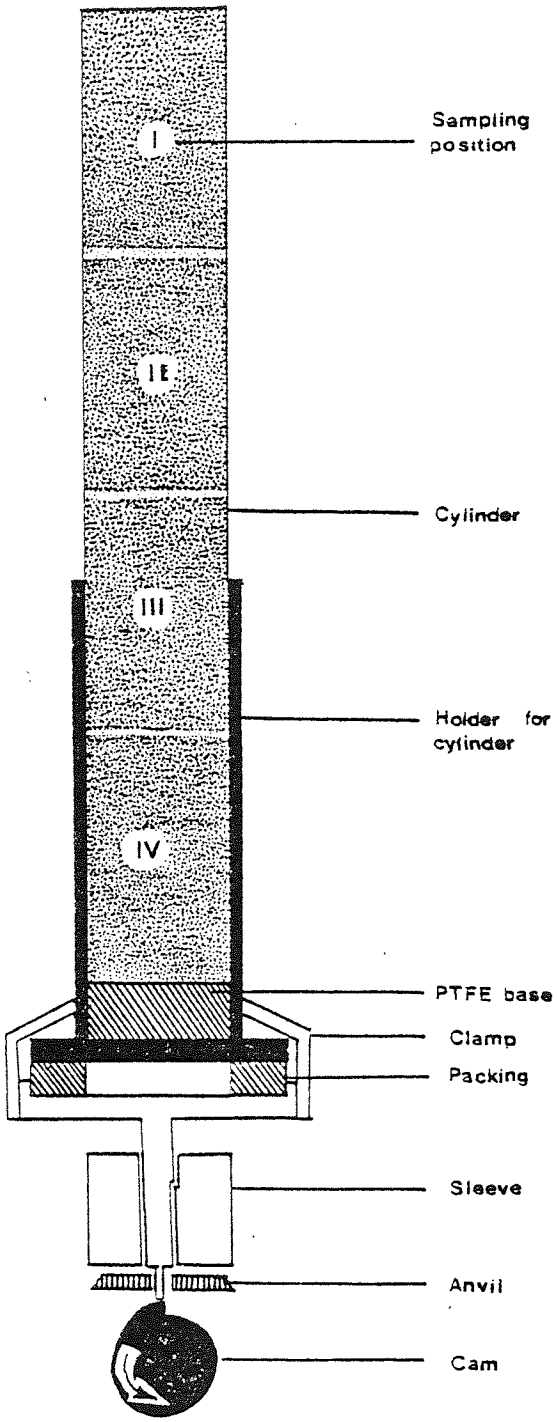

cylinder was filled with a fresh powder sample and located in the holder arrangement on the jolting volumeter, and the powder was then subjected to low frequency vibration of 4 Hz, saw-tooth waveform. This type of vibration was shown using mercury porosimetry to produce a non-dilating powder bed with interparticle void diameters between 10 and 100 μm which were generally smaller than the excipient particles, but large enough to allow any dislodged fine particles to move freely through the powder bed. After vibrating for 15,000 cycles, five powder samples were removed from each of four levels in the cylinder shown in Figure 56, zone I being at the top of the cylinder and zone IV at the base of the powder bed.

Samples were removed from the cylinder by forcing the P.T.F.E. plug up the cylinder until the powder level was just protruding above the top lip. A new powder surface was exposed by skimming off excess particles with a spatula. A 250 mg sample was taken across the whole central area of the exposed section. This sampling procedure was followed by formation of new sample areas until twenty samples had been removed and the cylinder was empty. Four replicate determinations were made for each experimental point. The samples were analysed for potassium sorbate using the U.V. spectrophotometric method described in the previous section, 4.1.

4.2.2 Results and Discussion

The coefficients of variation (CV%) of the vibrated powder mixes were compared with the theoretical coefficient of variation of a mixed system discussed in section 4.1.1 (Figure 57). The particles of potassium sorbate showed a greater tendency to segregate from particles of Dipac excipient than from Elcema G250. Since

Fig. 57
Mean coefficient of variation at different sampling positions, with 95% confidence limits for DiPac sugar ▨ and Elcema G250 □ ; X and Y are theoretical upper and lower 99% confidence limits for a random mix

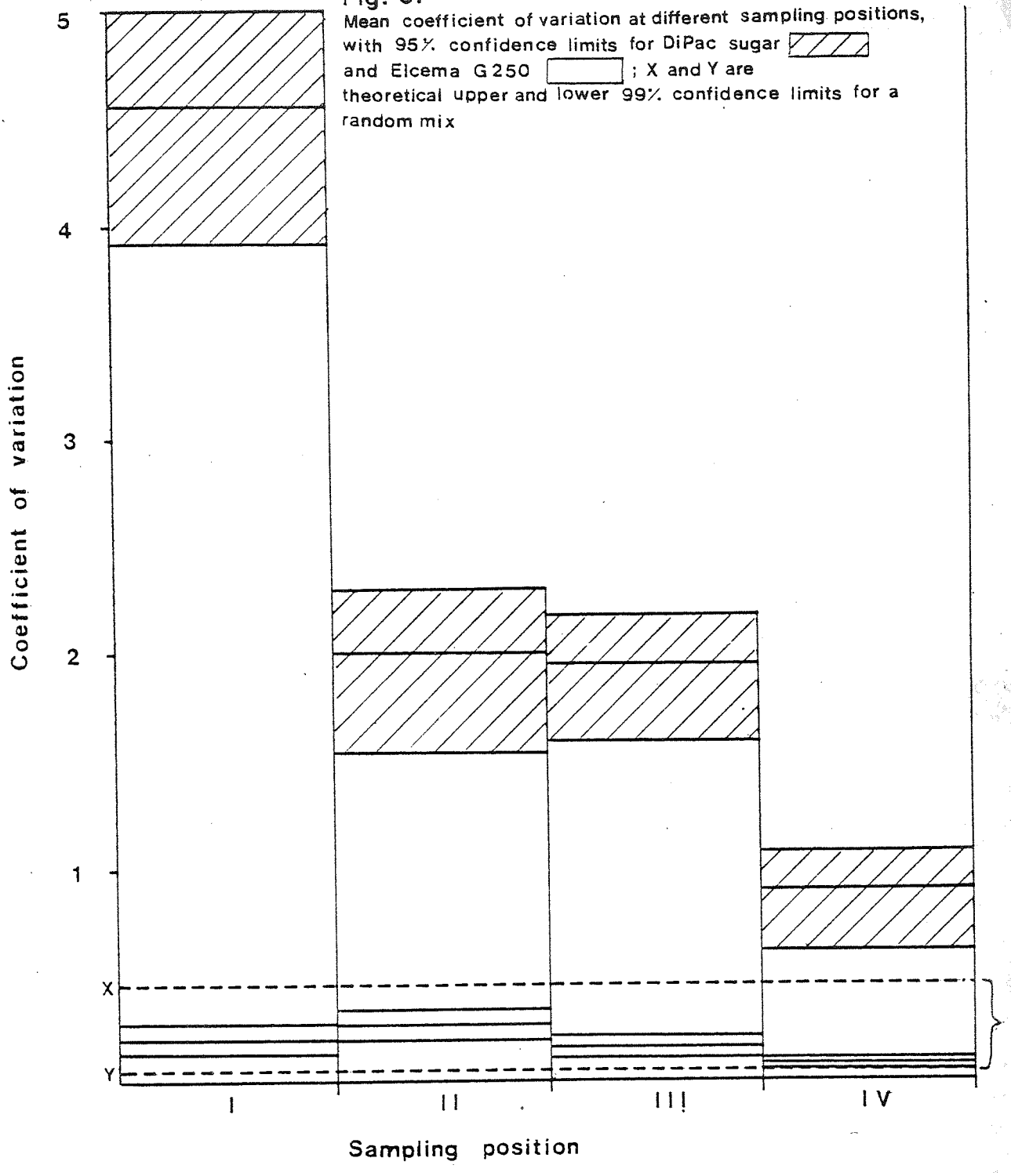

neither the Dipac nor the Elcema G250 excipient particles were able to move through the mix, segregation must have occurred by fine drug particles becoming dislodged from the excipient surface. The Elcema G250 particles had a more porous surface than Dipac so the larger pores in the Elcema may have trapped fine drug particles thus preventing them from becoming segregated when the powder was vibrated. The mechanism by which fine drug particles segregated from carrier particles such as the Dipac was called "constituent segregation" by Yip and Hersey (131) to distinguish it from another mechanism called "ordered unit segregation" where carrier particles with an excess or a deficiency of drug particles move to particular locations in the powder bed. Ordered unit segregation was minimised in the present model system by the low frequency vibrations producing a non-dilating powder bed in which movement was only possible by percolation of fines. The size of the interparticle voids was too small to allow coarse ordered units to percolate through the bed. The mix containing Dipac showed a tendency for potassium sorbate to segregate throughout the powder bed with no long-range segregation effects (discussed in section 4.3.2.2) or large accumulations of drug in any specific part of the vibrated cylinder. The coefficient of variation of the Dipac and potassium sorbate system increased towards the top of the cylinder, probably caused by larger void diameters in the top zone and increased movement of material being consolidated by the low-frequency vibrations.

As explained in section 3.3.4.3, the surface area of intra-particle pores accessible to fine adherent particles greater than 2 μm was larger for Elcema G250 (2,241 $cm^2.g^{-1}$) than for Dipac which had an accessible surface area of only 817 $cm^2.g^{-1}$ (Table 21). The intraparticle pore volume of Elcema was 0.52 $cm^3.g^{-1}$ which

was also considerably larger than that of Dipac at 0.10 $cm^3.g^{-1}$ (Table 17). Of the total number of fine particles, diameter d, in a mix, the theoretical fraction, f which will adhere to carrier particles, diameter D is given by the relationship (66):

$$f = n d^2 / 4 D^2 \qquad (87)$$

where n is the number of small particles adhering to each large particle. This relation assumes a close hexagonally-based packing of adherent particles as a monolayer on the surface of the carrier particles.

Using the experimental values for surface areas accessible to potassium sorbate particles, to obtain a more accurate assessment of carrier particle areas, f was greater than unity for both Elcema G250 and Dipac, showing that there were many more theoretical sites of adhesion than potential adherent particles. Thus, stereometrically, both Elcema G250 and Dipac were capable of carrying all the fine particles, but potassium sorbate appeared to have a stronger affinity for Elcema G250 than for Dipac particles in similar vibration conditions. This may be a result of the differences in surface physical properties of the two carrier powders, such as surface porosity and surface area which can influence the interparticle contact and modify the bond strengths formed by surface energy interactions of the two sets of particles.

The vibration segregation model based on a jolting volumeter and a sampling cylinder had limitations in that the vibration conditions could not be varied and this precluded its development for further studies of powder segregation. A second vibration model was designed based on an electromagnetic vibration unit.

4.3 Vibrational Powder Segregation Model

An electromagnetic vibration unit was substituted for the jolting volumeter to allow the vibration conditions to be varied so that the effect of different vibrations such as those produced by machinery rumble during tablet manufacture could be assessed. The brass cylinder with the P.T.F.E. plug caused some powder movement during the sampling process and there was some difficulty in removing similar representative samples from different powder mixes. The sampling tube was re-designed as a perspex cylinder split into twenty interlocking sections which stacked into a single column supported by an outer perspex cylinder to keep the column rigid during vibration. The excipient powders studied were the commercial excipients, Dipac and Emdex characterised in section 3.3 which were compared with the recrystallised lactose excipient characterised in Chapter 3.

4.3.1 Method

The individual perspex cylinders were stacked vertically and were located by interlocking joints (Figure 58(b)). When assembled, the twenty small cylinders were placed inside a retaining perspex cylinder and the powder mix was poured into the inner stack of cylinders. The total enclosed volume of the inner system was approximately 250 cm^3. After filling with powder a P.T.F.E. cap was placed over the cylinder head to prevent powder loss during vibration and the complete unit was clamped to the vibration table as shown in Figure 58(a). Following vibration the whole cylinder assembly was removed from the vibration unit and the P.T.F.E cap taken from the cylinder head. The inner cylinder was pushed out of the rigid outer tube and a powder sample was

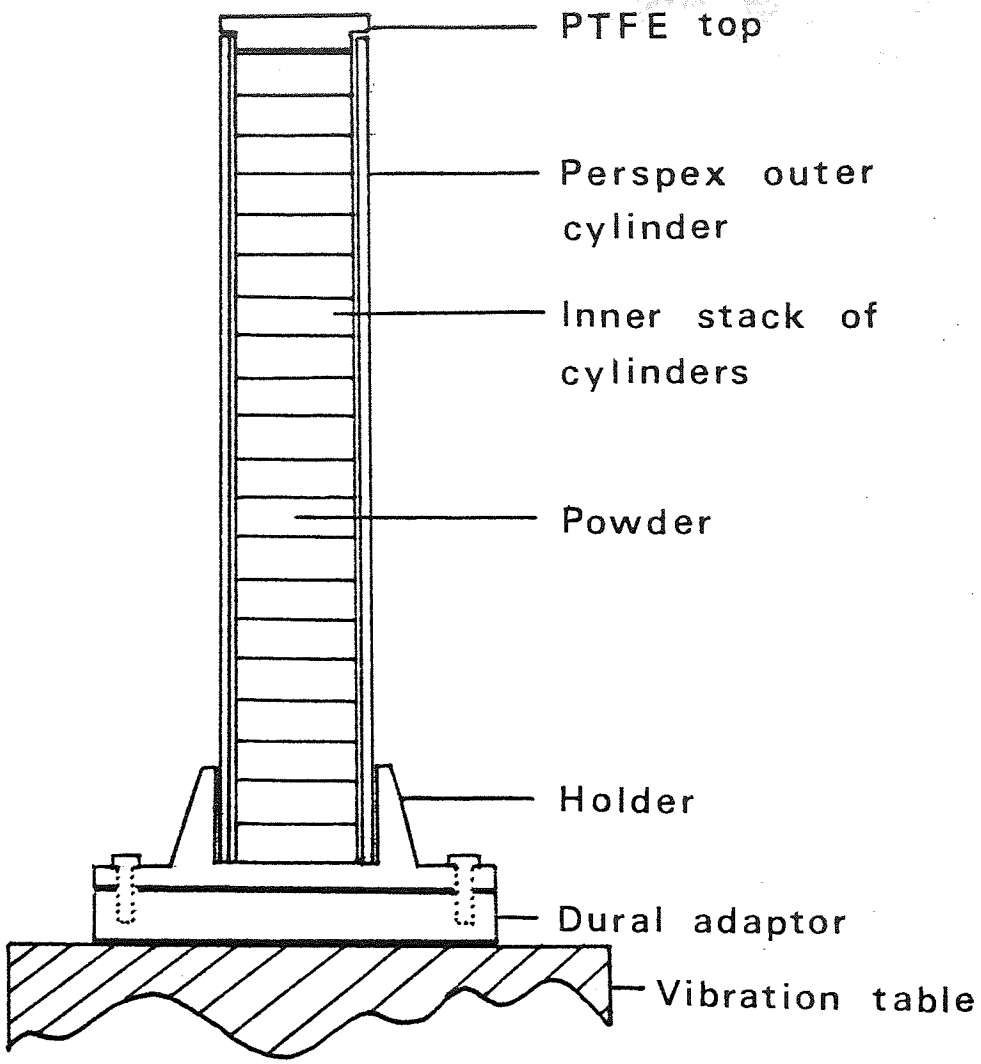

Figure 58(a). Arrangement of stacking cylinders assembled and fitted on the vibration unit.

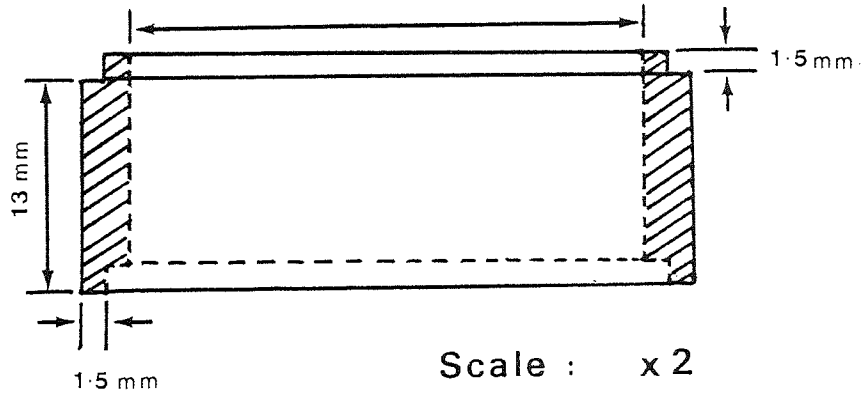

Figure 58(b). Detail of one perspex stacking unit.

taken from the highest level completely filled with powder by removing the upper stacking units. Further samples were taken by removing the next stacking unit down the cylinder. The interlocking cylinders were stacked with the protruding side of the joints uppermost; this rim protected the unsampled lower layer of powder when the upper cylinder was raised slightly and slid sideways to remove the powder sample. The scraping action by which the upper cylinders were removed ensured that there was minimum disturbance to the sample surfaces below. The powder samples contained potassium chloride as a model drug and because analysis was carried out by the autobalance conductance bridge method no dilutions were necessary. The use of a model drug, sampled and analysed directly was preferred to the use of tracer particles or radioactive techniques since this method did not introduce any extra components into the powder mix which could interfere with the formation of ordered units thereby affecting the final homogeneity of the system. The objective was to assess the likely influence of vibration on the drug content of individual pharmaceutical tablets.

The electromagnetic vibration unit is shown in Figures 59(a), (b). The powder container was vibrated sinusoidally on a vibration table where the conditions could be altered using associated control systems. The oscillator (Type TG 66A, Levell) generated sine waves with frequencies which could be varied from 20 Hz to over 20,000 Hz. The actual frequency used to vibrate the cylinder at any instant was shown by a frequency counter (Advance Ltd., London). The sine wave was fed to a power amplifier (Type 250 WLF, Derritron, London) which could alter other vibration conditions such as the energy, power, displacement velocity or acceleration.

The acceleration of the powder was measured directly and continuously using an accelerometer (Type DJB 101, Bruel and Kjoer, Naerum, Denmark) connected to a charge amplifier (Model DVA, Ling Dynamic Systems, Royston, U.K.) and a voltmeter (Advance Ltd., London). Changes in the vibrational acceleration produced resistance changes in the accelerometer which were transformed into voltage differences measured by the voltmeter. The differences between the waveform being fed into the vibration unit and that detected by the accelerometer were monitored using a double-beam oscilloscope (Type D61a, Telequipment, London). The cylinder containing the powder was bolted to the vibration table (type VP5b, Derritron, London) using a specially constructed dural adaptor unit (Figure 58). The adaptor kept the table and cylinder connected rigidly to the oscillating metal core beneath the vibration table. The vibration conditions were altered by a change in the electromagnetic field, the strength of the flux being governed by the signal from the power amplifier. The electromagnets were protected against over-heating by a fan which drew cool air over the coils.

For experiments requiring a random waveform a sine random generator (type 1024, Bruel and Kjoer, Naerum, Denmark) was connected into the system (represented by dotted circuit in Figure 59(a)) in place of the oscillator. The sine random generator produced a narrow frequency bandwidth randomisation of a central frequency sine wave. A 123 kHz carrier signal was modulated by a 3 kHz oscillator of randomly varying amplitude, from which a central sine wave was selected of say, 50 Hz varying randomly in a bandwidth of 10 Hz for example. Under these conditions the sine wave frequency at any instant could lie between 45 and 55 Hz.

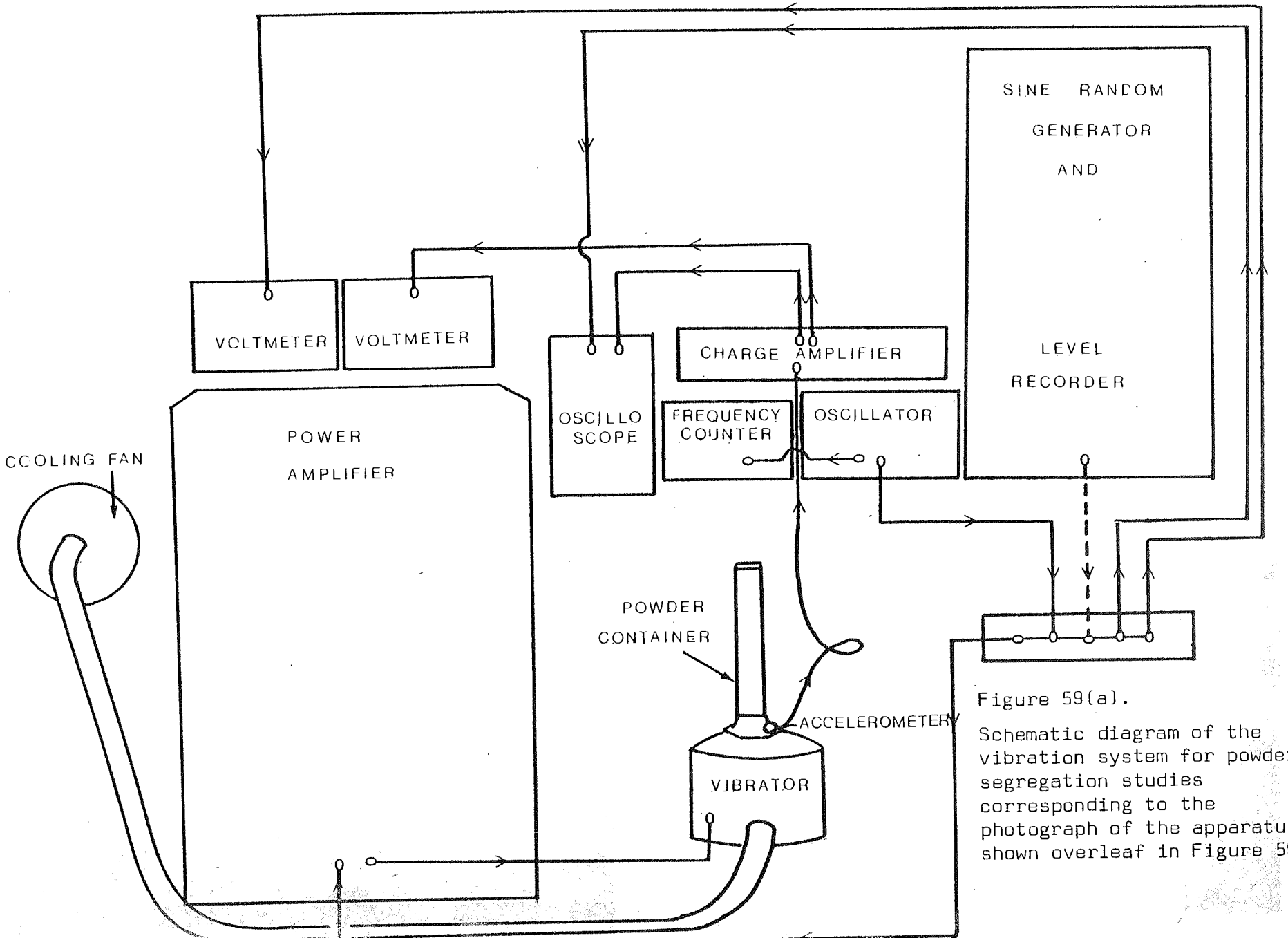

Figure 59(a).

Schematic diagram of the vibration system for powder segregation studies corresponding to the photograph of the apparatus shown overleaf in Figure 59(b).

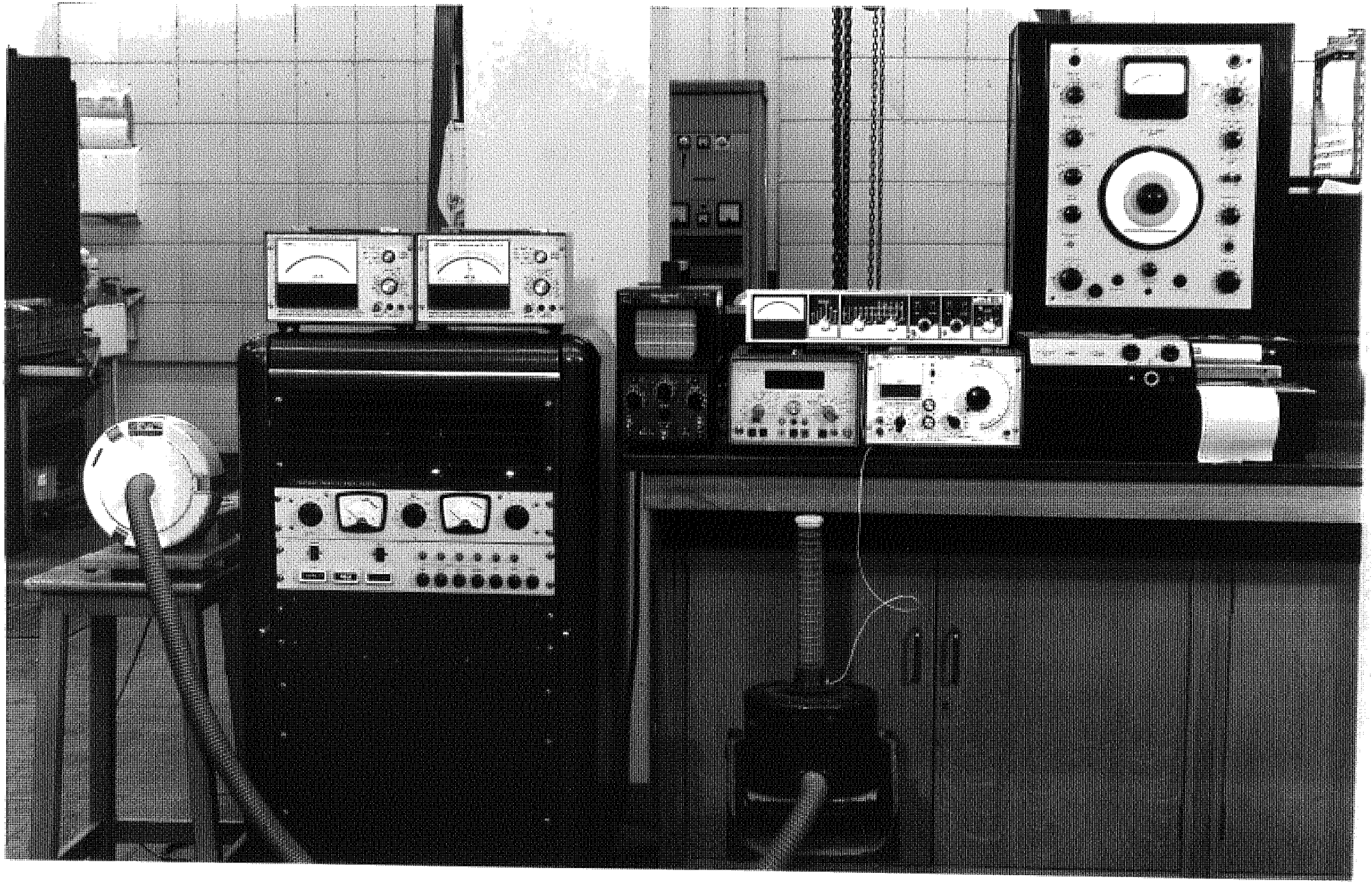

Both the central frequency and the bandwidth could be altered. In addition wide-band random vibrations could also be generated with a constant power spectral density in the frequency range 20 Hz to 20,000 Hz; this is termed white noise. In certain experiments a sine random generator was used in conjunction with a level recorder (type 2305, Bruel and Kjoer) to produce frequency-response curves of the vibrated powder systems which were used to identify resonant frequencies. The different instruments were connected according to the line diagram in Figure 60.

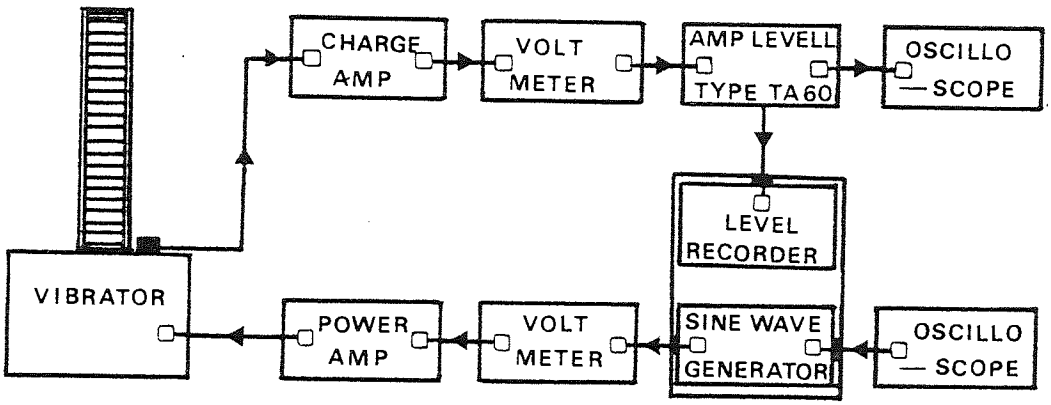

Figure 60. Schematic diagram showing circuits for producing and monitoring random vibrations in a powder cylinder.

4.3.2 Results and Discussion

4.3.2.1 Effect of Vibration, Time, Frequency and Acceleration Force on the Intensity of Powder Segregation

Powder mixes containing 0.5% fine potassium chloride particles adhering to coarse particles of Dipac, Emdex and recrystallised lactose excipients were each studied in the vibrational segregation model. Each powder mix was subjected to different vibration frequencies and acceleration forces for different periods of time.

All the drug and excipient powders were previously mixed to a homogeneity within the pharmacopoeial microdose specifications corresponding to coefficents of variation below 2%. The effect of the different vibration conditions on the segregation behaviour of the powder mixes was determined by calculating the coefficient of variation of samples analysed after vibration; any powder mixes with coefficients of variation greater than 2% following vibration were considered to have become segregated to an unacceptable extent.

The effects of different vibration frequencies and vibrational acceleration forces on powder segregation after different vibration times are shown by the three-dimensional curves in Figures 61 to 72. Note that the CV scale on the ordinate is the same in all these figures except Figure 72. The frequency of vibration was described by the number of complete cyclic displacements through which the powder container moved in one second and the vibrational acceleration force was the rate of change in cylinder velocity at that frequency. Although the movement of the individual powder particles was out of phase with the movement of the cylinder at certain frequencies and acceleration forces the particle motion was assumed to be related to that of the cylinder according to the models of Gutman (157) and Ryzhkov and Baskakov (156). At low acceleration forces the powder particles were observed to be not in flight during any part of the vibration cycle and the values of frequency and acceleration would therefore have been the same for both the container and the powder particles.

The powder mixes of Emdex and 0.5% w/w fine potassium chloride vibrated for five minutes at acceleration forces up to 3 G and frequencies from 20 to 1,000 Hz showed no significant segregation

tendency (Figure 61). At each of the vibration conditions the coefficients of variation remained well below 2%. As the vibration time was increased to fifteen minutes duration the coefficients of variation were found to increase slightly in powders vibrated at frequencies of 50, 100 and 500 Hz with an acceleration force of 3 G, although the segregation level still remained below the 2% pharmacopoeial specification level (Figure 62). A further increase in vibration time to thirty minutes produced slight segregation in powders vibrated at low frequencies such as 20 and 50 Hz with acceleration forces between 0.75 G and 3 G (Figure 63). As the vibration frequency increased, the segregation tendency decreased, even at the highest acceleration forces. A similar pattern occurred when the vibration time of the Emdex/potassium chloride mix was increased to 60 minutes duration (Figure 64). These results indicate that vibration of Emdex mixes containing 0.5% fine potassium chloride caused only slight segregation at low vibration frequencies, even when the vibration time was prolonged.

In mixes of recrystallised lactose, 250 - 500 µm size fraction, with 0.5% potassium chloride powder vibrated for 5 minutes in different conditions, there was only a slight segregation tendency (Figure 65). This small segregation only occurred in powders vibrated at the relatively high frequency of 500 Hz at acceleration forces above 1.5 G; no segregation was found in powders vibrated for 15 minutes at the same high frequencies (Figure 66). When the vibration time was increased to 30 minutes duration there was evidence of some segregation of fine potassium chloride powder from the lactose at vibration frequencies of 20 Hz at 1.5 G. There was also a slight, though less marked, increase in the coefficient

of variation with vibration forces of 3 G at high frequencies (Figure 67). This trend was continued when the vibration time was increased to 60 minutes, some segregation occurring at 20 Hz with an acceleration force of 1.5 G (Figure 68). At this 60 minute period there was a tendency for the fine potassium chloride to slightly segregate from the lactose at all vibration frequencies for acceleration forces of 1.5 G and above. Summarising these results for recrystallised lactose, mixed with 0.5% fine potassium chloride, an increase in vibration time from five minutes to 60 minutes caused a slight increase in segregation at higher acceleration forces.

Dipac was also mixed with 0.5% potassium chloride model drug, as described previously and subjected to different vibration conditions. After only five minutes vibration time there was a very considerable segregation of potassium chloride from Dipac (Figure 69). This was most marked at low vibration frequencies and high acceleration forces, the maximum coefficient of variation being reached in powders vibrated at a frequency of 50 Hz and an acceleration of 3 G. The segregation tendency of the Dipac powder mixes decreased at high vibration frequencies and low acceleration forces, which formed a low-level plateau region enclosing vibration conditions of 0.75 and 1.5 G at 100 and 500 Hz and extending to 3 G at 1000 Hz. After 15 minutes vibration time (Figure 70) this plateau region, in which there was no segregation, decreased to include only those powders vibrated at 0.75 G from 100 to 1000 Hz and at 1000 Hz from 0.75 G to 3 G. At all other vibration conditions there was an increased amount of segregation of potassium chloride from Dipac. The coefficients of variation increased with increasing acceleration force and decreasing frequency to a maximum value

under vibration conditions of 100 Hz and 3 G. At frequencies below 100 Hz, the segregation tendency decreased, but there was still a considerable effect. When vibration was extended to 30 minutes, the potassium chloride powder continued to become more segregated from the Dipac excipient (Figure 71). In addition to the increasing peak values for coefficient of variation, there was also more marked segregation at low acceleration forces and high frequencies. The only conditions which did not produce any segregation were 0.75 G and 1.5 G acceleration, at a frequency of 1000 Hz. When the vibration time was increased to 60 minutes, the fine potassium chloride powder became much more segregated from the Dipac (Figure 72). The maximum segregation effect in powder vibrated for 60 minutes was nearly twice that found in powders vibrated for only 30 minutes. This marked increase in the magnitude of powder segregation after prolonged vibration occurred in all vibration conditions for Dipac mixes; and there was some segregation tendency even at high frequencies and low G forces. All the vibration conditions produced some segregation of potassium chloride from Dipac powder.

At each vibration time the surfaces of the three-dimensional curves showed the same upward sweep from conditions producing little or no segregation such as those occurring at any frequency with low acceleration forces or for any acceleration at high frequencies, to a maximum at conditions composed of high acceleration forces and low vibration frequencies. The slopes of the surface leading to the conditions of maximum segregation become steeper with increasing vibration time. The surfaces of the three-dimensional segregation curves also became more convoluted after prolonged vibration and secondary maxima were produced at low frequencies (Figures 71 and 72).

These effects only became evident following prolonged vibration of the powder mix, probably because of the influences of resonance frequencies which were observed to produce density differences in some parts of the vibrated powder cylinder. In zones where density increases the corresponding decrease in the interparticle void spaces would limit the movement of powder particles in a manner similar to that found in Dipac powder consolidated by vibration in a jolting volumeter (section 4.2.2).

Although there was only a slight segregation tendency in systems containing 0.5% fine potassium chloride powder mixed with the excipients Emdex or recrystallised lactose, the three-dimensional segregation curves showed a similar upward trend at low frequencies and high acceleration forces to that found in mixes of Dipac and potassium chloride. However, the magnitude of segregation under all vibration conditions, even after prolonged vibration, was considerably less in mixes containing carrier particles of Emdex or recrystallised lactose than in those of Dipac, which also formed ordered mixes according to the criteria described in section 4.1.2. Emdex and recrystallised lactose formed ordered mixes with fine potassium chloride particles which did not show marked segregation tendencies during vibration despite having widely different particle size distributions and although the mixes were free-flowing; both these conditions were previously implicated in the worst cases of segregation in powders mixed by randomisation.

The results which Khan and Smalley (145) observed in powder systems containing a single massive lead sphere at the base of a cylinder containing finer sand particles, where the speed with which the lead sphere rose to the surface of the powder increased

with increasing acceleration force and decreasing vibration frequency, were found to be broadly similar to the segregation of powder systems studied here, although the mechanisms involved were different. The upward movement of coarser particles was observed not to be a prominent mechansism in ordered mixes of drug and excipients. It was also found that certain vibration conditions such as at low frequencies produced an increase in segregation compared with that predicted by Khan and Smalley. This was comparable to one of the conclusions of Harwood (147) from his studies of combinations of sand particles, although he attributed the segregating influence in a vibrating cylinder of powder to particle size differences of the constituent powders. This conclusion was in common with other segregation studies of vibrated and non-vibrated powder mixes. Williams (60) and Brown (116) considered that of all factors influencing segregation of powder mixes formed by randomisation the most important was the size difference between the constituent particles.

The results presented in this section show that this was not the case in powder mixes formed by ordering. Ordered mixes of drug and excipient powders contained widely different constituent particle size distributions and yet were possibly less prone to segregation than random mixes studied elsewhere whose constituent particle sizes differed only slightly. In one sense this phenomenon of ordered mixes could actually be used to determine or characterise their formation as well as to define their stability, or to quantify the extent of their existence in a partially ordered random or total mix.

The three coarse excipient powders had similar particle size distributions (section 3.3.3) and Emdex and recrystallised lactose formed non-segregating mixes with 0.5% fine potassium chloride, showing that this combination of constituent particle sizes can produce stable ordered mixes. However, Dipac, a powder with the same particle size range as Emdex or lactose, segregated from particles of potassium chloride. It is thought that the segregation tendency of Dipac mixes was mainly due to the mechanism of "constituent segregation". Once the fine particles of potassium chloride became dislodged from the coarse Dipac particles during vibration of the powder, the drug was free to move through the void spaces in the bed in an analogous manner to the mechanisms producing segregation of random mixes containing different constituent particle size distributions. "Constituent segregation" was considered to be the principle segregation mechanism in mixes of Dipac and potassium chloride powder for several reasons:

1. The two excipients which formed stable ordered mixes with potassium chloride had similar particle size distributions to the Dipac, which did not. All the different excipient particles should undergo similar movement when vibrated, but Dipac was the only one which showed a marked segregation tendency. All the excipient particles were mixed initially to the same degree of homogeneity and should therefore have had a comparable distribution of drug particles on individual carrier particles, so that re-location of Emdex or recrystallised lactose ordered units would have produced segregation of the same magnitude as that found in mixes of Dipac following vibration.

2. The particles of potassium sorbate segregated from Dipac carrier particles in a consolidating bed where no ordered unit

movement could occur.

3. Particles of potassium chloride segregated from Dipac in vibration conditions which did not cause overall particle movement.

4. The intensity of segregation observed in mixes of Dipac and potassium chloride was too large to be accounted for by ordered unit segregation. The concentrations of potassium chloride in different parts of the segregated powder bed would have required a wide discrepancy in the numbers of drug particles carried by different Dipac particles. Some Dipac particles would have had to carry 400% more drug particles than others, which would have required multilayer adsorption on certain carrier particle sizes. This type of discrepancy was not observed in scanning electron microscopy studies of the ordered mixes prior to vibration.

It is therefore reasonable to conclude that constituent segregation occurred by movement of dislodged drug particles, free to move through the powder mix. Whilst the fine potassium chloride particles remained adhered to the coarse carrier particles, segregation did not occur. The differences in segregation tendencies of the three excipient powders containing potassium chloride resulted from differences in the stability of the ordered mix formed between constituent particles, this being influenced by the surface properties of the different excipient carrier particles and their interactions with the fine adherent model drug particles. The surface properties which may be important in creating "active" sites of adherence include the carrier particle pore size distribution, pore volume, surface rugosity, surface area and accessible surface area, each of which affect the location of adherent particles and the degree of interparticle contact. The actual location of the adherent particles in surface cavities may

be sufficient to protect the fine particles against dislodgement during vibration. However, since van der Waals' and electrostatic forces are responsible for interparticle adhesion, the surface discontinuities such as pores and asperities may increase the stability of an ordered unit by altering the distribution of surface electrical charge, concentrating it around pores where fine particles become more tightly bound by a combination of increased interparticle contact area and a concentration of surface forces. It was shown in Chapter 3 that Dipac particles possessed fewer of these surface discontinuities than either Emdex or the highly porous, recrystallised lactose. Dipac mixes showed the greatest segregation tendency when vibrated at low frequency and high acceleration forces. However, segregation was increased at any vibration condition when only one of these conditions was present; for example, a small acceleration force of 0.75 G produced a significant segregation when combined with the low frequency of 20 Hz and similarly a high frequency of 1000 Hz produced significant segregation of powders vibrated with a high acceleration of 3 G. The increased segregation tendencies of powders vibrated at low frequency or high acceleration was caused by an increased particle flight time. Particle flight was observed to occur mainly in systems vibrated with acceleration forces greater than 0.75 G. Although particles were observed to be in flight above this acceleration at all the frequencies studied, from 20 Hz to 1000 Hz, the high frequencies produced infinitesimally short flight times. Some particle segregation was found in powders vibrated in sub-flight conditions both with the electromagnetic vibration model and the jolting volumeter model, but the magnitude of segregation found in non-dilating beds was considerably lower than that in powders

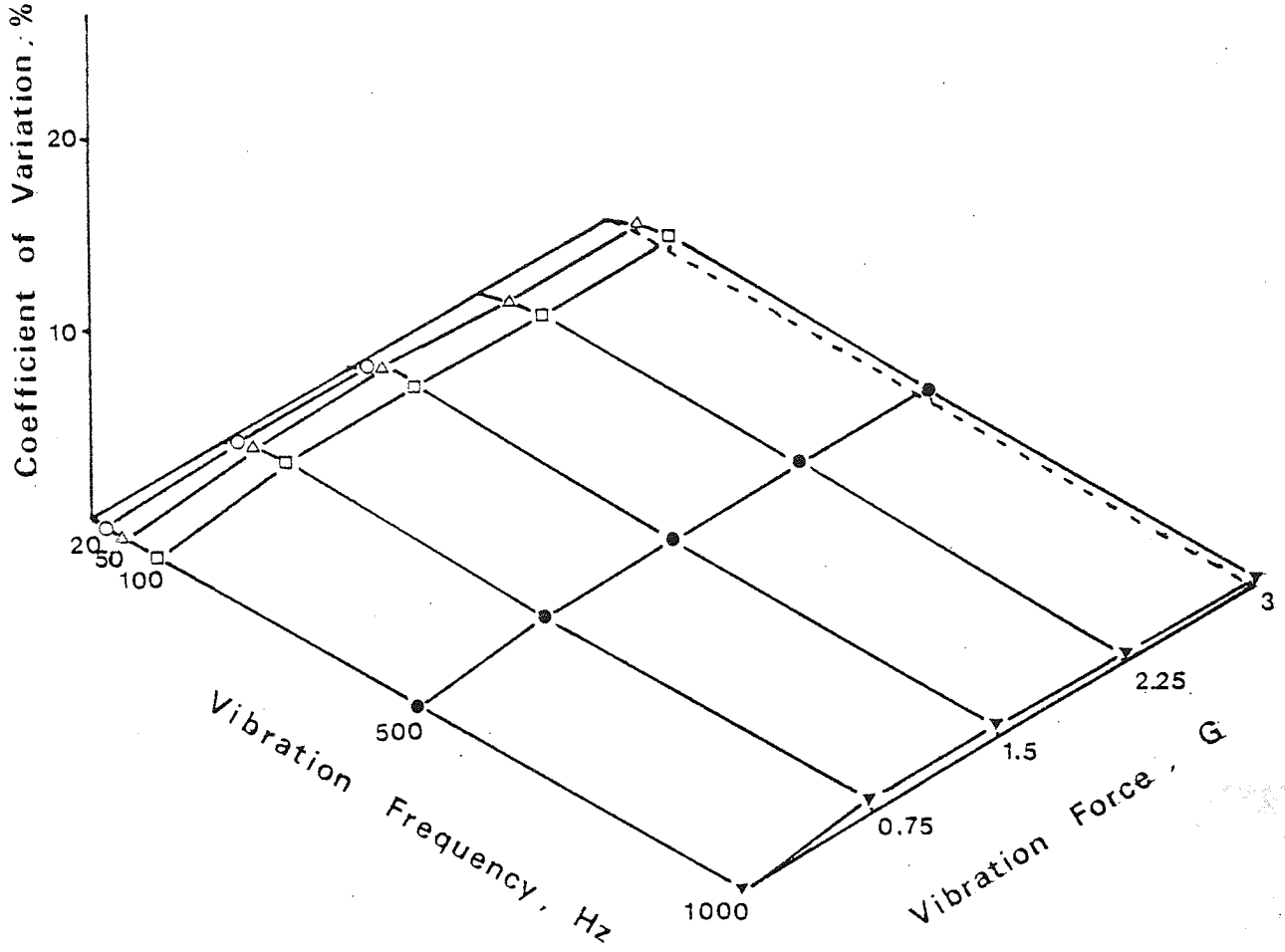

Figure 61. The coefficient of variation of 0.5% potassium chloride/Emdex mixes after 5 minutes vibration showing the effect of vibration frequency and acceleration force.

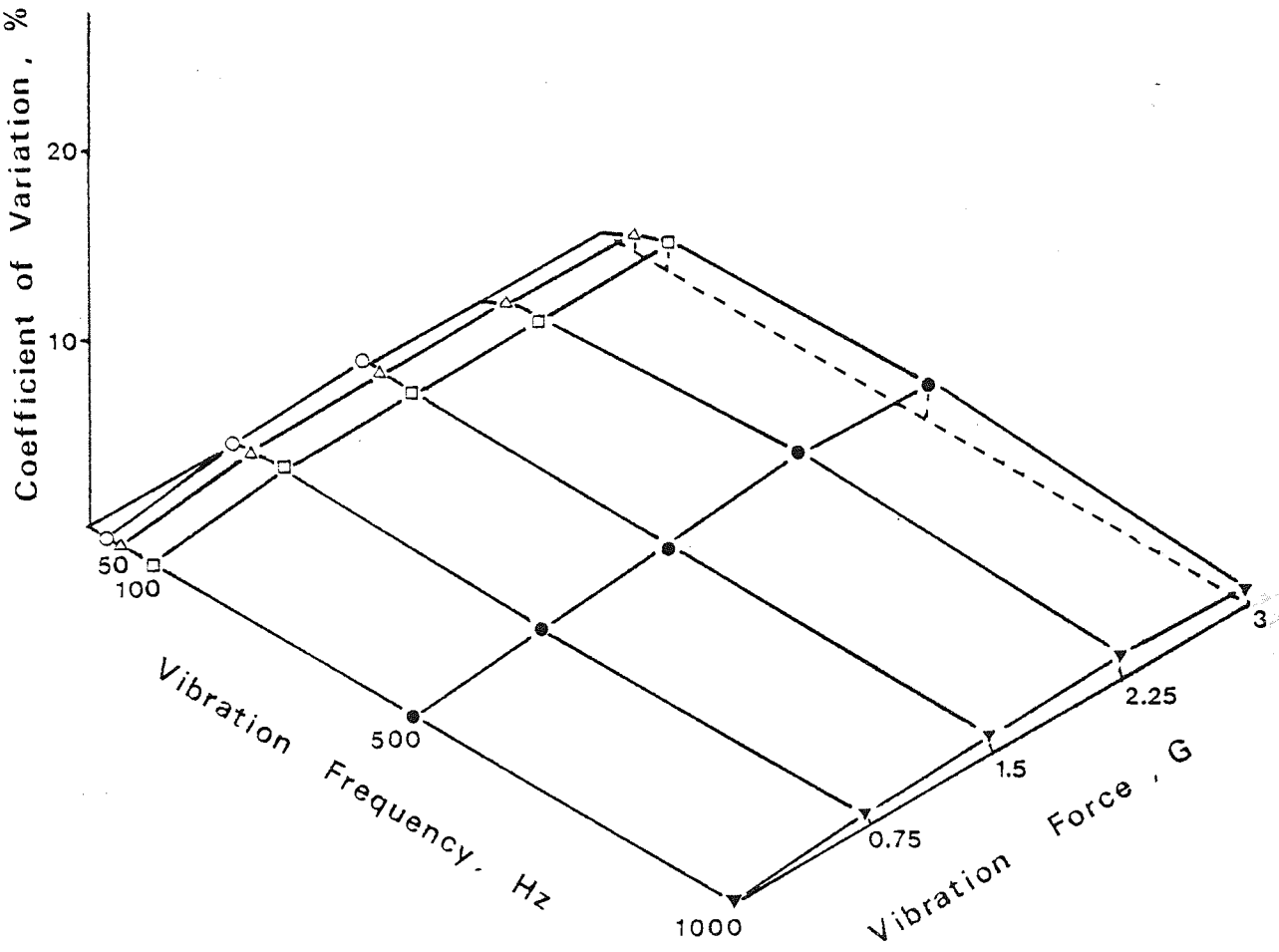

Figure 62. The coefficient of variation of 0.5% potassium chloride/Emdex mixes after 15 minutes vibration showing the effect of vibration frequency and acceleration force.

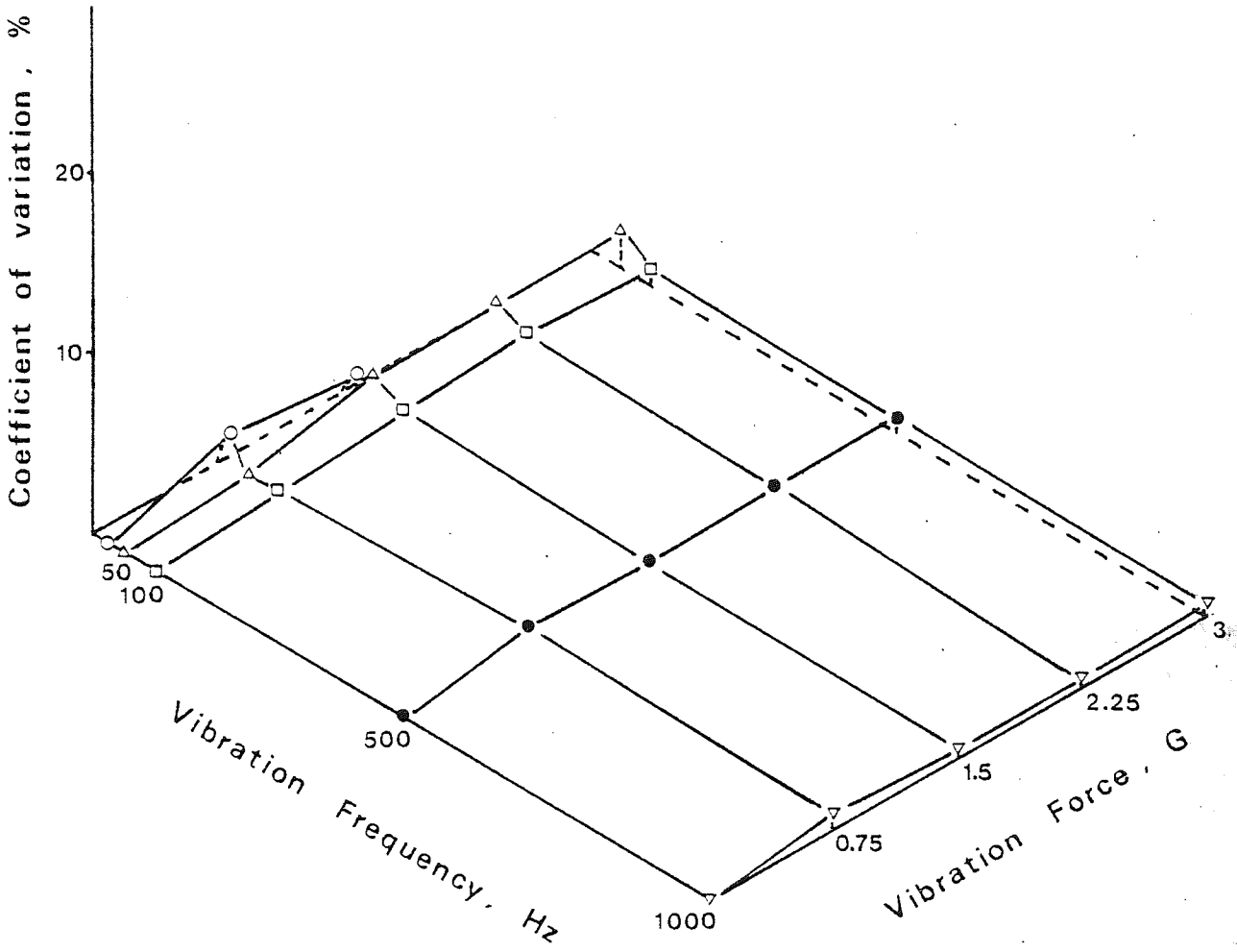

Figure 63. The coefficient of variation of 0.5% potassium chloride/Emdex mixes after 30 minutes vibration showing the effect of vibration frequency and acceleration force.

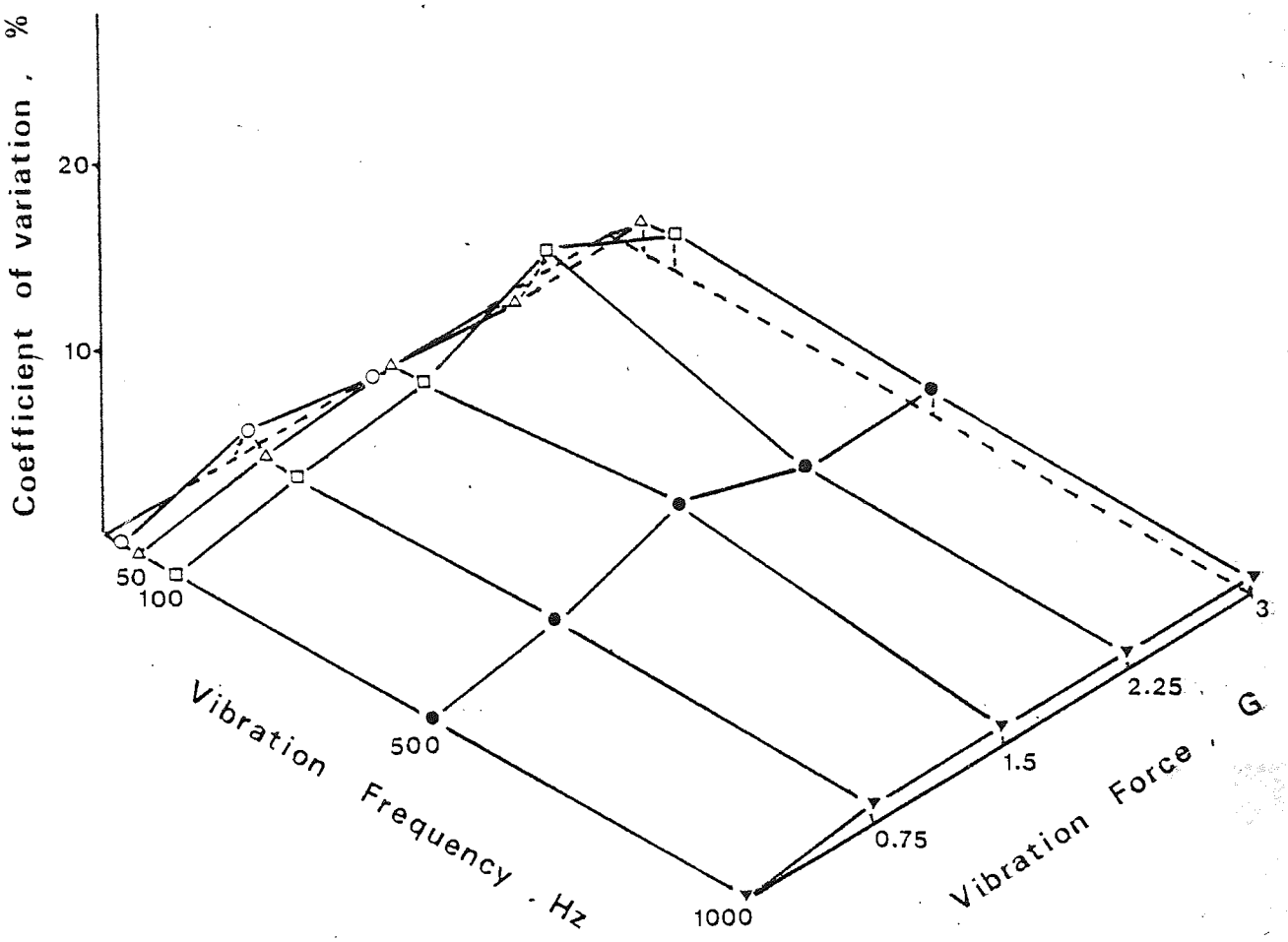

Figure 84. The coefficient of variation of 0.5% potassium chloride/Emdex mixes after 60 minutes vibration showing the effect of vibration frequency and acceleration force.

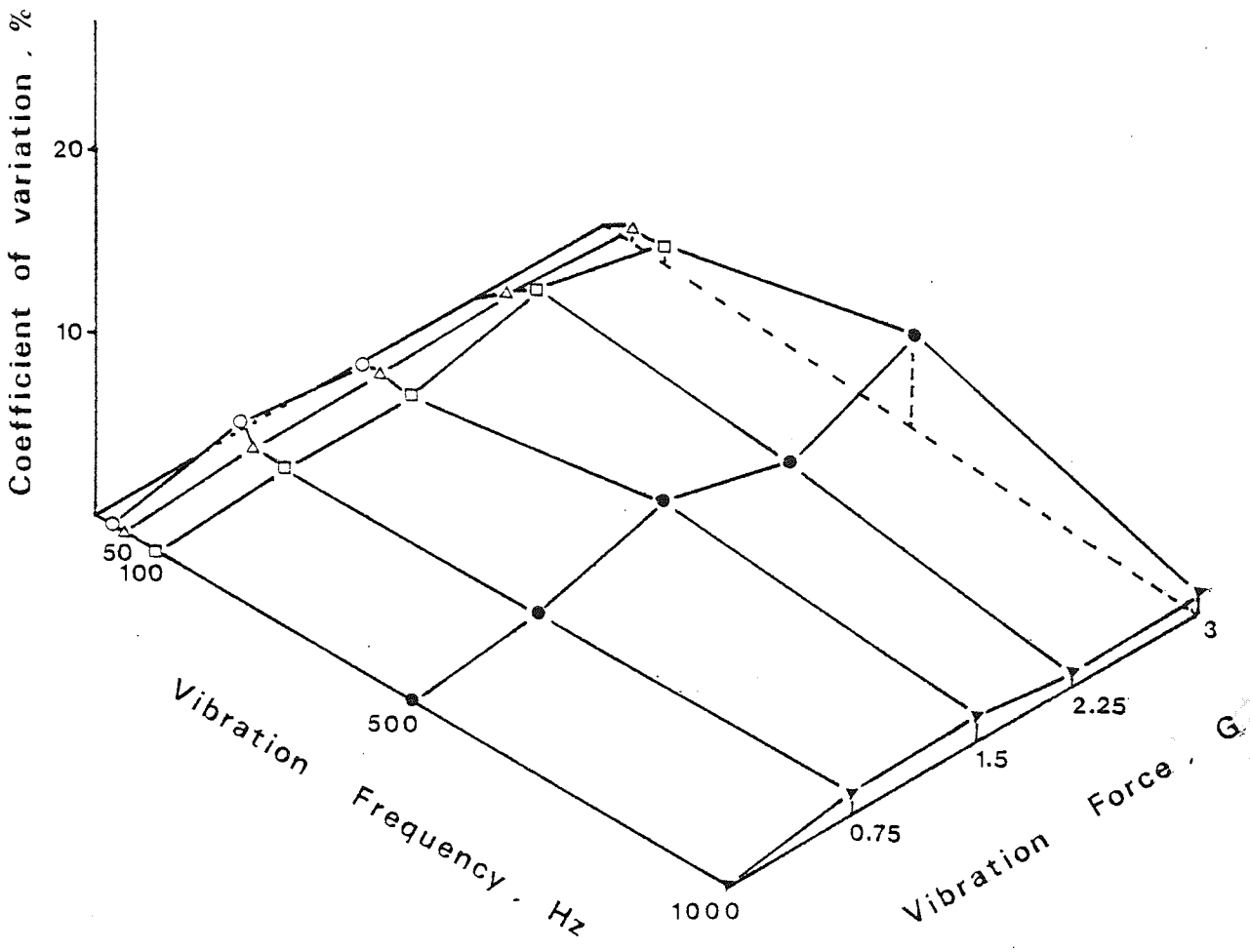

Figure 65. The coefficient of variation of 0.5% potassium chloride/recrystallised lactose mixes after 5 minutes vibration showing the effect of vibration frequency and acceleration force.

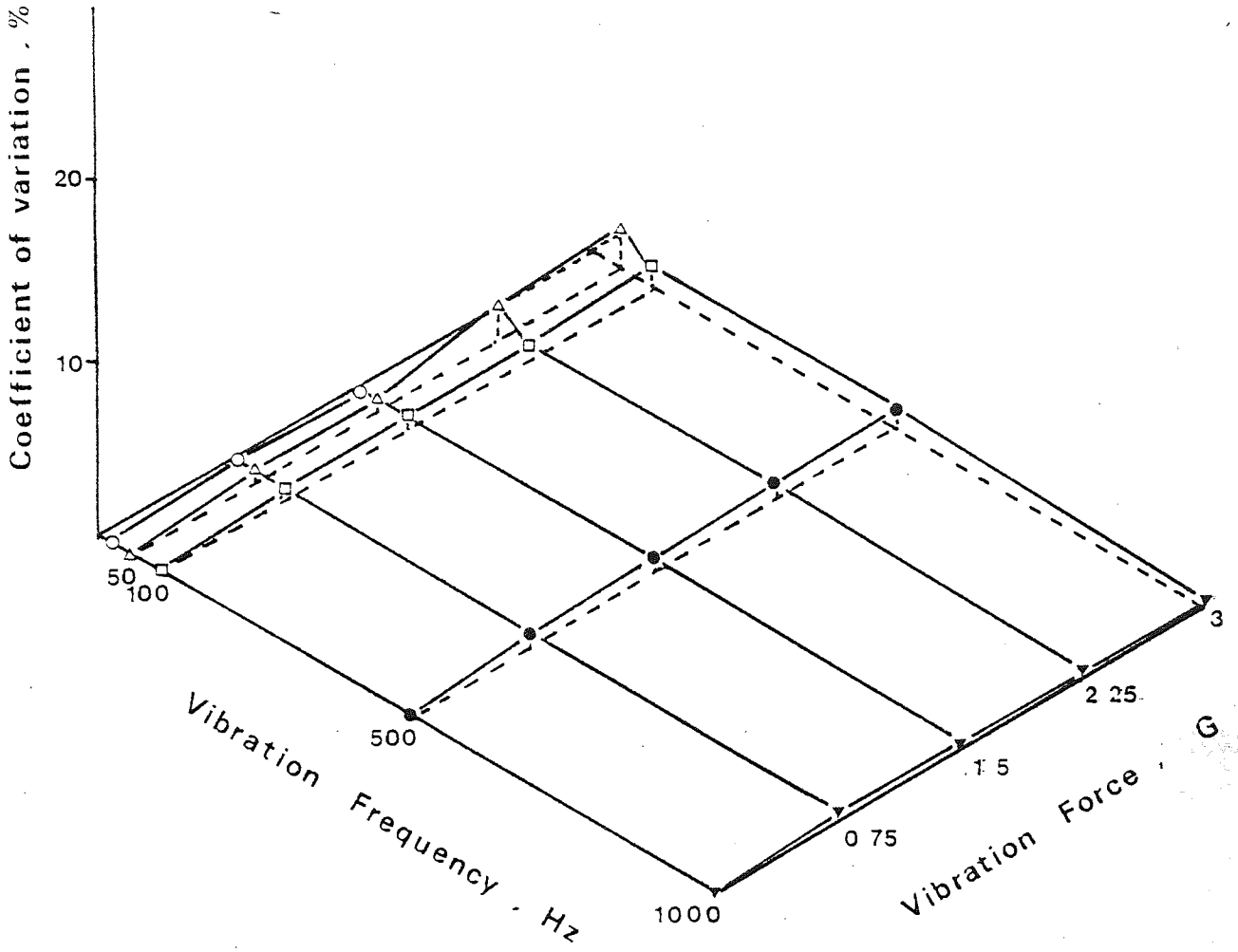

Figure 66. The coefficient of variation of 0.5% potassium chloride/recrystallised lactose mixes after 15 minutes vibration showing the effect of vibration frequency and acceleration force.

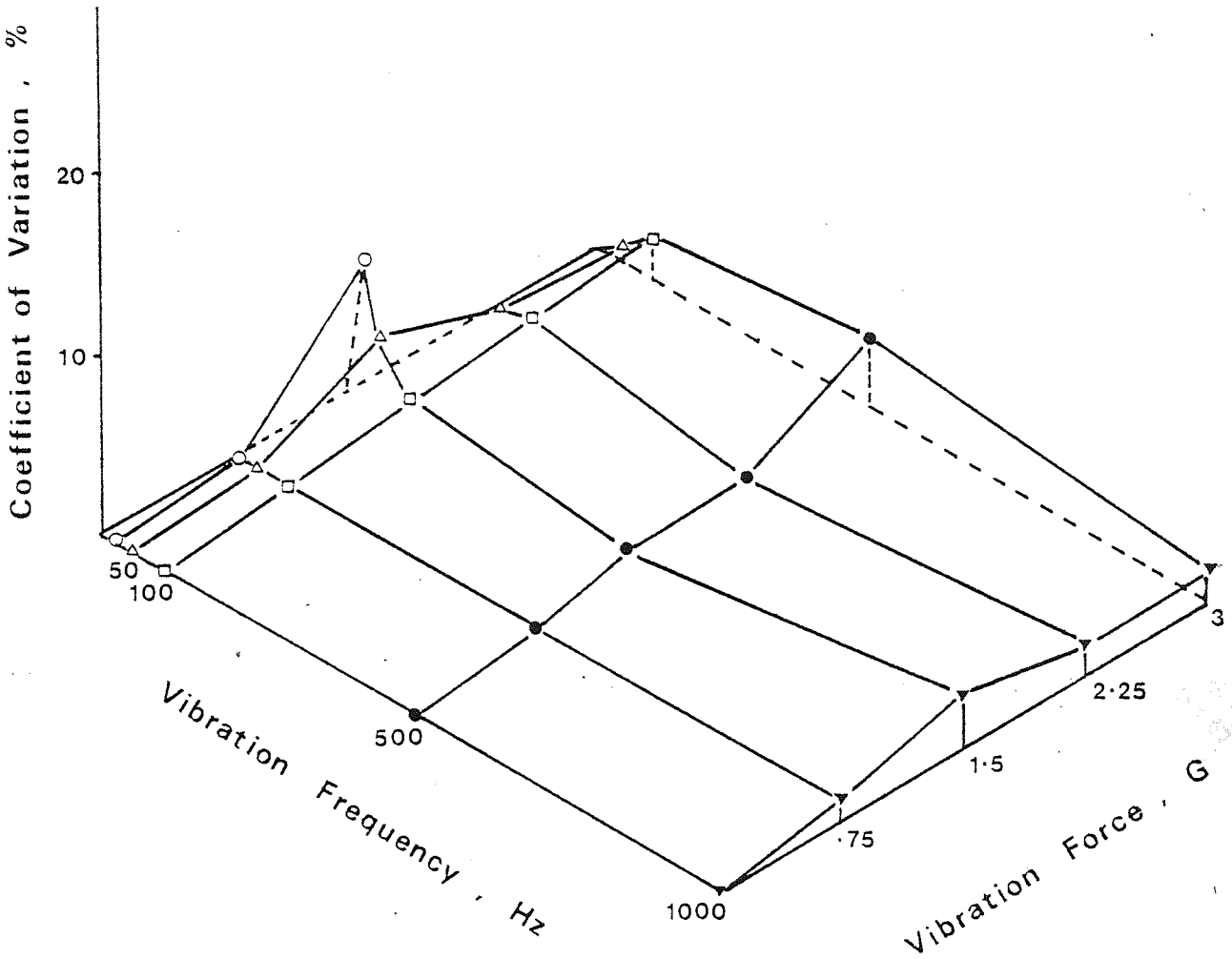

Figure 67. The coefficient of variation of 0.5% potassium chloride/recrystallised lactose mixes after 30 minutes vibration showing the effect of vibration frequency and acceleration force.

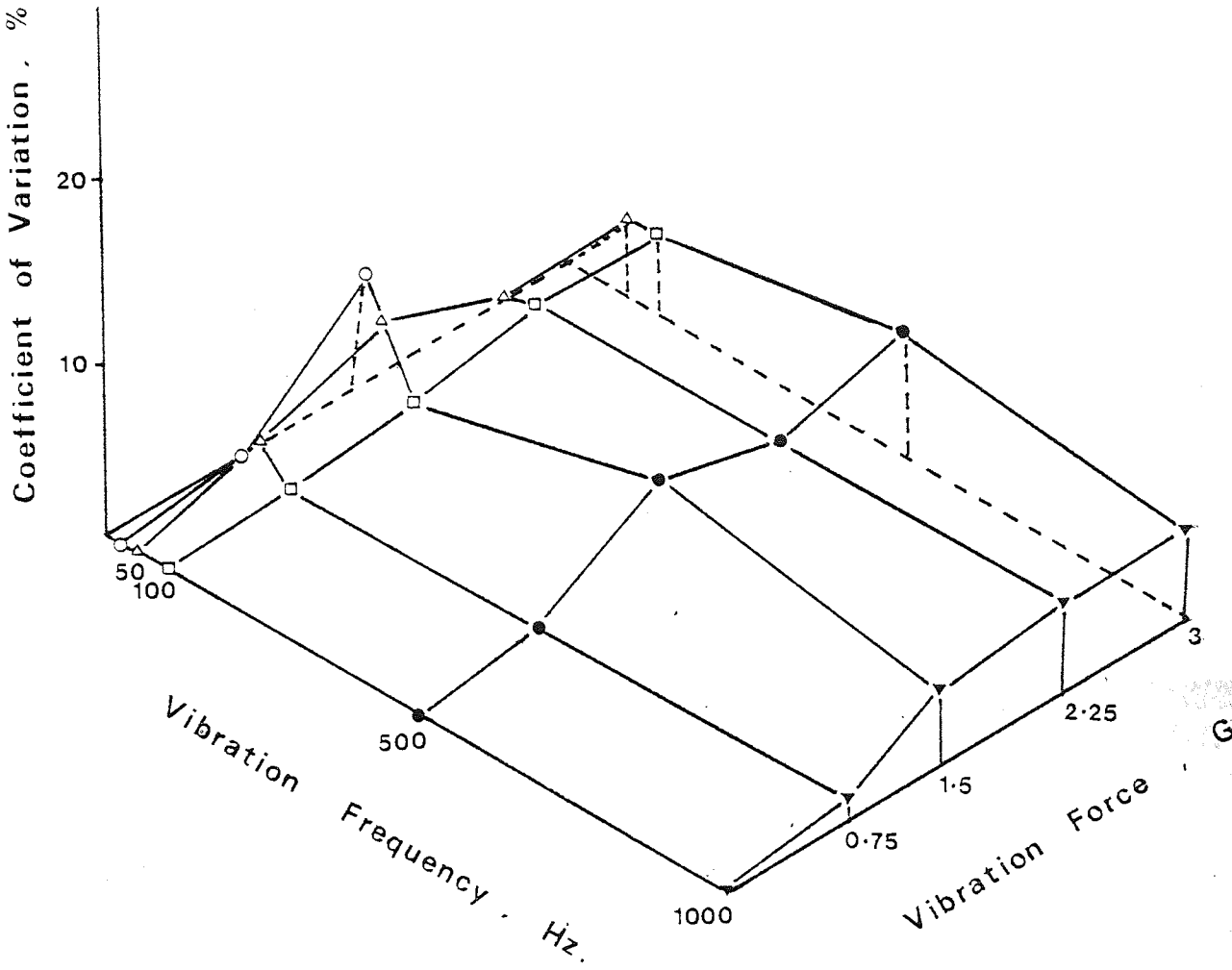

Figure 68. The coefficient of variation of 0.5% potassium chloride/recrystallised lactose mixes after 60 minutes vibration showing the effect of vibration, frequency and acceleration force.

Figure 69. The coefficient of variation of 0.5% potassium chloride/ Dipac mixes after 5 minutes vibration showing the effect of vibration frequency and acceleration force.

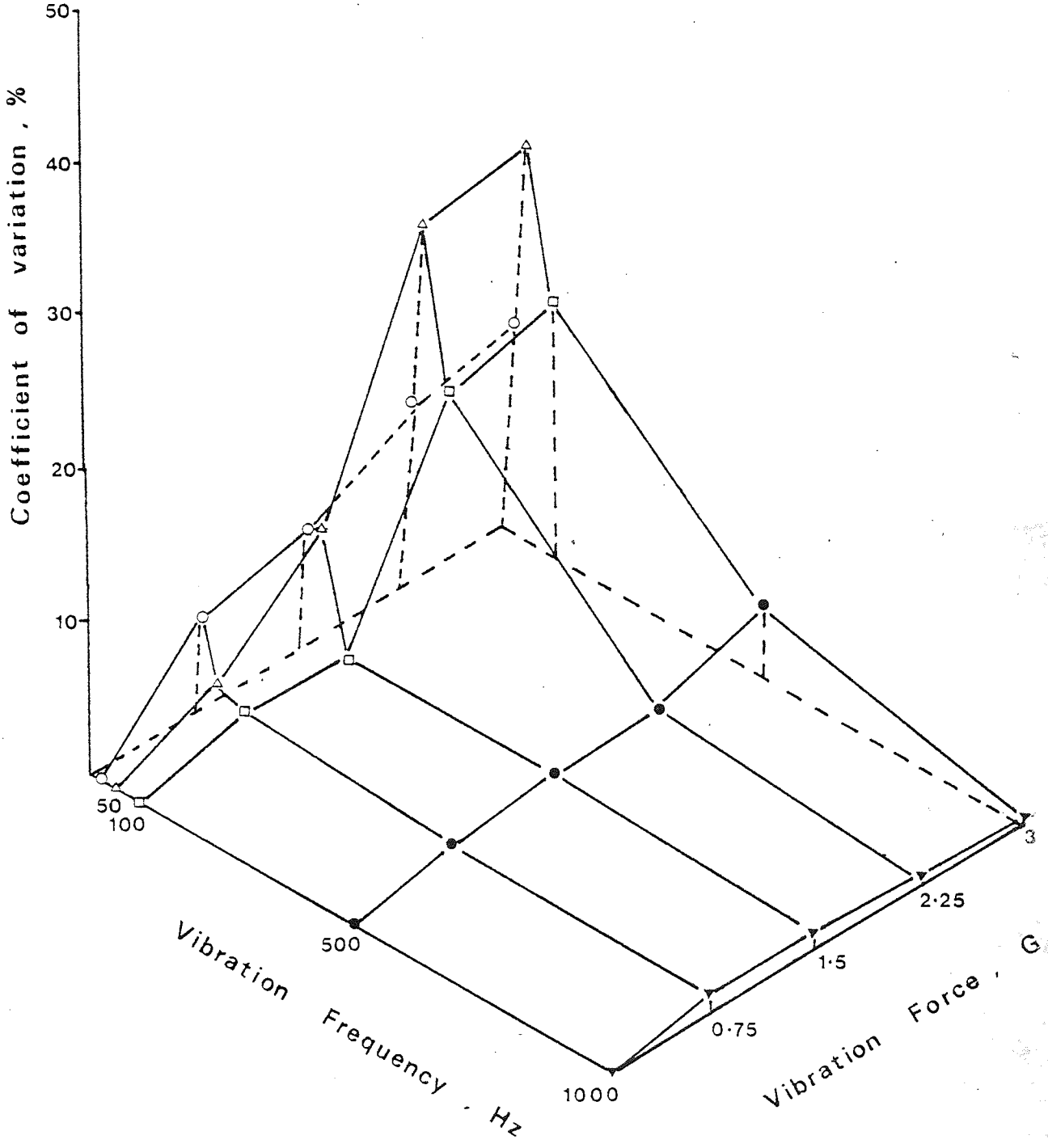

Figure 70. The coefficient of variation of 0.5% potassium chloride/ Dipac mixes after 15 minutes vibration showing the effect of vibration frequency and acceleration force.

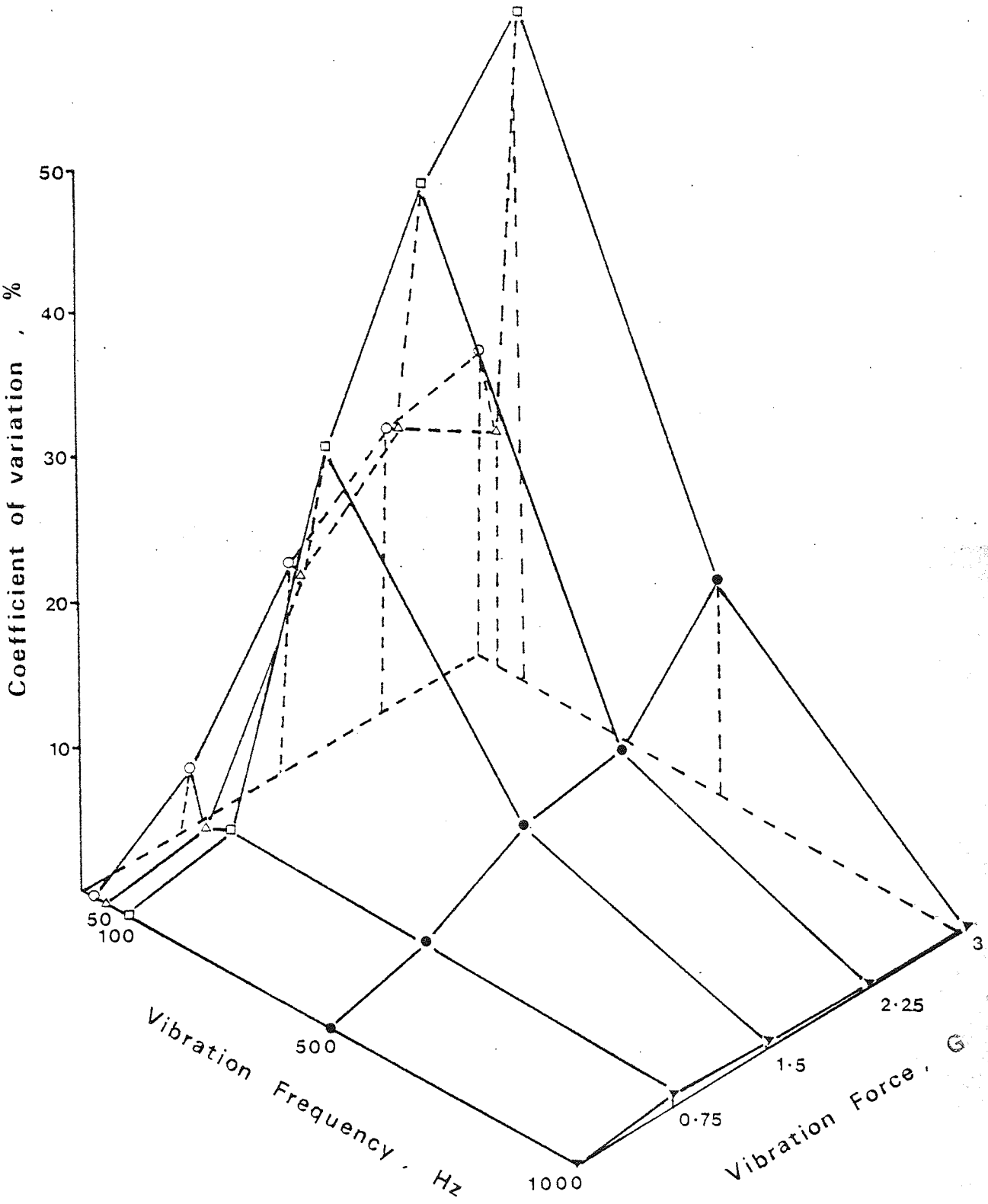

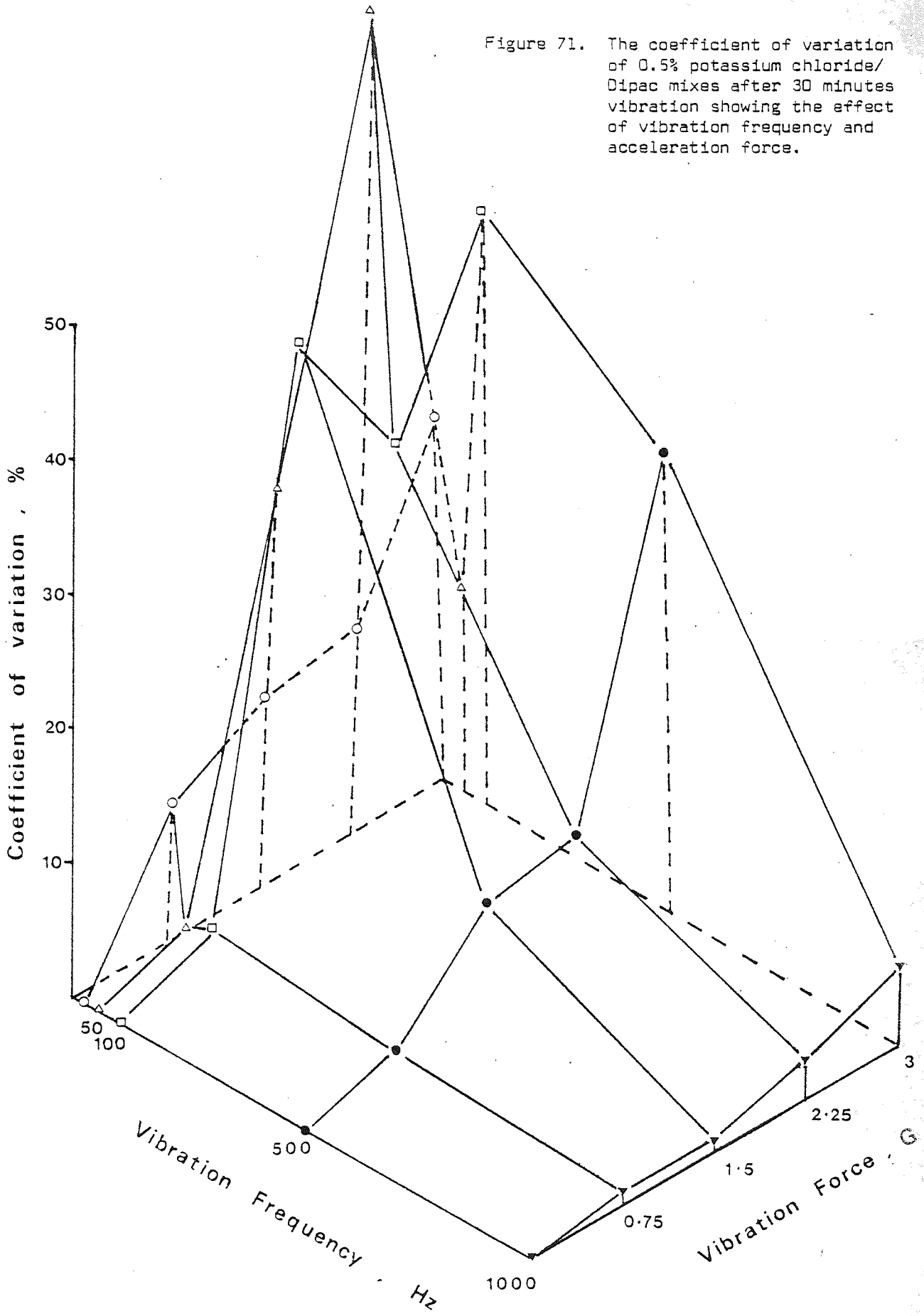

Figure 71. The coefficient of variation of 0.5% potassium chloride/ Dipac mixes after 30 minutes vibration showing the effect of vibration frequency and acceleration force.

Figure 72. The coefficient of variation of 0.5% potassium chloride/Dipac mixes after 60 minutes vibration showing the effect of vibration frequency and acceleration force.

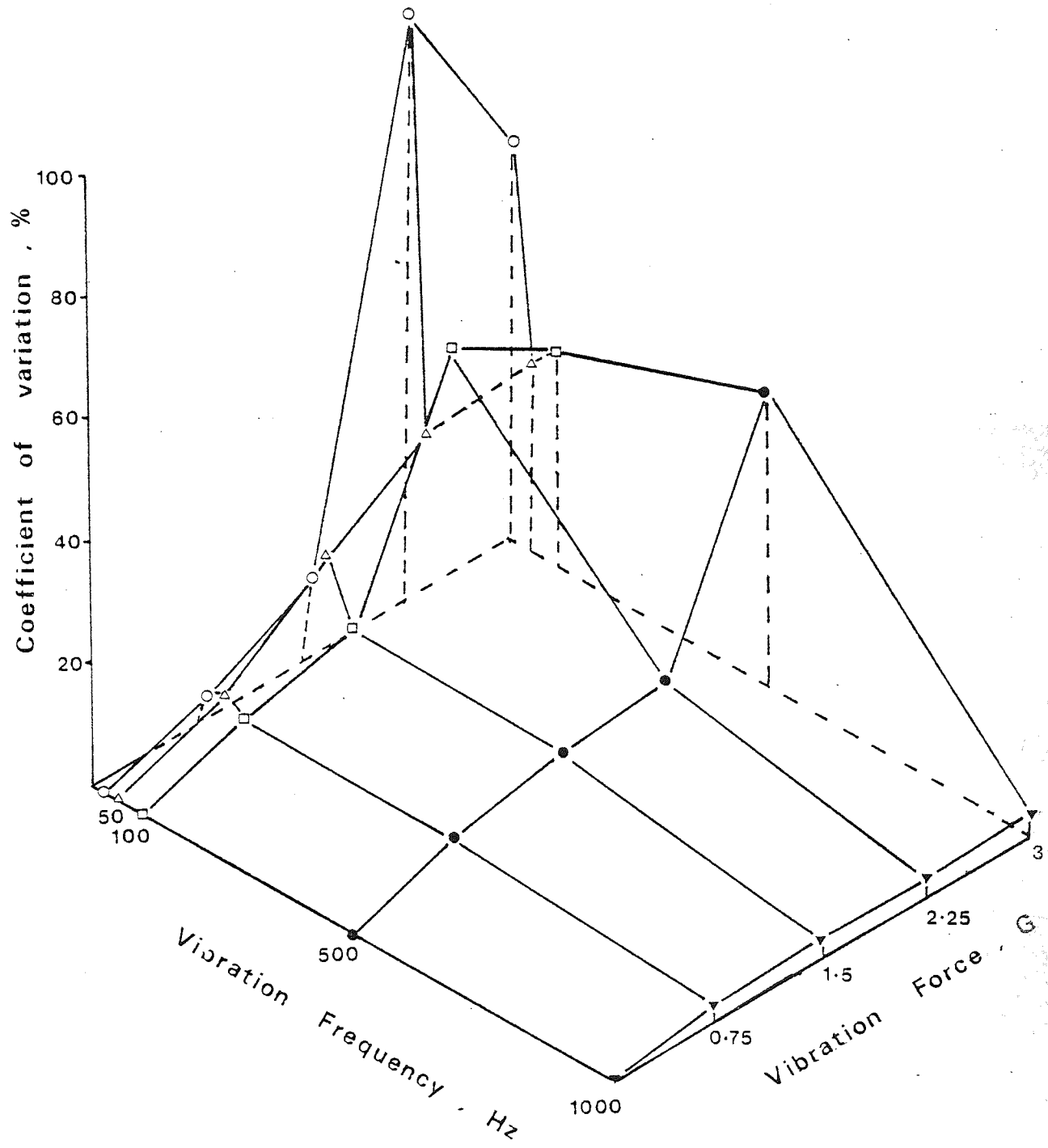

where particles were in flight.

Two types of powder flight were identified, one in which the powder bed was dilating and consolidating out of phase with the cylinder and another in which the powder was churning in the cylinder. These types of particle motion were similar to those described by Lawrence and Beddow (146) for powders filled into vibrating dies. In either of these conditions, particles were moving relative to one another, providing considerable opportunity for the adherent fine particles of potassium chloride to become dislodged by abrasion and move freely within the powder bed. The relative movement was greatest in the churning bed observed at high accelerations; these conditions produced the largest segregation tendencies. The increased segregation which occurred in dilating beds resulted from a combination of interparticle abrasion producing free drug particles which were then translocated more quickly. The mechanisms of particle translocation in dilating beds included percolation and trajectory segregation caused by particle flight in churning beds.

The three-dimensional curves represent the effect of changing vibration conditions on coefficients of variation and provide information about the intensity of segregation, but they are unable to reveal the actual locations of segregated particles in the powder bed under different vibration conditions. The coefficients of variation register the same intensity of segregation for drug particles whether located at the top of the powder bed or at its base and provide no information about the range of particle movement which Danckwerts called "scale of segregation".

4.3.2.2 Scale of Segregation

The scale of segregation defined by Danckwerts (174) and

described in Chapter 1 (section 1.4.7.2) was used to locate particle concentrations in a powder following vibration. Equation (55) was used to calculate the correlation coefficient, R(r):

$$R(r) = \frac{(x_1 - \bar{x})(x_2 - \bar{x})}{(x - \bar{x})^2} \qquad (55)$$

where $+1 > R(r) > -1$ and $\bar{x}$ is the mean drug concentration of all the samples taken from a mix. A graph of R(r), the correlation coefficient, against r, the distance separating samples taken from a mix, can show, for example, whether a depletion in drug content is associated with a depletion or increase in drug content in a part of the powder bed a distance r away. A value of R(r) = 0 shows that the relationship between drug concentrations a distance r apart is purely random (not significantly related) whereas a value of R(r) close to +1 shows that a similar concentration occurs in samples a distance r apart. Conversely, when R(r) = -1 the drug concentrations a distance r apart are related but a high concentration in one sample say is associated with a low concentration in the other sample. The discrepancy in each concentration from the mean is similar, but the values in each sample are on opposite sides of the mean.

The distribution of the fine model drug component, potassium chloride, was assessed according to concentrations at points, x_n. A large number of pairs of sample points, x_n and x_{n+r} were measured in sampling arrays with values of r from zero up to 19. The vibrated cylinder was used as a convenient array with sampling points a standard distance r apart corresponding to the height of one interlocking cylinder unit. The primary value of the array was taken as the first complete sampling level following vibration,

(x_n) and the remaining sampling positions were considered as secondary values ($x_n + r$). This procedure was repeated so that x_n became the next sampling level and all other levels became secondary values. In this way the correlation coefficients were calculated for each value of the sample separation distance, r. Figure 73 shows a correlogram of a vibrated mix of Dipac with a coefficient of variation of over 100% corresponding to the maximum segregation intensity shown in Figure 72. The correlogram shows that powder samples separated by distances less than about ten sampling positions (r = 10) had a composition well to one side of the average concentration. There was no significant association between samples separated by distances, r = 11 to r = 12. When the sample separation distance increased above r = 12 the values of R(r) became more negative, and at r = 16 and at r = 17 reached a minimum close to R)r) = -1. Correlation coefficients around -1 indicate a composition well to one side of the average at a given sampling point associated with a similar value on the other side of the average a distance r away. Danckwerts discounted values of R(r) less than zero, although Schofield (230) and Lacey and Mirza (175) used negative correlation coefficients to identify long-range segregation effects. Correlograms of samples removed from mixes of Dipac, Emdex and lactose with 0.5% potassium chloride were calculated and are shown in Figures 74 to 76. Each of the figures shows separate correlograms for powders vibrated at 50 Hz for 60 minutes with different acceleration forces. The correlograms had constantly changing slopes because of the changing relationship between samples different distances apart. Most of the powders showed some long-range segregation effects although the mix of

Figure 73. Correlogram of Dipac powder samples following vibration. R(r) is the correlation coefficient between samples different distances, r, apart calculated using equation 55.

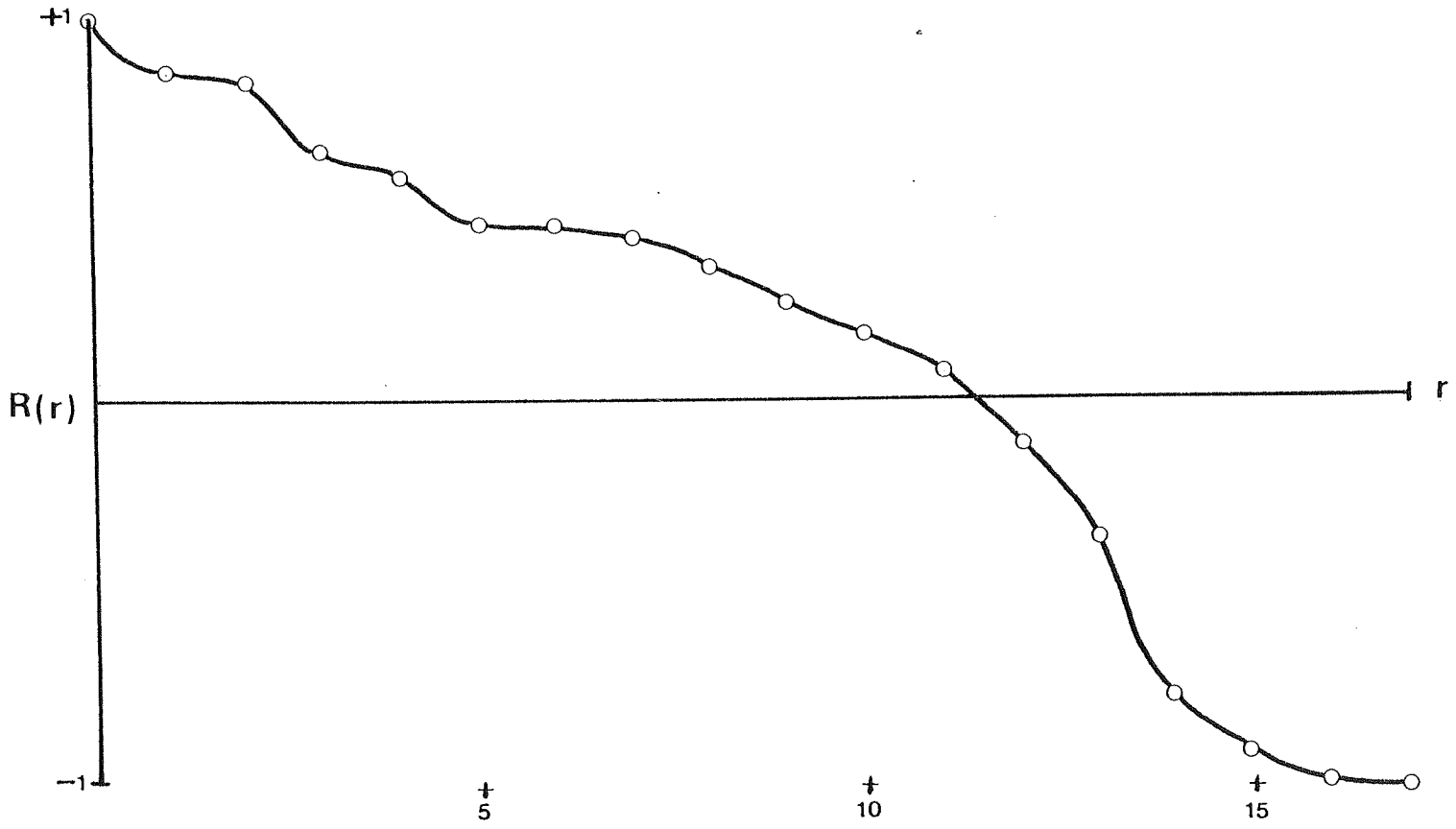

Figure 74. Correlograms of powder mixes containing Emdex carrier particles following vibration for 60 minutes at a frequency of 50 Hz and different accelerations.

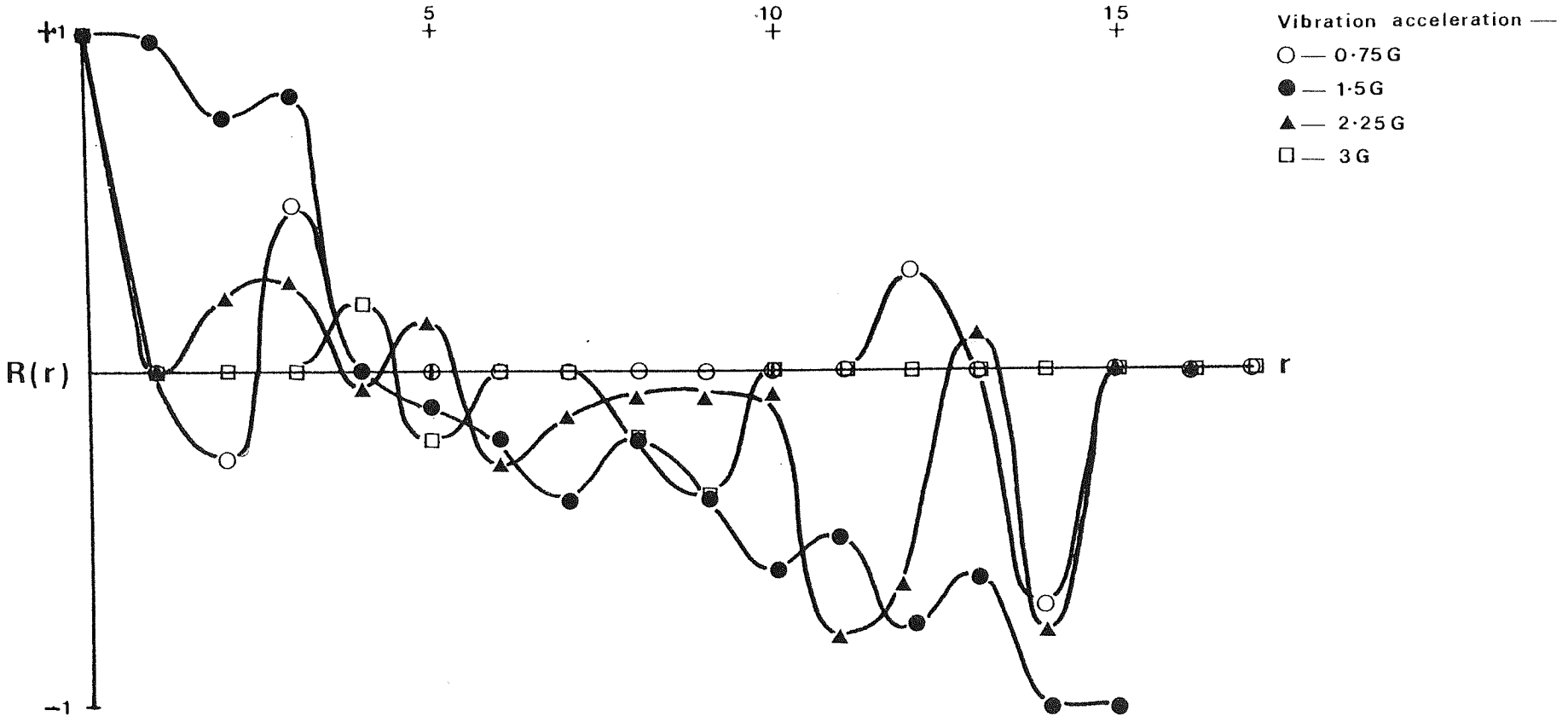

Figure 75. Correlograms of powder mixes containing Dipac carrier particles following vibration for 60 minutes at a frequency of 50 Hz and different accelerations.

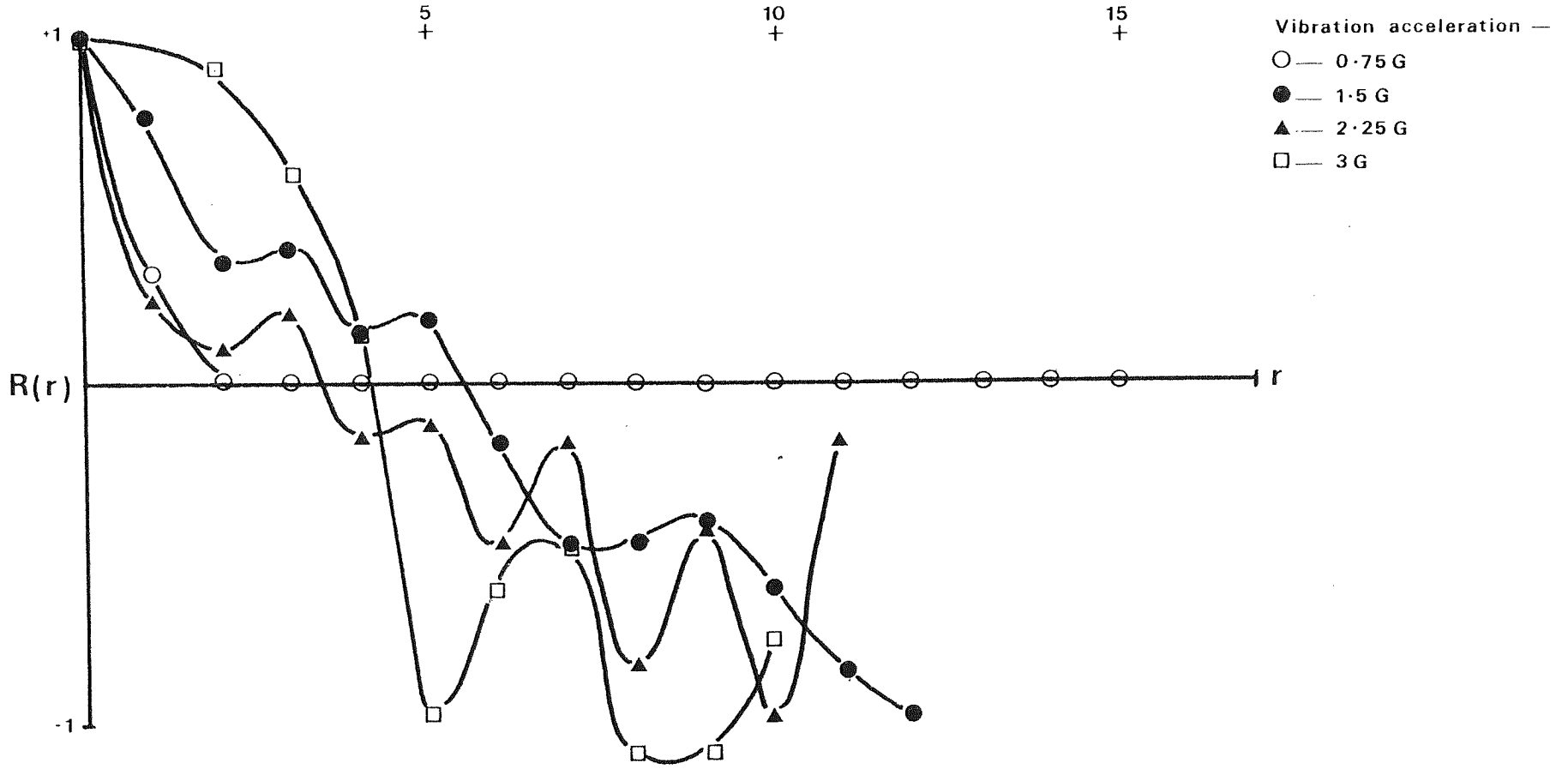

Figure 76. Correlograms of powder mixes containing Dipac carrier particles following vibration for 60 minutes at a frequency of 50 Hz and different accelerations.

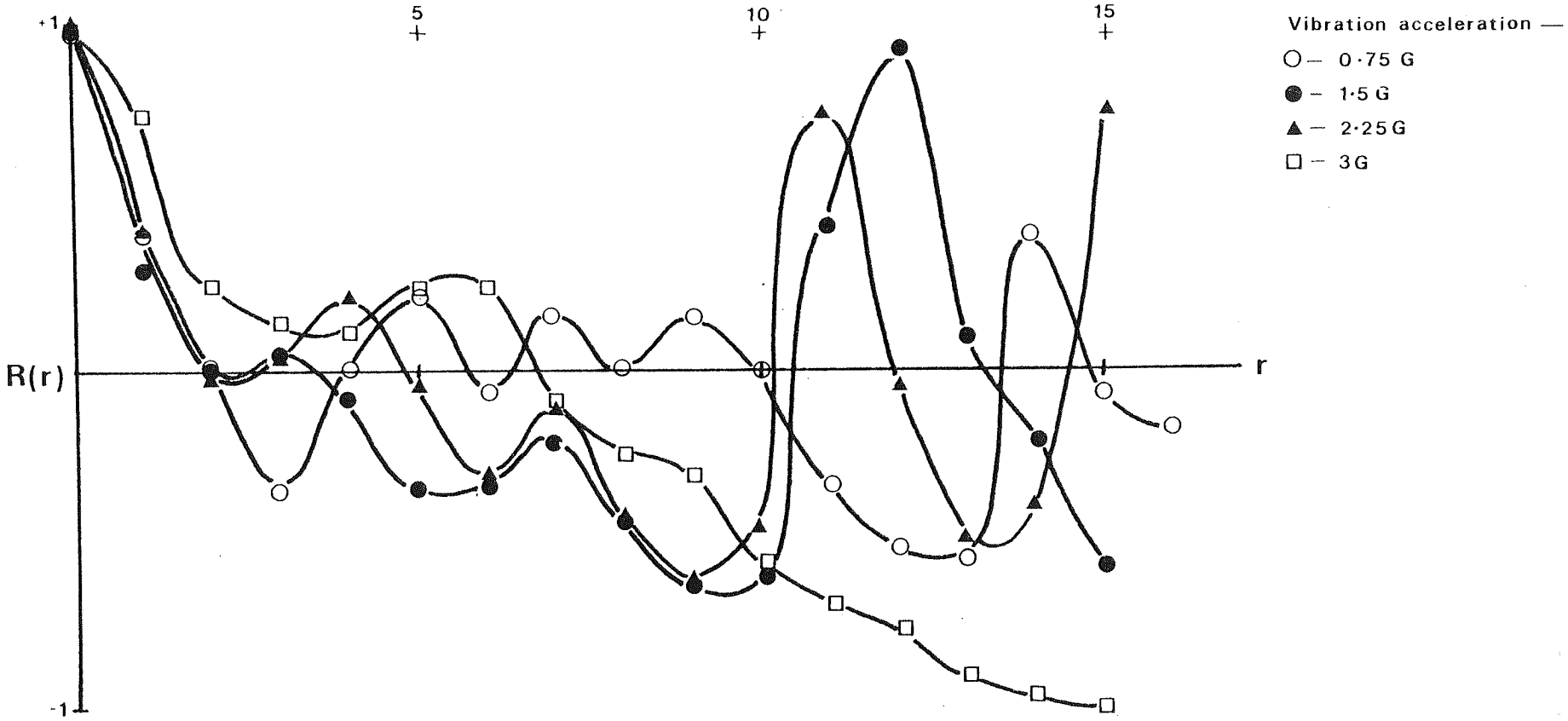

recrystallised lactose and potassium chloride showed a random relationship between samples separated by distances greater than r = 2. Some samples of Dipac separated by large distances showed that concentrations well to one side of the average could be associated with similar concentrations on the same side of the average as well as on the other side, over long distances. This type of correlogram also suggested that movement of drug particles was probably occurring simultaneously in opposite directions, an effect not previously considered. The major mechanism of powder movement is thought to have been percolation of fine particles down the powder bed but some upward movement may have occurred by trajectory segregation or a mechanism similar to diffusion. Neither the results for Emdex nor for recrystallised lactose particles suggested this type of movement to any large extent, although there was evidence of long-range movement which resulted in concentration differences on opposite sides of the mean when separated by distances greater than, r = 5.

The correlograms were developed by Danckwerts to calculate the scale of segregation, S_{seg}. The scale of segregation was defined as the area enclosed between the correlogram and the abcissa for values of r below the point at which R(r) first cuts the r axis ($R(r) = \zeta_1$) according to the following equation:

$$S_{seg} = \int_0^{\zeta_1} R(r).dr, \text{ where } R(\zeta_1) = 0 \qquad (88)$$

For this reason negative values were not considered in calculating the scales of segregation listed in Table 25:

Table 25. Scales of segregation of different drug and excipient mixes following vibration

Acceleration (G)	Scale of Segregation (S_{seg})		
	Emdex	Recrystallised Lactose	Dipac
0.75	0.063	0.085	0.154
1.5	0.307	0.227	0.180
2.25	0.063	0.096	0.184
3	0.063	0.302	0.212

The values for the scale of segregation of the different excipient systems had similar ranges. The scale of segregation is not the same as the intensity of segregation, thus the scale of segregation indicates the type of particle movement which occurs at any given intensity. The scale of segregation supplies information about the structure of the mixes, and values of S_{seg} will vary, for example, with the clump (aggregate) size of the potassium chloride particles distributed throughout the mix. The increasing scale of segregation in mixes of Dipac and potassium chloride subjected to increased acceleration forces showed that there was a gradual increase in the size of drug particle aggregates in the vibrated powder. If this hypothesis is correct Emdex and recrystallised lactose mixes showed a cyclic change in agglomerate or clump size with increasing vibration acceleration, and initial increases in clump size were followed by subsequent agglomerate breakdown. This type of changing pattern of clump formation and breakdown would indicate minor differences in the numbers of potassium chloride particles adhering to carrier particles in

different bed locations. As the carrier particles moved in the cylinder during vibration of the powder, these minor differences combined to produce the clumping effect disclosed by measurements of the scale of segregation. Alternatively, the vibrations may have caused dislodgement of some fine adherent drug particles which then formed agglomerates that were small enough to be re-dispersed by further vibrations.

The scales of segregation of different systems were compared using the following equation (230):

$$S_{seg\ 1,2} = \frac{\Sigma_r R(r)_1 . R(r_2)}{\{\Sigma_r R(r)_1^2\}^{\frac{1}{2}} . \{\Sigma_r R(r)_2^2\}^{\frac{1}{2}}} \qquad (89)$$

The similarity coefficient, $S_{seg\ 1,2}$, varies with $R(r)_1$, the correlation coefficient at a distance r for pattern 1 and $R(r)_2$ the correlation coefficient at the same distance for the pattern (correlogram) to be compared. The similarity coefficients had values between zero and ± 1, and were equal to unity in identical correlograms. Pattern 1 was taken as the reference correlogram for powders vibrated at 0.75 G acceleration and the subsequent correlograms were compared individually. Table 26 shows the relationship between correlograms obtained from measurements of powders vibrated at different acceleration forces.

None of the correlograms showed a good correlation with the reference vibration conditions; increasing acceleration forces produced changes in the scale of segregation probably by changing clump sizes of the model drug. The largest differences in similarity coefficients were found between correlograms produced by Dipac mixes.

Table 26. Similarity coefficients of different drug and excipient mixes following vibration for 15 minutes at 50 Hz

Acceleration (G)	Similarity Coefficient ($S_{seg\ 1,2}$)		
	Emdex	Recrystallised Lactose	Dipac
0.75	1.0	1.0	1.0
1.5	0.456	0.550	-0.191
2.25	0.607	0.554	0.449
3	0.644	0.458	0.500

Another similarity coefficient was obtained by comparing each correlogram with the correlogram of a mix with zero scale of segregation. Schofield (230) has shown that in this case equation (89) reduces to:

$$S_{seg\ 1} = \frac{1}{\left\{\Sigma R(r)_1^2\right\}^{\frac{1}{2}}} \qquad (90)$$

In these conditions each vibrated powder system was effectively compared with the scale of segregation in a mixed powder. Values of $S_{seg\ 1}$ close to unity indicate a system in which virtually no clumps of drug were present. Table 27 shows that the mixes of Dipac had a gradually decreasing similarity coefficient $S_{seg\ 1}$ as the acceleration of the vibrated powders increased.

The decreasing similarity between the scale of segregation of a Dipac/potassium chloride mix and that of a mixed system as the acceleration force increased was apparently caused by increasing clump size according to the results for scale of segregation in Table 25. The similarity coefficient $S_{seg\ 1}$ of

Table 27. Comparison of scales of segregation of various powder mixes with that of a completely mixed system.

Acceleration (G)	Similarity Coefficient ($S_{seg\ 1}$)		
	Emdex	Recrystallised Lactose	Dipac
0.75	0.733	0.951	0.647
1.5	0.400	0.461	0.501
2.25	0.593	0.539	0.521
3	0.882	0.369	0.392

of Emdex showed an initial decrease as the vibration acceleration increased but subsequently approached that of the mixed system. Systems containing clumps changed to ones with reduced clumping as acceleration force increased, because Emdex and lactose systems contained only small quantities of drug aggregates as shown by their low segregation intensities. Thus small changes in vibration conditions produced re-structuring of both the Emdex and recrystallised lactose systems with consequent formation or breakdown of aggregates. Relatively small changes in drug content produced large changes in the value of the similarity coefficient $S_{seg\ 1}$, due to the variance, $(x - \bar{x})^2$ used to calculate the correlation coefficients. The recrystallised lactose had a similarity coefficient $S_{seg\ 1}$ close to that of a non-clumped system at low vibration accelerations but the correlation apparently decreased and increased cyclically when the acceleration was subsequently increased. This trend of cyclic changes in the similarity coefficient with increasing acceleration may again have been caused by changes in the size of clumps which, like those in Emdex mixes, were small enough to break down and re-form without seriously affecting the overall powder homogeneity (determined previously by the coefficient of variation, section 4.3.2.1).

Danckwerts (174) also developed a relationship to determine the overall shape of any clumps or agglomerates formed in a mix, by comparing the volume of the clumps with that of a sphere of equivalent dimensions, according to the following equations:

$$V_{clump} = 2\pi \int_{0}^{\zeta_1} r^2 . R(r) . dr \qquad (91)$$

$$D_c = 3V_{clump}/4\pi S_{seg}^3 \qquad (92)$$

D_c, the clump shape coefficient was equal to unity when the aggregates were spherical. Although specific numerical values can be assigned to different clumps their relationship to actual geometrical shapes is a more difficult concept because of the ill-defined outlines which the clumps possess. Nevertheless, the clump shape coefficient can be used to differentiate between "streaky" (non-spherical) and "non-streaky" clumps. Table 28 shows the relationship between the calculated clump shape and the acceleration force, which the different mixes were subjected to during vibration.

Table 28. Clump shape coefficients D_c of different drug and excipient mixes following vibration

Acceleration (G)	Clump shape coefficient (D_c)		
	Emdex	Recrystallised Lactose	Dipac
0.75	2.39	1.31	2.22
1.5	3.83	3.03	1.29
2.25	2.39	7.34	1.44
3	2.39	3.92	14.52

All of the excipient/drug powder mixes formed clumps which were relatively "non-streaky" at low vibration accelerations. The recrystallised lactose clumps appeared to become relatively more "streaky" in powders vibrated at 2.25 G and Dipac mixes produced extremely "streaky" aggregates when vibrated with an acceleration of 3 G.

In addition to using the scale of segregation and other relationships developed by Danckwerts to describe the location of potassium chloride particles in a powder mix, another method was used, based on the deviation of individual sample concentrations from the mean drug concentration of all the powder samples. This technique was considerably simpler to use than the scale of segregation calculations and gave a direct assessment of the location of potassium chloride particles which could be related to the pharmacopoeial requirements for drug content uniformity.

4.3.2.3 Locations of Drug Concentrations in Powder Systems

The cylinder in which the powder mixes were vibrated was sampled at up to twenty different positions separated by equal vertical distances (Figure 58(a)). At each sampling level the drug concentration was determined and the difference from the overall sample mean was calculated. The deviation in concentration of individual powder samples from the mean was used to assess the drug distribution throughout the cylinder of vibrated powder. The relationship between the location of drug concentrations and specific parts of the powder bed was shown by plotting the deviation from the sample mean against the bed depth from which the sample was removed. Figures 77 to 91 show this relationship where the bed depth was represented by the sample number corresponding to

the cylinder unit from which each sample was removed. Sample number one was always removed from the first completely filled cylinder unit at the top of the powder bed and the sample number increased with the bed depth. The sample deviations were compared to the estimated appropriate pharmacopoeial specifications for microdose drug formulations (section 1.4.8) and this enabled the practical importance of individual sample deviations to be assessed based on a sample size of 200 mg and a nominal drug content of 1 mg (0.5%). Figures 77 to 81 show the concentrations of drug particles at different bed depths for Emdex/0.5% potassium chloride mixes vibrated in different conditions for different lengths of time. Figures 77 A, B, C and D show powders vibrated at low frequency, 20 Hz. At low acceleration forces around 0.75 G (Figures 77 A, B) there appeared to be a tendency for the upper parts of the powder bed to become depleted in potassium chloride content. This effect was most evident after prolonged vibration (Figure 77 B) where the potassium chloride lost from the top of the powder bed, accumulated lower in the cylinder and did not continue to fall any further. This drug depletion at the top of the powder bed was probably caused by the increased movement of individual particles in a mobile upper layer. The same tendency was also apparent, although less marked when the vibration acceleration was increased to 1.2 and 1.5 G (Figures 77 C & D), but the overall coefficients of variation of these powders did not exceed 2.3% (section 4.3.2.1). An increase in the vibration frequency to 50 Hz (Figure 78) also produced a general depletion in the potassium chloride content at the top of the powder cylinder. However, this only occurred after prolonged vibration of 30-60

minutes with accelerations of 0.75 G, 1.5 G and 2.25 G (Figure 78 B, D and F) and the depletion extended to a smaller depth than in powders vibrated at a frequency of 20 Hz. For higher acceleration forces, powder mixes vibrated at 50 Hz had a greater segregation tendency in the lower parts of the powder bed where short-range effects appeared to predominate (Figure 78 F, G and H); however again the overall coefficients of variation were low and did not exceed 2.2%. A very similar trend occurred in the Emdex systems vibrated at frequencies of 100 Hz (Figure 79); at the low acceleration forces of 0.75 G and 1.5 G, vibration for long periods produced a slight depletion in drug at the top of the cylinder, followed by a rise in drug content in the levels immediately below and a small long-range effect demonstrated by rises which occurred towards the cylinder base (Figure 79 B, C and D). This long-range segregation tendency was likely caused by a small amount of the fine drug powder percolating through the powder bed to the base without becoming re-ordered or blocked by local increases in bulk density. The extent or range of this percolation segregation effect appeared to be governed by the vibration time. At higher acceleration forces, the percolation effect was obscured by short-range segregation tendencies lower down the powder bed (indicated by larger deviations from the mean) caused by increased powder motion during the churning produced by the increased acceleration (Figure 79 F, G and H).

In Emdex mixes vibrated at 500 Hz there was again a slight depletion in drug content at the top of the cylinder (Figure 80); however under these conditions there was no evidence of the segregation tendencies towards the base of the powder bed found at high acceleration forces in powders vibrated at lower frequencies

(Figure 80 F, G and H). Most of the powders vibrated at 500 Hz had coefficients of variation not exceeding 1.9% and individual samples were within the pharmacopoeial limits for drug content. This was also true for Emdex mixes vibrated at a frequency of 1000 Hz (Figure 81), where almost all the powder samples were within the pharmacopoeial specification limits, indicating that there was virtually no segregation tendency at this high frequency. Powders vibrated at high acceleration forces for prolonged periods did not show any segregation effects at 1000 Hz frequency, probably because of the infinitesimal duration of particle flight which did not allow enough time or dilation space for segregation to occur.

Figures 82 to 86 show the corresponding data for powder samples containing 0.5% potassium chloride and recrystallised lactose.

There was only a slight segregation tendency in mixes vibrated at a frequency of 20 Hz, although a slight accumulation of potassium chloride at the top of the powder was observed (Figure 82, A, B, C and D). This increase in drug concentration was largest in recrystallised lactose vibrated with an acceleration of 1.5 G for 60 minutes (Figure 82 D) and may have been caused by slight accumulation of coarse carrier particles rich in adherent drug particles rising towards the powder surface. However, the increase may have been caused by free drug particles being thrown upwards in a type of "trajectory" segregation which could also be related to a diffusion segregation method discussed later.

When the frequency was increased to 50 Hz (Figures 83 A & B), powder mixes vibrated at 0.75 G for short times showed no segregation tendency, but for vibrations longer than 15 minutes duration an

increased drug concentration was again found at the top of the powder bed (Figure 83 C) and the corresponding depletion in drug content in other parts of the powder bed was found in samples as low down the bed as level 10. This reduction in drug depletion was evident over the upper two-thirds of the bed depth and suggests that upward movement of drug rich coarse carrier particles occurred from low down the powder bed; this particle movement was not restricted to particle exchange in the mobile upper layer near the powder surface. For acceleration forces above 0.75 G at frequencies of 50 Hz (Figure 83) this upward movement of drug particles was possibly obscured or replaced by fine particles of potassium chloride becoming segregated from lactose carrier particles by percolating down the powder bed; this net downward movement of drug particles caused a depletion in potassium chloride content in samples from the top of the powder cylinder (Figure 83 D, E, F, G and H). At the highest acceleration force of 3 G (Figure 83 I) the depletion in drug concentration at the powder surface produced a corresponding marked increase in potassium chloride concentration towards the base of the powder bed after prolonged vibration. However, although each of the vibration conditions caused some movement of drug particles, the overall segregation effect was small and the coefficient of variation did not exceed 5.7%. There was no segregation tendency in recrystallised lactose vibrated at 100 Hz and low acceleration forces (Figure 84 A & B) although when the acceleration increased to 1.5 G (Figures 84 C, D) there was a reduction in the drug concentration at the top of the cylinder caused by the percolation mechanism. As the acceleration force was further increased there was a proliferation of short-range

segregation effects lower down the cylinder after prolonged vibration (Figure 84 F, H) but the overall coefficients of variation remained low. In recrystallised lactose systems vibrated at a frequency of 500 Hz with low accelerations there was no tendency for segregation of potassium chloride (Figure 85 A, B). When the acceleration was increased to 1.5 G, a depletion in drug content was observed at the top of the powder bed and corresponding rises in drug concentration occurred at different points further down the cylinder (Figure 85 C). This effect was most noticeable after prolonged vibration (Figure 85 D) although the percolation distance of drug particles remained small; percolation may have been restricted by resonance effects in the vibrated cylinder producing an increase in bulk density in powder just below the surface of the bed (see later in this section). Below this level of probable increased density, percolation again occurred and there was a small accumulation of drug particles near the cylinder base. At higher acceleration forces (Figures 85 E, F) the segregation tendencies were mainly short range effects producing local increases or decreases in drug content in different parts of the powder bed. However, when the acceleration force was increased to 3 G (Figure 85 G & H) there was a long-range segregation tendency with drug content increasing near the powder base. In recrystallised lactose and drug mixes vibrated at 1000 Hz (Figure 86) there were few observable segregation tendencies, although in powders vibrated with an acceleration of 1.5 G for prolonged periods (Figure 86 D) there was a slight depletion in drug content near the powder surface and a corresponding sharp increase part way down the powder bed. This effect was probably caused by percolation of fine potassium chloride particles dislodged from carrier particles of recrystallised

lactose. Percolation of fine particles also appeared to be the predominant segregation mechanism of drugs in mixes of Emdex and recrystallised lactose subjected to vibrations of different intensity and duration. As was found when the segregation intensities of vibrated powders were measured by coefficients of variation (section 4.3.2.1), the results for Emdex and lactose mixes in Figures 77 to 86 did not exhibit marked segregation of individual powder samples in terms of deviation from the content uniformity limits required by British and U.S. pharmacopoeial standards.

The effect of vibration conditions on the segregation tendency of mixes of Dipac and 0.5% potassium chloride is shown in Figures 87 to 91. In Dipac vibrated at 20 Hz, there were several short-range effects producing marked segregation of potassium chloride together with two long range segregation effects which changed as the vibration acceleration increased (Figure 87 A to H). For powders vibrated at 0.75 G there was an increased drug concentration towards the top of the cylinder, with corresponding depletion in drug further down the powder bed (Figure 87 A, B). This effect was more noticeable in powders vibrated for 15 minutes at an acceleration force of 1.5 G (Figure 87 C). The sharp increase in drug content at the powder surface was followed by a depletion in concentration at all other bed depths and could have been caused by "ordered unit segregation" or by "constituent segregation". The number of fine potassium chloride particles which a single Dipac particle was theoretically capable of carrying in a stereometrically hexagonal close-packed monolayer was calculated from the following equation (66):

$$\eta = \frac{2\pi (D + d)^2}{\sqrt{3}.d^2} \qquad (93)$$

This number of adherent particles will be referred to here as the saturation level for the specific carrier particle material and is in this case equivalent to 3,995 fine potassium chloride particles adhering to each Dipac carrier particle. The theoretical number of adherent particles which each Dipac particle was required to carry to form an ordered mix with 0.5% potassium chloride was only 107, which is well below the saturation level. It was therefore clear that there existed many more theoretical adherence sites than potential adherent particles. However, for the increase in drug concentration at the powder surface shown by Figure 87 C to be produced by an ordered unit segregation mechanism, each ordered unit would have to carry at least 234 more potassium chloride particles, than carrier particles in the rest of the powder bed. Although this number is still considerably lower than the theoretical saturation level it required that some Dipac particles carried over twice as many drug particles as other, apparently identical, particles. In addition to this theoretical reasoning, a practical observation supported the view that the observed segregation in Dipac mixes as shown in Figure 87 C was not caused by the mechanism of ordered unit segregation; these observations were made on the powder cylinder after vibration and prior to sampling. It was noticed that the whole of the powder surface was covered in a layer of fine particles to a depth of about 4 mm which is equivalent to approximately one third of one sample level. This increased drug concentration at the powder surface therefore appears to have been caused by fine particles of potassium chloride becoming dislodged from carrier particles under the vibration conditions. The free fine particles could then travel up through the powder bed by a type of "trajectory"

segregation or "diffusion" mechanism.

Strek *et al.* (58) formulated a "law of diffusional segregation" in which they considered that the mass flow perpendicular to a given area was directly proportional to the concentration gradient in the mass transport direction, expressed by the following equation which is analogous to Fick's first law of diffusion:

$$\frac{\delta m}{\delta t} = \frac{D_s'}{tK} \cdot \delta c_s(r,t)/\delta r \qquad (94)$$

where D_s' is the segregation coefficient; t is time; K is a constant; $\delta m/\delta t$, the unit mass flow of the drug particles and $\delta_{c_s}(r,t)/\delta_r$, the boundary condition expressed as a function of the segregation tendency. Although any mechanism of diffusional segregation must work against an apparent concentration gradient, the conditions existing in the vibrated bed of drug and excipient particles extended the effective bed depth of the powder because prolonged particle flight produced and maintained bed dilation. Under these conditions the bed effectively extended into an area beyond the static powder surface. Fine particles of drug projected into this area by vibrations produced drug depletion in the region immediately below the sub-flight surface causing upward movement of particles by diffusion in a normal concentration gradient. During vibration the period during which free fine drug particles were not in flight was small but following vibration, when the bed again became static a fine layer of drug particles which had been fluidised above the bed now settled back onto the surface of the powder. The vigour of vibrofluidisation was often seen to produce a cloud of fine particles above the vibrating powder surface and during intense vibration the fine particles were forced out of the cylinder by

gas compression described in the model developed by Gutman (158). Vibrofluidisation was only observed in powders vibrated at low frequencies and this phenomenon has also been described by Harwood (147). Rowe et al. (141) described a fluidised system in which fine particles were displaced upwards through a packed bed of coarser particles; this occurred because of the lower fluidisation velocity of the finer particle component and because downward percolation was prevented by the upward air flow. When the fluidising air velocity increased, the coarse particles were also carried to the surface. In the vibration conditions used in this study, an increase in acceleration to 2.25 G and above produced vibrofluidisation of the Dipac particles as well as the fine potassium chloride particles; this caused upward displacement to become the dominant mechanism of segregation under these higher vibration acceleration conditions. Upward segregation of fine particles during fluidisation is due to entrainment of particles in the bubble wake or area immediately following the upward moving air bubble (223) and, although bubble formation may occur during intense vibration at low frequencies, it is more probable that upward movement occurs by some mechanism analogous to diffusion. The role of vibrofluidisation in this diffusion model of segregation was to create a reservoir of drug particles in a fluidised zone above the vibrating powder surface. The resulting depletion in drug concentration at the bed surface created the necessary concentration gradient for drug particles to rise to the powder surface, where they in turn were fluidised thus maintaining the gradient.

When vibrofluidisation occurred in the Dipac powder mixes vibrated at low frequencies, 20 - 100 Hz, it is likely that the two segregation mechanisms, downward percolation and upward diffusion,

occurred together - upward diffusion predominating in conditions producing particle flight in the fine drug fraction of the mix, and downward percolation predominating when vibrofluidisation conditions were intense enough to produce particle flight of the whole powder bed. Under vibration conditions where vibrofluidisation did not occur, percolation would be the sole segregation mechanism.

As shown earlier, no segregation occurred in Emdex powder mixes vibrated at low frequencies, and only a small amount of diffusive segregation was apparent in recrystallised lactose mixes: thus it seems that the effects of vibrofluidisation discussed above are only evident in ordered mixes where there are free fine particles of the adherent component.

The long-range segregation effect whereby drug particles moved to the surface of the powder bed became less pronounced as vibration time increased (Figure 87 D, E).

When the acceleration force was increased to 2.25 G there was an increase in drug concentration towards the base of the powder bed (Figure 87 F). This long-range downward segregation effect became very marked after prolonged vibration, producing intense overall segregation with coefficients of variation around 100% (Figure 87 G) presumably by percolation of large numbers of potassium chloride particles towards the powder base. The vibration conditions would dislodge fine drug particles from Dipac carrier particles. Once dislodged, the fines percolate down through the bed and may be unable to become re-ordered with different carrier particles because of the vibration conditions. During prolonged vibration there is sufficient time for a large quantity of drug particles to become dislodged and percolate right down to the cylinder base. A similar accumulation of fine drug particles in

the lower part of the cylinder occurred when the acceleration force was increased to 3 G (Figure 87 H, I). When the frequency was increased to 50 Hz (Figures 88A and B) there was only a small movement of drug particles vibrated at 0.75 G and there were no apparent long-range segregation effects. However, when the acceleration force was increased to 1.5 G there was marked segregation in all parts of the powder bed (Figure 88 C, D). Segregation was present as large short-range effects with a long-range tendency for drug particles to percolate downwards to a position mid-way down the cylinder, leaving a drug deficient area at the surface of the powder bed (Figure 88 C). This long-range effect became more marked during prolonged vibration and there was some evidence for a small amount of upward movement of drug particles from the bottom of the powder bed towards the middle of the cylinder (Figure 88 D). This was shown by a lowered drug concentration in the lower part of the cylinder following vibration for one hour. The apparent upward movement of fine potassium chloride particles may have been caused by a resonance effect in which an anti-node centred on the middle of the tube produced a static area of powder with mobile regions above and below it. Resonance of a system of a powder cylinder in forced vibration exists when any change, however small, in the frequency of excitation causes a decrease in the response of the system, i.e. a resonant frequency is defined as the frequency for which response is a maximum. Resonance produced in a system being subjected to forced vibration can therefore alternatively be defined as a decrease in the intensity of vibration in a system resulting from a change in the frequency of excitation (224).

Figure 92. Frequency response curve for a vibrated cylinder containing Dipac and potassium chloride powder.

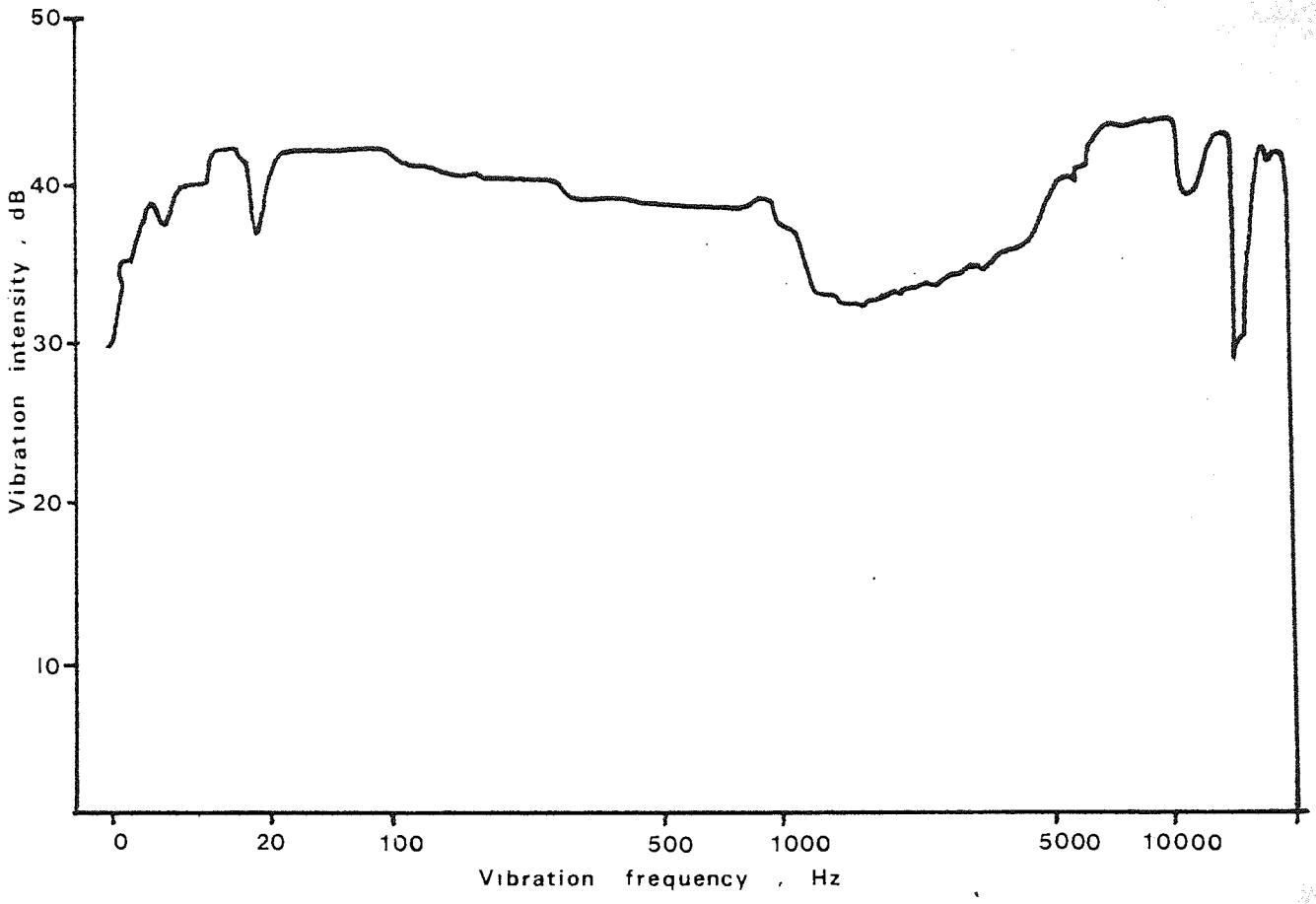

Figure 92 shows the frequency-response curve, independent of specific accelerations, for the vibrated cylinder containing Dipac and potassium chloride; the frequency response curves for Emdex and recrystallised lactose mixes were very similar to this. There were several resonance effects around the 20 - 50 Hz frequency range which could have been responsible for a change in the vibrational conditions within the powder beds.

As shown in Figure 88 E, when the acceleration force was increased to 2.25 G the resonance effect discussed above seems to have virtually disappeared since there was no marked deficiency of drug near the cylinder base. However there was still some short-range segregation producing increased drug concentration towards the middle of the vertical powder bed (Figure 88 E).

Associated with this was a slight long-range tendency for fine drug particles to move downwards away from the powder surface by percolation. This effect was increased when the vibration time was prolonged (Figure 88 F) and fine particles of potassium chloride percolated to the base of the powder bed. An increase in acceleration force to 3 G again produced considerable short-range segregation tendencies (Figure 88 G). As in powders vibrated with an acceleration of 2.25 G prolonged vibration (Figure 88 H) produced long-range segregation, where percolation of fines towards the cylinder base again occurred. In all the Dipac powders vibrated at 50 Hz the conditions produced very intense segregation so that samples had drug concentrations outside the content uniformity limits required by pharmacopoeial standards for microdose drugs.

The frequency was further increased to 100 Hz (Figure 89 A, B) and the small segregation tendency in powders vibrated at 0.75 G for 5 - 15 minutes increased when vibration was prolonged to 30 - 60 minutes. There was a tendency for a reduced drug concentration at the powder surface (Figure 89 B) which became more apparent when the vibration acceleration was increased to 1.5 G (Figure 89 C, D). However, as occurred in powders vibrated at 50 Hz with intermediate acceleration, there was a tendency for drug to accumulate near the middle of the cylinder and also further evidence of upward movement of drug particles from the base of the powder bed. This effect may again have been the result of resonance effects in the vibrated cylinder causing powder in separate sections of the bed to behave differently. When the acceleration force was increased to 2.25 G (Figure 89 E) the percolation mechanism again became dominant with fine drug particles moving downwards away from the top of the cylinder. The extent of

this long-range effect increased with prolonged vibration (Figure 89 F) and under these conditions the drug accumulated at the cylinder base. A similar pattern was found when the acceleration force was increased to 3 G (Figure 89 G, H) and there was an associated increase in the amount of drug particles percolating down through the powder bed under these more vigorous segregation condiitons. As in Dipac mixes vibrated at 50 Hz, the powders vibrated at 100 Hz produced intense segregation with coefficients of variation often around 40%, apparently caused mainly by the percolation mechanism. In comparison with the effects at lower frequencies, powder vibrated at 500 Hz appeared to have a smaller segregation tendency. For example, segregation effects were negligible in powders vibrated at 0.75 G (Figure 90 A) although some short-range percolation occurred when vibration was prolonged (Figure 90 B). When the acceleration force was increased to 1.5 G (Figure 90 C) there was only slight segregation after five minutes vibration time, but some short-range percolation of particles at the powder surface was evident after 15 minutes. The range of drug particle percolation increased with the vibration time as did the quantity of particles moving down the bed (Figure 90 D). An increase in vibration acceleration force to 2.25 G (Figure 90 E, F) produced no change in the depth the percolating particles reached, although the drug concentration at this level, about one third the distance down the cylinder, increased slightly. There was no segregation of particles below this level. A further increase in acceleration force to 3 G again produced little change in the depth to which the particles percolated (Figure 90 G, H). This may have been a result of some resonance in the vibrated cylinder or it could have been caused by the decreased flight

time of particles at 500 Hz. The marked segregation produced after prolonged vibration (Figure 90 H) suggested that large quantities of drug particles were being displaced from their carrier particles but only those in the upper parts of the cylinder had any freedom to segregate. Percolation of these particles ended just above the middle of the cylinder, probably due to increased bulk density of powder below this level reducing interparticle void spaces and preventing powder turbulence.

Using an accelerometer fixed to the side of the vibrating cylinder at different bed depths, the effect of resonance at a vertical frequency of 500 Hz and a vertical acceleration of 3 G was determined. The accelerometer measured the horizontal component of vibration acceleration. Figure 93 shows the horizontal acceleration of the powder cylinder at different bed depths. The level of maximum horizontal acceleration was found to correspond to sample level number eight which was also the point where a large amount of drug was concentrated following vibration. The large horizontal vibration component combined with the vertical vibration to increase the bulk density in the lower part of the cylinder probably by causing closer packing of particles and thus prevented free movement of dislodged fine particles of potassium chloride higher up the cylinder.

The decreased intensity of segregation produced by a vibration frequency of 500 Hz, was further reduced when the frequency was raised to 1000 Hz (Figure 91). At this high frequency there was only a small segregation tendency even at high acceleration forces after prolonged vibration although this was still more marked than in other excipient systems (Figure 91 F, H). The marked decrease in powder segregation was caused by the high frequency of vibration;

this limited the particle movement by reducing the duration of particle flight to minute fractions of a second. When segregation occurred it was in powders vibrated at high acceleration forces for prolonged periods (Figure 91 F, H). The segregation effects were short-range movements caused by small-scale percolation of drug particles. Since percolation can occur spontaneously (130), the higher vibration accelerations, 2.25 and 3 G, which produced segregation at 1000 Hz may have caused adherent drug particles to become dislodged from carrier Dipac particles, percolation subsequently occurring spontaneously.

To summarise the foregoing discussion, as in Emdex and recrystallised lactose subjected to different vibration conditions, the most common segregation mechanism affecting fine drug particles dislodged from Dipac carrier particles was percolation. At low frequencies there was a tendency for free drug particles to move upwards through the vibrated powder bed when vibrated, probably caused by a diffusion mechanism associated with specific resonance conditions and the creation of vibrofluidisation.

Segregation occurred by movement of free drug particles dislodged from the surface of carrier particles and there was no evidence to suggest that "ordered unit" segregation was a significant effect under these conditions. Both the vibration frequency and the acceleration force influenced the segregation mechanism. At some low frequencies the predominant segregation mechanism was diffusion, whereas at higher frequencies this changed to percolation. Percolation was also the main segregation mechanism in powders vibrated at low frequencies with accelerations greater than 1.5 G. At very high frequencies, vibration dislodged particles which segregated by spontaneous percolation.

Figures 77 to 91

Relationship between drug concentration at specific levels in powder beds following vibration under different vibration conditions.

b and p are the upper and lower content uniformity limits for B.P. preparations containing small quantities of potent drugs and represent a variation of ± 10% of the mean drug content.

u and s are the upper and lower content uniformity limits for U.S. pharmacopoeial microdose drug preparations and represent a variation of ± 15% of the mean drug content.

The captions on each figure define the drug/excipient system, vibration time, frequency (Hz) and the acceleration force (G).

The individual sample size = 200 mg corresponding to a nominal drug content of 1 mg.

The powder surface at the top of the cylinder is represented by sample number 1.

Figure 77. A. Emdex and potassium

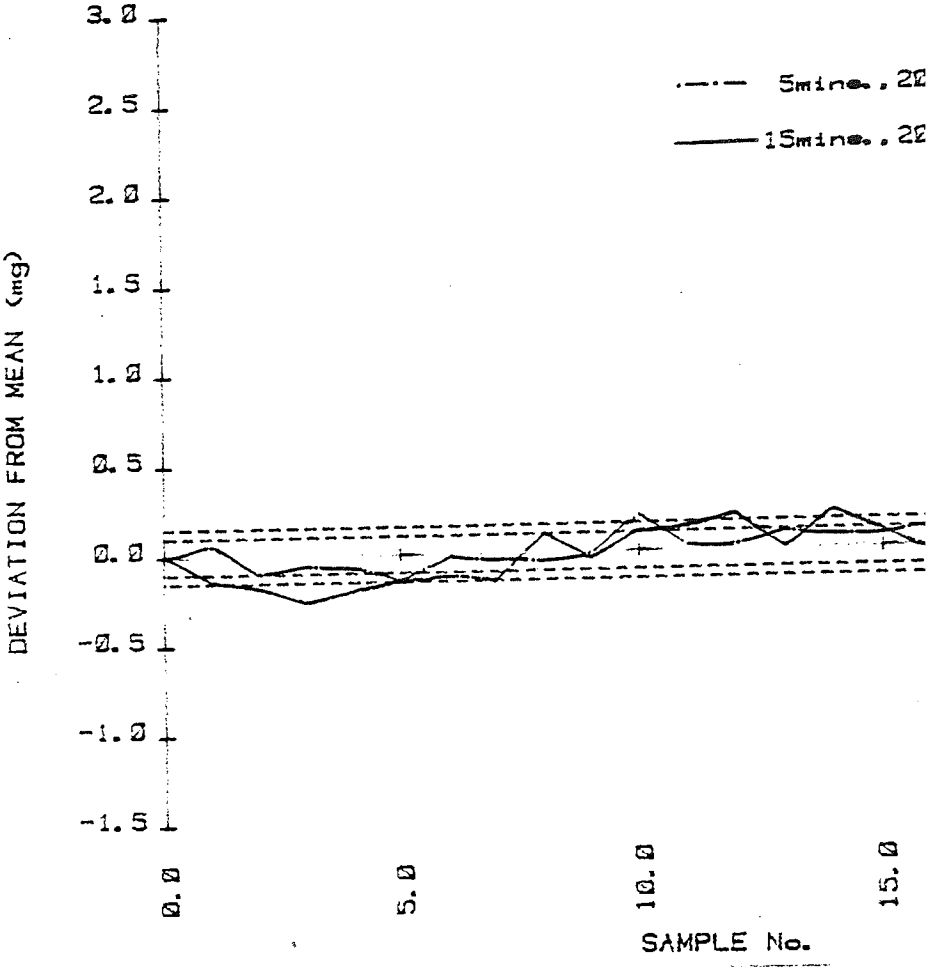

B. Emdex & potassium c

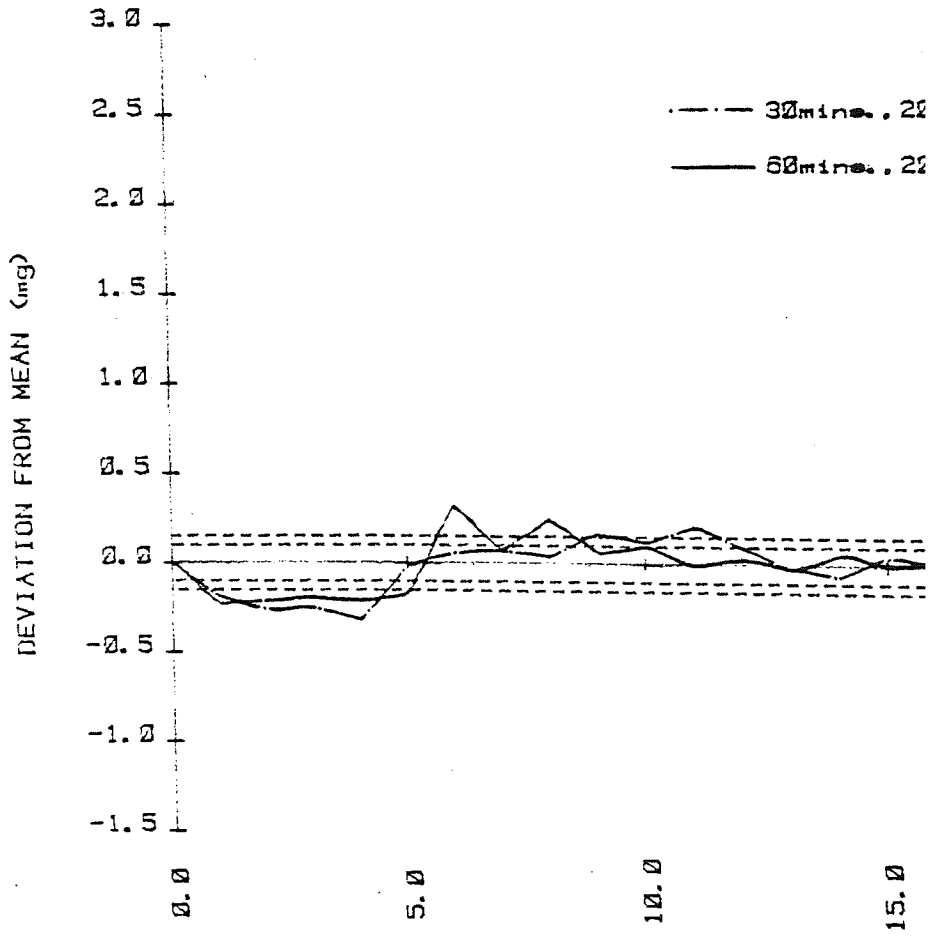

Figure 77. D. Emdex & potassium chloride 0.5%

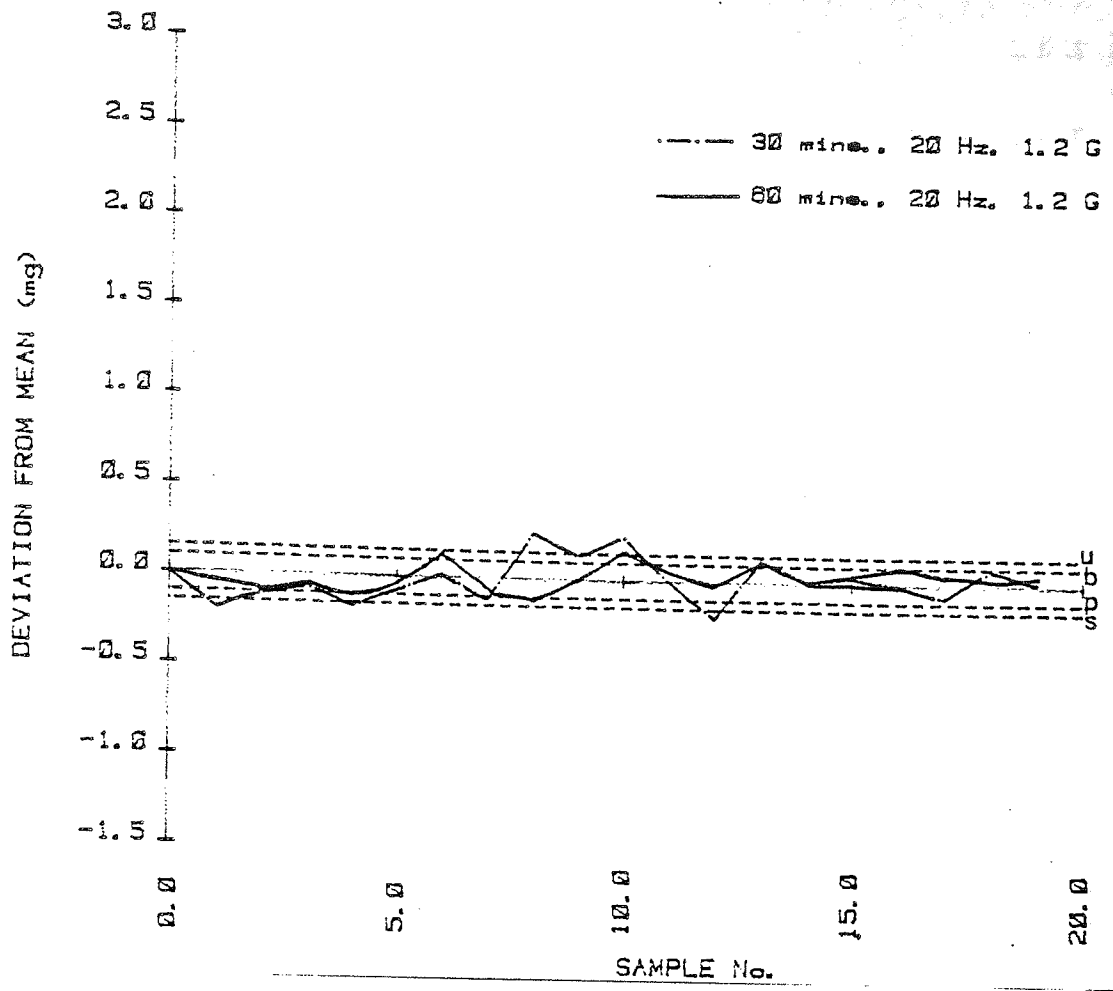

C. Emdex & potassium chloride 0.5%

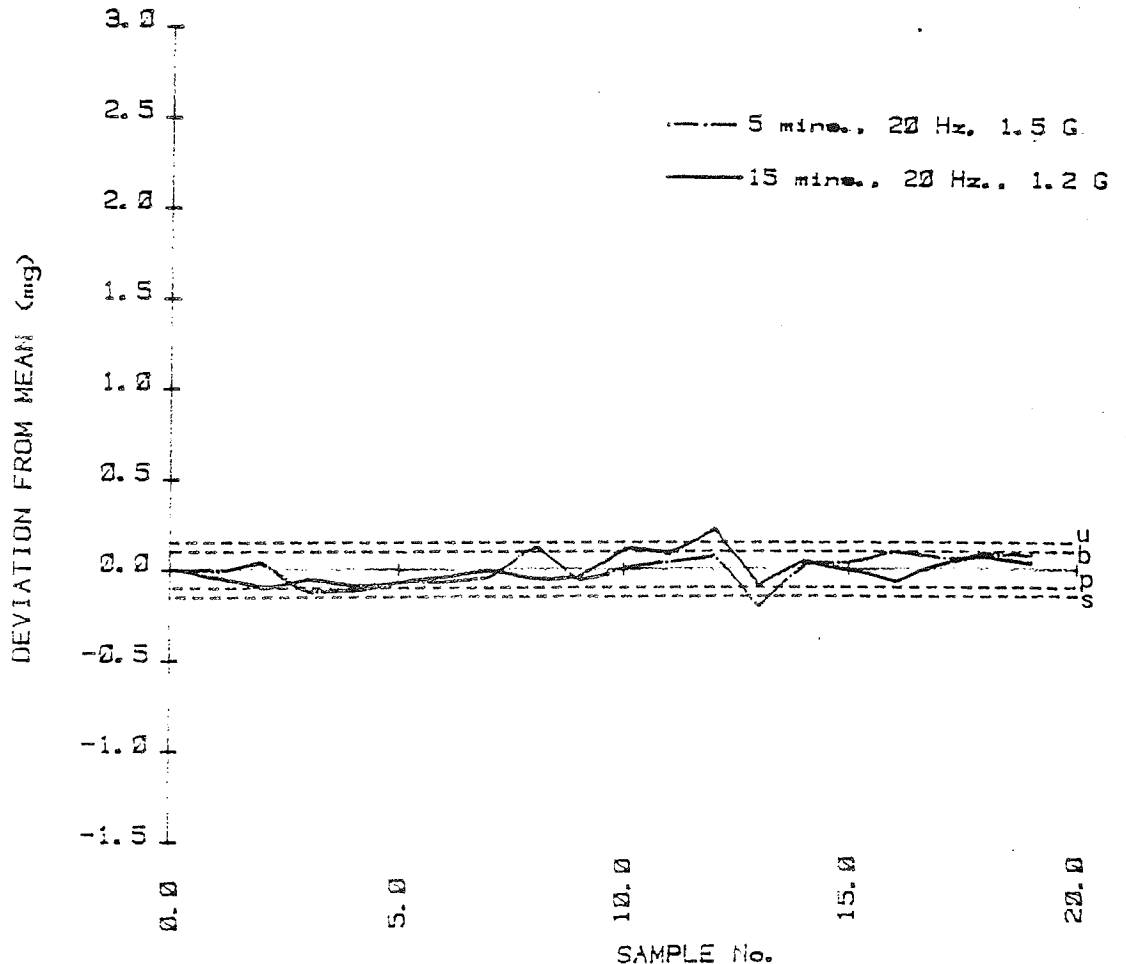

Figure 78. A. Emdex & potassium ch.

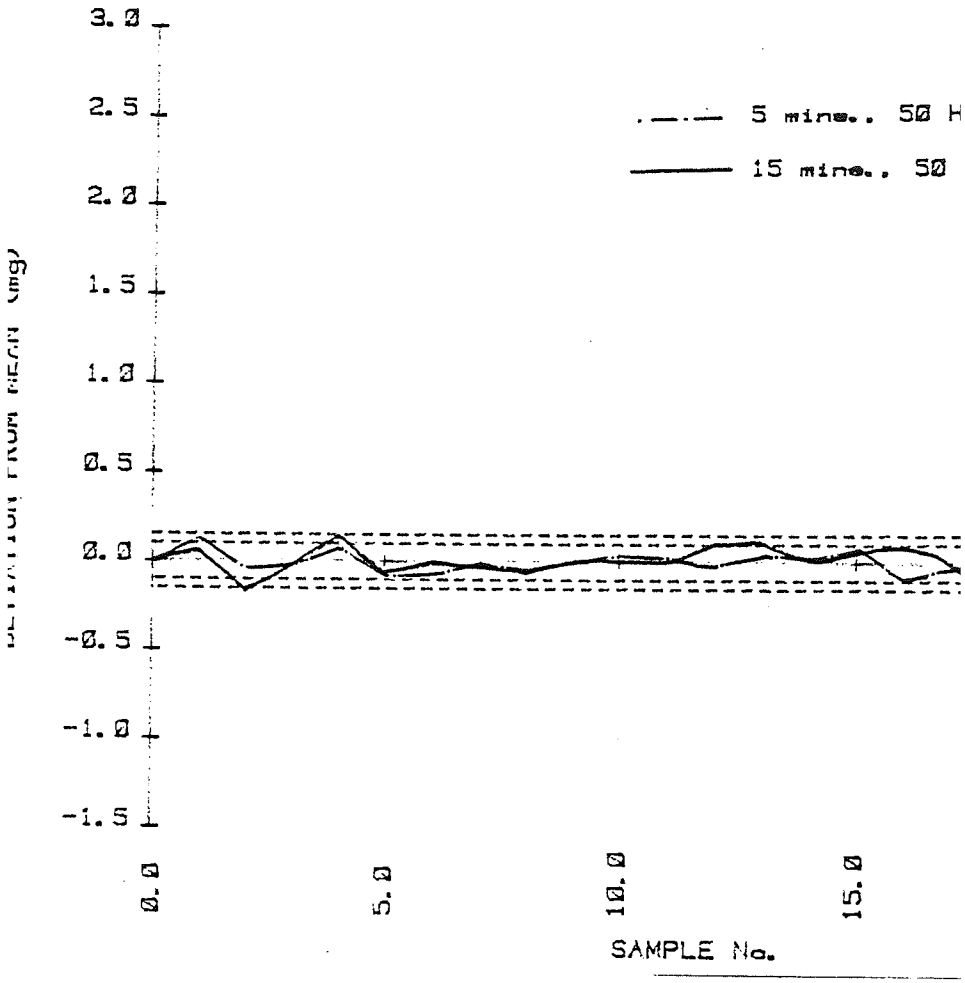

B. Emdex & potassium chlo

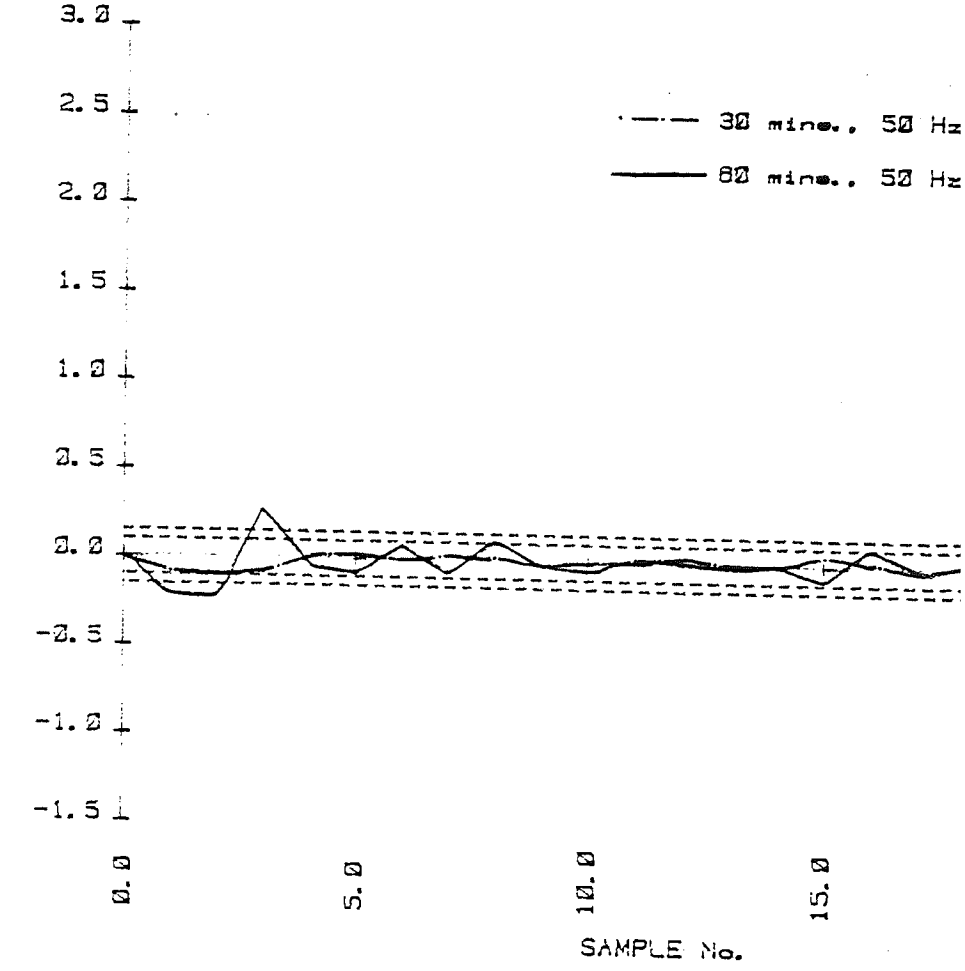

Figure 78. C. Emdex & potassium chloride 0.5%

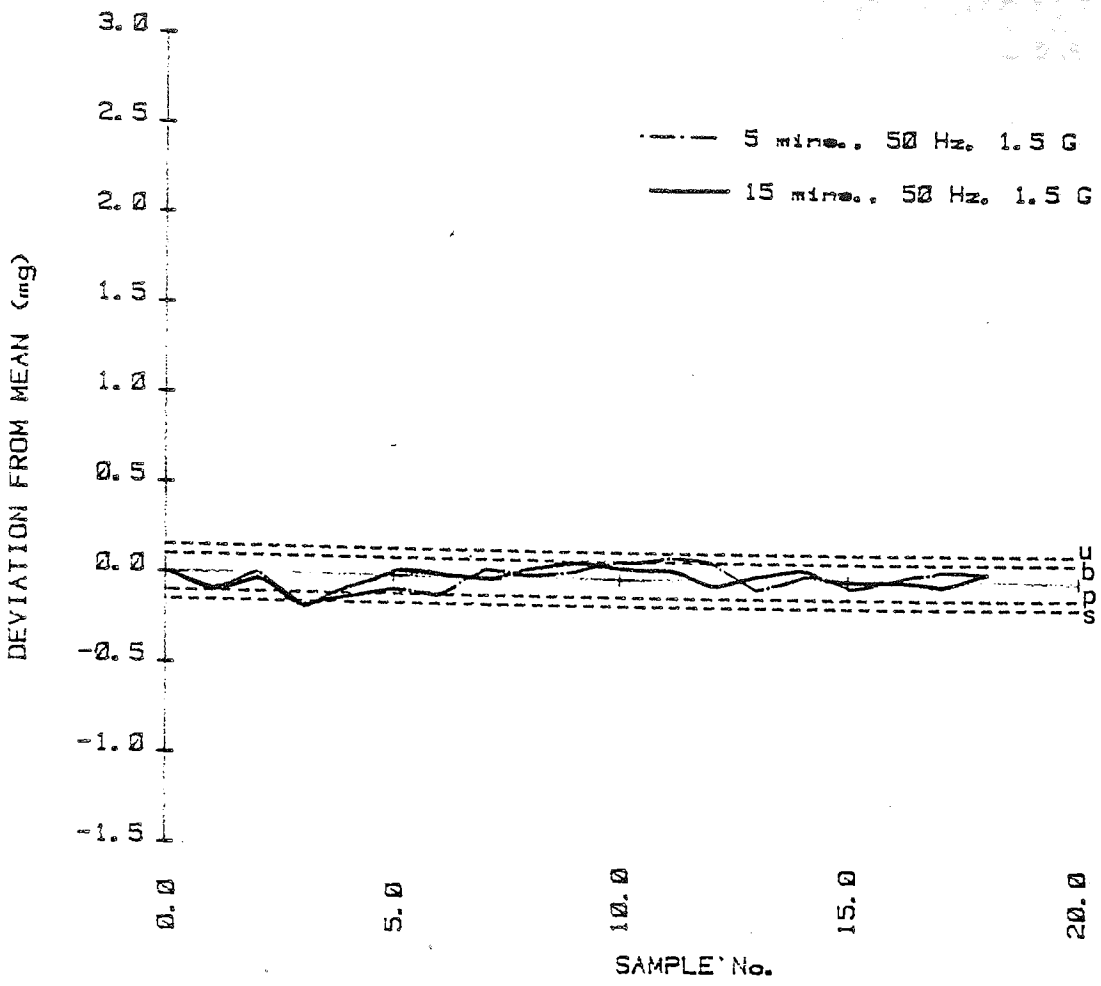

D. Emdex & potassium chloride 0.5%

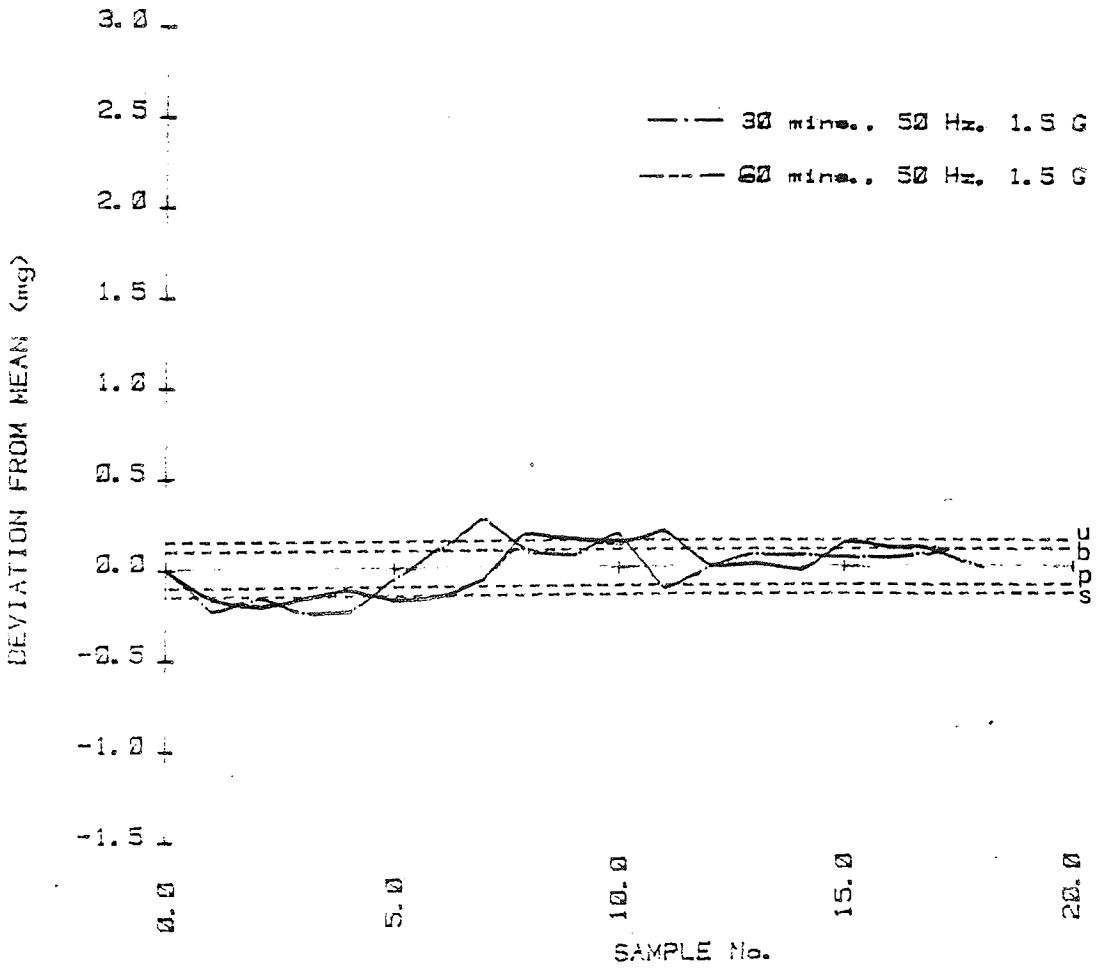

Figure 78. E. Emdex & potassium ch

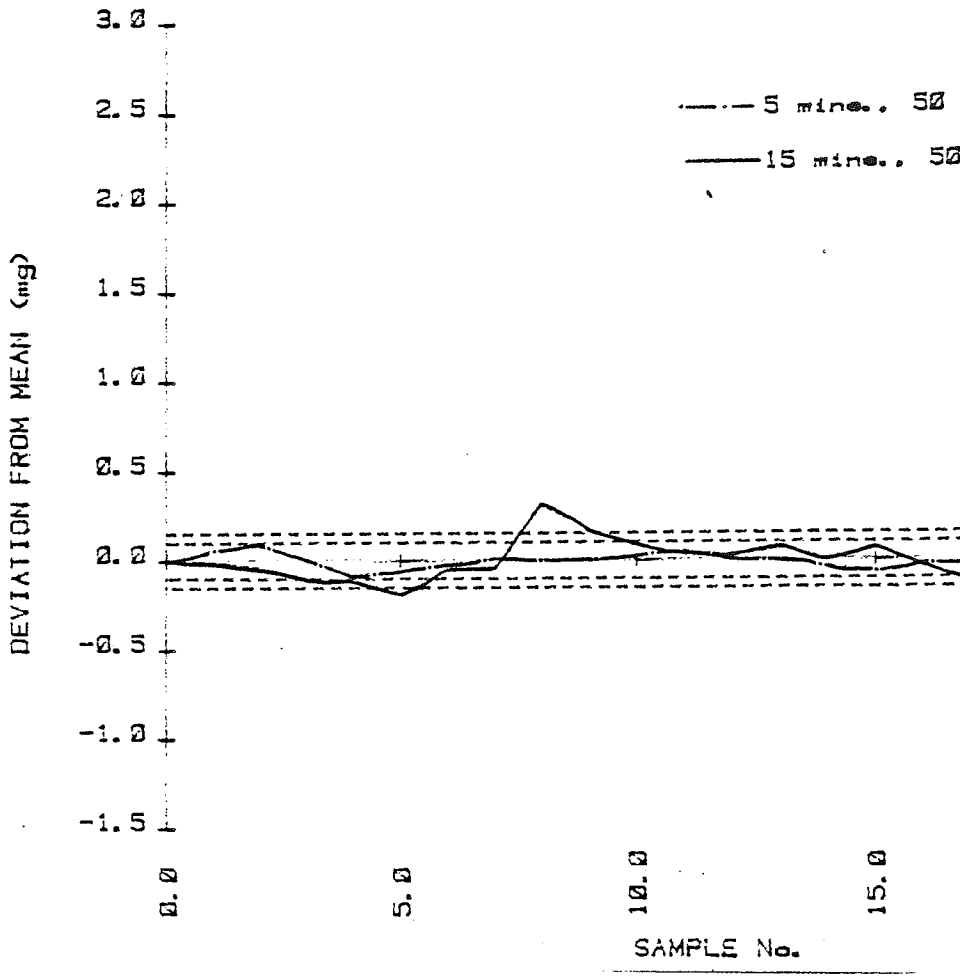

F. Emdex & potassium ch

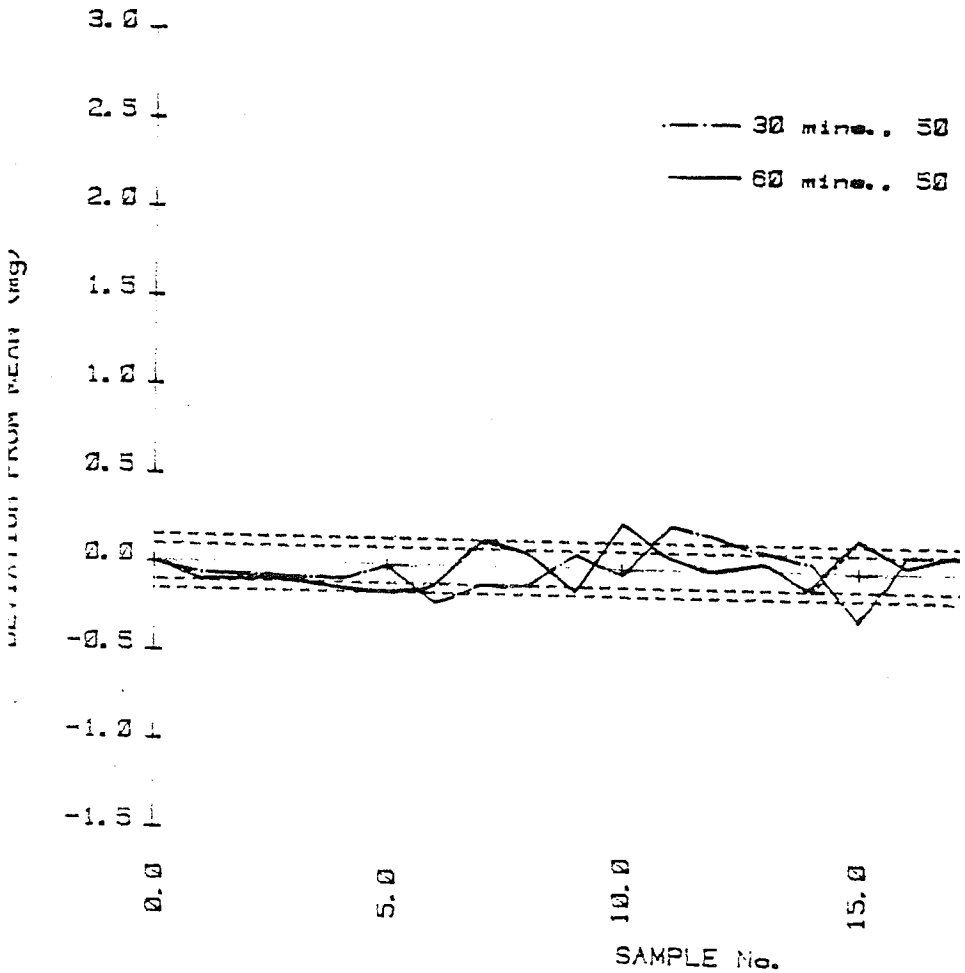

Figure 78. G. Emdex & potassium chloride 0.5%

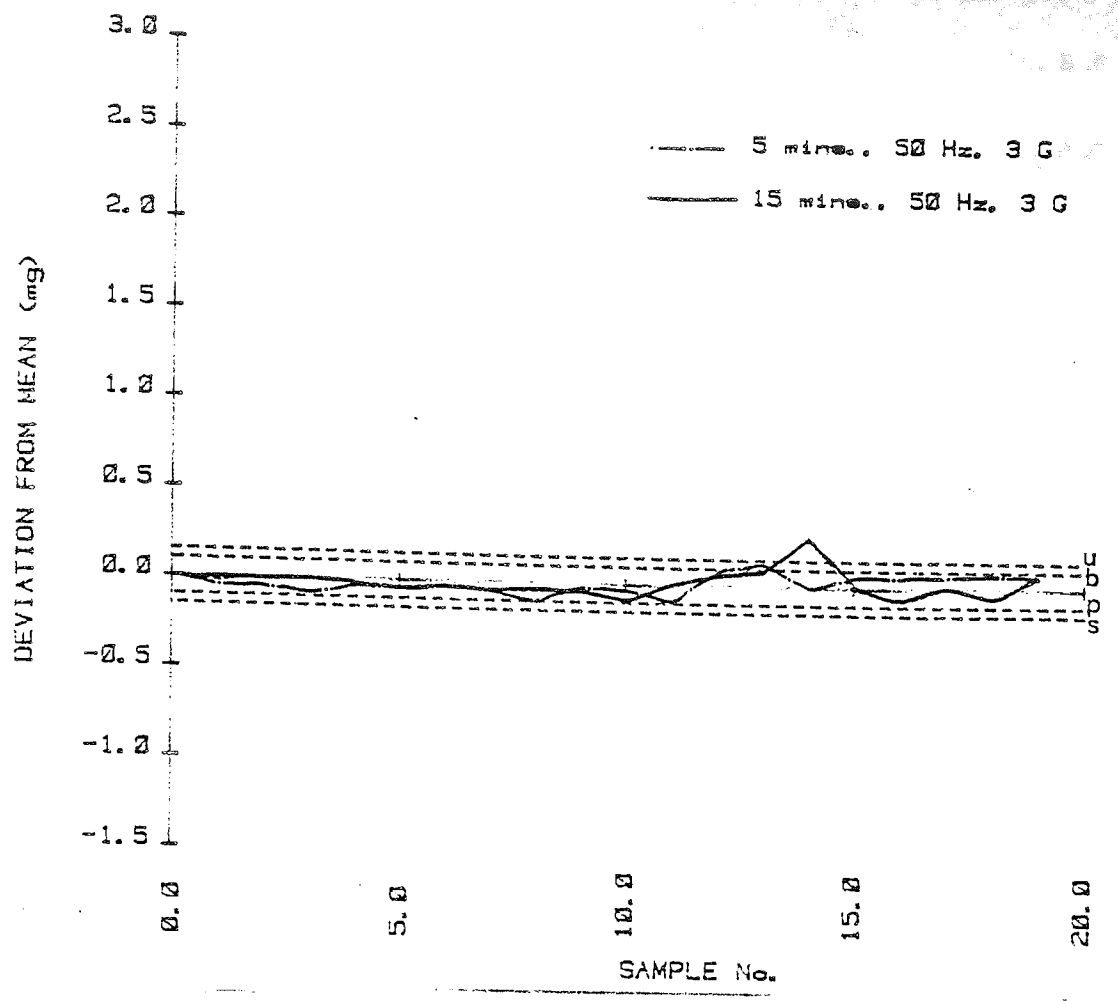

H. Emdex & potassium chloride 0.5%

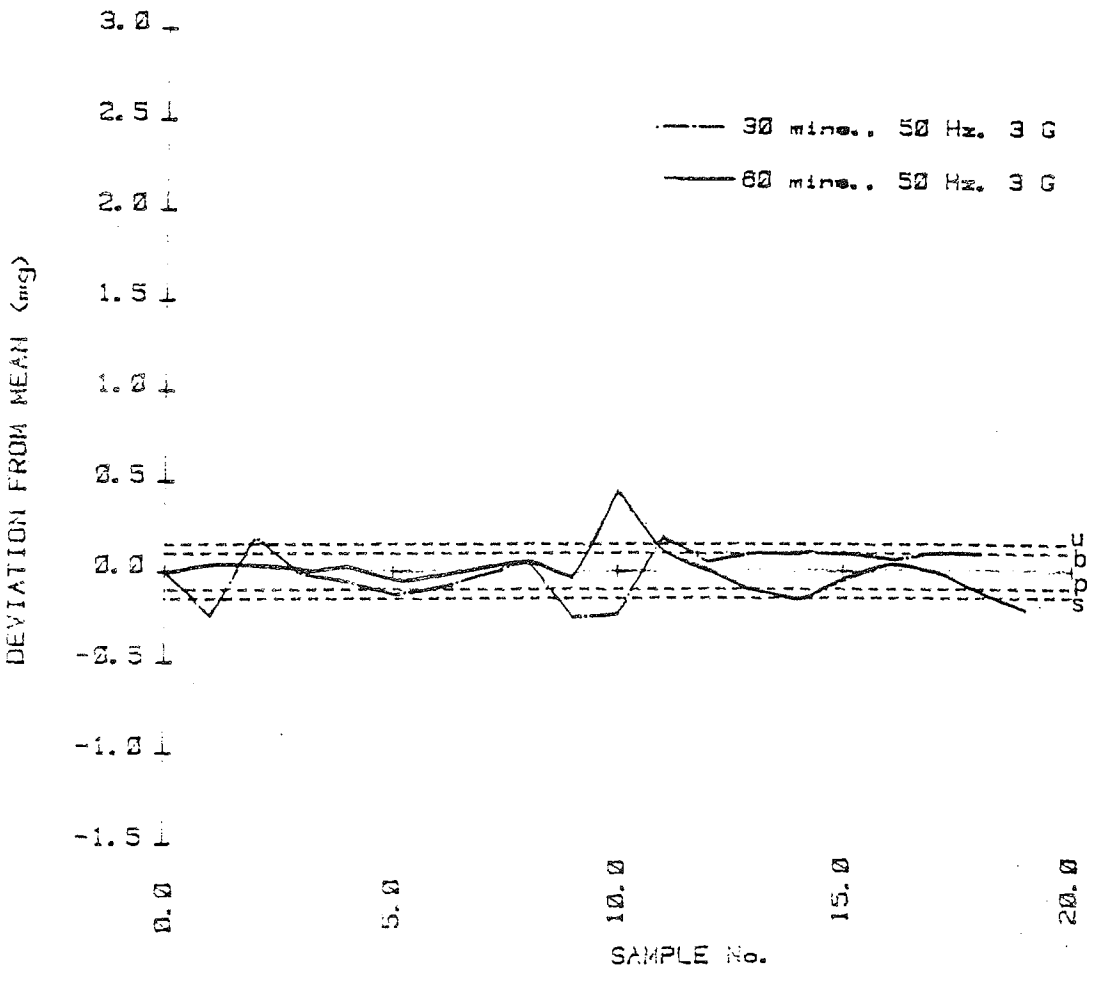

Figure 79 A. Emdex & potassium chlor

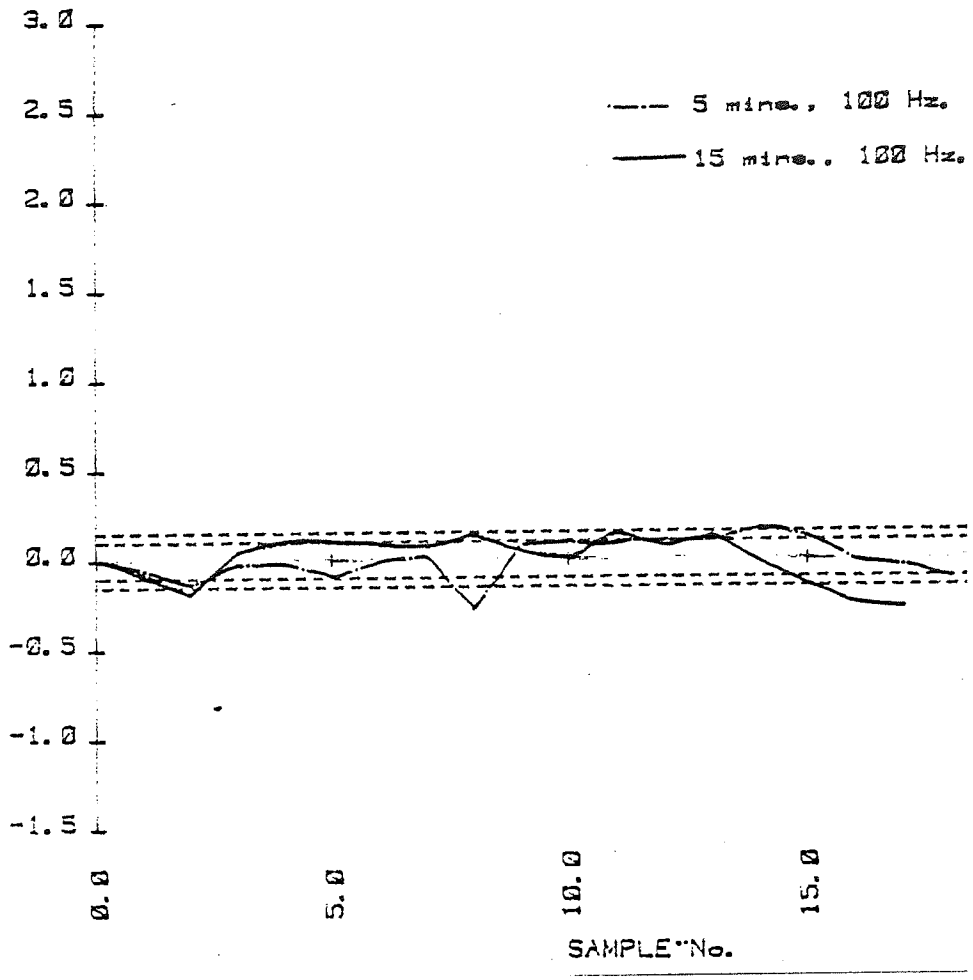

B. Emdex & potassium chlor

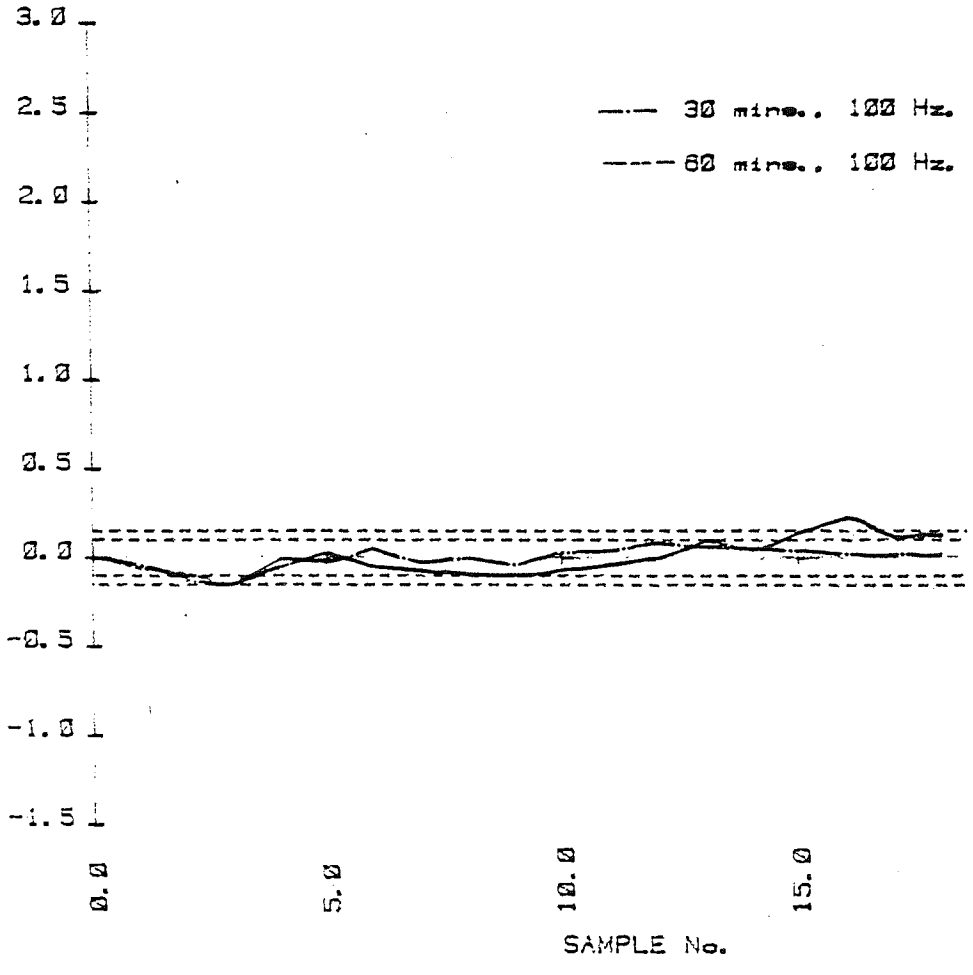

Figure 79. C. Emdex & potassium chloride Ø.5%

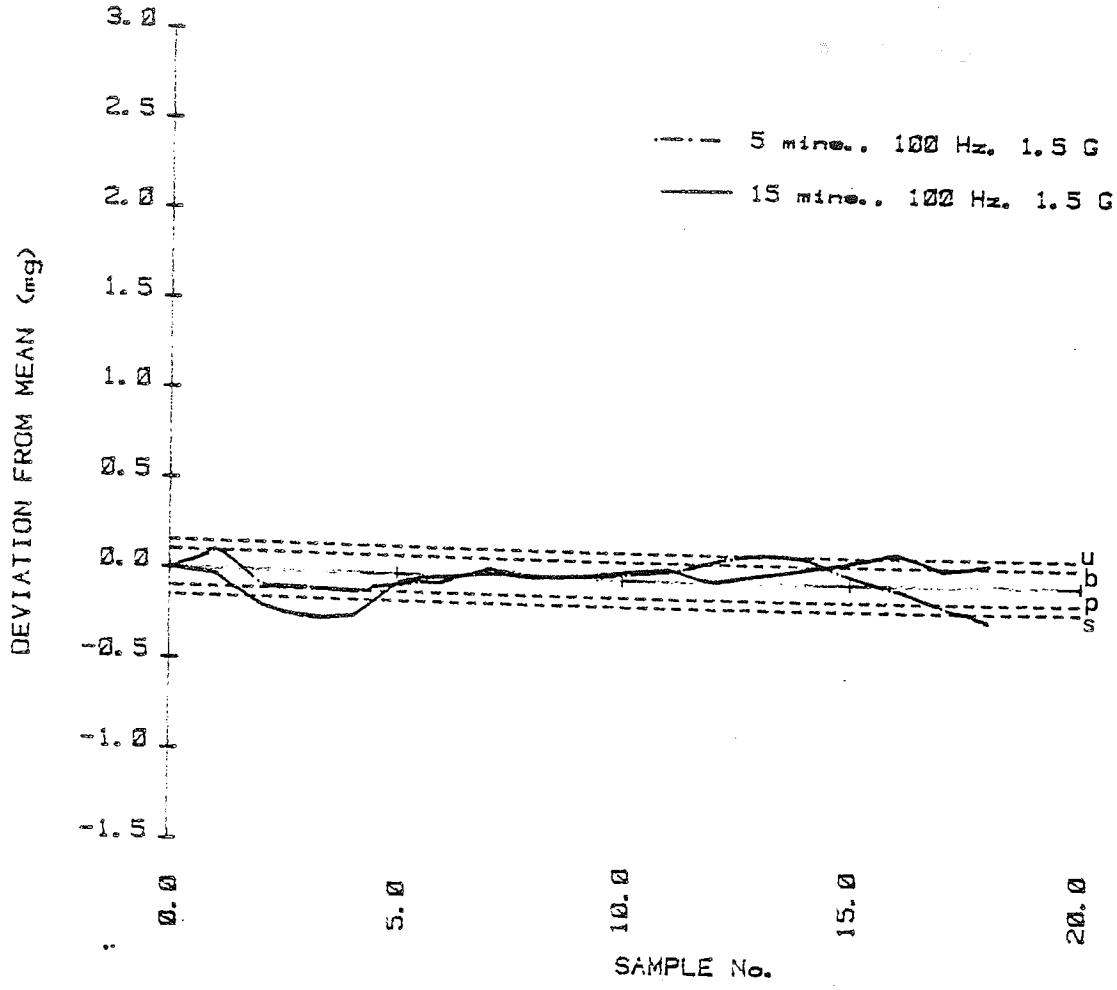

D. Emdex & potassium chloride Ø.5 %

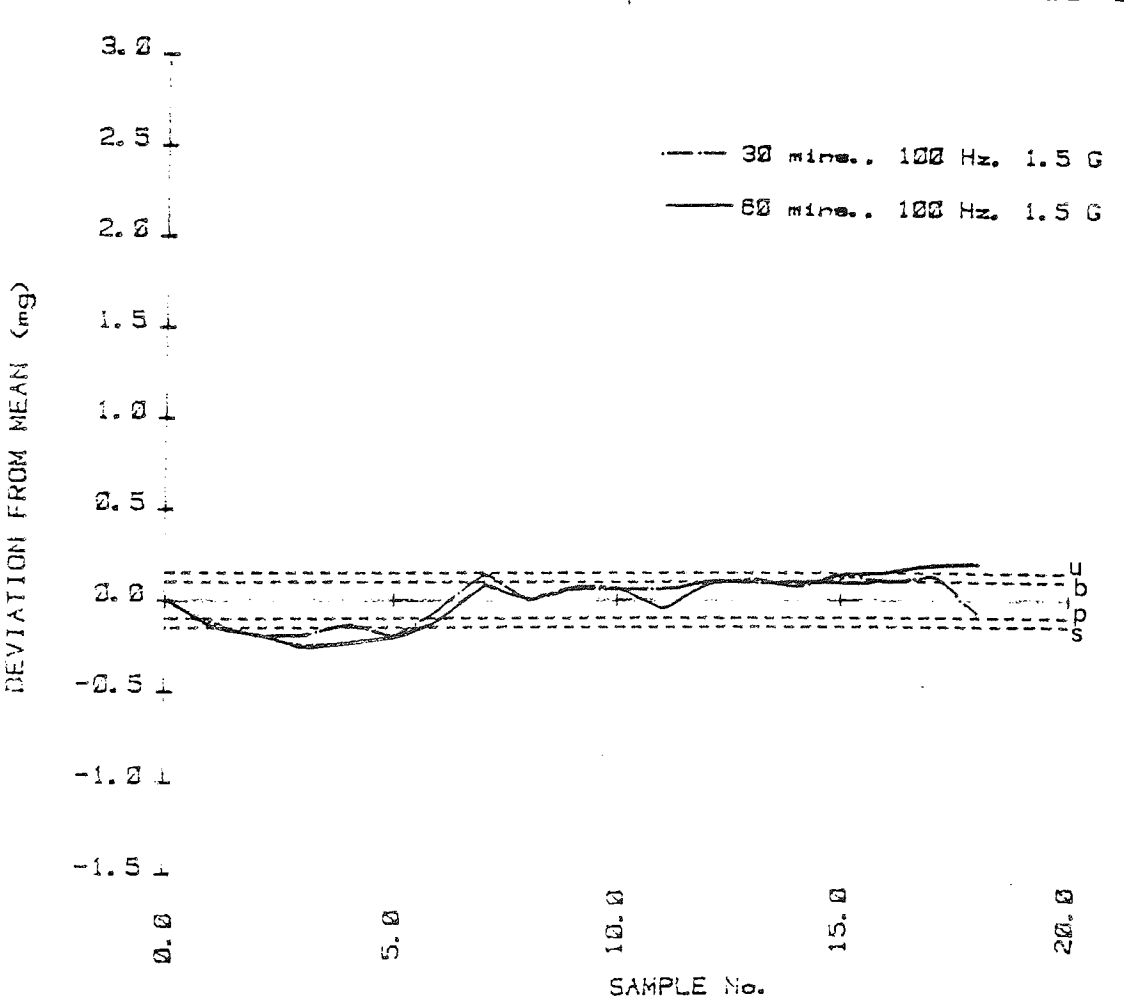

Figure 79. E. Emdex & potassium chlor

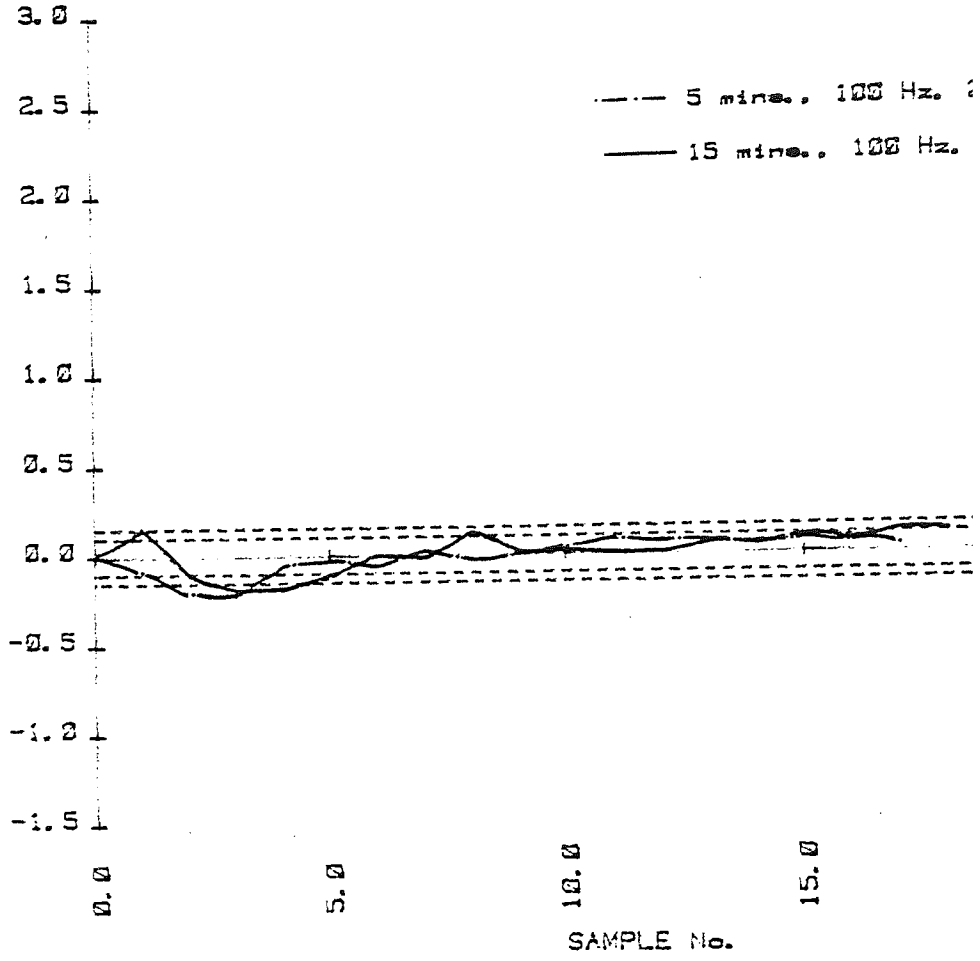

F. Emdex & potassium chlor

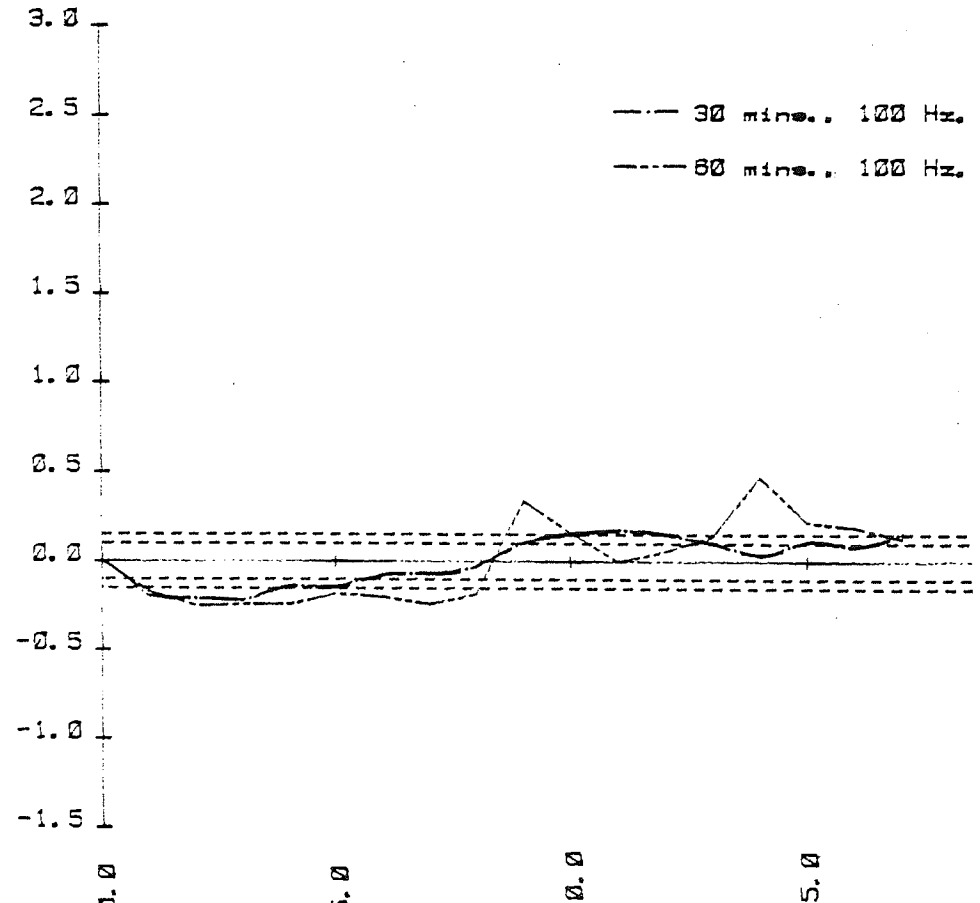

Figure 79. G. Emdex & potassium chloride 0.5%

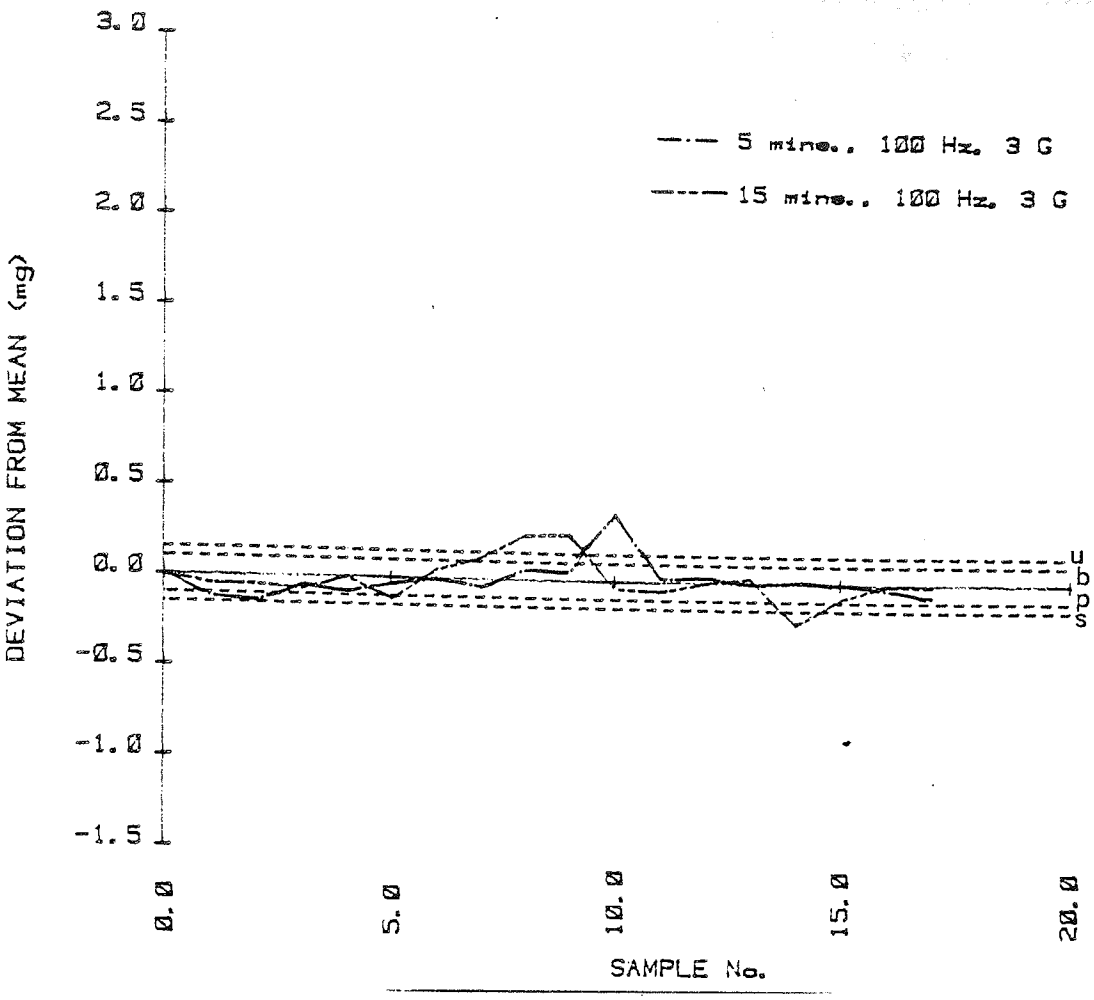

H. Emdex & potassium chloride 0.5%

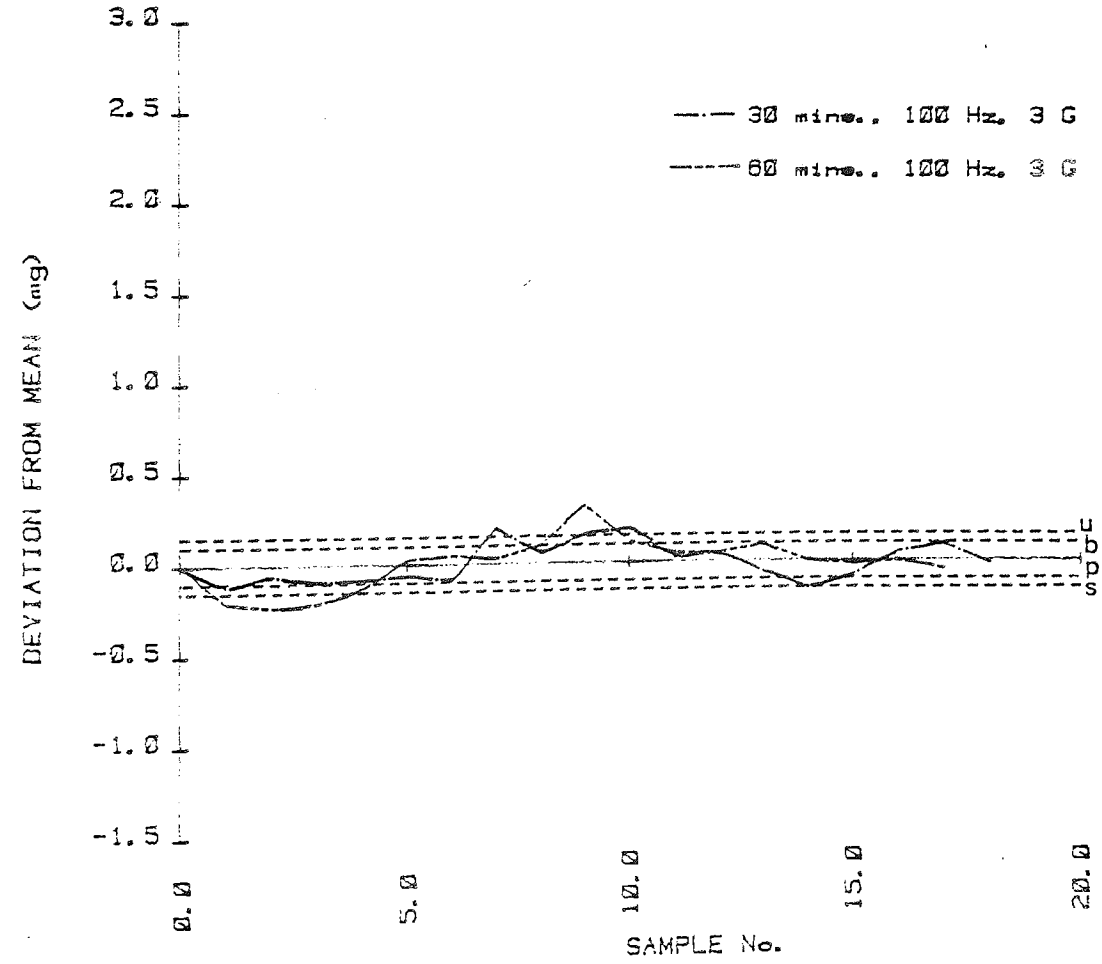

Figure 80.A. Emdex & ppotassium chloride

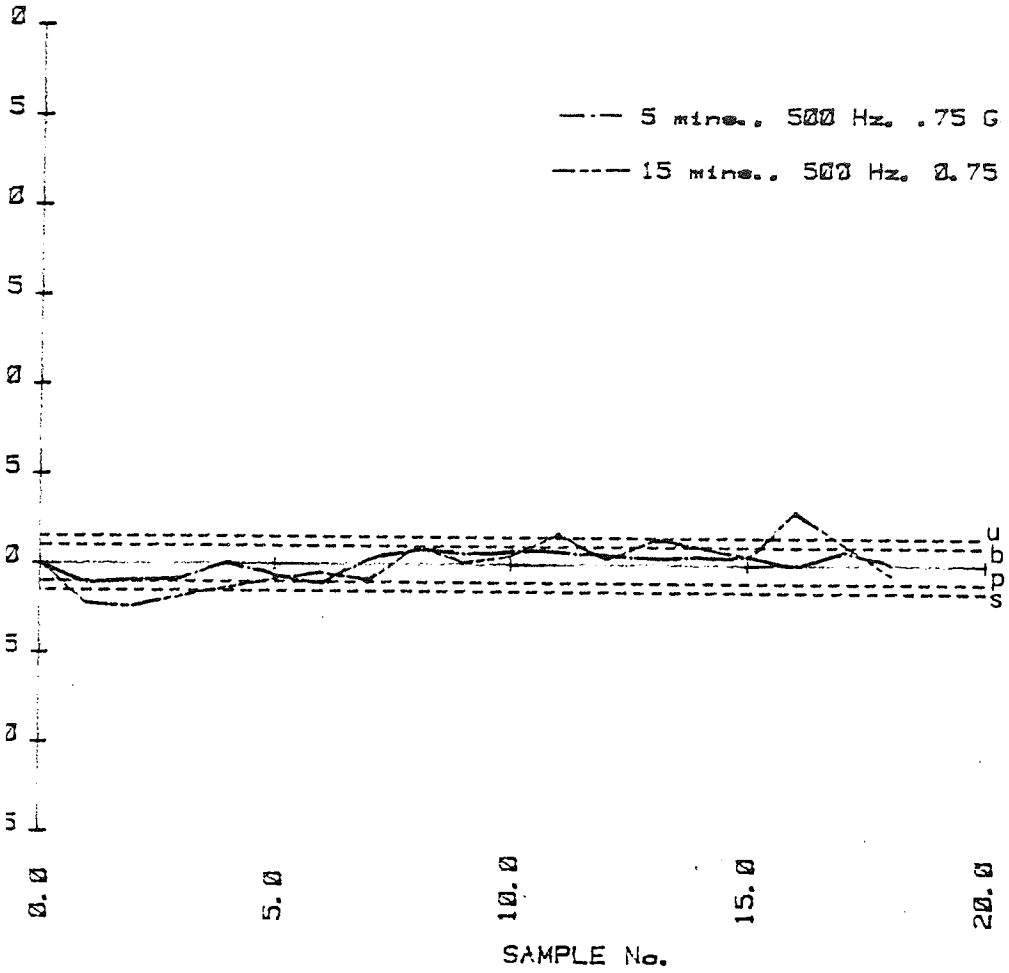

B. Emdex & potassium chloride

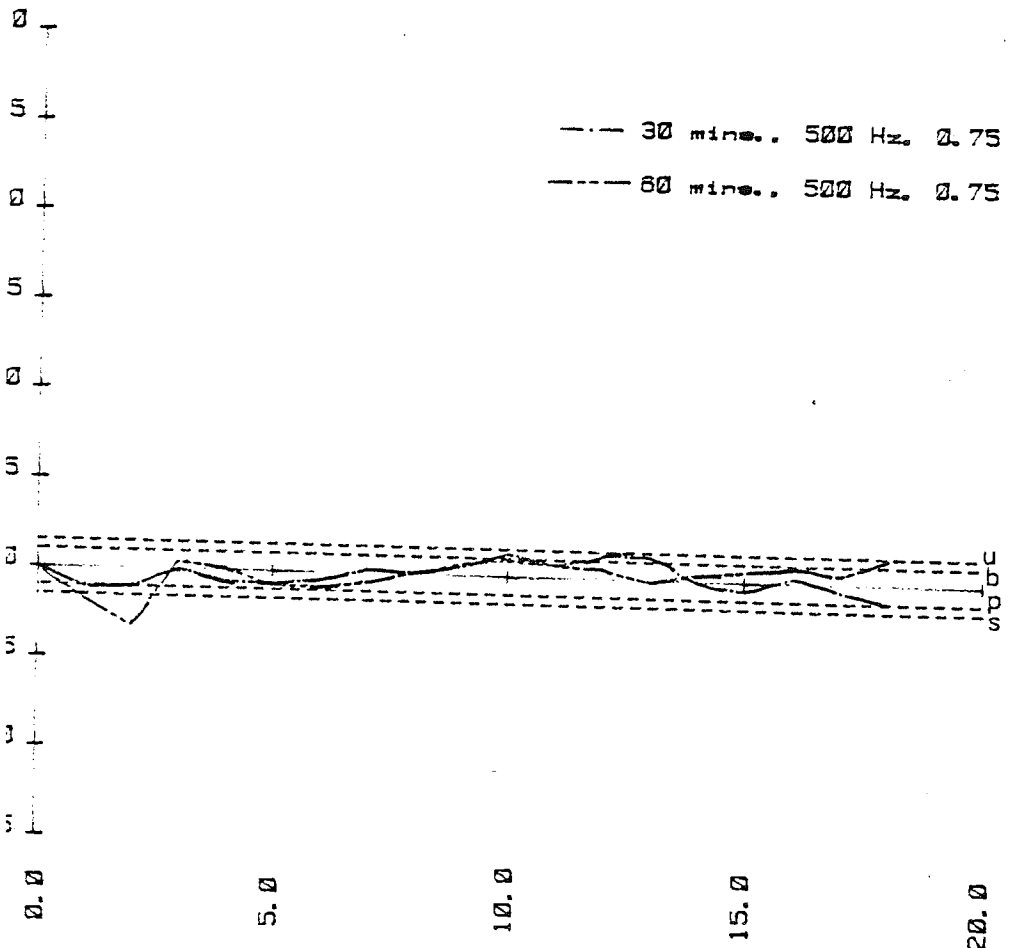

Figure 80. C. Emdex & potassium chloride 0.5%

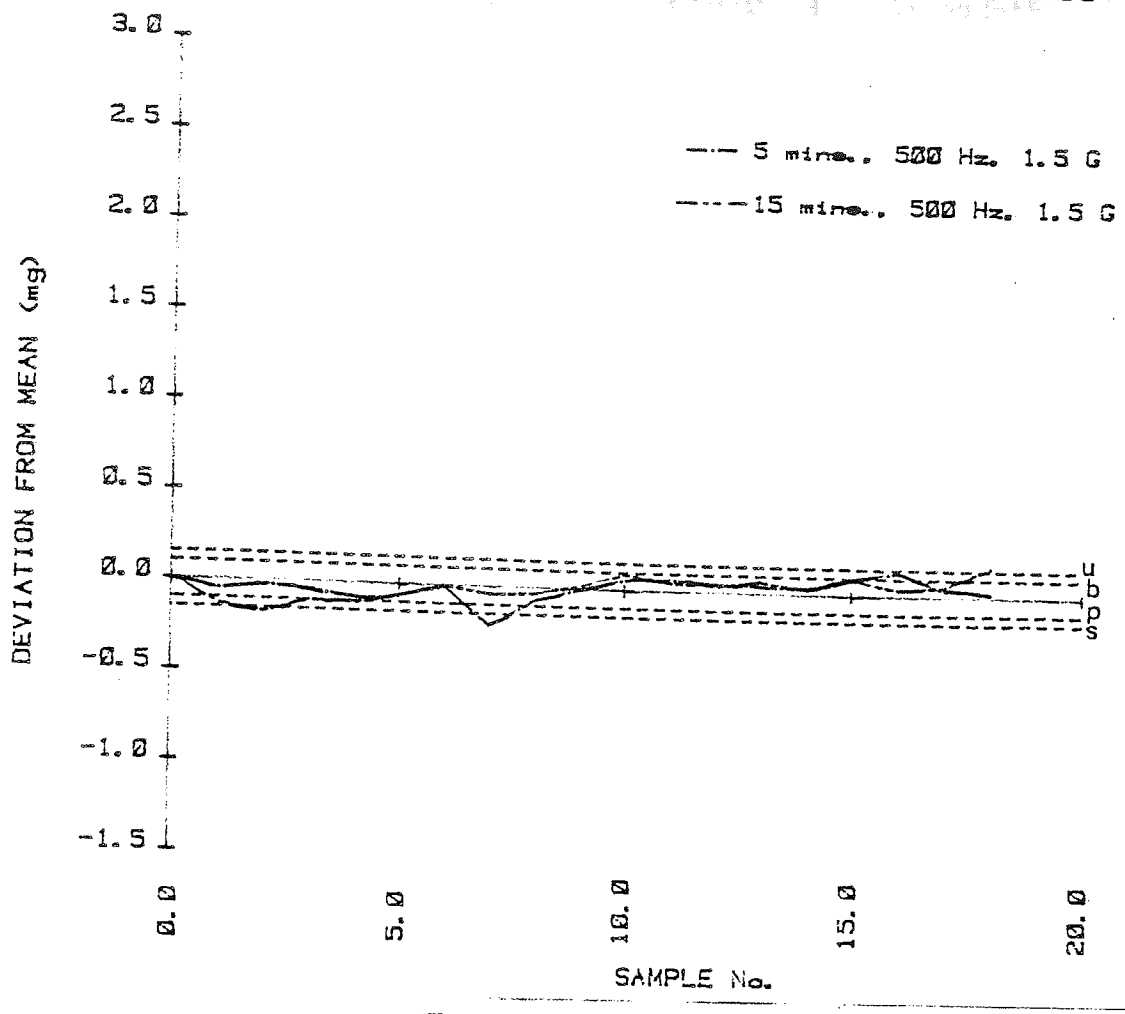

D. Emdex & potassium chloride 0.5%

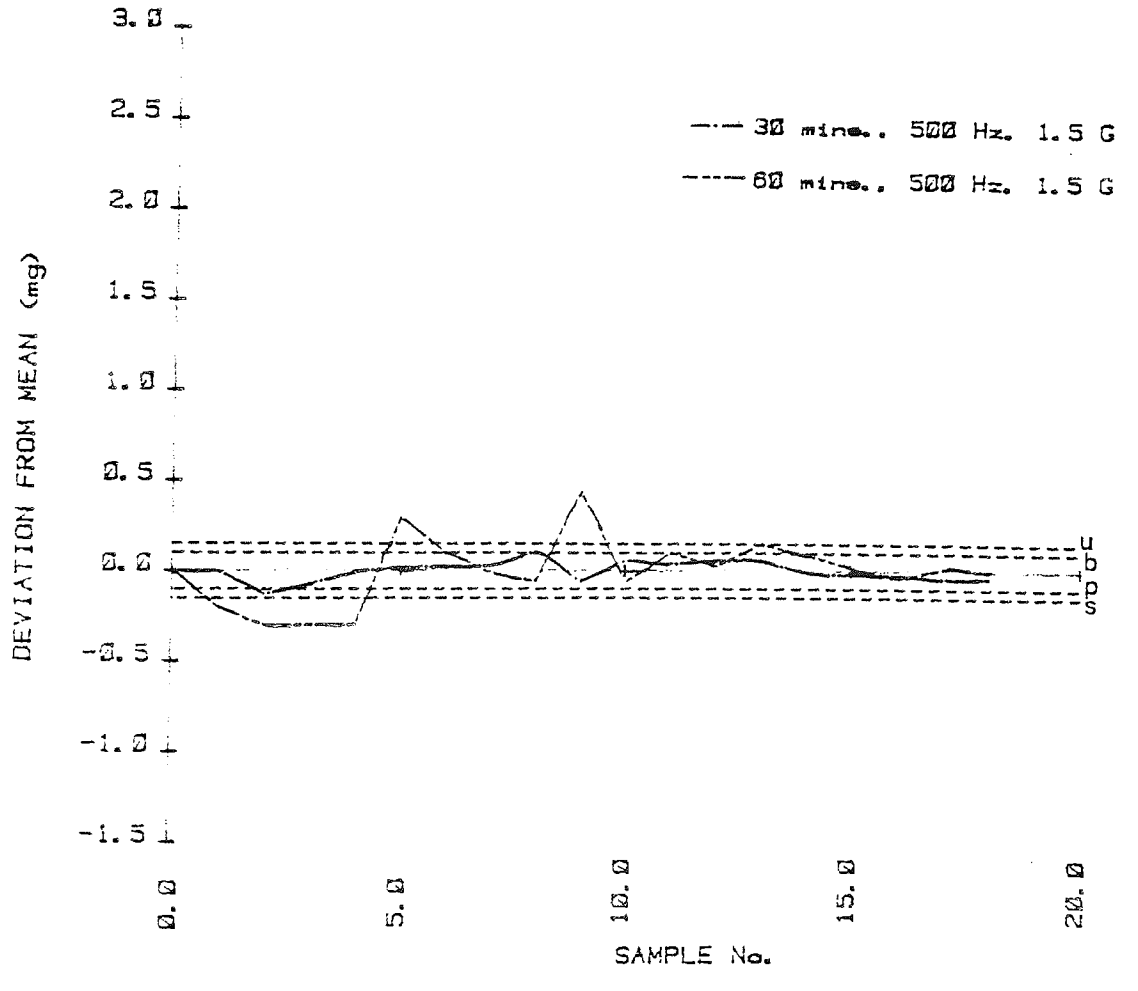

Figure 80. E. Emdex & potassium chlc

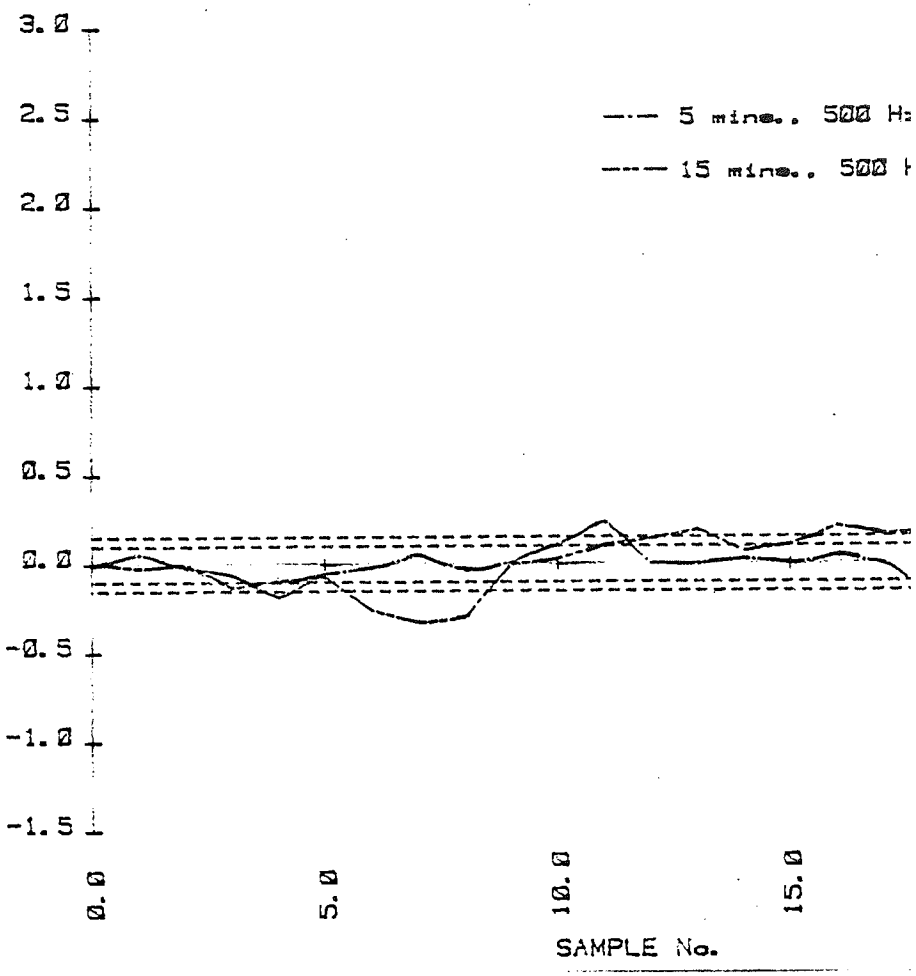

F. Emdex & potassium chlo

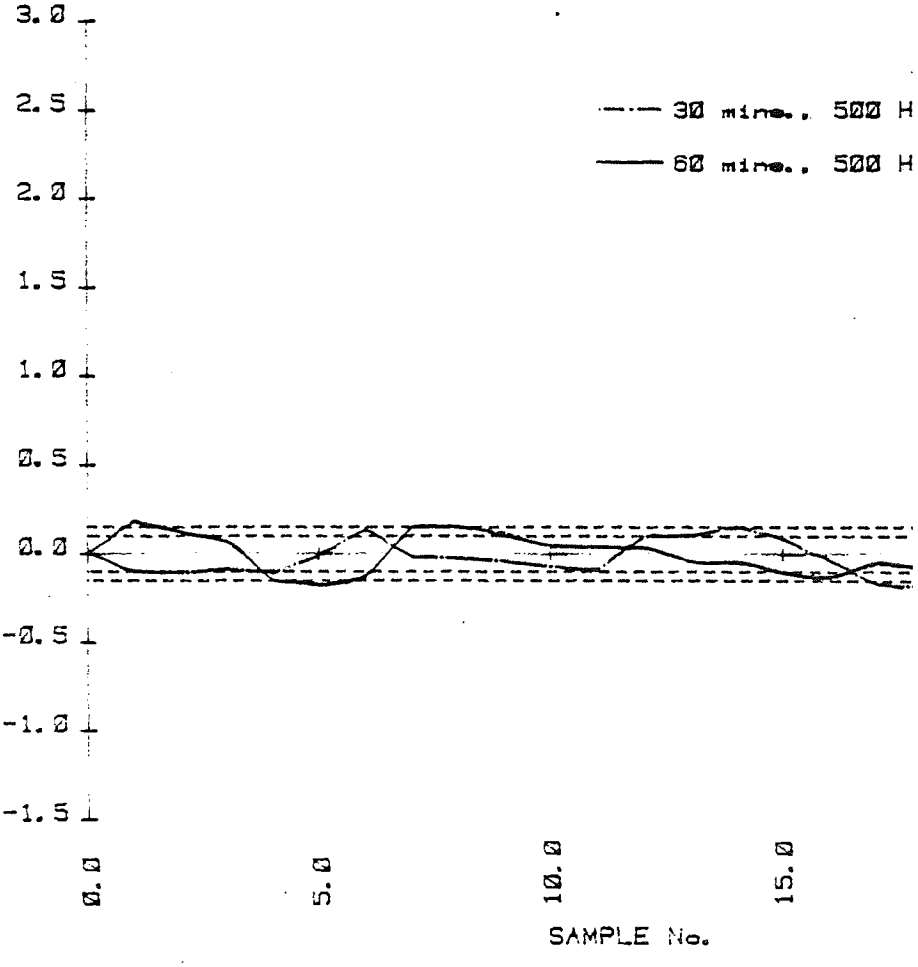

Figure 80. G. Emdex & potassium chloride 0.5%

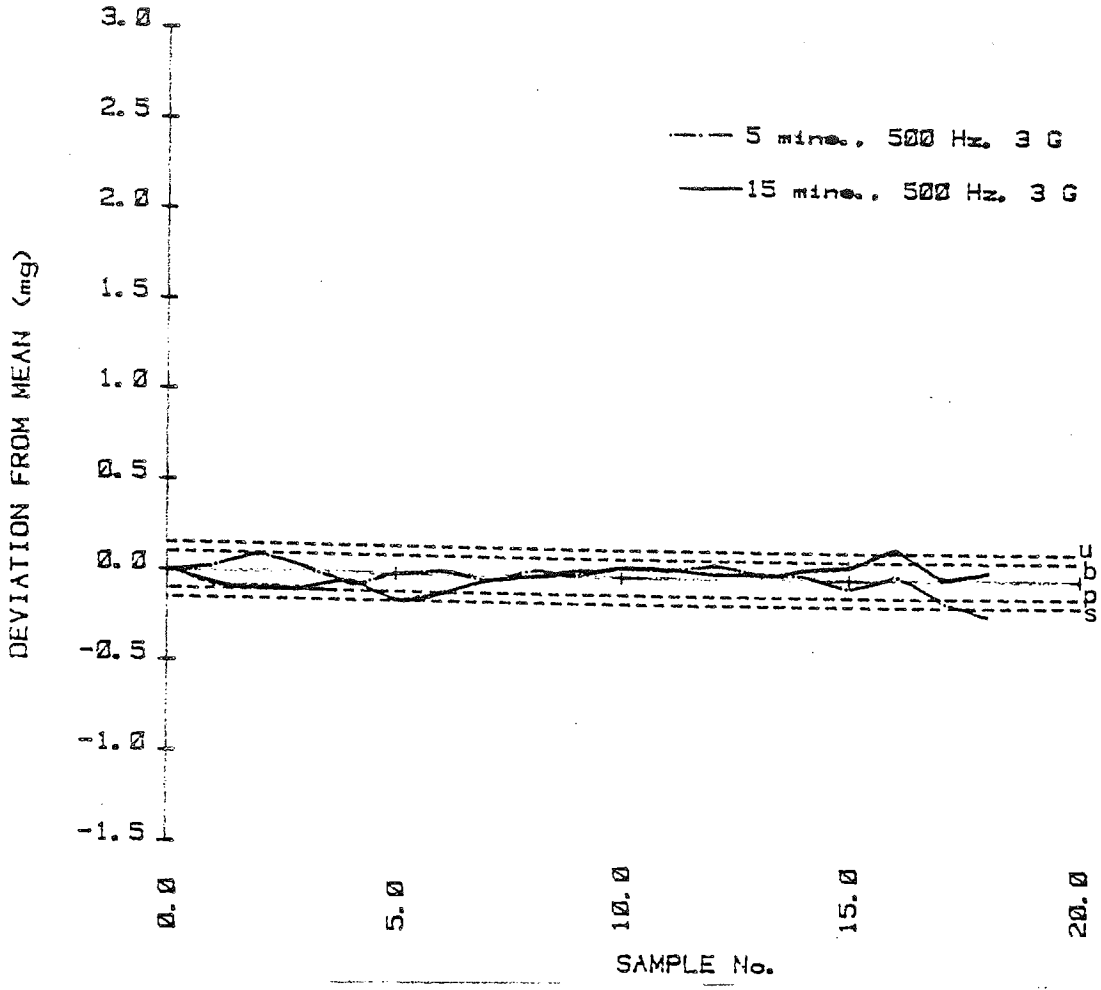

H. Emdex & potassium chloride 0.5%

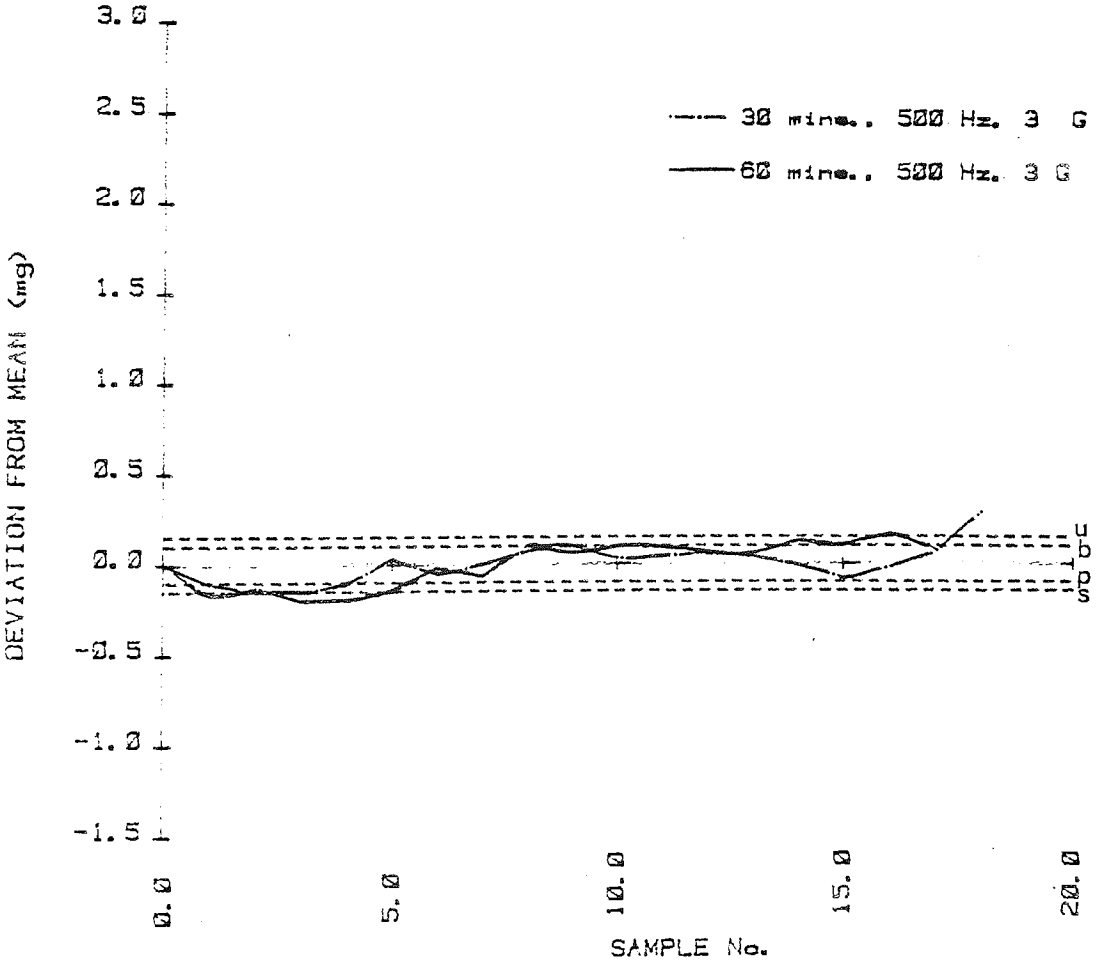

igure 81. A. Emdex & potassium chloride @

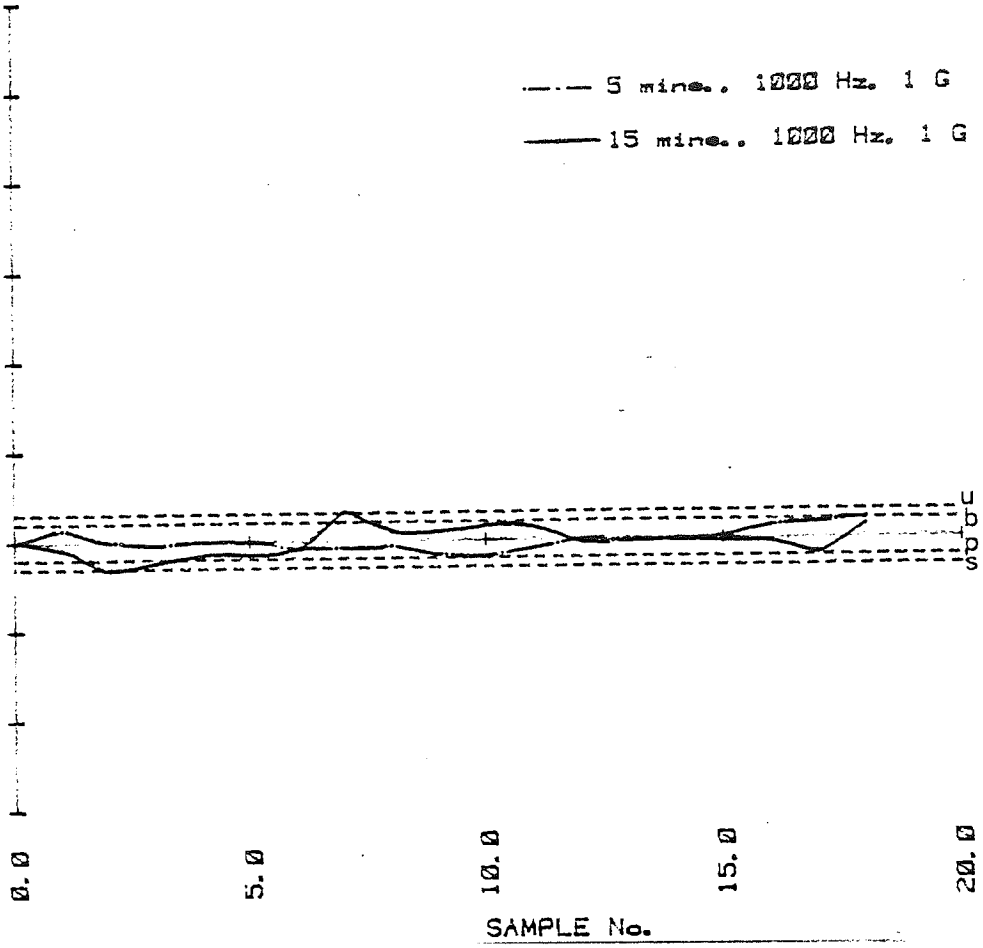

B. Emdex & potassium chloride @

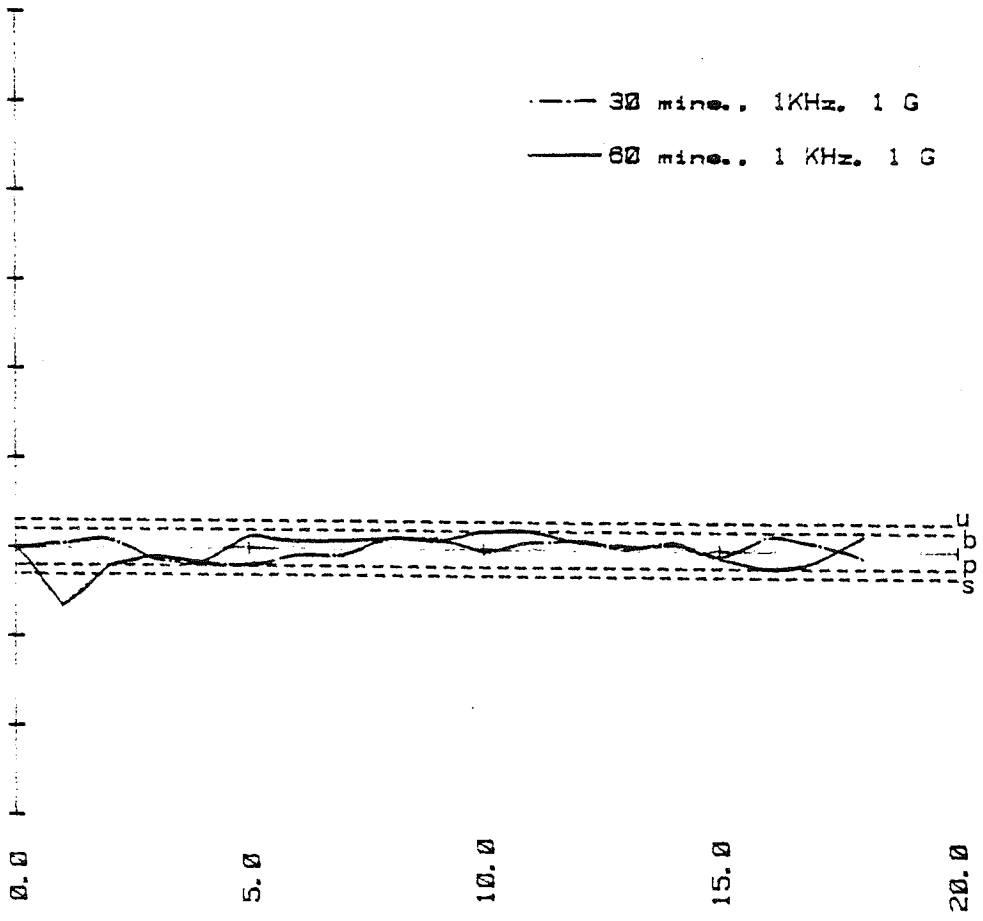

Figure 81.

C. Emdex & potassium chloride Ø.5%

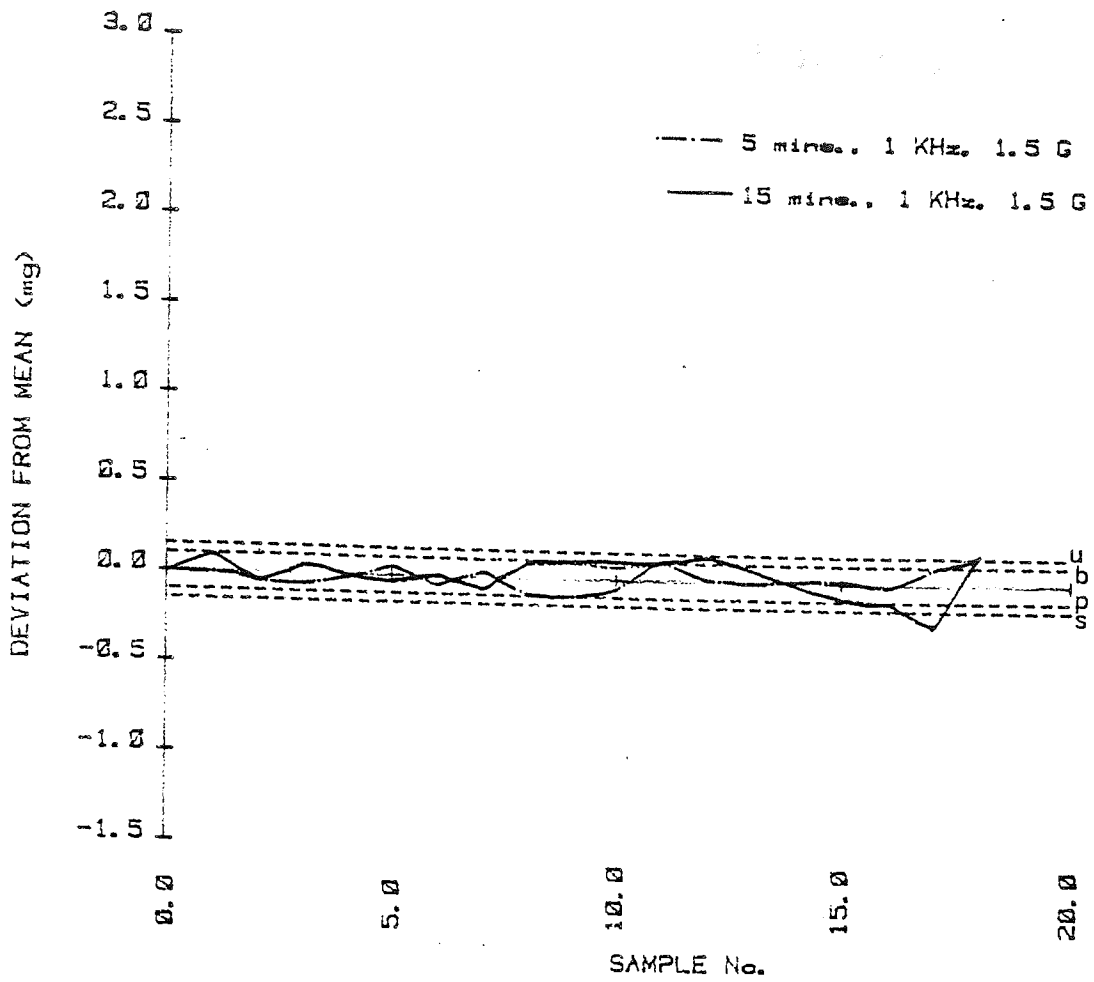

D. Emdex & potassium chloride Ø.5%

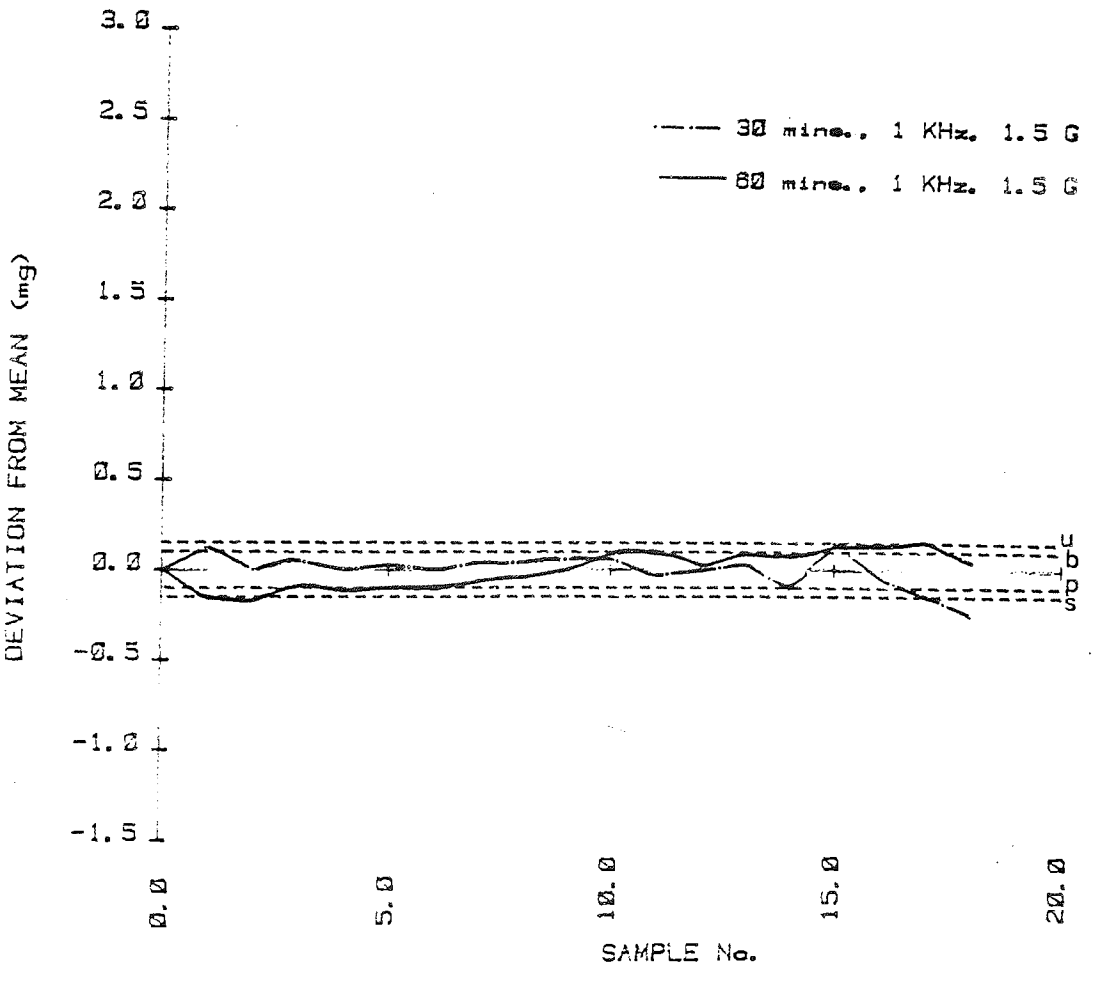

Figure 81.E. Emdex & potassium chloride

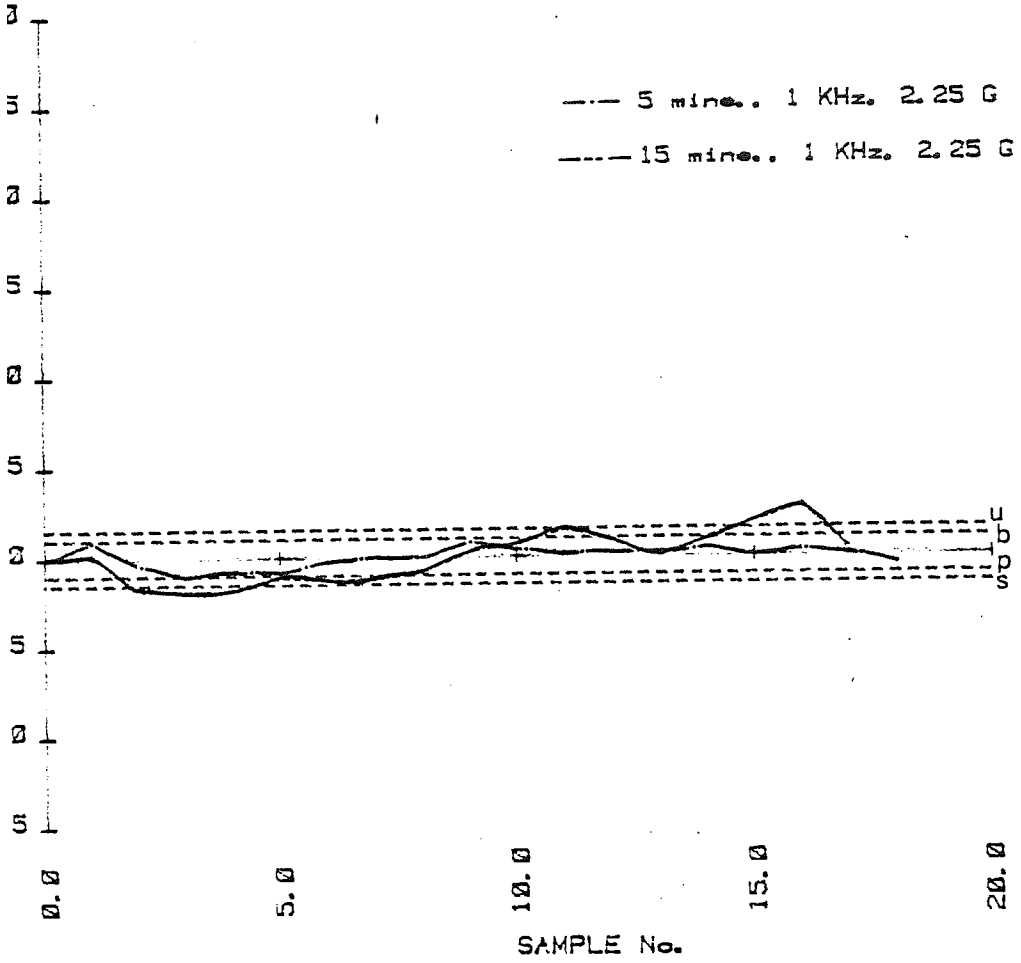

F. Emdex & potassium chloride

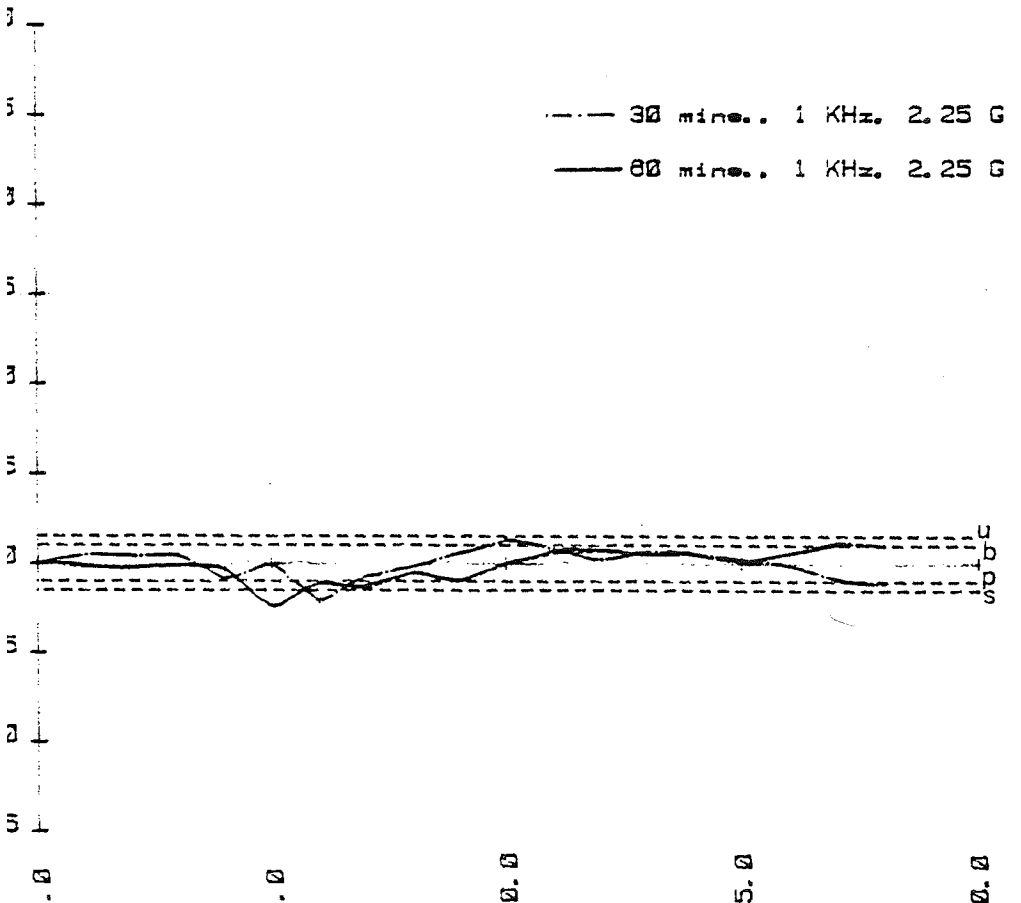

Figure 81. G. Emdex & potassium chloride Ø.5%

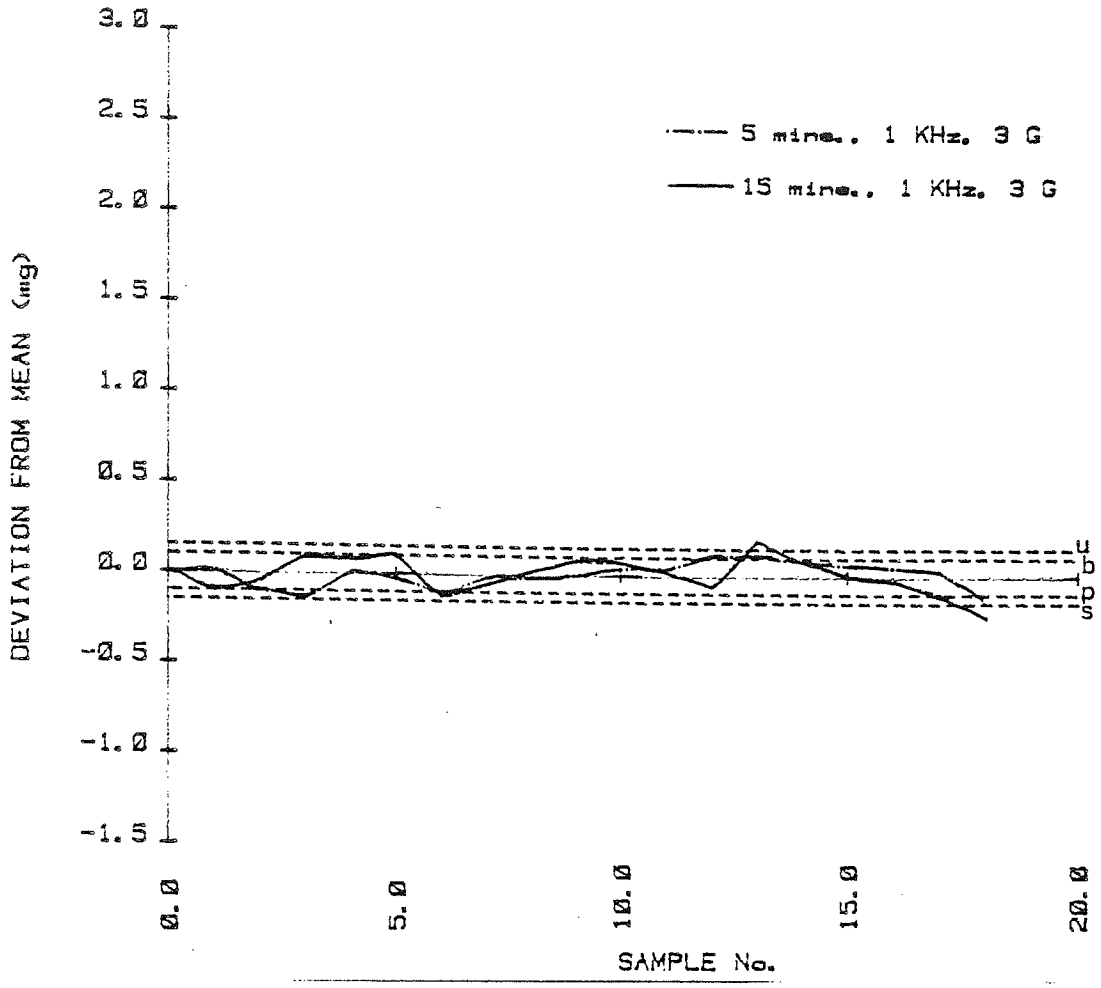

H. Emdex & potassium chloride Ø.5 %

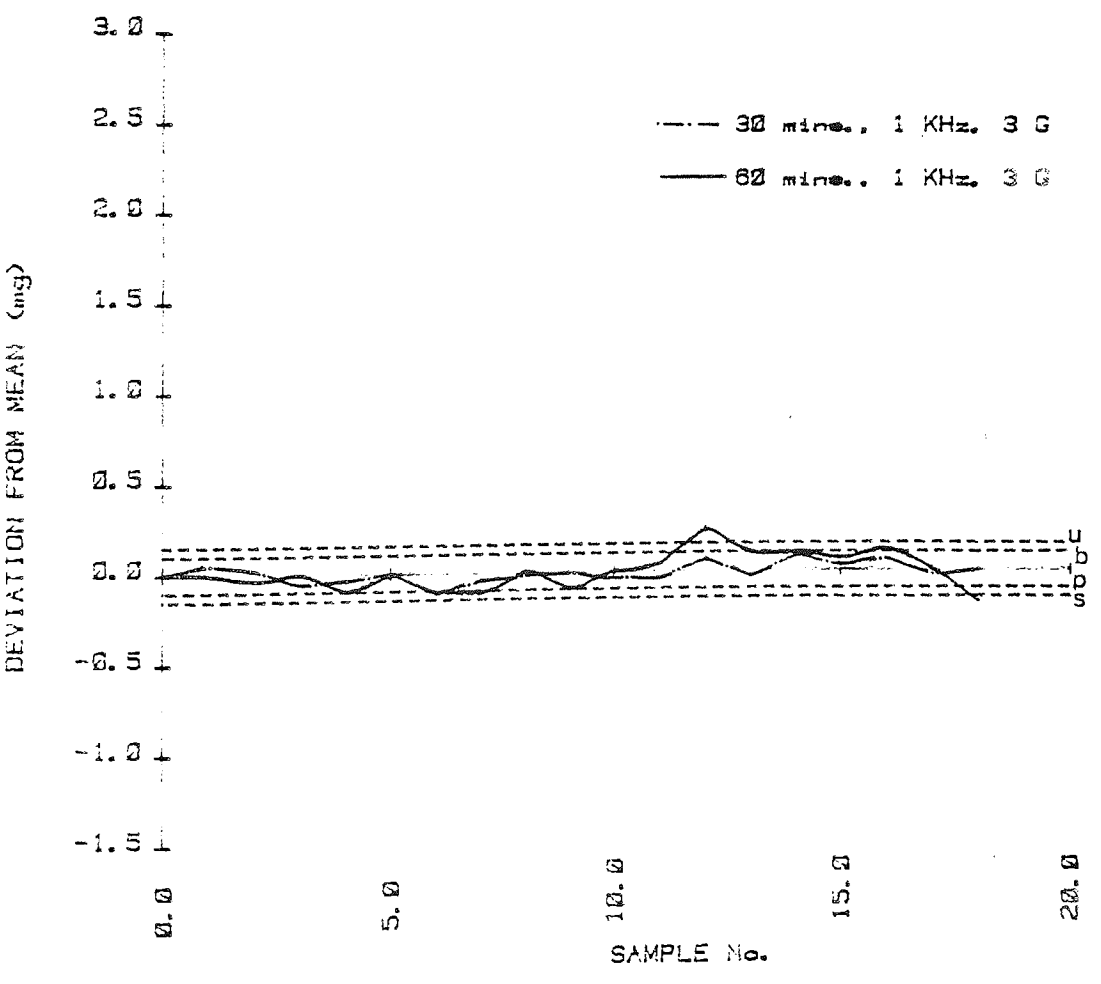

Figure 82. A. Lactose & potassium chloride 0.5%

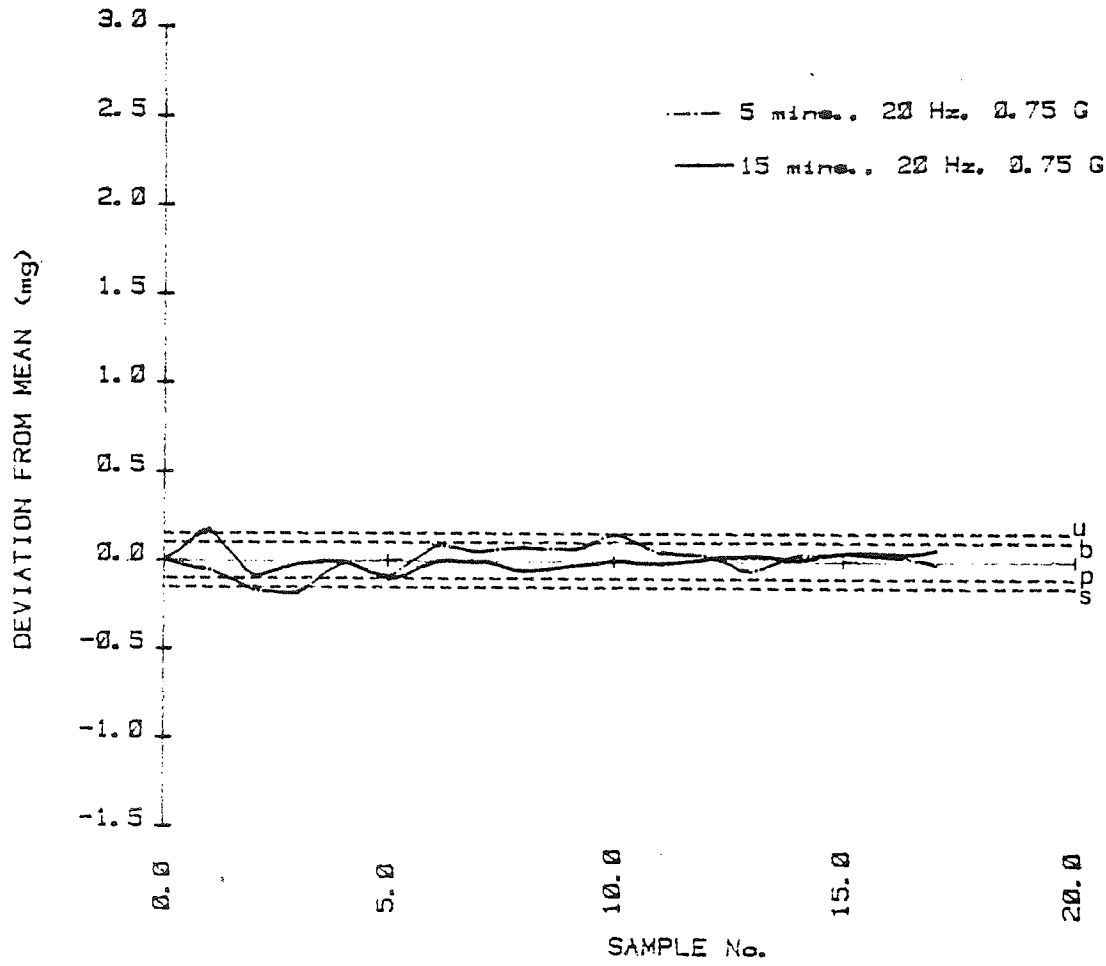

B. Lactose & potassium chloride 0.5%

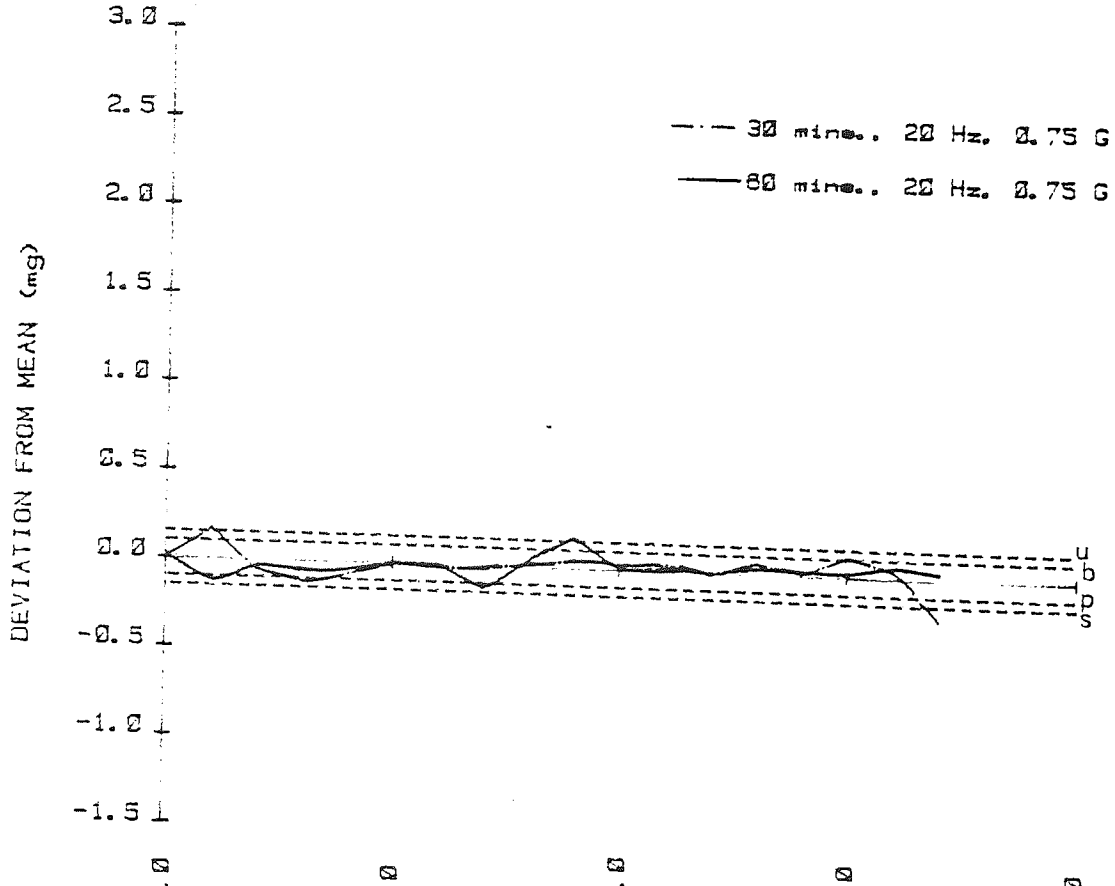

Figure 82. C. Lactose & potassium sorbate Ø.5

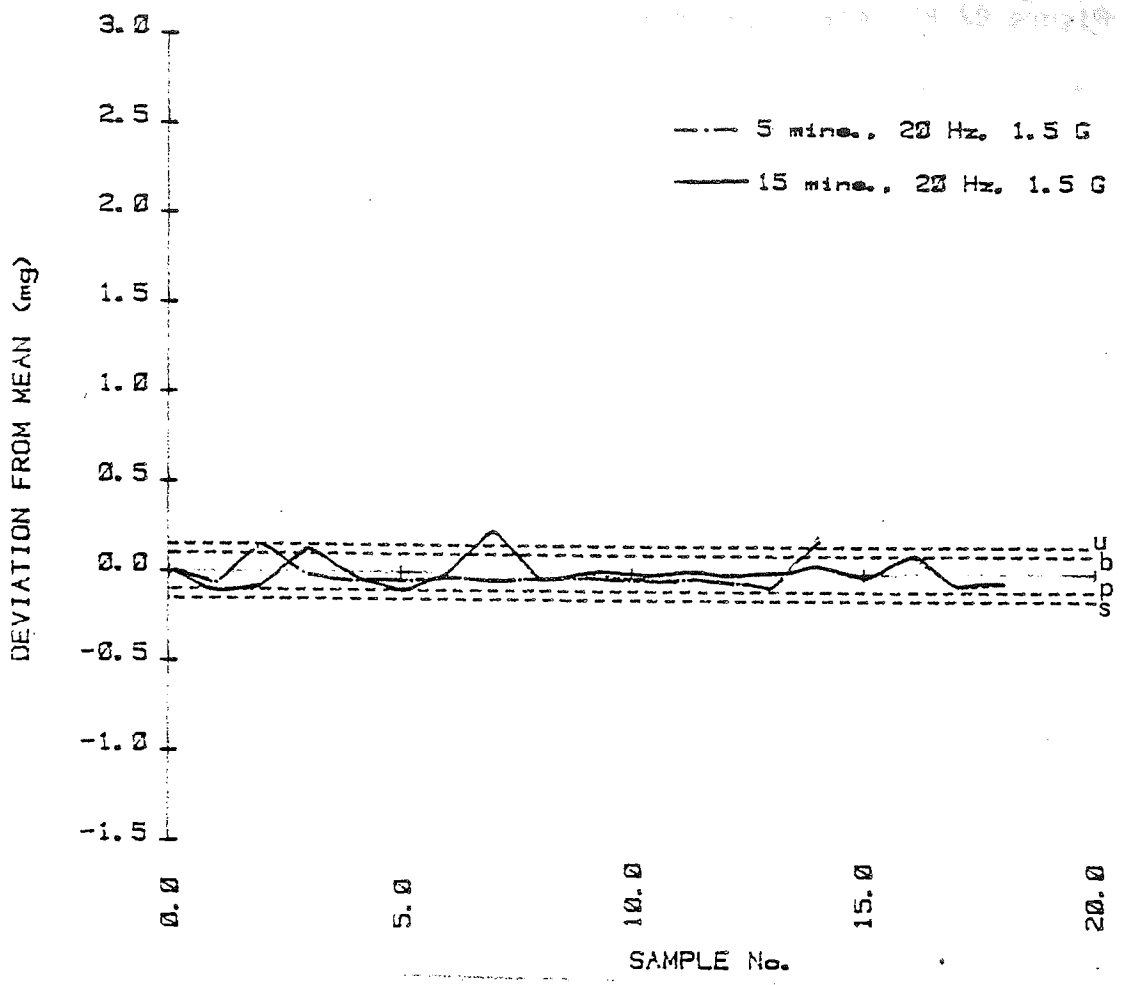

D. Lactose & potassium chloride Ø.

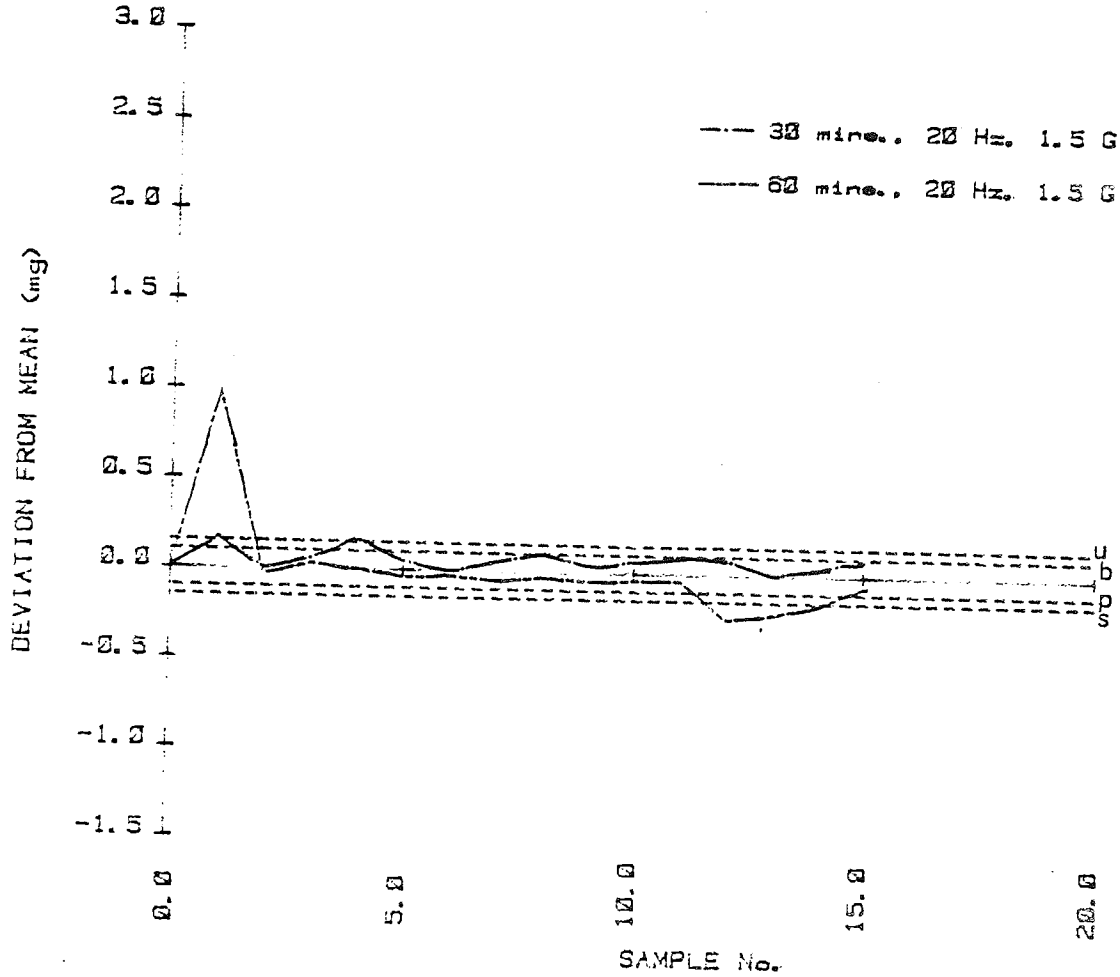

Figure 82/83 E/A. Lactose & potassium chloride Ø.5%

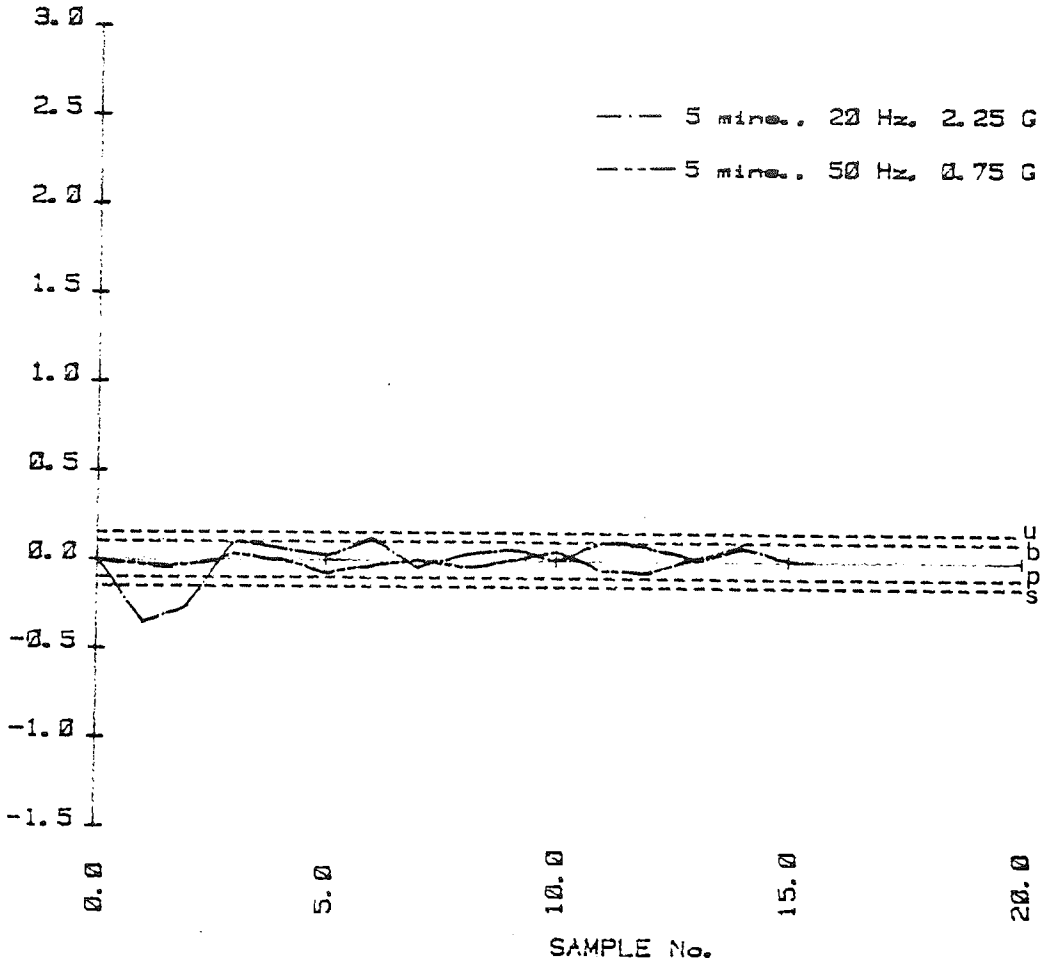

B. Lactose & potassium chloride .5%

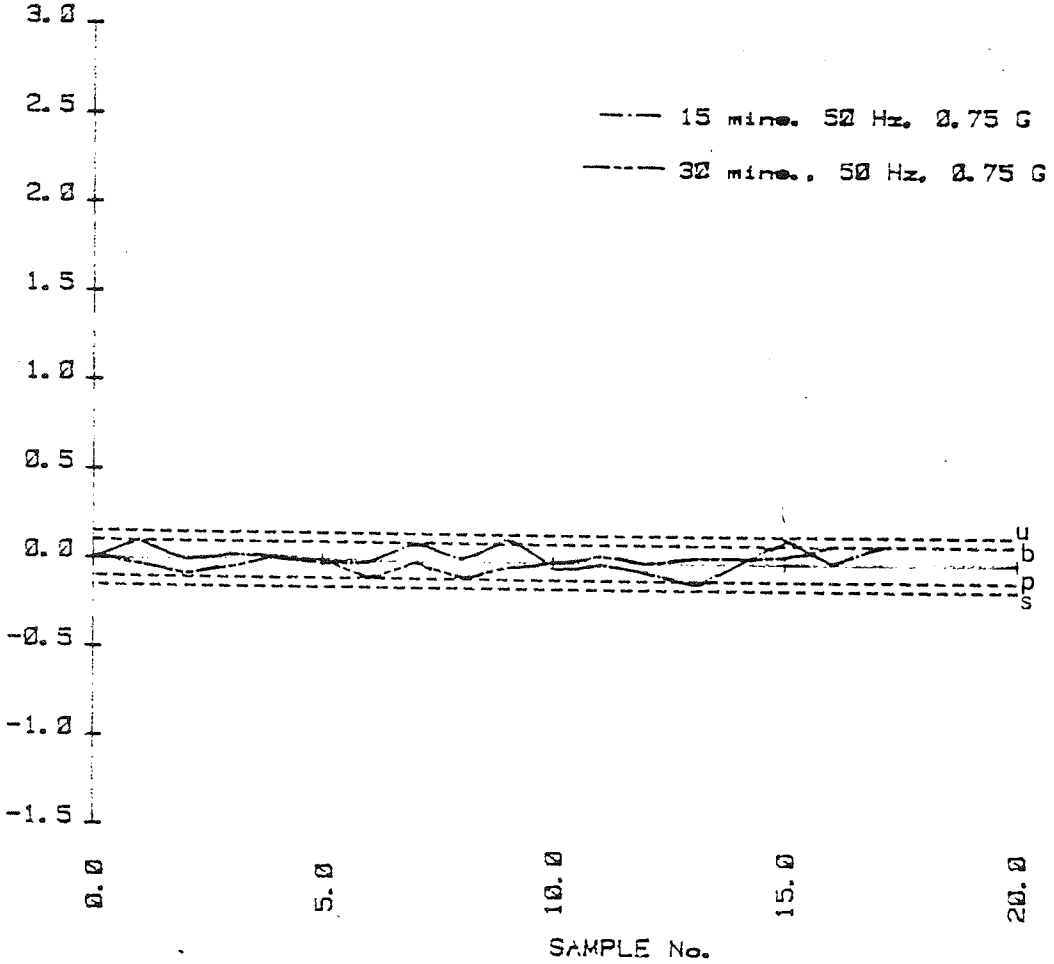

Figure 83. C. Lactose & potassium chloride .5%

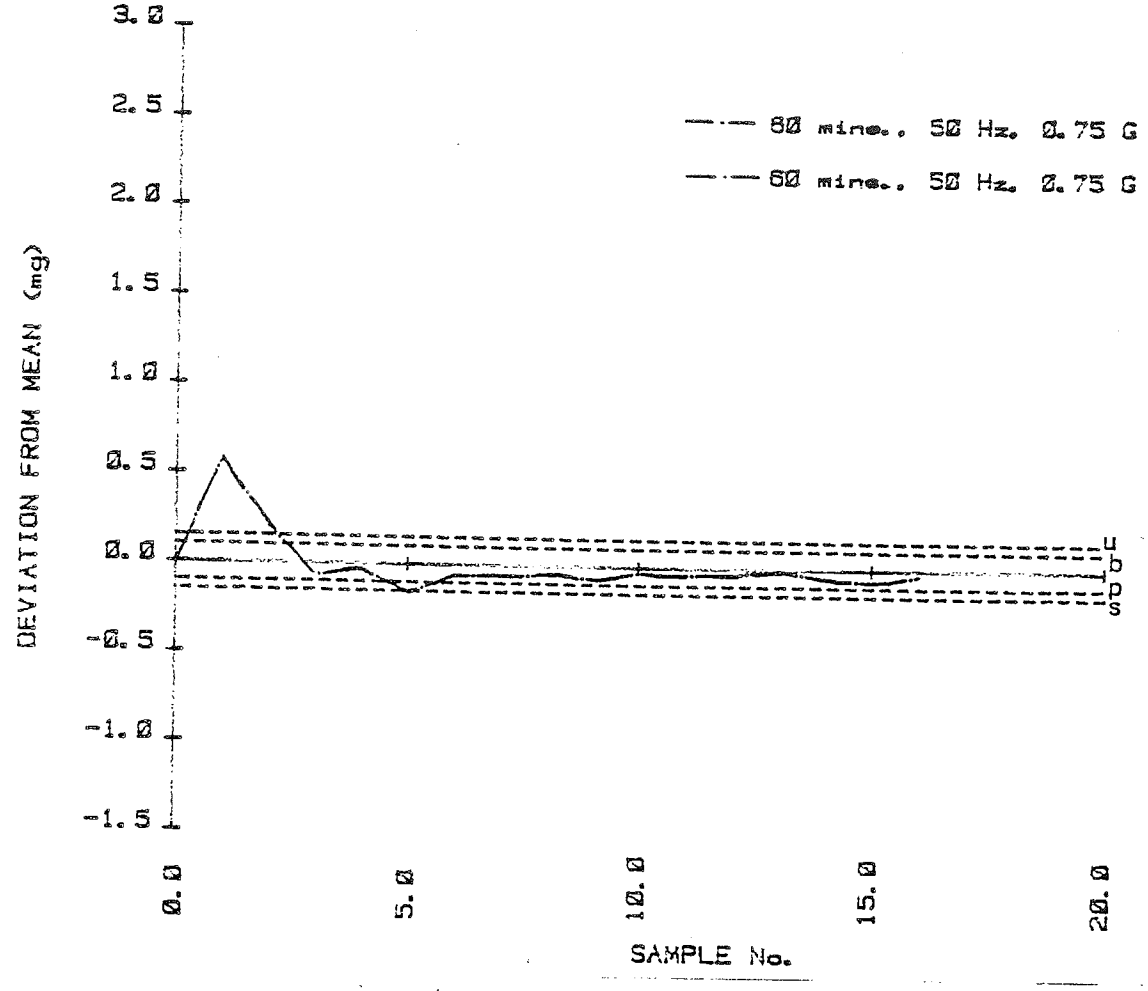

D. Lactose & potassium sorbate .5%

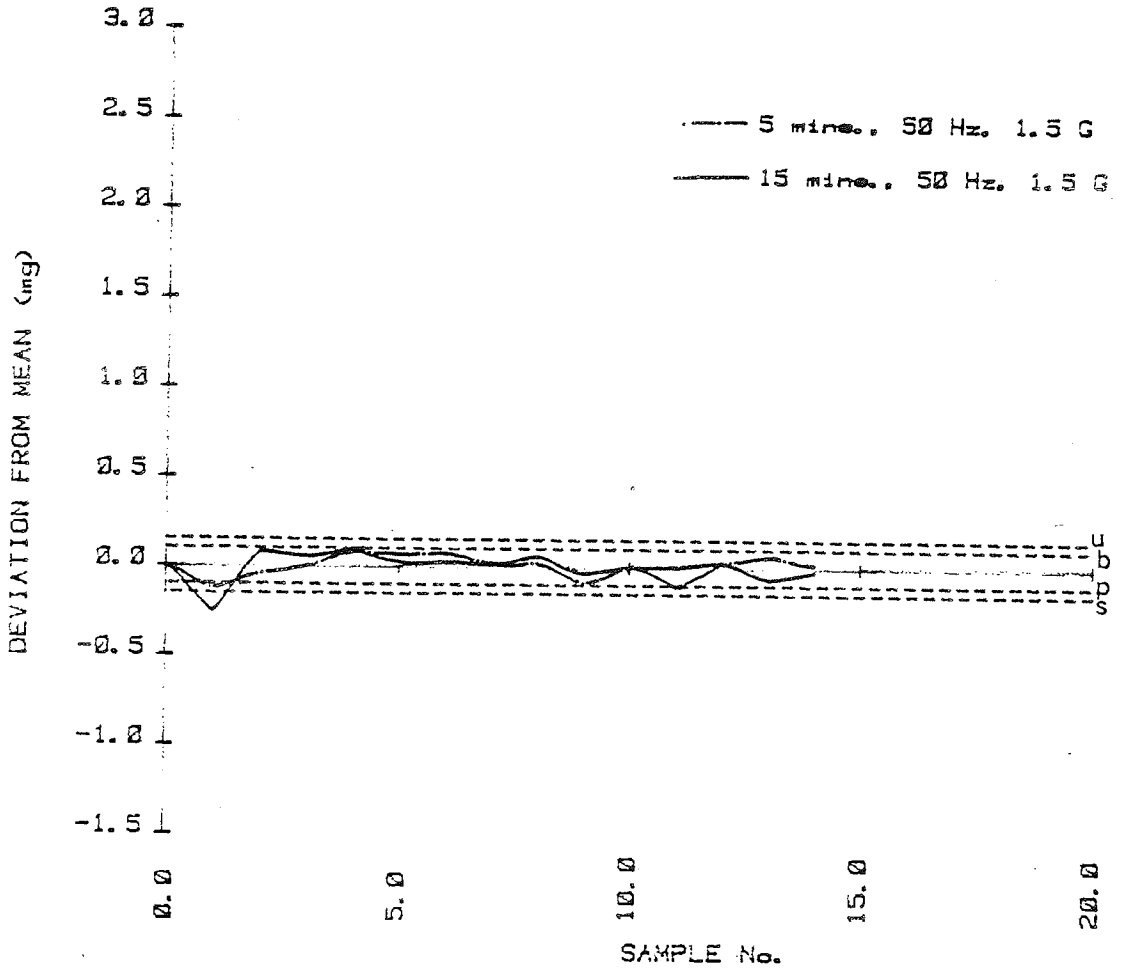

Figure 83. E. Lactose & potassium chloride .5%

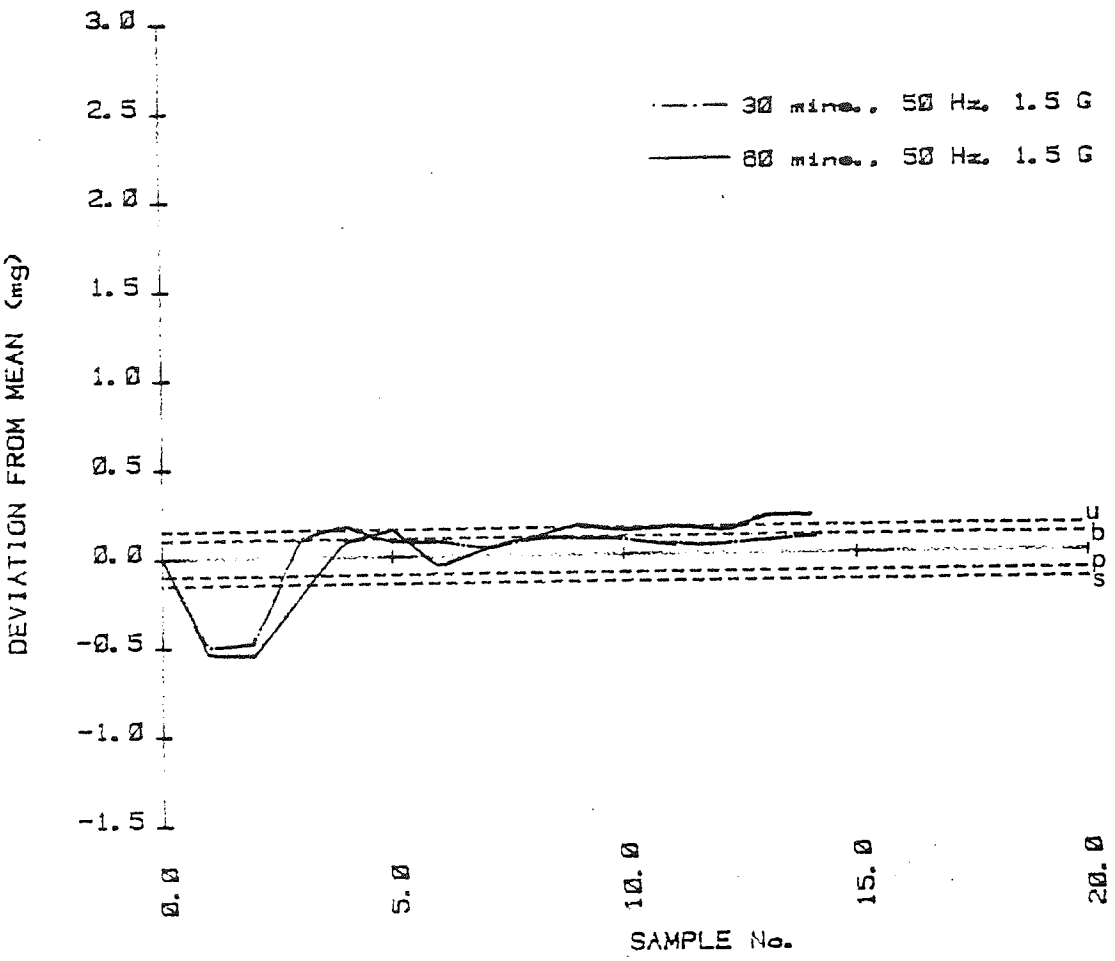

F. Lactose & potassium chloride .5%

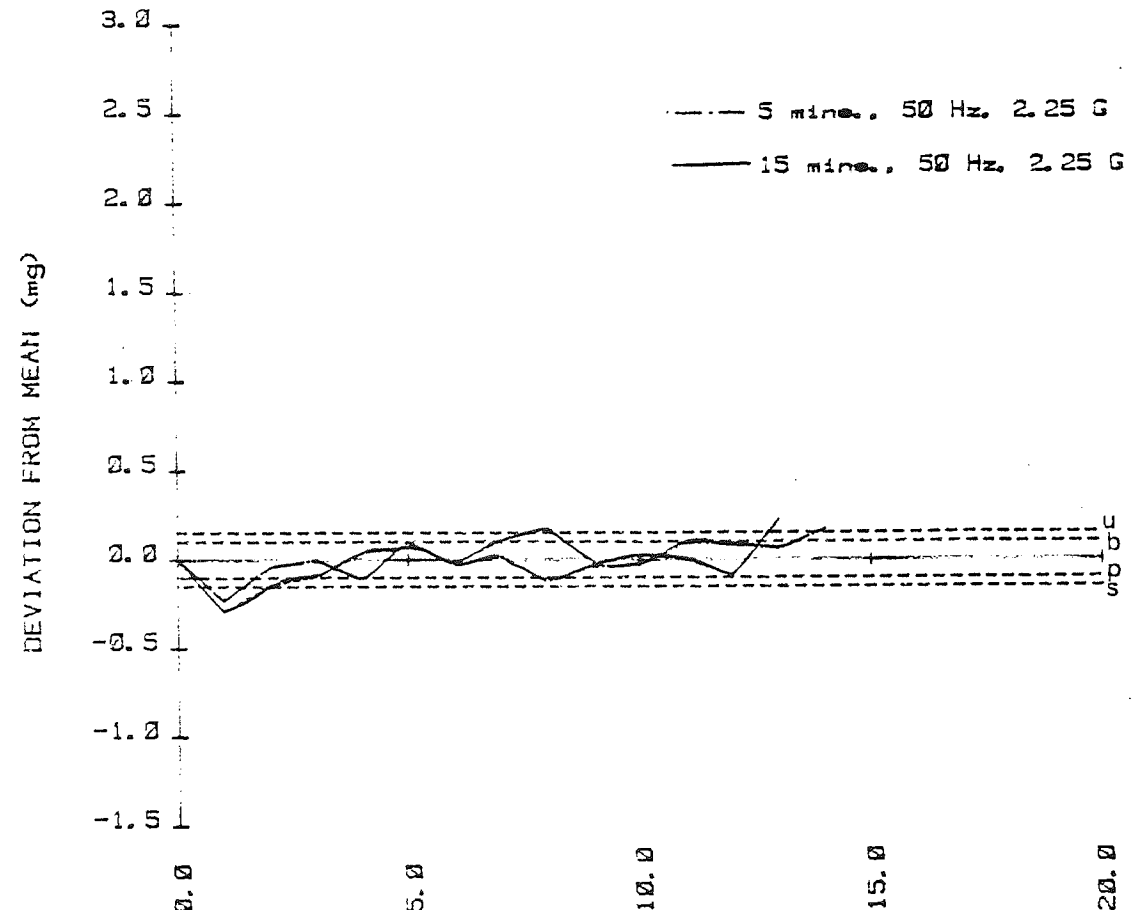

Figure 83. G. Lactose & potassium chloride .5

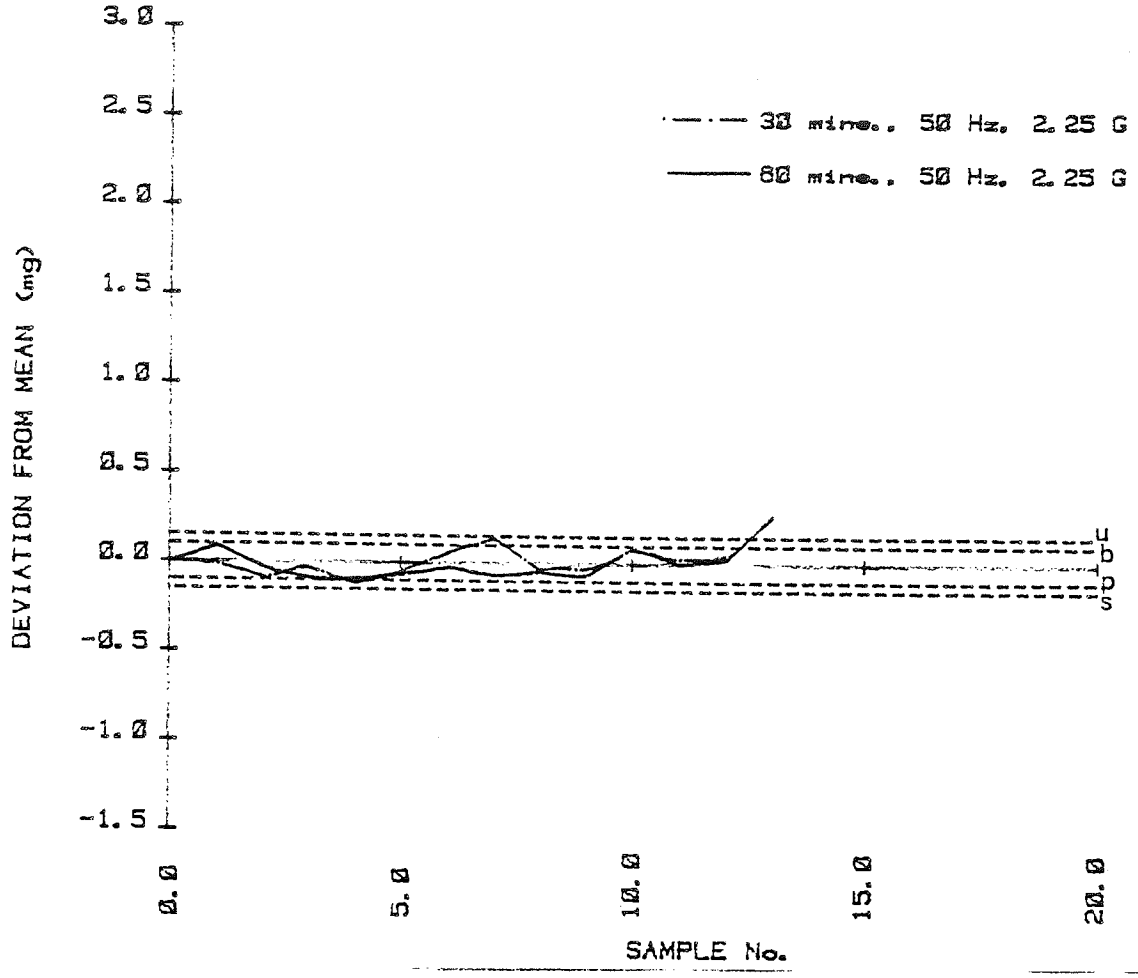

H. Lactose & potassium chloride .5

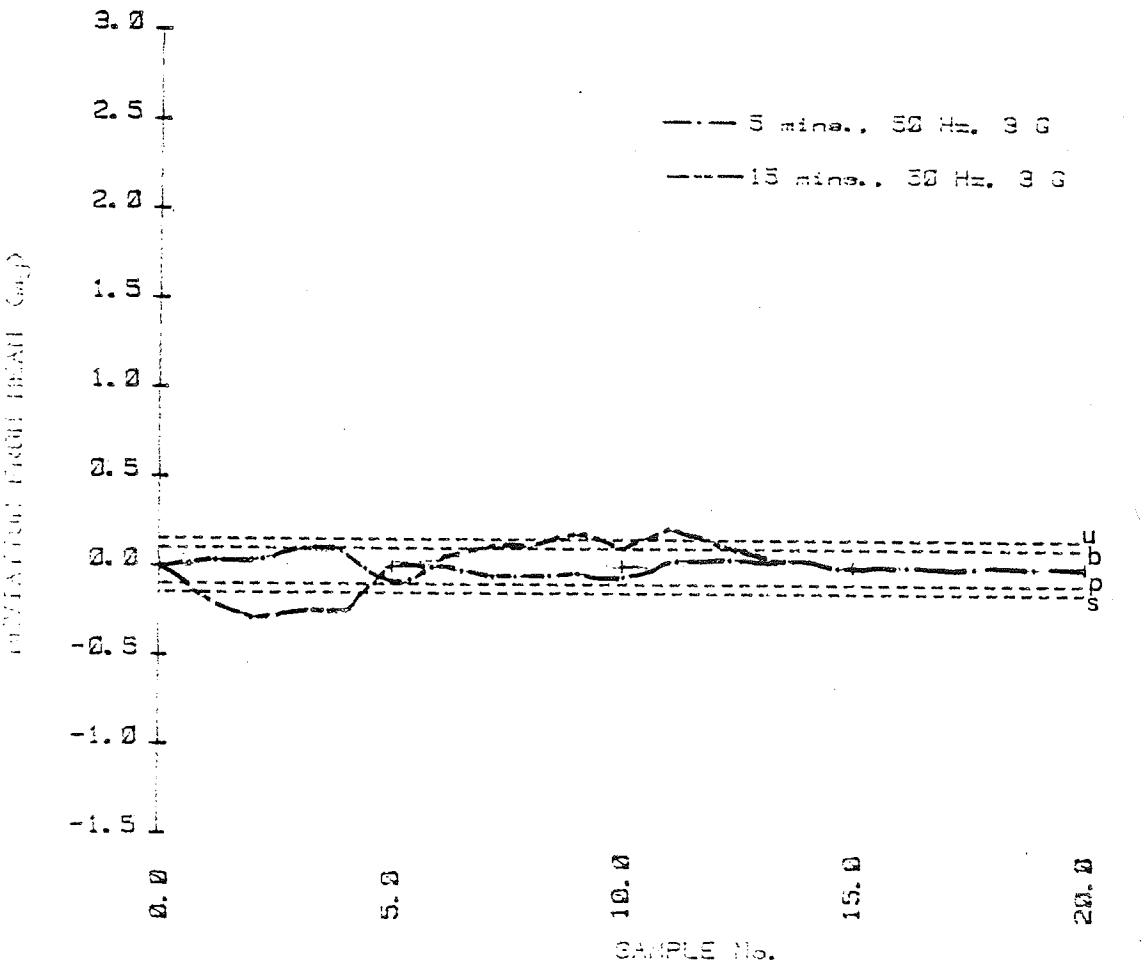

Figure 83. 1. Lactose & potassium chloride .5%

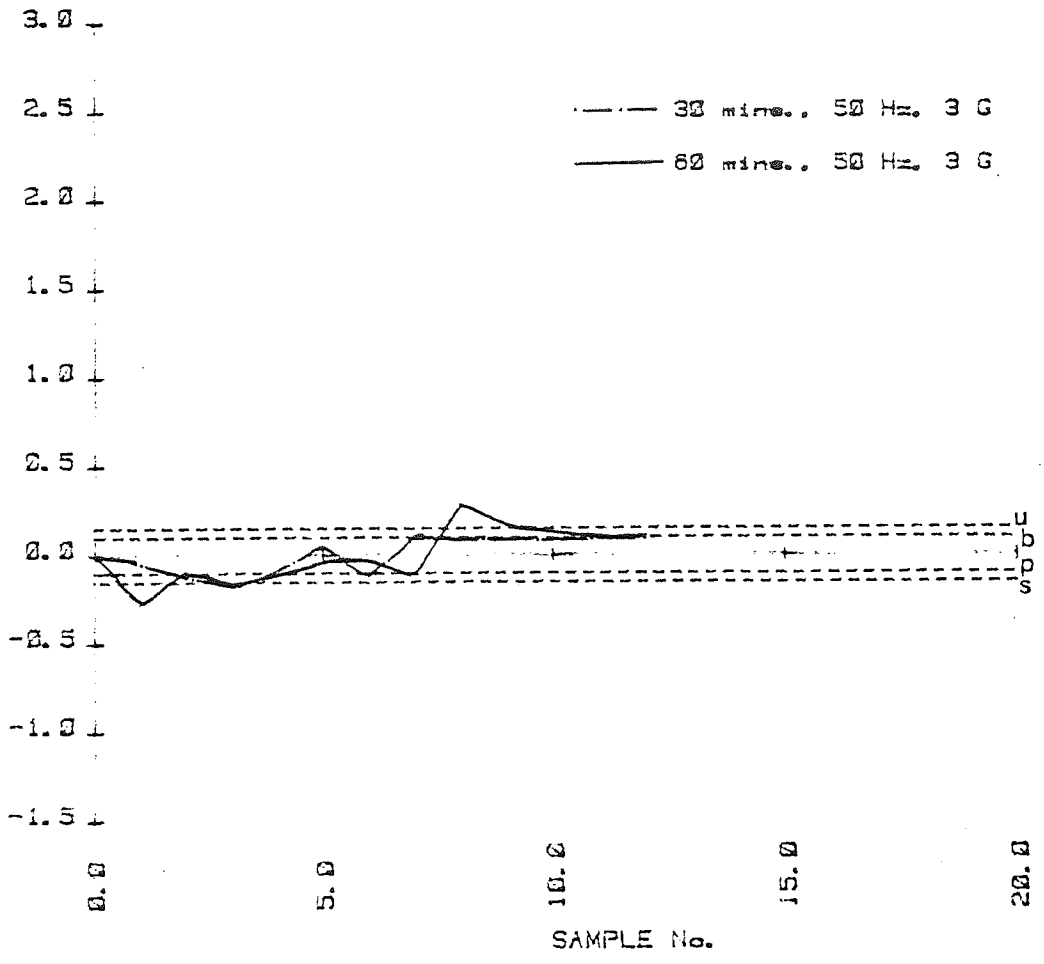

Figure 84. A. Lactose & potassium chloride .5%

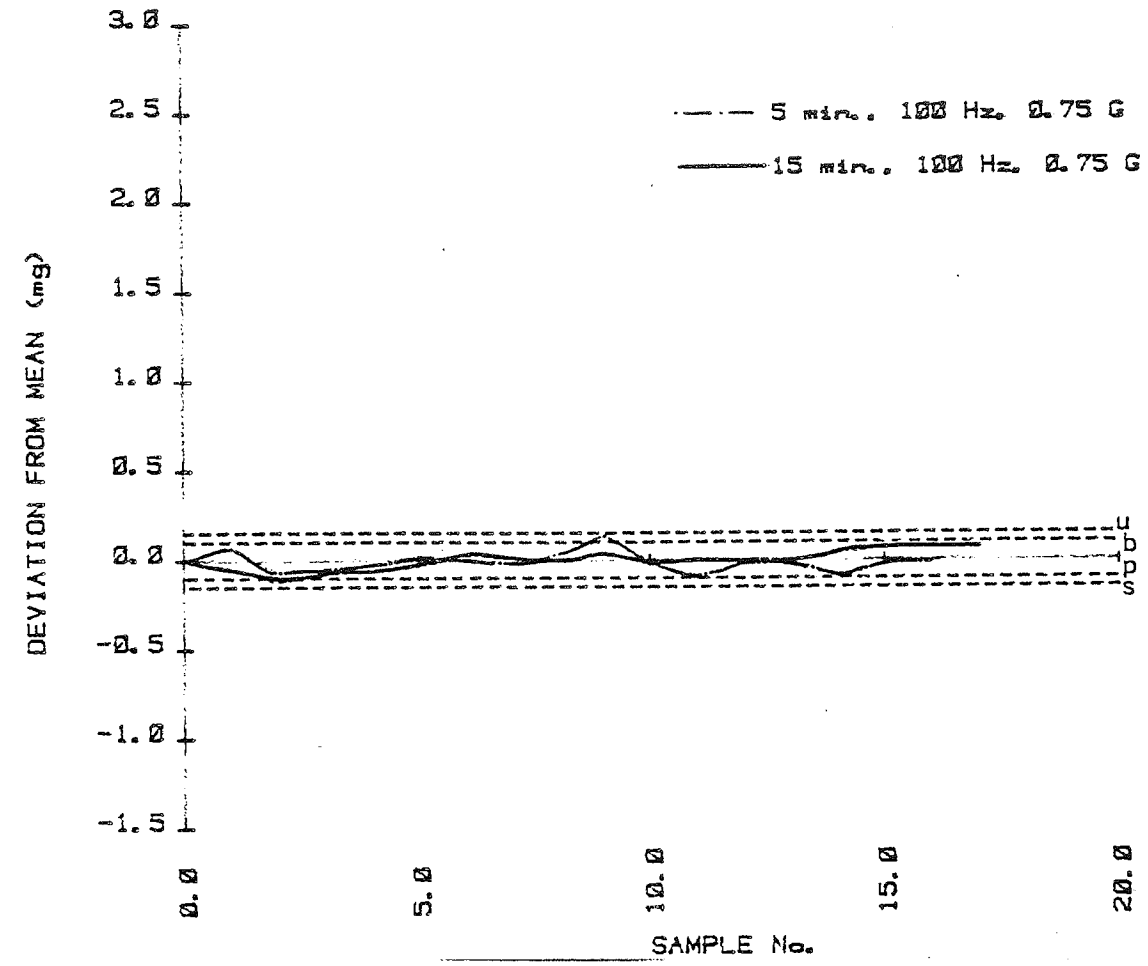

B. Lactose & potassium chloride .5%

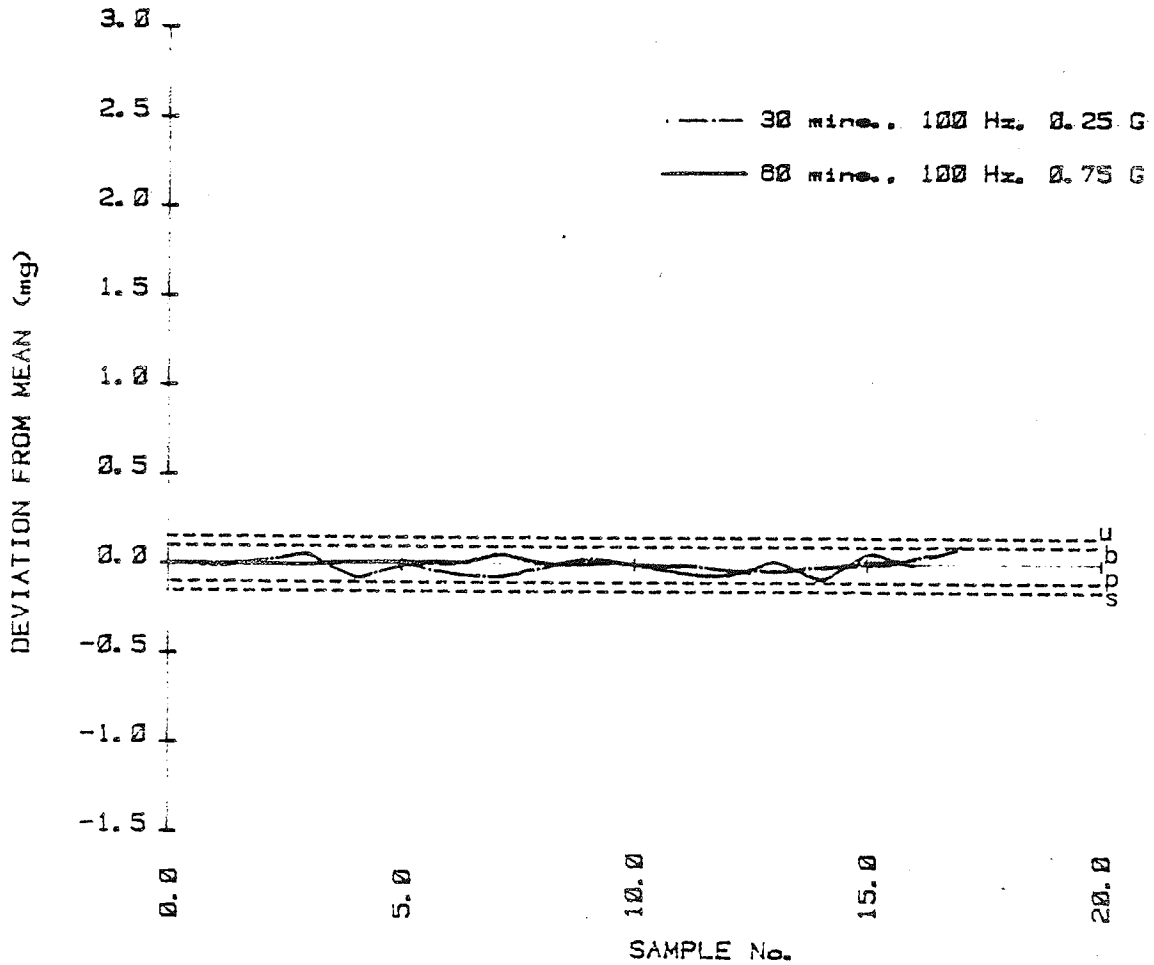

Figure 84. C. Lactose & potassium chloride .5%

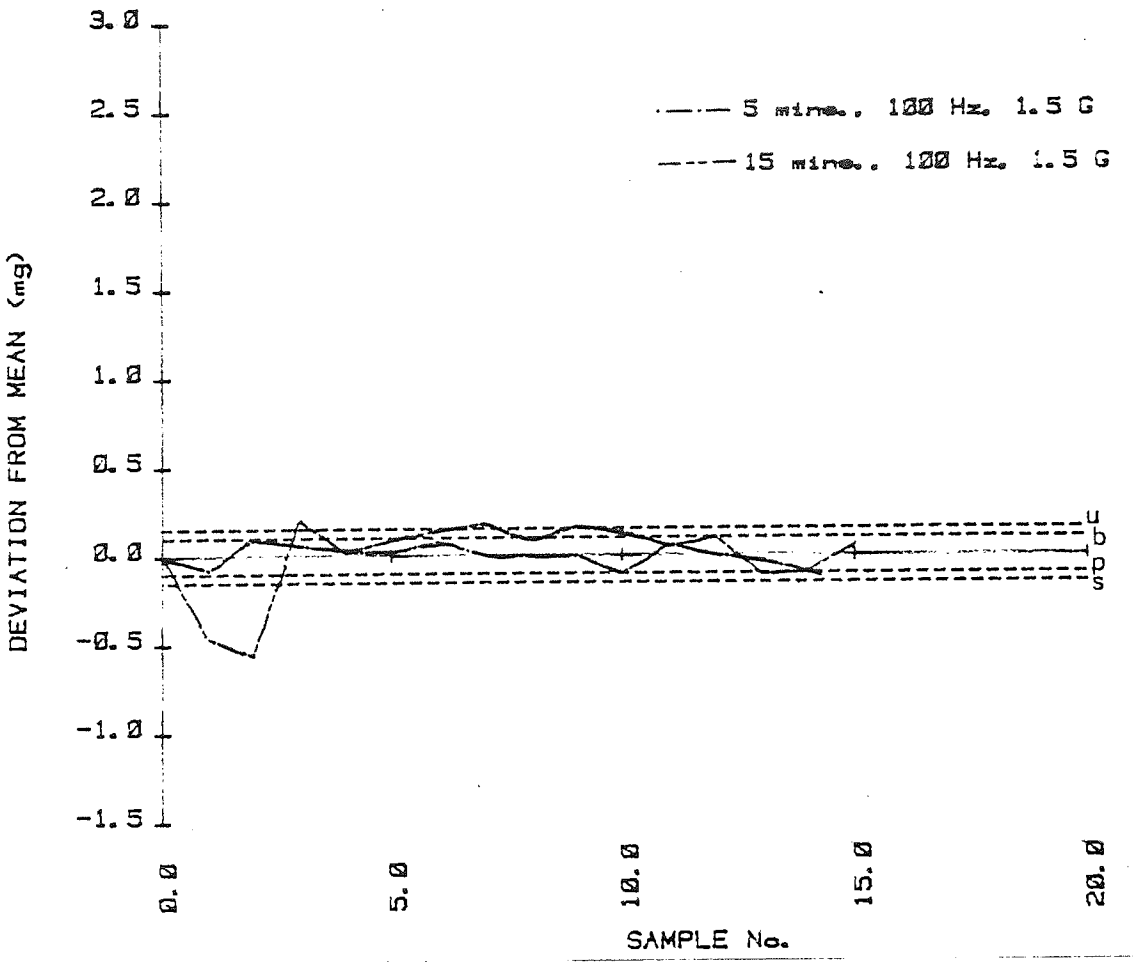

D. Lactose & potassium chloride .5%

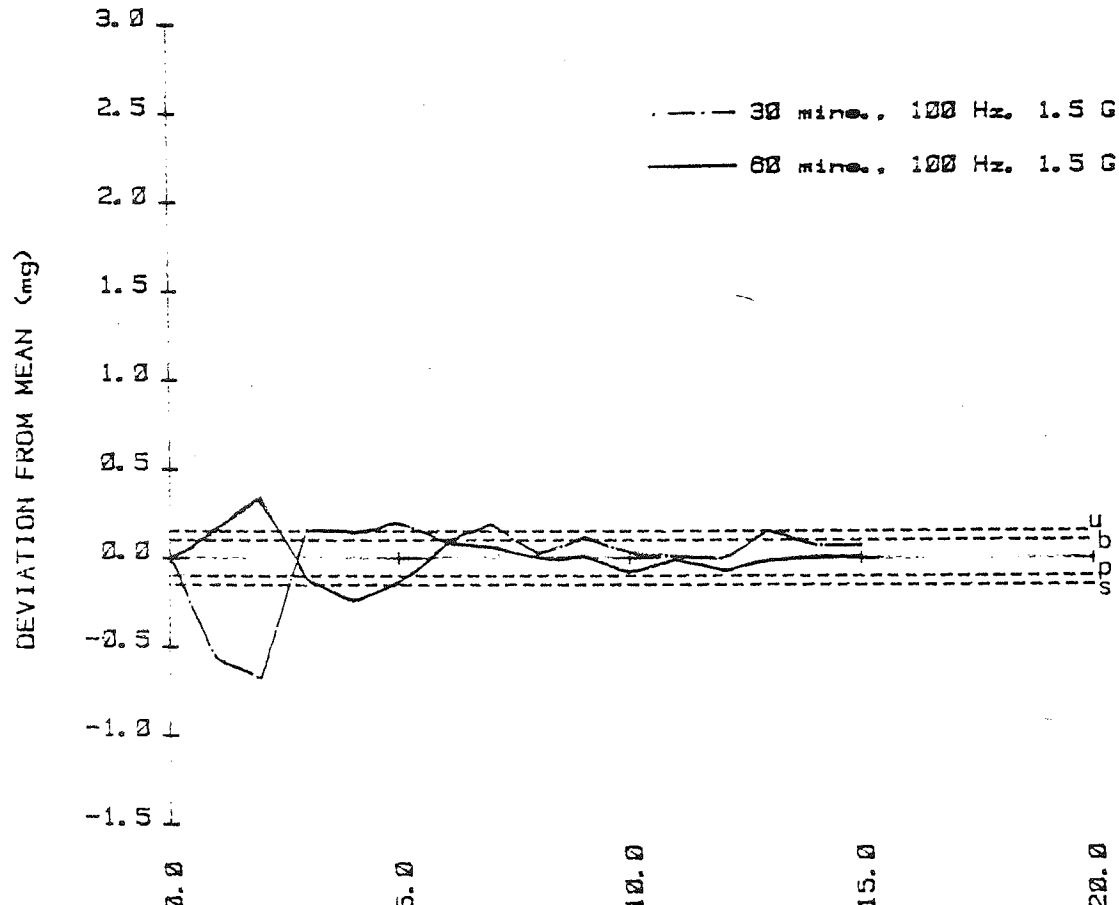

Figure 84. E. Lactose & potassium chloride .5%

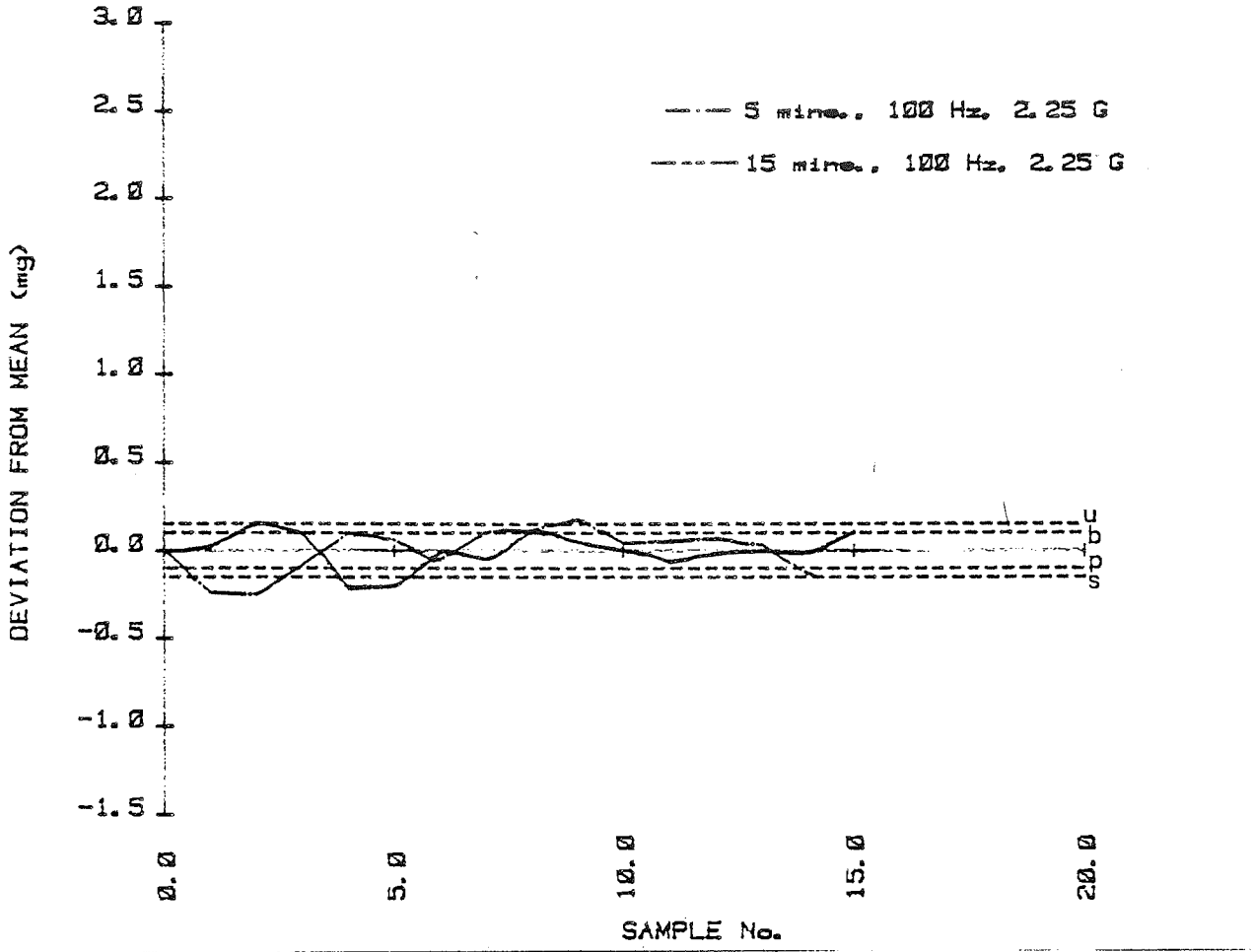

F. Lactose & potassium chloride .5%

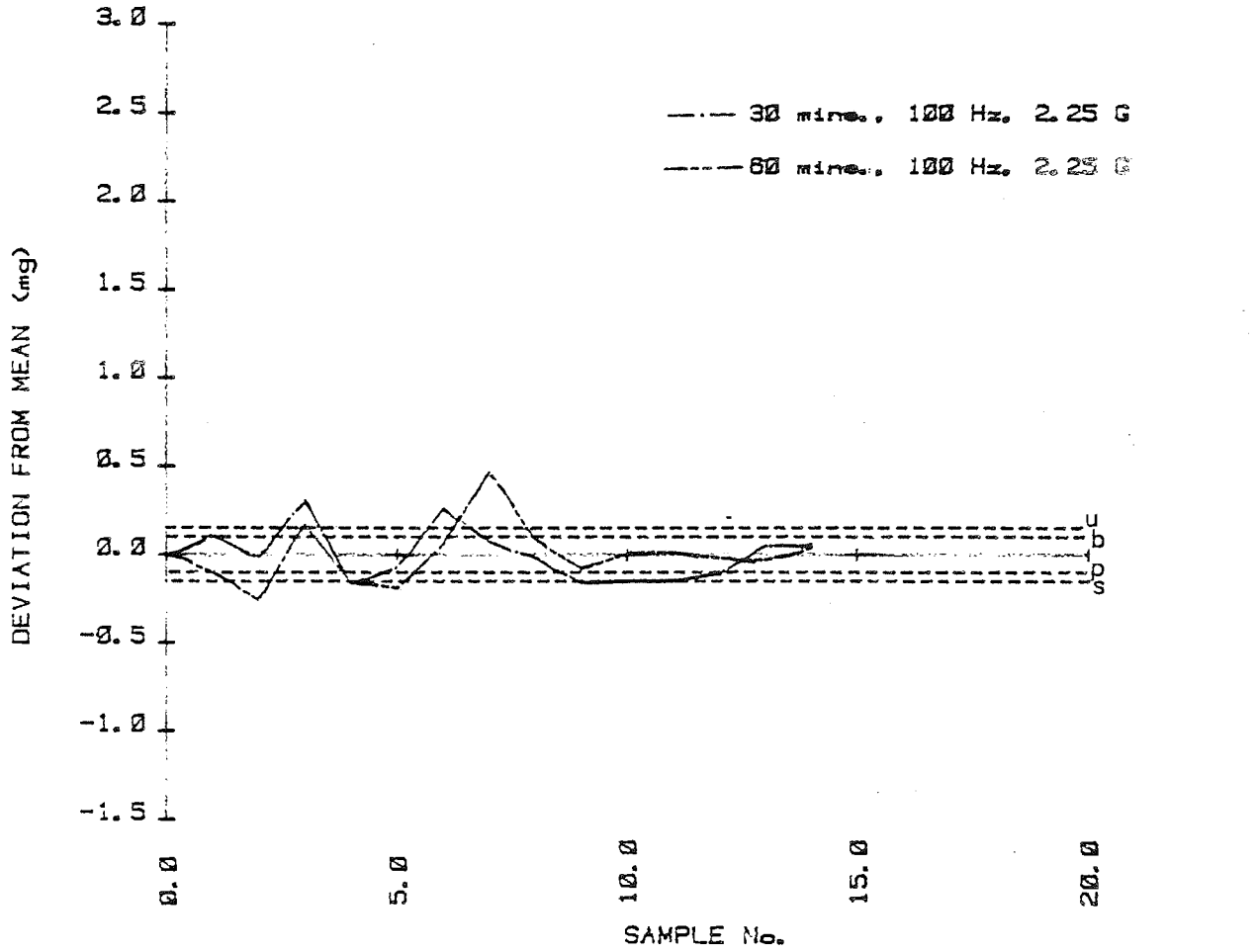

Figure 84. G. Lactose & potassium chloride .5%

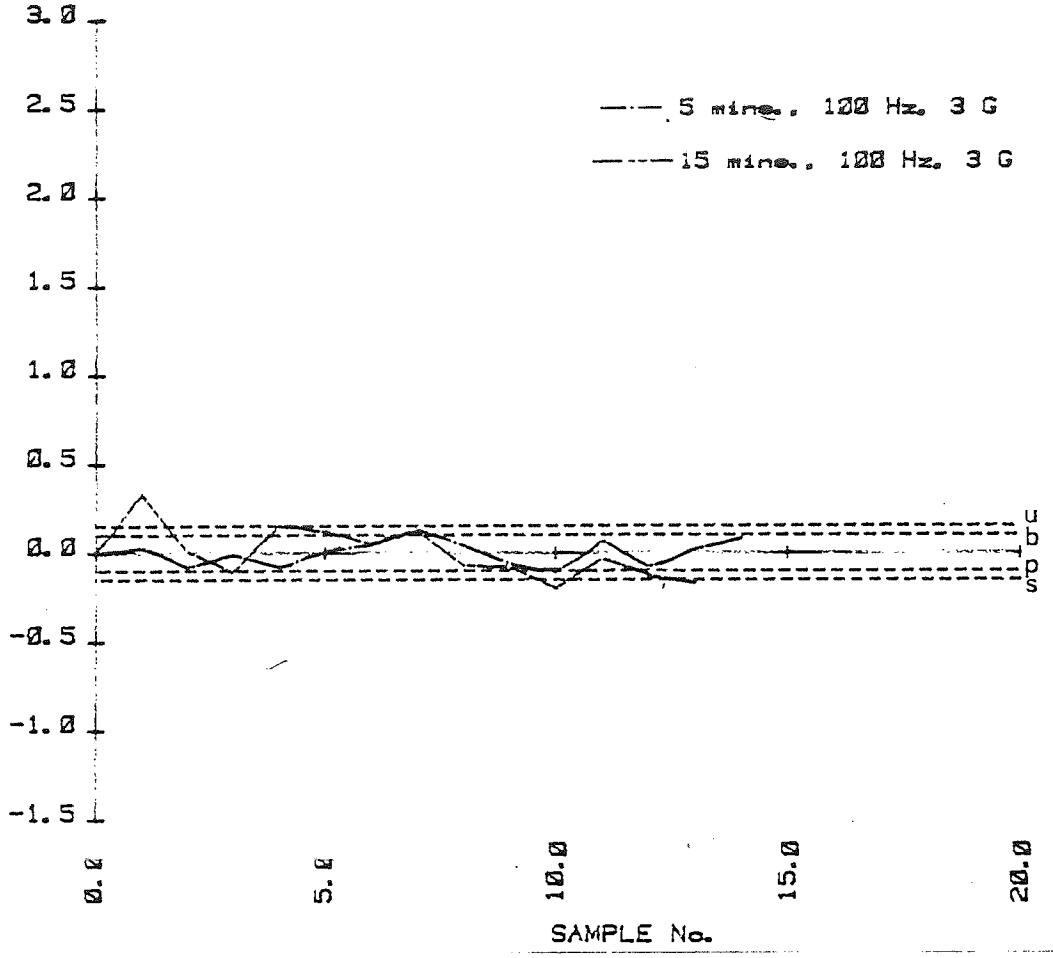

H. Lactose & potassium chloride .5%

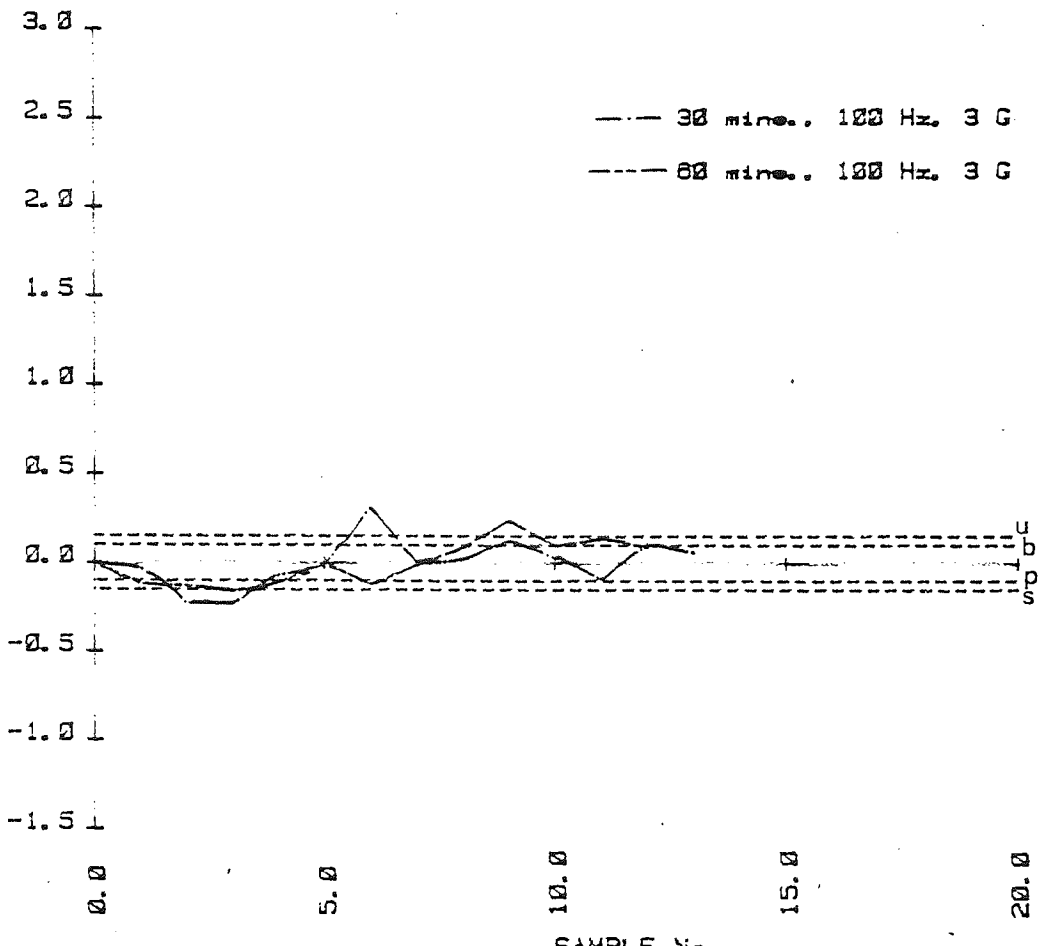

Figure 85.

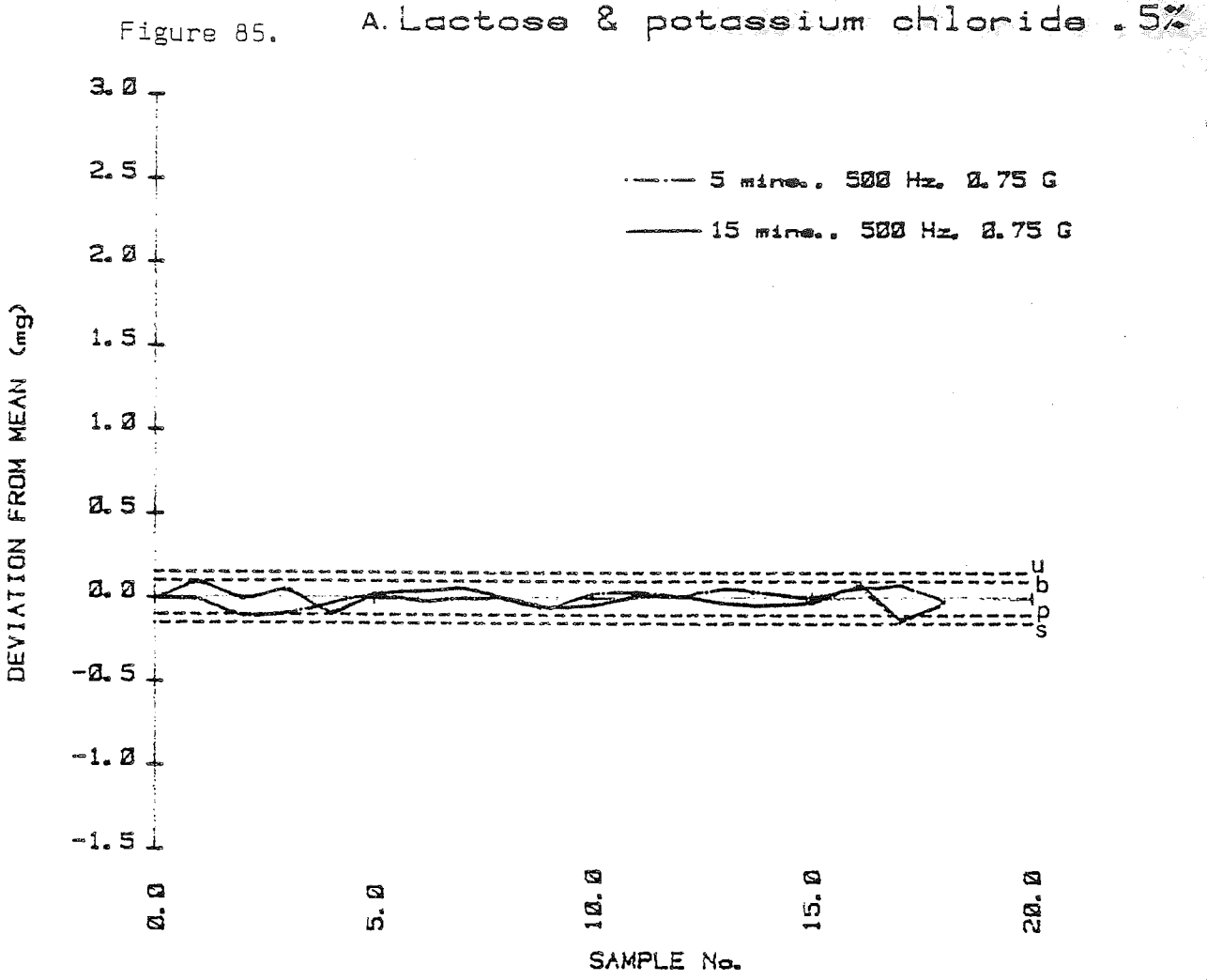
A. Lactose & potassium chloride .5%
5 mins., 500 Hz, 0.75 G
15 mins., 500 Hz, 0.75 G
DEVIATION FROM MEAN (mg)
3.0
2.5
2.0
1.5
1.0
0.5
0.0
-0.5
-1.0
-1.5
u
b
p
s
0.0
5.0
10.0
15.0
20.0
SAMPLE No.

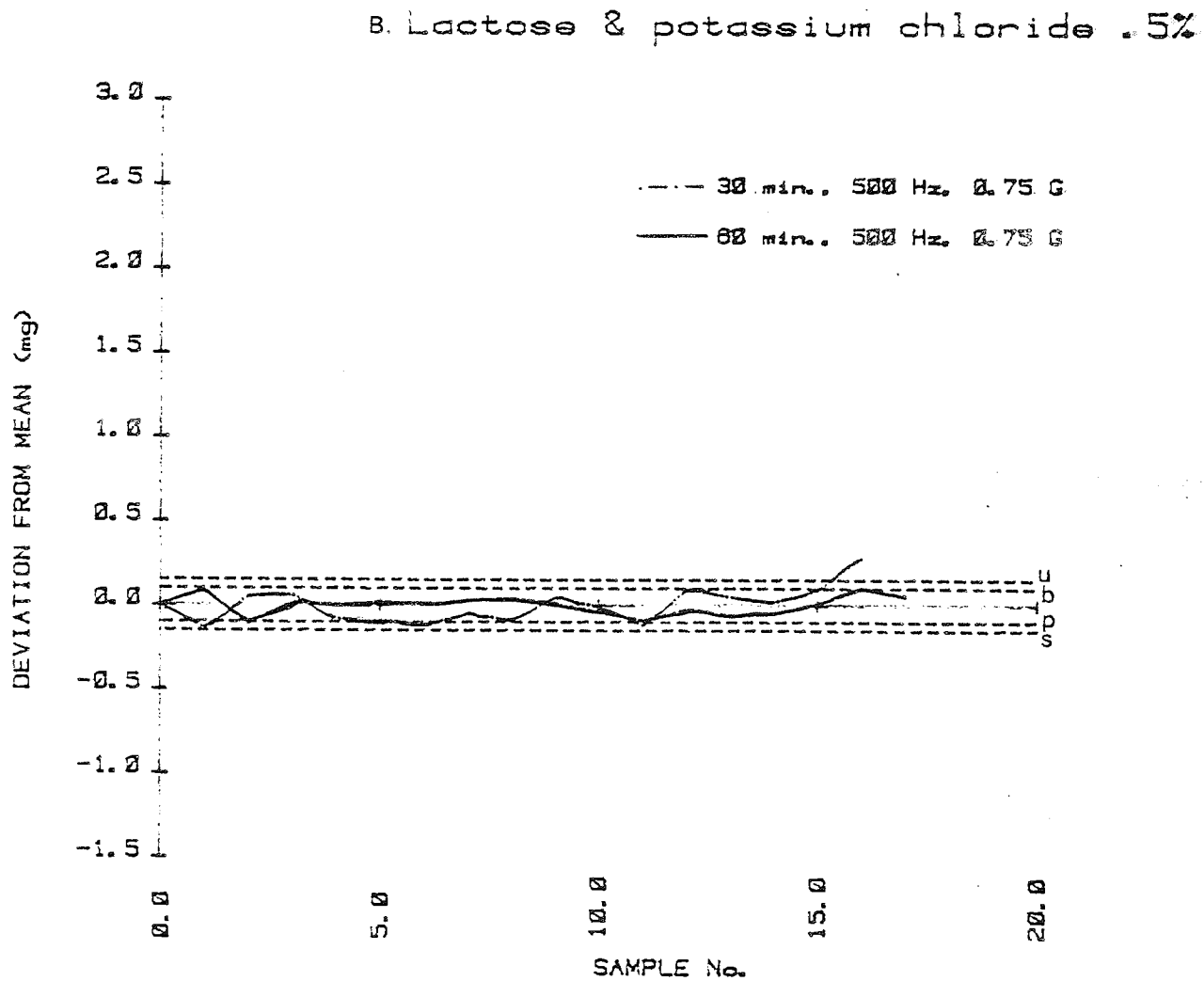
B. Lactose & potassium chloride .5%
30 min., 500 Hz, 0.75 G
60 min., 500 Hz, 0.75 G
DEVIATION FROM MEAN (mg)
3.0
2.5
2.0
1.5
1.0
0.5
0.0
-0.5
-1.0
-1.5
u
b
p
s
0.0
5.0
10.0
15.0
20.0
SAMPLE No.

Figure 85. C. Lactose & potassium chloride .5%

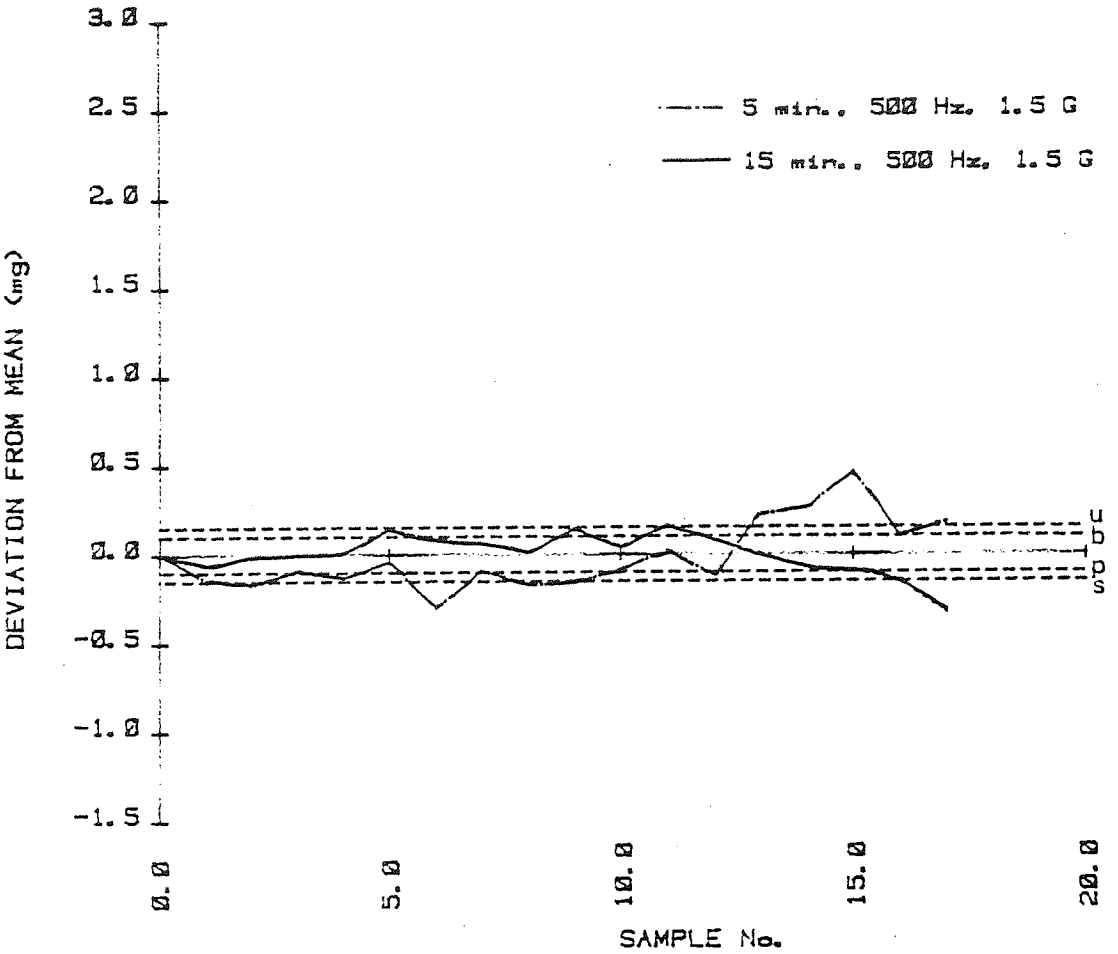

D. Lactose & potassium chloride .5%

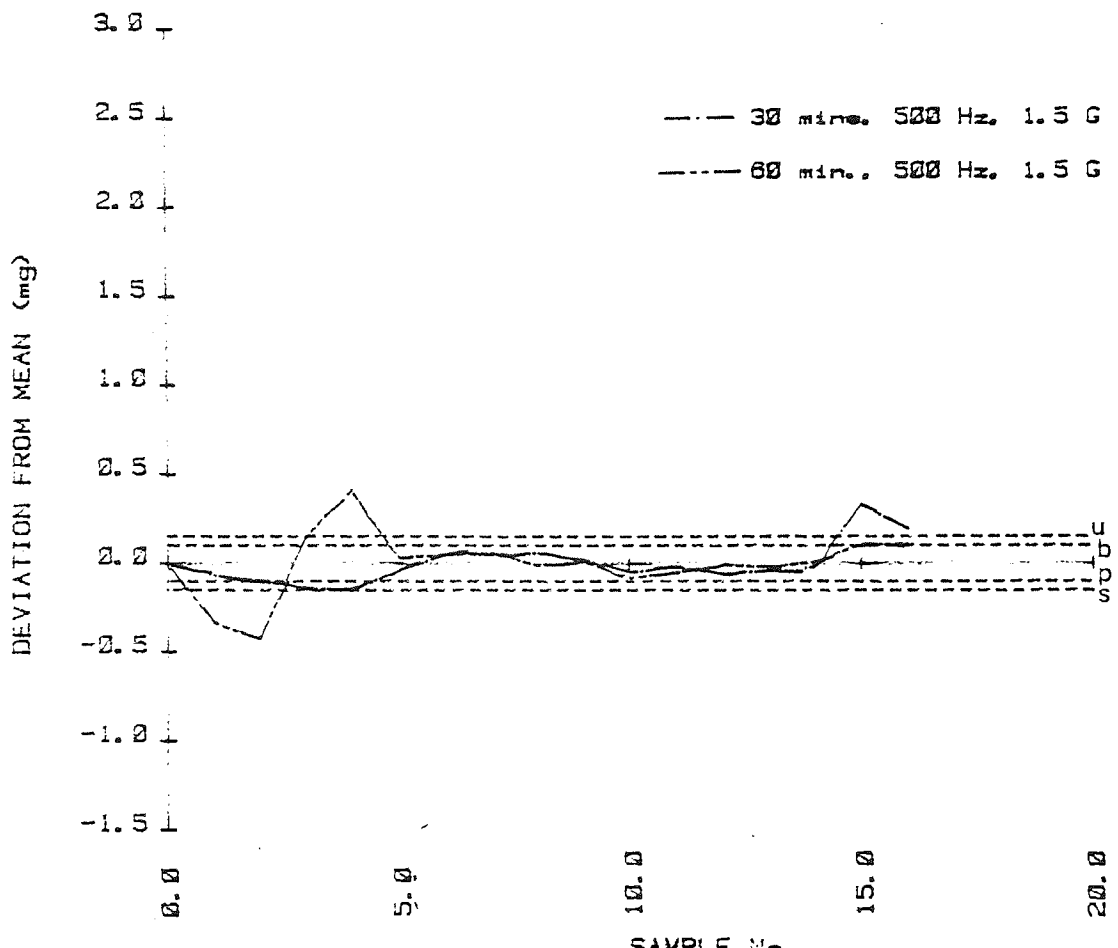

Figure 85.

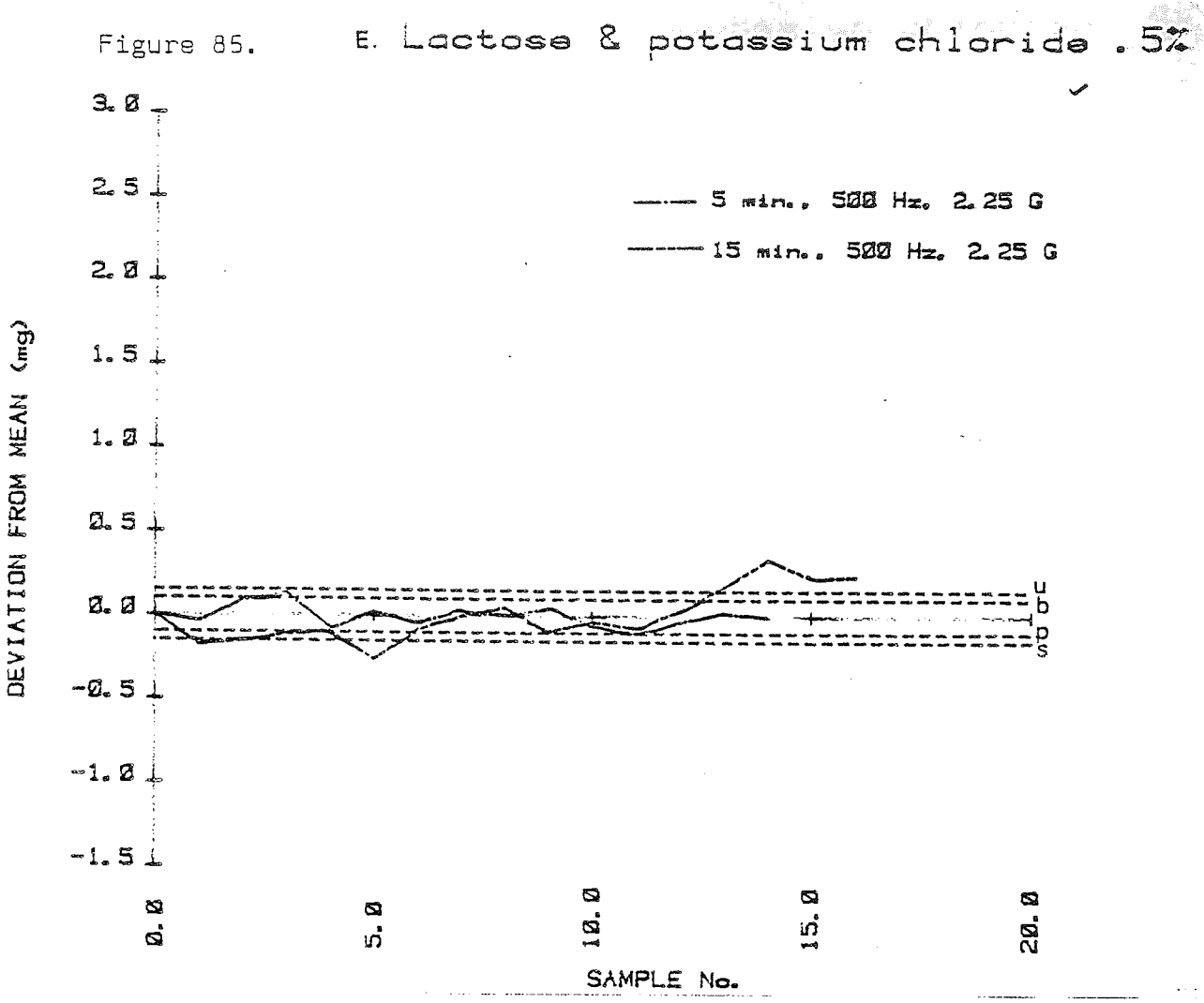
E. Lactose & potassium chloride .5%
5 min., 500 Hz. 2.25 G
15 min., 500 Hz. 2.25 G
DEVIATION FROM MEAN (mg)
3.0
2.5
2.0
1.5
1.0
0.5
0.0
-0.5
-1.0
-1.5
0.0
5.0
10.0
15.0
20.0
SAMPLE No.

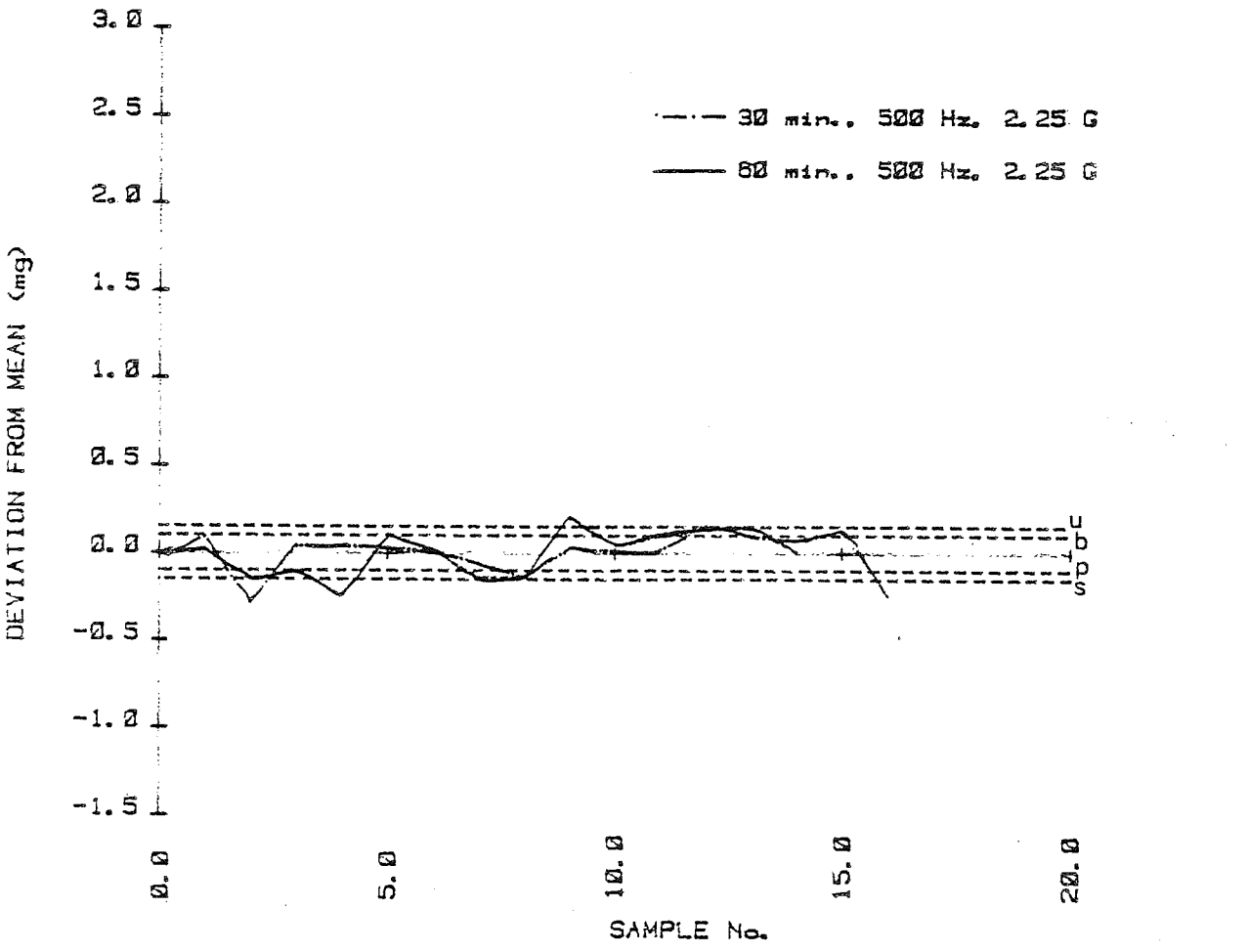
F. Lactose & potassium chloride .5%
30 min., 500 Hz. 2.25 G
60 min., 500 Hz. 2.25 G
DEVIATION FROM MEAN (mg)
3.0
2.5
2.0
1.5
1.0
0.5
0.0
-0.5
-1.0
-1.5
0.0
5.0
10.0
15.0
20.0
SAMPLE No.

Figure 85. G. Lactose & potassium chloride .5%

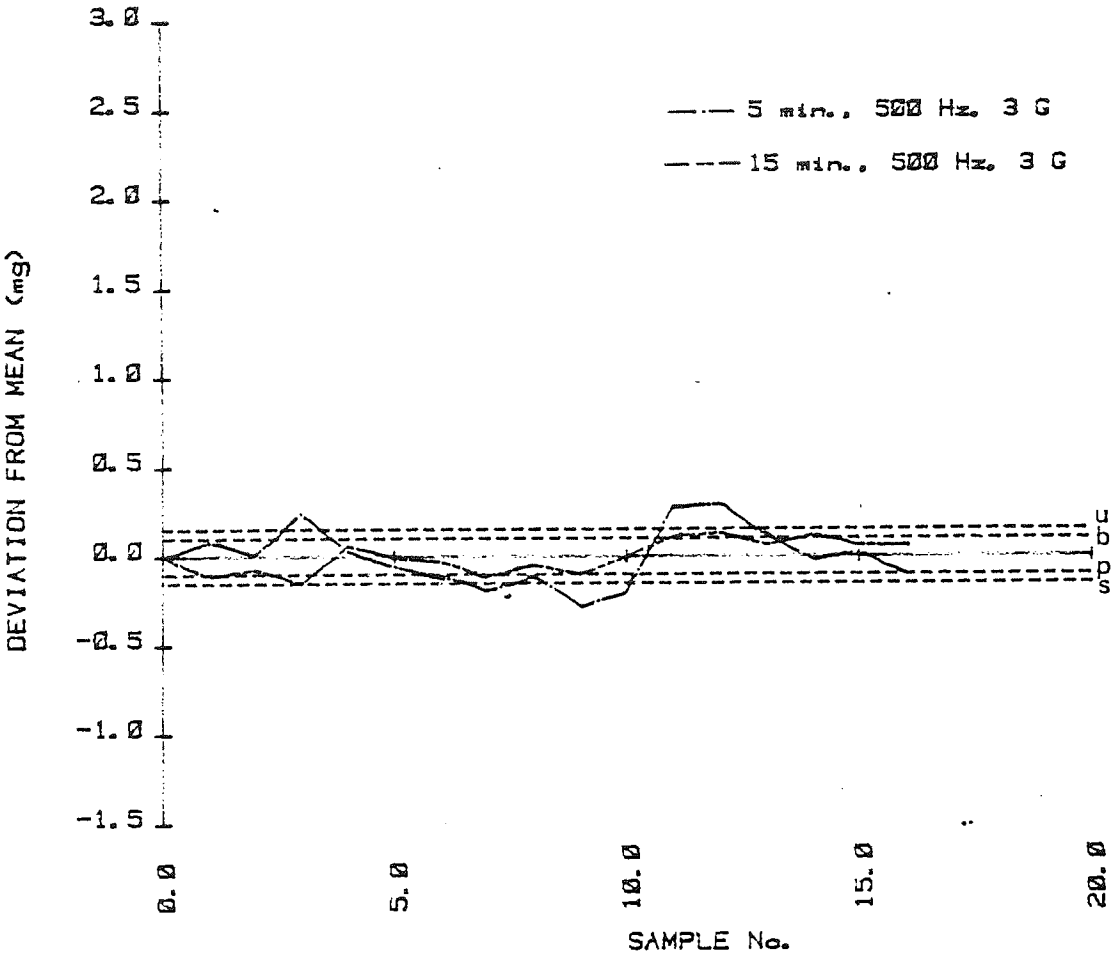

H. Lactose & potassium chloride .5%

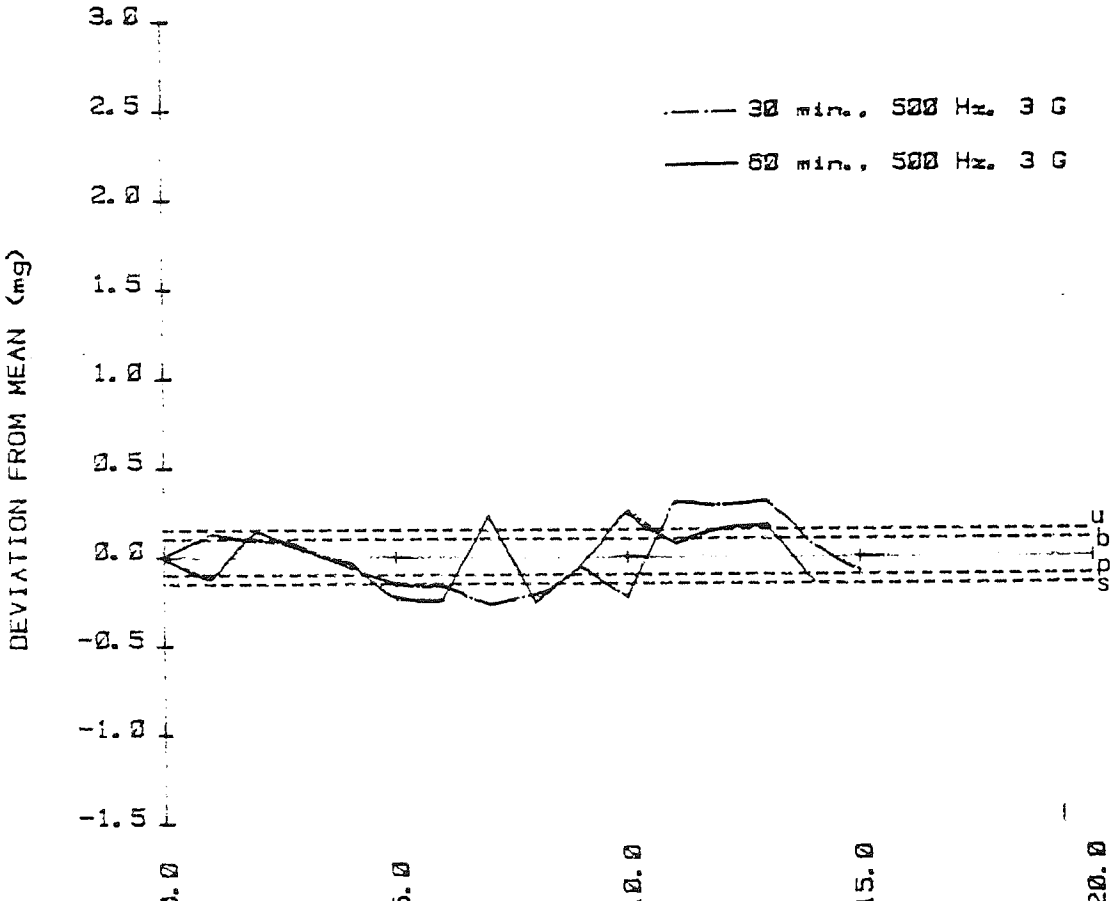

Figure 86.

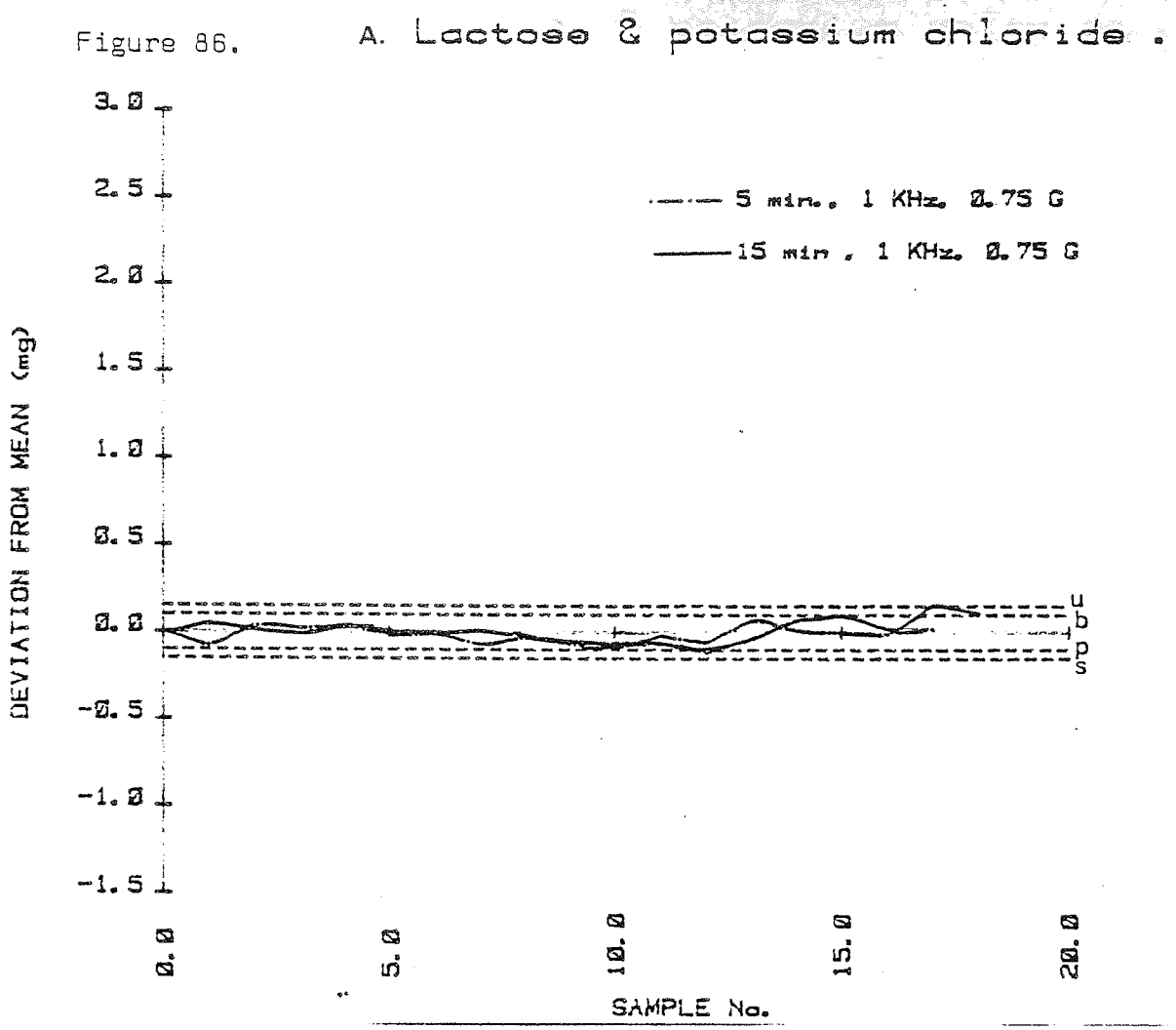
A. Lactose & potassium chloride .
5 min., 1 KHz, 0.75 G
15 min., 1 KHz, 0.75 G
DEVIATION FROM MEAN (mg)
3.0
2.5
2.0
1.5
1.0
0.5
0.0
-0.5
-1.0
-1.5
0.0
5.0
10.0
15.0
20.0
SAMPLE No.
upper
lower

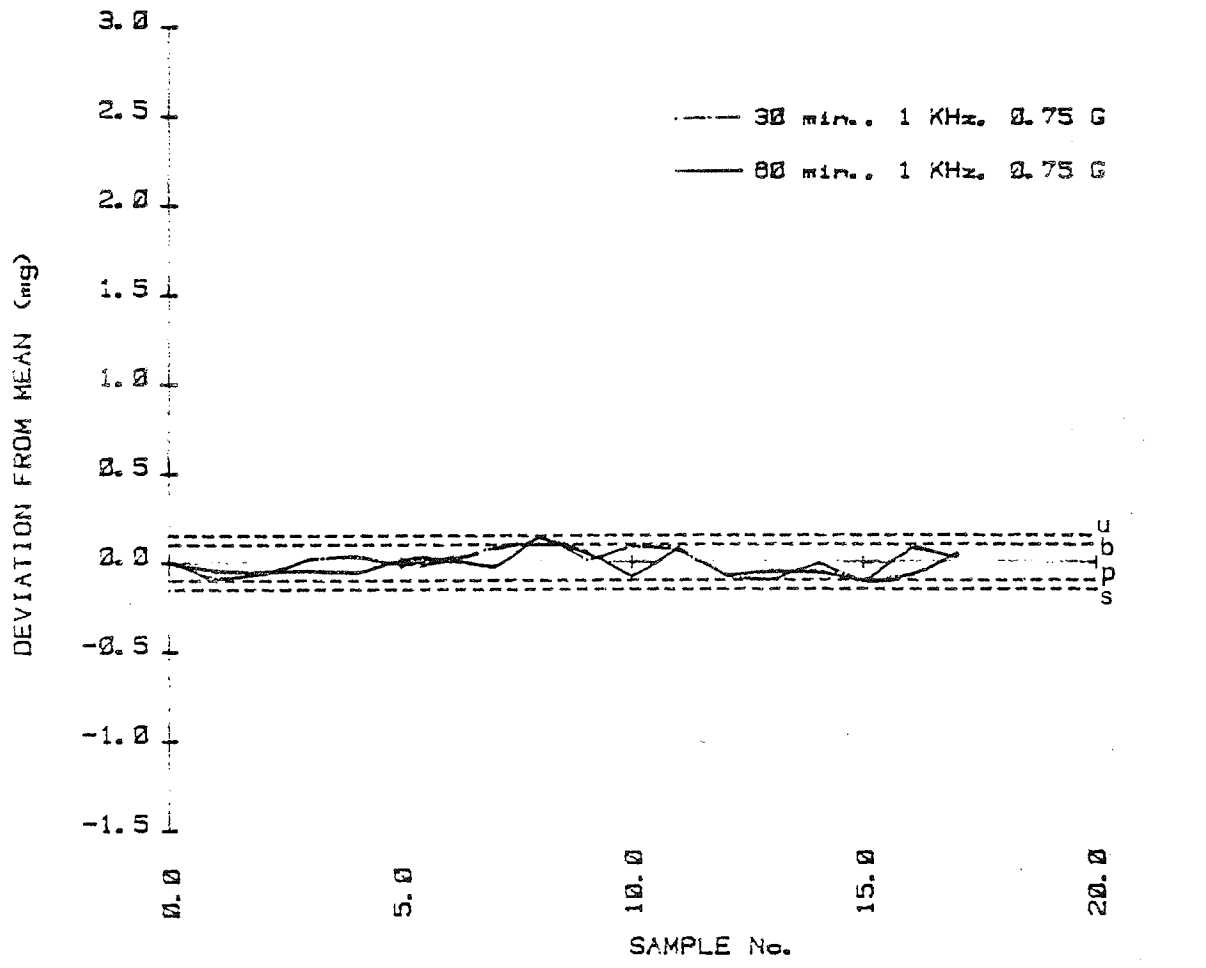
B. Lactose & potassium chloride .
30 min., 1 KHz, 0.75 G
60 min., 1 KHz, 0.75 G
DEVIATION FROM MEAN (mg)
3.0
2.5
2.0
1.5
1.0
0.5
0.0
-0.5
-1.0
-1.5
0.0
5.0
10.0
15.0
20.0
SAMPLE No.
upper
lower

Figure 86. C. Lactose & potassium chloride 0.5%

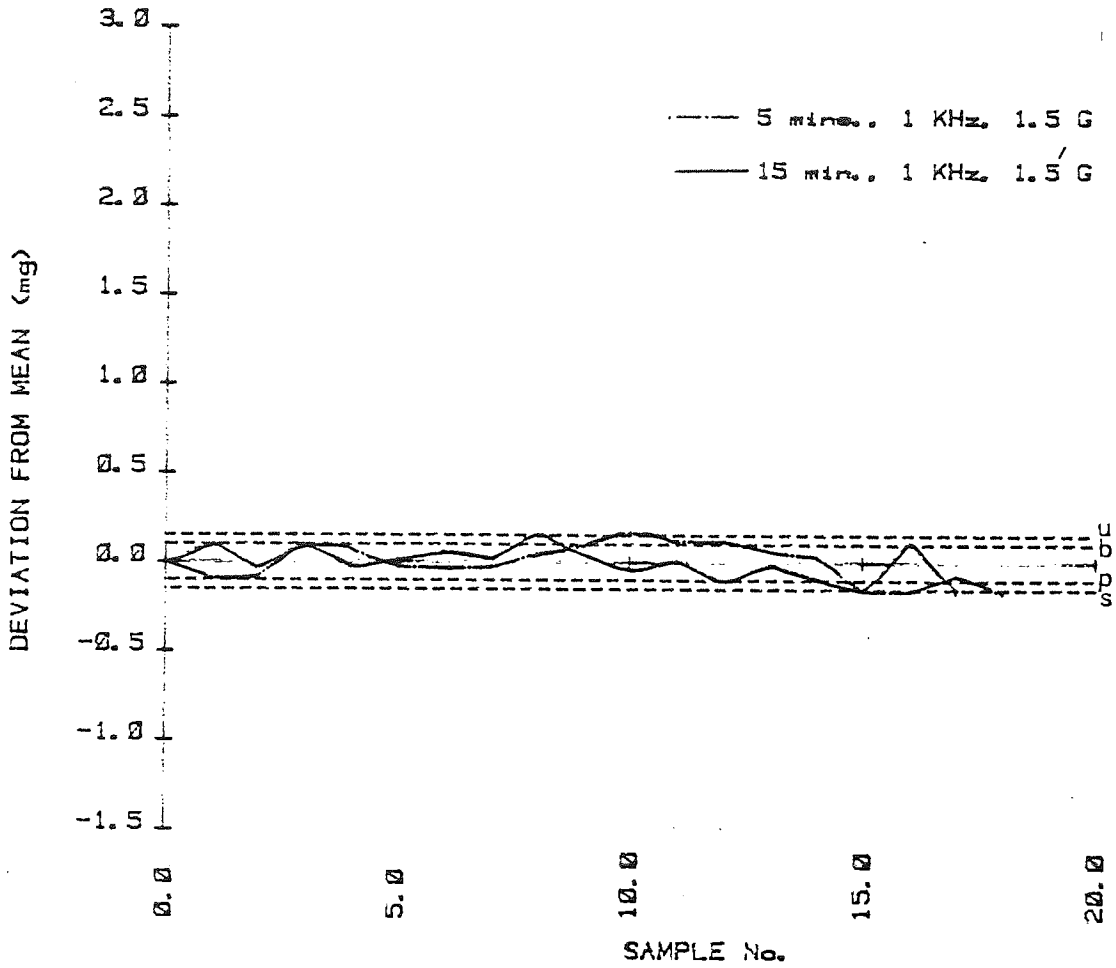

D. Lactose & potassium chloride .5%

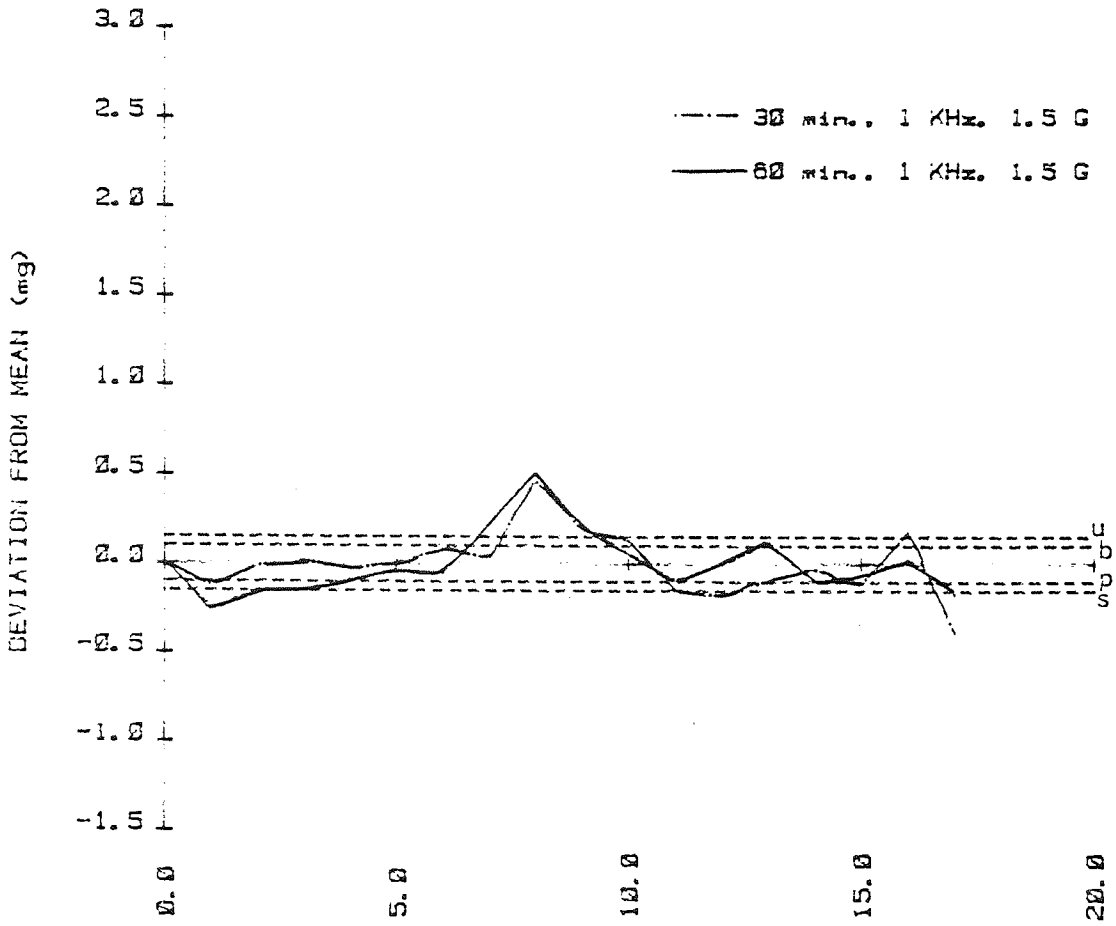

Figure 86. E. Lactose & potassium chloride .

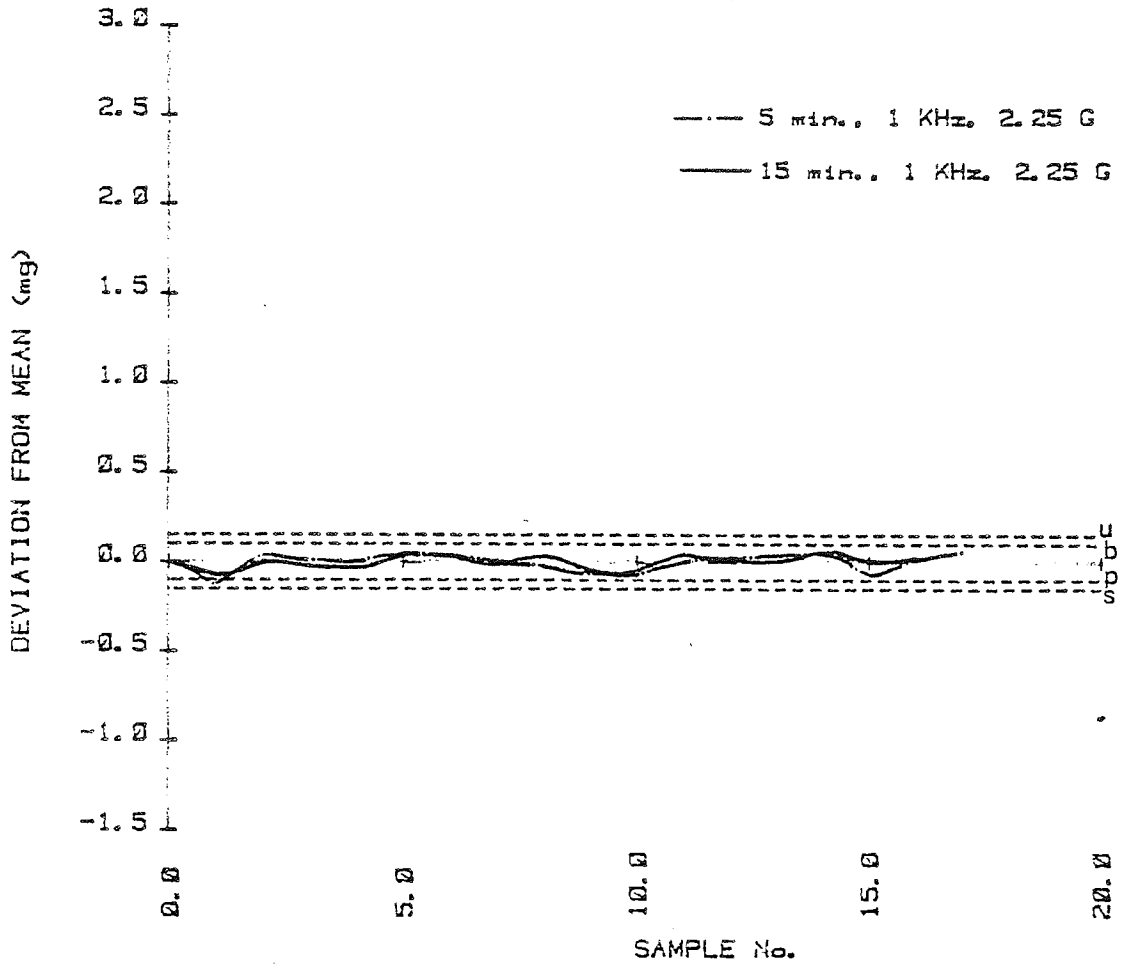

F. Lactose & potassium chloride .

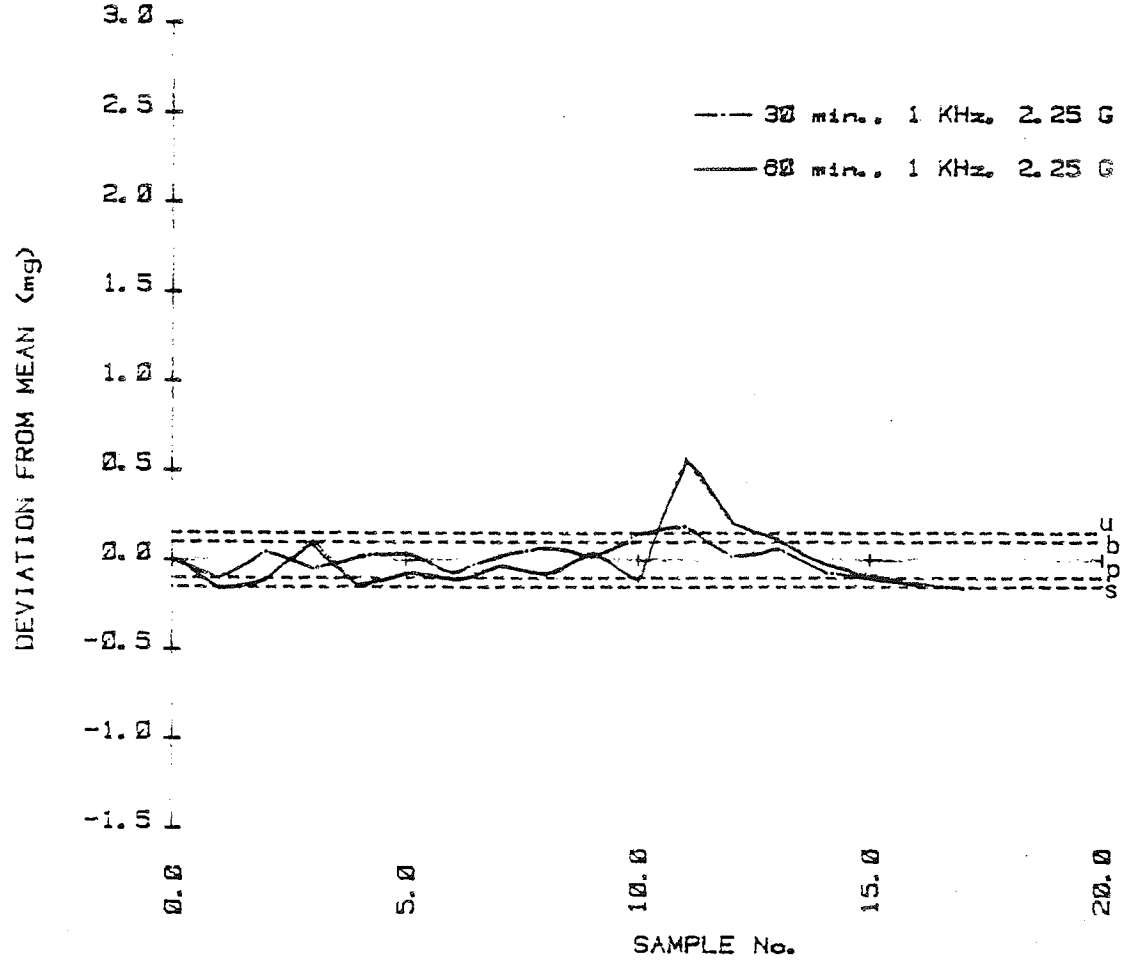

Figure 86. G. Lactose & potassium chloride .5%

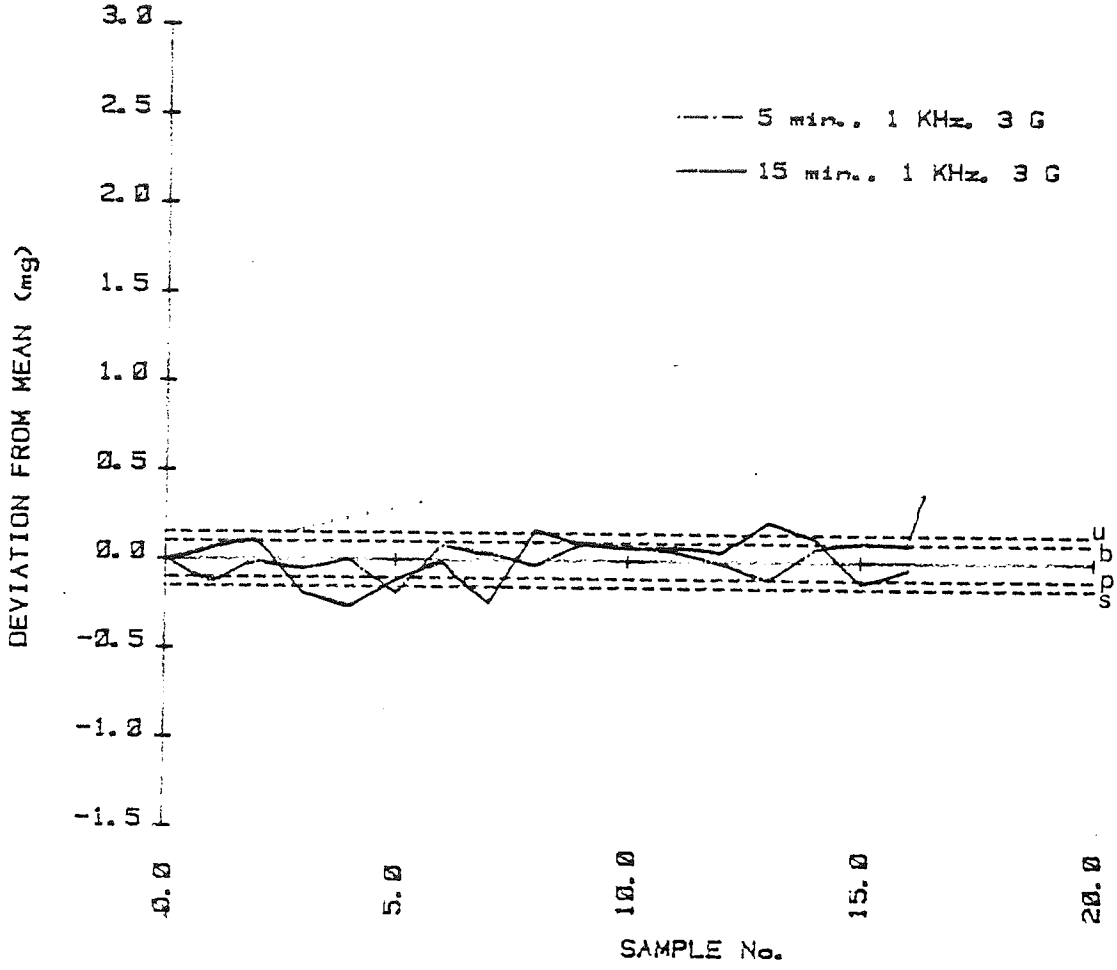

H. Lactose & potassium chloride .5%

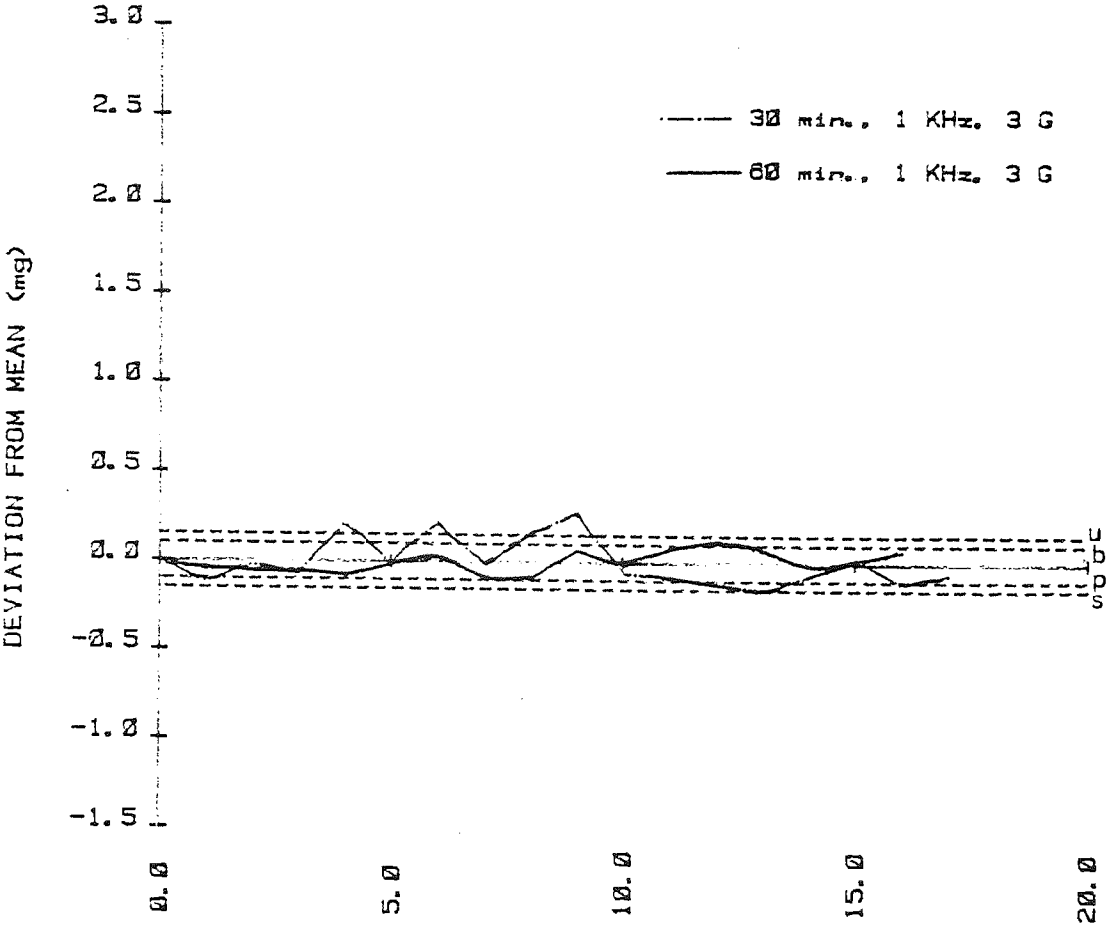

Figure 87. A. Dipac & potassium chloride .5 %

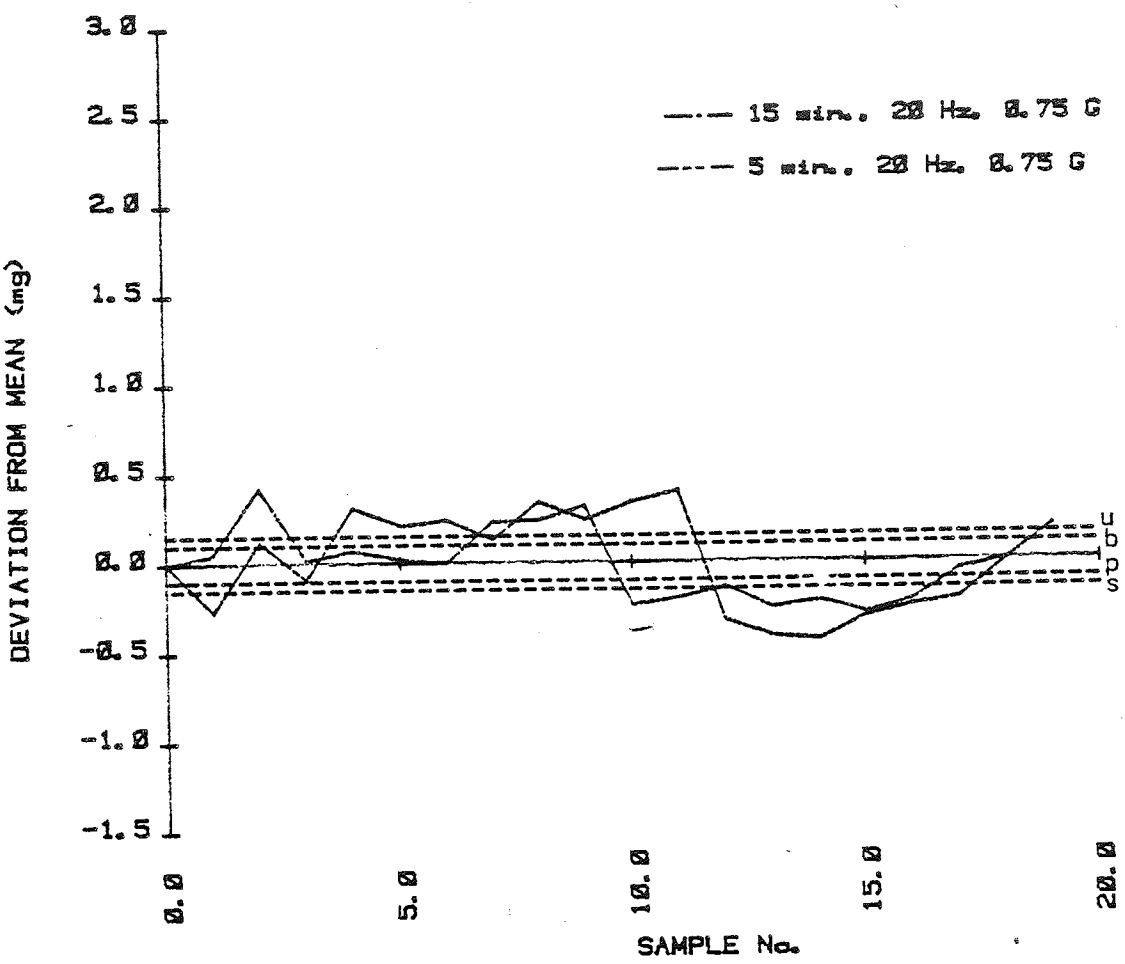

B. Dipac & potassium chloride .5%

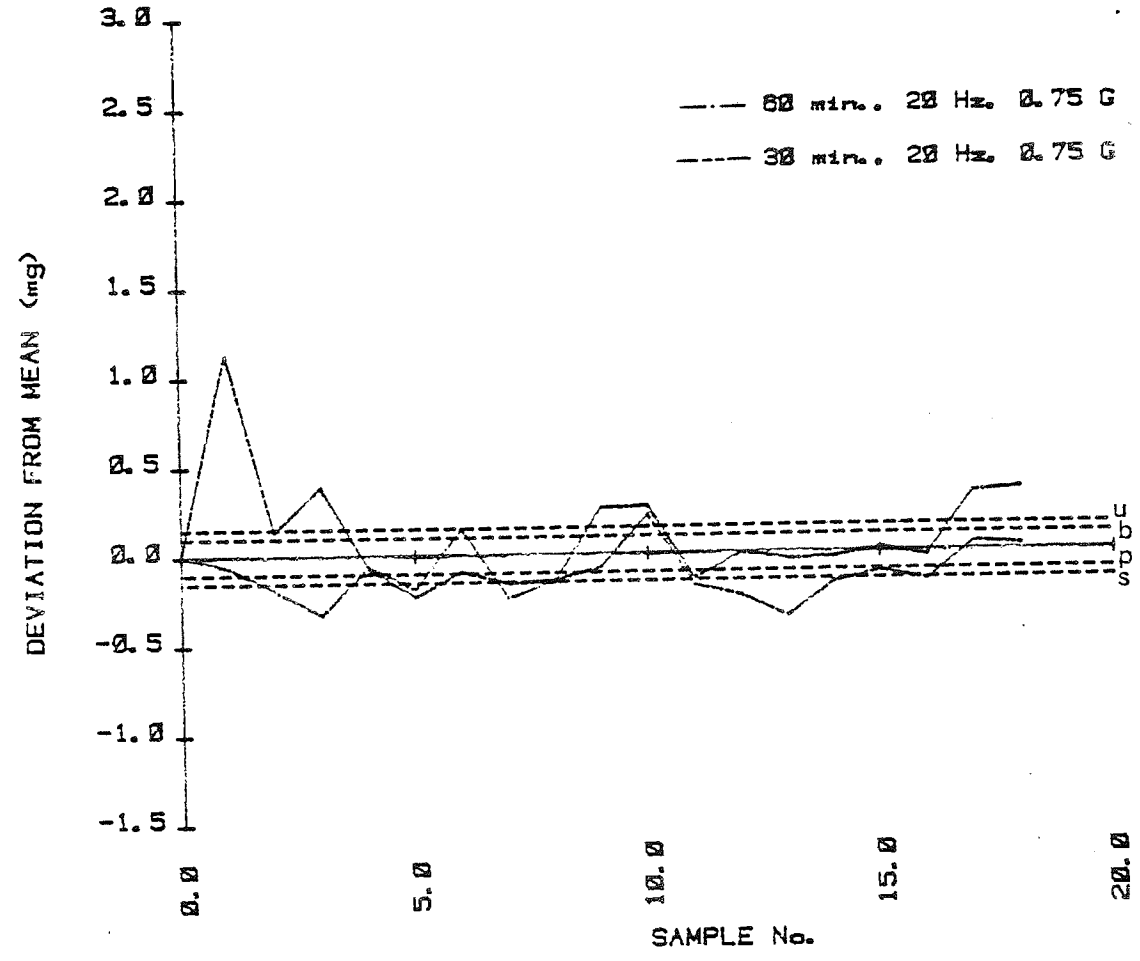

Figure 87.C. Dipac and potassium chloride .5 %

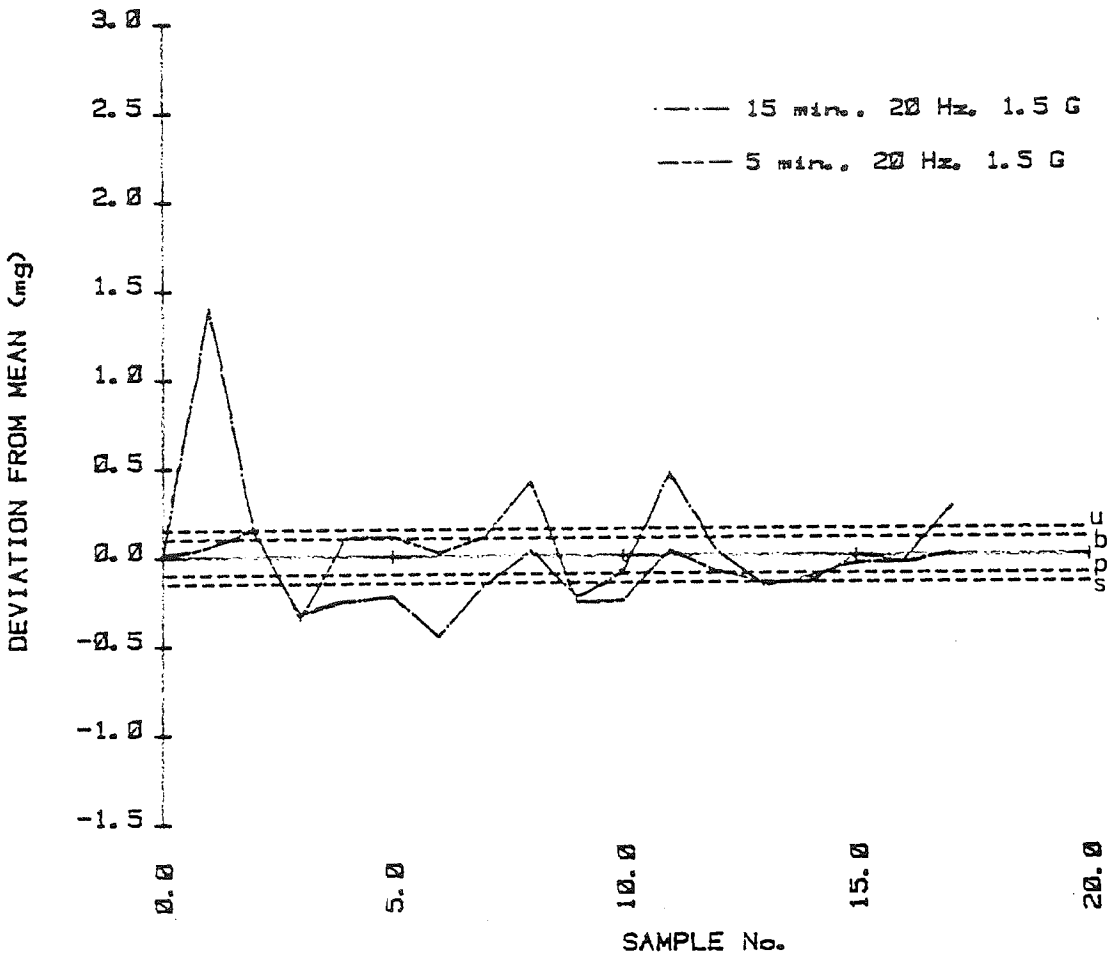

D. Dipac and potassium chloride .5%

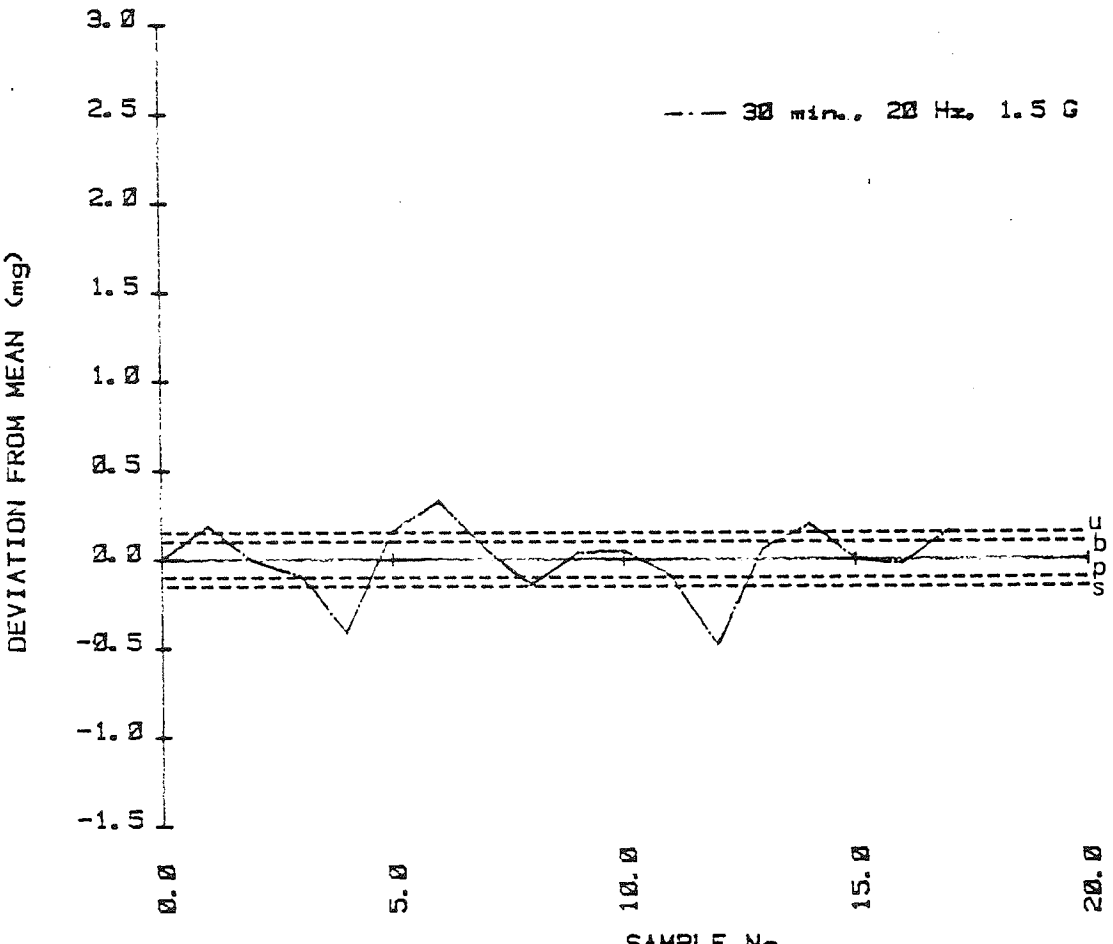

Figure 87. E. Dipac and potassium chloride .5%

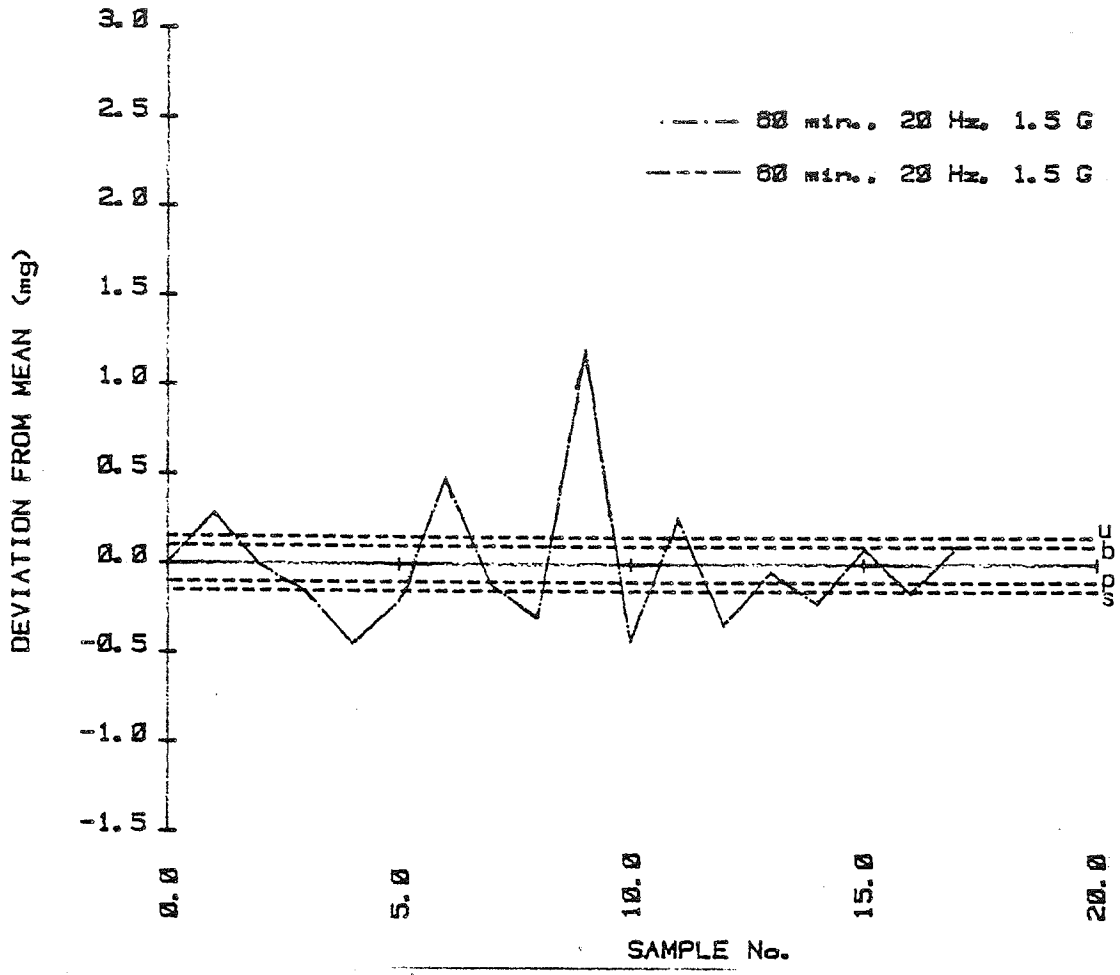

F. Dipac and potassium chloride .5%

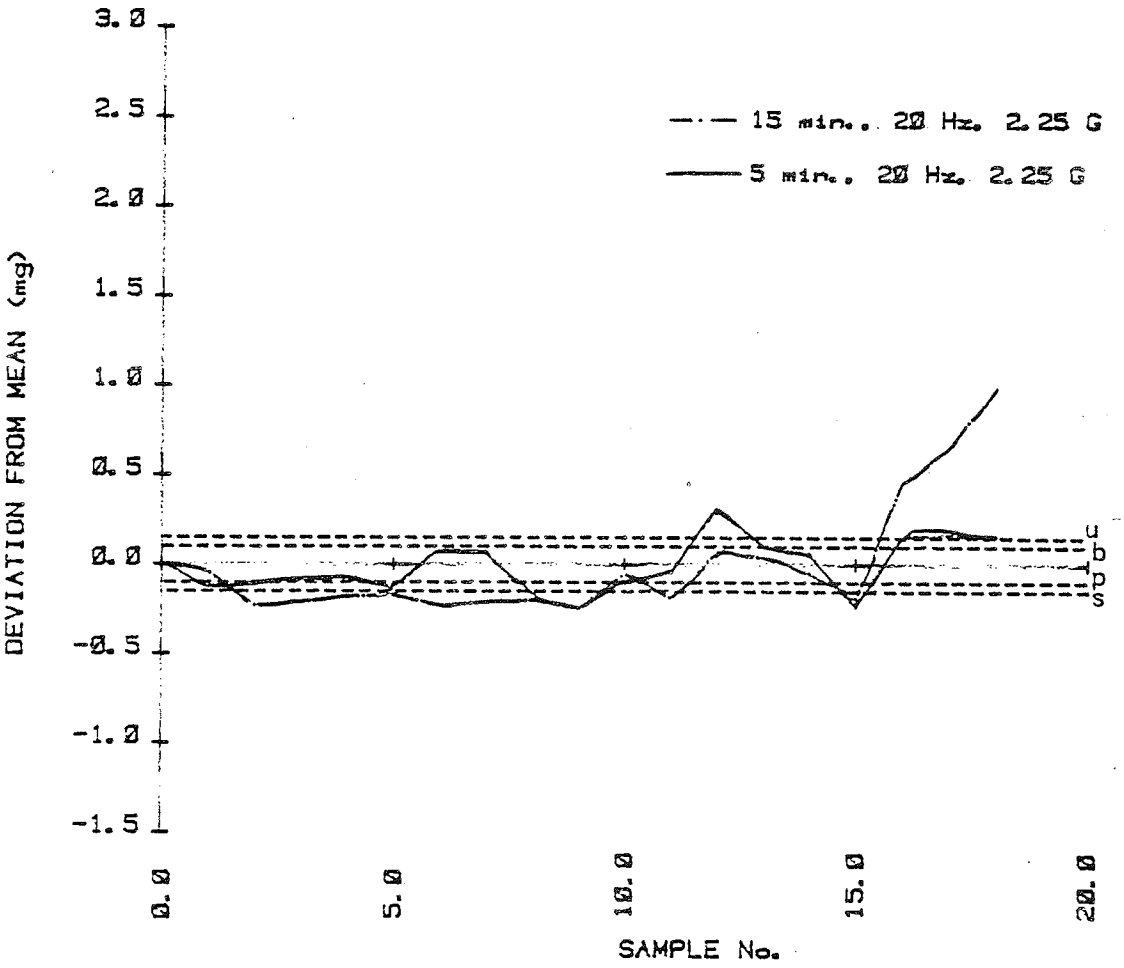

Figure 87.

G. Dipac and potassium chloride. 5%

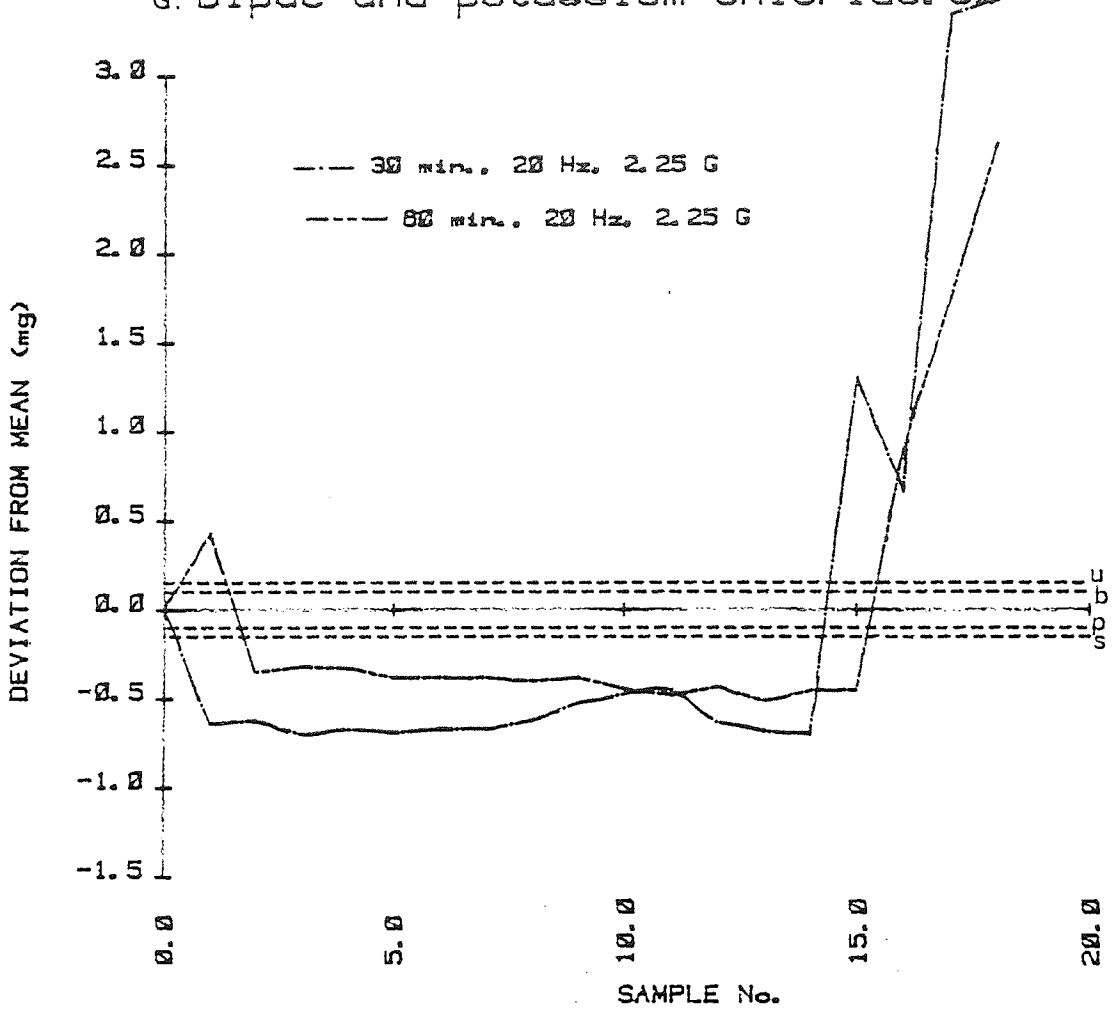

H. Dippac and potassium chloride .5%

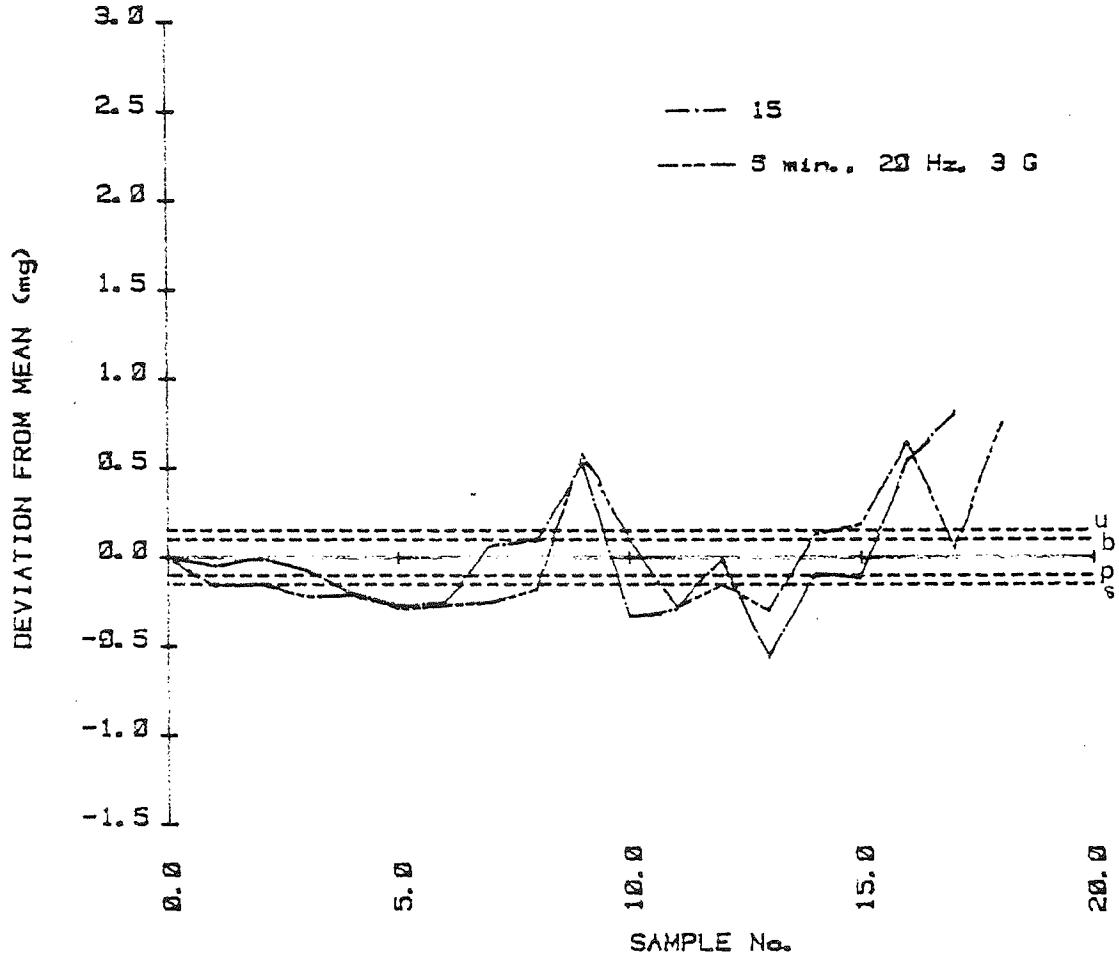

Figure 87. 1. Dipac and potassium chloride .5%

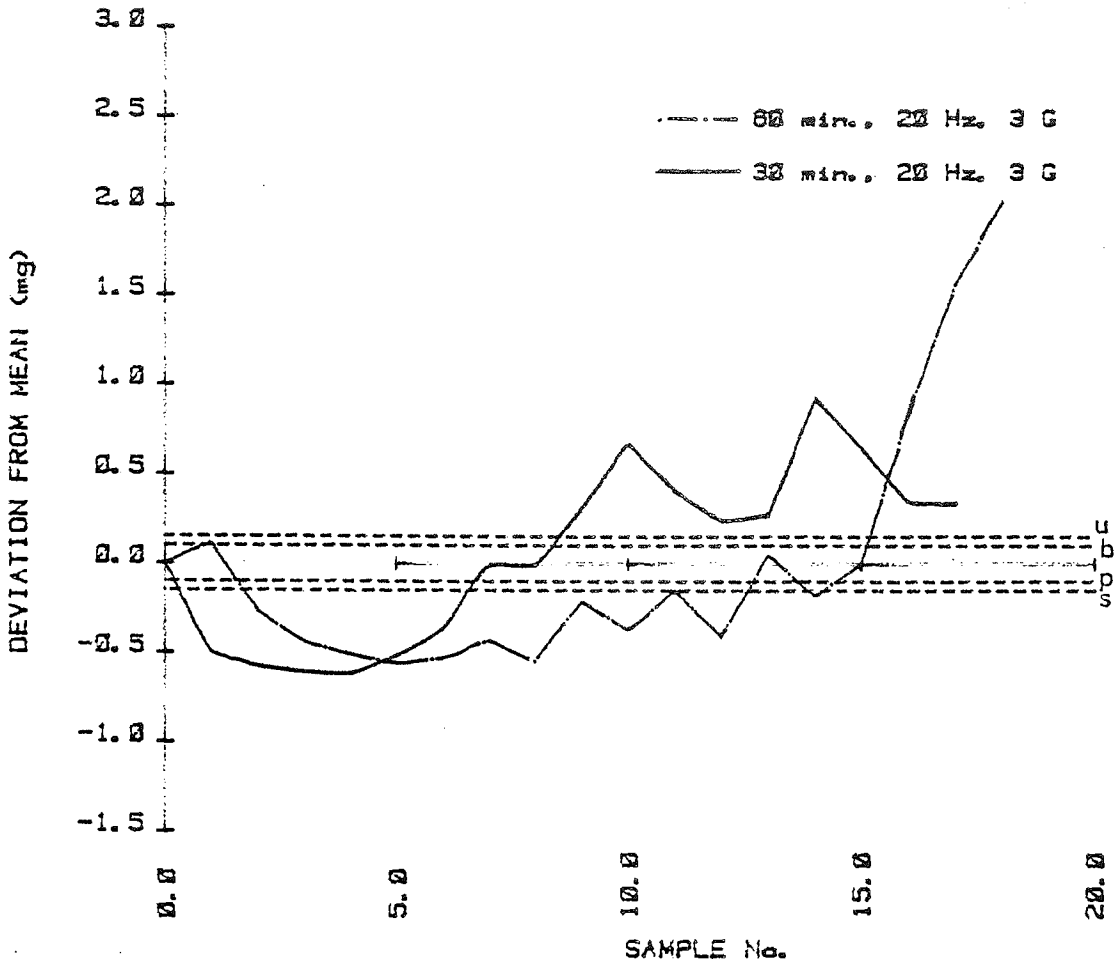

Figure 88. A. Dipac and potassium chloride .5%

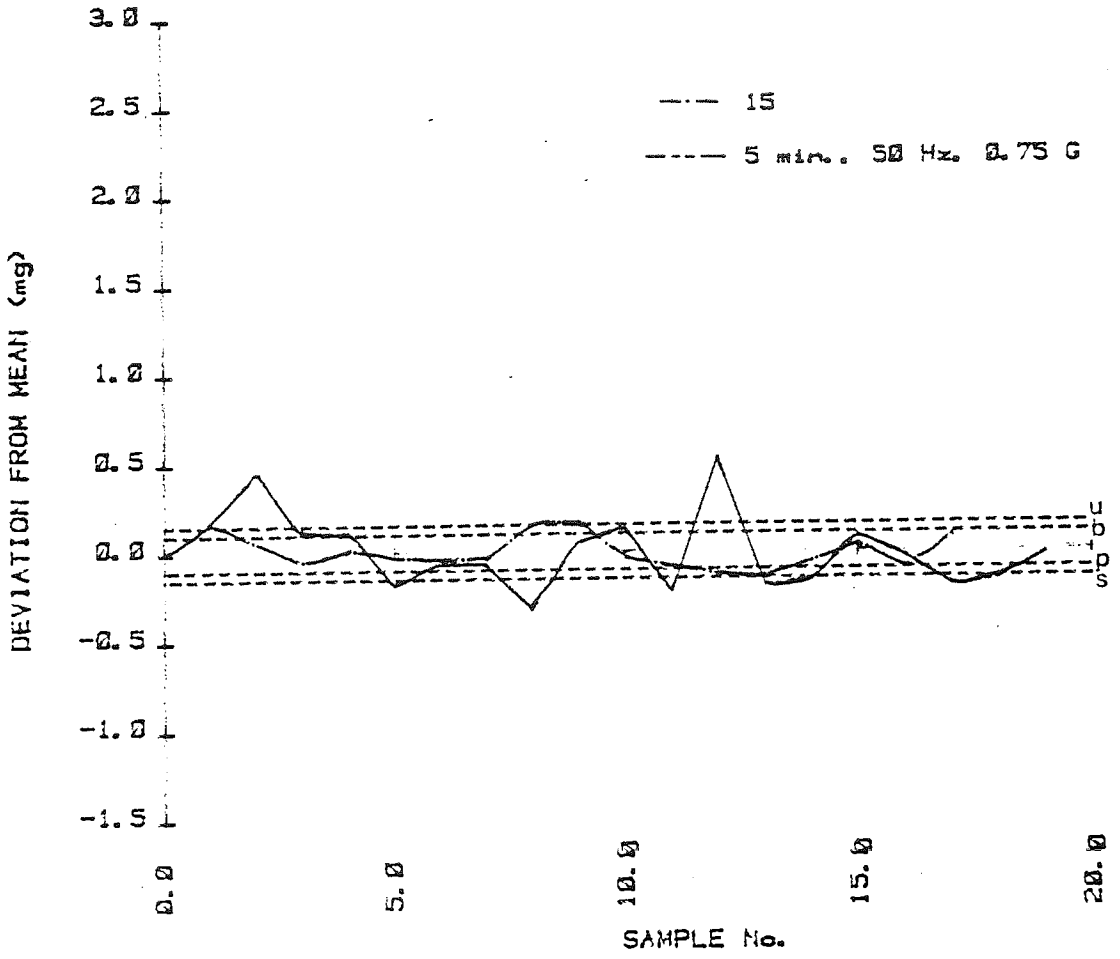

B. Dipac and potassium chloride .5%

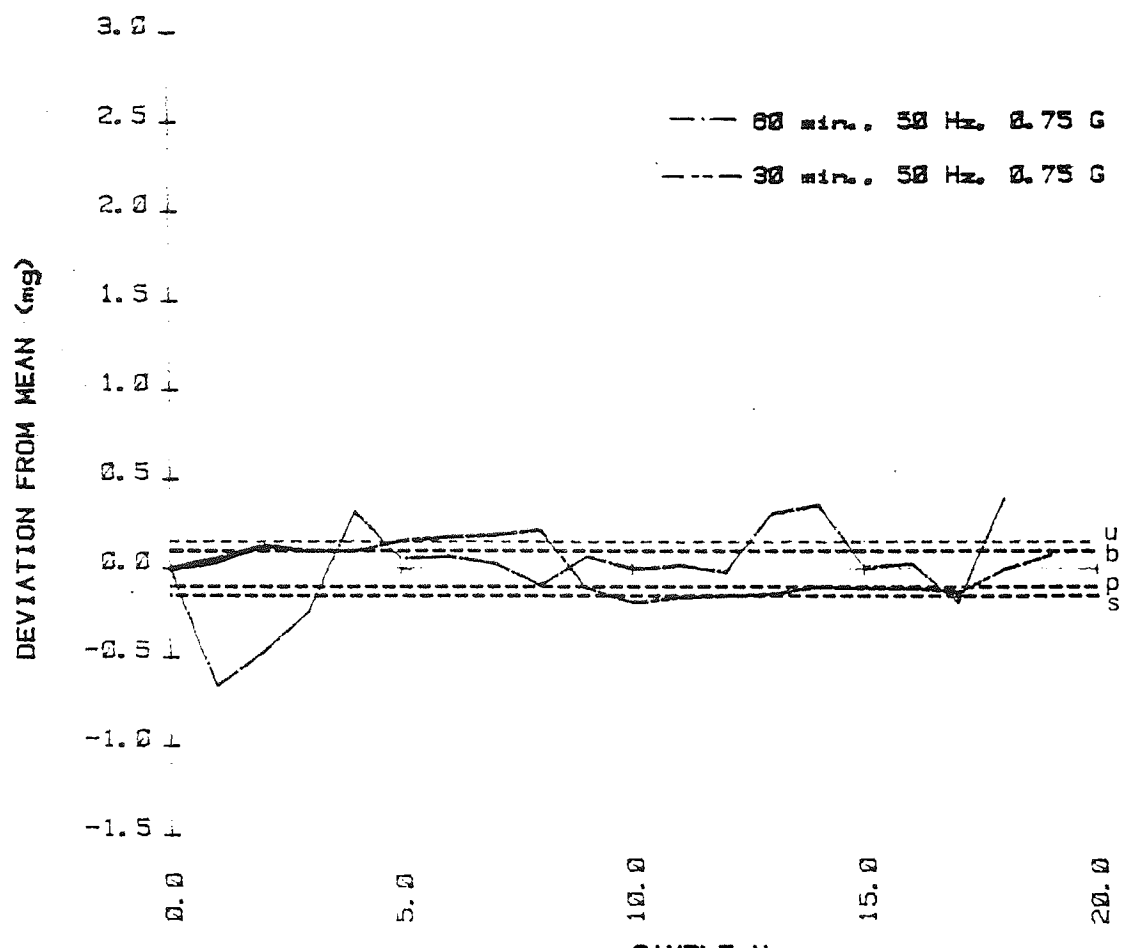

Figure 88. C. Dipac and potassium chloride .5%

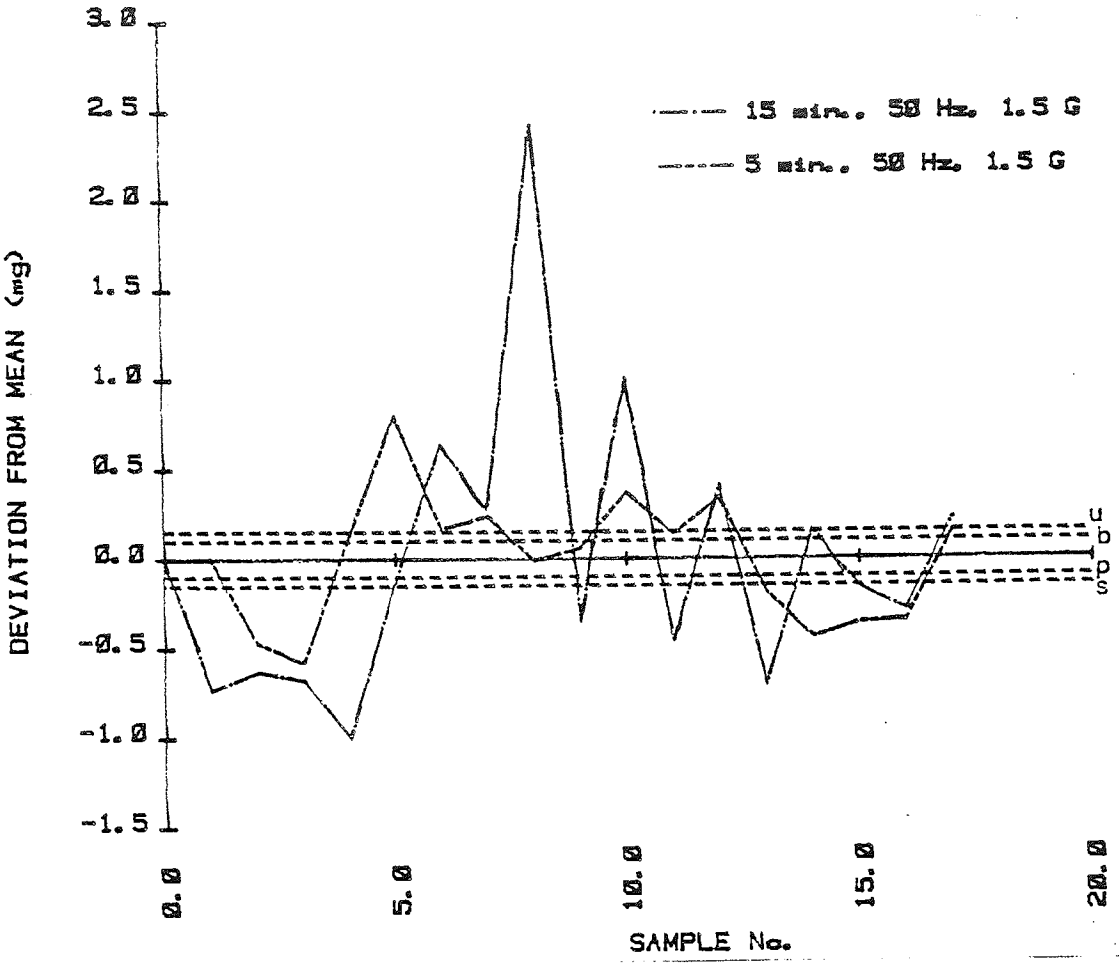

D. Dipac and potassium chloride .5%

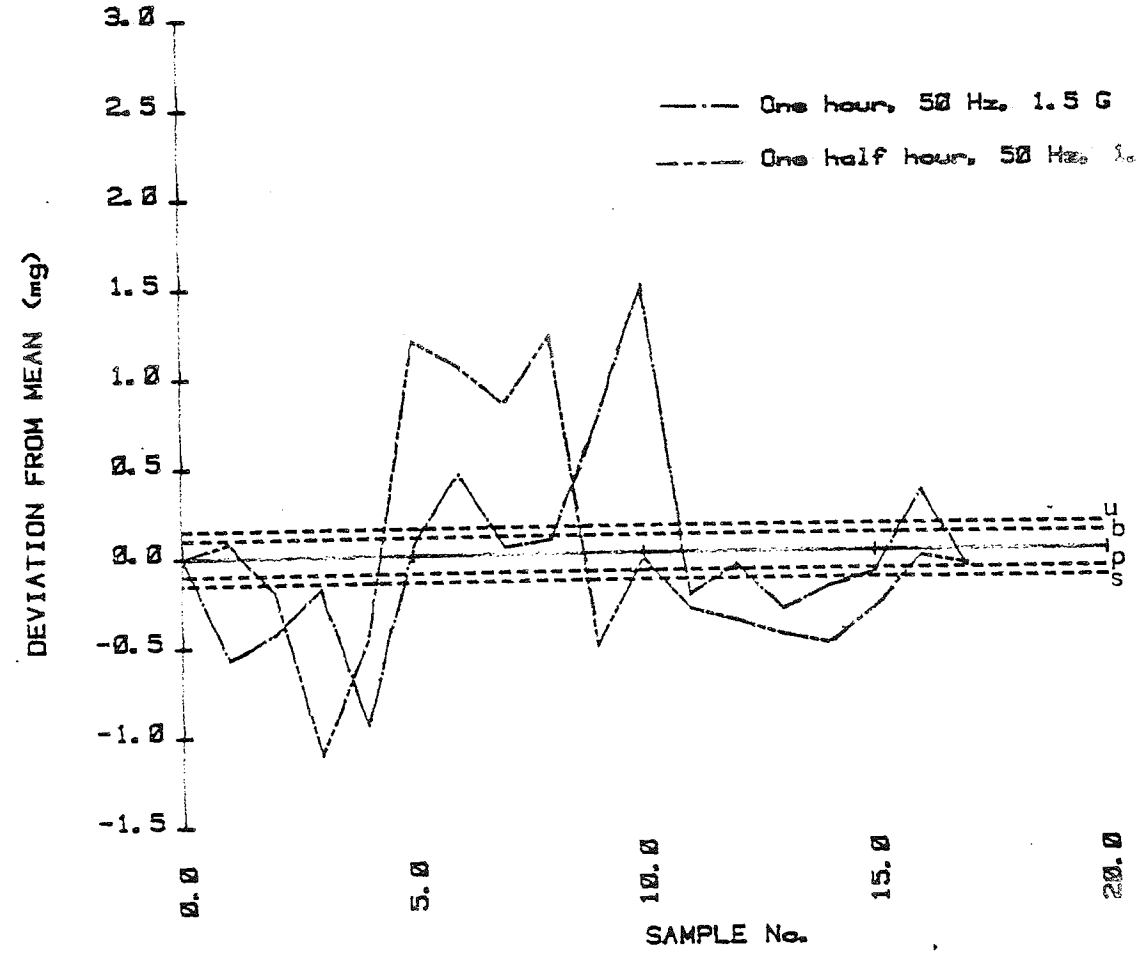

Figure 88 E. Dipac and potassium chloride .5%

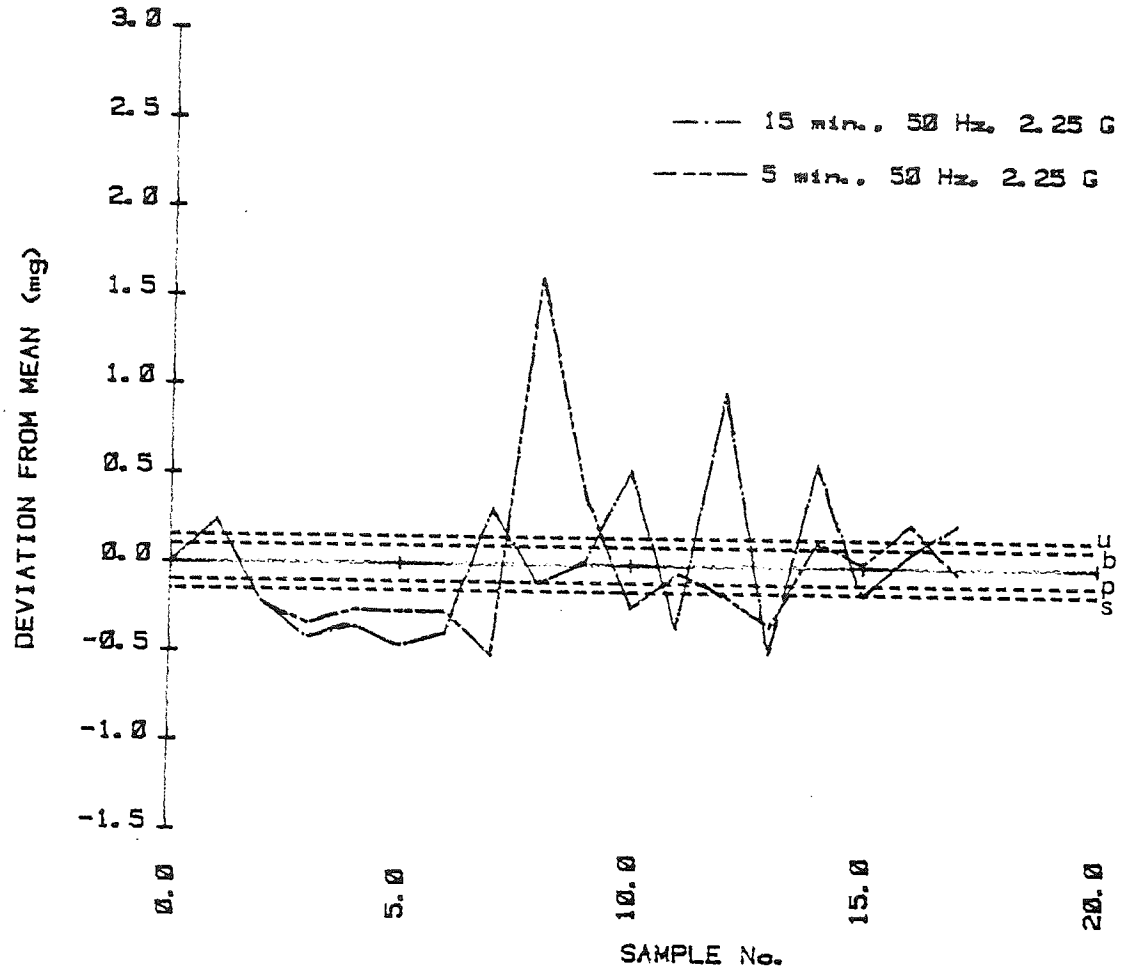

F. Dipac and potassium chloride .5%

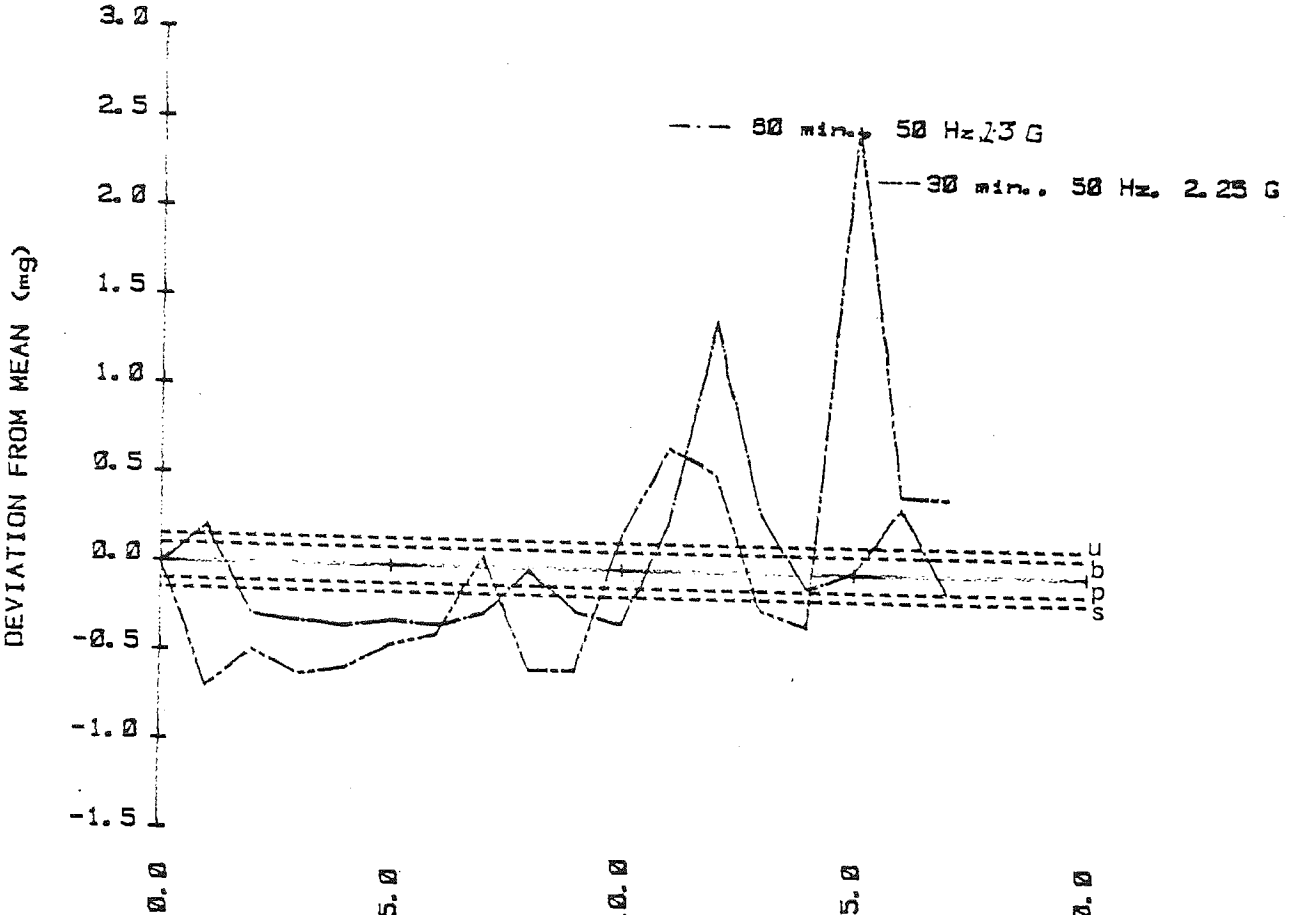

Figure 88. G. Dipac and potassium chloride .5%

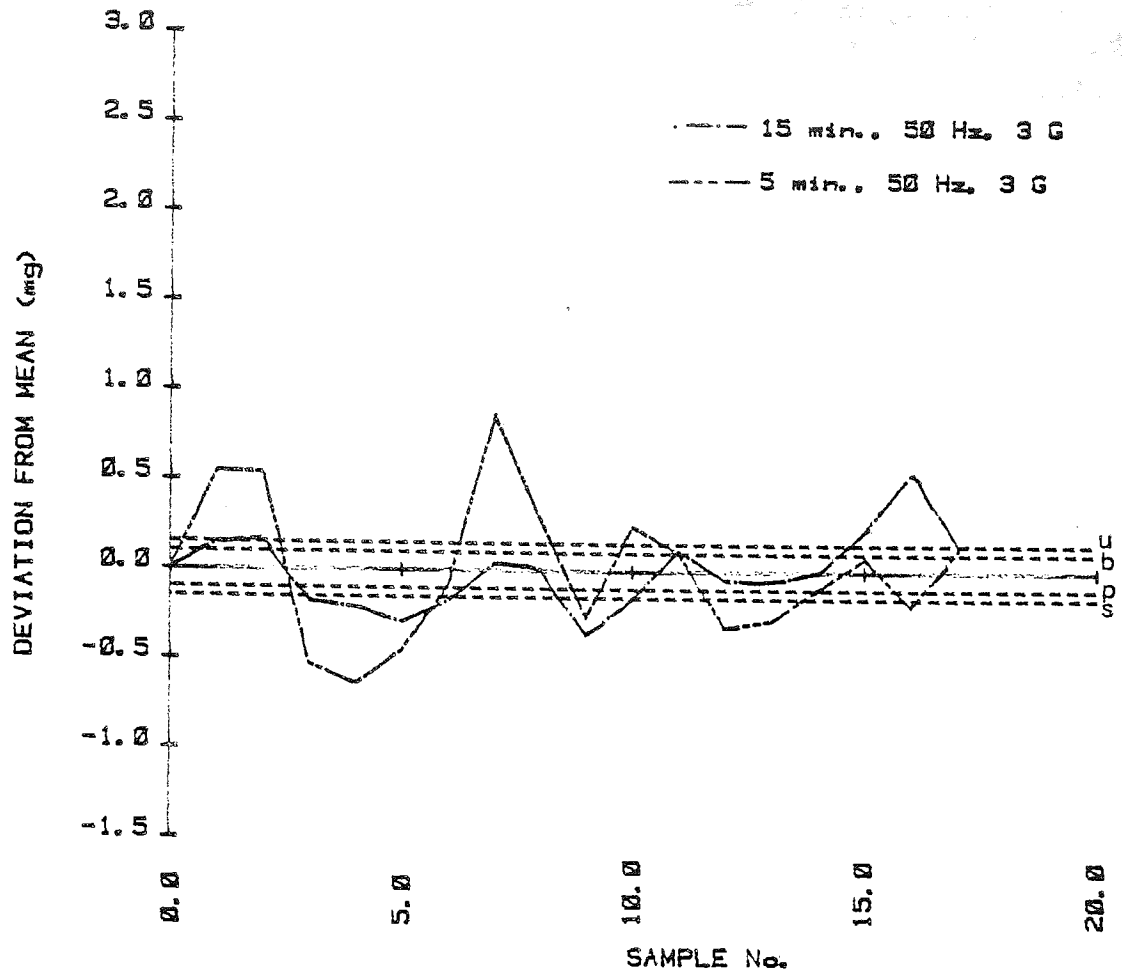

H. Dipac and potassium chloride .5%

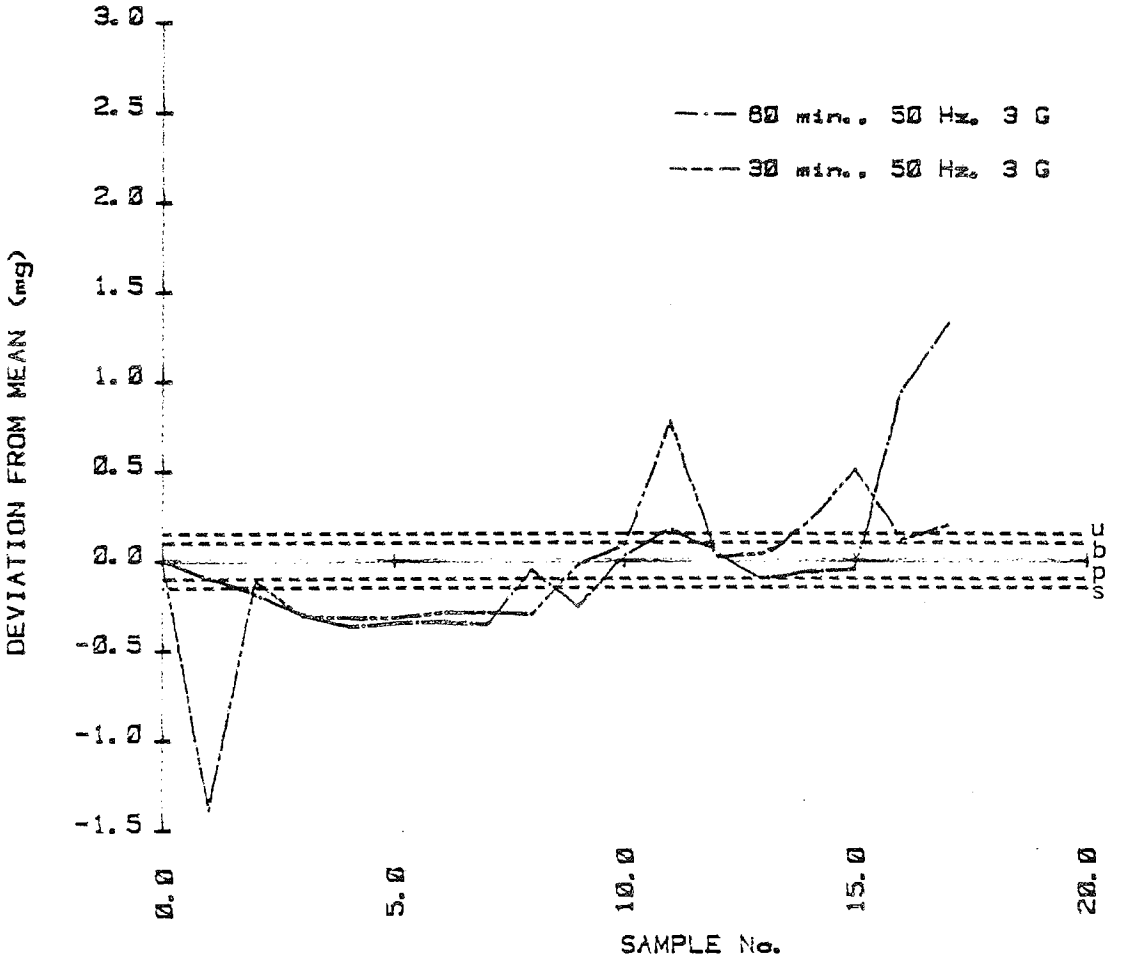

Figure 89. A. Dipac and potassium chloride .5%

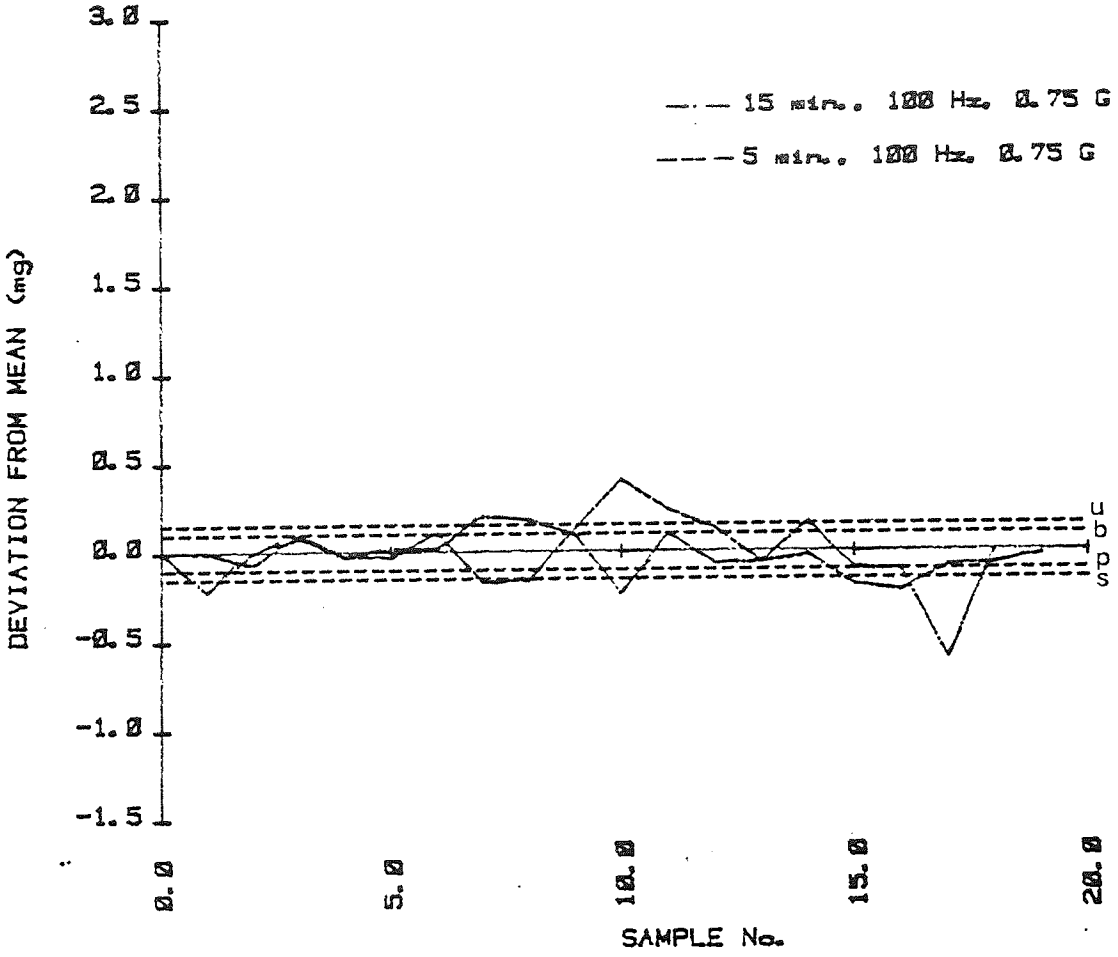

B. Dipac and potassium chloride .5%

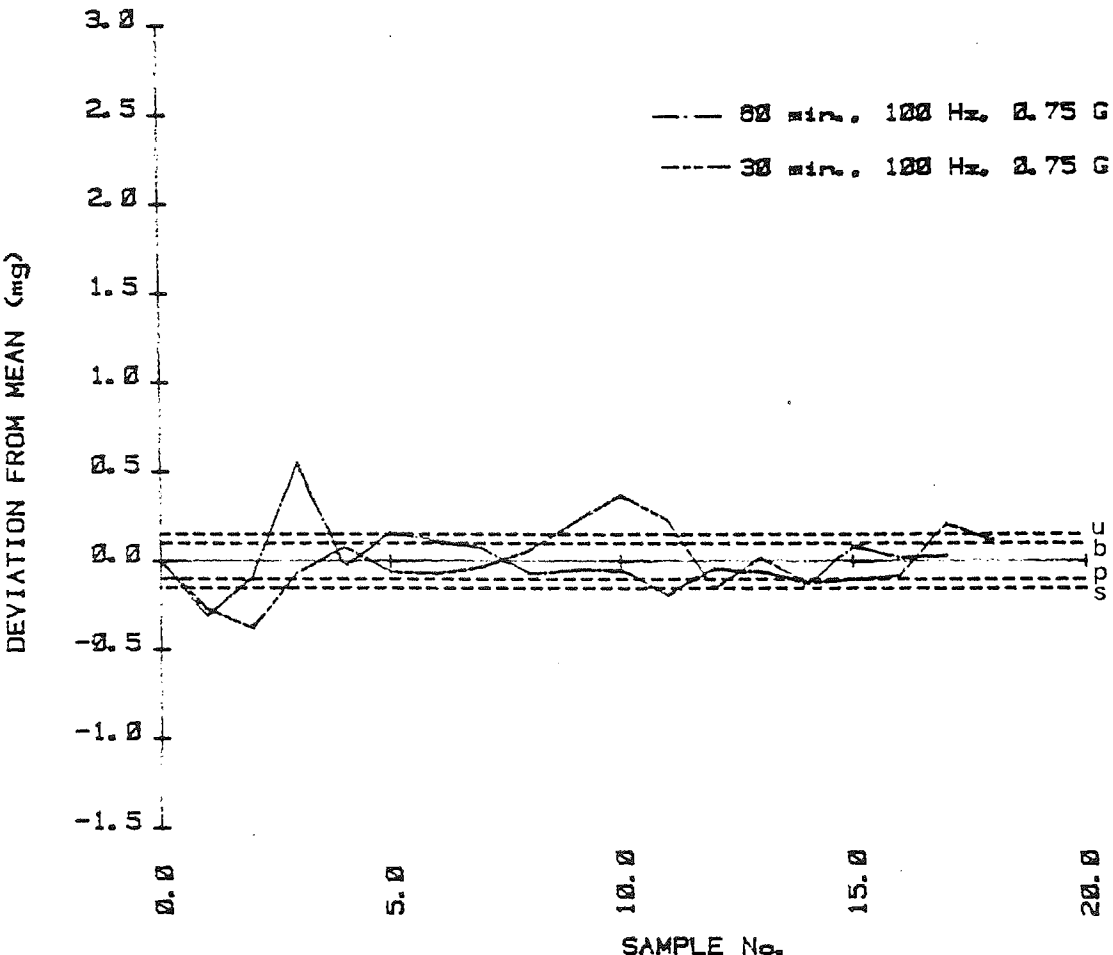

Figure 89.

C. Dipac and potassium chloride .5

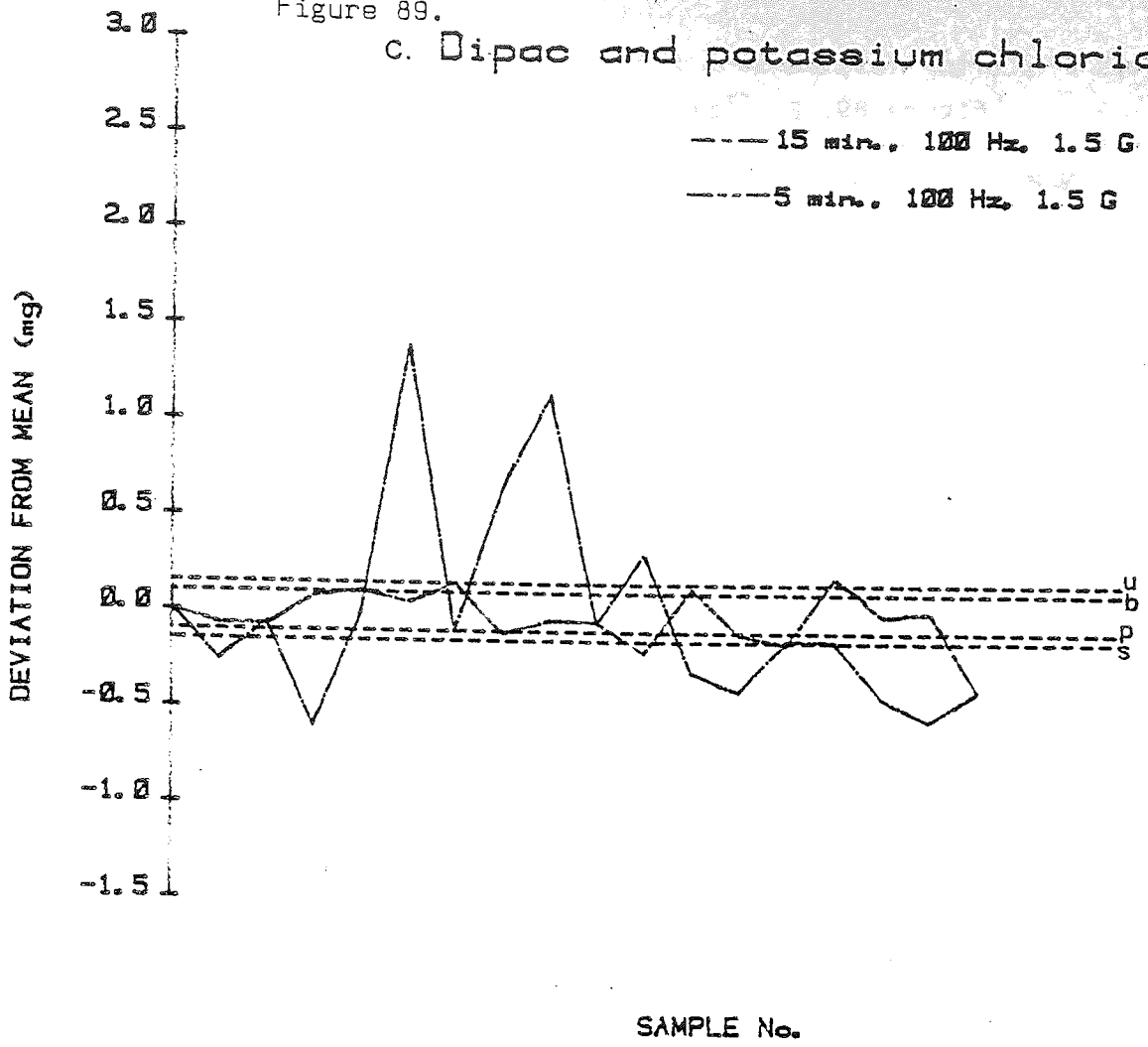

D. Dipac and potassium chloride .5%

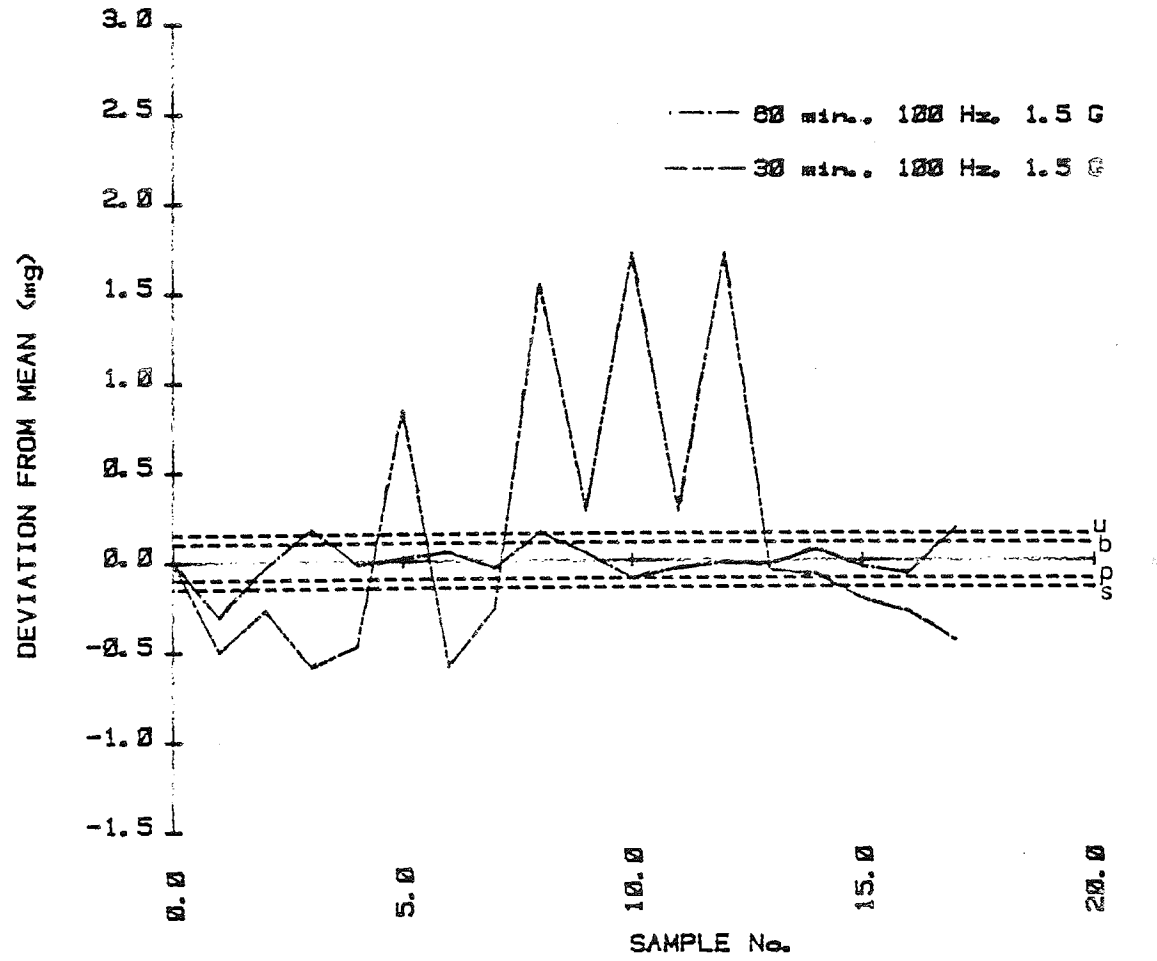

Figure 89. E. Dipac and potassium chloride .5%

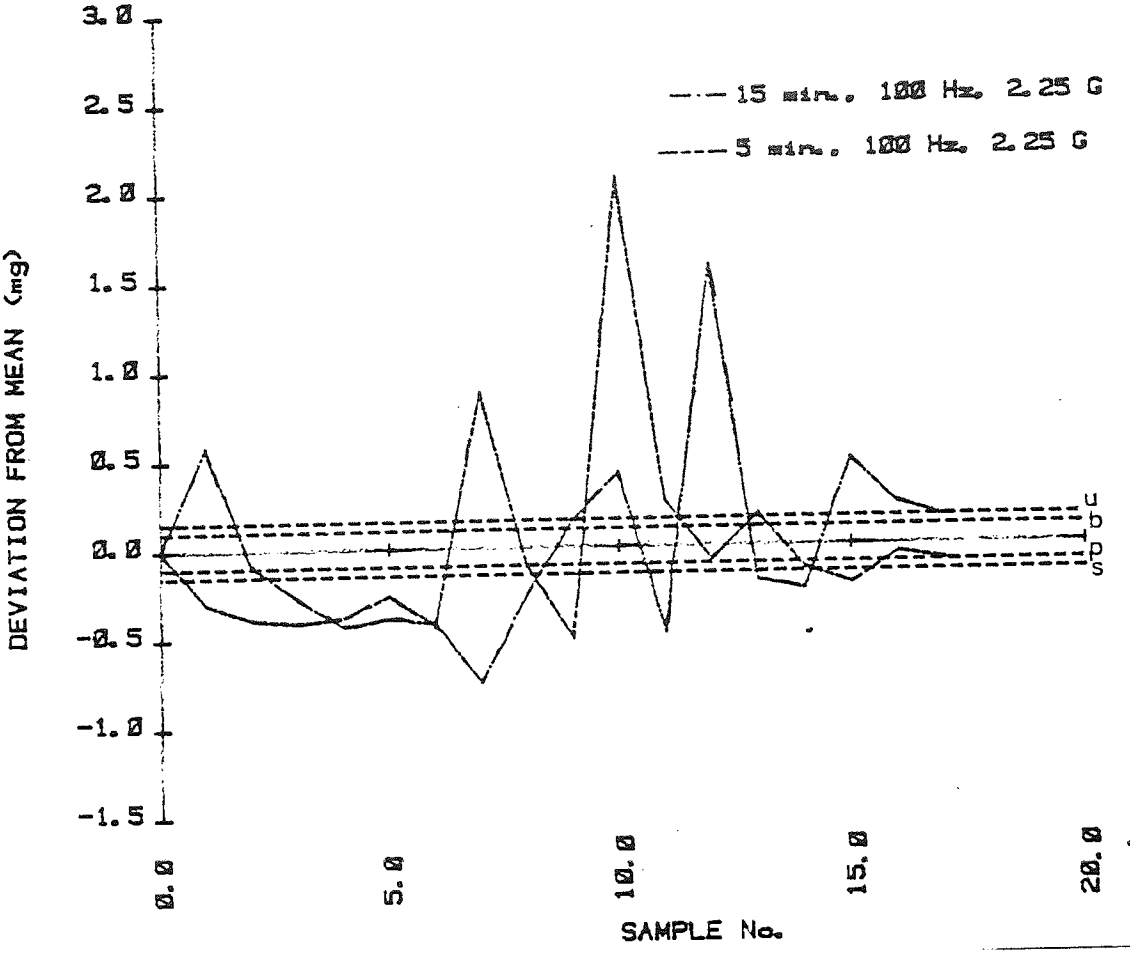

F. Dipac and potassium chloride .5%

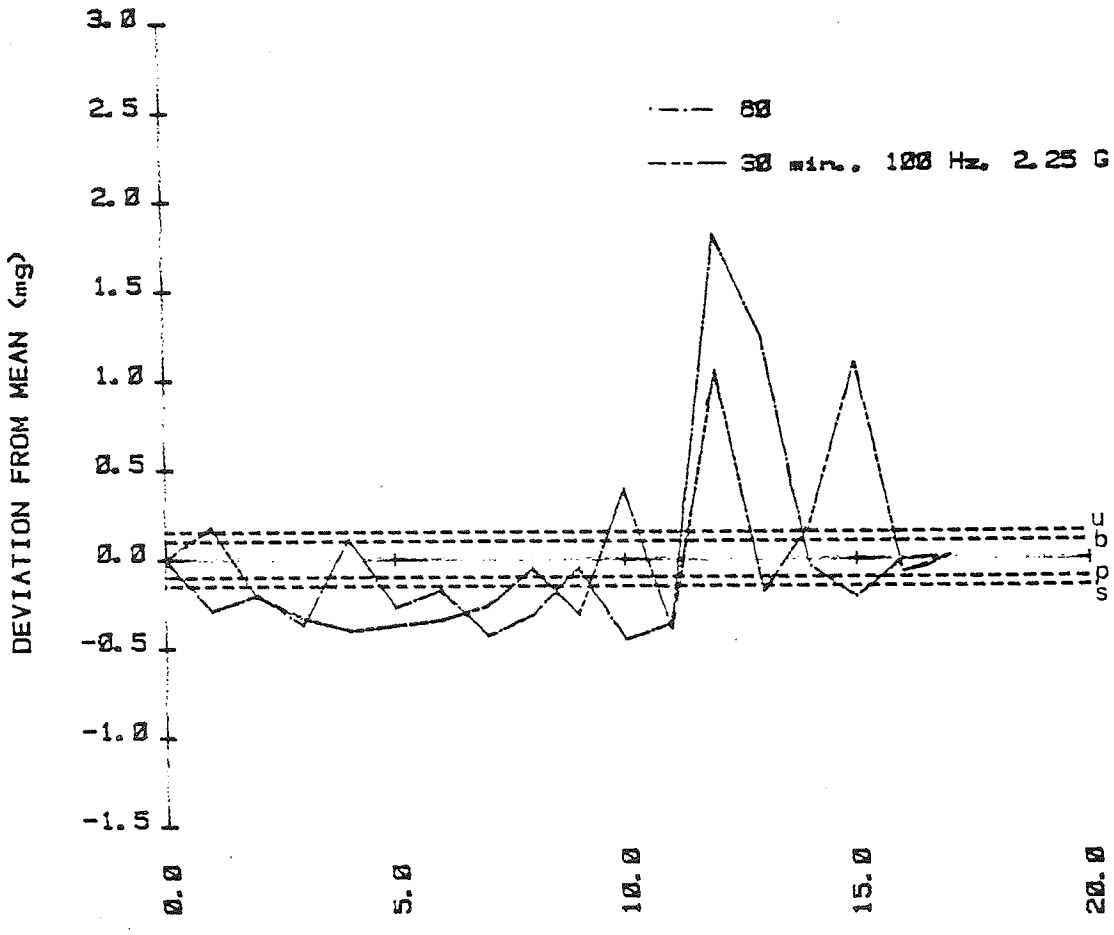

Figure 89. G. Dipac and potassium chloride .5%

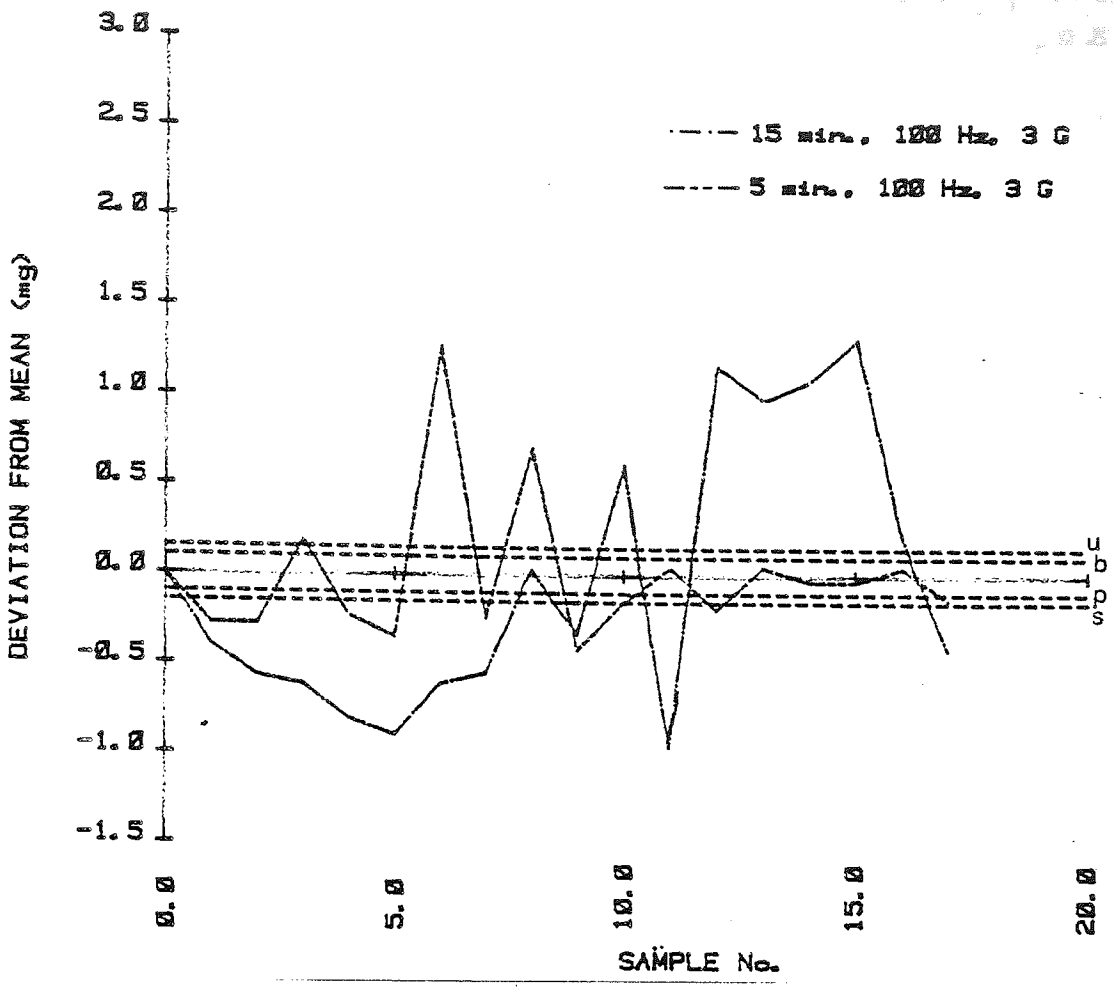

H. Dipac and potassium chloride .5%

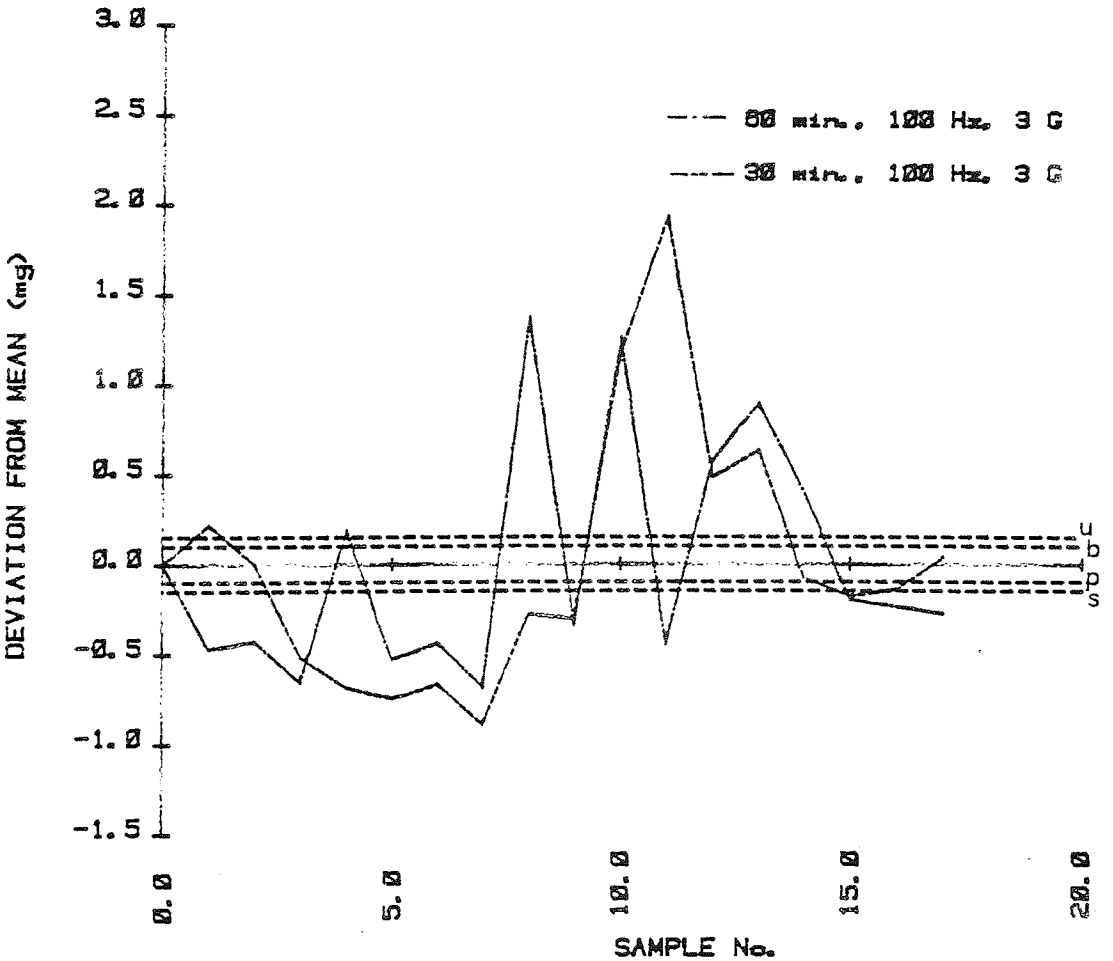

Figure 90.A. Dipac and potassium chloride .5%

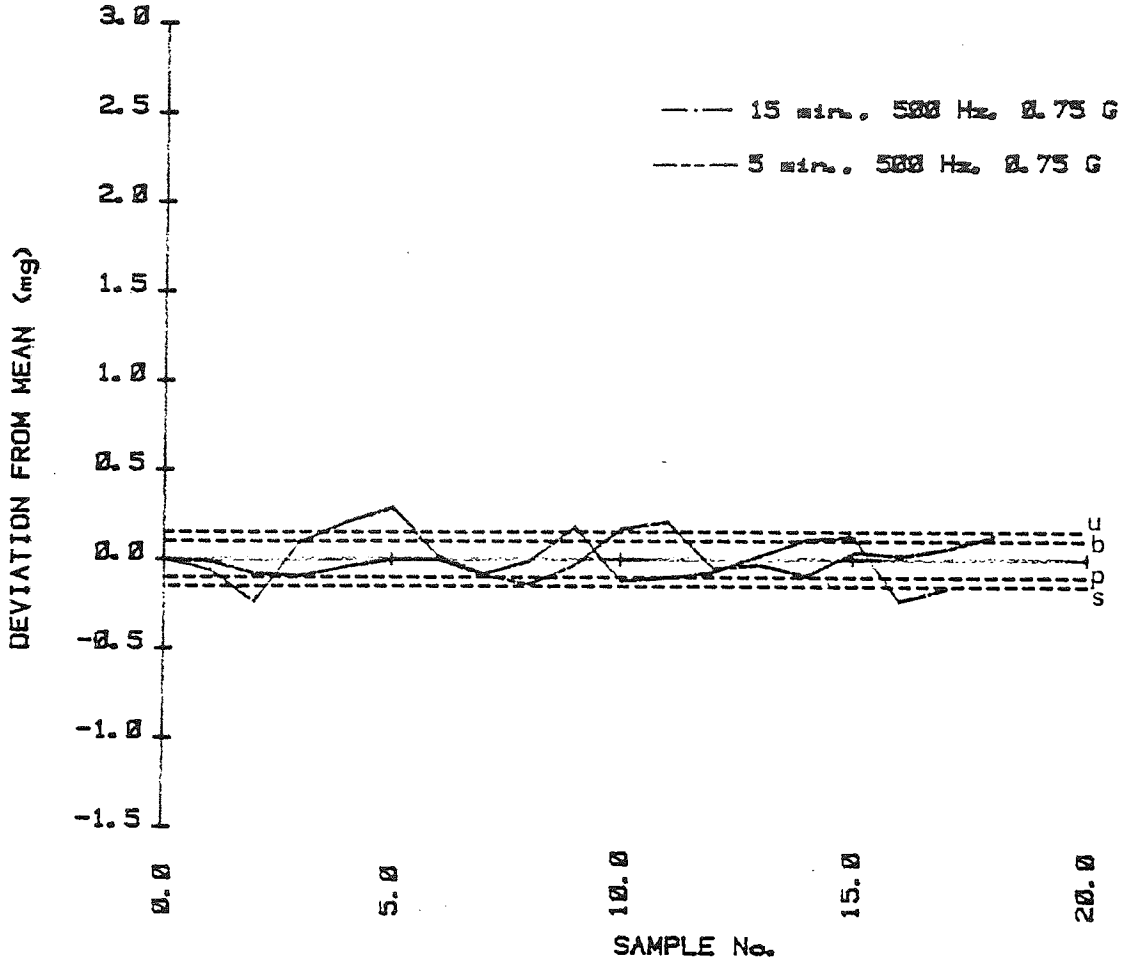

B. Dipac and potassium chloride .5%

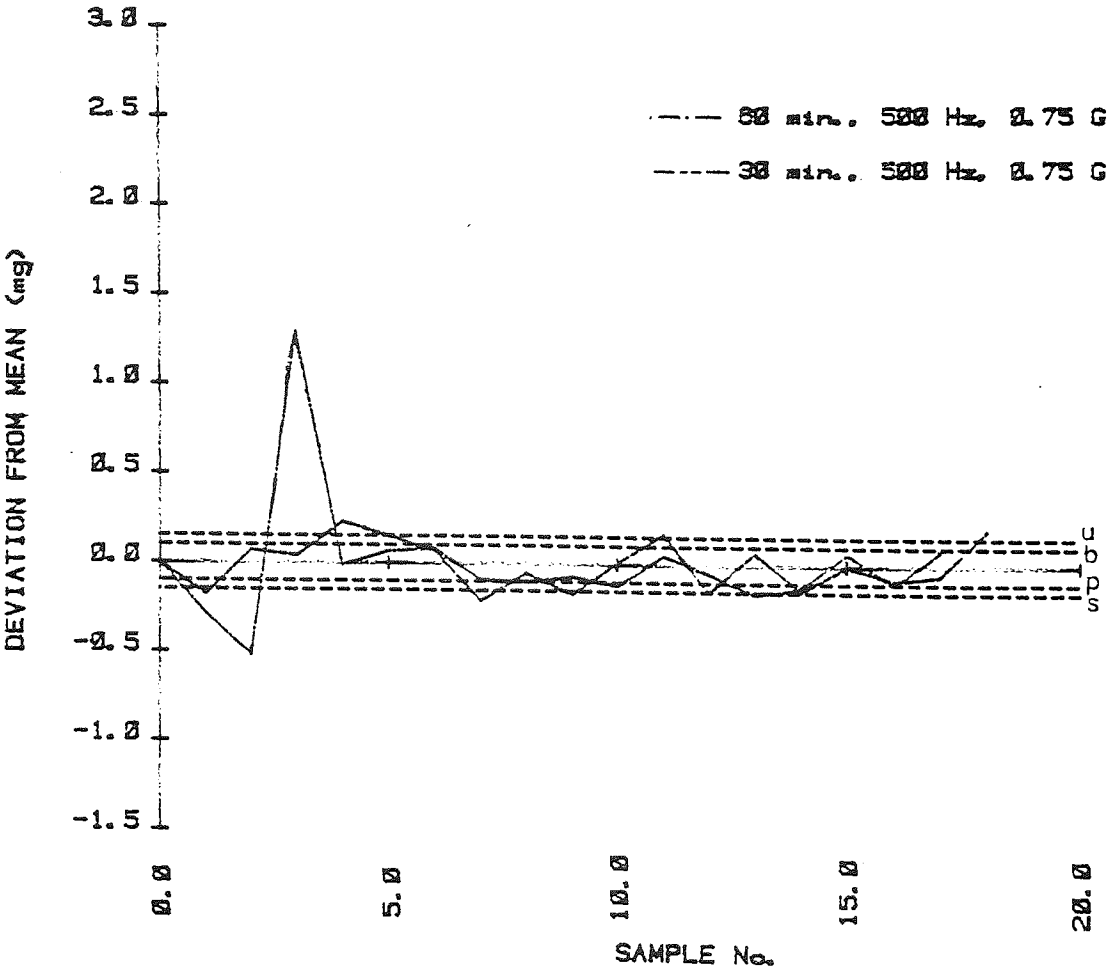

Figure 90.

C. Dipac and potassium chloride .5%

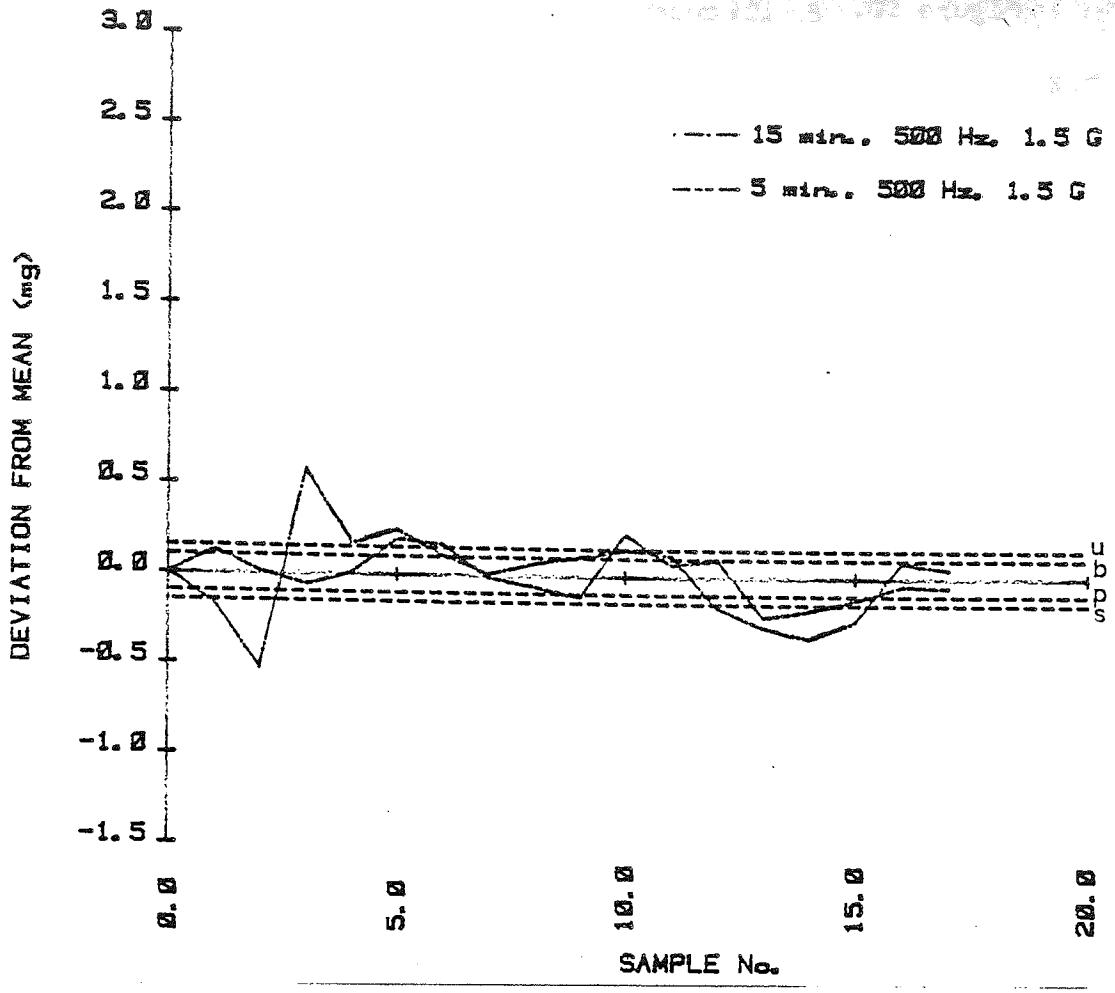

D. Dipac and potassium chloride .5%

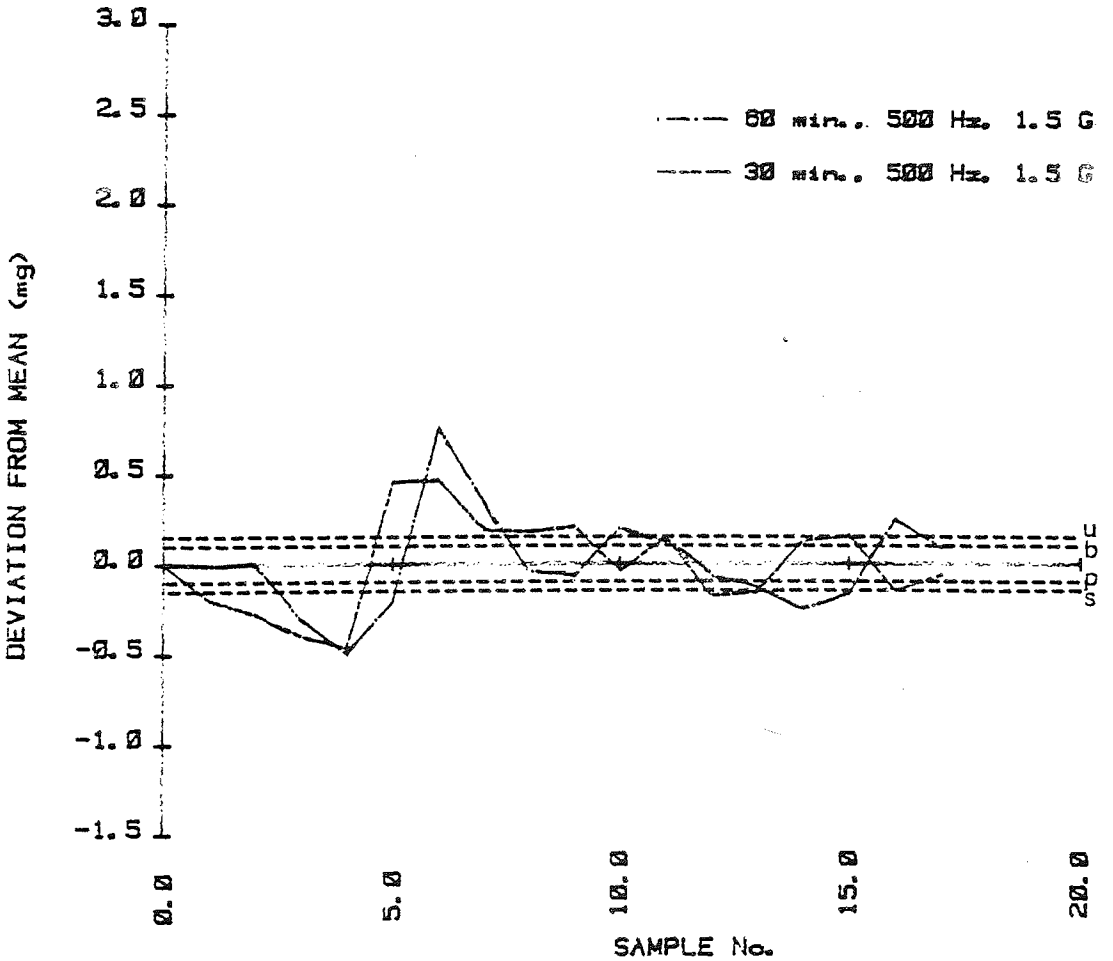

Figure 90. E. Dipac and potassium chloride .5%

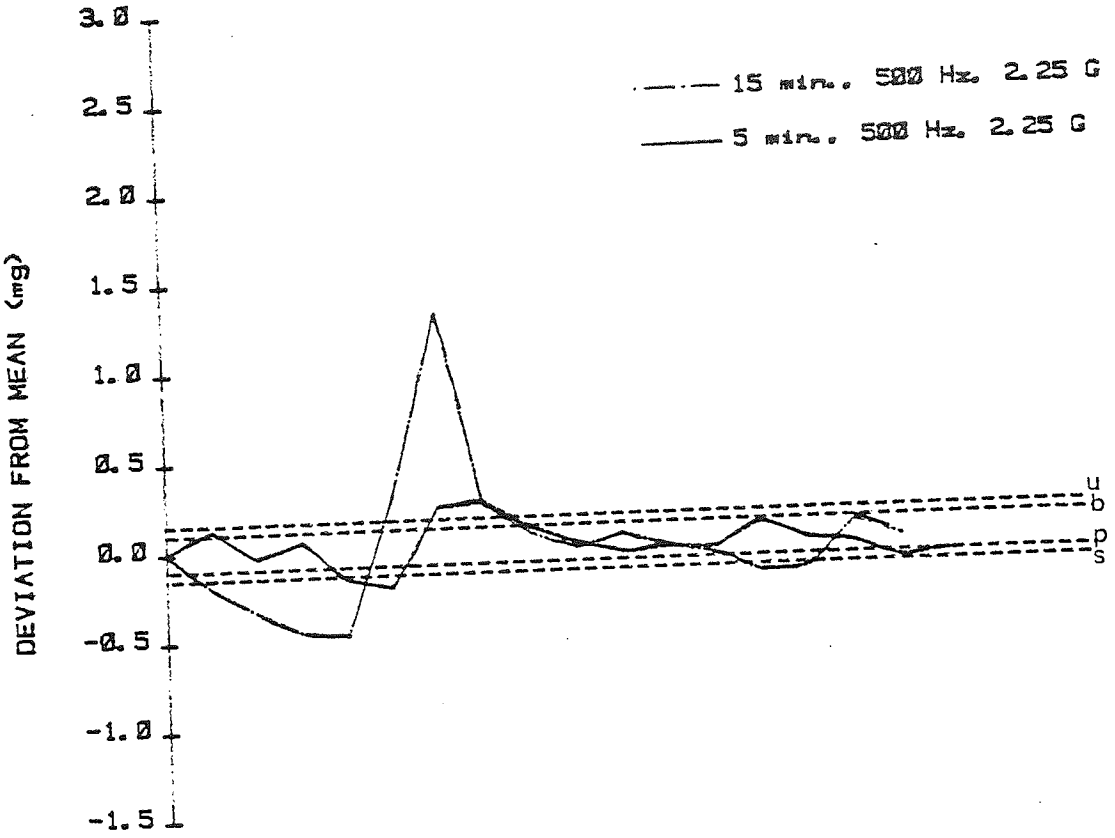

SAMPLE No.

F. Dipac and potassium chloride .5 %

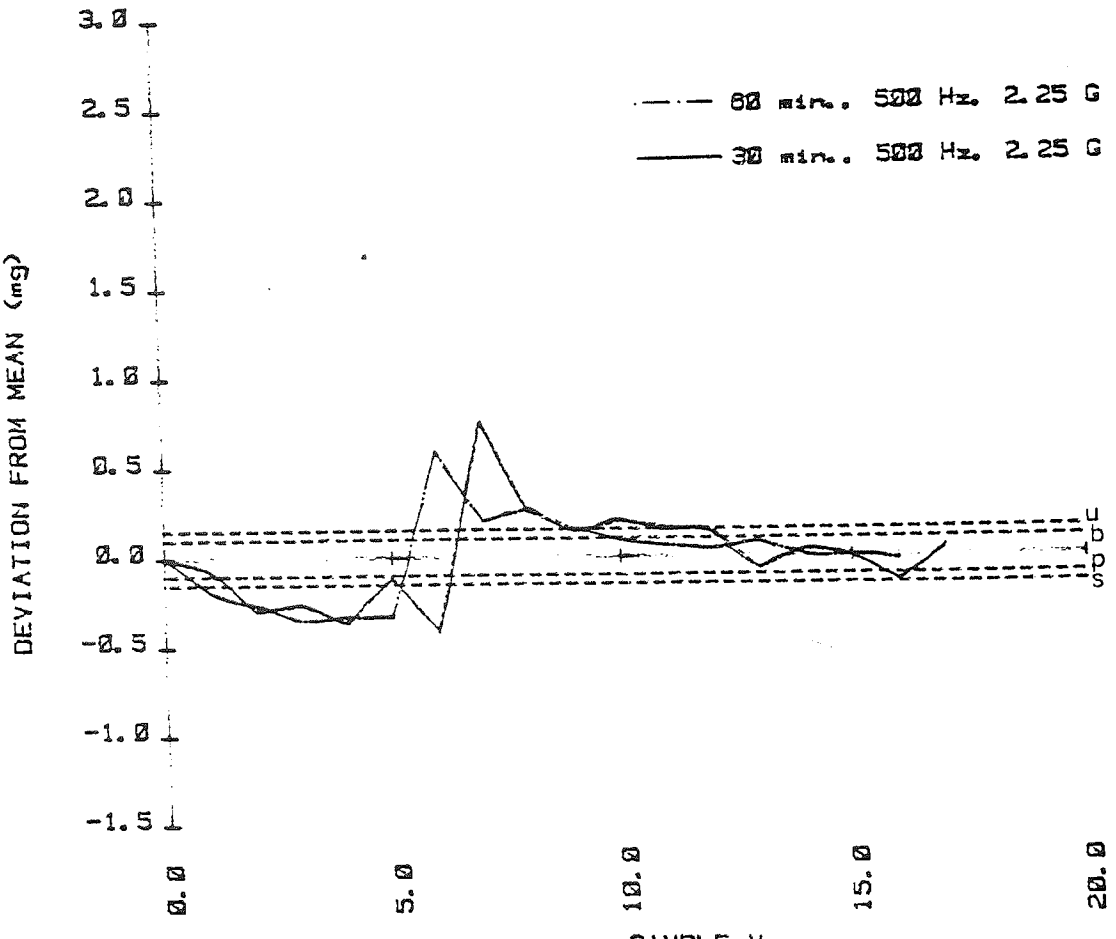

Figure 90. G. Dipac and potassium chloride .5%

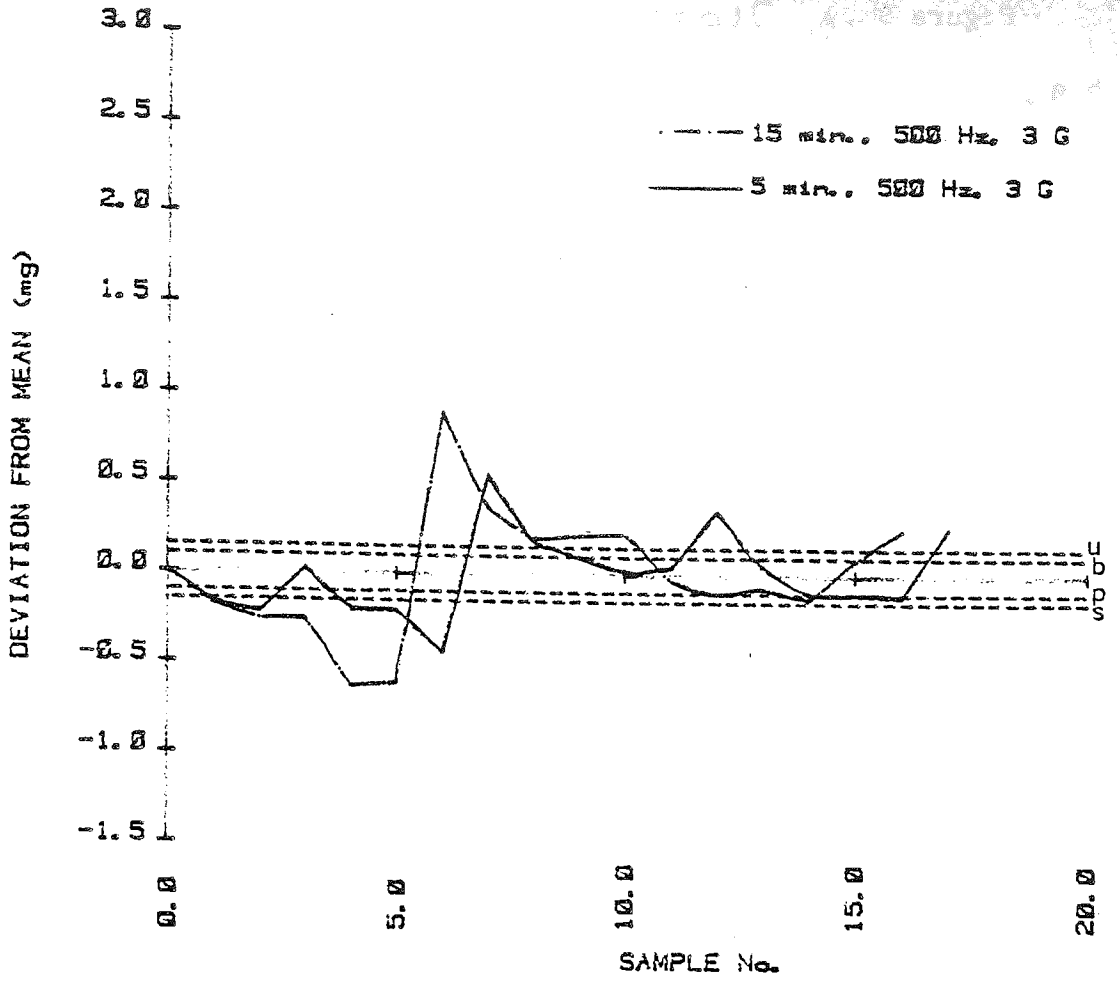

H. Dipac and potassium chloride .5%

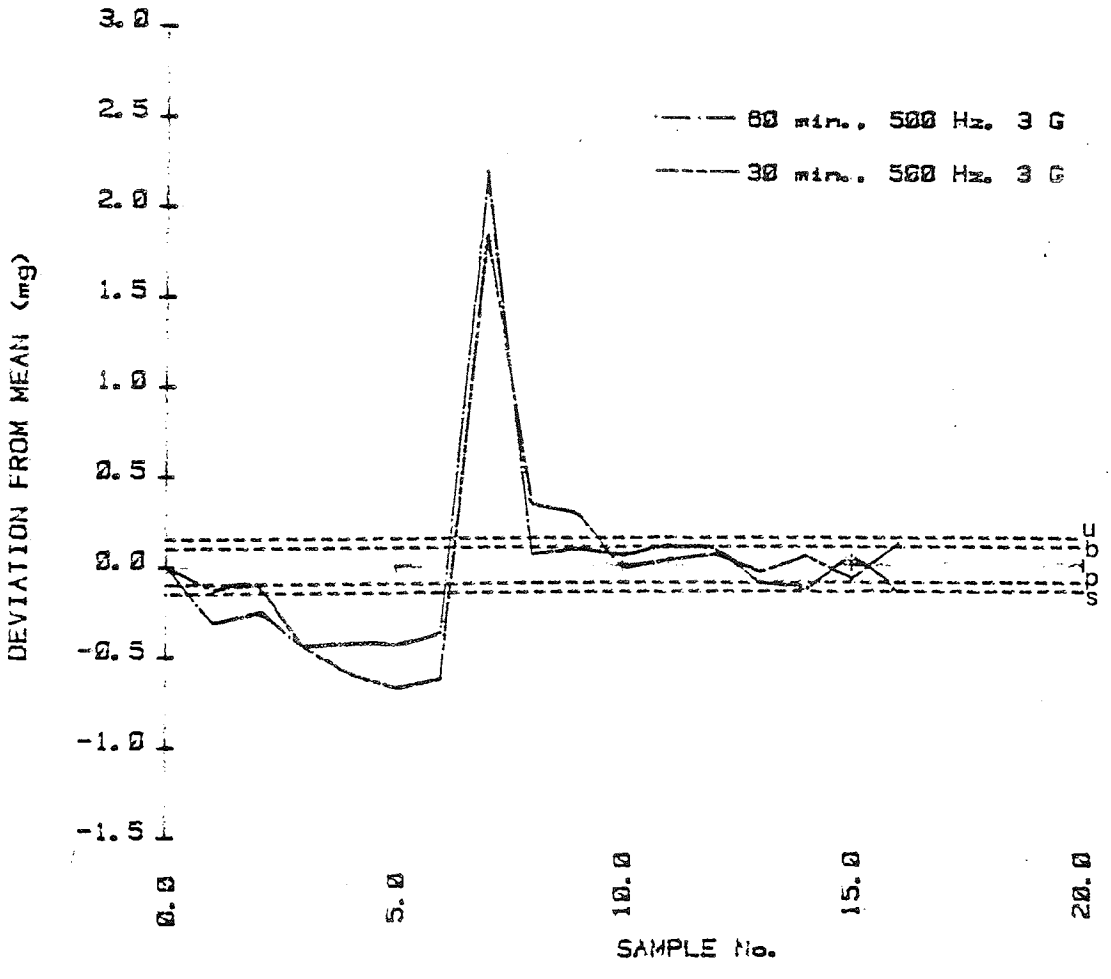

Figure 9(. A. Dipac and potassium chloride .5%

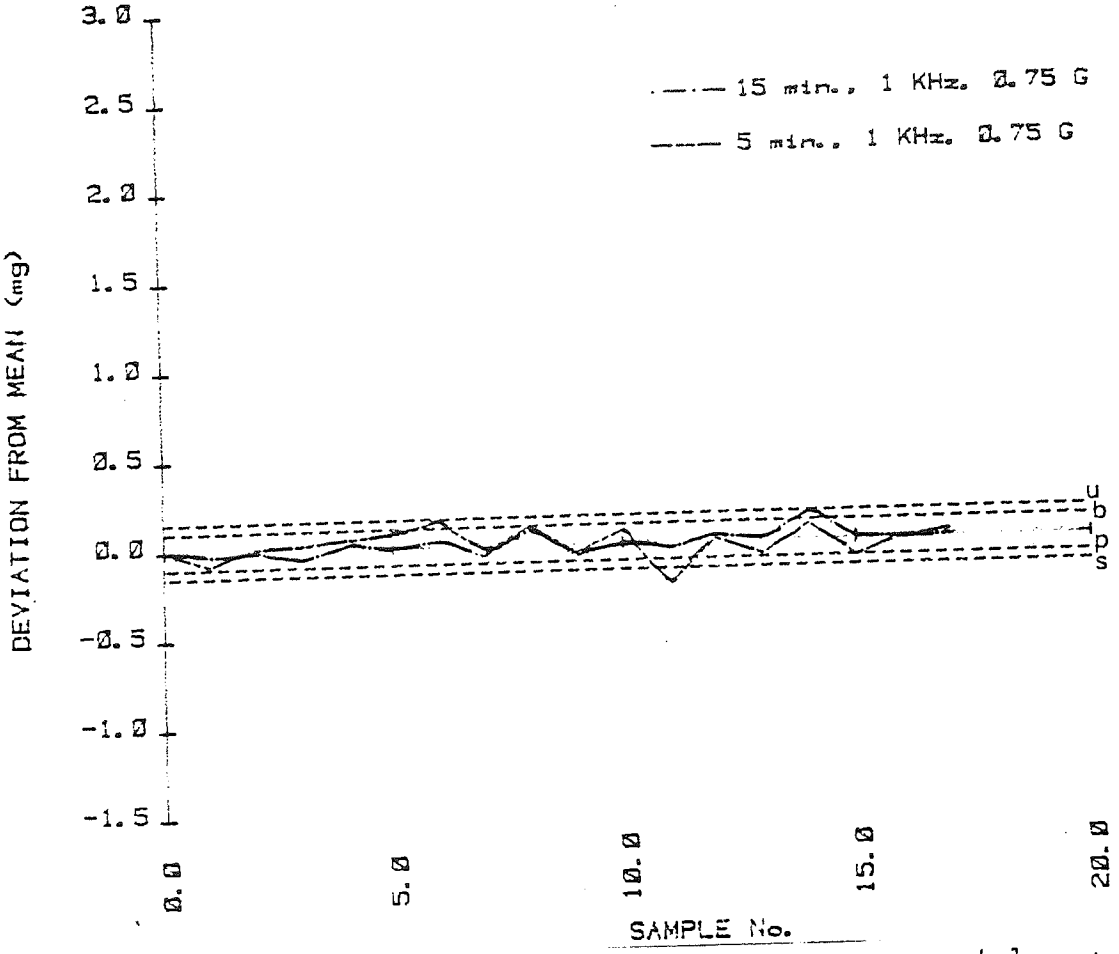

B. Dipac and potassium chloride .5%

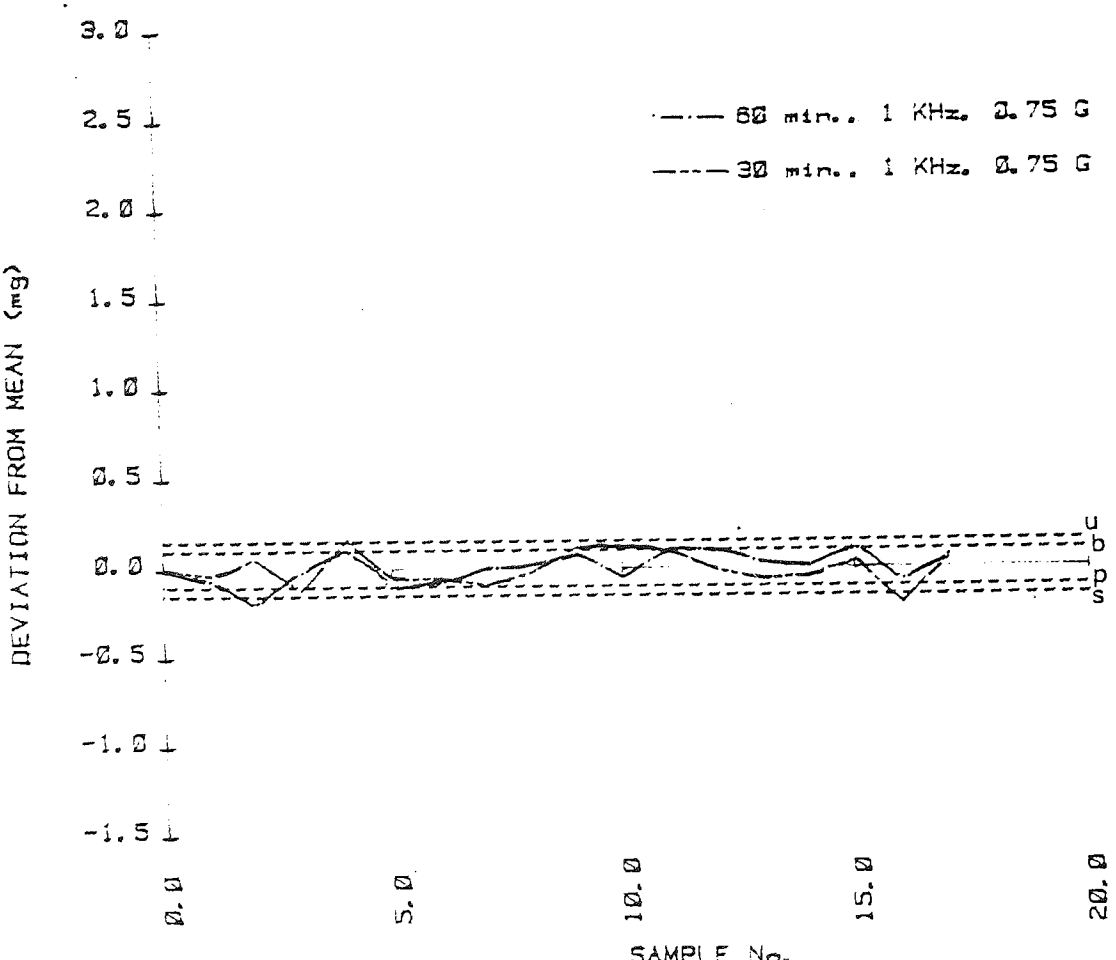

Figure 91. C. Dipac and potassium chloride .5%

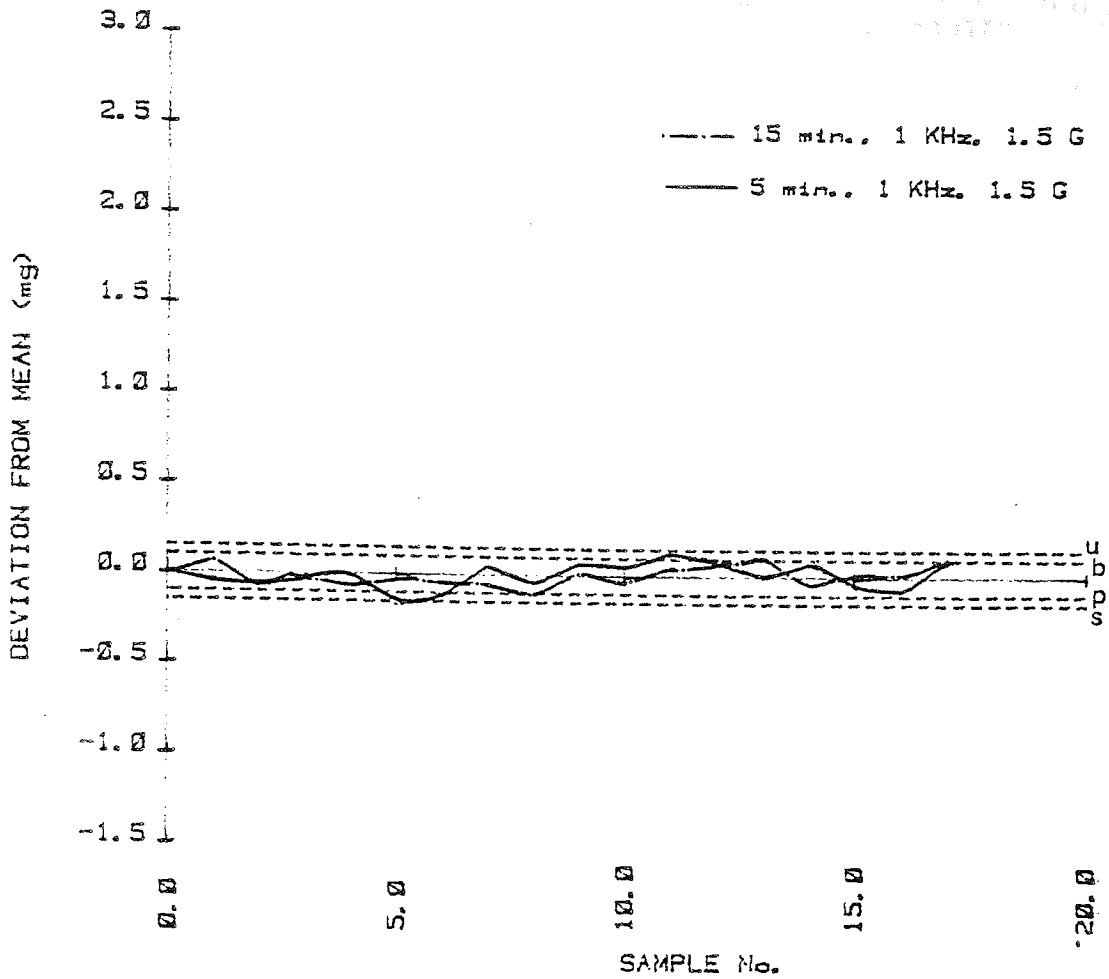

D. Dipac and potassium chloride .5%

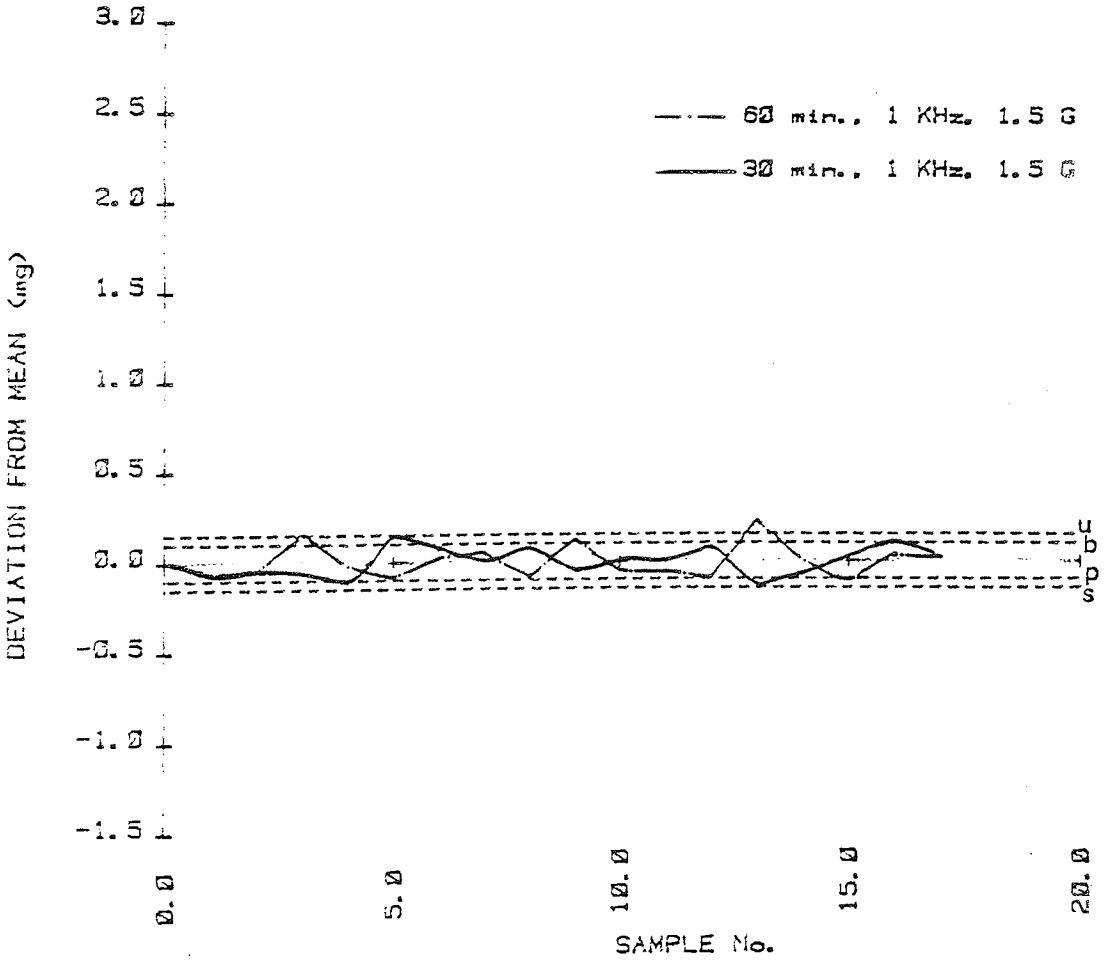

Figure 91. E. Dipac and potassium chloride .5%

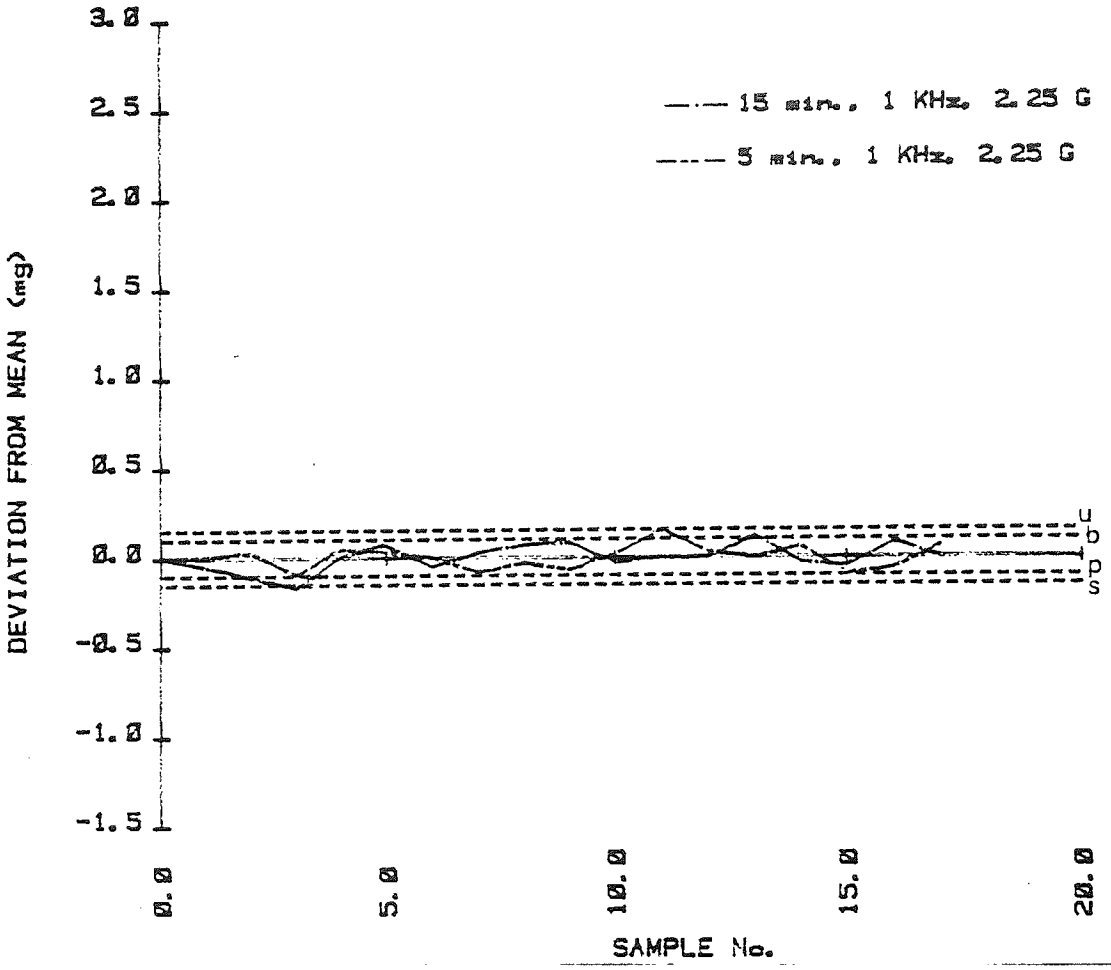

F. Dipac and potassium chloride .5%

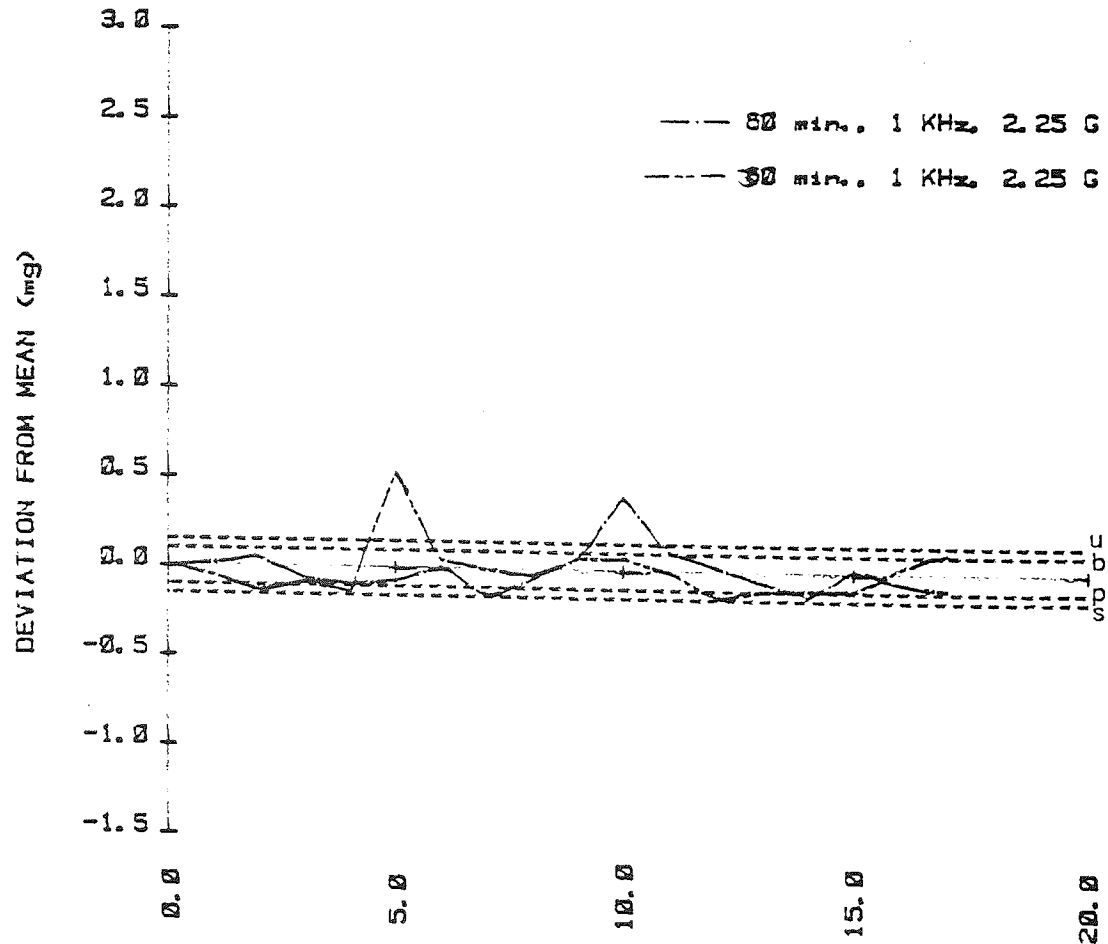

Figure 91. G. Dipac and potassium chloride .5%

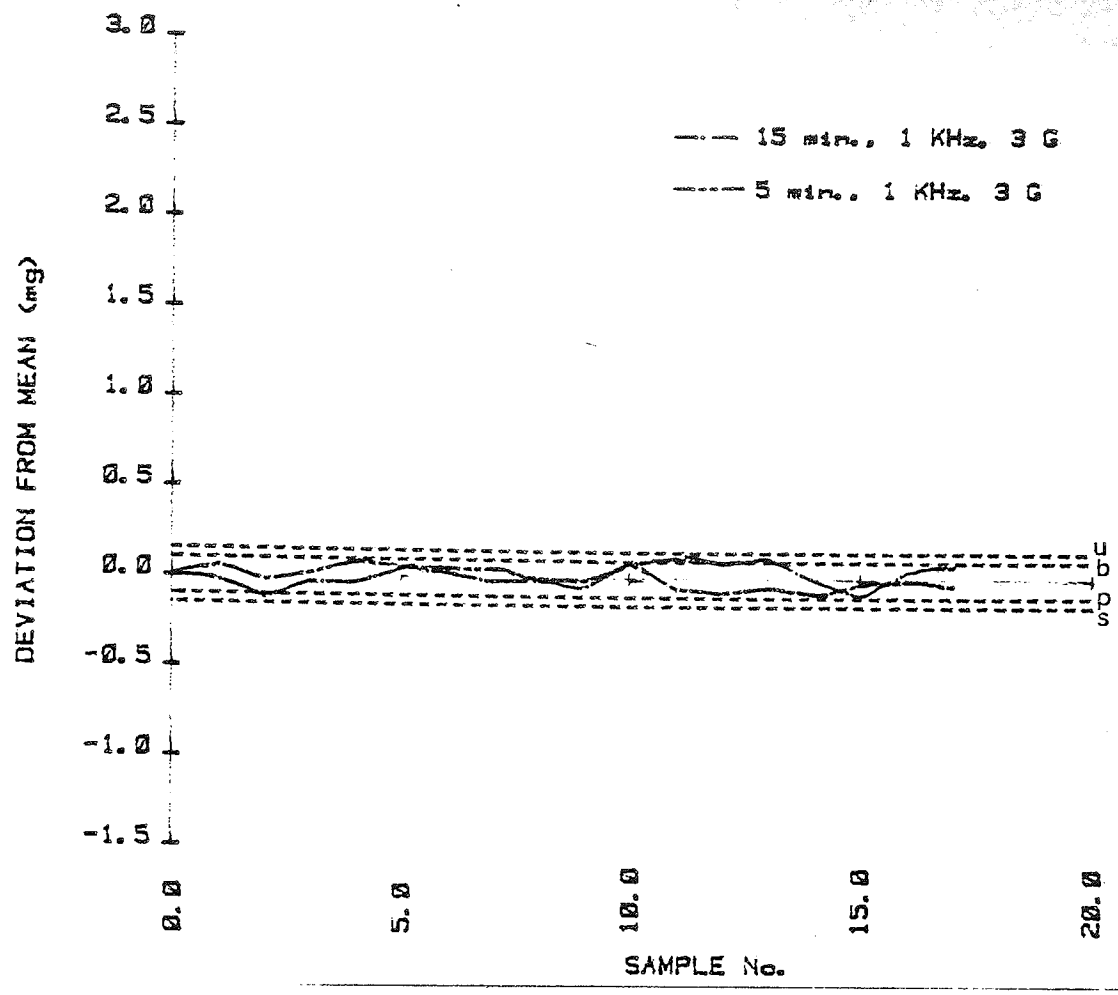

H. Dipac and potassium chloride .5%

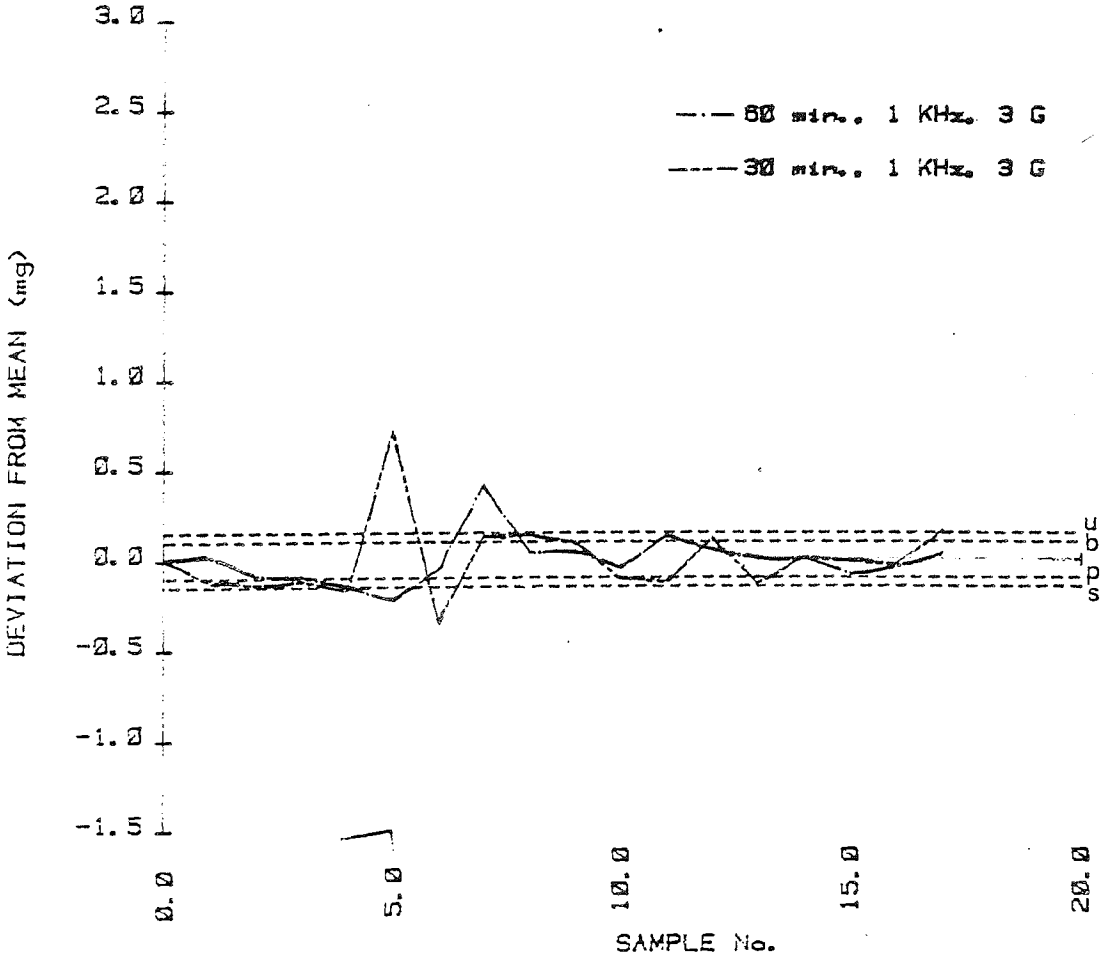

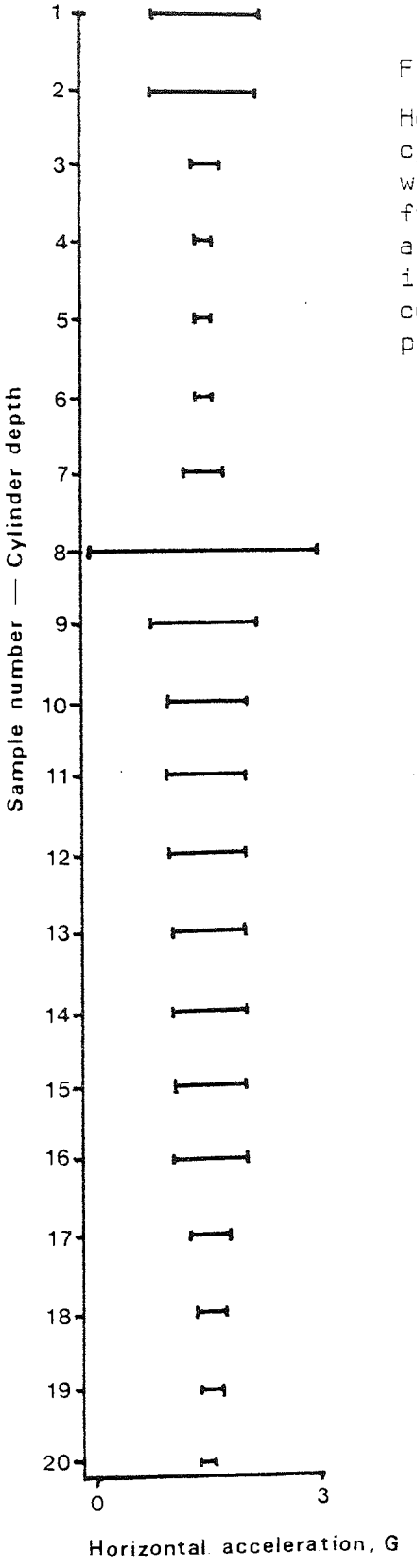

Figure 93.

Horizontal acceleration of powder cylinder at different bed depths when vibrated at a vertical frequency of 500 Hz and a vertical acceleration of 3 G. Sample 1 is at the top of the cylinder containing Dipac and 0.5% potassium chloride.

4.3.2.4 Displacement, Velocity, Energy, Power and Inertia

Other characteristics of vibration in cylinders containing powder mixes include such factors as: (i) the vertical displacement of the cylinder from its position at rest, (ii) velocity of vibration, (iii) vibrational energy, (iv) vibrational power and (v) the force of inertia of the system during vibration. Each of these characteristics can be measured directly or from mathematical treatment of the vibrations represented by the acceleration and frequency at a particular condition.

It was possible to produce any given displacement of the powder cylinder by different combinations of vibration frequency and acceleration force. In this way, the same displacement could be produced by vibrating the cylinder at low frequency and low acceleration, or by a higher frequency combined with a higher acceleration.

By combining a frequency of 50 Hz with an acceleration force of 0.75 G, a displacement of 0.59 mm was produced. The same displacement was also produced by 100 Hz vibrating at 3 G although, as explained earlier, this combination of conditions produced different segregation effects in the vibrated powder. The displacement induced by the lower frequency and acceleration caused a coefficient of variation in the powder mix of about 2% whereas the same displacement at higher frequencies and acceleration produced a coefficient of variation around 40%.

Figures 94 to 97 show the relationship between the vibration conditions and the segregation tendencies of different drug/excipient mixes. The segregation behaviour of the ordered mixes did not appear to be directly related to displacement or energy of vibration;

marked segregation occurred at very low energies and displacements, whereas at certain higher values the coefficient of variation decreased (Figures 94 and 96). Although the power of vibration and the vibration velocity did not display a linear relationship with the coefficient of variation, both factors caused an upward trend in the observed powder segregation with increasing power or velocity (Figures 95 and 97). The vibrational force of inertia (P_T) was calculated from the equation of Traustel reported by Matthée (135):

$$P_T = L_{VIB}^3 \cdot \rho_p \cdot b \qquad (95)$$

where L_{VIB} is the length of vibration (2 x displacement), ρ_p, the powder density and b, the acceleration. As with the previous factors there was no definite evidence of a relationship between inertia force and the segregation of different powder mixes.

All of the vibration conditions, including acceleration appear, we found, to be inter-dependent, but the vibration frequency appears to have been the single most important condition which influenced powder segregation, because of the resonance effects produced at certain frequencies.

4.3.2.5 Random Vibration

A sine random generator was used to produce random vibrations with different bandwidths, centred on specific frequencies. Figure 98 shows the random waveform produced by vibrations with a 30 Hz bandspread centred on a frequency of 50 Hz. Table 29 a, b, c, lists the centre-frequencies and bandspreads of random vibration signals used to vibrate the different powder mixes for fifteen minutes at 1.5 G acceleration. Centre frequencies with

Figure 94. Relationship between vibrational displacement and powder segregation in mixes of 0.5% potassium chloride with different excipients.

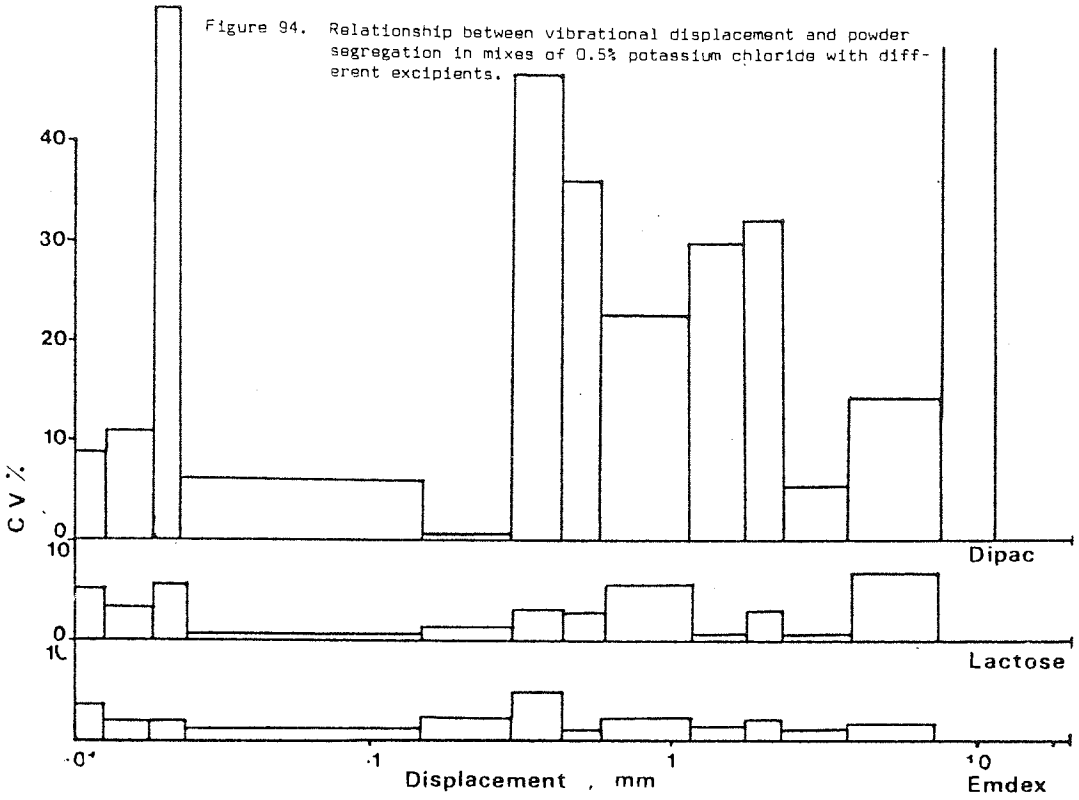

Figure 95.

Relationship between vibrational displacement and powder segregation in mixes of 0.5% potassium chloride with different excipients.

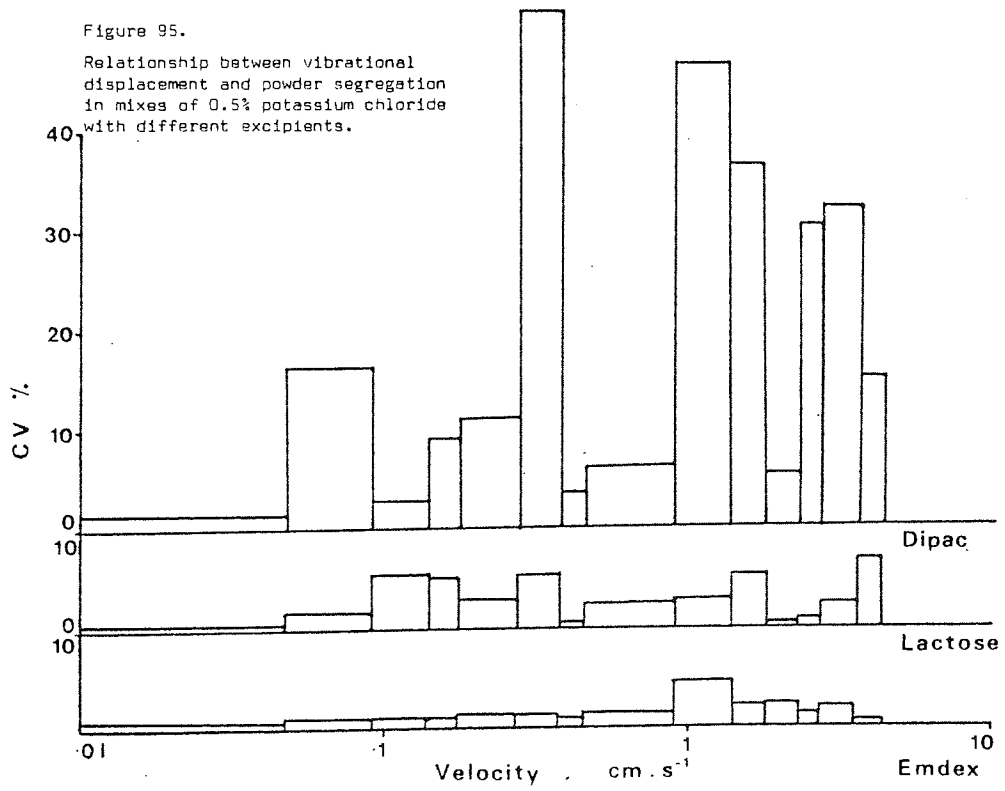

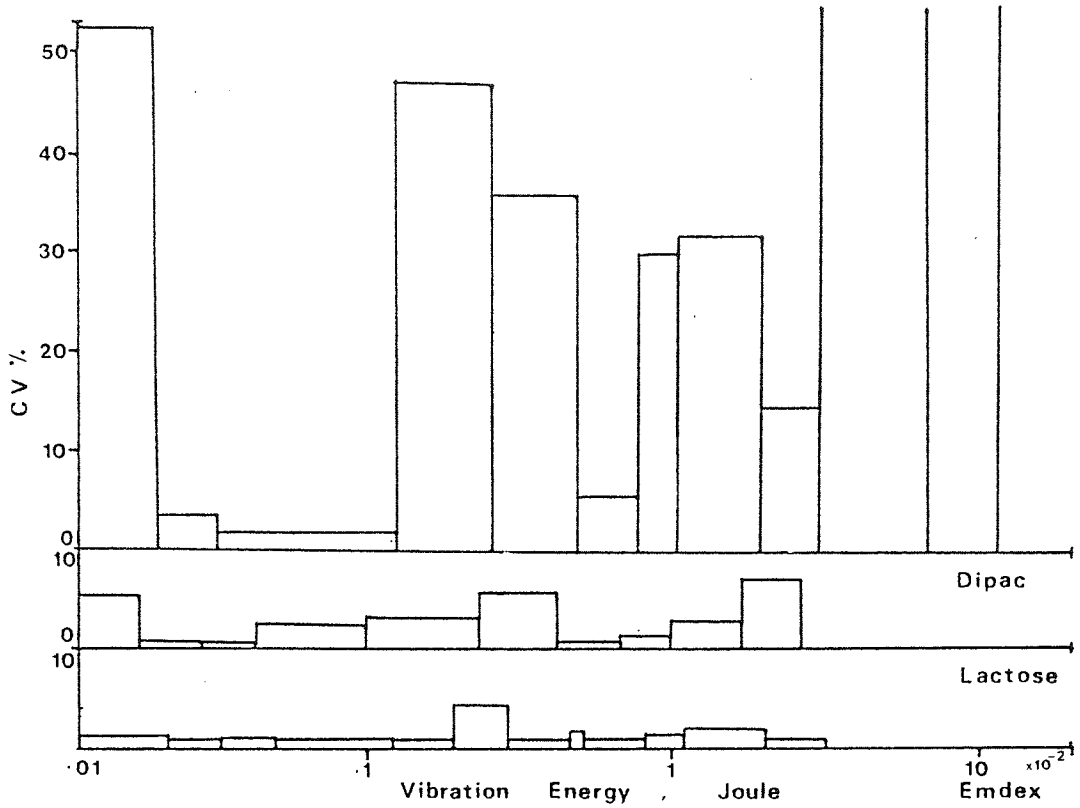

Figure 96. Relationship between vibrational energy and powder segregation in mixes of 0.5% potassium chloride with different excipients.

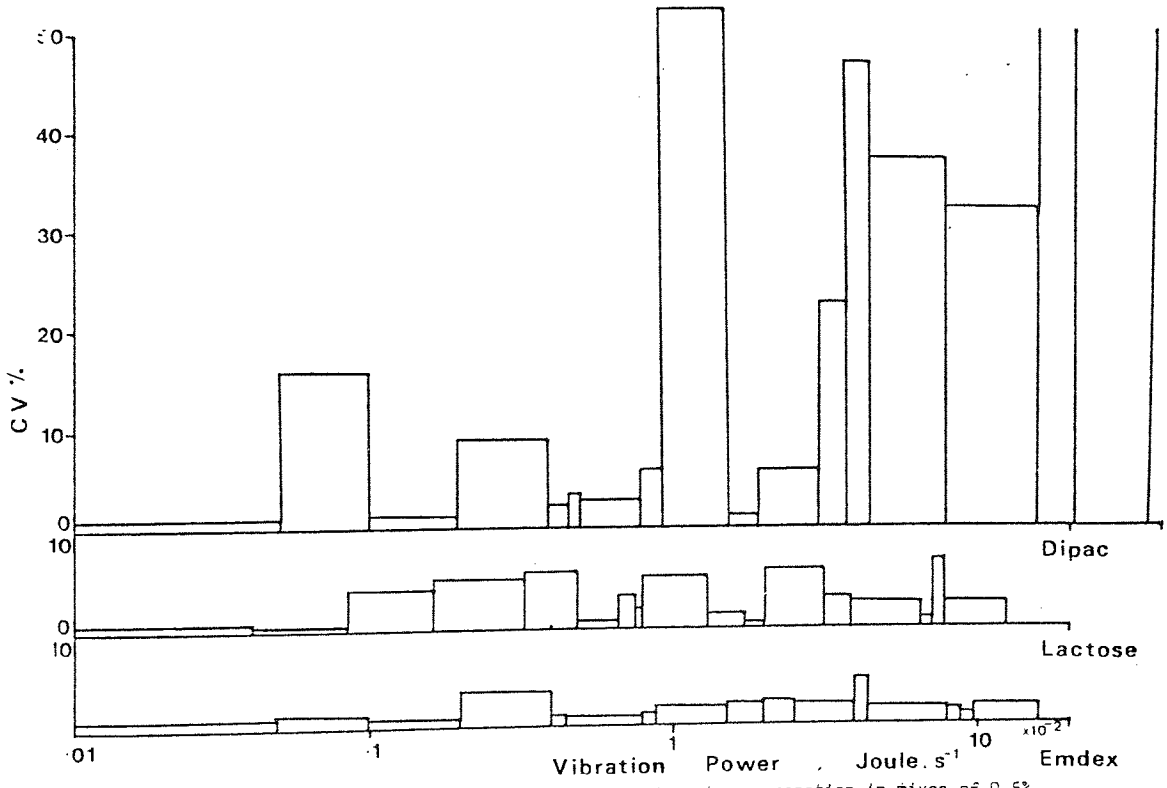

Figure 97. Relationship between power of vibration and powder segregation in mixes of 0.5% potassium chloride with different excipients.

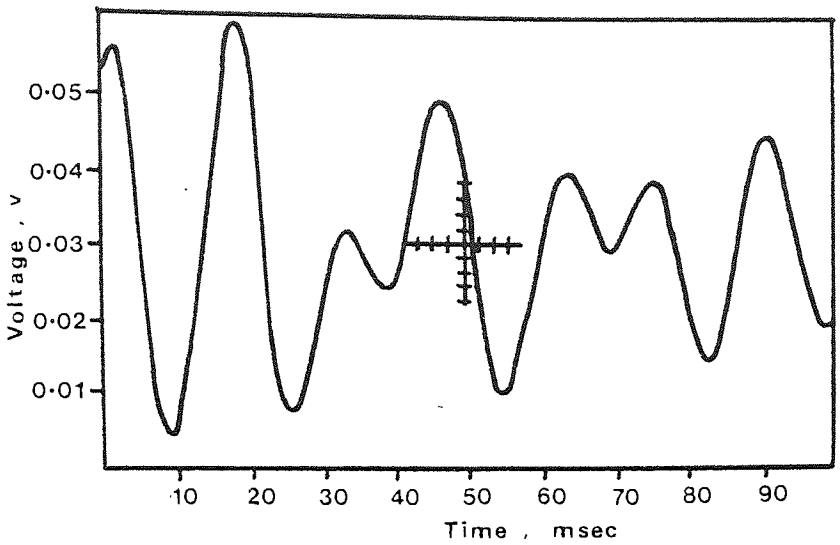

Figure 98. Random waveform recorded on an oscilloscope by vibration with a 30 Hz bandspread centred on a 50 Hz frequency signal

bandspreads of only 10 Hz were used to produce narrow-band random signals. *Narrow-band random* vibrations were capable of destroying any resonance effects such as the nodes and anti-nodes which were observed to produce lateral powder movement and turbulence affecting cylinders subjected to sine-wave vibrations.

A comparison of ordered mixes vibrated at a specific single frequency, with those subjected to random vibrations at the same centre-frequency, was used to assess the influence of resonance on the segregation tendencies of powder mixes. The Emdex and recrystallised lactose mixes with 0.5% potassium chloride did not segregate outside pharmacopoeial limits when vibrated randomly (Table 29 a, b). These systems showed a slight tendency to segregate at low centre-frequencies in a similar manner to the segregation found in powders subjected to low single-frequency vibrations. There was also a slightly larger segregation tendency in Emdex and lactose mixes vibrated randomly at a centre-frequency of 50 Hz

Table 29 Coefficients of variation (CV%) with upper and lower 95% confidence limits of different powder mixes subjected to sinusoidal random vibrations

(a) Emdex	Centre Frequency (Hz)	Bandwidth (Hz)	Mean CV(%)	Upper Limit	Lower Limit
Emdex and	50	10	0.44	1.10	-0.22
0.5% potassium	100	10	0.50	0.67	0.34
chlordide	500	10	0.40	0.57	0.23
	50	30	0.91	1.09	0.72
	White	Noise	0.52	1.61	-0.57

(b) Recrystallised Lactose	Centre Frequency (Hz)	Bandwidth (Hz)	Mean CV(%)	Upper Limit	Lower Limit
Recrystallised	50	10	0.24	0.77	-0.30
Lactose and	100	10	0.58	1.62	-0.46
0.5% potassium	500	10	0.04	0.05	0.03
chloride	50	30	0.63	1.31	-0.04
	White	Noise	0.05	0.07	0.02

(c) Dipac	Centre Frequency (Hz)	Bandwidth (Hz)	Mean CV(%)	Upper Limit	Lower Limit
Dipac and	50	10	3.48	6.21	0.74
0.5% potassium	100	10	1.87	2.85	0.90
chloride	500	10	0.20	0.38	0.03
	50	30	4.20	8.54	-0.13
	White	Noise	0.25	0.29	0.21

and a bandspread of 30 Hz, when compared with powders vibrated at the same centre-frequency but with the bandspread reduced to 10 Hz. This probably occurred because the larger bandspread introduced more low-frequency vibrations which have previously (section 4.3.2.3) been shown to increase the segregation tendency of ordered powder mixes. Mixes of Dipac and 0.5% potassium chloride showed a greater segregation tendency than either Emdex or recrystallised lactose mixes when randomly vibrated (Table 29(c)). The increased segregation which occurred in mixes of Dipac was similar to the increases found in vibration studies at single frequencies, although the magnitude of the segregation tendency was reduced under random vibration. Dipac mixes vibrated at 50 Hz single frequency had a coefficient of variation of 14.78% compared with 3.48% for mixes vibrated randomly at 50 Hz with 10 Hz bandspread, and 4.20% for those vibrated at 50 Hz with 30 Hz bandspread. The random vibrations probably caused less segregation because the powder cylinders were unable to vibrate at their natural frequencies long enough to produce resonance. The anomalous increase in powder segregation at the wider bandspread of 30 Hz was probably caused by the introduction of lower frequencies. This effect was destroyed by increasing the bandspread to include many higher frequencies (Figure 99). Broad-band random signals with a frequency range from 20 Hz to 20,000 Hz, referred to as white noise, were used to vibrate all the powder mixes. Even in mixes containing Dipac, there was no segregation tendency. Figures 100 to 102 show the effects of drug particle movement in the different powder mixes following random vibrations. Random vibration produced no overall segregation in mixes of Emdex and potassium chloride (Figure 100), but there was a slight loss of drug from the powder

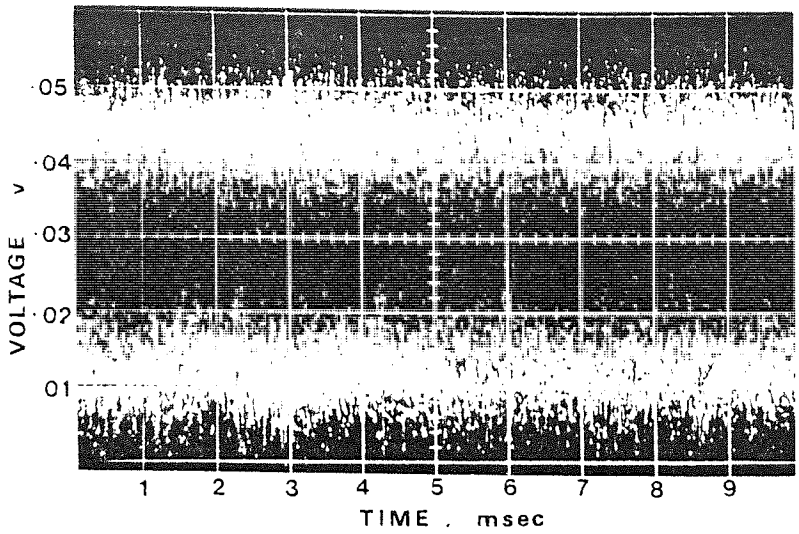

Figure 99. Broadband random vibrations from 20 Hz to 20,000 Hz (white noise)showing the similarity between the excitation waveform and the vibrator response.

surface in powders vibrated randomly with a centre-frequency of 50 Hz (Figure 100 A, B). The drug particles only percolated a short distance, being restricted to a layer of more mobile particles near the powder surface, and the powder movement involved was very small, most of the samples throughout the bed were within the pharmacopoeial limits for drug content uniformity.

In recrystallised lactose (Figure 101) subjected to random vibrations, only samples vibrated at a centre-frequency of 50 Hz with 30 Hz modulation and at 100 Hz showed any drug movement (Figure 101, B, C). At these lower frequencies there was a slight increase in drug content at the powder surface and an even smaller drop in concentration at the base. This may have been caused by some diffusional segregation but it is more probable that this small-scale effect was caused by ordered-unit segregation. At the lower centre-frequencies of randomly vibrated Dipac mixes (Figure 102), both short and long-range segregation

Figures 100, 101 and 102

Relationship between drug concentration at specific levels in powder beds following random vibration under different vibration conditions.

The captions on each figure define the drug/excipient system, vibration time and acceleration force (G) as well as the random vibration frequencies indicated by the centre-frequency (Hz) and the bandspread (modulation, in Hz).

The inner pair of dotted lines indicate the upper and lower content uniformity limits for B.P. preparations containing small quantities of potent drugs and represent a variation of ± 10% of the mean drug content.

The outer pair of dotted lines indicate the upper and lower content uniformity limits for U.S.P. microdose preparations and represent a variation of ± 15% of the mean drug content.

The individual sample size = 200 mg corresponding to a nominal drug content of 1 mg.

Fig 100 A Emdex & potassium chloride .5%

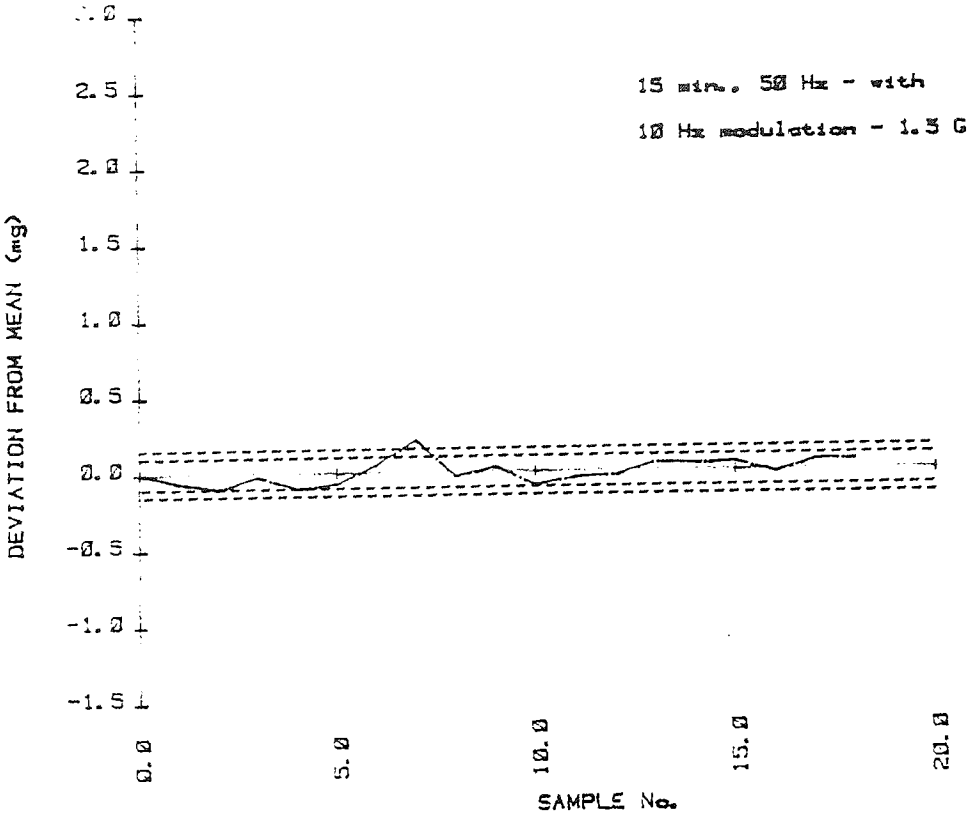

Fig 100 B Emdex & potassium chloride .5 %

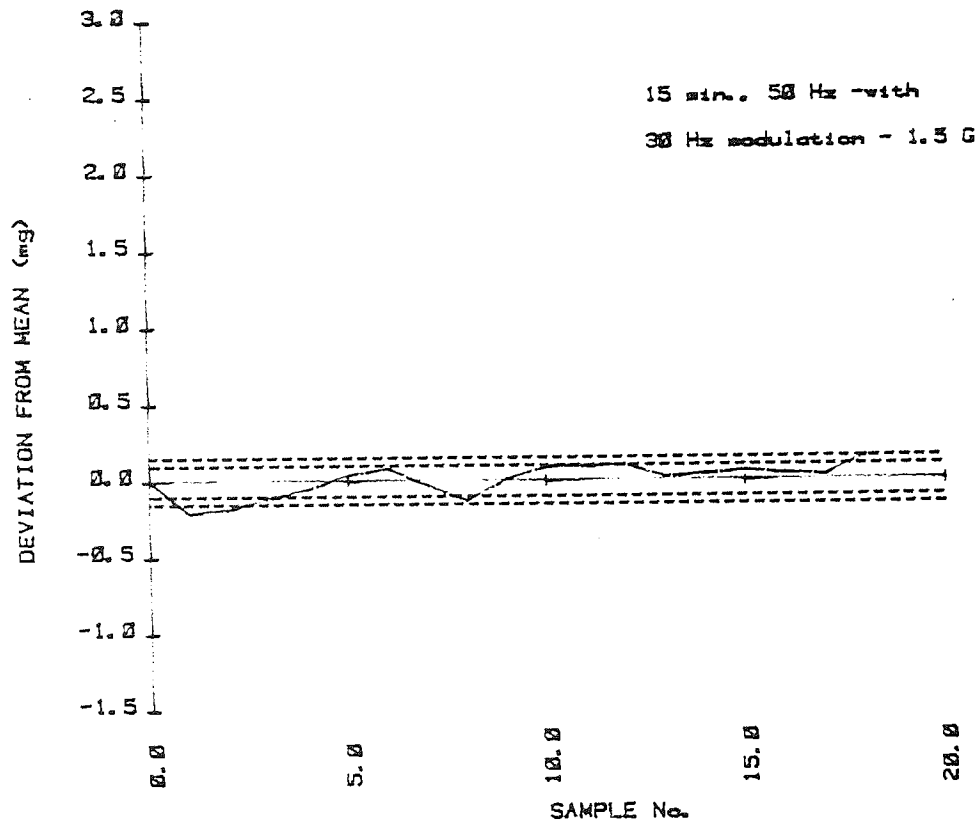

Fig 100 C Emdex & potassium chloride .5%

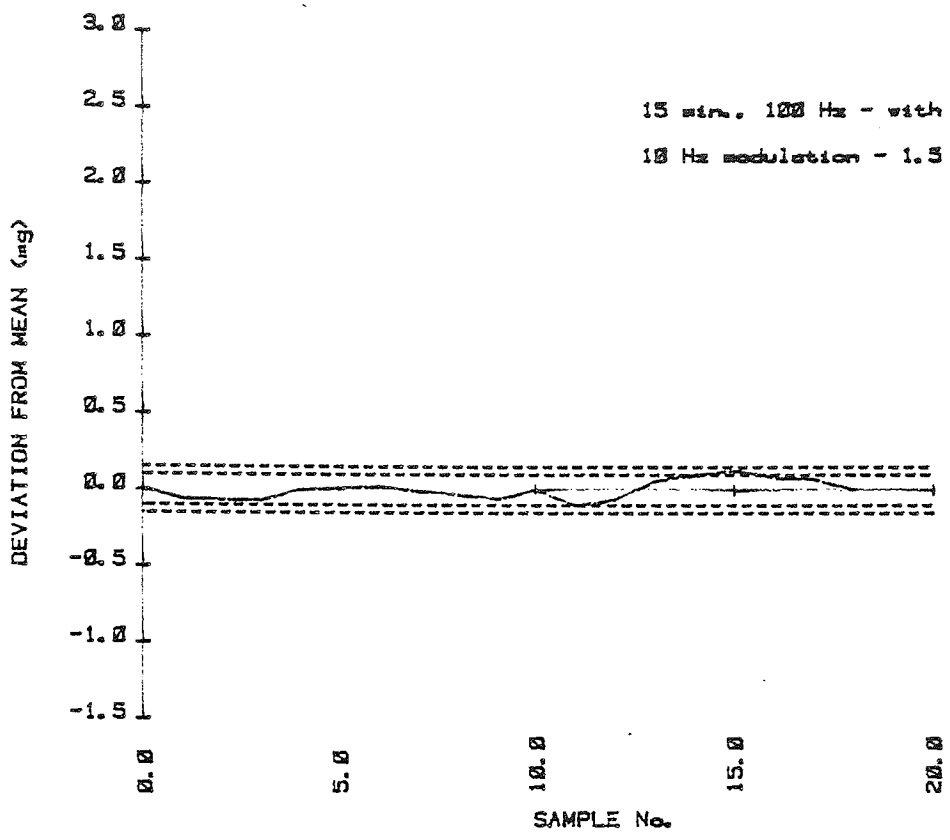

Fig 100 D Emdex & potassium chloride .5%

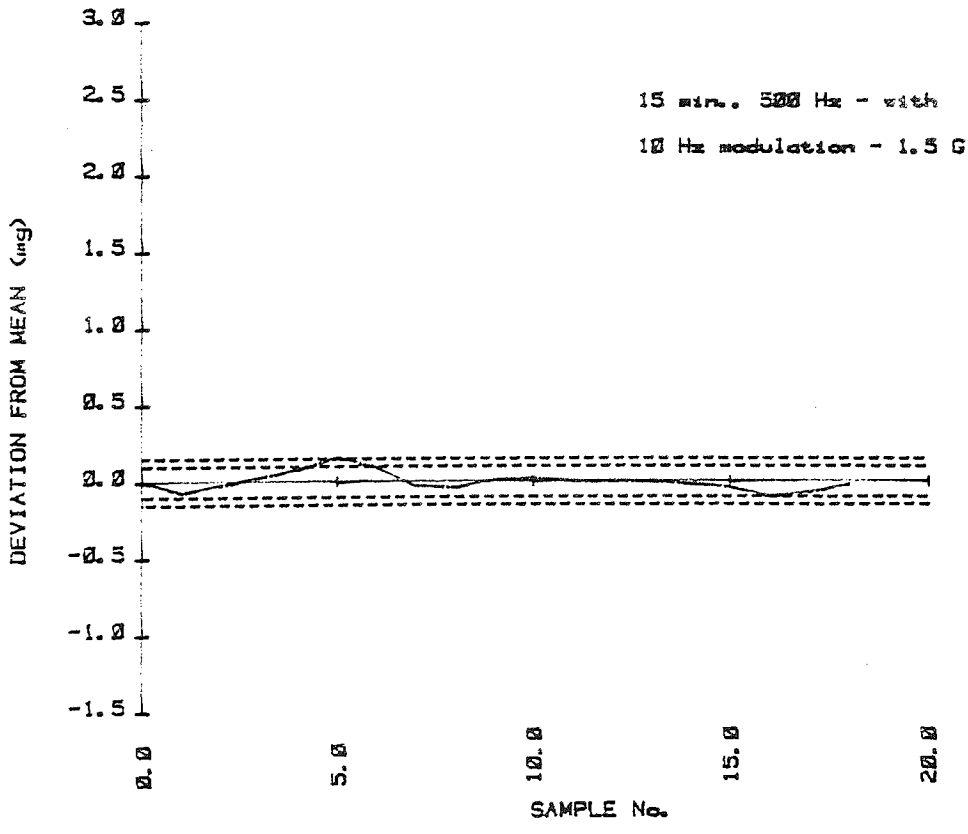

Fig 100 E Emdex & potassium chloride .5 %

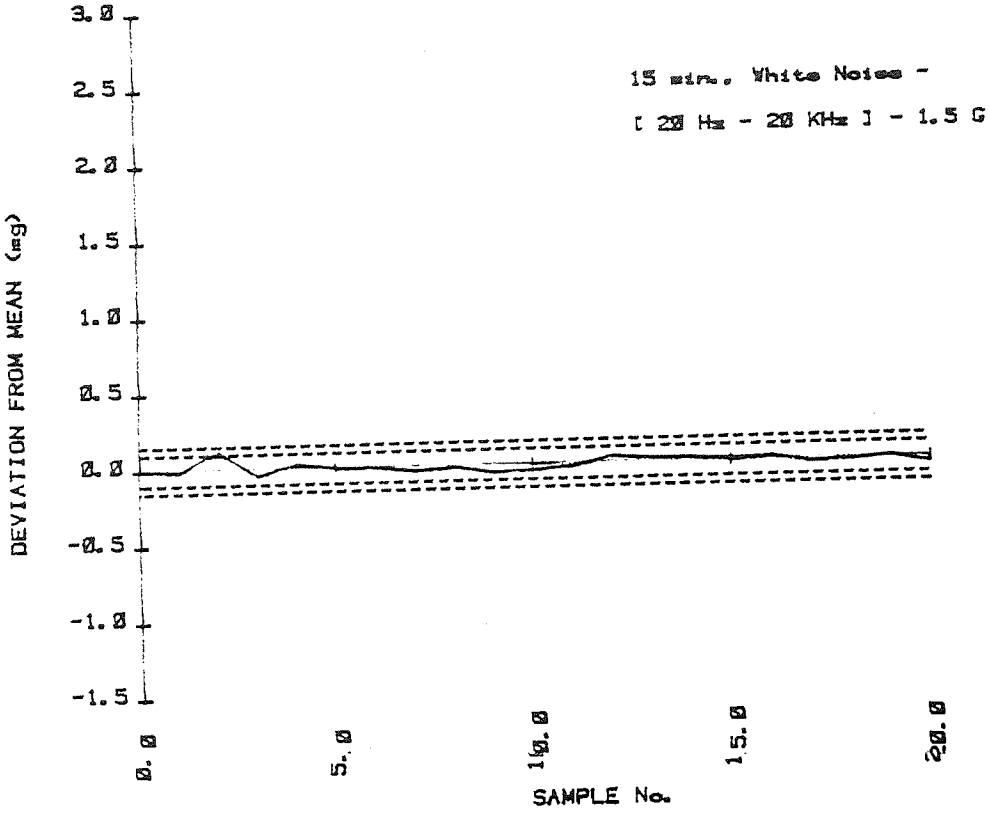

Fig 101 B Lactose & potassium chloride .5%

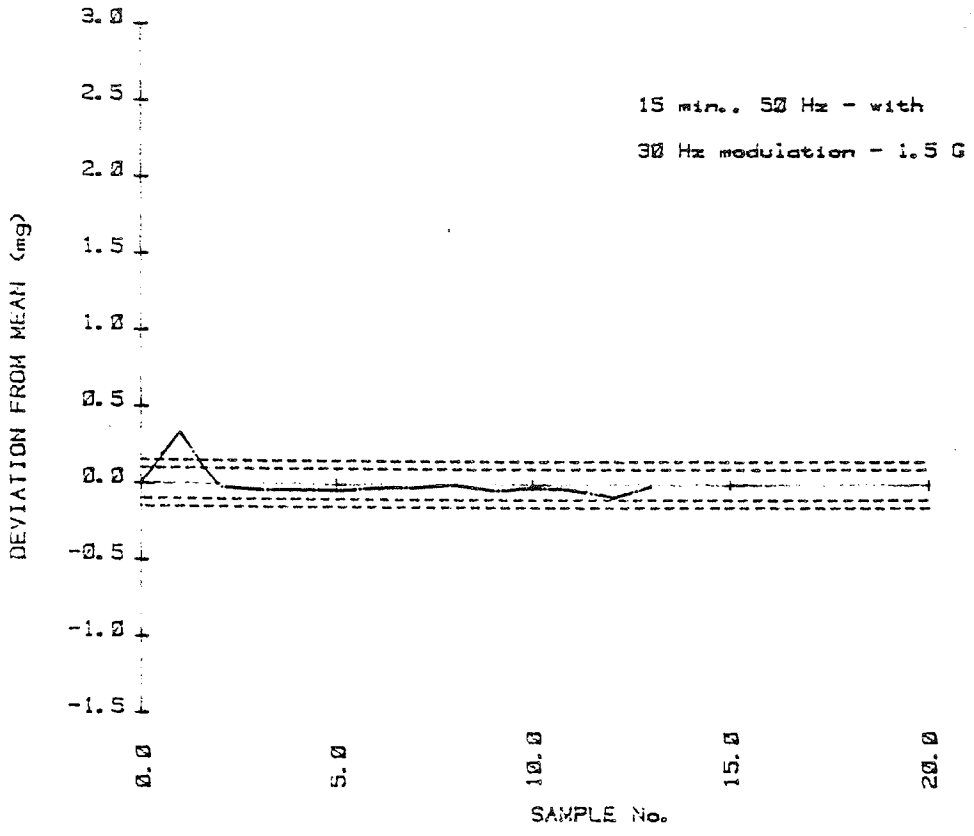

Fig 101 A Lactose & potassium chloride .5%

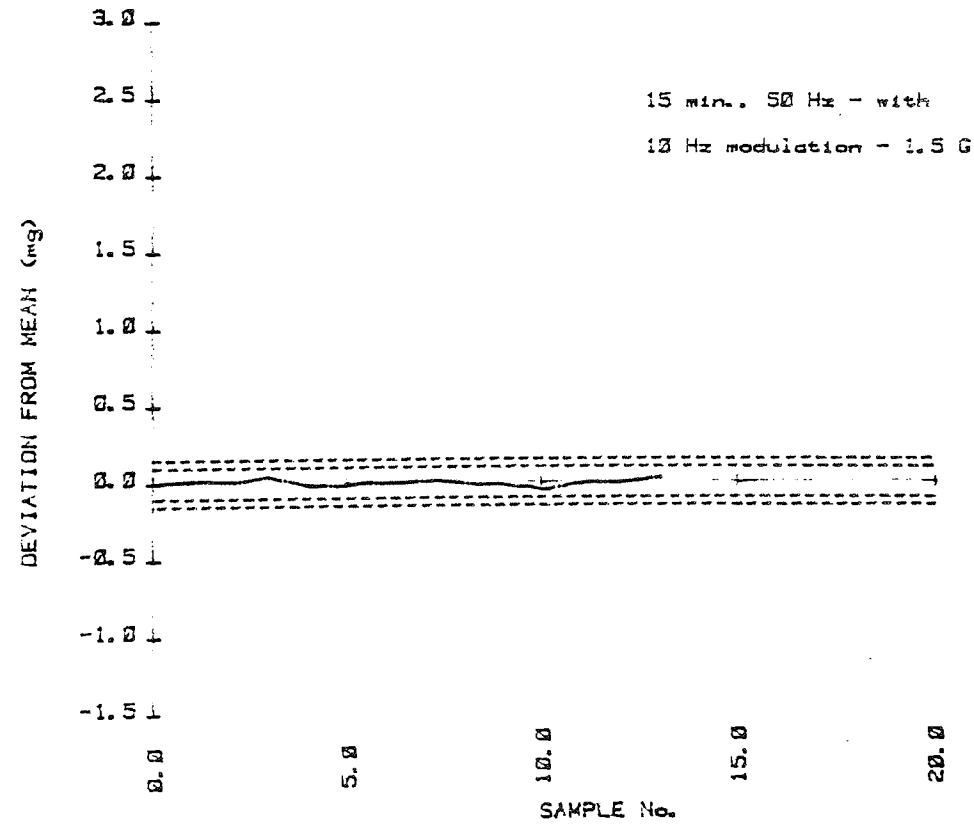

Fig 101 C Lactose & potassium chloride .5%

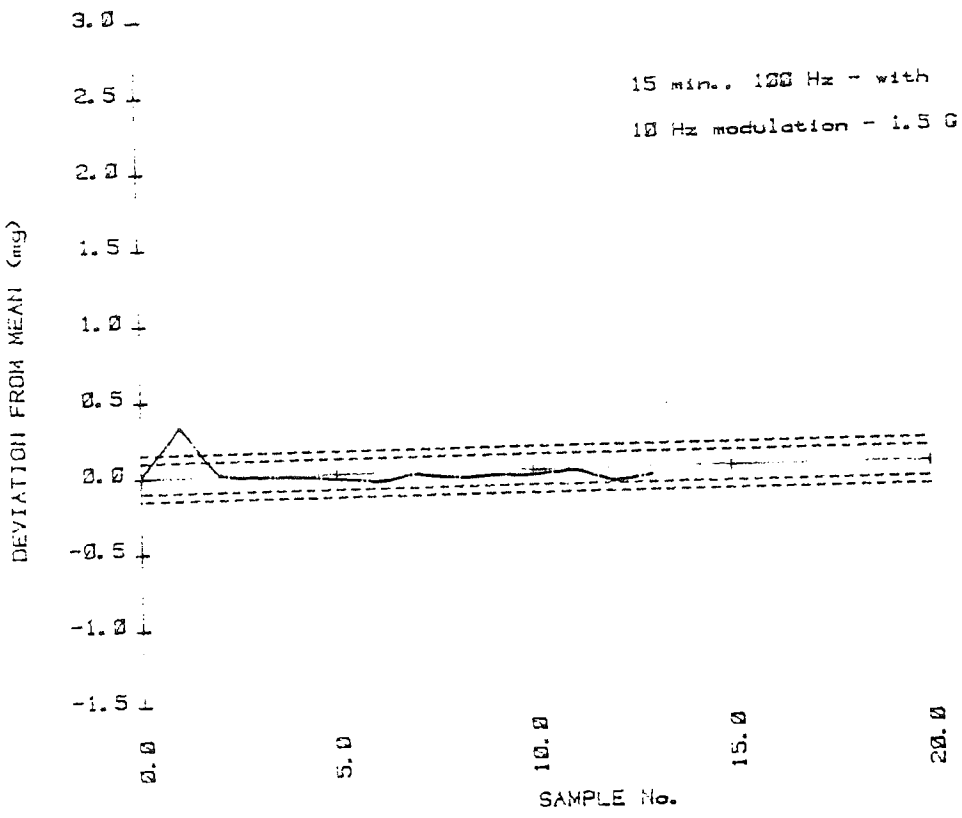

Fig 101 D Lactose & potassium chloride .5%

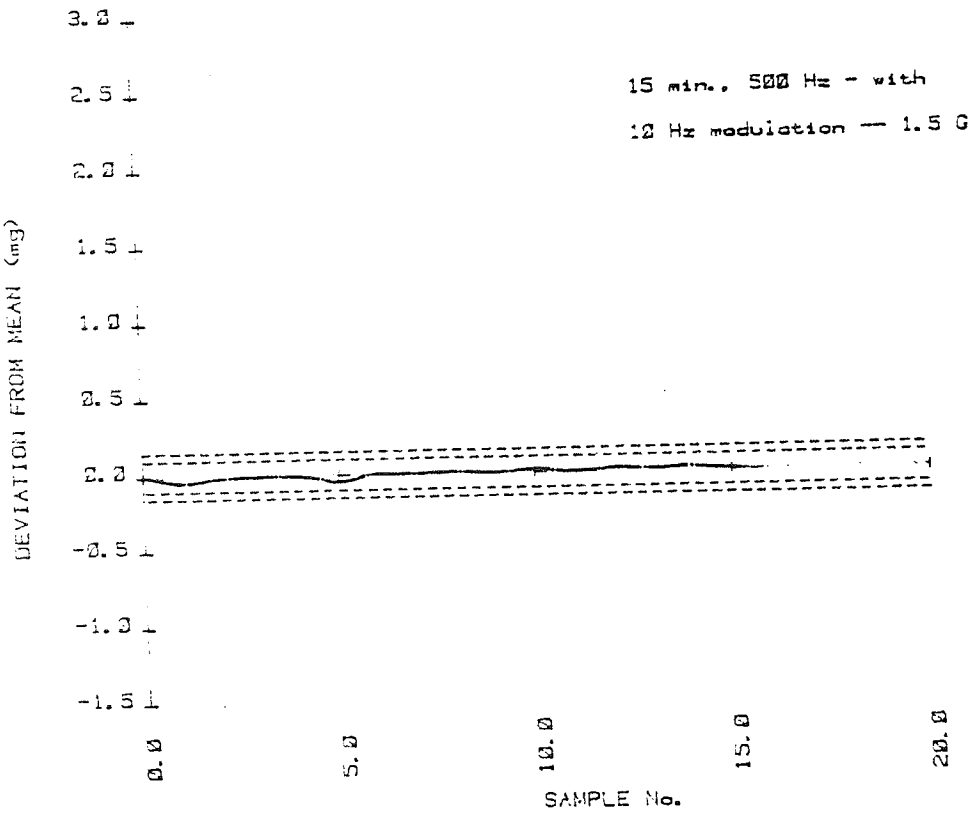

Fig 101 E Lactose & potassium chloride .5%

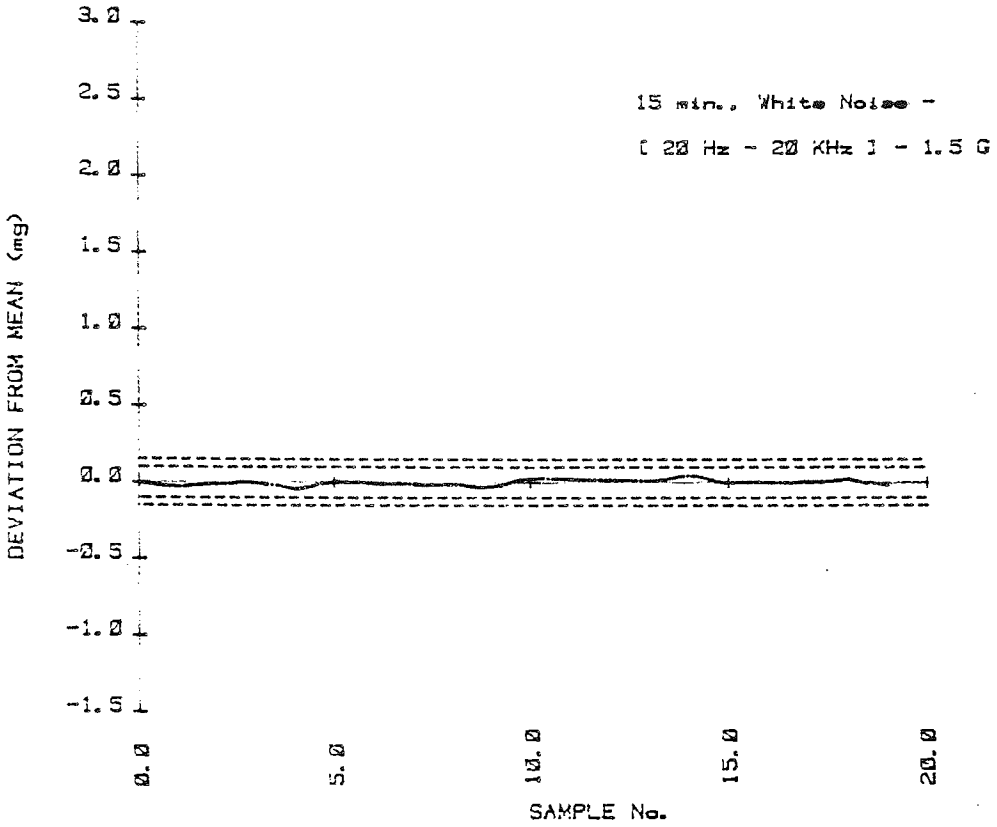

Fig 102 A Dipac and potassium chloride .5%

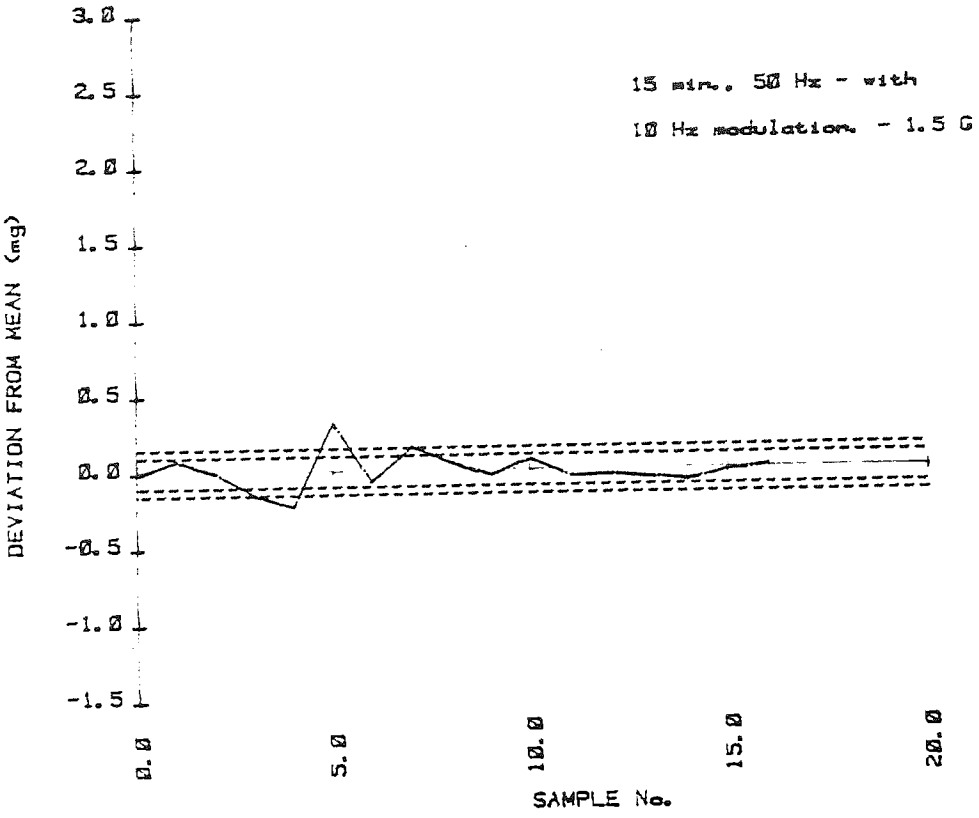

Fig 102 B Dipac and potassium chloride .5%

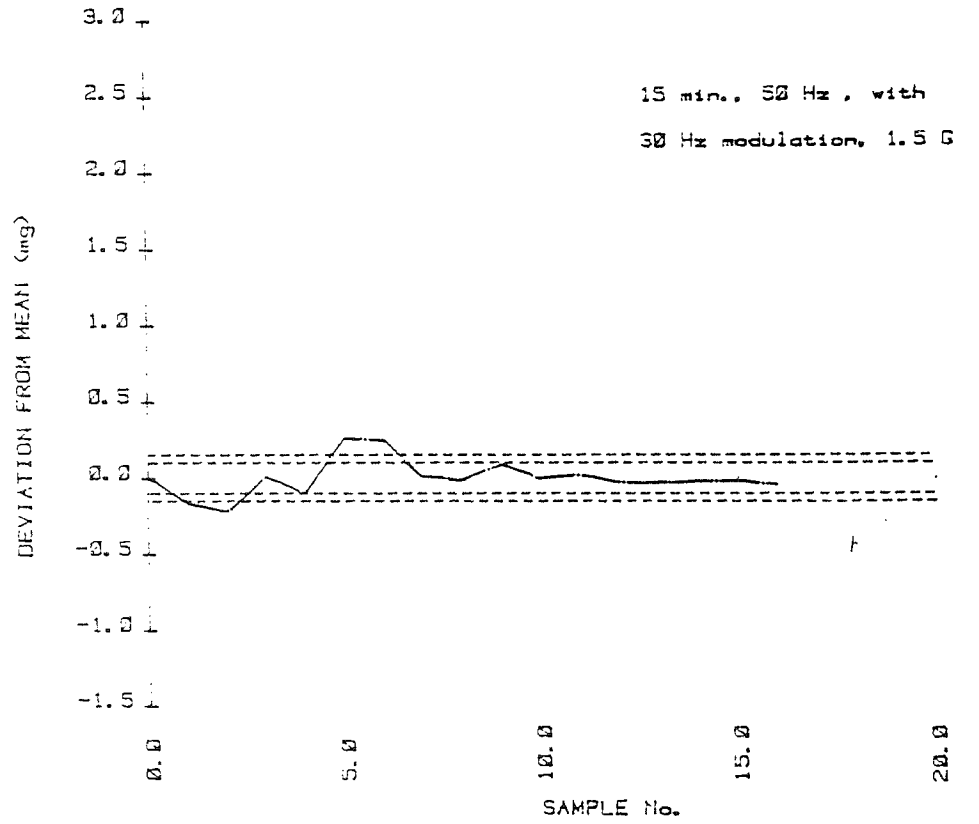

Fig 102 C Dipac and potassium chloride .5%

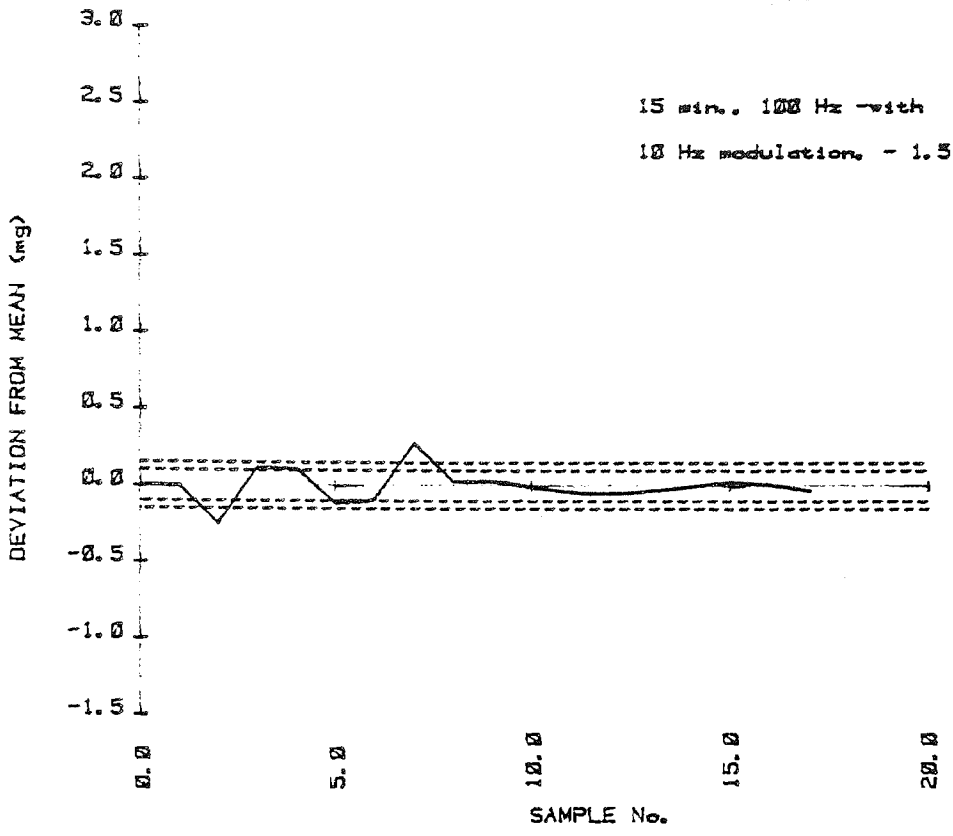

Fig 102 D Dipac and potassium chloride .5%

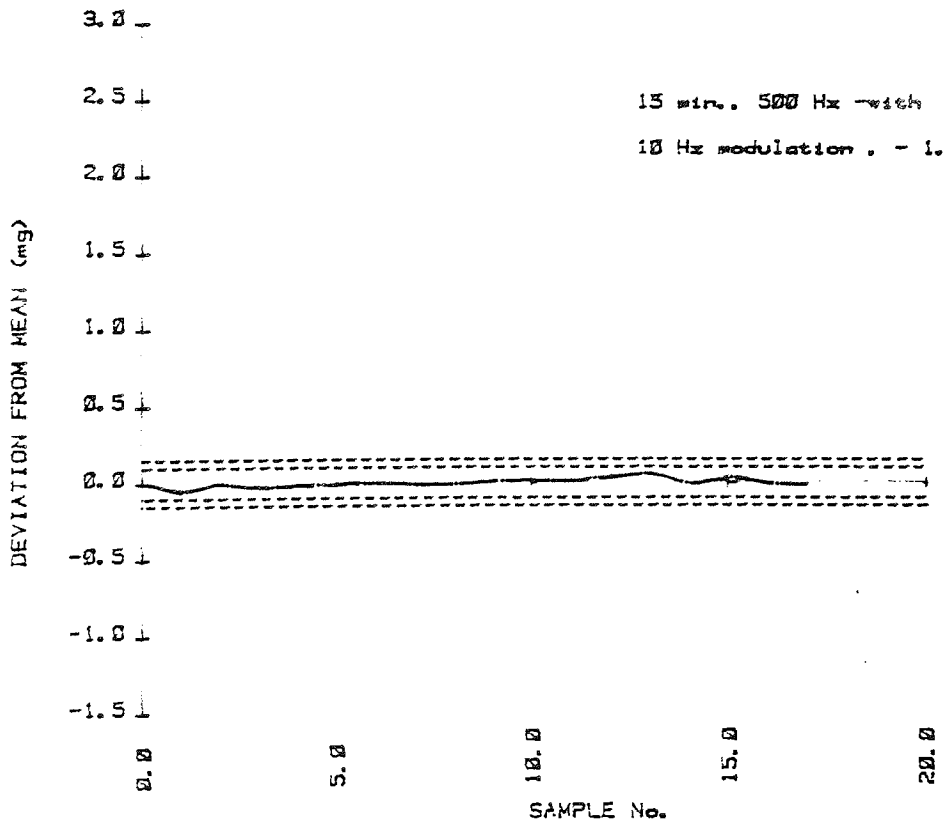

Fig 102 E Dipac and potassium chloride .5%

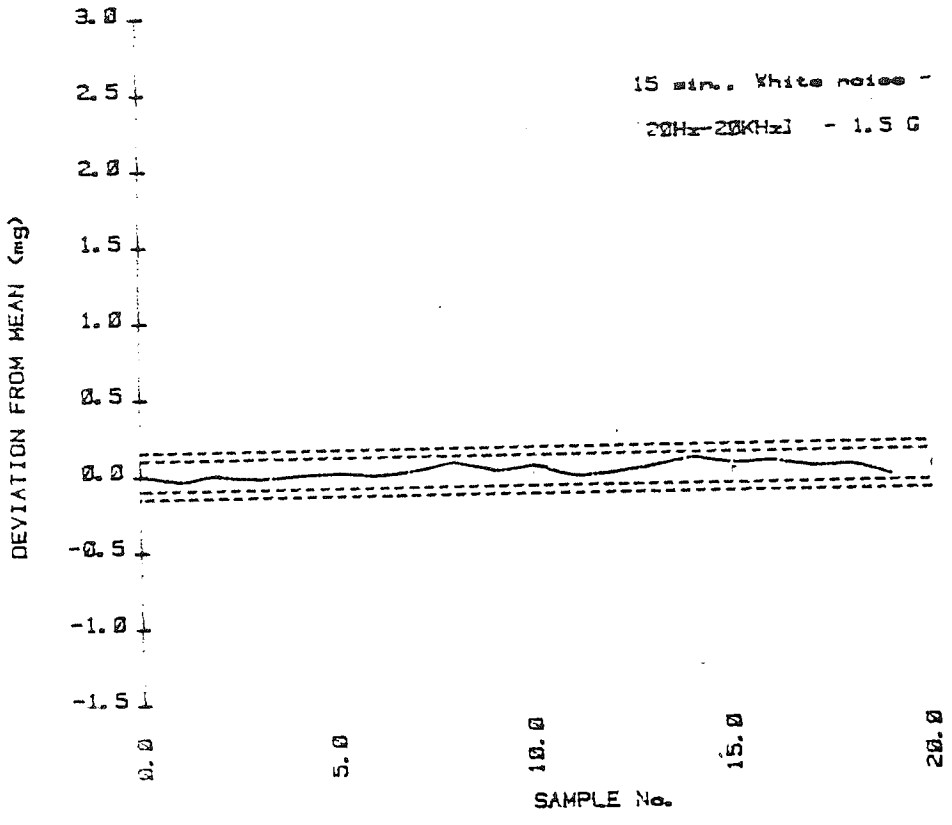

was present, although both were relatively small effects (Figure 102 A, B). The long-range segregation tendency was apparently caused by percolation of fine drug particles from the powder surface to the bottom of the upper mobile layer. In Dipac, as with the other excipient systems, the higher centre-frequencies of narrow-band random vibrations produced virtually no net movement of drug particles (Figures 100 D, 101 D and 102 D). This was also absent in all the different powder mixes subjected to broad-band random vibrations (white noise) at an acceleration of 1.5 G and all of the powder samples remained within the pharmacopoeial limits (Figures 100 E, 101 E and 102 E).

The results from this part of the vibration study suggest that random vibrations reduced powder segregation by preventing resonance effects. It may therefore be possible to reduce powder segregation in industrial systems by eliminating all non-random vibrations in processing equipment, as a more practical alternative to producing completely vibration-free conditions. The influence of vibrational resonance on the segregation of ordered powder mixes is thought to be exerted by production of increased interparticle abrasion caused by turbulence in parts of the powder bed.

4.3.2.6 Excipient Particle Size

To assess the influence of carrier particle size on the stability of ordered mixes different excipient particle size fractions were studied. The theoretical number of active adherence sites available on individual carrier particles increases with increasing particle diameter, according to equation (93). Therefore, by changing the carrier particle size whilst the adherent particle

size is maintained constant, one can alter the number of fine particles which each coarse particle is stereometrically capable of carrying; such a change may influence the stability of the ordered mixes formed with different carriers. This hypothesis was tested using recrystallised lactose powder as the carrier excipient in view of the wide differences in particle size distributions available. Six different carrier particle sizes were used with geometric mean diameters of 9.5 μm, 127 μm, 212 μm, 354 μm, 596 μm and 843 μm. This represented differences in the ratio of carrier to adherent particle size ratio ranging from about 1 : 1 to more than 100 : 1 and there was a corresponding difference in the drug saturation level at each carrier particle size as shown in Table 30.

Table 30 The number of adherent particles required to saturate the surface of carrier particles with different particle sizes according to Equation 93.

Excipient Particle Size (μm)	Saturation Level (no. of particles)
843	63,169
596	31,575
354	11,139
212	3,995
127	1,434
9.5	8

Each of the excipients of different particle size was mixed with 0.5% fine potassium chloride powder as described in section 4.1 and subjected to a range of different vibration frequencies from

50 Hz to 5000 Hz for 15 minutes at an acceleration force of 2 G. The segregation tendency of each powder mix was determined from the sample coefficients of variation following vibration (Figures 103 and 104). Fine potassium chloride particles mixed with fine lactose excipient particles of mean size 9.5 μm and 127 μm showed no segregation tendency following vibration (Figure 103). The coarser excipient particles with a diameter of 212 μm did not allow any marked segregation of drug particles although there was a slight segregation tendency in mixes vibrated at lower frequencies (Figure 103). The segregation of drug from excipient particles with diameters of 354 μm was greater than that produced in lower particle size excipients, (Figure 104). This trend continued in the two highest particle size excipient powders where segregation also increased with decreasing frequency (Figure 104).

Yip and Hersey (72) adapted Buslik's homogeneity index (Equation 29) to calculate the homogeneity of ordered mixes produced by different carrier particle sizes:

$$H_i = -\log W_o \qquad (29)$$

where W_o was taken as the weight of a single ordered unit. In an ordered mix, the relatively more massive carrier particle composes most of the ordered unit mass, i.e. $W_o \simeq W_c'$ (weight of single carrier particle). Therefore:

$$H_i = -\log W_c' \qquad (96)$$

where $W_c' = \pi D^3 \rho / 6 \qquad (97)$

Table 31 shows the theoretical values for absolute homogeneity, H_i, of different mixes containing various recrystallised

Figure 103. Relationship between vibration frequency and coefficient of variation of ordered mixes with different lactose carrier particle sizes vibrated at an acceleration of 2 G for 15 minutes.

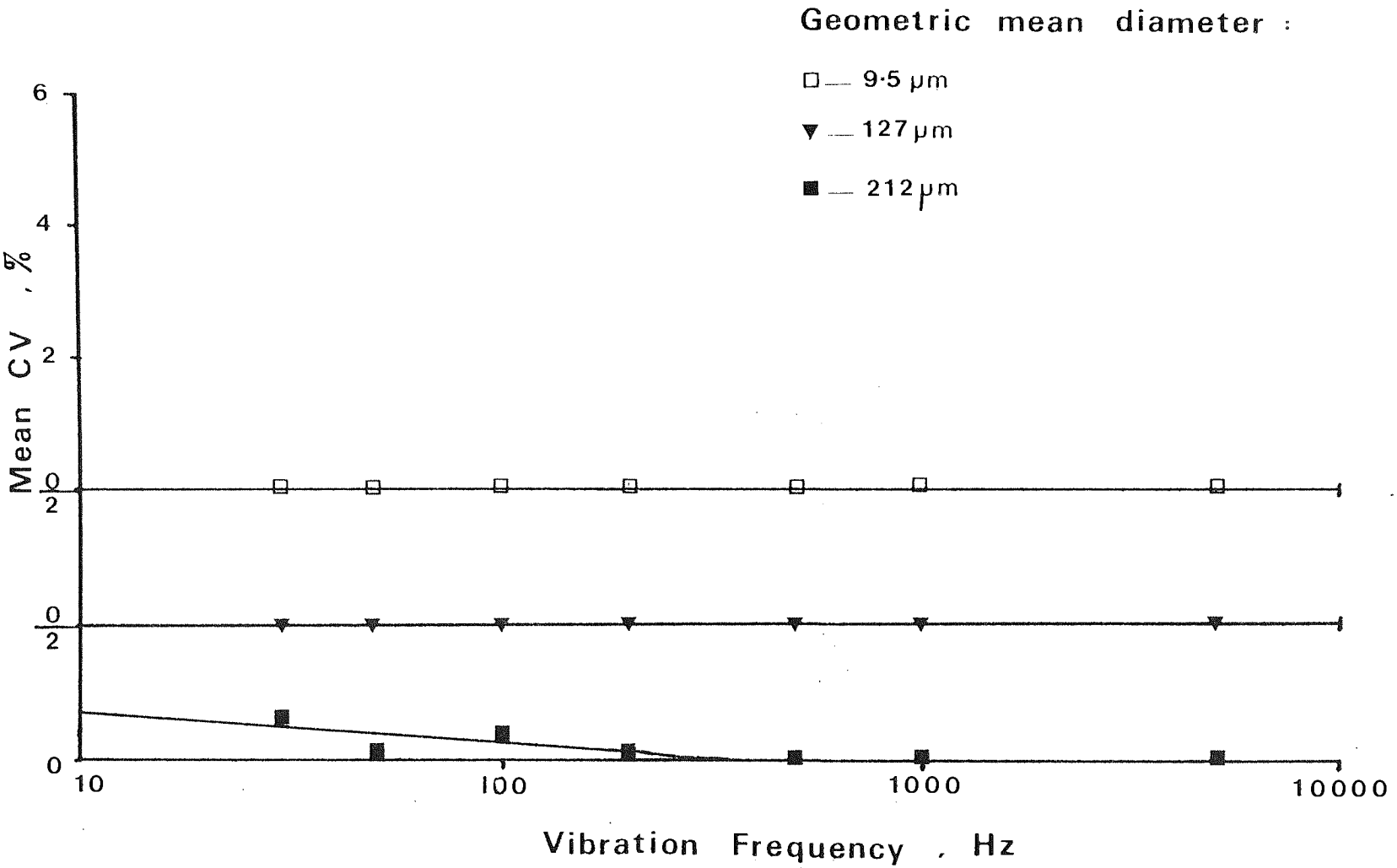

Figure 104. Relationship between vibration frequency and coefficient of variation of ordered mixes with different lactose carrier particle sizes vibrated an an acceleration of 2 G for 15 minutes.

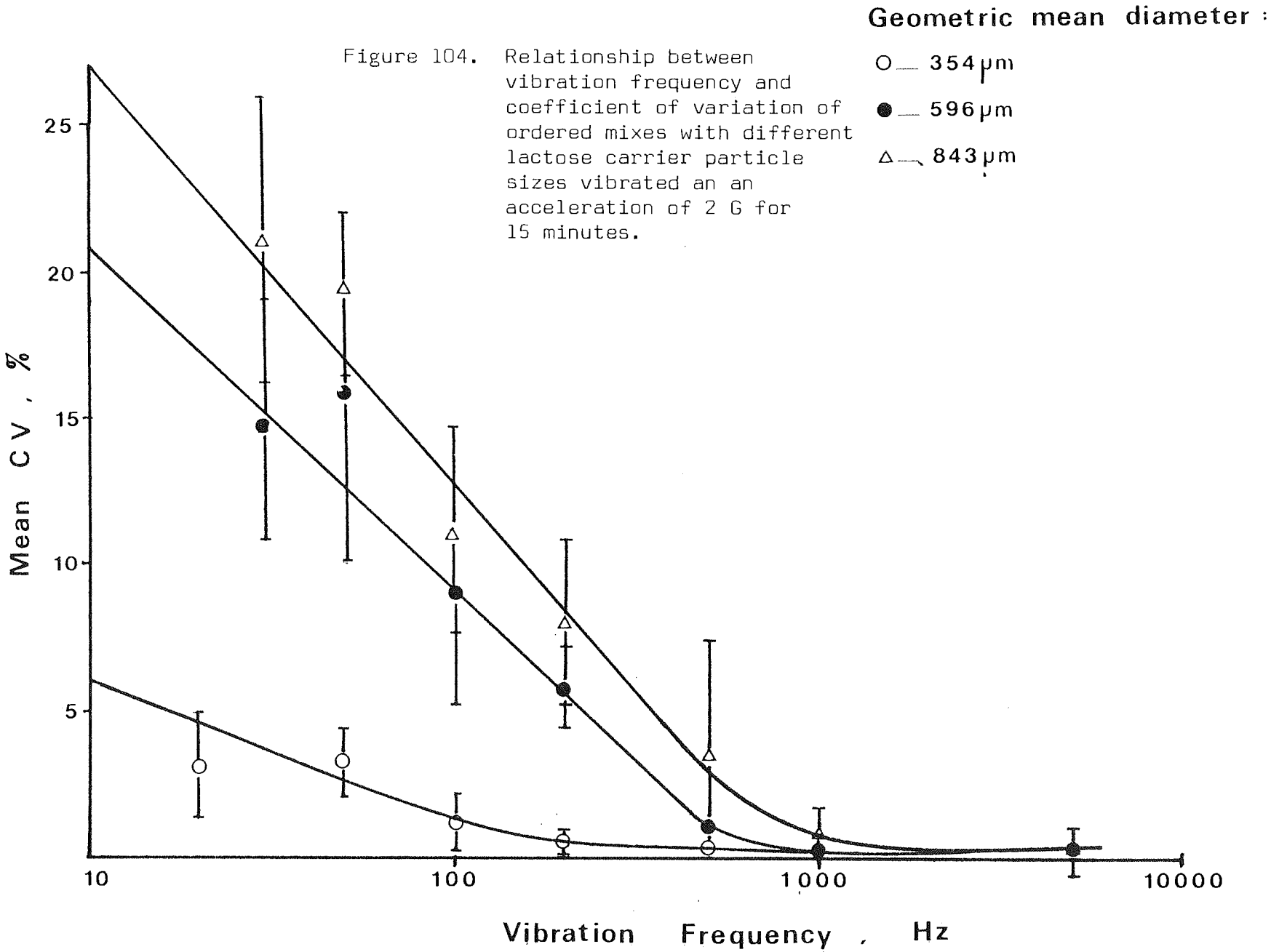

lactose carrier particle sizes. As the excipient particles became coarser the theoretical absolute homogeneity of the mixes decreases. The homogeneity of mixes containing carrier particles of 9.5 μm diameter decreased by a factor of 3×10^6 when the excipient particle size was increased to 843 μm.

Table 31 Changes in theoretical homogeneity, H_i, of ordered mixes with different carrier particle sizes

Particle Size (carrier), μm	Absolute Homogeneity H_i
9.5	9.17
127	5.79
212	5.13
354	4.46
596	3.78
843	3.33

However, the peak segregation which occurred in lactose excipient particles with diameters of 843 μm (Figure 104) was still considerably lower than the segregation tendency of mixes containing the less coarse Dipac excipient (Figure 71) under identical vibration frequency and acceleration conditions. This demonstrates that factors other than particle size control the segregation of ordered mixes. Each of the different particle size fractions of lactose appear to have formed ordered mixes with fine potassium chloride particles and the adherence forces with the different carrier particle sizes we also assumed to have been similar. It is thought that the vibration conditions dislodged similar quantities of drug particles from all of the

different particle size excipients (see later discussion, section 5.2.3) but the distances which the non-cohesive fraction of drug particles are able to travel is governed by the same factors which influence segregation of random mixes. Fine drug particles dislodged from carrier excipient particles will certainly have more freedom to segregate through a vibrated bed of coarse particles than in a cohesive bed of fine particles. The freedom of non-cohesive drug particle movement increased with increasing carrier particle size (Figures 103, 104); however there is only a small difference in segregation tendency between the two largest carrier particle sizes suggesting that further particle size increases would produce progressively smaller increases in powder segregation. The increased number of available carrier sites on individual particles of the coarser excipient powders did not increase the stability of the ordered mixes formed. Although the coarsest particles have many more adherence sites on each individual particle, the overall number of sites in the whole powder bed decreases with increasing particle size. Furthermore, under all the experimental conditions of carrier particle size evaluated, there were many more theoretical sites of adherence than potential adherent particles.

4.3.2.7 Effect of Drug Concentration

The concentration of potassium chloride model drug was altered to examine the effect of increasing the number of adherent particles, under different vibration conditions, on the stability of ordered mixes formed with Emdex, recrystallised lactose and Dipac. The drug content of the mixes was increased from 0.5% to 1, 2, 5 and 10% w/w. Although the 10% drug concentration was a

twenty fold increase over the 0.5% microdose level, all three excipients theoretically had sufficient adherence sites to form an ordered mix with all the fine drug particles present as a stereometric monolayer (Table 32).

Table 32 Theoretical number of fine drug particles each coarse particle carries (D_N) at different concentrations compared with saturation number of each carrier particle (S_N) according to equation 93.

% Drug Content	Emdex		Recrystallised Lactose		Dipac	
	D_N	S_N	D_N	S_N	D_N	S_N
0.5	106		183		106	
1	213	3,995	366	5,556	213	3,995
2	425		739		425	
5	1,133		1,910		1,133	
10	2,429		4,048		2,429	

The powder mixes composed of different proportions of drug and excipient particles were vibrated at a vibration acceleration of 2 G and frequencies ranging from 50 to 1000 Hz. The segregation tendencies of the different mixes following vibration was assessed from measurements of the sample coefficients of variation (Figures 105 to 107). In mixes containing Emdex and potassium chloride there was a marked increase in segregation when the drug content was increased from 0.5 to 1% (Figure 105). The intensity of segregation increased with decreasing vibration frequency. The segregation tendency of the vibrated Emdex mixes increased with increasing drug concentration to a maximum at 10%, and the vibration-

Figure 105. Relationship between vibration frequency, drug content and the segregation tendency of Emdex powder mixes. Acceleration force = 2 G, vibration time = 15 minutes. The different symbols are used for different drug concentration to facilitate interpretation of the three-dimensional area.

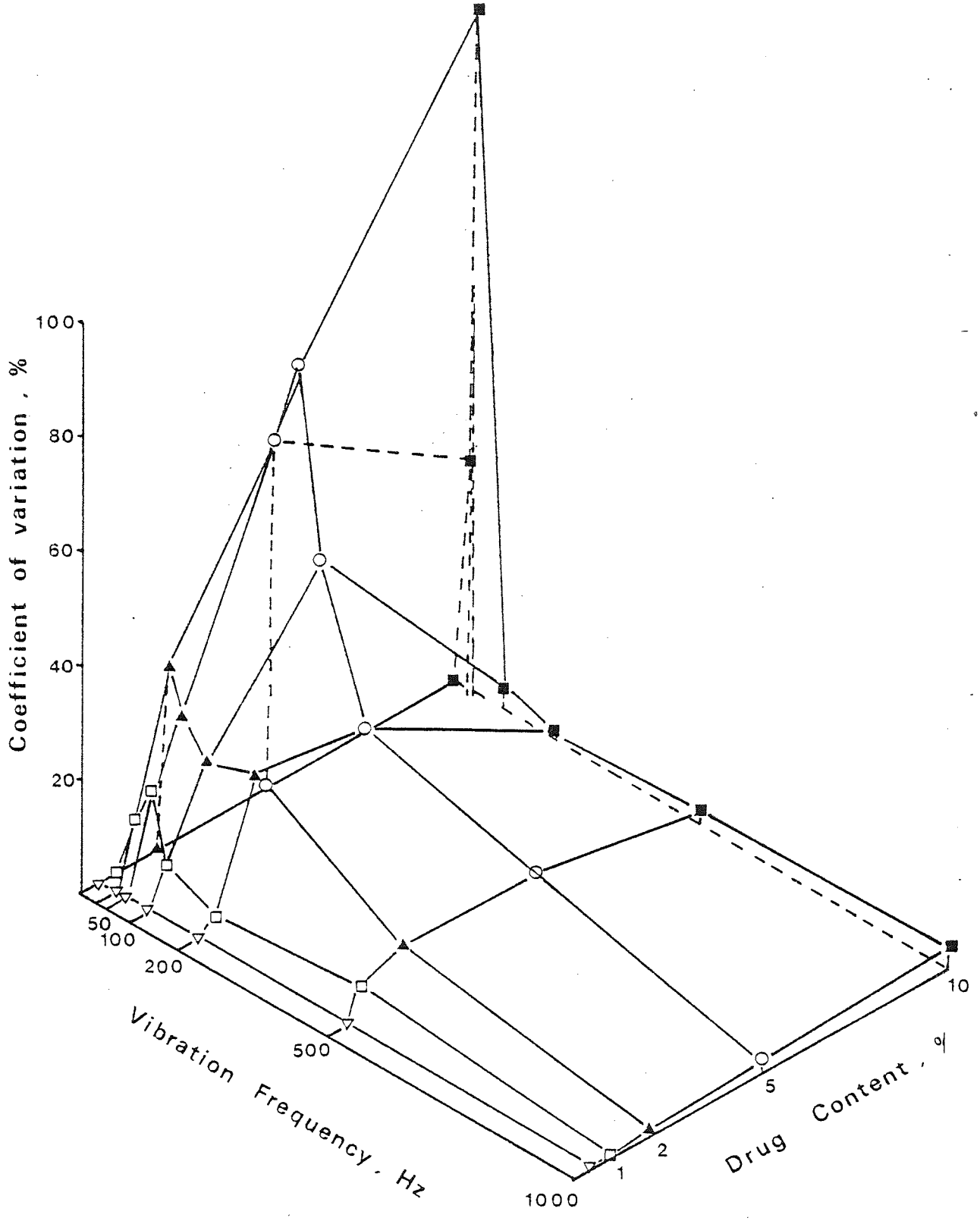

Figure 106. Relationship between vibration frequency, drug content and the segregation tendency of recrystallised lactose powder mixes. Acceleration force = 2G, vibration time = 15 minutes. The different symbols are used for different drug concentration to facilitate interpretation of the three-dimensional area.

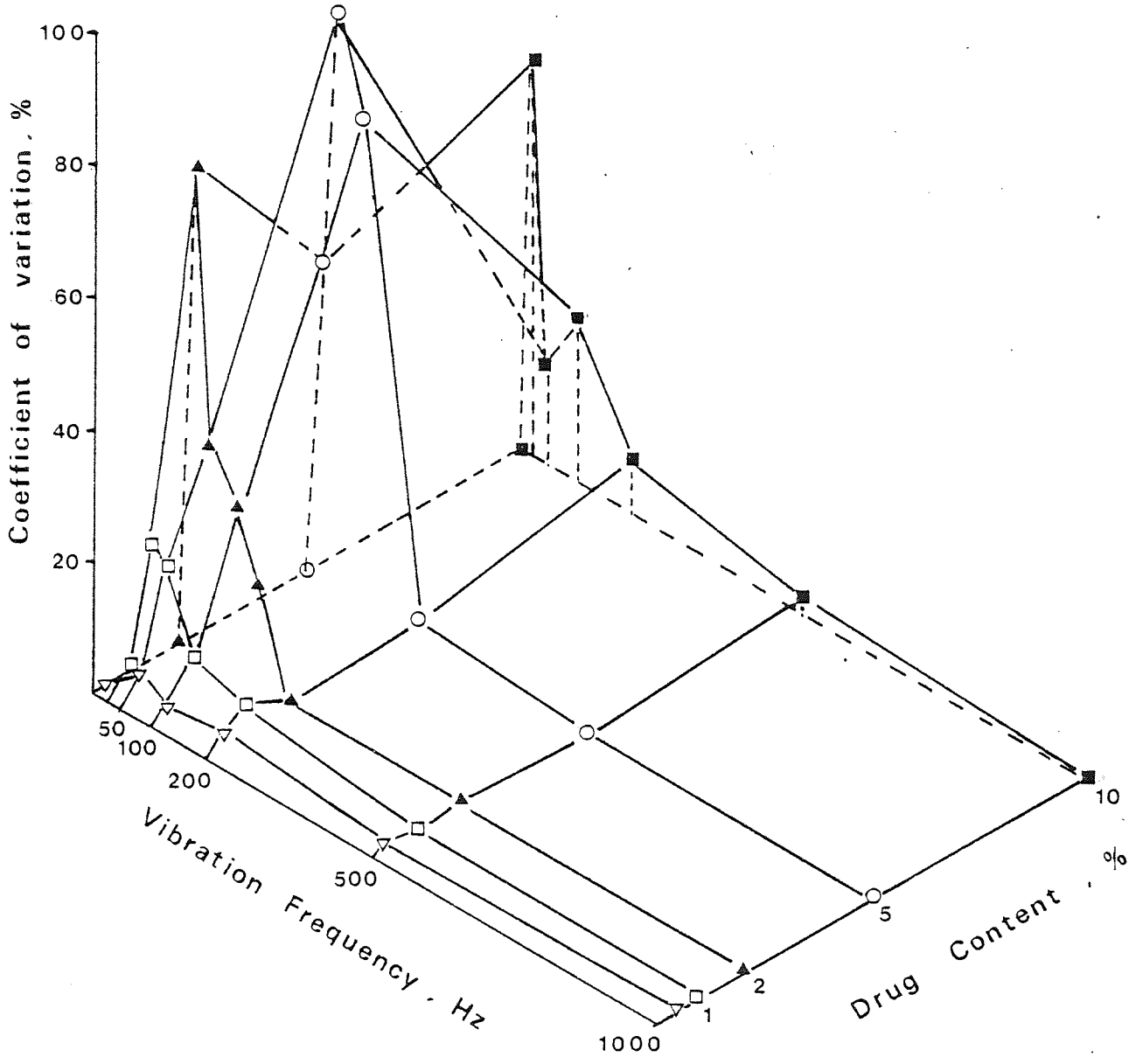

Figure 107. Relationship between vibration frequency, drug content and the segregation tendency of Dipac powder mixes. Acceleration force = 2 G, vibration time = 15 minutes. The different symbols are used for different drug concentrations to facilitate interpretation of three-dimensional area.

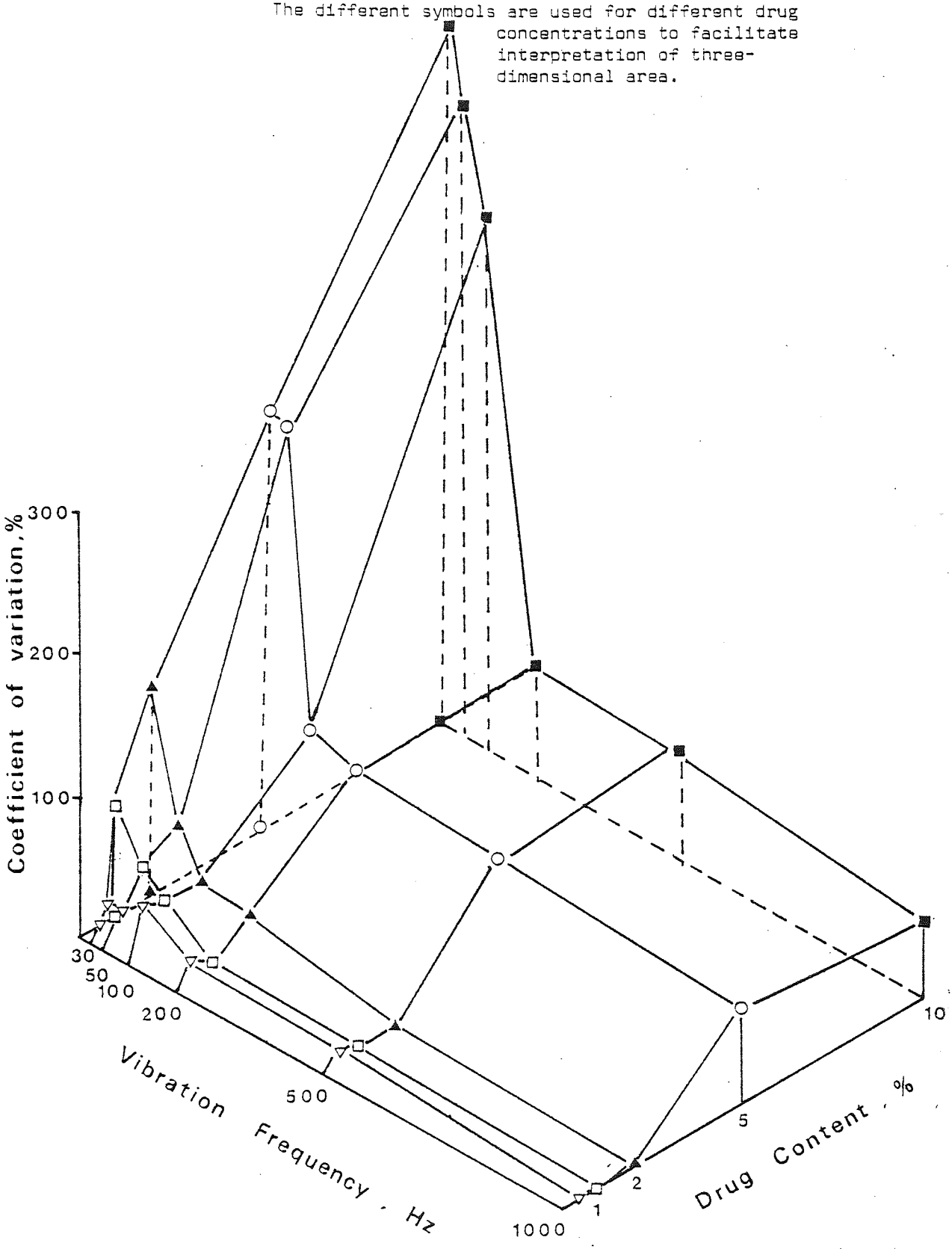

induced segregation was generally larger at low frequencies.

The three-dimensional curve representing the segregation of different drug concentrations mixed with recrystallised lactose excipient and vibrated at different frequencies is shown in Figure 106. As with the Emdex mixes, segregation increased with decreasing vibration frequency. There was also a marked increase in segregation in mixes containing up to 2% drug powder, but above this concentration the segregation pattern became complex in powders vibrated at low frequencies, and formed a plateau region at a coefficient of variation of 80-100%. This was the maximum segregation produced in mixes of recrystallised lactose and was considerably lower than the maximum coefficients of variation for vibrated Emdex systems. The coefficients of variation for the lactose mixes containing more than 2% drug, showed few large increases under any vibration conditions, and this may have been caused by the carrier particles losing the same number of adherent particles from both high and low drug concentration mixes. As the number of drug particles carried by each excipient particle increased, there was a fall in the actual percentage of adherent particles which became dislodged, unlike the Emdex particles which continued to lose increasing numbers of drug particles with increasing drug concentration.

The Dipac/potassium chloride mixes showed marked segregation for all drug concentrations and at all vibration frequencies (Figure 107). The lower vibration frequencies caused the most drug segregation and this became extreme in mixes containing 10% drug, vibrated at frequencies lower than 100 Hz. In all the excipient systems tested there was a distinct change in the amount

of segregation produced by vibration frequencies below 200 Hz and those above 200 Hz. Below 200 Hz the segregation became more marked. Nevertheless in Dipac mixes containing 5 and 10% drug, there was considerable segregation following vibration at 200, 500 and 1000 Hz. The drug adhering to Dipac particles showed a far greater tendency to segregate at high drug concentrations than that mixed with Emdex. Of the mixes with higher drug concentrations, recrystallised lactose appeared to allow the least segregation. The influence of different vibration frequencies on the segregation of mixes with increased drug concentrations was similar to that found previously in mixes containing only 0.5% potassium chloride. The low frequencies had the greatest effect on segregation; this is because the increased flight time, particle movement and abrasion lead to fine adherent particles becoming dislodged more easily and percolating more quickly through the powder bed, with the net effect of increased segregation. Table 32 showed that even at the highest drug concentrations the excipient particles were stereometrically capable of carrying all the drug particles. If all of these sites were "active" and formed adherence points for the fine drug particles, the coefficients of variation should have remained at similar low values for the different drug concentrations tested. The general increase in segregation with increasing drug concentration showed that only a small proportion of the excipient particle surfaces were suitable as adherence sites for formation of stable ordered mixes. The lower segregation intensity of recrystallised lactose mixes suggests that the more porous, rougher particle surfaces of this excipient are capable of forming more active adherence sites than the less porous Emdex particles.

The most intense and extreme segregation occurred in powders containing drug particles mixed with the relatively smooth Dipac particles.

4.3.3 Vibration in Pharmaceutical Processing Equipment

A system was developed to analyse the frequency and acceleration of vibrations produced by pharmaceutical process machinery during various stages of mixing and tableting, so that a comparison could be made with the vibration conditions producing segregation in the model systems studied previously.

An accelerometer was connected to a tunable band pass filter (type 1621, Bruel and Kjoer) which filtered out frequencies in the range 0.2 Hz to 20,000 Hz and passed on a specific pre-selected frequency to a precision sound level meter (type 2203, Bruel and Kjoer) which measured the corresponding vibration acceleration. An accelerometer with a permanent magnet attached to the base was used to measure the vibration frequencies and accelerations by placing the accelerometer on different flat metal surfaces of the process equipment, such as the tableting machine feed hopper, feed-frame and the main pressure roller bearings. Several different types of tableting machines were monitored, equipped with different quantities of punches and dies and rotating at different turret speeds. Accelerometers connected to the hopper and feed frame of a Manesty RD rotary tableting machine (Manesty Machines, Speke, U.K.) produced different vibration signatures (Figure 108). The hopper vibrated at two principle frequencies around 200 Hz and 2500 Hz with corresponding peak accelerations of 0.75 G and 2.5 G. There were also two broad-band vibrations around 50 Hz at 0.23 G and 800 Hz at 0.68 G. The tableting machine feed-frame vibrated less intensely at one main frequency around 3,000 Hz with an

Figure 108. Vibration signals measured on the hopper, O, and the feed frame, ▲ , of a Manesty RD tableting machine.

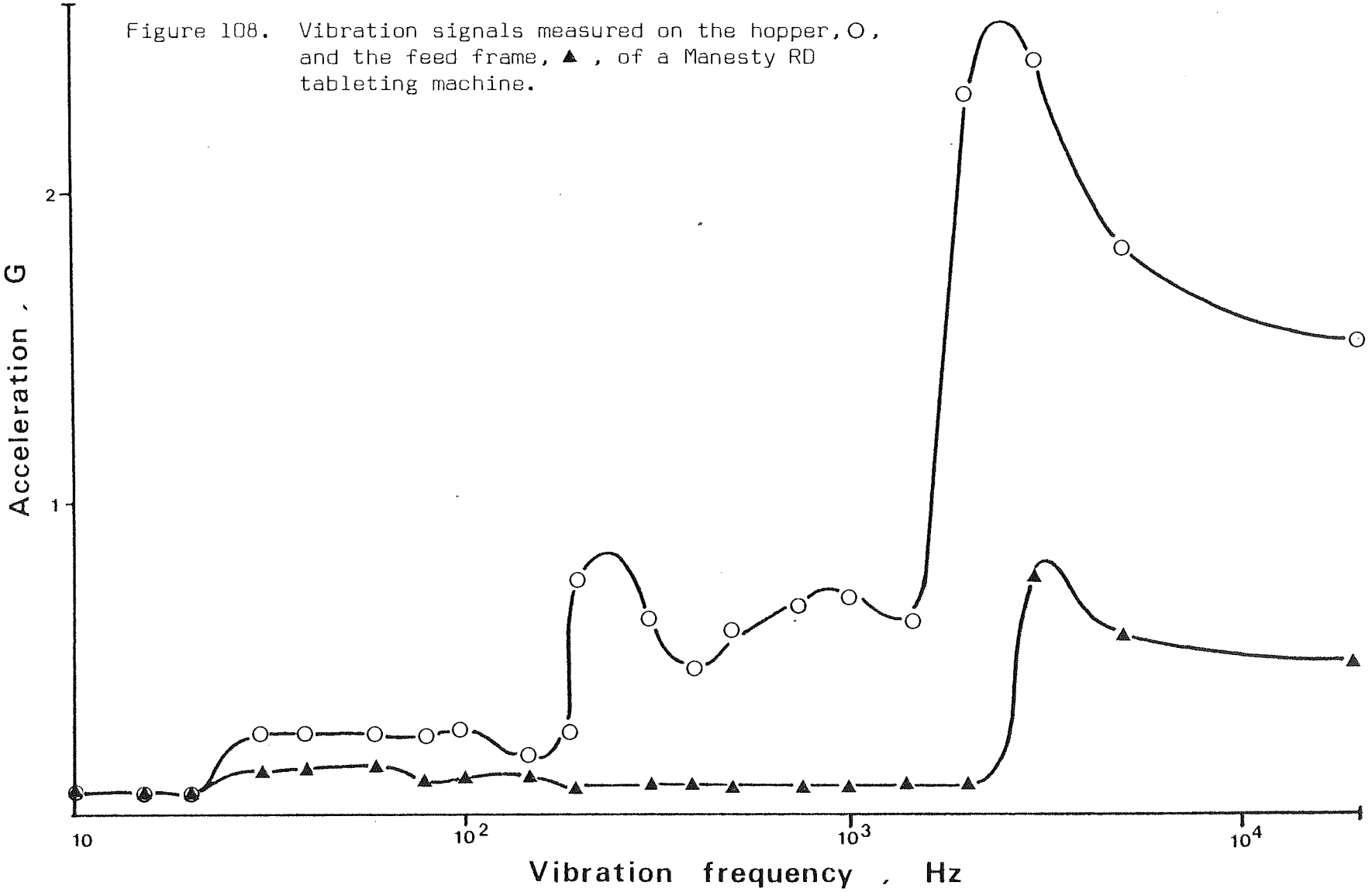

acceleration of about 0.8 G.

A similar difference in vibration measurements was found at separate points in a double station tableting machine with smaller diameter compression tooling (Manesty BB3B). Figure 109 shows the vibrations measured in the front feed frame and front hopper at different turret speeds with nine sets of punches and dies (one-third full tooling). The vibrations which occurred in the front hopper of the double rotary machine were found at two main frequencies: 150 Hz with 0.16 G acceleration and at 300 Hz with 0.12 G acceleration. The front feed-frame vibrated more intensely with a peak acceleration at 3000 Hz. At a turret speed of 18 r.p.m. this peak acceleration was 1.25 G. A similar high value occurred at 22 r.p.m., although there was a slight reduction in vibration frequency. A further increase in turret speed to 26 r.p.m. produced a vibration acceleration of 1.6 G at 2,000 Hz, and at 28 r.p.m. the acceleration increased to 3.2 G at the same frequency. These changes in vibration frequency and acceleration were caused by changes in the damped and un-damped oscillations of the tableting machine at different speeds, usually referred to as machinery rumble. Another change in the vibration signature of the tableting machine was produced by compressing tablets using a full complement of punches and dies (27 sets). The vibrations were measured on the rear hopper and feed frame of the double rotary (Figure 110). The hopper vibrated at one main frequency centred at 350 Hz with a maximum acceleration of 0.4 G. The rear feed frame vibrated strongly at three main frequencies: 9 Hz; 200 Hz and 5,000 Hz with corresponding accelerations of 0.6 G, 4.5 G and 2 G.

Figure 109. Vibration signals measured on the front hopper at 18 r.p.m. ▲ , and on the front feed-frame at 18 r.p.m., ○; 22 r.p.m., ▼ ; 26 r.p.m., □ ; and 28 r.p.m., ■ of a Manesty BB3B rotary tableting machine with 9 sets of punches and dies.

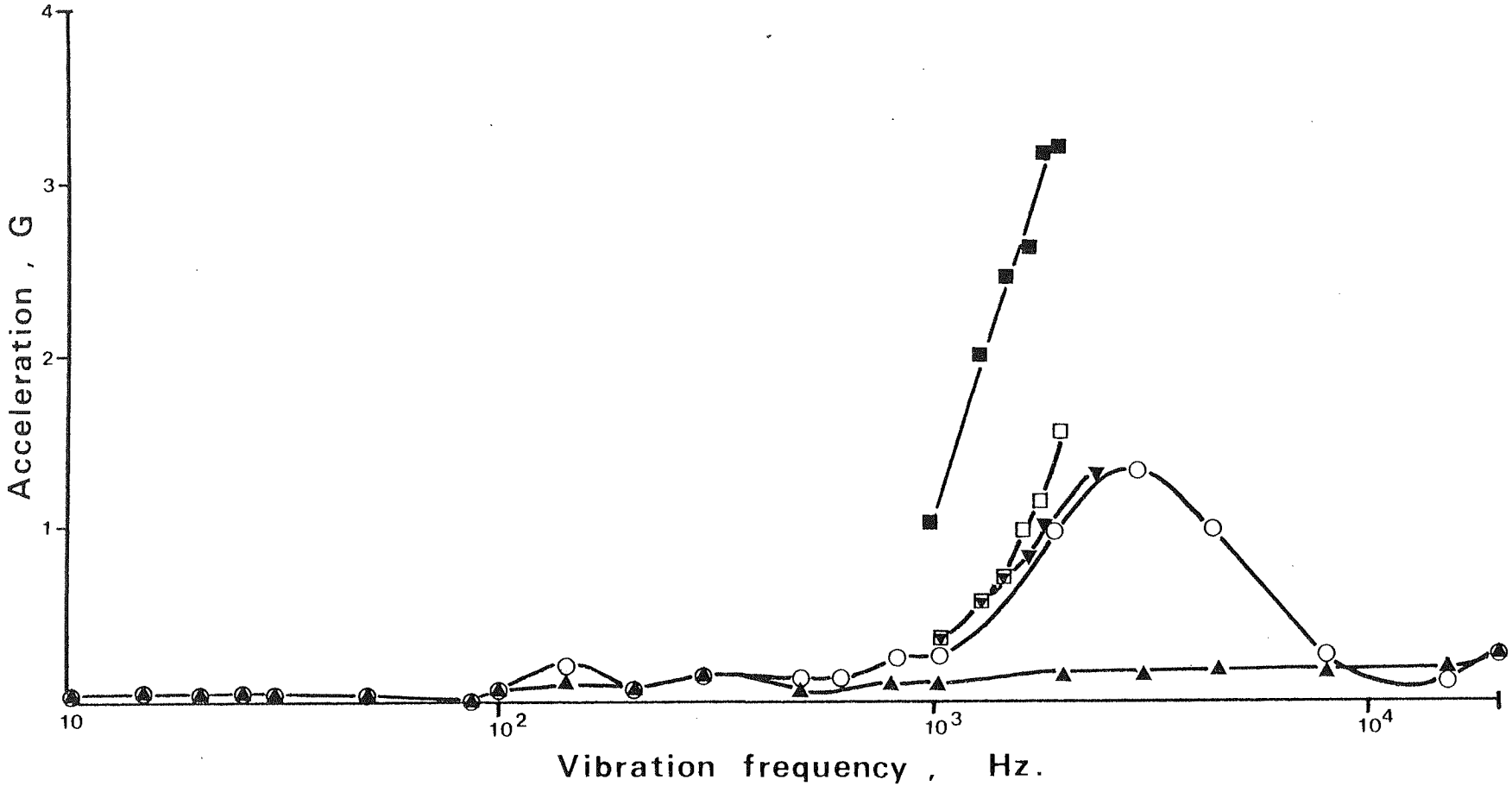

Figure 110. Vibration signals measured on the rear hopper, □ ; and the rear feed-frame, ● of a Manesty BB3B rotary tableting machine with a complete set (27) of punches and dies.

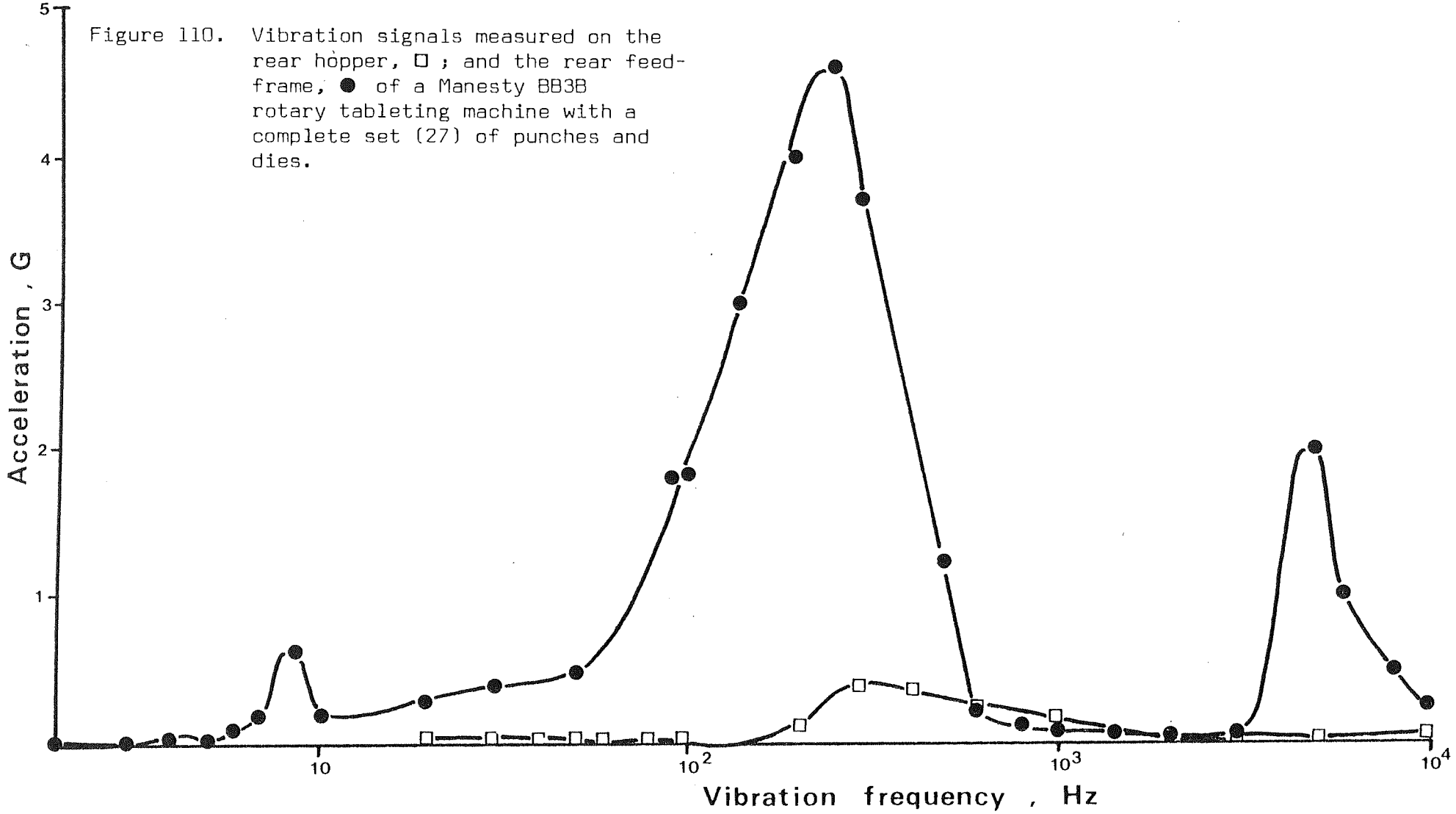

Figure 111. Vibration signals measured on the third hopper, ▼ and the upper main pressure roller bearing, O of a Manesty Layerpress rotary tableting machine.

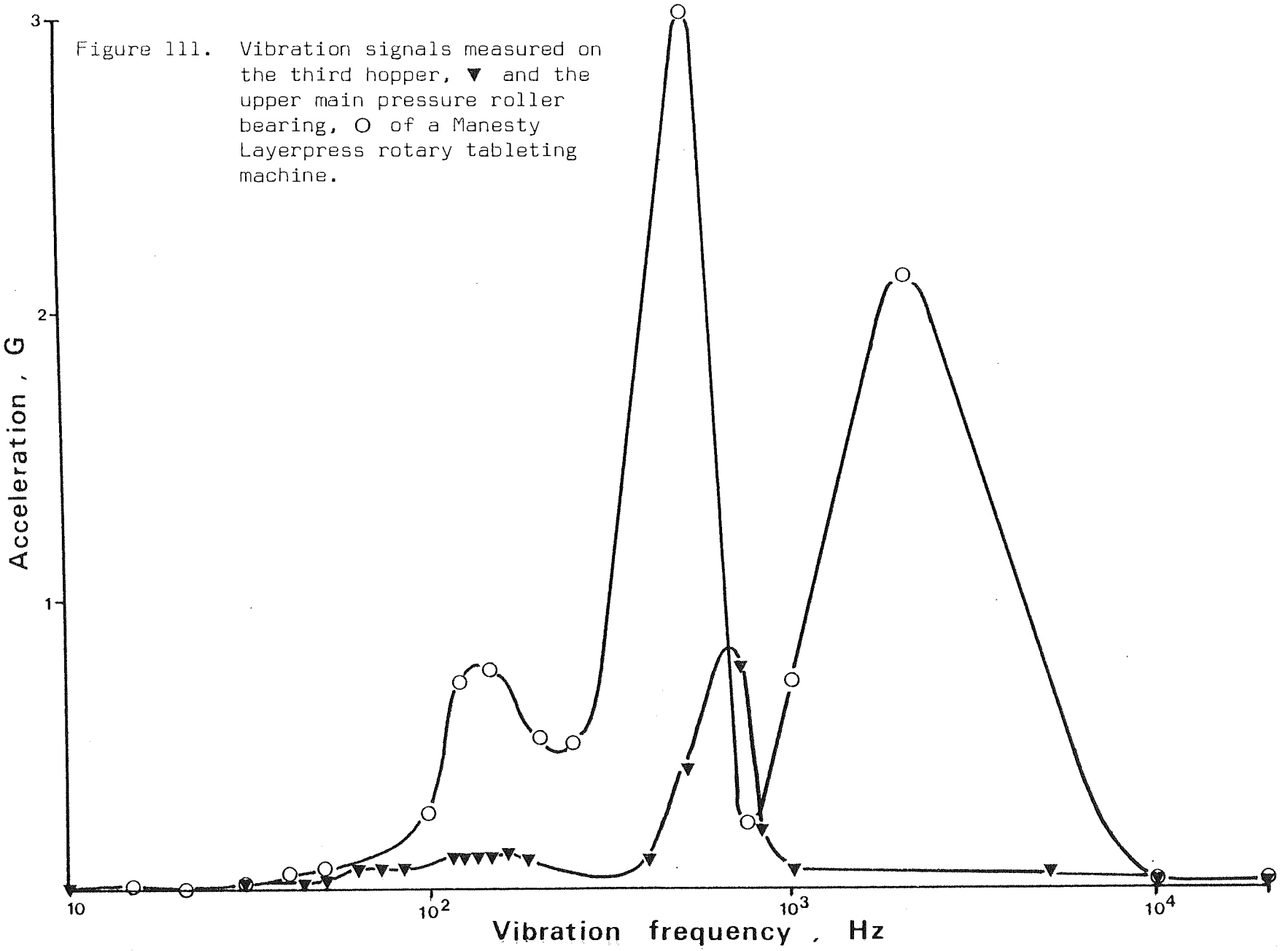

A third tableting machine capable of making layered tablets, was also tested (Manesty Layerpress). The tableting machine had two pre-compression stages and a single final compression stage. Vibration measurements were made on the top main pressure roller bearing (close to the force-feeding unit) and on the third hopper feeding the last layer before final compression (Figure 111). The hopper vibrated at two principle frequencies around 100 Hz with an acceleration of 0.25 G and at 700 Hz with an acceleration of 0.8 G. The pressure roller bearing vibrated at three main frequencies, 150 Hz, 500 Hz and 2,000 Hz with vibration accelerations of 0.78 G, 3 G and 2.1 G respectively.

In addition to the different tableting machines, a powder mixer, the Nauta mixer, was also tested (Nautamix Co., Haarlem, Holland). Vibrations on the bottom mounting frame were measured. Figure 112 shows the vibrations produced with the mixer half-full

Figure 112. Vibration signals measured on a Nauta mixer half-filled, ▲ and completely filled, ○ with dry powder.

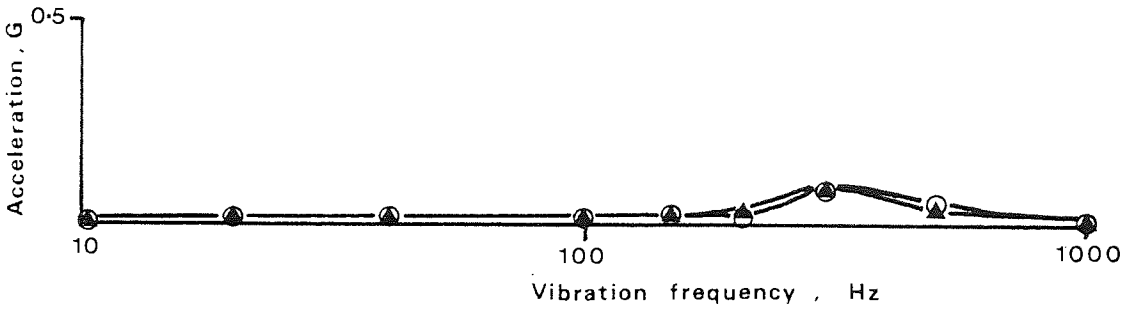

and fully charged. The charge-size made little difference to the vibrations which consisted of a single frequency at 300 Hz with an acceleration of 0.1 G.

Although the Nautamixer was virtually vibration-free, several of the tableting machines had points on the hopper or feed-frame

which vibrated at frequencies and accelerations within the range previously tested in the model system. Both the hopper and the feed-frame are points at which powder mixes are particularly susceptible to segregation. The model systems showed that drug and excipient powder mixes had segregation tendencies which were increased by combinations of low-vibration frequency and high acceleration such as those found in the rear feed-frame of the Manesty BB3B (Figure 110) and on the top pressure roller bearing of the Manesty Layerpress (Figure 111). Despite the segregation produced when some powder mixes are vibrated, vibratory force-feeders are still frequently used to promote powder discharge from bins and bulk hoppers (227, 228, 229). The results obtained in the present study demonstrate that the vibration conditions produced by all types of pharmaceutical machinery should be examined in relation to their potential effect on the powder systems being processed. In particular, various types of tableting machine produced vibration conditions in the range previously shown (section 4.3.2) to cause segregation of several different ordered mixes.

4.4 General Discussion

All of the different powder mixes showed the greatest segregation tendency when subjected to low frequency vibration. Segregation at any particular frequency was also intensified by increased acceleration. The velocity and power of vibration were also linked to segregation tendency but other characteristics such as displacement, energy and inertia of vibration appeared to have less influence on the segregation of ordered powder mixes. Interpretation of the results indicated that percolation of free fine drug particles was the predominant segregation mechanism.

The percolation mechanism only affects free drug particles and the largest observed effect was in the mobile layer close to the powder surface, although in more violent vibration conditions, drug particles percolated to the base of the powder bed.

Vibration at certain low frequencies and intermediate acceleration forces, caused upward movement of free fine drug particles by a mechanism of diffusional segregation. There was no evidence that movement of ordered units caused marked segregation. Increasing vibration time caused an increase in the distance which particles percolated or diffused. The distances through which particles moved were also affected by resonance effects produced in the vibrating powder system at certain frequencies. Resonance formed nodes and anti-nodes in the cylinder which produced horizontal vibrations at some points in the powder bed, causing churning or densification. In the areas of the powder where churning occurred, particle abrasion caused increased constituent segregation and the free drug particles percolated distances which were sometimes reduced by closely-packed sections of the powder bed, densified by the resonance effects. From calculations of the scale of segregation and the deviation of individual sample concentrations from the mean value for the powder bed, it was shown that both long-range and short-range segregation occurred in most of the vibrated powders. Even in powders where the segregation intensity was very low there was some particle movement producing long-range segregation effects.

The different excipients showed different segregation tendencies when mixed with the model drug particles. In all vibration conditions,mixes of drug with the coarse excipient, Dipac were most susceptible to segregation. Mixes containing

Emdex or recrystallised lactose appeared to have much lower segregation tendencies and were virtually unaffected in most vibration conditions. Since each of these three excipients had similar particle size distributions, differences in segregation tendency were not dependent on particle size differences of the ordered units. Particle size only influenced segregation after the fine drug particles became dislodged from the coarser carrier particles, and under these conditions, the segregation mechanisms appeared to be similar to those associated with segregation of random mixes. Percolation of the fine drug particles also increased with increasing carrier particle size, probably due to a reduction in bulk density of the bed producing large interparticle voids. The main factor opposing segregation was adherence of the fine drug particles to the coarse carrier particles. The theoretical number of fine particles capable of adhering to carrier particles as a monolayer was not a useful description of the ability of excipients to form stable ordered mixes, since Dipac, Emdex and the recrystallised lactose could each carry similar numbers of particles and at 0.5% drug concentration there were many more theoretical sites than fine drug particles available to occupy them. This suggested that only a small proportion of the total particle surface was involved in forming "active" adherence sites. These areas of active adherence are presumed to include surface discontinuities such as large pores, surface asperities or the accessible areas associated with these regions. The theoretical volume of the potassium chloride particles was 0.52 ml. g^{-1} compared with pore volumes of 0.1 $ml.g^{-1}$ for Dipac, 0.64 $ml.g^{-1}$ for Emdex and 1.25 $ml.g^{-1}$ for recrystallised lactose particles. Each of the excipients thus had a large enough pore volume to entrap

all the fine drug particles which formed only 0.5% by weight of the total mix. It is assumed that only a small proportion of the total pore volume will be suitable to form active adherence sites, therefore excipient particles such as Emdex and Lactose which have high pore volumes will also have a greater number of active adherence sites than the relatively less porous Dipac. The increased segregation which occurred in Emdex mixes containing drug concentrations above 0.5% may have been caused by saturation of the active sites with adherent drug particles, free fine drug particles would then have produced segregation by one of the mechanisms described in section 4.3.2. In contrast the lower segregation tendency of recrystallised lactose at high drug concentrations may have been due to the much larger accessible pore volume of these carrier particles than either Dipac or Emdex, producing a concomitant increase in the number of active adherence sites. Fine particles occupying pores would be more strongly adhered to the carrier due to a larger surface area of contact with the excipient particle. The role of surface asperities in forming ordered mixes (84) was less important than other factors since Emdex particles were less rough than those of Dipac and yet the latter allowed more segregation of drug particles. The moisture content of the excipient particles appeared to be unimportant for the formation of a stable ordered mix. Recrystallised lactose had a low moisture content as did Dipac powder, whereas Emdex had a higher percentage moisture. The segregation tendency of Emdex mixes was unaffected when the moisture content of the powder was reduced.

Stephenson and Thiel (225) also found that changes in moisture content did not affect the formation of ordered mixes despite

possible changes in the forces responsible for stabilising the mixes. In the systems studied here the moisture contents were sufficiently low for all the ordered mixes to have been stabilised by combinations of van der Waals and electrostatic forces (226).

The mixing time required to form ordered mixes was found by others to be generally about 15 minutes (70, 72, 84, 132, 225). However in the systems studied here, different mixing times were required to form ordered mixes of 0.5% drug and the various excipient powders. It was found that Emdex and recrystallised lactose formed perfect ordered mixes after about 30 minutes mixing, whereas Dipac required almost 120 minutes. This apparent relationship between the stability of an ordered mix and the mixing time extended to ordered mixes formed between higher concentrations of drug and excipient. Ordered mixes containing 10% drug and excipient took 540 minutes to form with Dipac which had an extreme segregation tendency; 310 minutes with Emdex which also produced marked segregation and only 180 minutes for recrystallised lactose which segregated least. A similar pattern emerged for the intermediate drug concentrations. The increased mixing time which was required to form ordered mixes may be related to the surface electrical activity of the different excipients, as well as to other surface properties such as porosity. Powders which have few large surface pores to entrap drug particles will require a much greater surface electrical charge to hold adherent particles on the surface. This electrostatic charge could have been built up triboelectrically, by interparticle friction or friction of particles against the mixer surface. Some triboelectric charging will occur during mixing of powders in the Y-cone blender, thus a prolonged mixing time may have

allowed the relatively smooth Dipac particles to acquire an increased surface charge. This could also apply to Emdex, the particles of which were insufficiently porous to trap the large numbers of fine particles present when mixed with the higher concentrations of drug.

The amount of segregation found in the different drug/ excipient mixes varied according to the vibration conditions. Combinations of low vibration frequencies, 20, 30, 50 and 100 Hz with high accelerations, 2.25 and 3 G caused the greatest segregation of different ordered mixes. Vibration frequencies and accelerations were shown to be comparable to the vibrations measured in different tableting machines during the routine production of pharmaceutical tablets. In order to reduce or prevent segregation of ordered mixes it was shown to be desirable to minimise or eliminate non-random vibrations.

Chapter 5

Determination of Interparticle Forces in Powder Mixes*

The ability of excipients such as Emdex, recrystallised lactose and Dipac to form ordered mixes and the stability of those mixes when subjected to different vibration conditions described in the previous chapter, was attributed to the strength of the surface adhesive forces between different particles.

A method was developed by Krupp (187) to determine the forces of adhesion of fine spherical particles to plane metal substrates. Krupp mounted a metal substrate, such as a gold or silver plate, covered in adherent fine metal spheres, vertically in a specially-modified ultracentrifuge rotor tube. Following rotation in an ultracentrifuge the number of metal spheres removed from the metal substrate was counted through a window in the specially constructed cell using a microscope.

A similar method and apparatus were also used by St. John and Montgomery (244) to measure the adhesion of gold and silver spheres to gold and silver plane substrates. A modification of these methods was used in the present study to determine the adherence of fine drug particles to coarse carrier particles.

5.1 Method

Because of the similarity between the microscopic appearances of both drug and excipient adherent particles and also in view of the rough surface of the coarse excipient particles, visualisation by microscope could not be used to determine the quantities of

---

*Practical work carried out with Prof. J. A. Hersey and Mr. F. K. Lai at V.C.P., Melbourne, Australia.

fine salicylic acid particles used as a model drug removed by ultracentrifugation. It was decided to use a chemical method to quantify the amount of drug removed from the carrier particles. Since the carrier powder could not be clamped in position like the plane metal substrates used by previous investigators, coarse particles with adherent fine particles (ordered units) were fixed to a scanning electron microscope stub using strong adhesive. The stub was then clamped in the measuring cell and the rotor was placed in an ultracentrifuge (Model L2-65B, Beckman Instruments, California, U.S.A.). Several types of strong adhesives were used to fix the carrier powder to the stubs, but none were able to withstand the extremely high forces exerted in the ultracentrifuge; consequently all the carrier particles were lost from the stub surface. An alternative method of retaining the ordered units during ultracentrifugation was developed using the following modification of a technique used by Donald (196).

Figure 113 shows the final design of the measurement cell used to quantify the forces of adhesion in ordered powder mixes. The specimen sample from the ordered mix was placed in the holder hemisphere of the split sphere and the screen was placed over the powder (Figure 113a). The collector hemisphere was then screwed on to the holder hemisphere and the complete split-sphere was placed in the perspex cradle located at the bottom of the ultra-centrifuge tube. The position of the split-sphere was adjusted in the cradle so that the screen was normal to the axis of rotation when the ultracentrifuge tube was placed in the rotor (Beckman model 40.2) shown in Figure 113b. The perspex top unit was fitted over the split-sphere and the ultracentrifuge tube cap tightened on with a torque wrench. The securing screw was then screwed down on to the split-sphere to keep it in position during ultracentrifugation.

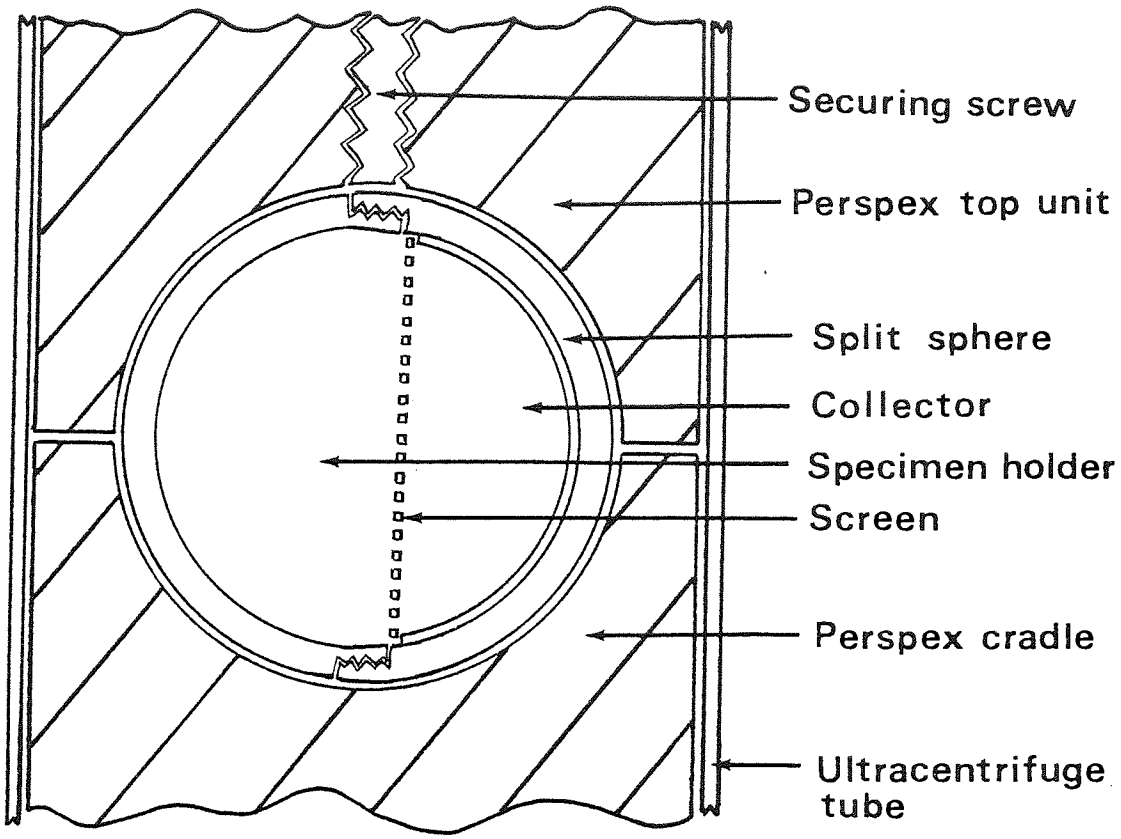

Figure 113(a) Detail of the split sphere arrangement used to hold powder samples in the ultracentrifuge rotor.

Figure 113(b) Diagram showing location of the specially-modified ultracentrifuge tube in the ultracentrifuge rotor assembly.

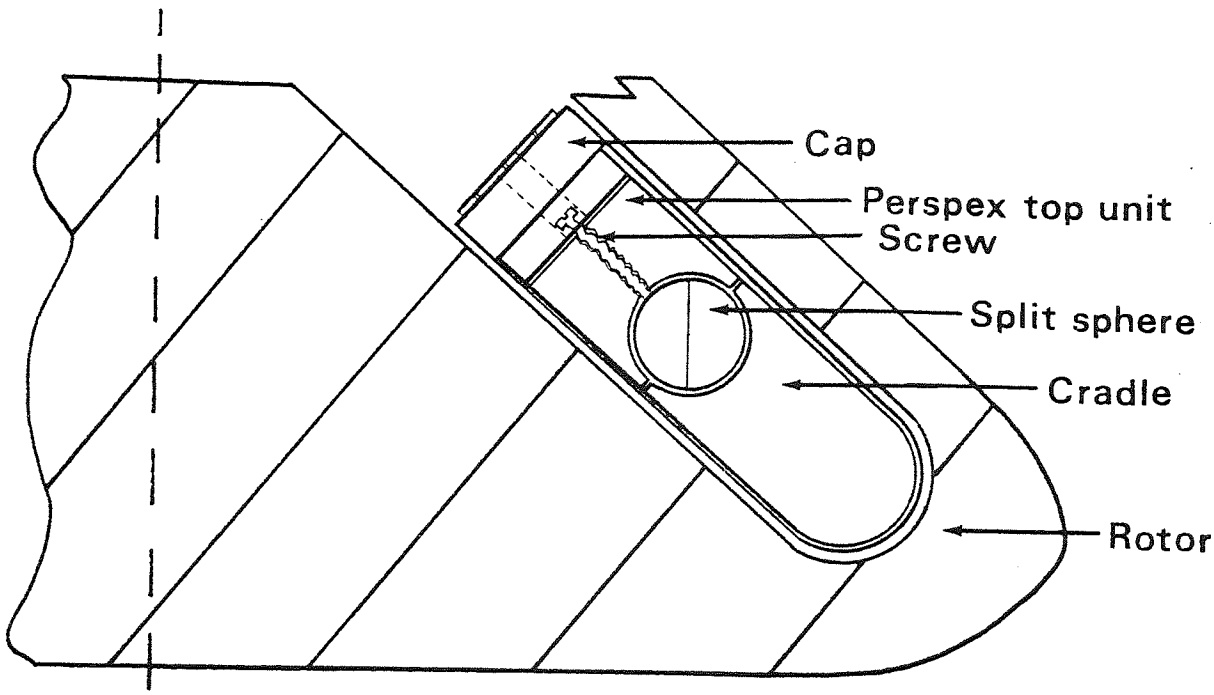

The assembled modified ultracentrifuge tube was placed in the rotor and aligned so that the screen was perpendicular to the angle of rotation with the collector hemisphere facing outwards (Figure 113b).

During ultracentrifugation the ordered mix in the specimen holder was forced against the 50 μm wire mesh screen which was fine enough to retain the smallest ordered units but coarse enough to let any fine drug particles removed from carrier particles through into the collector hemisphere. The rotor was maintained at the desired run speed for one minute. This was found by experimental trials to be long enough to allow all the fine particles to travel through the sieve mesh once they were dislodged by the forces exerted during ultracentrifugation.

Following ultracentrifugation, the tube was removed from the rotor, the cap was taken off and the perspex top carefully lifted out without disturbing the split sphere. A glass rod with double-sided adhesive tape on one end was used to remove the split sphere from the perspex cradle. The specimen holder and screen were then unscrewed from the collector hemisphere which was washed out into a volumetric flask using an aqueous solution containing 50% absolute alcohol to dissolve any salicylic acid particles which had been dislodged from the carrier particles and passed into the collector hemisphere during ultracentrifugation. Because the quantities of salicylic acid to be analysed were minute, a high resolution ultraviolet spectrophotometer was used (Cary 118, U.S.A.). This instrument allowed absorptions in the required spectral band to be analysed to four places of decimals. The slit width of the spectrophotometer was adjusted automatically and the analysis period was 0.1 seconds with a useful absorption range of 0 to 0.1. Quartz cells were used to hold the analysis samples and these were

balanced internally from manual settings. The absorbance of specimen samples was measured at a wavelength of 300 nm. For each ultracentrifuge experiment approximately 12 mg of the selected ordered mix containing the "drug" (salicylic acid) and excipient was used. This quantity of powder sample was the largest mass suitable for introduction into the specimen holder without causing blockage of the sieve mesh or prolonging the time taken for dislodged particles to travel through the apertures of the screen. The different powder samples were spun at ultracentrifuge rotor speeds of 2,500; 5,000; 10,000; 15,000; 20,000; 25,000 and 30,000 r.p.m.

The spin speeds were controlled automatically by the ultracentrifuge to within ± 1% of the recorded setting from 10,000 r.p.m. to 30,000 r.p.m. and within 100 r.p.m. from 5,000 r.p.m. to 10,000 r.p.m. These rotor speeds corresponded to known separation forces acting on the ordered units in the specimen cell as listed in Table 33:

Table 33 Relationship between rotor speeds and the forces acting on ordered units in the specimen cell

Rotor Speed (r.p.m.)	Relative Centrifugal Force (R.C.F.) (G)	Force Field ($N.g^{-1}$)
2,500	365.4	0.36
5,000	1461.6	1.43
10,000	5846.4	57.29
15,000	13154.4	128.91
20,000	23385.6	229.18
25,000	36540.0	358.09
30,000	52416.4	513.68

In terms of earth's gravity, the relative centrifugal force (R.C.F.) or number of times gravity acting on the ordered units was calculated from the following equation:

$$R.C.F. = \omega^2.r'/980 \qquad (98)$$

where ω was the angular velocity given by:

$$\omega = \pi / 30 \times \text{rotor speed (r.p.m.)} \qquad (99)$$

and r' was the distance of the ordered unit from the axis of rotation. The increasing forces acting on the ordered units with increasing rotation speeds separated different numbers of drug particles according to the force and the drug excipient mix being tested. The adhesion forces which must have existed between the drug particles and the carrier to resist separation from ordered units under the influence of different removal forces (Table 18) were calculated.

5.2 Results and Discussion

The concentration of drug particles removed from ordered units was related to the speed at which the samples were rotated. The amount of drug particles remaining adhered to the carrier particles was calculated as a percentage of the total drug concentration in the original ordered mix and was related to the force of adhesion between drug and excipient particles.

5.2.1 Interparticle Forces in Ordered Units of Microdose Preparations

An ordered mix of 1% salicylic acid was made with each of several excipients, including Dipac, Emdex and recrystallised lactose powders. In addition to the excipients tested previously,

another powder was used, sucrose (CSR, Victoria, Australia). Ordered mixes of sucrose with salicylic acid (66, 67, 71, 72, 74, 82) and of sucrose with other model drugs (70, 84) have been widely reported in the literature, and it was desired to compare the forces stabilising these ordered mixes with those formed with the other three excipients tested, Emdex, recrystallised lactose and Dipac. The sucrose grade used consisted of crystals with a particle size range of 420 to 625 µm, which was slightly coarser than most of the other excipients tested. The sucrose crystals were flat-faced, non-re-entrant cuboids and, despite being smooth surfaced, the sucrose crystals were theoretically unsaturated at a drug concentration of 1% fine particle salicylic acid. The mean particle radius of the salicylic acid powder was 2.5 µm (micronised by West Australian Institute of Technology, Department of Pharmacy). The ultracentrifuge rotation speeds used to examine the different powder mixes produced separation forces of up to 514 $N\,g^{-1}$ in the ordered units of drug and excipient particles. Under these extreme conditions, the drug and excipient particles in ordered units that remained intact following rotation at the maximum speed must have been bound together with forces of adhesion exceeding 1200 m.dyne (1.2×10^{-8} N). The following expression was used to calculate the adhesion force at any particular separation force or rotor speed (186):

$$F_{adhesion} = M_o.\omega.r' \qquad (100)$$

where $F_{adhesion}$ is the force of adhesion between adherent drug particles and excipient carrier particles; M_o, the mass of ordered units; ω, the angular velocity; r', the distance of the ordered units from the axis of rotation.

Figure 114 shows the relationship between the quantity of drug particles adhering to the sucrose carrier excipient particles and the force of adhesion. The median adhesion force where 50% of drug particles are bound to the surface of sucrose particles was approximately 300 m.dyne (3×10^{-3} N) and the amount of drug still adhered to ordered units at the maximum applied separation force of 514 N g^{-1} was 20%. The adhesion profile of sucrose and salicylic acid was very similar to that of recrystallised lactose containing 1% salicylic acid particles in an ordered mix (Figure 115). The median adhesive force of recrystallised lactose particles and salicylic acid particles was approximately 300 m.dyne (3×10^{-3} N) and the amount of drug particles bound to recrystallised lactose particles with adhesion forces exceeding 1200 m.dyne (1.2×10^{-2} N) was 20%. Figure 115 also shows the adhesion profile of 1% salicylic acid and Emdex ordered mixes. The median adhesive force of Emdex particles and salicylic acid particles was greater than 1200 m.dyne (1.2×10^{-2} N) and even at the maximum measurable adhesion force of 1200 m.dyne produced by applied separation forces of 514 $N.g^{-1}$, more than 60% of the fine drug particles were still adhered to Emdex carrier particles. The adhesion profile of Dipac and 1% salicylic acid ordered mixes differed from those produced by ordered mixes containing sucrose, recrystallised lactose and Emdex carrier particles (Figure 115). The shape of the adhesion force relationship for Dipac consisted of a curve with an initial parabolic section at low adhesion forces and a second curve-section which appeared to suggest an asymptotic approach to zero drug content. The Dipac particles and salicylic acid particles had a median adhesion force of 700 m.dyne (7×10^{-3} N) and the amount of drug particles bound to Dipac particles with adhesion forces

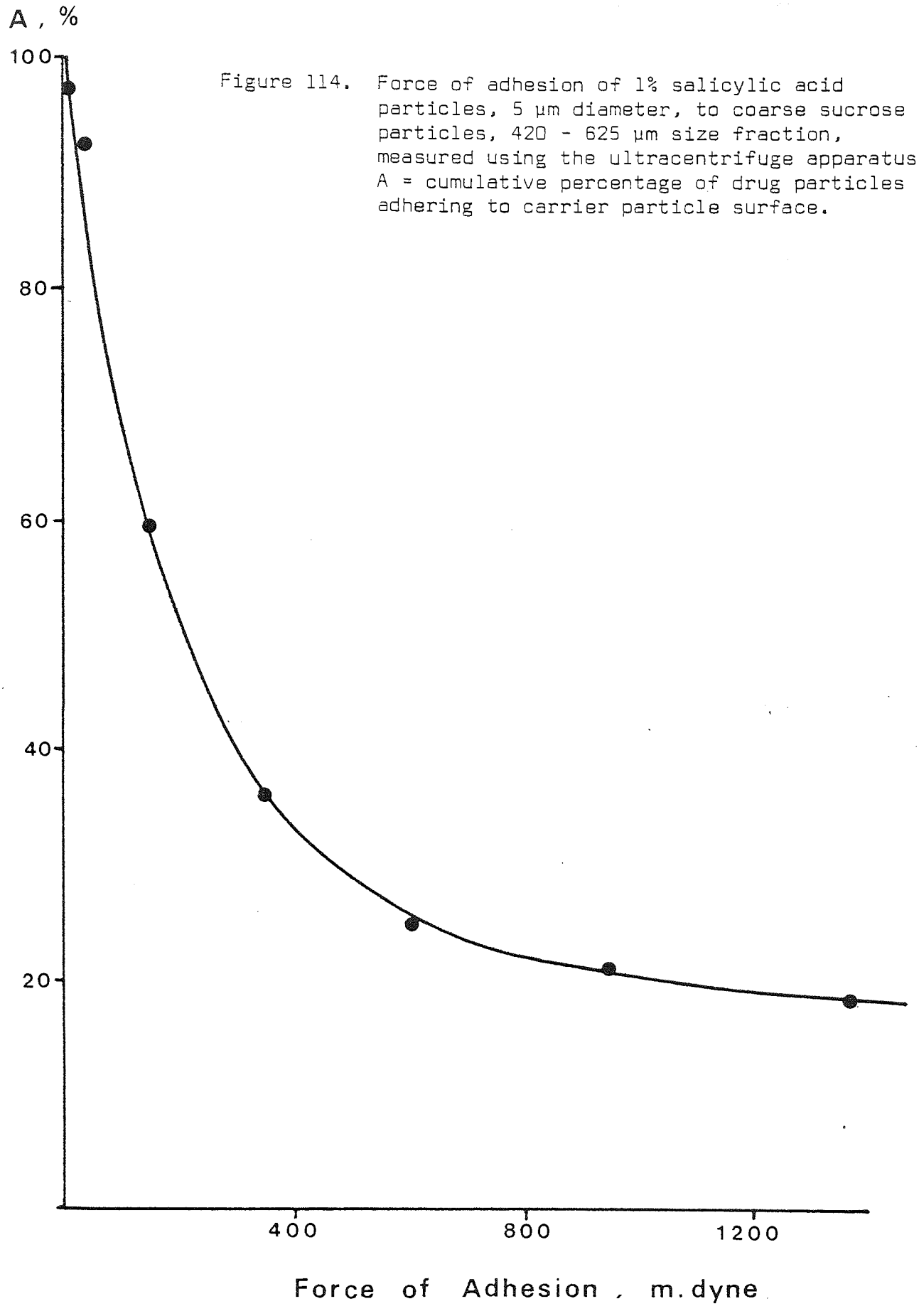

Figure 114. Force of adhesion of 1% salicylic acid particles, 5 µm diameter, to coarse sucrose particles, 420 - 625 µm size fraction, measured using the ultracentrifuge apparatus. A = cumulative percentage of drug particles adhering to carrier particle surface.

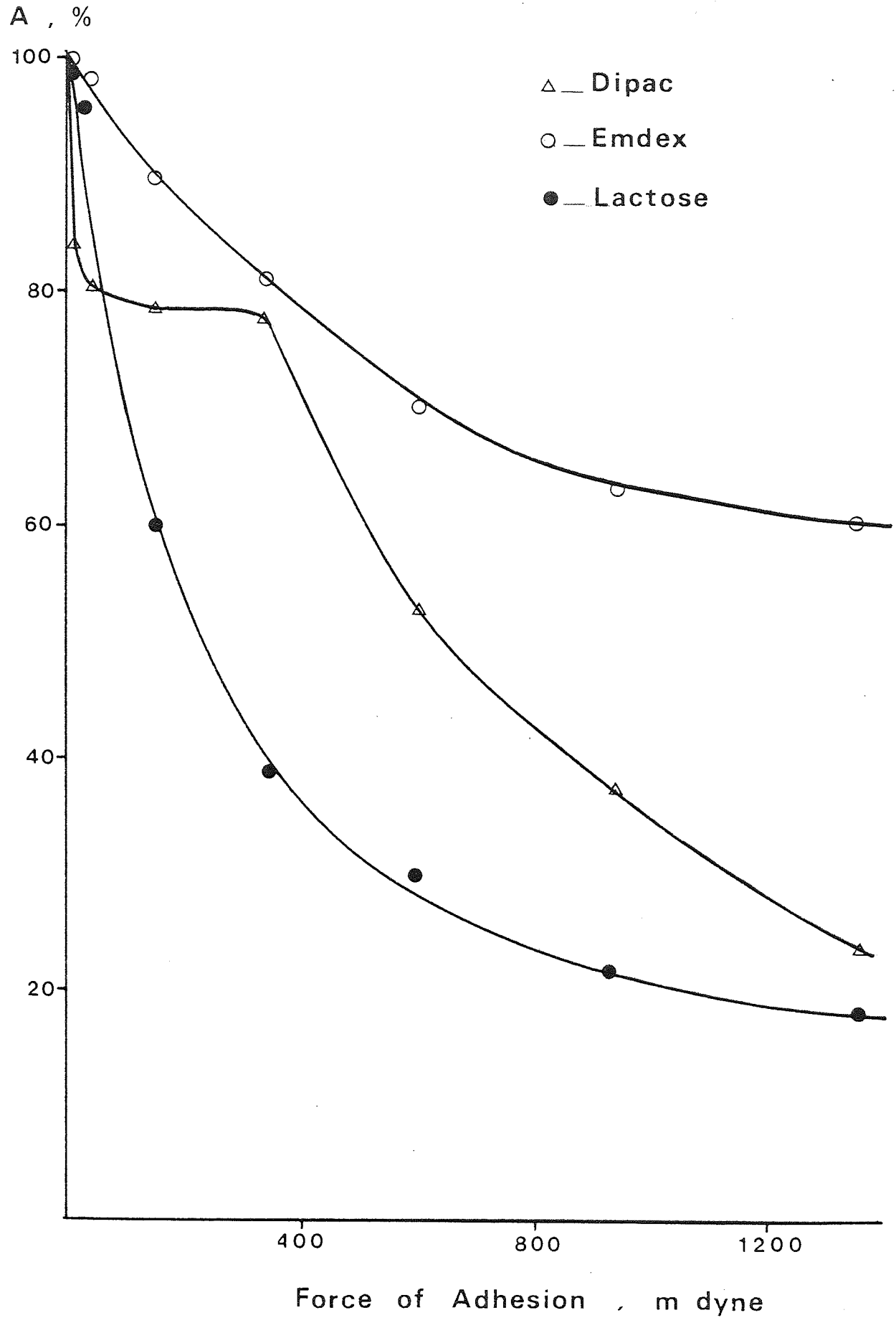

Figure 115. Force of adhesion of 1% salicylic acid particles, 5 µm diameter, to different excipient particles. A = cumulative percentage of drug particles adhering to carrier particles.

in excess of 1360 m.dyne was 25% of the total drug content. The first section of the adhesion profile showed an initial rapid loss of large amounts of drug particles from ordered units containing Dipac particles; about 20% of the fine salicylic acid contained in the ordered mix was separated from carrier particles by applied forces of removal less than 1.5 N g^{-1}. This low separation force corresponded to ordered units with drug and Dipac particles which were bound together by adhesion forces of less than 38 m.dyne. The same separation force of 1.5 N g^{-1} when applied to ordered mixes containing carrier particles of sucrose, recrystallised lactose and Emdex removed only about 5% of adherent salicylic acid particles.

Of the four ordered mixes containing different carrier powders, Emdex appeared to form the most stable ordered mixes with 1% salicylic acid and most ordered units appeared to be bound by strong adhesion forces. Since only 35% of the fine drug particles were adhered to Emdex carrier particles with forces less than 1360 m.dyne, large-scale constituent segregation of these ordered mixes would be extremely unlikely even at very high applied spearation forces such as those produced by intense vibration. However, ordered mixes containing 1% salicylic acid and Dipac lost about 20% of their fine drug particle content at very low separation forces and these salicylic acid particles would be free to move through a powder bed. This large amount of weakly held fine drug particle fraction could be responsible for the large constituent segregation tendency produced in ordered mixes containing Dipac particles, when subjected to different vibration conditions (section 4.3.2). The ordered mixes formed between 1% salicylic

acid and carrier particles of either sucrose or recrystallised lactose appeared to have an intermediate stability at low separation forces between the tightly bound ordered units containing Emdex and the larger proportion of weakly held drug and Dipac particles. The sucrose and recrystallised lactose systems had a lower median force of adhesion than either Emdex or Dipac. However the amount of drug remaining adhered to sucrose or recrystallised lactose carrier particles with a force larger than 1360 m.dyne (1.36×10^{-2} N) was less than the amount adhering to Emdex although similar to that of Dipac ordered mixes. The amount of initial drug loss from ordered units held together by forces less than 38 m.dyne (3.8×10^{-4} N) in sucrose and recrystallised lactose was less than in Dipac but similar to that in Emdex ordered mixes.

5.2.2 Effect of Drug Concentration

Ordered mixes containing 2% fine salicylic acid particles were made with sucrose, Emdex, recrystallised lactose and Dipac carrier particles and 5% salicylic acid mixes were made with Emdex, recrystallised lactose and Dipac. Each ordered mix was subjected to the same applied separation forces ranging from 0.36 N g^{-1} at 2,5000 r.p.m. to 513.68 N g^{-1} at 30,000 r.p.m. In several of the ordered mixes containing 2% salicylic acid, the adhesion profiles changed from those obtained for ordered mixes containing only 1% salicylic acid. Ordered mixes of 2% salicylic acid and sucrose carrier particles had an adhesion profile with an initial steep curve which subsequently became shallower and then formed a second differently sloping curve (Figure 116) which was similar to that found in the ordered mix of Dipac and 1% salicylic acid (Figure 115).

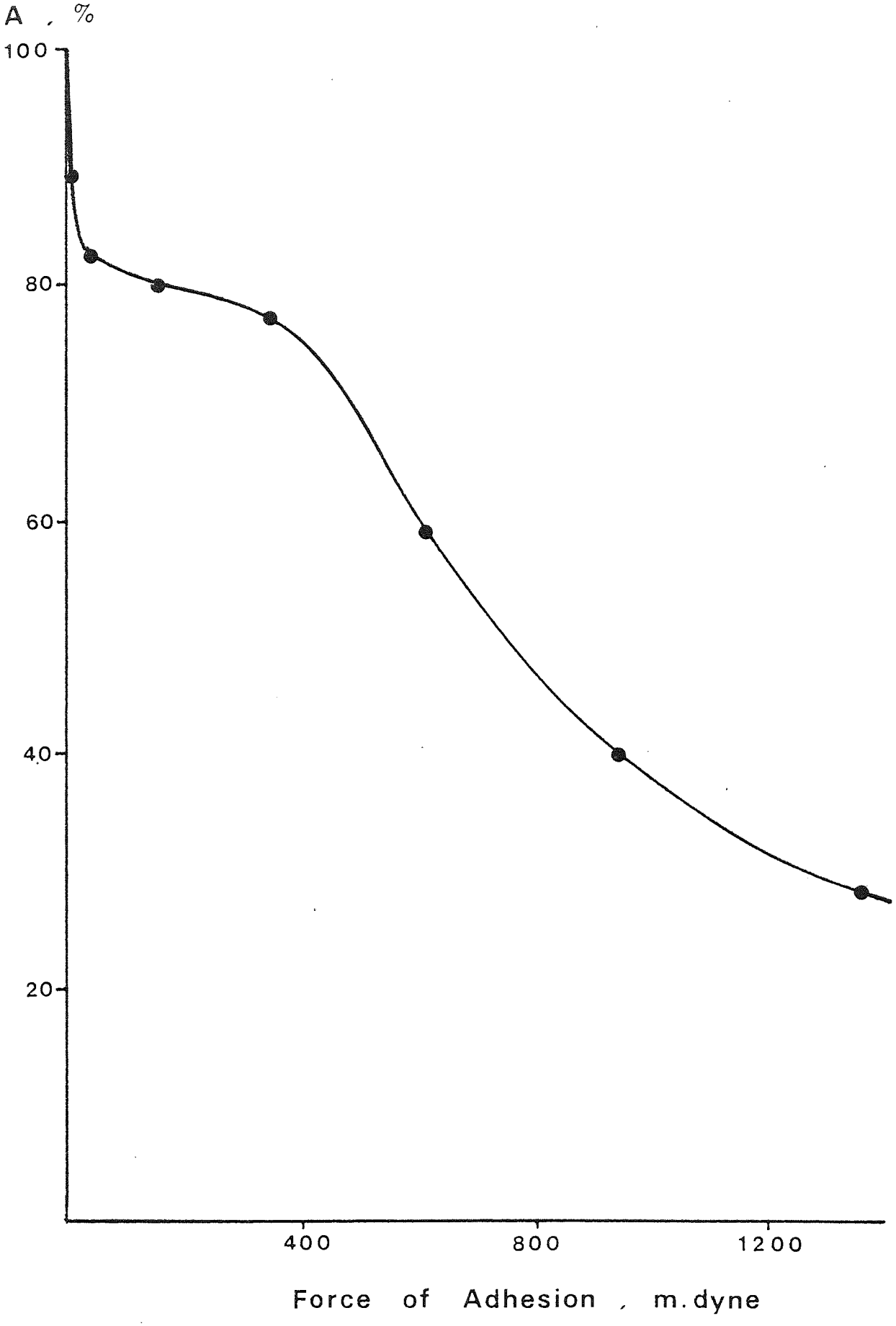

Figure 116. Force of adhesion of 2% salicylic acid particles, 5 µm diameter, to sucrose particles, 420 - 625 µm size fraction, measured using the ultracentrifuge apparatus. A = cumulative percentage of drug particles adhering to carrier particle surface.

The first steep section of the curve corresponded to the loss of large quantities of weakly-bound salicylic acid particles from the surface of the sucrose carrier particles. As with 1% salicylic acid and Dipac ordered mixes, the quantity of drug lost by sucrose particles was 20% of the total salicylic acid content and was removed by an applied separation force of less than 1.5 $N.g^{-1}$ which corresponded to a maximum adhesion force of only 38 m.dyne, for these loosely bound fine drug particles. In the second section of the curve, the slope was less steep than the one produced by an ordered mix containing 1% salicylic acid and sucrose, and the percentage of drug remaining adhered to the carrier surface at applied forces greater than 514 $N.g^{-1}$ was nearly 30% of the total drug content.

As with the sucrose/salicylic acid system, the ordered mixes of Emdex and 2% salicylic acid also appeared to contain a disproportionately high quantity of weakly bound fine drug particles dislodged from carrier particles by very low applied separation forces (Figure 117). An ordered mix of Emdex and 1% salicylic acid powder had only 1.8% of the total drug particle content adhered to carrier particles with adhesion forces less than 38 m.dyne. However, in powder mixes containing 2% salicylic acid the corresponding figure was nearly 9%. There was an associated decrease in the median adhesion force, from more than 1360 m.dyne in 1% drug/Emdex mixes to about 900 m.dyne in ordered mixes containing 2% salicylic acid. The amount of drug remaining adhered to Emdex carrier particles with adhesion forces greater than 1360 m.dynes decreased from 60% in ordered mixes containing 1% salicylic acid to 40% of the total drug content in mixes containing 2% salicylic acid. Although Emdex and 2% salicylic acid ordered

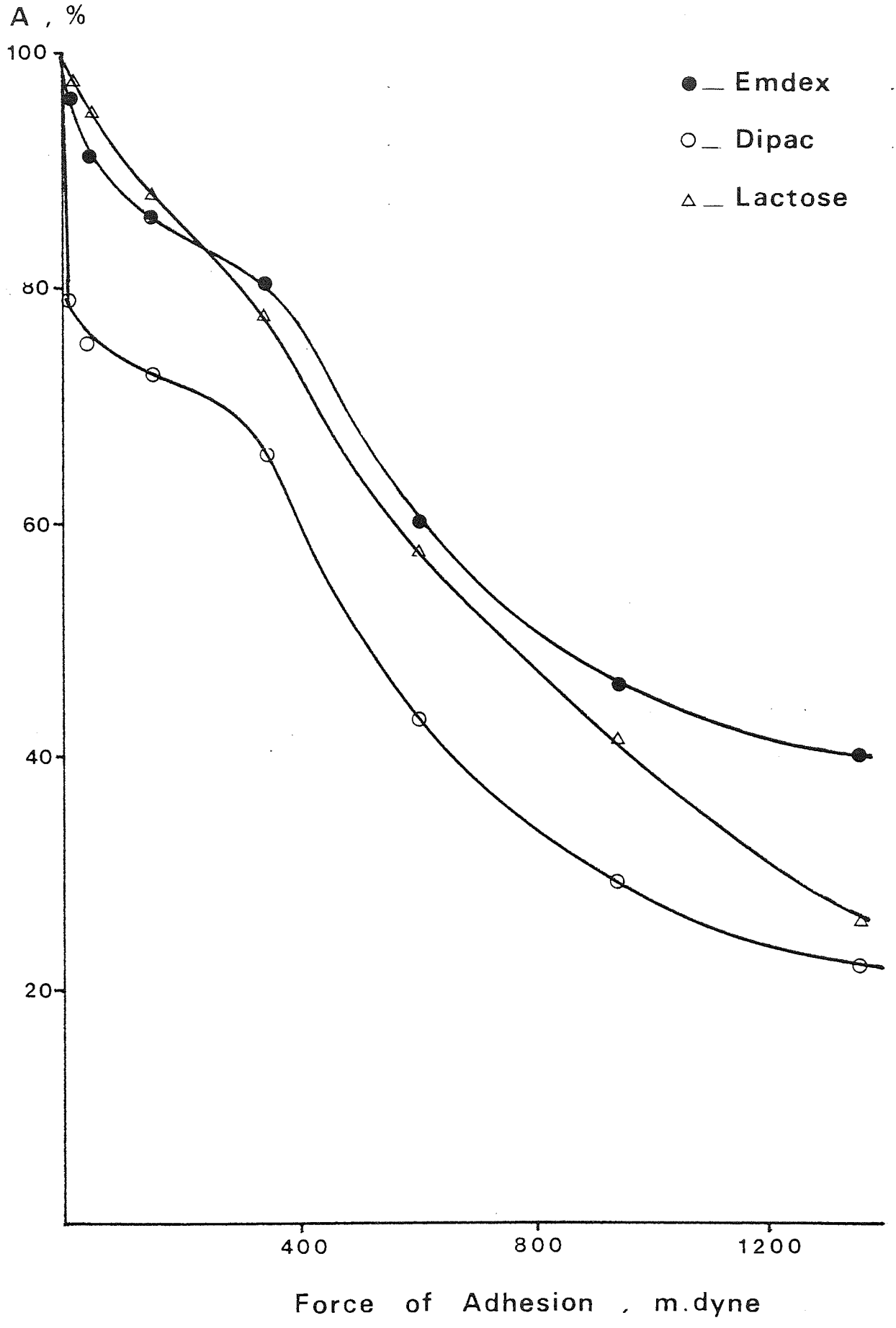

Figure 117. Force of adhesion of 2% salicylic acid particles, 5 µm diameter, to different excipient particles. A = cumulative percentage of drug particles adhering to carrier particle surface.

mixes displayed a similar adhesion profile to that found with Dipac and 1% drug, the particles of salicylic acid were less strongly bound to Dipac carrier particles than to Emdex (Figure 117). The increase in drug content to 2% salicylic acid powder in mixes containing Dipac caused a larger percentage of fine drug particles to be lost from the carrier particles at low applied separation forces. Between 25 and 30% of the fine salicylic acid particles were bound to Dipac carrier particles with adhesion forces of less than 38 m.dyne ($3.8\ N^{-4}$). As with ordered mixes made up of 2% salicylic acid and Emdex, the Dipac mixes showed a decrease in the median force of adhesion and a decrease in the amount of drug particles adhering to the carrier particles with forces larger than 1360 m.dyne, although this effect was less marked with ordered mixes containing Dipac carrier particles than those of Emdex.

Unlike the ordered mixes with increased drug content described above, 2% salicylic acid and recrystallised lactose showed only very slight evidence of a two-phase adhesion profile. The median force of adhesion increased from about 300 m.dyne to about 750 m.dyne in ordered mixes of 2% salicylic acid/lactose (Figure 117) and the amount of drug adhering to the recrystallised lactose carrier particles with adhesion forces in excess of 1360 m.dyne showed corresponding increase from 20% to about 30% of the total drug content. However, this latter trend did not continue in ordered mixes of recrystallised lactose containing an even higher concentration of 5% salicylic acid (Figure 118).

In these ordered mixes with 5% drug content, the recrystallised lactose carrier particles appeared to lose larger quantities of drug particles than might have been expected at intermediate

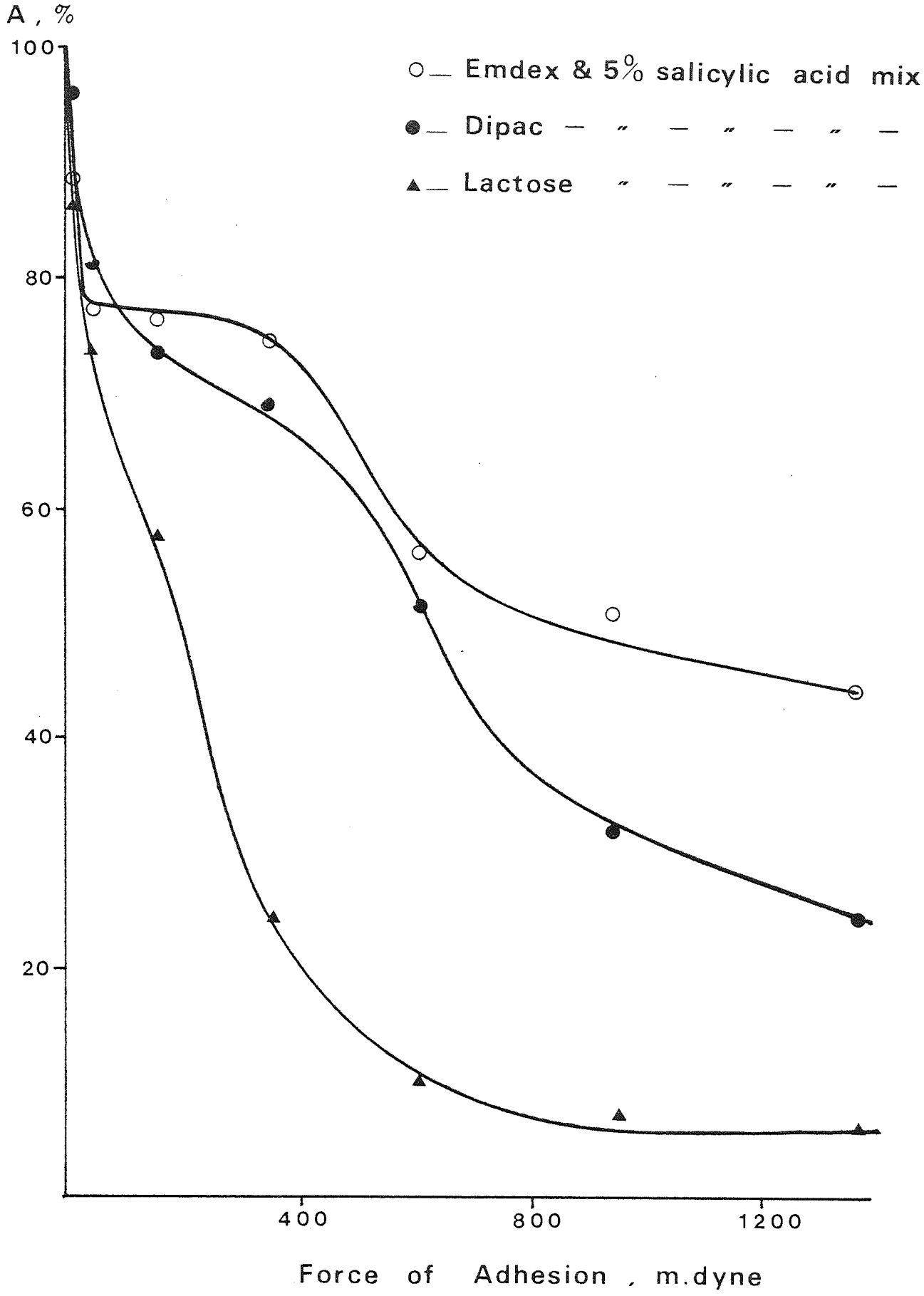

Figure 118. Force of adhesion of 5% salicylic acid particles, 5 µm diameter, to different excipient particles. A = cumulative percentage of drug particles adhering to carrier particle surface.

separation faces. In fact, this rapid and massive decrease in salicylic acid content was not caused by separation from recrystallised lactose particles. It was caused by the fragile nature of the recrystallised lactose spherulites shown by the friability measurements in Chapter 3, which led to fragmentation of the coarse particles at higher applied forces above 151 m.dyne, corresponding to an applied force of 57 N g^{-1}. The break-up of the recrystallised lactose particles probably caused individual dendrites to be forced through the sieve mesh still carrying their adhering drug particles.

The other two excipients, Emdex and Dipac, that were used to form ordered mixes with 5% salicylic acid showed an even greater tendency than mixes containing less drug to lose large numbers of fine particles at different applied separation forces (Figure 118). In ordered mixes formed between Emdex and 5% salicylic acid over 20% of the fine drug particles adhered to carrier particles with forces less than 38 m.dyne (3.8×10^{-4} N) compared with less than 10% adhered with this force in the mixes containing 2% salicylic acid. Dipac and 5% salicylic acid had approximately 20% of the total drug concentration bound to carrier particles with adhesion forces less than 38 m.dyne. Associated with this disproportionately high loss of loosely bound drug particles there was a lag period which followed the initial decrease. The extent of this lag period which followed the loss of a large quantity of weakly bound drug particles, varied but there was relatively little further loss of drug particles from carrier particles until the end of the lag period, despite a continuous increase in removal force.

The length of the lag period appeared to be related to the slope of the second phase of the curve and the lag nearly always

ended at a value of adhesion force of approximately 400 m.dyne, where extrapolation of the second curve back along the same slope crossed the y-axis at a point where A = 100%. This projected curve is represented by slope (a) in Figure 119 which shows the lag section of the 2% salicylic acid/sucrose adhesion profile as a dotted line. Extrapolation of the initial steep curve before the start of the lag period showed that a much weaker adhesion profile could have been predicted from the behaviour of the sucrose and 2% salicylic acid ordered mix at low adhesion forces (curve (b), Figure 119). The different ordered mixes which displayed an adhesion profile similar to the curve with a dotted section shown in Figure 119 appeared to be constituted from a composite of two systems - one in which the adhesion forces were high and the other in which adhesion forces were lower.

Although the results for ordered mixes containing recrystallised lactose and 5% salicylic acid were affected by the break-up of friable carrier crystals, the overall adhesion profile did not display the composite constitution linked with the loss of weakly-bound drug particles from ordered units.

5.2.3 Effect of Excipient Particle Size

The effect of the particle size of excipients used as carrier particles for adherent drug particles on the adhesion force between drug and excipient was studied in ordered mixes containing 1% salicylic acid powder. Two carrier particle size fractions were used, 500 to 710 μm recrystallised lactose powder (Figure 120); these results could be compared with the data for the 250 - 500 μm size fraction obtained previously. The larger particle size fraction of recrystallised lactose formed ordered mixes with

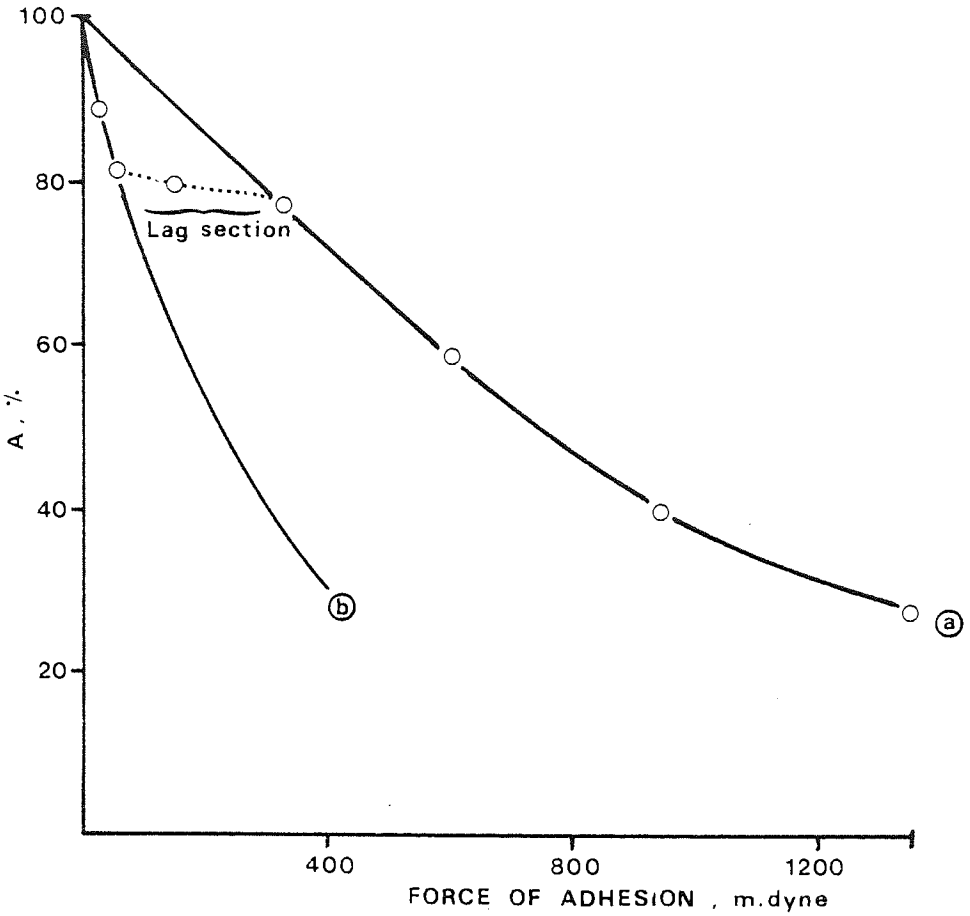

Figure 119. Diagram showing composite nature of adhesion curve. Curve a, the second part of the adhesion profile extrapolated back to A = 100%, and b the initial part of the profile extrapolated to show the probable low adhesion forces of particles following this curve. Curves a & b are linked by the "lag section". A = cumulative percentage of drug particles adhering to carrier particles.

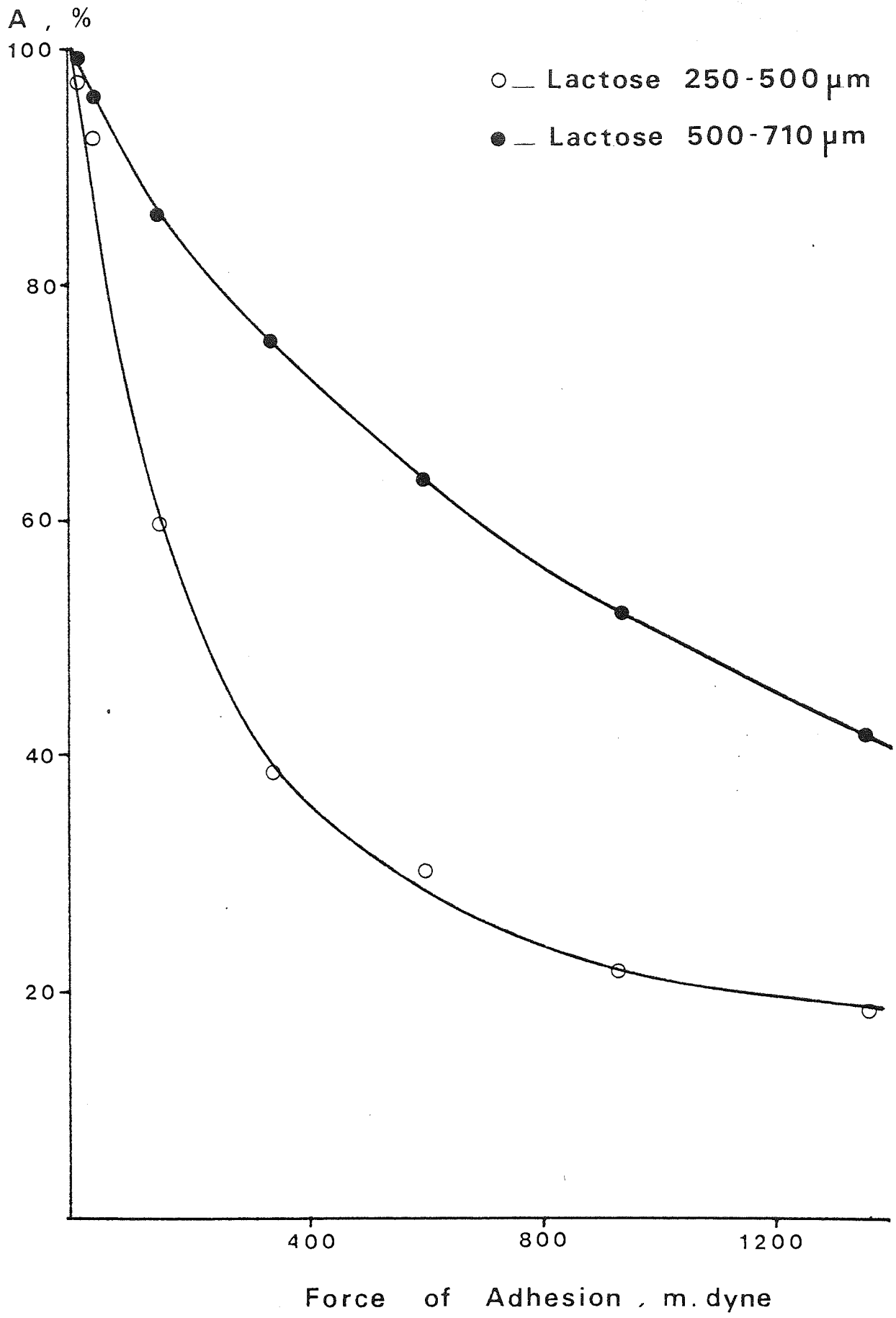

Figure 120. Force of adhesion of 1% salicylic acid particles, 5 µm diameter, to different size fractions of recrystallised lactose. A = cumulative percentage of drug particles adhering to carrier particles.

salicylic acid having larger interparticle adhesion forces than the smaller particle size lactose fraction. The difference in the percentage of fine salicylic acid particles remaining adhered to the recrystallised lactose carrier particles increased with increases in the applied separation force.

In the finer size fraction of recrystallised lactose, the median force of adhesion between carrier particles and fine salicylic acid particles was about 250 m.dyne (2.5×10^{-3} N), whereas the equivalent median force of adhesion for the coarser size fraction was 1,000 m.dyne (1.0×10^{-2} N). There was also a difference in the amount of fine drug particles remaining adhered to each of the different carrier particle size fractions subjected to high separation forces. In ordered mixes containing 250 - 500 µm recrystallised lactose, only 20% of the fine salicylic acid was bound to carrier particles with adhesion forces greater than 1360 m.dyne, compared with over 40% of drug particles which remained adhered to 500 - 710 µm lactose particles.

The differences between the forces of adhesion found in ordered mixes based on fine carrier particles and those containing coarse recrystallised lactose were not predicted from calculations of the theoretical number of adherence sites (Tables 30 and 32); such calculations suggested that both sizes of carrier particles were stereometrically capable of binding all the fine particle drug fraction. As with the results obtained in Chapter 4 (sections 4.3.2.6 and 4.3.2.7) the differences in adhesion forces found between different carrier particle sizes suggested that the actual number of "active" adherence sites was only a small fraction of the number of theoretical sites, derived from the quantity of fine adherent particles which could be packed in a close hexagonal

monolayer around a large particle. The experimental differences in force of adhesion suggested that the larger carrier particles had a greater number of "active" sites per unit surface area and that these "active" sites were also capable of binding adherent particles more strongly than those on the finer carrier particle fraction. The larger recrystallised lactose particles had more surface discontinuities, such as increased surface roughness, a higher number of asperities and greater quantities of large pores; these discontinuities would be capable of modifying the electrostatic charge distribution of the particles and would enhance the interparticle adhesion forces within ordered units.

Fine drug particles, attracted to these surface discontinuities on the larger lactose particles by the high localised electrical charge would also benefit from increased protection against external applied separation forces provided by physical barriers such as pore walls or surface asperities. Fine particles trapped in pores or beside asperities were prevented from being rolled, slid or pulled off the carrier particle surface by the applied separation forces. St. John (186) proposed that fine particles were attached to the carrier surface by an adhesive force normal to the substrate surface and a tangential component due to electrical inhomogeneities around surface discontinuities. When a separation force was applied to these particles, the two component stabilising forces caused the fine particles to roll and thereby broke the adhesive bond. This model implied that the adhesive force and couple were higher statically (while stuck in a groove, pore, etc.) than dynamically (while rolling on a plane surface). Figure 121 shows the distribution of forces around a fine adherent particle lodged in a surface pore or discontinuity.

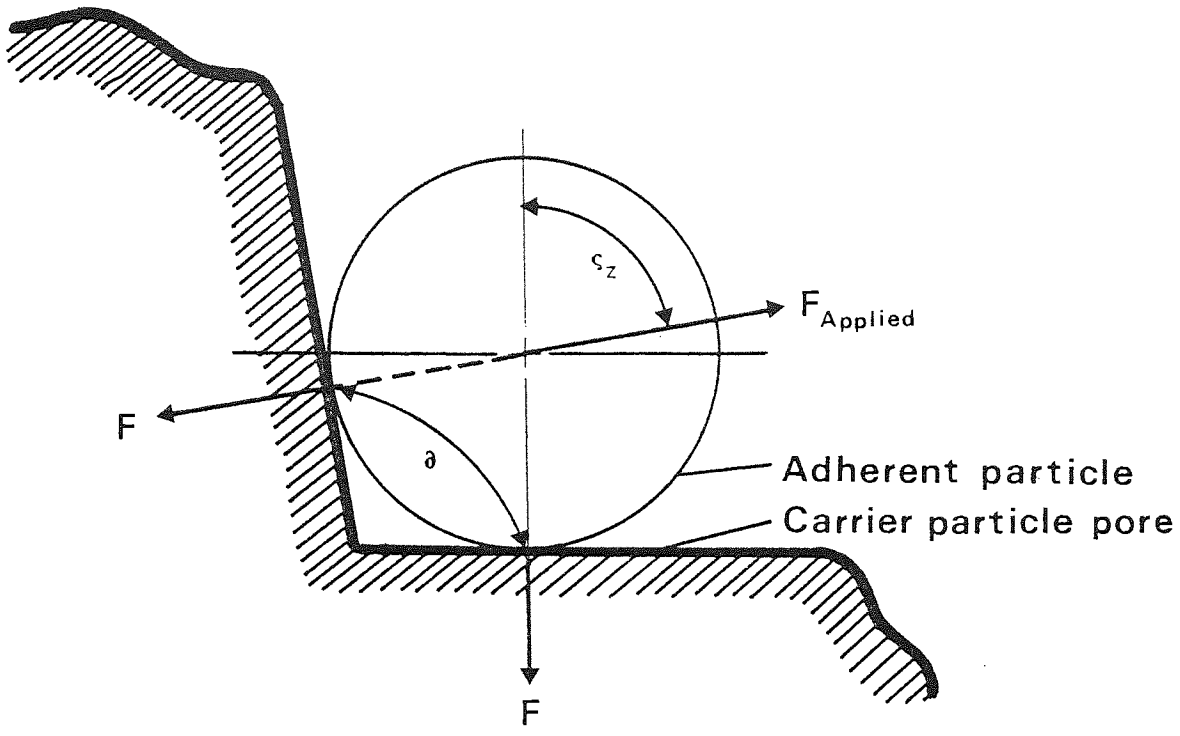

Figure 121. Schematic diagram showing location of adherent particles in carrier particle pores by different combinations of forces. δ is the cleft angle of the pore, ζ_z, the zenith angle, F_1 and F_2 the adhesive forces and $F_{applied}$ the separation force.

The wedge angle, δ, and the zenith angle, ζ_z, are related to the adhesion forces, F_1 and F_2, and the applied separation force, $F_{applied}$, by the following relationships (186):

$$F_1 / F_{applied} = \sin \zeta_z / \sin (180 - \delta) \qquad (101)$$

$$F_2 / F_{applied} = \cos \zeta - \{\sin \zeta_z . \cos(180 - \delta) / \sin (180 - \delta)\} \qquad (102)$$

Equations 101 and 102 assume a static rigid-body model without any adhesive couples or equal and parallel adhesive forces acting in opposite directions at the point of contact. In the experimental test method utilised in the present study (Figure 113); the zenith

angle, ζ_z, varied from 0^o to 360^o and the wedge angle, δ, varied from 0^o to 180^o. Fine particles trapped in pores in the carrier hemisphere facing away from the sieve mesh (screen) dividing the split sphere had zenith angles from 180^o to 360^o. The relative contributions of the two static adhesive forces to the adhesive couple acting against the applied separation force were calculated, and are listed in Table 18 a and b, according to the appropriate zenith and wedge angles.

The zenith angles in brackets indicate that the signs of the adhesive couples should be reversed from those shown in the table; thus for zenith angles between 270^o and 340^o an increase in the applied "separation" force actually increased the adhesive couple. If the zenith angle was 90^o, adhesion was due to an adhesive couple since the applied force was purely tangential whereas if the zenith angle had no tangential component, the adhesion was due to an adhesive force acting upwards from the carrier surface normal to the applied force. Carrier particles with smooth surfaces were represented in Table 33 by wedge angles of 0^o or 180^o and the adhesion between drug and excipient particles in these cases was due to a single adhesive force acting normal to the carrier surface. Therefore, carrier particles with a sufficiently porous surface to entrap fine drug particles benefited from an increased adhesion produced by a static adhesive couple, as well as an increased adhesive force resulting from the concentration of electrostatic charge around surface discontinuities. The increased force of adhesion in ordered units containing coarse recrystallised lactose particles would explain the results presented in Figure 120.

Table 18(a) Zenith angles* and wedge angles related to $F_1/F_{applied}$

Zenith angle (Degrees)	Wedge angles (degrees)										$F_{applied}$
	0, 180	10, 170	20, 160	30, 150	40, 140	50, 130	60, 120	70, 110	80, 100	90	
0, 180, 360	0	0	0	0	0	0	0	0	0	0	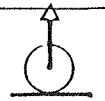
10, 170 (350, 190)	0	1	0.51	0.35	0.27	0.23	0.20	0.18	0.18	0.17	
20, 160 (340, 200)	0	1.97	1	0.68	0.53	0.45	0.39	0.36	0.35	0.34	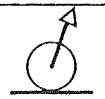
30, 150 (330, 210)	0	2.88	1.46	1	0.78	0.65	0.58	0.53	0.51	0.5	
40, 140 (320, 22)	0	3.7	1.88	1.29	1	0.84	0.74	0.68	0.65	0,64	
50, 130 (310, 230)	0	4.41	2.24	1.53	1.19	1	0.88	0.81	0.78	0.77	
60, 120 (300, 240)	0	4.99	2.53	1.73	1.34	1.13	1	0.92	0.88	0.87	
70, 110 (290, 250)	0	5.41	2.75	1.88	1.46	1.23	1.09	1	0.95	0.94	
80, 100 (280, 260)	0	5.67	2.88	1.97	1.53	1.29	1.14	1.05	1	0.98	
90 (270)	0	5.76	2.92	2	1.56	1.31	1.15	1.06	1.02	1	

Table 18(b) Zenith angles* and Wedge angles related to $F_2/F_{applied}$

Zenith Angle	0, 180	10, 170	20, 160	30, 150	40, 140	50, 130	60, 120	70, 110	80, 100	90	$F_{applied}$
0 (180) 360	1	1	1	1	1	1	1	1	1	1	
10 (170) (190) 350	0.98	0	0.51	0.64	0.73	0.79	0.84	0.88	0.91	0.98	
20 (160) (200) 340	0.94	-1	0	0.35	0.53	0.65	0.74	0.82	0.88	0.94	
30 (150) (210) 330	0.87	-1.97	-0.51	0	0.27	0.45	0.58	0.68	0.78	0.87	
40 (140) (220) 320	0.77	-2.88	-1	-0.34	0	0.23	0.37	0.53	0.65	0.77	
50 (130) (230) 310	0.64	-3.71	-1.47	-0.68	-0.27	0	0.20	0.36	0.51	0.64	
60 (120) (240) 300	0.50	-4.41	-1.88	-1	-0.53	-0.23	0	0.18	0.35	0.50	
70 (110) (250) 290	0.34	-4.99	-2.24	-1.29	-0.78	-0.45	-0.2	0	0.18	0.34	
80 (100) (260) 280	0.17	-5.41	-2.53	-1.53	-1	-0.65	-0.39	-0.18	0	0.17	
90, 270	0	-5.67	-2.75	-1.73	-1.19	-0.84	-0.58	-0.36	-0.18	0	

*Zenith angles in brackets have equivalent forces with reversed signs

5.2.4 Effect of Drug Particle Size

To evaluate the effect of drug particle size, ordered mixes containing sucrose carrier particles and 1% salicylic acid powder were made, varying the particle size of the 1% model drug. Four different particle size fractions of salicylic acid powder were used: 53 - 75 μm; 75 - 90 μm; 90 - 105 μm and 105 - 120 μm. The different size fractions of salicylic acid were obtained by sieving in an air-jet sieve (Alpine, Augsburg, W. Germany).

The forces of adhesion which bound the different particle sizes of salicylic acid to the carrier sucrose particles (420 - 625 μm diameter) are shown in Figures 122 and 123. The two fine drug powders with particle sizes of 53 to 75 μm and 75 μm to 90 μm diameter (Figure 122) had similar adhesion profiles. The median adhesion forces binding the fine salicylic acid particles (53 - 75 μm and 75 - 90 μm diameter) to the coarse sucrose particles was about 580 m.dyne (5.8×10^{-3} N), and the amount of fine drug particles adhered to carrier particles with adhesion forces larger than 1360 m.dyne (1.36×10^{-2} N) was about 12% of the total salicylic acid content for both these fine size fractions. The adhesion profiles shown in Figure 122 were of the same type as the composite curve shown in Figure 119. However the results for the two larger particle sizes of salicylic acid, 90 to 105 μm and 105 to 120 μm diameter (Figure 123) did not display curves with a composite constitution and, for these coarser drug particles, the median adhesion forces larger than 1360 m.dynes were higher than for the two smaller particle sizes. This may have been partly due to the larger particle sizes of dislodged salicylic acid having more difficulty in passing through the 120 μm sieve mesh dividing the split sphere (Figure 113) than the smaller particles.

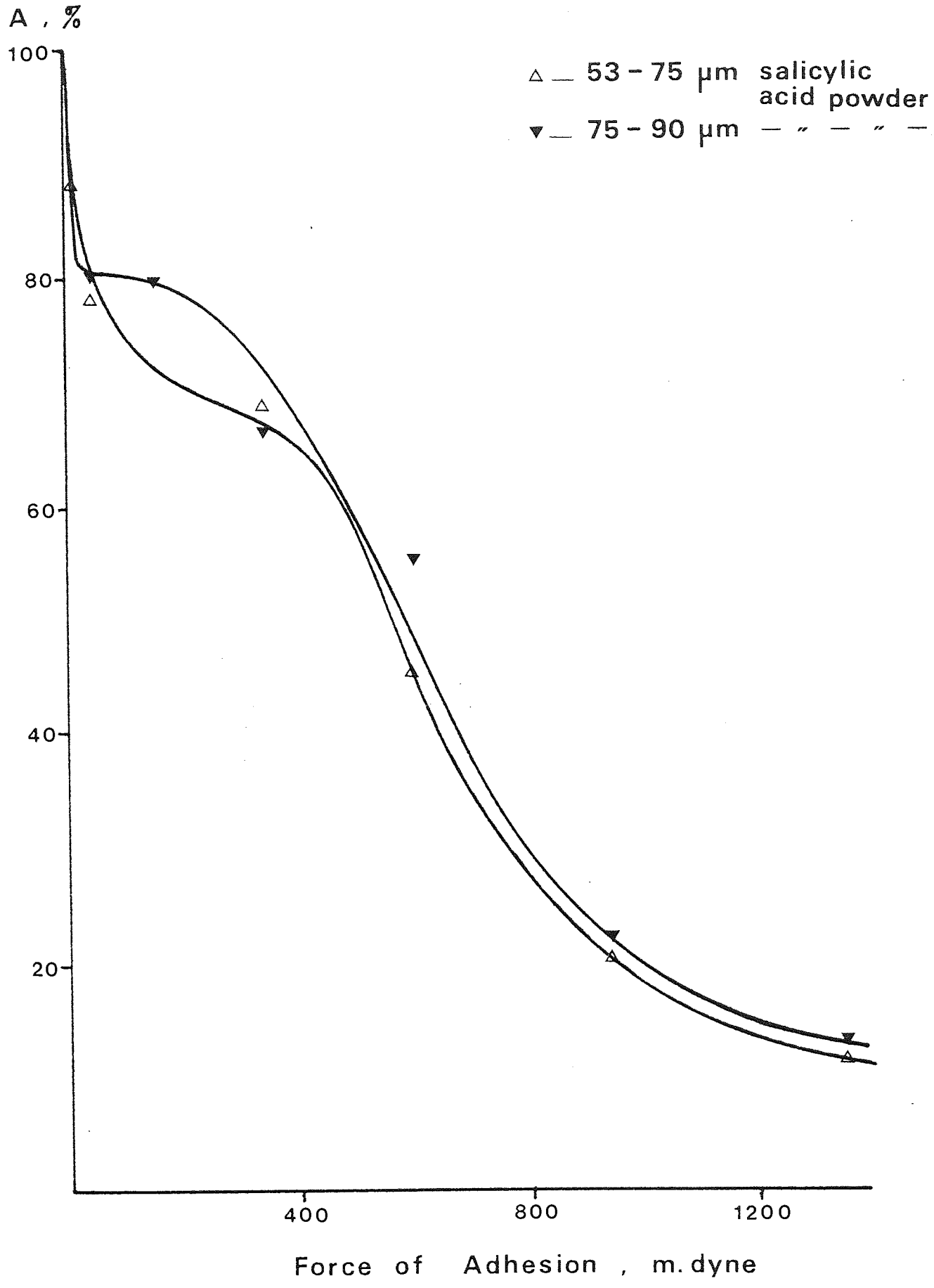

Figure 122. Force of adhesion of 1% salicylic acid particles of different size fractions, to sucrose carrier particles, 420 - 625 µm size fraction. A = cumulative percentage of drug particles adhering to carrier particles.

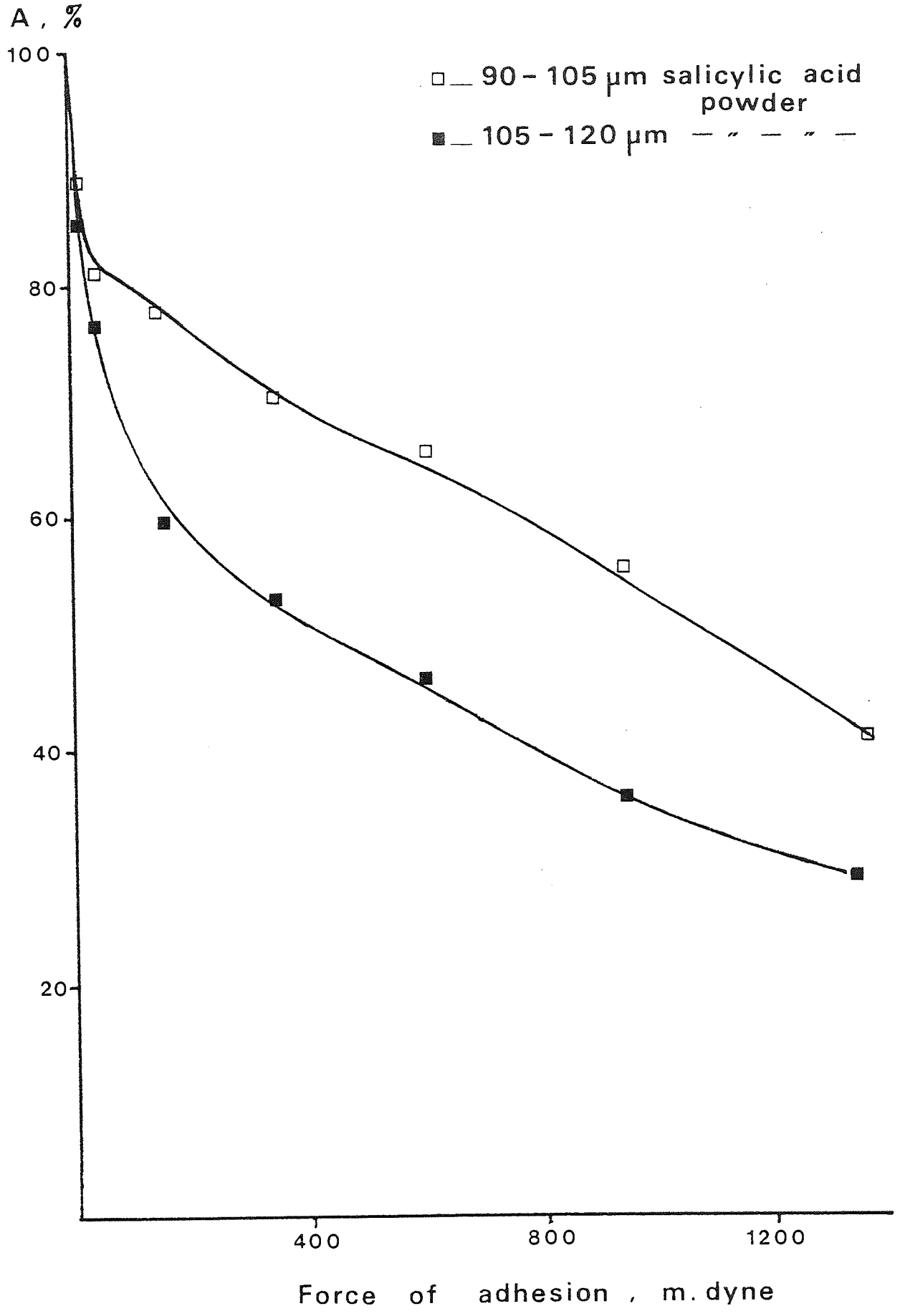

Figure 123. Force of adhesion of 1% salicylic acid particles of different size fractions, to sucrose carrier particles, 420 - 625 µm size fraction. A = cumulative percentage of drug particles adhering to carrier particles.

In ordered units composed of adherent drug particles with diameters from the 5 µm size used previously to 90 µm, the median adhesion force varied with the first power of the drug particle radius in a rectilinear log-log relationship (Figure 124).

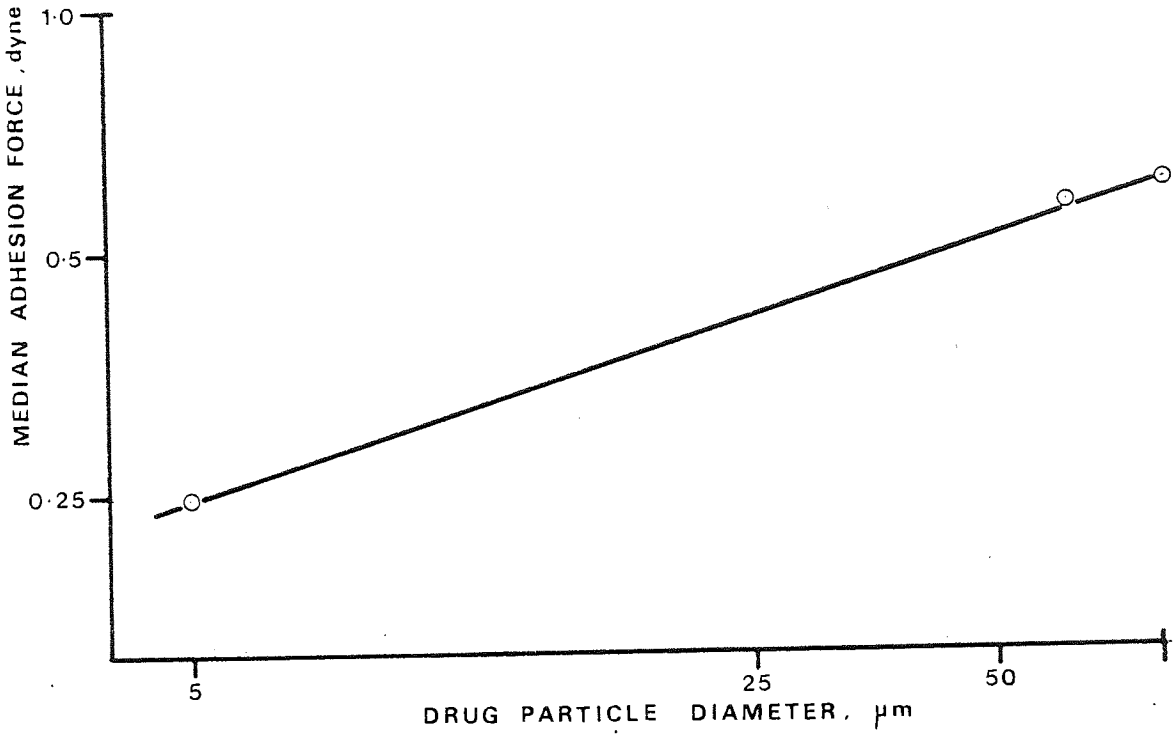

Figure 124. Median adhesion forces of salicylic acid particles of different sizes to sucrose carrier particles, 420 - 625 µm size fraction.

This association between adherent particle radius and the force of adhesion was also found by St. John (186) with fine gold spheres in the size range 10 µm to 60 µm diameter, adhering to a plane gold substrate. The increase in adhesion force of the larger adherent drug particles is attributable to increasing contact area and increased plastic deformation of the carrier particle surface which was shown by Krupp (187) to increase interparticle adhesive bonding. The relationship between drug particle diameter and adhesion force departed from a first-power affinity in drug particles larger than 90 µm diameter.

This may have been caused by the larger particle size drugs not "fitting" in to surface pores or irregularities. Such steric effects would markedly reduce the number of "active" sites for larger adherent particles. Alternatively, the departure from a first-power relationship may have occurred because the drug particle diameter approached the sieve mesh dimensions causing interference with the movement of salicylic acid particles through the screen dividing the split sphere (Figure 113).

5.2.5 Ternary Mixes

Different third components were added to ordered mixes containing 1% salicylic acid powder and 420 - 625 μm size fraction sucrose crystals. The powders used as third components in different mixes were selected in view of their possible practical applications as minor ingredients in pharmaceutical direct compression systems. The effect of the third components on the adhesion forces binding salicylic acid particles (5 μm diameter) was studied using the ultracentrifuge apparatus. The minor ingredients used as third components were: magnesium stearate, a tableting lubricant; talc, a flow aid and tableting lubricant and maize starch, a binding agent in wet massing processes and a disintegrant. The third components were added to ordered mixes previously formed between sucrose and salicylic acid.

5.2.5.1 Effect of Magnesium Stearate Concentration

Ordered mixes containing 1% salicylic acid were made with sucrose carrier particles and different concentrations of fine magnesium stearate powder of 0.5%, 1%, 2%, and 4% of the total weight of the binary powder mix. Most of the adhesion profiles produced by the ternary mixes containing magnesium stearate were

composites of two separate curves, similar to the one shown in Figure 119. Ordered mixes of sucrose/salicylic acid contains 0.5% fine magnesium stearate lost 20% of the salicylic acid 'drug' particles at applied separation forces less than 57 Ng^{-1}, which was equivalent to adhesion forces less than 151 m.dyne (Figure 125). In ordered mixes with a magnesium stearate concentration of 1% w/w, the proportion of weakly adhered drug particles increased and more than 40% of the total salicylic acid content was adhered to ordered units with forces less than 38 m.dyne (Figure 125). At a concentration of 2% magnesium stearate, more than 40% of the total salicylic acid content of the ternary mix was adhered to sucrose carrier particles with forces less than 38 m.dyne (Figure 126), and nearly 30% were bound in ordered units by adhesion forces of less than 9.5 m.dyne. The amount of weakly held salicylic acid particles increased further in ordered mixes containing 4% magnesium stearate, where about 40% of the total salicylic acid content of the mix was bound in ordered units by adhesion forces of less than 9.5 m.dyne (Figure 126).

Although an increase in magnesium stearate concentration appeared to produce an increase in the amount of weakly bound drug particles, there was also a proportion of more strongly-bound salicylic acid particles which appeared to be unaffected by the concentration of magnesium stearate in the ordered mix. The median adhesion force of drug particles bound to ordered units in mixes containing 0.5% magnesium stearate was 650 m.dynes and this force decreased to about 150 m.dyne in mixes with 1% magnesium stearate content (Figure 125). However, the median drug adhesion force again increased in ordered mixes containing 2% and 4% magnesium stearate to a value of 250 m.dyne.

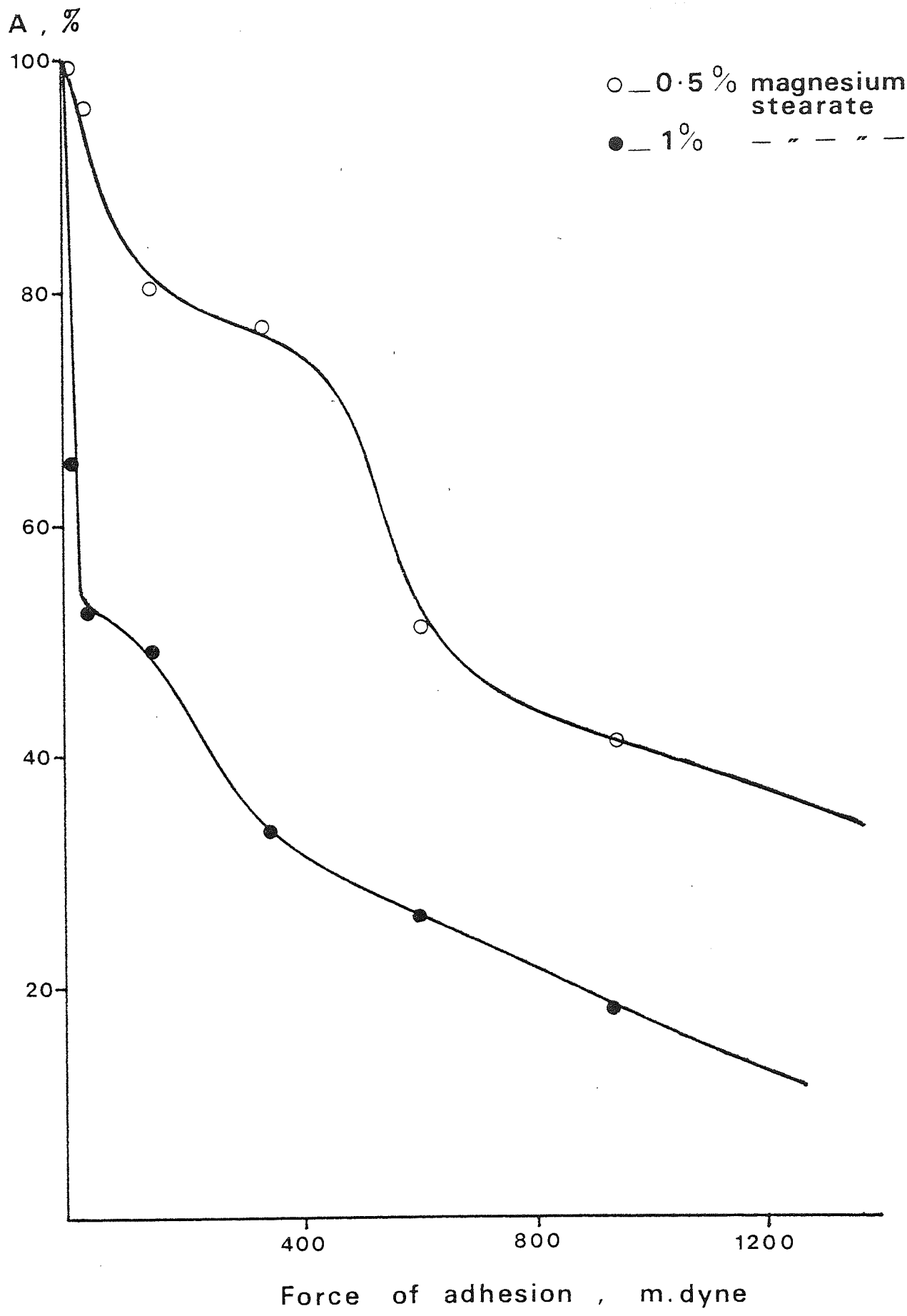

Figure 125. Force of adhesion of 1% salicylic acid particles, 5 μm diameter to sucrose carrier particles in ordered mixes also containing different magnesium stearate concentrations. A = cumulative percentage of drug particles adhering to carrier particles.

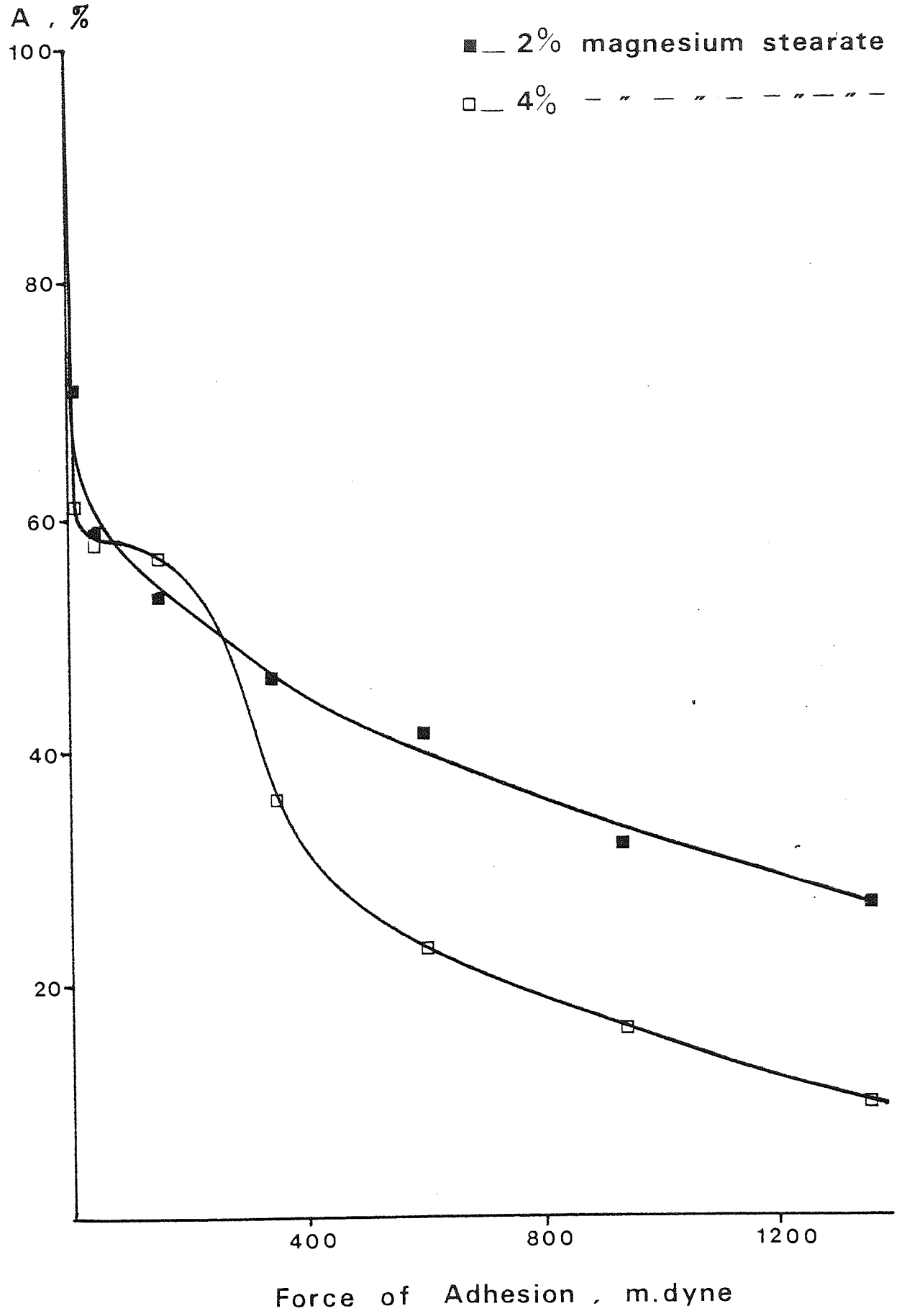

Figure 126. Force of adhesion of 1% salicylic acid particles, 5 μm diameter, to sucrose carrier particles in ordered mixes also containing different magnesium stearate concentrations. A = cumulative percentage of drug particles adhering to carrier particles.

Lai and Hersey (134) studied the variance of samples removed from ordered mixes containing coarse sucrose, fine salicylic acid and magnesium stearate. They found that addition of magnesium stearate to the ordered mixes increased sample variance of the drug content and they proposed a mechanism for this action which they called "stripping". According to this segregation mechanism, magnesium stearate particles displace fine salicylic acid particles from their binding sites on the coarse carrier particles.

This effect of magnesium stearate may result from its ability to alter the electrostatic charge and charge distribution on the surface of the sucrose carrier particles. The work reported in Chapter 6 of this thesis supports this hypothesis. Magnesium stearate was found to carry a positive electrostatic charge whereas salicylic acid and sucrose carrier particles had negative electrostatic charges. Compared with the more electronegative salicylic acid, positively-charged magnesium stearate particles would have a greater affinity for the negatively-charged surface of the carrier sucrose particles.

An increase in magnesium stearate concentration caused increased numbers of adherent drug particles to be displaced. This occurred because of the increased number of binding sites occupied by magnesium stearate particles leading to a reduction in the number of sites available for adhesion of salicylic acid particles. The magnesium stearate appeared to displace the more weakly-bound drug particles from ordered units whereas the more strongly adhered salicylic acid particles remained attached to sucrose carrier particles.

5.2.5.2 Effect of Starch and Talc Powder

To evaluate the effect of alternative third-components ordered mixes were made with 1% salicylic acid, 5 µm diameter, and coarse sucrose crystals, 420 - 625 µm size fraction, plus either starch or talc as the third component fine powder. The ternary ordered mixes contained 2% of either starch or talc particles and the effect of these additional ingredients on the stability of each ordered mix was studied using the ultracentrifuge system. Once again the drug adhesion profile of the ternary ordered mix containing 2% starch (Figure 127) was similar to the composite curve shown in Figure 119.

The median force of adhesion and the amount of drug particles adhered to carrier particles with forces larger than 945 m.dyne were both increased in ternary mixes containing 2% starch compared with equivalent binary ordered mixes without any starch content. However, about 15% of the total salicylic acid content of the ordered mix was bound to sucrose carrier particles with adhesion forces less than 38 m.dyne (Figure 127) compared with only 8% of the drug content in the equivalent binary mixes without starch (Figure 114). Thus it appears the starch particles caused some displacement of weakly bound salicylic acid particles from sucrose carrier particles, although this effect was smaller than that found in ternary mixes containing an equivalent percentage of magnesium stearate.

The drug adhesion curve in ordered mixes containing 2% talc as the ternary component was different from the curves produced by addition of either magnesium stearate or starch powder (Figure 127). The talc appeared to stabilise the ordered mix of 1% salicylic acid and sucrose and therefore reduced the amount of drug particles

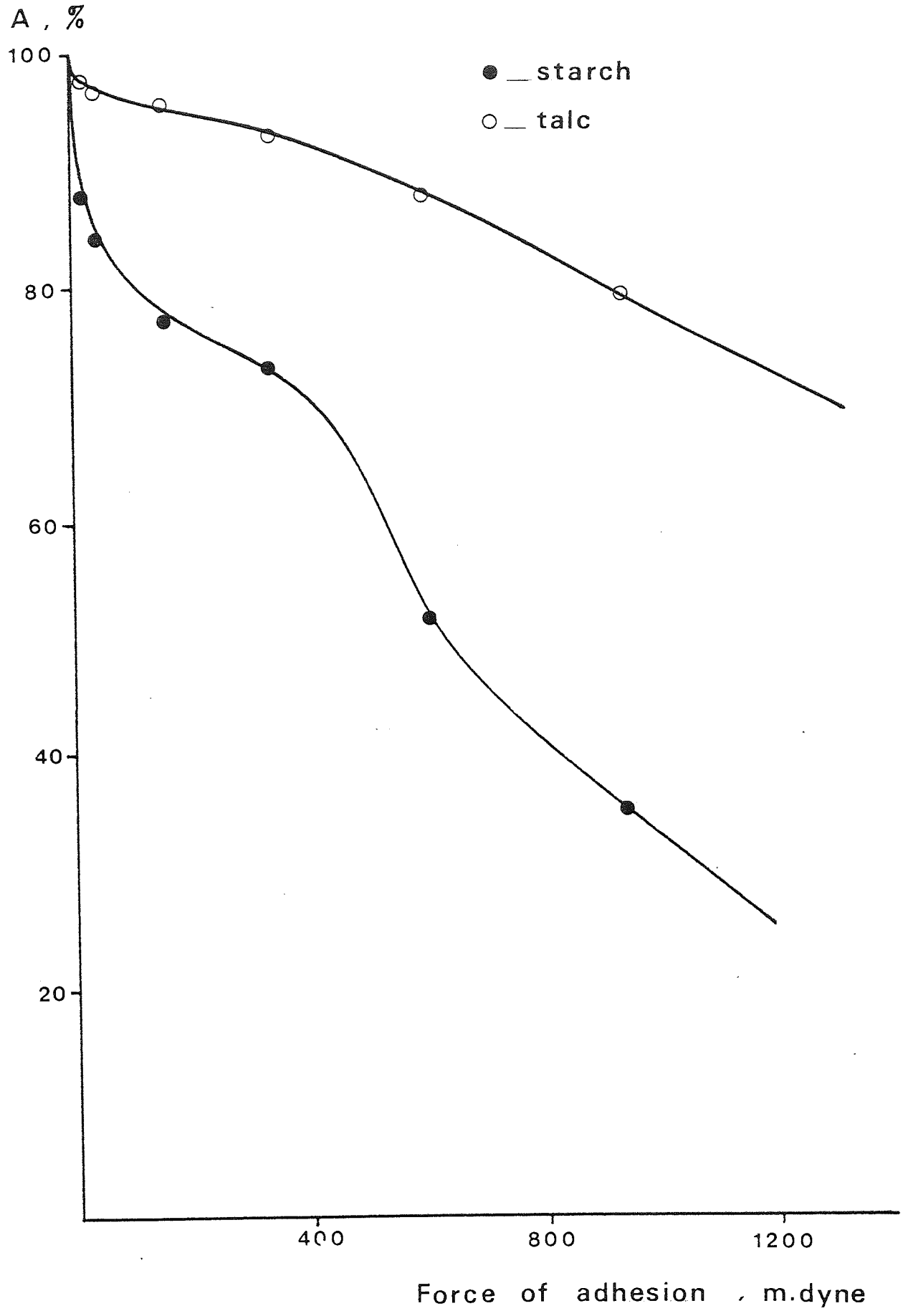

Figure 127. Force of adhesion of 1% salicylic acid particles, 5 µm diameter, to sucrose carrier particles in ordered mixes also containing 2% of a third component, either starch or talc. A = cumulative percentage of drug particles adhering to carrier particles.

lost from ordered units and generally increased the interparticle forces of adhesion. Only 20% of the total number of salicylic acid particles were removed from ordered units at the maximum applied separation force of 358 $N.g^{-1}$ compared with over 80% of the drug content lost from carrier particles in the corresponding binary ordered mixes of salicylic acid and sucrose powder subjected to the same applied separation force (Figure 114). The marked stabilising effect of talc in ordered mixes of salicylic acid and sucrose may result from a modification of the electrostatic charge interaction between the three components in an opposite manner from that produced by magnesium stearate or starch particles as shown later in Chapter 6.

The different adhesion forces in ordered mixes of salicylic acid drug particles and sucrose containing a third component suggest that the effect of either formulation additives on the segregation tendency of pharmaceutical mixes should be assessed. In formulations where one or more excipients are found to cause "stripping" of drug from carrier particles the constituent excipient powders should be altered where necessary to produce the optimum adhesion profile for maintaining adequate homogeneity of individual drug formulations.

5.3 General Discussion

The precision of adhesion force measurements using the ultracentrifuge technique was assessed using the relationship developed by St. John (186) for spherical adherent particles:

$$P_R = M_p.\alpha' = 4\pi a_r^3 \alpha'.\rho^o / 3 \qquad (103)$$

where P_R is the precision of the method; ρ^o, the adherent particle density; M_p, the adherent particle mass; α', the shock forces

produced by handling, assumed to be less than 10 G and a_r, the adherent particle radius. For fine particles of salicylic acid, 5 μm diameter, adhering to the carrier excipient particles used in the present study, the precision of the ultracentrifuge method was found to be of the order of 1×10^{-3} m.dyne.

An expression relating the theoretical force of adhesion, F^P, between two sets of particles was developed by Krupp (187):

$$F^P = \hbar\bar{\omega}^2 / 64\pi^3 . Z_o^5 . H(t) \qquad (104)$$

where Krupp's estimate of the cohesive van der Waals constant was taken as $\hbar\bar{\omega}$ = 2eV and in this study the constant of the drug and excipient was taken as being between $\hbar\bar{\omega}$ = 1.4 and 2eV; Z_o was the distance of maximum force of adhesion (adhesional distance) between the adherents, which could not be calculated, but was assumed by Krupp to be 4×10^{-10} m and H(t) the hardness of the carrier particles estimated to be less than 10^8 dyn / cm^{-2}. From these values, the estimated theoretical median adhesion forces binding ordered units of salicylic acid and excipient carrier particles was between 100 and 200 m.dynes. The experimentally determined median adhesion forces for salicylic acid and sucrose particles was of the same order as the predicted theoretical adhesion force (Figure 114). However, the less smooth surfaces of Emdex, recrystallised lactose and Dipac had larger median adhesion forces than the theoretically estimated value and this was probably caused by the static adhesive couple present in excipient particles with surface pores adding to the adhesive forces as demonstrated in section 5.2.3.

The type of adhesion profile shown in Figure 119 was associated with a disproportionately large amount of drug particles

being weakly bound to carrier particles, and was found in certain ordered mixes containing higher drug concentrations, as well as in mixes constituted from larger particle size drug powders and in ordered mixes containing certain third component excipient powders. Supporting the results for mixes of Dipac and drug powders which were shown to be unstable when vibrated (Chapter 4), the adhesion curves of Dipac and salicylic acid showed the presence of large quantities of weakly bound drug particles; as a result the adhesion profile was a composite of two separate curves which appeared to be associated with a combination of stable and unstable ordered units. The loss from the carrier surface of large quantities of drug particles which were weakly-bound in ordered units plus a second, more strongly adhered set of drug particles as shown by composite curves such as that in Figure 119, indicated incomplete ordering or ordered units which were unstable when external forces were present. The latter two conditions appear to be represented by a "pseudo-random" set of fine drug particles, weakly bound and therefore easily removed from carriers, and a "truly ordered" set of more strongly adhered particles capable of withstanding high applied separation forces. The "pseudo-random" particle fraction occurred in a set of particles fine enough to be considered cohesive but which were unable to form adequate interparticle bonds with larger particles because of a deficiency in "highly active" sites. The loosely-bound particles would be free to move through a powder mix individually or in fine particle agglomerates in a manner previously discussed in the section on constituent segregation of drug particles in Chapter 4. Although not totally random, since fine particles could become re-ordered with new carriers or agglomerated with different drug particles after any interparticle

collision the mix does have a random element. The above explanation can also be applied to the vibrational segregation tendencies of Emdex mixes containing higher drug concentrations above 2% (Chapter 4). In mixes of 5% drug and Emdex the carrier particles were not sufficiently porous to carry all the drug particles on "highly active" sites and a percentage were therefore only weakly bound to the Emdex surface. This weakly held fraction became "pseudo-randomised" under certain vibration conditions. In the cases of both the Dipac/drug mix, and the Emdex/drug mixes containing higher drug concentrations segregation of constituent fine drug particles was promoted by dislodgement of large numbers of weakly bound adherent particles. Conversely, the recrystallised lactose excipient particles were capable of carrying all the drug particles and therefore did not display the composite curve but formed strong adhesive bonds with a large proportion of the fine drug particle fraction. The adhesion profile obtained for recrystallised lactose of large particle size (500 - 710 μm) showed that these more porous carrier particles formed stronger adhesive bonds between drug and excipient than the smaller particle size fraction of recrystallised lactose. The increase in segregation tendency of vibrated mixes with increasing excipient particle size (section 4.3.2.6) was attributed to an increased mobility of any dislodged fine particles due to larger interparticle voids. The adhesion profiles obtained for these large carrier particles suggests that this was the most probable explanation since the fine particles were bound more strongly to large carrier particles.

Other ordered mixes with composite adhesion profiles include those formed with ternary mixes of magnesium stearate, where the lubricant powder appeared to displace drug particles leaving them

free to move "pseudo-randomly" and cause constituent segregation. As with other mixes with a composite adhesion profile, the truly ordered components prevented complete segregation of the drug particle fraction from the excipient particle fraction.

A powder mix with an adhesion profile which shows a steady decrease in the percentage of drug particles bound to carrier particles with increasing adhesion forces, appears to be less likely to produce marked segregation than mixes with a composite adhesion profile which indicates large quantities of weakly adhered particles. This general rule seems to apply even when the composite adhesion profile shows the presence of a larger amount of drug particles bound to carrier particles with high adhesion forces. Fine drug particles adhered to carrier excipient particles appear to be susceptible to segregation by external applied forces when a substantial proportion of the total drug content is bound in ordered units with forces less than 200 m.dyne.

Chapter 6

6. Triboelectrification and Contact Electrification of Powder Particles

6.1 Measurement of Surface Electrical Charge

In the absence of an externally applied electrical field, particles which come into contact with other particles or surfaces, whether they are metal or non-metal can acquire a charge which is retained when the surfaces separate. When two dissimilar metals are placed in contact, a potential difference is produced such that electrons will move more easily from say, metal A to B than from metal B to A. The potential difference is called the contact potential. If metal B is separated from metal A, then the isolated metal A will be positively charged and B will be negatively charged (231). When the two surfaces, A and B are non-conductors they can still become charged in a similar manner.

Triboelectrification, in which charging occurs by interaction of moving surfaces, was discussed in Chapter one (section 1.5.2). Although triboelectrification is capable of producing large quantities of charged particles by frictional interactions it is difficult to distinguish this effect from the phenomenon of contact charging described above (232) and the two effects are often treated as a single phenomenon. Both contact and frictional electrification contribute to the electrostatic charge measured when powders are blown off a surface such as in the system studied by Rudge (198).

In the present study the surface electrical charges of several pharmaceutical powders were measured when poured from two different insulating surfaces. The same powders were tested which had been studied in previous experiments on vibrational segregation

of ordered mixes (Chapter 4) and in the determination of interparticle forces in ordered mixes (Chapter 5).

6.1.1 Method

Each powder was tested individually, the charge on the particles being measured by pouring a known weight of powder on to a specially constructed static charge detector. It was realised that some of the measured charge was gained in pouring from the container and that the actual residual charge on a powder depends on the specific conditions of measurement and prior storage. These measurements of static charge were carried out in order to assess the magnitude and sign of charges on particles used as constituent powders in the formation of ordered mixes.

A Faraday well was used to measure the static charge on the different powder particles and was specially constructed in brass according to the design shown in Figure 128. The static charge produced on the Faraday well was measured using an electrometer (Type 610C, Keithley Instruments, Cleveland, U.S.A.). The powder under test was poured into the inner brass container of the Faraday well (Figure 128) so that the base was fairly uniformly covered in powder. The weight of powder used in each charge determination was measured using an analytical balance. Four replicate determinations of particle charge were made for each powder using different samples.

Powders were poured into the Faraday well off a glass surface in the form of a 250 cm^3 glass beaker (J. A. Jobling, Greenford, U.K.) and also off a plastic surface in the form of a 250 cm^3 polyethylene beaker (Azlon Labplex, from Fisons Scientific Apparatus, Loughborough, U.K.). The rate of pouring was kept as constant as

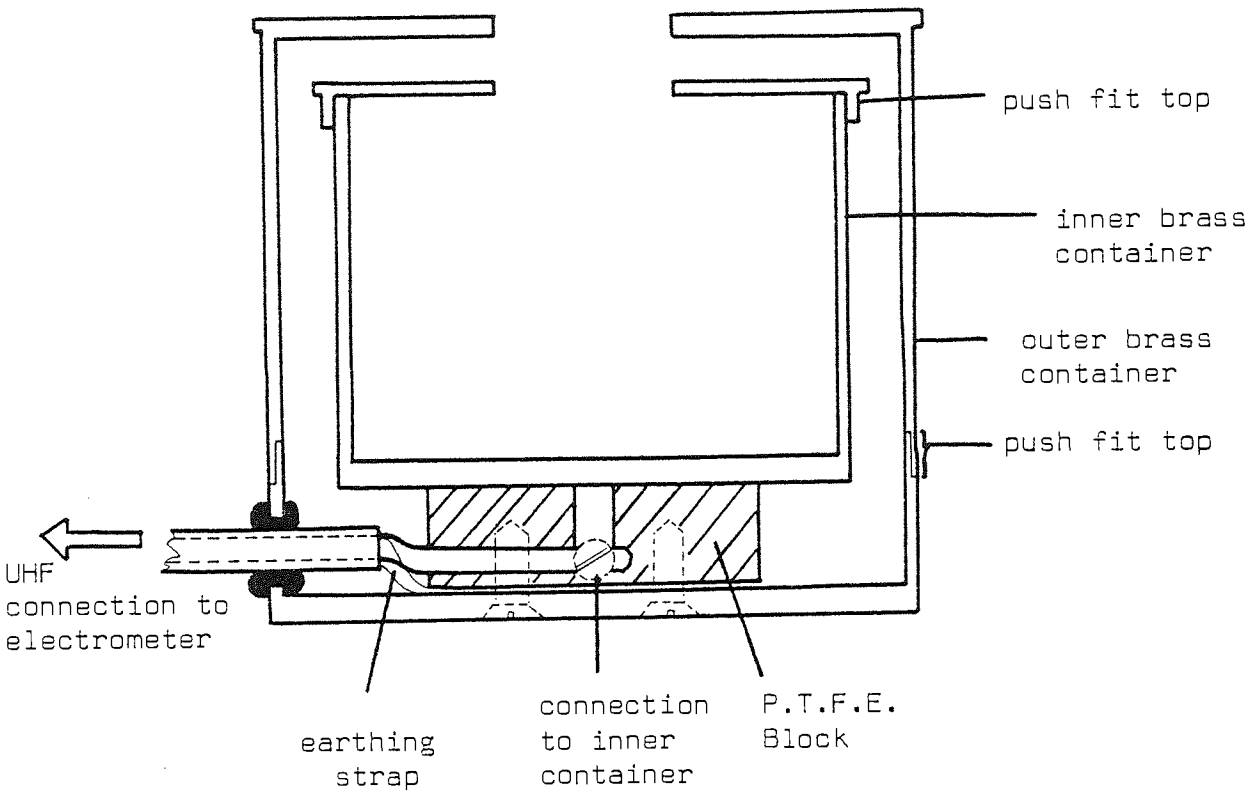

Figure 128. Front elevation of Faraday Well, constructed for determinations of static charges on powder particles.

possible for all samples in an attempt to achieve reproducible and comparable experimental conditions. The Faraday well was connected to the electrometer using a teflon-insulated UHF-type connector to prevent charge leakage. All the powders used in the determinations of static charge were measured following undisturbed storage for several weeks in sealed glass containers at room temperature. No special procedures were carried out to clean particle surfaces since the object of these experiments was to determine the charge characteristics of powders in conditions as close as possible to those existing during normal pharmaceutical processing. The samples used in other experiments reported in this thesis had also been stored under similar conditions.

6.1.2 Results and Discussion

The mean static charges on the different powders poured into the Faraday well off a glass surface were determined (Table 34). The upper and lower 95% confidence limits of the mean charge and the variance of the measured values about the mean were also calculated and are shown in Table 34. There was a significant difference in the magnitude of the powder particle charges although the majority of powders tested carried a negative electrostatic charge, including all the excipients used as carrier particles in mixing/segregation studies.

Table 34 shows that the potassium chloride powder carried a negative charge of 13×10^{-9} $C.g^{-1}$. The three different excipient powders, Dipac, Emdex and recrystallised lactose (250 - 500 μm size fraction) also charged negatively (Table 34).

Table 34. Mean specific charges of different powders measured after pouring off a glass surface. Values are expressed in terms of 10^{-9} C.g^{-1} to facilitate comparison of charges on different powders. Values are mean of five separate determinations.

Powder Sample	Mean Specific Charge (10^{-9} C.g^{-1})	95% confidence limits	Variance
Dipac	-7.6	± 1.6	0.76
Emdex	-1.2	± 0.45	0.06
Recrystallised lactose 250 - 500 µm size fraction	-2.9	± 0.7	0.15
500 - 710 µm	-0.63	± 0.14	0.56
710 - 1000 µm	-0.4	± 0.17	0.83
180 - 250 µm	-7.6	± 2.1	1.36
90 - 180 µm	-9.7	± 3.8	4.31
0 - 90 µm	-7.7	± 0.88	23.39
Potassium Chloride	-13.0	± 1.1	38.09
Elcema G250	-16.0	± 1.2	63.31
Sucrose	-2.4	± 0.94	0.26
Salicylic Acid	-25.0	± 1.8	0.96
Starch	+0.13	± 0.09	0.24
Potassium Sorbate	+3.2	± 0.39	4.44
Magnesium Stearate	+8.8	± 1.0	0.31
Talc	-2.7	± 0.47	6.46

The larger the difference in magnitude of the electropositive and negative charges of two sets of powder particles, the larger will be the mutual attraction. This is best shown using a triboelectric series which is analogous to an electrochemical series. Although a triboelectric series is specific to the conditions under which the powders were tested, the series gives an indication of the possible interaction between different powders. The further apart powders with different charge signs are in the series the greater is their likely mutual attraction. Table 35 shows the triboelectric series constructed from the values given in Table 34.

From the triboelectric series shown in Table 35 it can be seen that the model drug, potassium chloride was more electronegative than any of the three carrier excipient powders, Dipac, Emdex or recrystallised lactose, 250 - 500 µm size fraction.

Dipac was followed next by recrystallised lactose, 250 - 500 µm size fraction, but this excipient powder was five times less electronegative than potassium chloride powder. The least electronegative of the three carrier excipients was Emdex which was approximately ten times less electronegative than the potassium chloride. The finer particle size fractions of recrystallised lactose were more electronegative than the larger particle sizes; however if electronegativity was calculated in terms of charge per particle this

Table 35. Triboelectric series of different types of drug and excipient powders poured off a glass surface

Electronegative	Salicylic acid (adherent, drug)
	Elcema G250 (carrier, excipient)
	Potassium Chloride (adherent, drug)
	Recrystallised lactose 90-180 µm (carrier, excip)
	Recrystallised lactose 0-90 µm (carrier, excip)
	Recrystallised lactose 180-250 µm (carrier, excip)
	Dipac (carrier, excipient)
	Recrystallised lactose 250-500 µm (carrier, excip).
	Talc (glidant, excipient)
	Sucrose (carrier, model excipient)
	Emdex (carrier, excipient)
	Recrystallised lactose 500-710 µm (carrier, excip)
	Recrystallised lactose 710-1000 µm (carrier, excip)
	Starch (disintegrant excipient)
	Potassium sorbate (adherent, model drug).
Electropositive	Magnesium Stearate (lubricant, excipient)

would reverse the positions in the triboelectric series.

Table 34 shows the adherent drug, potassium sorbate to be electropositive whereas both Dipac and Elcema G250 were both electronegative. However, Elcema G250 was far more electronegative than Dipac powder. Under these conditions, the potassium sorbate would be attracted more by Elcema G250 particles than by Dipac when poured from a glass surface.

In measurements of interparticle adhesion forces made in Chapter 5, ordered mixes were formed between the adherent drug, salicylic acid, which was the most electronegative powder in the triboelectric series (Table 35) and the excipient powders, Dipac, Emdex, sucrose and recrystallised lactose (250 - 500 µm and 500 - 710 µm particle size fractions).

The fine powders used as additives in ternary ordered mixes (section 5.2.5) included magnesium stearate (section 5.2.5.1) and starch and talc (section 5.2.5.2). The magnesium stearate and starch powders both de-stabilised ordered units containing salicylic acid as a model drug and caused a marked decrease in interparticle adhesion forces. Both magnesium stearate and starch powders were electropositive and would be strongly attracted to both drug and excipient powders.

This could cause adherent drug particles to be replaced on the carrier surface by magnesium stearate particles, especially if ordered mixing occurred by dynamic rearrangement of the fine particles on the carrier surfaces.

In addition, the strong attraction between magnesium stearate and drug particles would tend to cause stripping of the drug particles from the excipient surface as predicted by Lai and Hersey (134).

In contrast, the talc appeared to stabilise ordered mixes of drug and sucrose excipient particles (section 5.2.5.2). Talc was found to have a very similar electronegativity to sucrose; the carrier excipient (Table 34) sucrose had a mean static charge of -2.4×10^{-9} C.g^{-1} and talc had a surface charge of -2.7×10^{-9} C.g^{-1}. Since the talc had a similar order of electronegativity to the excipient particles, the surface charge of the talc was unable to disrupt the binary ordered mix already formed between sucrose and salicylic acid. This stabilising effect prevented the ordered units from separating when subjected to high removal forces in an ultracentrifuge (section 5.2.5.2).

As indicated earlier, using different experimental conditions it may well be impossible to reproduce the rank order of powders in the triboelectric series presented in Table 35; this is partly due to the complex nature of powder surfaces (231). For comparison Table 36 shows the results for a similar set of pharmaceutical powders measured independently (233) in a separate laboratory.

The absolute values for surface charges did not coincide with those obtained in the experiments described above (Table 34). Nevertheless, the signs of the charges were the same and the order of magnitude of the charges were similar.

In addition to determining the surface charge on the various drugs and excipients poured off a glass surface, the measurements were repeated using a plastic surface to pour the powders into

Table 36. Static charges on the surfaces of several different pharmaceutical powders as measured by M. J. Pearse (233)

Sample	Specific charge ($C.g^{-1}$)
Recrystallised Lactose (250 - 500 µm fraction)	-6.4×10^{-9}
Elcema G250	-5.1×10^{-9}
Avicel PH 101	-2.4×10^{-9}
Magnesium stearate	$+4.7 \times 10^{-9}$
Original lactose powder	-2.5×10^{-9}

the Faraday well. The results are shown in Table 37 and reveal that using a different surface altered the sign of the surface charge on the powders as well as the charge magnitude.

Table 37. Mean specific charges of different powders measured after pouring off a plastic surface

Powder Sample	Mean specific Charge(10^{-9} $C.g^{-1}$)	95% Confidence limits	Variance
Dipac	- 6.1	± 0.32	0.03
Emdex	+ 4.7	± 0.40	4.29
Recrystallised lactose 0 - 90 µm	+ 17.0	± 1.8	0.91
90 - 180 µm	+ 24.0	± 1.7	0.75
180 - 250 µm	+ 30.0	± 0.64	0.11
250 - 500 µm	+ 16.0	± 1.6	0.79
500 - 710 µm	+ 28.0	± 3.6	3.84
710 - 1000 µm	+ 7.7	± 1.0	0.27
Recrystallised lactose (whole size range)	+ 11.0	± 1.5	0.65
Potassium chloride (> 45 µm)	- 0.21	± 0.4	4.80
Potassium chloride (< 45 µm)	- - 6.9	± 0.15	0.62

Whereas in powders poured off a glass surface, most of the particles charged negatively, the reverse was true in pouring powders off a plastic surface. Both Emdex and all the particle size fractions of recrystallised lactose displayed charge reversal and all of the powders became less electronegative when poured off a plastic surface (Table 37). This occurred because glass and plastic (polyethylene) are at opposite ends of a triboelectric series (Table 38) as shown by Hendrick (231)

Table 38. Typical triboelectric series reported by Hendrick (231). The materials at the top of the series are positive with respect to those lower in the series

Glass
Quartz
Mica
Wool
Cat's fur
Silk
Cotton
Wood
Amber
Resins
Metals
Polystyrene
Polyethylene
Teflon

Glass is more electropositive than most materials and will therefore produce electronegative image charges on most other surfaces,whereas

plastic is more electronegative and tends to produce electropositive separation charges on other powder surfaces as shown in Table 37. Triboelectrification of two dissimilar surfaces in mutual contact occurs by transfer of electrons from one material to another. When the surfaces are two dissimilar metals such as, for example, caesium and tungsten the electron transfer occurs until the Fermi levels are aligned. The Fermi levels indicate the positions of conduction electrons which have an unexcited energy level in comparison with a reference level outside the metal known as the "vacuum" energy level (Figure 129). For caesium in isolation, the separation energy, or in other words the difference between the Fermi level to vacuum level, is 3.04×10^{-9} J (Figure 130a) whereas tungsten has an energy of 7.2×10^{-19} J (Figure (130a) in isolation. When the two metal surfaces are brought together, electron transfer occurs until the Fermi levels are equal. To reach this state tungsten has lost electrons and thus becomes positive whereas caesium has gained electrons and becomes negative (Figure 130b). The potential observed externally is the difference between the two work functions (separation energies referred to earlier) which is 4.16×10^{-9} J in this example (231). The same electron transfer occurs for insulators although the exact mechanism is not well understood, and only electrons close to the surface of insulators such as most drug and excipient powders, are probably involved in the charging process. The difference in the work functions between two materials A and B will be $\Phi_A - \Phi_B$, and where material A is strongly electropositive such as glass, most powders will lose electrons and become electronegative whereas a strongly electronegative material A, such as polyethylene, will act as an electron

Figure 129. Definition of the work function, Ø, in relation to the vacuum and Fermi energy levels of a metal.

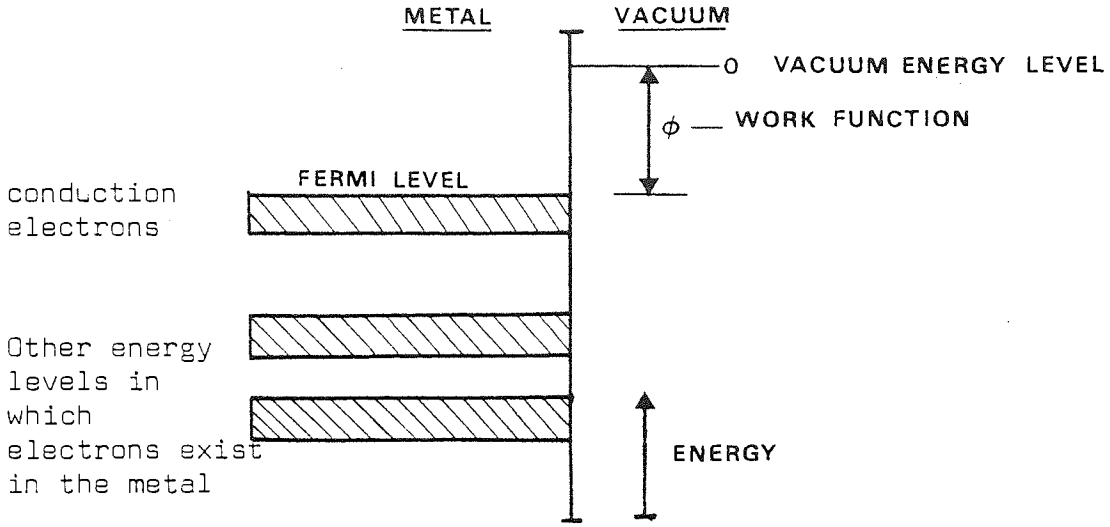

Figure 130. Mechanism of contact charging using 2 metals, caesium and tungsten as examples $Ø_C$ & $Ø_t$ are the work functions of casesium and tungsten respectively.

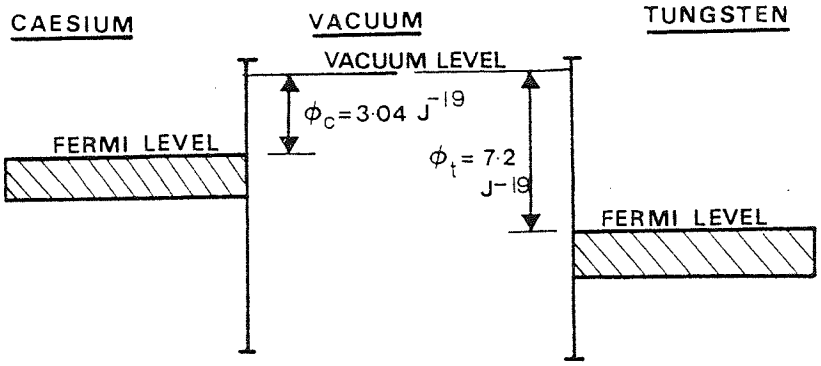

(a) Energy levels of caesium and tungsten in isolation

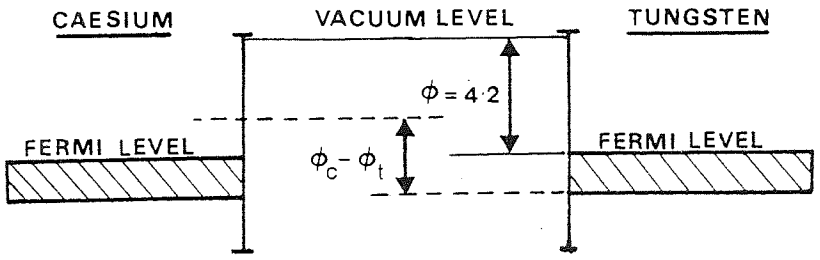

(b) Energy levels of caesium and tungsten in contact

donor to other powder surfaces which thus become electropositive. Exceptions to these two examples occur when powders are more electropositive than glass or more electronegative than plastic.

In the context of ordered mixing, there are significant implications from the finding that polyethylene surfaces produced a positive charge or weakened the electronegative charges on the surfaces of pharmaceutical powders. The ordered mixes produced in Chapter 4 between the model drug potassium chloride and either Emdex, Dipac or recrystallised lactose powders were formed in a Y-cone blender constructed in perspex. Table 37 shows that whereas potassium chloride powder remained electronegative, the Emdex and recrystallised lactose powders became strongly electropositive when poured off a plastic surface. This change in sign and strength of the surface static charge on the carrier particles, Emdex and recrystallised lactose would increase the attraction for the electronegative particles of potassium chloride. In contrast, according to Table 37, the Dipac powder particles remained electronegative and would therefore be less strongly attracted to the weakly electronegative potassium chloride.

Thus, from the measurements obtained by pouring off electronegative (plastic) surfaces, Emdex and recrystallised lactose would be more strongly attracted to particles of potassium chloride powder than Dipac. This may partly account for the increased stability of Emdex and recrystallised lactose ordered mixes when subjected to vibration (Chapter 4) or to removal forces in an ultracentrifuge (Chapter 5), compared with the unstable ordered mixes containing Dipac. Particles of Dipac and potassium chloride had similar work functions as indicated by their specific charges and were therefore not attracted to one another.

6.2 Triboelectric Charging

The modification of surface charge in the study described in the previous section was mainly caused by contact charging with only a small contribution from frictional electrification. The frictional charging of powder particles, that is true triboelectrification, can be used to increase the static charge on particle surfaces. Triboelectric charging has the advantages over another electrostatic charging method known as corona charging in that explosion hazards resulting from spark-over are reduced, and the influence of humidity on charging efficiency is minimal and under normal conditions does not need to be controlled (234). There are several different methods of triboelectric charging powder particles including rotating drums, vibrating chutes, fluidised beds and pneumatic systems such as the electrocyclojet and the air cyclone (202). Of these, the air cyclone is reported to produce the most reproducible charge densities and a specific particulate charge which is at least an order of magnitude greater than that attained by friction on a vibrating chute (202).

6.2.1 Method

A brass cyclone was specially constructed as shown in Figure 131. The dimensions shown in Figure 131 used to construct the cyclone utilised in these experiments were not the only possible combinations. Table 39 shows the various dimensions of cyclones constructed by others, standardised by comparison with the cylinder diameter used in each design. The cyclone used in these experiments (Number 6, Table 39) was constructed to produce the maximum contact between individual particles and the cyclone wall. In each experiment the vortex finder was set at a height to remove

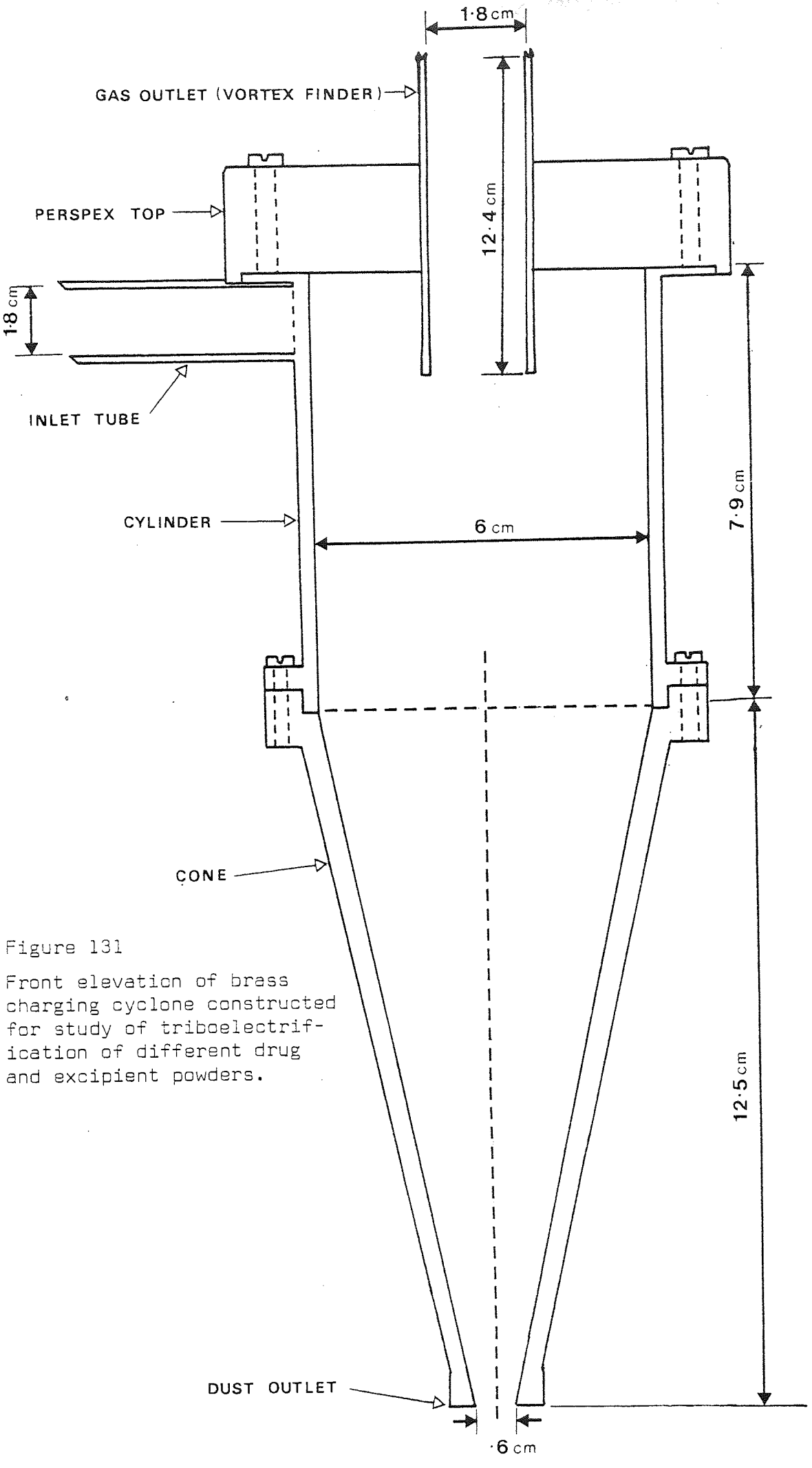

Figure 131

Front elevation of brass charging cyclone constructed for study of triboelectrification of different drug and excipient powders.

the inner vortex of air without removing any of the charged particles. In this way the gas outlet acted as an exit for all the fluidising air whilst the dust outlet at the base acted as an exit for all the charged particles.

The material used to construct the cyclone was brass and should ideally be chosen according to its work function which should fall between the work functions of the two powder components to be charged so that the ordered mix subsequently formed would be as stable as possible due to the maximum mutual attraction between ordered units. The use of a metal in the construction of the charging cyclone has the advantage that it can be earthed to prevent charge build-up and minimise possible hazards such as non-uniform triboelectrification of different particles and in the worst case, spark-over. A perspex cyclone was used by Pope et al. (201) to charge different mineral powders but they found that the unearthed perspex produced less reproducible charges than a nickel-coated brass cyclone.

Figures 132 a and b show the arrangements of the specially constructed triboelectric charging apparatus. The air-flow used to carry the powder particles in to the charging cyclone was supplied from a blower (Model TL91, BVC Ltd., Leatherhead, U.K.) and the flow rate could be adjusted according to the differential pressure indicated by the manometer. Air from the blower entered the apparatus via the flow box, packed with expanded polystyrene chips to ensure turbulence. The emergent turbulent air stream passed to the charging cyclone down a horizontal glass tube. A vertical side arm was connected through ground-glass joints to a funnel opening into a pressurised perspex container. A second blower (Model 79E42891, Costech Ltd., St. Albans, U.K.) was used

Figure 132

(Fig. 132(a) photograph of apparatus shown in (b)). (b) Diagram showing the assembled charging apparatus with the charge measuring apparatus in position.

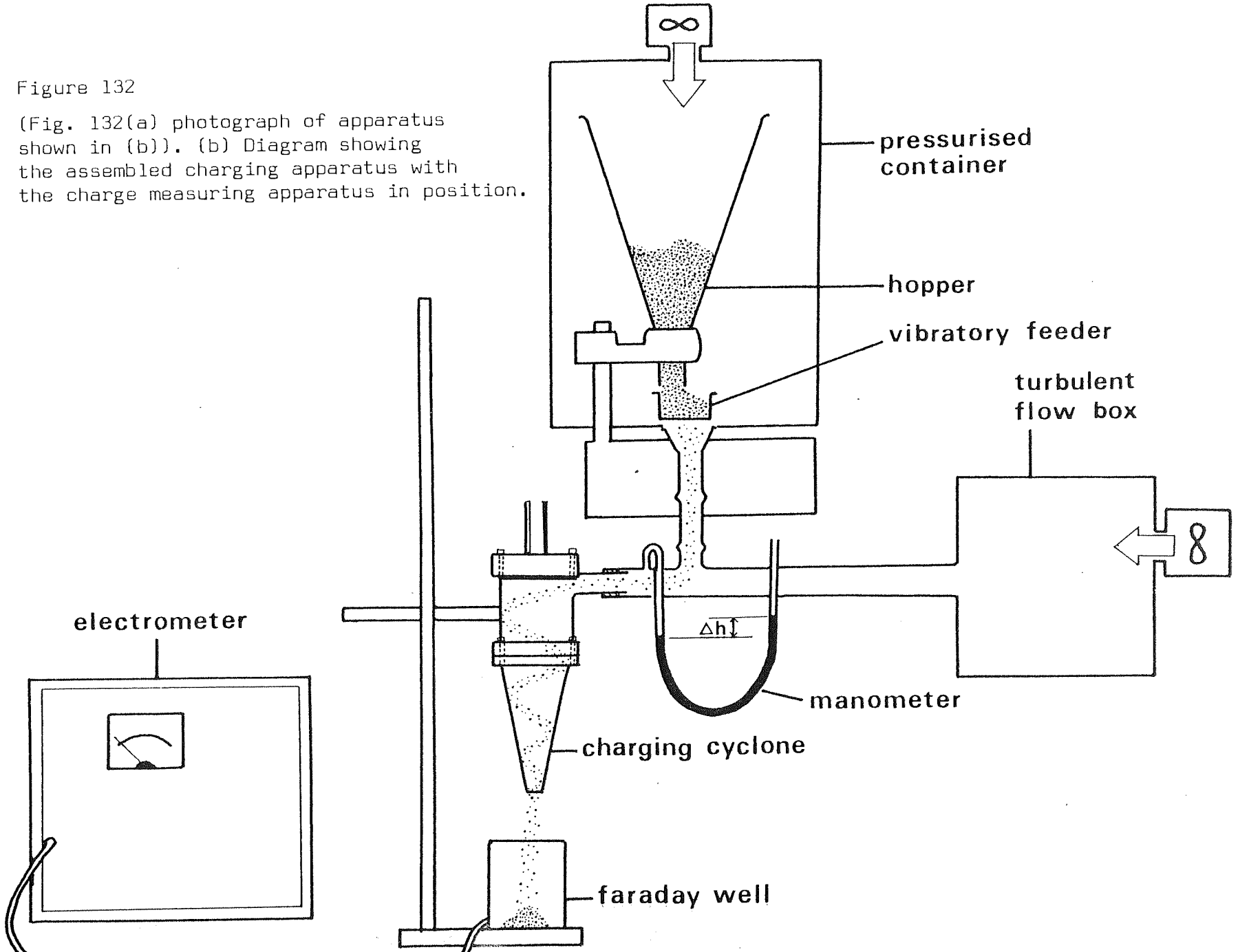

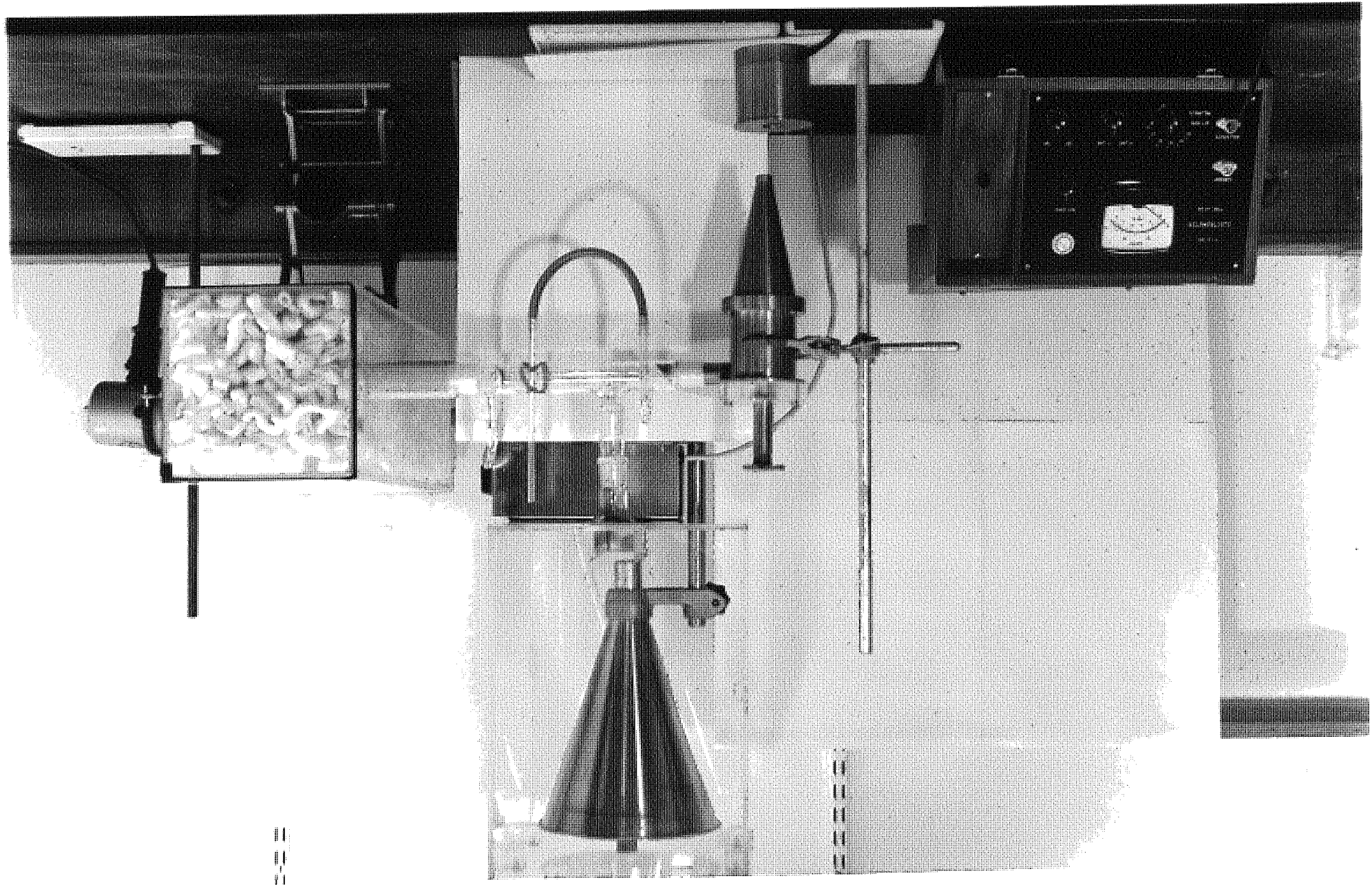

Table 39. Dimensions used by various investigators for construction of cyclones. (Dimensions represent proportions of cylinder diameter, D, within a cyclone specification.)

No.	Inlet Height	Cylinder Diameter	Cylinder Length	Cone Length	Inlet Width	Gas Outlet Diameter	Gas Outlet Depth	Dust Outlet Diameter	Reference Source
1	-	D	1.35 D	1.8 D	-	0.5 D 0.4 D	-	-	235
2	0.5 D	D	1.5 D	2.5 D	0.2 D	0.5 D	0.5 D	0.38 D	236
3	0.75 D	D	1.5 D	2.5 D	0.38 D	0.75 D	0.88 D	0.37 D	236
4	0.5 D	D	2.0 D	2.0 D	0.25 D	0.5 D	0.63 D	0.23 D	237
5	0.32 D	D	1.3 D	2.2 D	0.32 D	0.3 D	0.96 D	0.1 D	238
6	0.25 D	D	1.3 D	2.1 D	0.3 D	0.3 D	Variable	0.1 D	Fig. 131

to provide a pressure gradient so that powder, fed into the glass funnel from the hopper via the vibratory feeder was injected into the horizontal air stream and was not blown back into the pressurised perspex container. Powder particles were injected into the horizontal glass tube at a constant rate by the vibratory feeder and were pneumatically carried into the charging cyclone in air suspension. The particles were directed to the cyclone wall and impinged tangentially. Following the initial wall impact the particles fell helically down towards the dust outlet in constant frictional contact with the cyclone wall. At the cyclone base the triboelectrically charged particles left through the dust outlet whereas the air formed an inner upward vortex which was removed at the top of the cyclone through the gas outlet. After charging in the cyclone the particles were collected in the Faraday well connected to a Keithley model 610C electrometer. The triboelectric charge acquired by the sample was determined as described in section 6.1.1 except that powder was introduced direct from the cyclone to the Faraday well without pouring off an intermediate surface. The drug and excipient powders used in Chapters 4 and 5 whose charge densities had been measured as discussed in section 6.1, were charged triboelectrically using the cyclone apparatus.

6.2.2 Results and Discussion

The static charges induced triboelectrically on the surfaces of the different drug and excipient powders are shown in Table 40. The pressure of the air stream used to transfer the powders into the cyclone was kept constant at approximately 62 mm and the feed rate of powder was adjusted to the values recorded in Table 40 to produce the maximum specific charge on the different powder particles.

Table 40. Different drug and excipient powders charged triboelectrically in an earthed brass cyclone. The pneumatic air stream was kept at a constant flow rate indicated by a differential pressure of 62 mm. Values are expressed in terms of 10^{-9} $C.g^{-1}$ to facilitate comparison with Table 34

Powder Sample	Mean Specific Charge (10^{-9} $C.g^{-1}$)	95% Confidence Limits	Mean Specific Charge Rate (Current, Amp)	Variance	Mean Flow Rate ($g.s^{-1}$)
Dipac	-130.0	± 23	6.3×10^{-9}	0.02	0.20
Emdex	-1,300.0	± 46	45×10^{-9}	0.06	0.23
Recrystallised lactose 250 - 500 µm size fraction	-130.0	± 35	7.8×10^{-9}	0.04	0.13
Recrystallised lactose 500 - 710 µm size fraction	-470.0	± 16	29×10^{-9}	0.01	0.07
Recrystallised lactose 710 - 1000 µm size fraction	-360.0	± 63	13×10^{-9}	0.13	0.04
Potassium chloride	-550.0	± 110	54×10^{-9}	0.34	0.14
Elcema G250	-330.0	± 100	20×10^{-9}	0.30	0.05
Sucrose	-510.0	± 230	3.7×10^{-9}	1.73	0.35
Starch	-200.0	± 120	2.6×10^{-9}	0.44	0.19
Magnesium Stearate	+17	± 14	39×10^{-9}	2.03	0.003
Talc	-49	± 26	0.85×10^{-9}	0.64	0.17

When compared with the previous results (Tables 34 and 37), the results in Table 40 show that the electronegativity of all of the powders was increased by triboelectric charging. Static charges on most of the powders were increased by a factor of at least ten by triboelectrification compared with the charge measured by pouring the powders off a glass slope (Table 34). The only powder which was charged positively by triboelectrification was magnesium stearate and the charge increased from $+8.8 \times 10^{-9}$ $C.g^{-1}$ when poured off glass to $+17 \times 10^{-9}$ $C.g^{-1}$ by triboelectric charging. The starch powder which carried a weak positive charge of $+0.13 \times 10^{-9}$ $C.g^{-1}$ when poured off glass, became electronegative (-200×10^{-9} $C.g^{-1}$) when charged triboelectrically. The excipients Dipac, Emdex and recrystallised lactose used as carrier powders in the formation of ordered mixes with potassium chloride, increased in electronegativity. Dipac increased from -7.6×10^{-9} $C.g^{-1}$ when poured off glass, to -130×10^{-9} $C.g^{-1}$ when charged triboelectrically and recrystallised lactose (250 - 500 µm size fraction) increased from -2.9×10^{-9} $C.g^{-1}$ off glass to -170×10^{-9} $C.g^{-1}$ by triboelectrification. The electronegative static charge on Emdex excipient particles increased more than either Dipac or recrystallised lactose from -1.2×10^{-9} $C.g^{-1}$ off glass by a factor of 1,000 to $-1,300 \times 10^{-9}$ $C.g^{-1}$ when charged triboelectrically.

The mean specific charge rate in column 4 of Table 40 is synonymous with the measured current since Coulomb per second is a definition of the ampère. The current is affected by the flow rate of powder into the charge cyclone as well as the charge picked up by triboelectrification. The powder flow rate influenced particle charge by affecting the quantity of individual particle frictional contacts with the cyclone wall.

The excipient powders, Dipac, Emdex and recrystallised lactose (250 - 500 μm, 500 - 710 μm and 710 - 1000 μm size fractions) were used as well as the drug powder, potassium chloride, to study the effect of powder feed rate and differential air pressure (air velocity) on the charge density. Table 41 shows the effect of feed rate on the triboelectrification of potassium chloride. When poured off a glass surface the measured charge of potassium chloride was negative. At a flow rate of 0.14 $g.s^{-1}$ and 63 mm air pressure, the potassium chloride was triboelectrically charged negatively. However, when triboelectrification was continued for 35 seconds or longer, charge reversal occurred and the potassium chloride became electropositive. Table 41 shows that varying the powder flow rate altered both the mean specific charge and the time at which charge reversal occurred. At the maximum flow rate of 4.63 $g.s^{-1}$, charge reversal was instantaneous and the potassium chloride had a mean specific charge of $+65 \times 10^{-9}$ $C.g^{-1}$. Intermediate flow rates produced charge reversal at between 0 and 35 seconds, usually at approximately 5 seconds (Table 41). The process of charge reversal could have occurred as a result of particles of potassium chloride rubbing on other potassium chloride crystals rather than on the brass cylinder wall which became coated with a fine layer of potassium chloride particles. At high feed rates this process of self-charging and coating occurred instantaneously, whereas at low feed rates charge reversal took proportionately longer. However it is also possible that charge reversal occurred as a result of mechanical fracture of potassium chloride crystals during triboelectrification. This mechanism is known to produce massive particle charging in crystals such as mica (231). If fracture charging occurred during triboelectrification

Table 41. Effect of feed rate on the triboelectrification of potassium chloride powder (<45 μm diameter)

Mean Flow Rate ($g.s^{-1}$)	Mean Specific Charge (10^{-9} $C.g^{-1}$)	95% Confidence Limits	Variance	Mean Specific Charge Rate (Current, Amp.)	Differential Air Pressure (mm)	Charge Reversal Conditions	
						Maximum Electronegative Charge ($C.g^{-1}$)	Time at which charge reversal occurred (s)
0.14	-550	± 11	0.34	54×10^{-9}	63	Not measured	35
0.71	+34	± 3.4	5.30	1.7×10^{-9}	63	-100×10^{-9}	1 - 4
0.97	+70	± 4.2	0.21	3.9×10^{-9}	63	0	0
4.63	+65	± 3.9	3.59	25×10^{-9}	63	-100×10^{-9}	5 - 6

of potassium chloride, high feed rates would be more likely to increase the effect by raising the interparticle collision rate. This is analogous to size reduction in a fluid energy mill where particles are fractured by interparticle collisions.

Increasing the feed rate during triboelectrification of Dipac powder did not produce charge reversal (Table 42). At an air pressure of 62 mm the maximum negative triboelectric static charge on Dipac particles was produced with a feed rate of 0.13 $g.s^{-1}$. Above this feed rate, fewer individual Dipac particles come into contact with the cyclone wall and frictional charging decreases as the feed rate increases. At powder flow rates below 0.13 $g.s^{-1}$, the static charge fell to -20×10^{-9} $C.g^{-1}$ at 0.04 $g.s^{-1}$, probably as a result of fewer interparticle collisions during triboelectrification. The effect of varying the velocity of the pneumatic air stream on the triboelectric charging of Dipac particles is also shown in Table 42. At lower air velocities, represented by a differential pressure of 45 mm, the mean specific charge reached a maximum value of -470×10^{-9} $C.g^{-1}$. At much reduced air velocities such as those producing a 20 mm differential pressure, the specific charge fell to around -220×10^{-9} $C.g^{-1}$. Part of the contribution to the triboelectric charge on a particle comes from impact with the cyclone wall. At very low air speeds the impact force would be reduced and thus the triboelectric charge would also fall. The maximum surface charge on Dipac particles was found in optimum conditions produced by an air pressure of 45 mm and a feed rate of 0.21 $g.s^{-1}$ (Table 42).

Emdex powder particles gained their lowest frictional charge of -390×10^{-9} $C.g^{-1}$ by charging with a maximum mass feed rate of 1.81 $g.s^{-1}$ at 63 mm air pressure. At the same air pressure

Table 42. Effect of feed rate and differential air pressure on the triboelectrification of different excipient powders

Powder Sample	Mean Feed Rate ($g\ s^{-1}$)	Differential Air Pressure (mm)	Mean Specific Charge ($10^{-9}\ C\ g^{-1}$)	95% Confidence Limits	Variance	Mean Specific Charge Rate (10^{-9} amp
Dipac	0.04	62	-20	±2.5	1.85	0.07
	0.13	62	-230	±9.9	0.29	0.11
	0.14	20	-220	±7.8	0.18	0.17
	0.20	62	-130	±2.3	0.02	6.3
	0.21	45	-470	±3.9	4.47	0.55
	0.71	62	-48	±2.5	1.88	2.7
	3.56	62	-23	±2.8	0.02	3.4
Emdex	0.19	75	-1,200	±18.4	0.01	58
	0.23	63	-1,300	±45.7	0.06	45
	0.63	63	-780	±14.8	0.64	73
	1.81	63	-390	±8.9	0.23	150
Recrystallised Lactose, 250 - 500 µm size fraction	0.02	56	-560	±24.5	1.77	9.5
	0.13	58	-190	±58.8	0.10	12
	0.13	64	-130	±35.3	0.04	7.8
	0.31	56	-66	±22.7	1.53	3.5
Recrystallised Lactose, 500 - 710 µm size fraction	0.07	62	-470	±15.9	0.01	29
	0.18	63	-310	±82.7	0.20	23
	0.95	63	-68	±8.7	0.22	6.8
Recrystallised Lactose, 710 - 1000 µm size fraction	0.04	63	-360	±63.0	0.13	13
	0.28	63	-230	±49.0	0.07	25
	1.38	63	-94	±8.7	0.22	15

a reduction in feed rate increased the triboelectric charge.

In recrystallised lactose (250 - 500 μm size fraction), the triboelectric charge was increased when the air pressure was reduced at a given feed rate (Table 42). The increase in surface charge occurred as a result of the same quantity of powder coming into more prolonged frictional contact with the cyclone walls. A reduction in feed rate whilst maintaining the air pressure further increased the electrostatic charge. This occurred as a result of increasing the quantity of individual particle-cyclone wall triboelectric contacts. Conversely, an increase in feed rate at the same air pressure caused a marked decrease in the surface charge on the lactose particles. The decreased charge was caused by a lower number of individual particles coming into triboelectric contact with the brass cyclone due to the presence of a larger bulk of powder passing through the system at the increased feed rate.

A coarser particle size fraction of recrystallised lactose, 500 - 710 μm, developed a surface charge similar to particles in the 250 - 500 μm size fraction when triboelectrified using an air pressure of 63 mm and a powder flow rate of 0.18 $g.s^{-1}$ Table 43). The electrostatic charge decreased when the feed rate of the 500 - 710 μm size fraction was increased. As in previous experiments the charge decreased with an increase in feed rate as a result of reduced intimate particle contact with the cyclone wall. Conversely, the increased particle contact caused by reducing the powder flow through the cyclone increased the triboelectric charge.

The coarsest size fraction of recrystallised lactose, 710 - 1000 μm, had a similar triboelectric charge range to the other

size fractions of recrystallised lactose powder. As expected from previous results, increasing the powder flow rate reduced the static charge, whereas decreasing the feed rate produced an increase in static surface charge to -3.6×10^{-7} C.g^{-1} (Table 42).

6.3 Charge Retention

The degree of retention of an increased static charge produced by triboelectrification on particle surfaces is important in assessing firstly the likely residual interparticle attractions after different lengths of time and secondly the problems which a highly electrostatic powder bed could cause during subsequent powder processing. The residual potential (or charge), V_p, at time t_c, can be derived theoretically by treating the charged particle as a condenser of capacity C_c, with a leakage resistance, R, given by the equation (205):

$$V_p = V_{po}\, e^{-tc/RC_c} \qquad (105)$$

where V_{po} is the original potential or charge on the particles. The product $R.C_c$ is commonly referred to as the time constant τ of the condenser (sometimes known as the charge relaxation time constant). τ is the time taken for the potential or charge to fall to $V_{po}.e^{-1}$ or 0.369 of the initial value. Walton (205) derived the following expressions to calculate the time constant, τ, from the potential and the rate of fall of potential at any time:

$$RC_c = \tau = \frac{-V_p}{dV_p/t_c} \qquad (106)$$

For a condenser formed by a powder with a dielectric resistivity ρ_r measured in electrostatic units and a dielectric constant, k, the time constant, τ, in seconds, is given by:

$$\tau = \frac{\rho_r . k}{4\pi} \qquad (107)$$

This becomes:

$$\tau = \frac{\rho'_r . k}{4\pi . 9 \times 10^{11}} \qquad (108)$$

where ρ'_r, the volume resistivity is measured in ohm. cm^{-1} and τ is in seconds.

Walton (205) claimed that this relationship for charge retention was independent of the geometry of the condenser (particle shape). However if the condenser loses charge by surface conduction as well as by bulk conduction, the value of the time constant will be smaller than that indicated by the above formulae.

Using equation (108) to calculate the charge decay period of the excipient powders studied here, the approximate time for 63% discharge (τ) from excipient particles is 2.94 minutes which is close to the value of 3 minutes given by Harris (239) as the half-period for charge decay of most organic powders. The equivalent time constant, $\bar{\tau}$, for potassium chloride powders is approximately 4.4 minutes according to equation (108).

6.4 Triboelectric Charging as an Ordered Mixing Process

Surface electrostatic charges described in section 6.1 appeared to influence the stability of ordered mixes formed between drug and excipient particles. For example, particles of Dipac and potassium chloride particles theoretically had a low mutual electrostatic attraction and these two powders formed ordered mixes which segregated when subjected to different vibration conditions (section 4.3.2.1). Conversely, particles of

Emdex were predicted to have a higher electrostatic attraction for particles of potassium chloride, and these two powders were found to form stable ordered mixes. Ordered mixes were formed by triboelectrically charging drug and excipient particles simultaneously in the apparatus shown in Figure 132. The powders were then subjected to vibration conditions previously shown to produce a marked segregation tendency for the specific ordered mix being examined (section 4.3.2). The segregation tendency of ordered mixes following triboelectrification were compared with the segregation of the same ordered mix without triboelectric charging.

6.4.1 Method

The excipients studied included Emdex, Dipac and recrystallised lactose (particle size fractions 250 - 500 µm and 710 - 1000 µm) mixed with the drug, potassium chloride. Ordered mixes were studied containing ½% potassium chloride with Dipac, ½% potassium chloride with recrystallised lactose, 710 - 1000 µm size fraction and 10% ordered mixes of potassium chloride with Dipac, Emdex and recrystallised lactose, 250 - 500 µm size fractions. The drug and excipient powders were mixed initially in a mortar using a glass rod in place of the pestle to reduce attrition. The surface of the container and stirrer were chosen to produce the lowest frictional and contact charging effect. The use of a perspex blender was avoided because of the unusual surface charges produced by plastic surfaces. Following mixing, a sample of powder was filled into the sampling cylinder described in section 4.3 but not vibrated, and the homogeneity of the ordered mix was assessed by comparing the drug content in different stacking units

of the sampling cylinder, on the basis of the coefficient of variation. A homogeneous ordered mix was assumed to have been formed when the coefficient of variation of powder samples was less than 2%. When this homogeneity was achieved the powder mix was filled into the hopper of the triboelectric charging apparatus (Figure 132).

The particular conditions of triboelectrification such as air velocity and feed rate were chosen to optimise the mutual attraction of the drug and excipient powders being processed. Conditions were used which were previously shown to produce the largest possible electropositive charge on potassium chloride particles and the largest possible electronegative static charge on the excipient particles. The results obtained in section 6.3 were used to select the optimum triboelectric charging conditions for the various drug and excipient powder mixes. The charged ordered units emerging from the dust outlet of the cyclone were directed straight into the sampling cylinder (section 4.3) and the coefficient of variation of each triboelectrically charged mix was again determined.

The process of triboelectrification followed by filling into the sampling cylinder was repeated for each ordered mix and each mix was then subjected to vibration for 15 minutes by the method described in section 4.3.1. Following vibration, the homogeneity of the triboelectrically charged ordered mixes was again assessed.

6.4.2 Results and Discussion

The conditions such as flow rate and air pressure used to charge the various drug and excipient ordered mixes triboelectrically in the brass charging cyclone are shown in Table 43. Table 43

also shows the resultant specific charges and charge rates or currents of the different ordered mixes. In each powder mix, the overall charge on the ordered units was negative since the majority of particles in the mixes were electronegative excipient powders which predominated over the small electropositive contribution of

Table 43. Triboelectric charging conditions of different drug and excipient ordered mixes

Powder Sample	Specific Charge ($C.g^{-1}$)	Specific Charge rate (Current, amp.)	Flow Rate ($g.s^{-1}$)	Air Pressure (mm)
Dipac & 0.5% potassium chloride	-28×10^{-9}	5.1×10^{-9}	5.1	63
Recrystallised lactose (710-1000 µm size fraction) & 0.5% potassium chloride	-150×10^{-9}	38×10^{-9}	0.88	63
Dipac & 10% potassium chloride	-22×10^{-9}	3.7×10^{-9}	5.1	63
Emdex & 10% potassium chloride	-120×10^{-9}	42×10^{-9}	0.22	63
Recrystallised lactose (250-500 µm size fraction) & 10% potassium chloride	-93×10^{-9}	5.3×10^{-9}	0.20	63

the potassium chloride particles even when the drug content was 10% of the total powder mass. The net negative charge on each 2-component system resulted from a residual negative charge remaining when the Fermi levels of the potassium chloride and excipient particles in ordered units became energetically equal (section 6.1.2) following charging.

The vibration conditions chosen to examine the stability of ordered mixes formed between triboelectrically charged powders

were those which caused the greatest segregation tendencies on the corresponding ordered mixes which had not been triboelectrically charged. For this reason the vibration conditions were combinations of low frequencies and high acceleration forces, usually 50 Hz and 2.25 G.

Table 44 shows the frequencies and acceleration forces used to vibrate the different powder mixes along with the corresponding coefficients of variation of mixes charged triboelectrically and those not subjected to triboelectric charging.

Of the excipient powders Emdex, Dipac and recrystallised lactose (250 - 500 μm size fraction) that were used to form ordered mixes with 0.5% potassium chloride, only Dipac showed marked segregation (section 4.3.2.1). For this reason an ordered mix of Dipac and 0.5% potassium chloride powder was charged triboelectrically and subjected to vibration at 50 Hz and 2.25 G. Under these conditions a similar ordered mix of Dipac and 0.5% potassium chloride, not triboelectrically charged, showed marked segregation - having a coefficient of variation of 61.48% with high error limits meaning that the actual segregation value could lie between CV = 33.18% and CV = 89.78% (with 95% confidence). Following triboelectric charging of the same system, vibration at 50 Hz and 2.25 G produced a much reduced segregation tendency indicated by a coefficient of variation of only 6.9% (Table 44). In addition to a lower coefficient of variation, the error limits were also greatly reduced.

Of the other excipients mixed with 0.5% potassium chloride and subjected to different vibration conditions in section 4.3, the recrystallised lactose, 710 - 1000 μm particle size fraction, underwent the most marked segregation represented by a coefficient of variation of 19.57% when vibrated at 50 Hz and 2.25 G (Table 44).

Table 44. Segregation tendencies of different ordered mixes subjected to various vibration conditions with and without prior triboelectrification. (Coefficient of variation = CV)

	Vibration frequency (Hz)	Vibration acceleration (G)	Without charging		With triboelectric charging	
			CV(%)	Error Limits	CV(%)	Error Limits
Dipac and 0.5% potassium chloride	50	2.25	61.48	± 28.3%	6.9	± 1.4%
Recrystallised lactose (710 - 1000 µm size fraction) & 0.5% potassium chloride	50	2.25	19.57	± 5.5%	3.9	± 0.85%
	30	2.25	21.15	± 13.5%	13.2	± 1.8%
Dipac and 10% potassium chloride	50	0.75	-	-	3.1	-
	50	2.25	500.1	±175.6%	17.9	± 1.95%
Emdex and 10% potassium chloride	50	2.25	118.9	± 4.5%	7.4	± 1.4%
Recrystallised lactose (250 - 500 µm size fraction) & 5% potassium chloride	50	2.25	93.2	± 0.2%	13.5	± 3.3%

When the same ordered mix was triboelectrically charged prior to vibration at 50 Hz and 2.25 G, the segregation tendency was reduced to 3.9% (Table 44). A further sample of this same ordered mix of 0.5% potassium chloride and recrystallised lactose, was also subjected to vibration at 30 Hz and 2.25 G. Under these conditions, triboelectric charging of the powder mixes prior to vibration reduced the segregation tendency from a CV of 21% to one of 13.2%.

The ordered mixes of drug and excipient powders which showed the greatest segregation tendencies when vibrated were those which contained 10% fine drug content. Results of vibration studies with powder mixes containing 10% potassium chloride plus Emdex, Dipac or recrystallised lactose (250 - 500 µm, size fraction) were presented in section 4.3.2.7. The 10% potassium chloride and Dipac ordered mixes subjected to vibration at 50 Hz and 2.25 G had a segregation tendency represented by a coefficient of variation of 500.1% with very high error limits such that the mean coefficient of variation could vary by as much as ± 175% (Table 44). This extremely high CV of 500.1% for Dipac was reduced to 17.9% (± 2%) by triboelectrically charging the same ordered mix prior to vibration (Table 44). Vibrating a separate sample of the same triboelectrically charged ordered mix at 0.75 G and 50 Hz produced very little segregation represented by a coefficient of variation of only 3.1% (Table 44).

An ordered mix containing 10% potassium chloride and Emdex had a high segregation tendency when vibrated at 50 Hz and 2.25 G (section 4.3.2.7) shown by a coefficient of variation of 118.9% (Table 44). When this Emdex mix was triboelectrically charged before vibration the coefficient of variation was reduced to 7.4%.

Ordered mixes of 5% potassium chloride and recrystallised lactose, 250 - 500 μm particle size fraction, had a high segregation tendency when vibrated at 50 Hz and 2.25 G (section 4.3.2.7). When the ordered mix was triboelectrically charged before vibration the mean coefficient of variation was reduced from 93.2% to 13.5%.

In all the ordered mixes studied, the coefficients of variation were markedly reduced by triboelectrically charging the drug and excipient powders prior to vibration. Triboelectric charging of the ordered mixes did not prevent the coefficient of variation increasing above the 2% level indicating that the powders were still segregated after vibration.

6.4.2.1 Mechanisms Producing Increased Particle Adhesion Following Electrostatic Charging

Several mechanisms are thought to be responsible for triboelectric charging reducing the segregation tendency of ordered mixes containing drug and excipient. Triboelectric charging increased the quantity of free electrons on the surface of the drug particles whilst it reduced the quantity of electrons on the surface of the excipient particles. The resulting increase in electrostatic forces and van der Waals forces created an increased mutual attraction between the drug and excipient particles in ordered units which produced several effects including increased cohesion.

Cross (250) outlined some of the effects which produce particle adhesion following electrostatic charging; these include Coulomb forces, dipole forces and molecular forces:

a) Coulomb forces: The Coulomb forces are the electrostatic adhesion forces made up of a charge component q and a mono-ionised field component, E_m:

$$F_{MAX} = q.E_m \qquad (109)$$

The charge, q, is the maximum charge per particle which was shown by Pauthenier (241) to be given by

$$q = 4\pi\varepsilon'_o.a_q^2.E_m \cdot p_d \qquad (110)$$

where a_q is the particle radius and p_d is a constant related to the dielectric constant, ε'_o, of the powder:

$$p_d = 1 + 2\left(\frac{\varepsilon'_o - 1}{\varepsilon'_o + 2}\right) \qquad (111)$$

The so-called Pauthenier limit approaches the corona point of a powder; this is the point at which the powder charge is greater than the resistivity of air and spark-over occurs. For a 40 μm diameter particle the Pauthenier limit is equivalent to a maximum charge of approximately 6×10^{-14} C per particle. Triboelectric charging of drug and excipient powders produced maximum particle charges below the Pauthenier limit and thus the true force (F_{MAX}) would be much lower than that calculated from equation (109). Even in powders which have maximum charges at the Pauthenier limit the Coulomb force produced would be less than 3×10^{-7} N and would not be sufficient alone to account for the observed adhesion.

b) Dipole forces: Powder particles held in a high ionisation field will have an induced dipole moment. The maximum dipole moment will be approximately:

$$4/3\pi a_q^3 (\varepsilon' - 1)\, \varepsilon'_o.E_m \qquad (112)$$

but where discharging predominates over charging this will reduce

to zero. Assuming uniform charging, the force on the dipole or maximum field gradient (F_g) is given by:

$$F_g = p_d.dE_m/dx \qquad (113)$$

where E_m is the field at a point a distance x from the substrate (excipient) surface.

The estimated dipole force, around 1.5×10^{-7} N for powders of the dimensions used in the present study was low and was probably not large enough to account for the increased adhesion following triboelectric charging, since the field gradient was small in a layer with a thickness less than 40 μm.

c) Molecular forces: Van der Waals forces were previously discussed in section 1.5.1.2 and were shown to act between any two molecules due to the instantaneous dipole in one molecule inducing a dipole moment in the other molecule. The force was shown to vary with distance according to the inverse 7th power over distances less than 20 nm and inverse eighth power over larger distances. Thus, the van der Waals forces between 2 macroscopic bodies depend critically on the true contact area between them. For two perfectly smooth spheres of radius, a_q, the adhesion is given by:

$$F^o_{vdw} = \frac{H.a_q}{12.Z_o}2 \qquad (114)$$

where H, is the Hamaker constant ($\approx 10^{-19}$ J) and Z_o is a separation constant (≈ 0.4 nm), F^o_{vdw} is less than 1×10^{-6} N although Dahneke (242) estimates the true adhesion force to be increased by a factor of at least 20 for materials with a low Young's modulus where surface flattening is produced. Harper (243) suggested

that at first contact a surface asperity could be represented mathematically by an approximation to a cone with its tip in contact with a plane surface of the adherent particle. As soon as there is any appreciable contact pressure between the surfaces the asperities deform plastically, forming small areas of true contact. The electrostatic forces described immediately above (a and b), particularly Coulomb forces, may be instrumental in producing this initial plastic deformation which brings the drug and excipient particles into close enough contact to increase the interparticle van der Waals adhesion forces. The radius of contact area r_c of two smooth spheres diameter D' pressed together by a load P_L is given by (240):

$$r_c = 0.723 \left(P_L . D' \left[\frac{1 - \nu_1^2}{E\,y1}\right] + \left[\frac{1 - \nu_2^2}{Ey2}\right]\right)^{\frac{1}{3}} \qquad (115)$$

where ν is the Poisson ratio and Ey the Young's modulus of each sphere.

For glass $r_c = 4 \times 10^{-8}$ m whereas for plexiglass (plastic) $r_c = 1 \times 10^{-7}$ m. For particles of drug and excipient with even lower Young's moduli the contact area may be further increased and thus van der Waal's force between flattened spheres given by the following expression will also be increased:

$$F^o_{vdw} = \frac{H.a_q}{12 Z_o^2} . 1 + \frac{2h}{Z_o} \qquad (116)$$

where h is the height of the flattened portion.

In particles with rough surfaces the true contact area is even more difficult to estimate. In the previous chapter and in section 1.5.1, interparticle bonding was discussed. Krupp (187) and Kattler et al. (193) explained their experimental results

for interparticle adhesion by consideration of van der Waals forces. Although it is difficult to prove the involvement of van der Waals' forces in producing increased adhesive forces between drug and excipient powder particles this is probably the dominant mechanism involved.

d) Other forces: Other factors apart from those affecting particle charge relationships need to be considered in assessing the influence of passing powders through a charging cyclone. Probably the most important is the effect referred to by Harper (243) as "hot-spot" formation. Hot-spots are produced on particles during triboelectric charging and can lead to localised high temperatures which can rise to 100^{o}C and can cause chemical changes and produce co-valent bonding between certain powder surfaces. In addition, triboelectric charging can cause cold-welding between metal particles although this effect can probably be discounted as a bonding mechanism in the drug and excipients studied here.

6.5 Conclusions

Drug and excipient powders were found to develop surface charges by processes such as contact and frictional electrification. The surface charges on powder particles were implicated in the formation of the ordered mixes studied previously, and in preventing their subsequent segregation or separation.

When measured after pouring off a glass surface most drug and excipient powders were found to charge electronegatively whereas when poured off a polyethylene surface many of the same powders were charged electropositively.

Excipients such as Emdex and recrystallised lactose which formed stable ordered mixes with drug powders such as potassium

chloride, had different charge signs . Conversely, Dipac which formed unstable mixes with drug powders had a comparable electronegative charge with, for example, potassium chloride.

It was thought that the effect on the stability of an ordered mix caused by the addition of a third component, such as magnesium stearate may have been due to the electrostatic charge on the third component. If the charge was similar to that of the carrier excipient the ordered mix could be stabilised but if the third component had a different charge than either the drug or the carrier excipient then the ordered mix could be destabilised producing segregation of the constituent powders.

In comparison with electrostatic charges on different drug and excipient powders when poured off a glass surface the charges were increased by a factor of at least 100 when measured after triboelectric charging.

The conditions used to produce triboelectrification were found to affect the specific charges of different powders. It was found that reducing the air pressure at a given feed rate increased the triboelectric charge. This increased charge occurred as a result of prolonged powder residence in the cyclone producing longer contact between particles and the cyclone walls. A reduction in feed rate whilst maintaining the air pressure further increased the electrostatic charge by producing a more intimate contact between particles and the cyclone walls.

By selecting conditions of triboelectrification which produced the optimum interparticle attraction between drug and excipient particles, the stability of the ordered mixes so formed was enhanced. Systems which produced the most marked segregation when vibrated under certain conditions described in Chapter 4 were re-tested

following triboelectrification. In each case the segregation of the vibrated ordered mixes was markedly reduced by triboelectric charging of the drug and excipient powders prior to vibration.

Triboelectrification was thought to increase the stability of ordered mixes by increasing the interparticle attractive forces such as Coulomb forces and van der Waal's forces.

Chapter 7

General Discussion

The results presented in this thesis show that the formation of a stable ordered mix is dependent on the properties of the excipient powder which acts as a carrier for adherent drug particles. The influence of the carrier excipient particles on the formation of stable ordered mixes can be sub-divided into two major categories: the effect of the surface structure of excipient particles on the segregation potential of ordered mixes and the effect of surface electrical charge on the stability of ordered mixes. Optimisation of these two properties was shown, in Chapters 4 and 6, to produce extremely stable, non-segregating ordered mixes between different drug and excipient particles. By controlling the surface properties of excipient particles in relation to the physical characteristics of drug particles in a specific pharmaceutical formulation it should be possible to form a non-segregating, free-flowing, direct compression formulation which produces tablets of low-dose drugs with high content uniformity.

7.1 Carrier Particle Surface Structure

The results presented in Chapter 4 showed that certain ordered mixes of drug and excipient powders became segregated when subjected to vibrational acceleration and frequencies typical of those found in some pharmaceutical processing equipment. Systems were especially prone to segregation when high G forces were applied at low frequency. Segregation of drug from excipient particles occurred by the mechanism of "constituent" segregation described by Yip and Hersey (131). At a given drug concentration the differences in segregation tendency of the various ordered

mixes were attributed to differences in the surface properties of the excipient particles. Excipients which had extremely irregular surfaces with high porosities and high surface roughness were found to produce ordered mixes which were more resistant to vibrational segregation than excipients with smoother, less irregular surfaces.

It was shown (Chapter 4) that, in the systems studied, there were many more adherence sites on the different excipient carrier particles than fine drug particles available to occupy these sites. Thus it appears that only a small proportion of the excipient particle surface was actually involved in the formation of an ordered unit. These locations on the carrier surface are termed "active sites" (84) and their frequency of occurrence appears to be related to the excipient particle porosity and surface area. Particles such as recrystallised lactose produced by the methods described in Chapter 2, which have a high porosity, surface area and surface roughness, produced ordered mixes which were resistant to segregation when subjected to vibration (sections 4.3.2.1, 4.3.2.2 and 4.3.2.3). However, particles with a relatively smooth, non-porous surface such as Dipac, formed fewer active adherence sites and the fine drug particles consequently segregated when vibrated (section 4.3.2). The number of active adherence sites on an excipient carrier particle also influenced the concentration of drug which could be introduced into an ordered mix without de-stabilising the system and causing segregation. The highly porous recrystallised lactose appeared to be able to carry many more fine adherent particles than the less porous Emdex and Dipac excipient powders. Recrystallised lactose formed ordered mixes

with higher drug concentrations (5 and 10%) which were more resistant to vibrational segregation than those produced by either Emdex or Dipac particles (section 4.3.2.7). The mechanism by which porous carrier particles produce non-segregating ordered mixes is influenced by the physical barrier of the pore walls preventing the fine particles from becoming dislodged by abrasion during vibration or other powder movement. More importantly, the location of fine particles in clefts such as in pores or behind surface asperities, increases the force of adhesion between drug and excipient particles as discussed in Chapter 5.

The static adhesive couple formed between the drug particle and the excipient surface is increased according to the cleft angle in which the fine particle is located. Unstable ordered mixes, such as those shown to segregate when subjected to vibration (Chapter 4) were found to have a composite adhesion profile with a steep initial curve linked to a second curve with a different slope by a so-called "lag-section" during which period few drug particles were lost (section 5.2.3). The steep initial curve was indicative of the loss of large quantities of weakly-bound drug particles from the excipient surface in mixes which had a high segregation tendency. These loosely-bound particles are presumed to be those which are unable to become located in suitable pores or clefts on the excipient surface with suitable dimensions to produce strong adhesive couples. Consequently these weakly-bound drug particles form a reservoir of drug free to move through the powder bed, giving rise to segregation when vibrated. The quantity of this weakly-bound drug fraction determines the intensity of segregation produced under given conditions. Crystallisation of lactose from supersaturated solutions containing industrial

methylated spirit produced particles with highly irregular surfaces (Chapter 2). Increasing the surface porosity of excipient particles by a crystallisation method such as that described in Chapter 2, reduced the segregation of ordered mixes containing fine drug particles.

7.2 Surface Electrical Charge

Another factor which influences the stability of ordered mixes is the surface electrical charge on the constituent particles.

Drug and excipient powder particles had different electrostatic surface charges (section 6.1) and the sign and magnitude of the static charges in a powder was shown to differ according to the surface with which the powder had just made contact. In section 4.4 the time required to produce uniform ordered mixes was related to the stability of the mixes when subjected to vibration. It was found that the more unstable the ordered mix, the longer the mixing time required to produce a homogeneous system. This phenomenon was thought to be linked with triboelectrification of the powder surfaces. Excipients such as Dipac which had a low surface porosity normally formed few active sites and it may be that these particles required prolonged frictional contact in the perspex Y-cone blender to increase the surface charge and thus increase the mutual attraction between drug and excipient particles. Table 37 (section 6.1.2) shows that particles of Emdex and recrystallised lactose charge strongly electropositive when contacted with a polyethylene surface, whereas "drug" particles such as potassium chloride charged electronegative. Thus recrystallised lactose and Emdex would have a greater affinity for drug particles and the mixing times would be decreased

accordingly. However, Dipac, which remained electronegative when contacted with a plastic surface required prolonged tumbling in the perspex Y-cone blender to bring drug and excipient particles together in a uniform ordered mix.

The importance of charges on drug and excipient particle surfaces in the formation of stable ordered mixes was further demonstrated in section 6.4. Using a triboelectric charging cyclone the magnitude of the surface electrostatic charges on various excipients was increased. In addition, the tribo-electrification of the model drug, potassium chloride caused charge reversal which meant that all the excipients were strongly electronegative whereas the drug was electropositive. The increased mutual attraction between drug and excipient particles produced ordered mixes that had an increased resistance to segregation.

The results presented in this thesis suggest that it is possible to optimise the application of the ordered mixing process in the formulation of direct-compression tablets. Non-segregating ordered mixes can be formed by using excipient particles with porous surfaces. In formulations where such porous particles cannot be used, or where the quantity of drug in the formulation exceeds the number of active sites normally capable of producing static couples strong enough to prevent dislodgement of the adherent particles, the stability of the ordered mix can be increased by optimisation of the surface electrical charges in terms of magnitude and sign. The mutual attraction between drug and excipient particles can be increased by triboelectrification on a suitable surface governed by the work functions of the drug and excipient powders. Triboelectrification can be achieved by

using a suitable charging apparatus such as an air cyclone or by prolonged mixing in a tumbling blender.

The investigation described here provides a basis for the study of the effect of particle properties, including their surface charges, on the type of mix produced and on the resistance of that mix to segregation.

Using triboelectrification, it should be feasible to produce extremely stable ordered mixes, resistant to intense segregation conditions, between many different types of particles and incorporating larger proportions of drug.

Chapter 8

Conclusions

Recrystallisation of lactose from solutions containing industrial methylated spirit produces irregular powder particles with increased porosity, surface area and surface roughness (Chapter 2). Recrystallised lactose had a more irregular surface than any of the commercial excipients, Emdex, Dipac and Elcema G250 which had comparable particle size distributions. The content of IMS in the crystallising solution ('mother liquor') had a marked effect on the surface properties of the lactose spherulites recovered. At a concentration of 80% IMS in the crystallising solution, lactose spherulites were recovered with maximum pore surface area, specific surface area, surface roughness and porosity.

Ordered mixes can be formed between many different types of particles but not all are resistant to segregation. The stability of ordered mixes formed between different fine drug and coarse excipient particles is determined by their surface properties. Powders such as Emdex and recrystallised lactose which contained porous particles of highly irregular shape, formed non-segregating ordered mixes when tested in a vibrational segregation model. Conversely, the relatively smooth particles of Dipac formed ordered mixes which segregated during vibration. The different vibration conditions influenced the intensity and scale of segregation in a given ordered mix. A combination of low vibration frequencies and high acceleration forces caused the greatest segregation tendencies in different ordered mixes.

The differences in segregation tendency of the various ordered mixes, containing excipient particles with different

surface properties such as porosity, are also influenced by surface electrical properties such as electrostatic and van der Waals molecular forces. The porous excipient surfaces provide sites for adherence of fine drug particles located by electrostatic couples which are increased by the cleft angle and maintained by intermolecular adhesion forces. The interparticle adhesion forces measured by the ultracentrifuge method were largest in those ordered mixes which did not segregate when vibrated.

Increasing the mutual attraction between drug and excipient particles by triboelectrification also increased the stability of the ordered mixes they formed. Since the electrostatic charge imparted to the drug and excipient particles by triboelectrification quickly decayed, it is thought that the main effect produced by triboelectrification was to bring the drug and excipient particles into closer contact by virtue of the increased electrostatic forces. The long-term increase in interparticle adhesion forces was probably due to an increase in the effective van der Waals molecular forces. The instantaneous close contact due to attraction between particles carrying different charges and the resultant interparticle collision combined to reduce the interparticle gap and increased the contact area by plastic deformation of the two contacting surfaces. The increased intimate contact between the drug and excipient particles, increased the effective van der Waals adhesive forces by a factor of at least twenty and is probably sufficient to explain the increased stability of the ordered mixes produced by triboelectric charging.

In particular, ordered mixes containing for example 10% "drug" (potassium chloride) and Oipac or Emdex, previously found to

exhibit very marked segregation when vibrated, were shown to have an extremely reduced low segregation tendency when triboelectrically charged prior to vibration.

When ordered mixing is used to produce a direct compression formulation, the surface physical characteristics and surface electrical properties of the different components should be determined.

The excipient used as the major diluent should have a powder surface which is as irregular and porous as possible within the limits set by tableting and flow requirements. In addition, the drug and excipient particles should have surface charges which are widely different in magnitude and/or sign. The results presented in this thesis suggest that the process of triboelectrification can be used to increase the stability of an ordered mix that shows a tendency to segregate under certain conditions.

References

1. J. Cooper, "Inert" components of pharmaceutical preparations. Drug Devel. and Industrial Pharmacy, 5, 293-334 (1979).
2. J. E. Rees, Characterisation of Pharmaceutical Particulate Materials. Boll. Chim. Farm., 116, 125-141 (1977).
3. D. A. Dean, Unit Dose. Manuf. Chemist and Aerosol News, 51, 25-30 (1980).
4. W. C. Gunsel and J. L. Kanig, in Theory and Practice of Industrial Pharmacy, L. Lachman, H. Lieberman & J. L. Kanig, Editors, Lea & Febiger, New York (1976).
5. R. Cohn, R. Nessel and G. Reier, An Evaluation of Direct Compression Excipients. Paper presented to the Industrial Pharmacy Section, 113th Annual Meeting, A.Ph.A., Dallas, U.S.A. April 25-29 (1966).
6. A. Ingale, Recent Advancements in Direct Compression Tableting, The Eastern Pharmacist, 22, 45-48 (1979).
7. R. F. Shangraw, Raw Materials of Natural Origin in Solid Dosage Forms. I. Drug and Cosmetic Industry, June, 68-82 (1978).
8. R. F. Shangraw, Raw Materials of Natural Origin in Solid Dosage Forms. II. Drug and Cosmetic Industry, July, 34-42 and 83-84 (1978).
9. J. L. Kanig, New techniques in the direct compression of pharmaceutical tablets. Paper presented to the Emcompress Symposium, London (1970).
10. E. Mendell, Direct Compression Concepts, Tablet Disintegration, Capsule filling. Proceedings of Direct Compression Symposium London, 22 April, (1975).

11. R. N. Duvall, K. T. Koshy and R. E. Dashiell, Comparative evaluation of dextrose and spray-dried lactose in direct compression systems. J. Pharm. Sci., 54, 1196-1200 (1965).

12. M. Traisnel, Formulation Methodology in Direct Compression. Proceedings of Direct Compression Symposium, London, 22 April (1975).

13. A. B. Selkirk, The Effect of Massing Time on drug concentrations in different sized granules. J. Pharm. Pharmacol., 26, 554-555 (1974).

14. M. S. Spring, The Segregation of granules during tableting. J. Pharm. Pharmacol., 29, 513-514 (1977).

15. British Pharmacopoeia. Her Majesty's Stationary Office, London (1973).

16. D. Train, Pharmaceutical Aspects of mixing solids. Pharm. J., 185, 129-134 (1960).

17. R. E. Moskalyk, L. G. Chatten, C. E. Cox & M. Pernarowski, Uniformity of drug dosage in compressed tablets. J. Pharm. Sci., 50, 650-657 (1961).

18. J. W. Mullin, Crystallisation. Butterworths, London, 2nd Edition (1972).

19. W. L. McCabe & R. P. Stevens, Rate of Growth of Crystals from aqueous solutions. Chem. Eng. Progr.. 47, 168-174 (1951).

20. C. F. Abegg, J. D. Stevens & M. A. Larson, Crystal size Distributions on Continuous Crystallisers when Growth Rate is Size Dependant. A.I.Ch.E.J., 14, 118-122 (1968).

21. J. Nyvlt, Growth of Crystals not Obeying the McCabe ΔL Law. Collect. Czech. Chem. Commun., 44, 2173-2183 (1979).

22. E. P. K. Ottens & E. J. DeJong, A model for secondary nucleation in a stirred vessel cooling crystalliser, Ind. & Eng. Chem. Fundam., 12, 179-184 (1973).

23. M. J. L. Whiting, Crystal habit modification studies with succinic acid in selected solvents. Ph.D. Thesis, University College London, May (1976).

24. J. K. Haleblian, Characterization of habits and crystalline modification of solids and their pharmaceutical applications, J. Pharm. Sci., 64, 1269-1288 (1975).

25. J. L. Torgeson and J. Strassburger, Growth of oxalic acid single crystals from solution: solvent effects on crystal habit, Science, 146, 53-55 (1964).

26. R. J. Davey, R. I. Ristic and B. Zizic, Growth rate dispersion in the growth of ADP crystals from aqueous solution particle growth processes. Instn. Chem. Engrs. 6th Annual Research Meeting, London (1979).

27. M. B. Shah, Agglomeration in a crystallising system particle growth processes. Instn. Chem. Engrs. 6th Annual Research Meeting, London (1979).

28. B. L. Herrington, Some physical properties of lactose. I. The spontaneous crystallisation of supersaturated solutions of lactose. J. Dairy Sci., 17, 501-518 (1934).

29. B. L. Herrington, Some physico-chemical properties of lactose. II. Factors influencing the crystalline habit of lactose. J. Diary Sci., 17, 533-542 (1934).

30. F. Majd and T. A. Nickerson, Effects of alcohols on lactose solubility. J. Dairy Sci., 59, 1025-1032 (1976).

31. S. G. Lim and T. A. Nickerson, Effect of methanol on the various forms of lactose J. Diary Sci., 56, 843-848 (1973).

32. A. S. Michaels and A. van Kreveld, Influence of additives on growth rates in lactose crystals. Nederlands Melk-en Zuiveltijdschrift, 20, 163-181 (1966).

33. J. E. Rees, Mixing of particulate solids to ensure homogeneity of dosage forms: the need for a critical approach to pharmaceutical process development. Boll. Chim. Farm., 116, 445-462 (1977).

34. M. H. Cooke, D. J. Stephens and J. Bridgwater, Powder mixng - a literature survey. Powder Technol., 15, 1-20 (1976).

35. J. A. Hersey, Powder mixing theory. Proceedings 1st Int. Conf. on Powder Technol. in Pharmacy, Basel, Switzerland (1978).

36. J. E. Rees, Mixing as a criterion in process development. Manuf. Chemist and Aerosol News, 46, 23-28, Dec. (1975).

37. C. C. Yeung, Fine powder mixing, M. Pharm. Thesis, Victorian College of Pharmacy, Melbourne, Australia, March (1979).

38. S. S. Weidenbaum and C. F. Bonilla, A fundamental study of the mixing of particulate solids. Chem. Eng. Progr., 51, 27J-36J (1955).

39. P. M. C. Lacey, The mixing of solid particles. Trans. Instn. Chem. Engrs., 21, 53-59 (1943).

40. K. Stange, Die Mischgüte einer Zufallmischung als Grundlage zur Beurteilung von Mischversuchen. Chemie Ing. Techn., 6, 331-337 (1954).

41. K. R. Poole, R. F. Taylor and G. P. Wall, Mixing powders to fine-scale homogeneity: studies of batch mixing. Trans. Instn. Chem. Engrs., 42, T305-T315 (1964).

42. M. C. R. Johnson, Particle size distribution of the active ingredient for solid dosage forms of low dosage. Pharm. Acta Helv., 47, 546-559 (1972).

43. H. G. Kristensen, Statistical properties of random and non-random mixtures of dry solids. Part I. A general expression for the variance of the composition of samples. Powder Technol., 7, 249-257 (1973).

44. A. B. Manning, Theory of sampling granular material for determination of size distributions. J. Inst. Fuel, 11, 153-158 (1937).

45. D. Buslik, Mixing and sampling with special reference to multi-sized granular materials. A.S.T.M. Bull., 165, 66-73 (1950).

46. N. Harnby, The estimation of the variance of samples withdrawn from a random mixture of multi-sized particles. Chem. Eng., 214, CE270-CE271 (1967).

47. J. P. Beaudry, Blender efficiency. Chem. Eng., 55, 112-114 (1948).

48. P. J. Lloyd and P. C. M. Yeung, Mixing of Powders. Chem. Process. Eng. Oct. 57-61 (1967).

49. D. Train, Mixing of pharmaceutical solids, the general approach. J. Am. Pharm. Assoc. Sci. Ed., 49, 265-271 (1960).

50. C. F. Jenkin, The pressure exerted by granular material: an application of the principle of dilatancy. Proc. Roy. Soc. A 131, 53-89 (1941).

51. J. Bridgwater, Fundamental powder mixing mechanisms. Powder Technol., 15, 215-236 (1976).

52. P. M. C. Lacey, Developments in the theory of particle mixing. J. Appl. Chem., 257-268 (1954).

53. A. Brothman, G. N. Wollan and S. M. Feldman, New analysis provides formula to solve mixing problems. Chem. Metall. Eng., 52, 102-106 (1945).

54. W. Weydanz, Zeitlicher Ablauf Einen Mischungsvoranges. Chemie Ing. Techn., 72, 343-354 (1960).

55. C. W. Yip, Ordered powder mixing. M. Pharm. Thesis, Victorian College of Pharmacy, Melbourne, Australia (1977).

56. A. M. Scott and J. Bridgwater, Interparticle percolation. A fundamental solids mixing mechanism. Ind. & Eng. Chem. Fundam. 14, 22-27 (1975).

57. D. S. Cahn and D. W. Fuerstenau, Simulation of diffusional mixing of particulate solids by Monte Carlo techniques. Powder Technol., 1, 174-182 (1967).

58. F. Strek and A. Rochowiecki. A mathematical model of mixing of particulate solids. Powder Technol., 20, 243-248 (1978).

59. F. H. H. Valentin, The mixing of powders and pastes: some basic concepts. Chem. Eng., 208, CE99-CE1044 (1967).

60. J. C. Williams, The mixing of dry powders. Powder Technol., 2, 13-20 (1968/69).

61. R. Hogg, D. S. Cahn, T. W. Healy and D. W. Fuerstenau, Diffusional mixing in an ideal system. Chem. Eng. Sci., 21, 1025-1038 (1966).

62. J. C. Williams, The properties of non-random mixtures of solid particles. Powder Technol., 3, 184-194 (1970).

63. H. G. Kristensen, The characterisation of non-random mixtures. Part III. Theory of mixture correlograms. Arch. Pharm. Chemi. Sci. Ed., 1, 102-118 (1973).

64. H. G. Kristensen, The characterisation of non-random mixtures. Part V. A general model expressing the state of a non-random mixture. Arch. Pharm. Chemi. Sci. Ed., 1, 145-163 (1973).

65. H. G. Kristensen, The characterisation of non-random mixtures. A Survey. Powder Technol., 13, 103-113 (1976).

66. J. A. Hersey, Ordered mixing - a new concept in powder mixing practice. Powder Technol., 11, 41-44 (1975).

67. C. W. Yip and J. A. Hersey, Ordered powder mixing. Nature, 262, 202-203 (1976).

68. F. H. H. Valentin, Mixing of powders, pastes and non-Newtonian fluids. Chem. Proc. Eng., 48, 69-71 (1967).

69. D. J. Craik and B. F. Miller, The flow properties of powders under humid conditions. J. Pharm. Pharmacol. Suppl., 10, 136T-142T (1958).

70. D. N. Travers and R. C. White, The mixing of micronised sodium bicarbonate with sucrose crystals. J. Pharm. Pharmacol., 23, 2605-2615 (1971).

71. J. A. Hersey, Preparation and properties of ordered mixtures. Aust. J. Pharm. Sci., 6, 29-31 (1977).

72. C. W. Yip and J. A. Hersey, Perfect powder mixtures. Powder Technol., 16, 189-192 (1977).

73. P. Thanomkiat, P. J. Stewart and P. S. Grover, Influence of carrier particle size on Prednisone-direct compression vehicle ordered mixes. Powder Technol., 24, 97-98 (1979).

74. C. C. Yeung and J. A. Hersey, Ordered powder mixing of coarse and fine particulate systems. Powder Technol., 22, 127-131 (1979).

75. N. Orr, Assessment of an ordered mix. Powder Technol., 24, 105-106 (1979).

76. C. C. Yeung and J. A. Hersey, Criteria for ordered mixtures. Powder Technol., 24, 107 (1979).

77. D. Buslik, A proposed universal homogeneity and mixing index. Powder Technol., 7, 111-116 (1973).

78. J. Verraes, Mixing of cohesive powders. Proc. Int. Conf. on Powder Technol. in Pharmacy, Basel, June (1979).

79. J. A. Hersey, Recent development in ordered powder mixing. Paper presented to Mixing & Mixtures Symposium, Institute of Drug Technol., Melbourne, Australia, Nov. (1979).

80. C. Ampolsuk, J. V. Mauro, A. A. Nyhuis, N. Shah and C. I. Jarowski, Influence of dispersion method on dissolution rate of digoxin-lactose and hydrocortisone-lactose triturations. I. J. Pharm. Sci., 63, 117-118 (1974).

81. M. J. Crooks, Manufacture and quality control of microdose drug delivery systems. Aust. J. Pharm. Sci., N55, 25-31 (1976).

82. M. J. Crooks and R. Ho, Ordered mixing in direct compression of tablets. Powder Technol., 14, 161-167 (1976).

83. T. M. Jones, The effect of glidant addition on the flowability of bulk particulate solids. J. Soc. Cosm. Chem., 21, 483-500 (1970).

84. D. N. Travers, Some observations on the ordered mixing of micronized sodium bicarbonate with sucrose crystals. Powder Technol., 12, 189-190 (1975).

85. R. Huttenrauch and I. Keiner, Influence of lattice defects upon mixing processes. Powder Technol., 22, 289-290 (1979).

86. J. A. Hersey, When disorder leads to order in powder mixing. Powder Technol., 24, 109 (1979).

87. R. Huttenrauch and I. Keiner, Producing lattice defects by drying processes. Int. J. Pharmaceutics, 2, 59-61 (1979).

88. J. A. Hersey, Powder mixing by frictional pressure: specific example of use of ordered mixing. J. Pharm. Sci., 63, 1960 (1974).

89. C. C. Yeung and J. A. Hersey, Powder homogenisation using a hammer mill. J. Pharm. Sci., 68, 721-724 (1979).

90. N. A. Orr and E. Shotton, The mixing of cohesive powders. Chem. Eng., 269, 12-18 (1973).

91. M. C. R. Johnson, The effect of particle size upon mixture homogeneity. Pharm. Acta Helv., 50, 60-63 (1975).

92. M. C. R. Johnson and J. J. Cullinan, An example of ordered and random mixing in a two component powder mixture. Paper presented to 37th Int. Congress of Pharm. Sci. of F.I.P. The Hague, Holland, 5-9 Sept. (1977).

93. M. C. R. Johnson, Powder mixing in direct compression formulation by ordered and random processes. J. Pharm. Pharmacol., 31, 273-276 (1979).

94. M. C. R. Johnson, Powder mixing in direct compression formulation. Proc. Int. Conf. on Powder Technol in Pharmacy, Basel, Switzerland, June (1979).

95. J. A. Hersey, W. J. Thiel and C. C. Yeung, Partially ordered randomised powder mixtures. Powder Technol.,

96. L. Bates, Some aspects of handling powders in mechanical equipment. J. Soc. Cosm. Chem., 20, 693-703 (1969).

97. M. J. Griffin, Mixing and blending powders. Paper presented at Powtech 77. 4th Int. Powder Technol. & Bulk Solids Conf. Paper 5-6, Part II (1977).

98. Editorial, Smoothing out the flow - latest mixing and grinding techniques. Manuf. Chem. and Aerosol News, 50, 49-52 (1979).

99. J. C. Williams and M. A. Rahman, The continuous mixing of particulate solids. J. Soc. Cosm. Chem., 21, 3-36 (1970).

100. J. C. Williams, Continuous mixing of solids. A Review. Powder Technol., 15, 237-243 (1976).

101. P. Cook and J. A. Hersey, Powder mixing in the tabletting of fenfluramine hydrochloride; evaluation of a mixer. J. Pharm. Pharmac., 26, 298-303 (1974).

102. P. Cook and J. A. Hersey, Evaluation of a Nauta mixer for preparing a multi-component mixture. Powder Technol., 9, 257-261 (1974).

103. J. Bridgwater, D. F. Bagster, S. F. Chen and J. H. Hallam, Geometric and dynamic similarity in particle mixing. Powder Technol., 2, 198-206 (1968/69).

104. J. Novosad, Studies on granular materials. Pt. I. Kinematics of granular material mixed by a mechanical impeller. Collect. Czech. Chem. Commun., 29, 2681-2696 (1964).

105. K. W. Carley-MaCaulay and M. B. Donald, The mixing of solids in tumbling mixers - I. Chem. Eng. Sci., 17, 493-506 (1962).

106. A. Kaufman, Mixing of solids. Experiments with tumbling blenders. Ind. & Eng. Chem. Fundam., 1, 104-106 (1962).

107. C. W. Yip and J. A. Hersey, Powder mixing in a revolvocube mixer. Aust. J. Pharm. Sci., 6, 49-52 (1977).

108. C. W. Yip and J. A. Hersey, The revolvocube as a powder mixer. Proc. & Chem. Eng., 30, 33-34 (1977).

109. C. W. Yip and J. A. Hersey, Ordered or random mixing: choice of system and mixer. Drug. Devel. and Ind. Pharm., 3, 429-438 (1977).

110. N. Harnby, A comparison of the performance of industrial solids mixers using segregating material. Powder Technol., 1, 94-102 (1967).

111. A. R. Rogers and J. A. Clements, The examination of segregation of granular materials in a tumbling mixer. Powder Technol., 5, 167-174 (1971/72).

112. J. C. Williams and M. I. Khan, Selecting particulate solids mixers from segregating measurement data. Br. Chem. Eng., 17, 101 (1972).

113. M. D. Faiman and E. G. Rippie, Segregation kinetics of particulate solids systems. III. Oependence on agitation intensity. J. Pharm. Sci., 54, 719-722 (1965).

114. J. C. Williams, The segregation of particulate materials. A Review. Powder Technol., 15, 245-251 (1976).

115. J. C. Williams, The segregation of powders and granular materials. J. Univ. Sheffield Fuel Soc., 14, 29-35 (1963).

116. R. L. Brown, The fundamental principles of segregation. J. Inst. Fuel, 13, 15-19 (1939).

117. R. L. Brown and J. C. Richards, Principles of powder mechanics. Int. Series of Monographs in Chem. Eng. Vol. 10, Pergamon Press, Oxford (1970).

118. J. L. Olsen and E. G. Rippie, Segregation kinetics of particulate solid systems. I. Influence of particle size and particle size distribution. J. Pharm. Sci., 53, 147-150 (1964).

119. J. C. Williams and M. I. Khan, The mixing and segregation of particulate solids of different particle size. Chem. Eng., 269, 19-25 (1973).

120. L. R. Lawrence and J. K. Beddow, Powder segregation during die filling. Powder Technol., 2, 253-259 (1968/69).

121. D. J. Stephens and J. Bridgwater, The mixing and segregation of cohesionless particulate materials. Part II. Microscopic mechanisms for particles differing in size. Powder Technol., 21, 29-44 (1978).

122. C. D. Ripple, R. V. James and J. Rubin, Radial particle size segregation during packing of particulates into cylindrical containers. Powder Technol., 8, 165-175 (1973).

123. E. G. Rippie, J. L. Olsen and M. D. Faiman, Segregation kinetics of particulate solids systems. II. Particle density-size interactions and wall effects. J. Pharm. Sci., 53, 1360-1363 (1964).

124. K. I. Syskov and T. Lyan, Investigation of the process of segregation in ore - coal mixtures. Koks i Khimiya translated in Coke and Chemistry USSR, 2, 5-9 (1960).

125. T. Tanaka, Segregation models of solids mixtures composed of different densities and particle sizes. Ind. & Eng. Chem. Proc. Des. & Dev., 10, 332-340 (1971).

126. H. Campbell and W. C. Bauer, Cause and cure of de-mixing in solid - solid mixtures. Chem. Eng. Sept. 12, 179-189 (1966).

127. E. G. Rippie, M. D. Faiman and M. K. Pramoda, Segregation kinetics of particulate solid systems. 4: Effect of particle shape on energy requirements. J. Pharm. Sci., 56, 1523 (1967).

128. J. R. Johanson, Particle segregation and what to do about it. Chem. Eng., 85, 183-188 (1978).

129. A. P. Campbell and J. Bridgwater, The mixing of dry solids by percolation. Trans. Instn. Chem. Engrs., 51, 72-74 (1973).

130. J. Bridgwater and N. D. Ingram, Rate of spontaneous inter-particle percolation. Trans. Instn. Chem. Engrs., 49, 163-169 (1971).

131. C. W. Yip and J. A. Hersey, Segregation in ordered powder mixtures. Powder Technol., 16, 149-150 (1977).

132. L. Bryan, Y. Rungvejhavuttaya, P. J. Stewart, Mixing and de-mixing of microdose quantities of sodium salicylate in a direct compression vehcile. Powder Technol., 22, 147-151 (1979).

133. J. C. Samyn and K. S. Murthy, Experiments on powder blending and unblending. J. Pharm. Sci., 63, 370-375 (1974).

134. F. K. Lai and J. A. Hersey, A cautionary note on the use of ordered powder mixtures in pharmaceutical dosage forms. J. Pharm. Pharmacol., 31, 800 (1979).

135. H. Matthée, Segregation phenomena relating to bunkering of bulk materials: theoretical considerations and experimental investigations. Powder Technol., 1, 265-271 (1967/68).

136. C. Schofield, Using hoppers to blend powders. Proc. Technical Sessions, Vol. II. Powder Europa, Wiesbaden, W. Germany, Jan. (1980).

137. P. N. Rowe and A. W. Nienow, Particle mixing and segregation in gas-fluidised beds. A Review. Powder Technol., 15, 141-147 (1976).

138. A. W. Nienow, P. N. Rowe and A. J. Agbim. The role of particle size and density differences in gas fluidised beds through Fan and Chang, (140).

139. J. C. Williams, The mixing of solid particles. Pharm. Ind., 34, 816-820 (1972).

140. L. T. Fan and Y. Chang, Mixing of large particles in 2-dimensional gas fluidised beds. Can. J. Chem. Eng., 57, 88-98 (1979).

141. P. N. Rowe, A. W. Nienow and A. J. Agbim, The mechanisms by which particles segregate in gas fluidised bed-binary systems of near spherical particles. Trans. Instn. Chem. Engrs., 50, 310-323 (1972).

142. W. J. Thiel, The mechanical stability of mixtures when fluidised. Paper presented to Mixing & Mixtures Symposium, Institute of Drug Technology, Melbourne, Australia, Nov. (1979).

143. The Pharmaceutical Codex (Incorporating the British Pharmaceutical Codex), Eleventh edition, Pharmaceutical Press, London (1979).

144. A. A. Hirst, Co-ordination of theories of gravity separation. Trans. Inst. Min. Eng., 94, 93-113 (1937).

145. A. Khan and I. J. Smalley, Observation of particle segregation in vibrated granular systems. Powder Technol., 8, 69-75 (1973).

146. L. R. Lawrence and J. K. Beddow, Some effects of vibration upon powder segregation during die filling. Powder Technol., 2, 125-130 (1968/69).

147. C. F. Harwood, Powder segregation due to vibration. Powder Technol., 16, 51-57 (1977).

148. J. A. Hersey and I. Krycer, Fine grinding and the production of coarse particulates. Chem. Eng., 351, 837-840 (1979).

149. J. C. Williams and G. Shields, The segregation of granules in a vibrated bed. Powder Technol., 1, 134-142 (1967).

150. R. B. Hudson, M. L. Jansen and P. B. Linkson, Batch sieving of deep particulate beds on a vibratory screen. Powder Technol., 2, 229-240 (1969).

151. K. Shinohara and T. Tanaka, Mechanism of sieving under tapping based on solids flow. Ind. & Eng. Chem. Proc. Des. & Dev., 14, 8-11 (1975).

152. D. S. Parsons, Particle segregation in the fine powders by tapping as simulation of jostling during transportation. Powder Technol., 13, 269-277 (1976).

153. M. T. Turczyn, Pros and cons of broadband random vibration for product/package tests. Package Development and Systems. July/Aug., 20-22 (1979).

154. J. W. Nunziato and E. K. Walsh, One dimensional shock waves in uniformly distributed granular materials. Int. J. Solids Struct., 14, 681-689 (1978).

155. W. Kroll, Forschung auf dem Gebiete des Ingen-jeurwesens, 20, 2 (1954) trans. in R. Gutman, Trans. Instn. Chem. Engrs., 54, 174-183 (1976).

156. A. F. Ryzhkov and A. P. Baskakov, Equation of motion of the material in a shaker. Inzhenerno-Fizicheskii Zhurnal, 27, 15-22 (1974) transl. in J. Eng. Phys., 27, 798-803 (1976).

157. R. G. Gutman and J. F. Davidson. Darcy's Law for Oscillatory flow. Chem. Eng. Sci., 30, 89-95 (1975).

158. R. G. Gutman. Vibrated beds of powders: Pt. I. A theoretical model for the vibrated bed. Trans. Instn. Chem. Engrs., 54, 174-183 (1976).

159. J. F. G. Harris and A. M. Hildon, Reducing segregation in binary powder mixtures with particular reference to oxygenated washing powders. Ind. Eng. Chem. Proc. Des. Dev., 9, 363-367 (1970).

160. S. S. Weidenbaum, Mixing of solids. Adv. Chem. Eng., 2, 209-324 (1958).

161. C. Schofield, The definition and assessment of mixture quality in mixtures of particulate solids. Powder Technol., 15, 169-180 (1976).

162. N. Harnby, The statistical analysis of particulate mixtures. Part 2. The application of social survey statistical techniques to solids mixing problems. Powder Technol., 5, 155-165 (1971/72).

163. N. Harnby, The statistical analysis of particulate mixtures. Part I. The sampling of mixtures and the resultant precision of estimates based on the sample. Powder Technol., 5, 81-86 (1971/72).

164. C. Schofield and F. H. H. Valentin, The use of measures based on the standard deviation in the assessment of mixture quality. Chem. Eng. Sci., 23, 661-662 (1968).

165. L. T. Fan, S. J. Chen and C. A. Watson, Solids mixing. Ind. & Eng. Chem. Ann. Revs., 62, 53-69 (1970).

166. L. T. Fan and R. H. Wang, On mixing indices. Powder Technol., 11, 27-32 (1975).

167. M. D. Ashton and F. H. H. Valentin, The mixing of powders and particles in industrial mixers. Trans. Instn. Chem. Eng., 44, T166-T188 (1966).

168. H. Rumpf and K. Sommer, Varianz der stochastischen Homogenitaet bei Koernermischungen und Suspensionen und praktische Ermittlung der Mischguete. Chem. Ing. Tech., 46, 257 (1974).

169. J. B. Gayle, O. L. Lacey, J. H. Gary, Mixing of solids. Chi-squared as a criterion. Ind. and Eng. Chem., 50, 1279-1282 (1958).

170. P. V. Danckwerts, Theory of mixtures and mixing. Research, Science and its application in industry, 6, 355-361 (1953).

171. H. G. Harvey, General Research Report no. 1. The mixing of solids with particular reference to fine powders and allied systems. Special Projects & Testing Services Ltd. Esher & Manchester (1979) and Supplement (1979).

172. L. E. Marc de Chazal and Yen-Chi Hung. A study of the effect of sample size on the analysis of powder mixtures. A.I.Ch.E.J., 14, 169-173 (1968).

173. H. G. Kristensen, Statistical properties of random and non-random mixtures of dry solids. Part II. Variance - sample size relationships derived by autocorrelation theories. Powder Technol., 8, 149-159 (1973).

174. P. V. Danckwerts, The definition and measurement of some characteristics of mixtures. Appl. Sci. Res. Section A, 3, 279-296 (1953).

175. P. M. C. Lacey and F. S. M. A. Mirza, A study of the structure of imperfect mixtures of particles. Part I. Experimental technique. Powder Technol., 14, 17-24 (1976).

176. P. M. C. Lacey and F. S. M. A. Mirza, Part II. Correlation analysis, ibid., 25-34.

177. C. H. Chou, J. R. Johnson and E. G. Rippie, Polydisperse particulate solids mixing and segregation: non-stationary Markov chains. J. Pharm. Sci., 66, 104-110 (1977).

178. United States Pharmacopoeia, Vol. XIX, Published by The U.S.P. Convention Inc., Printed by Mack Co., Philadelphia, U.S.A. (1975).

179. J. A. Hersey, Powder mixing: theory and practice in pharmacy. Powder Technol., 15, 149-153 (1976).

180. J. A. Hersey, Assessment of homogeneity of powder mixtures. J. Pharm. Pharmacol., 19, 1685-1765 (1967).

181. J. A. Hersey, Monitoring homogeneity. Drug Devel. Commun., 1, 119-132 (1974/75).

182. J. A. Hersey and P. C. Cook, Homogeneity of pharmaceutical dispersed systems. J. Pharm. Pharmacol., 26, 126-133 (1974).

183. J. A. Hersey, Application of a proposed universal homogeneity and mixing index to tabletting operations. Powder Technol., 10, 97-98 (1974).

184. J. A. Hersey, P. C. Cook, M. Smyth, E. A. Bishop and E. A. Clarke, Homogeneity of multicomponent powder mixtures. J. Pharm. Sci., 63, 408-416 (1974).

185. M. C. R. Johnson, Particle-size requirements related to content uniformity of solid dosage forms. J. Pharm. Sci., 63, 1961-1963 (1974).

186. D. F. St. John, Adhesion of small metal spheres to plane metal substrates. Ph.D. Thesis, Michigan State University (1969).

187. H. Krupp, Particle adhesion. Theory and experiment. Advan. Colloid Interface Sci., 1, 111-239 (1967).

188. W. R. Smythe, Static and dynamic electricity, 3rd Edition, McGraw-Hill, New York (1972).

189. H. C. Hamaker, The London - van der Waals attraction between spherical particles. Physica, 4, 1058-1072 (1937).

190. J. E. Kiefer and V. A. Parsegian, An easily calculable approximation for the many body van der Waals attraction between 2 equal spheres. J. Colloid & Interface Sci., 57, 580-582 (1976).

191. D. K. Donald, Electrostatic contribution to powder-particle adhesion. J. Appl. Phys., 40, 3013-3019 (1969).

192. E. M. Lifshitz, The theory of molecular attractive forces between solids. Soviet Physics J.E.T.P., 2, 73-83 (1956).

193. W. Kottler, H. Krupp and H. Rabenhorst, Adhesion of electrostatically charged particles. Zeitschrift Angewandte Physik, 24, 219-223 (1968).

194. D. K. Donald and P. K. Watson, The influence of electric fields on particle adhesion in xerographic developer mixtures. Photographic Science and Engineering, 14, 36-41 (1970).

195. B. M. A. Bozorg and G. E. Klinzing, Adhesion of alumina powder to glass surfaces. Can. J. Chem. Eng., 57, 665-659 (1979).

196. D. K. Donald, Contribution of charge to powder particle adhesion. J. Adhesion, 4, 233-245 (1972).

197. A. D. Moore, Electrostatics. Sci. Am., 226, 47-58 (1972).

198. W. A. D. Rudge, On the electrification associated with dust clouds. Philosophical Magazine, 25, 481-494 (1913).

199. W. A. D. Rudge, On the electrification produced during the raising of a cloud of dust. Proceedings of the Royal Society, Series A, 90, 256-272 (1914).

200. H. Masuda and K. Iinoya, Electrification of particles by impact on inclined metal plates. A.I.Ch.E.J., 24, 950-956 (1978).

201. M. I. Pope, F. Satta, D. I. Sutton and M. J. Pearse, Factors affecting the triboelectric charging of mineral particles. Proc. 11th Int. Mineral Processing Congress, Cagliari, Italy, 213-228 (1975).

202. M. J. Pearse and A. D. Read, Triboelectric separation. A dry process for separating particulate mixtures. Warren Spring Laboratory Report, LR 223 (MP), (1976).

203. M. J. Pearse and M. I. Pope, The triboelectric separation of quartz-calcite and quartz-apatite powders after chemical conditioning. Powder Technol., 17, 83-89 (1977).

204. F. J. Feltham, Second thoughts on the Hansen Electrostatic filter. Filtration & Separation, Sept/Oct., 467-469 (1976).

205. W. H. Walton, First report on the electrical characteristics of resin impregnated filters. Porton Report No. 2465, Chemical Defence Establishment, Porton Down (1940).

206. K. A. Nielsen and J. C. Hill, Collection of inertialess particles on spheres with electric forces. Ind. & Eng. Chem. Fundam., 15, 149-156 (1976).

207. K. A. Nielsen and J. C. Hill, Capture of particles on spheres by inertial and electrical forces. Ind. & Eng. Chem. Fundam., 15, 157-163 (1976).

208. Medicine in the 1990's. Office of Health Economics No. 11, 14441 (1965).

209. The European Pharmacopoeia, (European Treaty Series No. 50), Published by Maisonneuve S.A., Sainte-Ruffine, France (1971).

210. Pavel Jelen and S. T. Coulter, Effects of supersaturation and temperature on the growth of lactose crystals. J. Food Sci., 38, 1182-1185 (1974).

211. V. R. Phillips, The quantitative recovery of crystals from mother liquor in experiments on crystallisation from solution. Chem. & Ind., 16 Nov., 922-924 (1974).

212. J. W. Mullin and H. M. Ang, Effect of ultrasonics on crystal agglomerates: test for the degree of agglomeration. Chem. & Ind., 3 Aug., 622-623 (1974).

213. E. O. Whittier, Lactose and its utilization: A review. J. Dairy Sci., 27, 505-537 (1944).

214. R. L. Carr, Classifying flow properties of solids. Chem. Eng., 72, 69-72 (1965).

215. H. H. Hausner, Friction conditions in a mass of metal powder. Int. J. Powder Metall., 3, 7-13 (1967).

216. M. Kahlweit, On the ageing of dendrites. Scripta Metallurgica, 2, 251-254 (1968).

217. J. J. Reeves and T. Z. Kattamis, A model for isothermal dendritic coarsening. Scripta Metallurgica, 5, 223-229 (1971).

218. H. M. Rootare and C. F. Prenzlow, Surface areas from mercury porosimeter measurements. J. Phys. Chem., 71, 2733-2736 (1967).

219. H. Heywood, Particle shape coefficients. J. Imp. Coll. Chem. Eng. Soc., 8, 25-33 (1954).

220. M. H. Rubinstein and P. Musikabhumna, A universal friability test for tablet granules. Pharm. Acta, 53, 125-129 (1978).

221. D. R. Beaman and J. A. Isasi, Electron beam microanalysis - Part I. The fundamentals and applications. Materials Research and Standards, November, 8-78 (1971).

222. D. R. Beaman and J. A. Isasi, Electron beam microanalysis - Part II. Experimental considerations and quantitative analysis. Ibid., December, 12-56 (1971).

223. P. N. Rowe, A. W. Nienow and A. J. Agbim, A preliminary quantitative study of particle segregation in gas-fluidised beds - binary systems of near spherical particles. Trans. Instn. Chem. Engrs., 50, 324-333 (1972).

224. C. M. Harris and C. E. Crede, Shock and Vibration Handbook. 2nd Edition, McGraw-Hill, New York (1976).

225. P. L. Stephenson and W. J. Thiel, The effect of humidity on the production of ordered mixtures. Powder Technol., 25, 115-119 (1980).

226. M. C. Coelho and N. Harnby, Moisture bonding in powders. Powder Technol., 20, 201-205 (1978).

227. P. Fairbank, Assisted mass flow discharge of bulk particulate materials. Proceedings Technical Sessions, Vol. I, Powder Europa, Wiesbaden, January 1980.

228. P. C. Arnold and A. S. Kaaden, Reducing hopper wall friction by mechanical vibration. Powder Technol., 16(1), 63-66 (1977).

229. K. Shinohara and T. Tanaka, Effect of tapping on flow of particles from storage vessels. Ind. & Eng. Chem. Process Design, 14, 1-8 (1975).

230. C. Schofield, Assessing mixtures by autocorrelation. Trans. Instn. Chem. Engrs., 48, T28-T34 (1970).

231. C. D. Hendricks, Charging macroscopic particles in electrostatics and its applications, Chapter 4, Edited by A. D. Moore, Wiley Interscience, New York (1973).

232. L. B. Loeb, Static electrification, page 166, Springer, Berlin (1958).

233. M. J. Pearse, Personal communication (1978).

234. M. J. Pearse and M. I. Pope, The separation of Quartz-Dolomite powders using a triboelectric technique, Powder Technol., 14, 7-15 (1976).

235. R. R. Greenfield, Filtration and Separation, May/June, 304-309 (1973)

236. Separation of Dust from Gases, E.E.U.A. Handbook No. 19, pages 26-37, Constable and Co., London (1967).

237. J. H. Berry, Chemical Engineers Handbook, 4th Edition, pages 20-69, McGraw-Hill, New York (1963).

238. M. J. Pearse, Unpublished work, Portsmouth Polytechnic (1975).

239. S. T. Harris, The technology of powder coatings, Edited by E. C. Roberson, Portcullus Press, London (1976).

240. J. Cross, Adhesion of electrostatic powder coatings, Inst. Phys. Conf. Series No. 27, Chapter 3, 202-213 (1975).

241. M. Pauthenier, J. Phys. Radium Ser., 7, 590-598, (1932).

242. B. Dahneke, The influence of flattening on the adhesion of particles. J. Colloid & Interface Science, 40, 1-13 (1972).

243. W. R. Harper, Contact and frictional electrification, Clarendon Press, Oxford (1967).

244. D. F. St. John and D. J. Montgomery, Adhesion of small metal spheres to plane metal substrates. J. Appl. Phys., 42, 663-668 (1971).